Titre: Title:	Inelastic response of steel roof deck diaphragms under simulated dynamically applied seismic loading
Auteur: Author:	Eric Martin
Date:	2002
Type:	Mémoire ou thèse / Dissertation or Thesis
Référence: Citation:	Martin, E. (2002). Inelastic response of steel roof deck diaphragms under simulated dynamically applied seismic loading [Master's thesis, École Polytechnique de Montréal]. PolyPublie. https://publications.polymtl.ca/8854/

URL de PolyPublie: PolyPublie URL:	https://publications.polymtl.ca/8854/
Directeurs de recherche: Advisors:	Robert Tremblay, & Colin Rogers
Programme: Program:	Unspecified

UNIVERSITÉ DE MONTRÉAL

INELASTIC RESPONSE OF STEEL ROOF DECK DIAPHRAGMS UNDER SIMULATED DYNAMICALLY APPLIED SEISMIC LOADING

ÉRIC MARTIN
DÉPARTEMENT DES GÉNIES CIVIL, GÉOLOGIQUE ET DES MINES
ÉCOLE POLYTECHNIQUE DE MONTRÉAL

MÉMOIRE PRÉSENTÉ EN VUE DE L'OBTENTION
DU DIPLÔME DE MAÎTRISE ÈS SCIENCES APPLIQUÉES
(GÉNIE CIVIL)
NOVEMBRE 2002

UNIVERSITÉ DE MONTRÉAL

ÉCOLE POLYTECHNIQUE DE MONTRÉAL

Ce mémoire intitulé :

INELASTIC RESPONSE OF STEEL ROOF DECK DIAPHRAGMS UNDER SIMULATED DYNAMICALLY APPLIED SEISMIC LOADING

présenté par : MARTIN Éric
en vue de l'obtention du diplôme de : Maîtrise ès sciences appliquées
a été dûment accepté par le jury d'examen composé de :

M. LÉGER Pierre, Ph.D., président
M. TREMBLAY Robert, Ph.D., membre et directeur de recherche
M. ROGERS Colin, Ph.D., membre et codirecteur de recherche
Mme McCLURE Ghyslaine, Ph.D., membre

REMERCIEMENTS

Je tiens à remercier tous ceux qui ont contribué à la réalisation de ce projet et plus particulièrement :

M. Robert Tremblay, directeur de recherche, et M. Colin Rogers, codirecteur de recherche, pour leurs conseils et aide précieuse apportés tout au long du projet.

Je remercie chaleureusement toute l'équipe technique du Laboratoire de Structures de l'École Polytechnique : M. Gérard Degrange, M. Denis Fortier et M. Patrice Bélanger. Je remercie aussi Wei Yang pour son aide apportée à la réalisation des montages expérimentaux.

Je voudrais remercier également le Conseil de recherche des sciences naturelles et du génie du Canada (CRSNG), le Bureau Canadien de la soudure (CWB), l'Institut Canadien de la Construction en Acier (ICCA), le Canadian Sheet Steel Building Institute (CSSBI), le Steel Deck Institute (SDI), Hilti et le Groupe Canam-Manac pour leurs contributions à ce projet.

RÉSUMÉ

Les procédures de conception parasismique actuelles pour les diaphragmes de toit en acier ne permettent pas de déformation inélastique dans le pontage métallique. Ainsi, les normes requièrent que les éléments verticaux de transfert des charges latérales (ex. : contreventements) soient dimensionnés comme éléments dissipateurs d'énergie. Il n'est pas possible pour le moment de considérer les diaphragmes comme éléments dissipateurs d'énergie dû au manque d'information sur le comportement sismique de ces éléments.

Face à cette problématique, un projet de recherche a été mis en branle à l'École Polytechnique de Montréal. Un objectif du projet de recherche est de déterminer des facteurs reliés à la ductilité, R_d, selon le type de diaphragme. Différents types de connecteurs sont considérés : des vis, des clous et des soudures pour les connecteurs à la structure, et des vis, des soudures et poinçons pour les connecteurs de couture. Une première série d'essais a été réalisée sur des diaphragmes sous des chargements monotoniques et quasi-statiques par Essa *et al.* (2001).

Mon projet de recherche avait pour objectif d'évaluer le comportement inélastique de diaphragmes en acier sous des chargements sismiques. Il comportait deux étapes principales : une partie analytique qui avait pour but d'évaluer la demande sismique et une partie expérimentale pour permettre d'examiner le comportement des éléments de diaphragme sous la demande sismique évaluée dans la partie analytique.

Des modèles numériques de bâtiments en acier ont été construits à l'aide du logiciel Ruaumoko. Le comportement hystérétique des diaphragmes a été modélisé à l'aide des données provenant des tests quasi-cycliques. Des bâtiments de différentes grandeurs ont été dimensionnés pour l'Est et l'Ouest du Canada. De plus, la conception des bâtiments a été réalisée pour différents facteurs de ductilité, R_d, en vue d'obtenir les niveaux de

ductilité en fonction de la charge de calcul. Des analyses non-linéaires sous une série de mouvements de sol historiques et artificiels ont été effectuées, et on a obtenu des historiques de la distortion et des forces de cisaillement dans le diaphragme.

À partir de ces résultats, des protocoles de chargement ont été développés pour chacun des facteurs reliés à la ductilité, R_d, considérés et pour l'Est et l'Ouest canadien.

Dix-neuf tests au total ont été réalisés sur un montage horizontal de 6.10 m x 3.66 m, dont 6 tests monotoniques et 13 tests sous les chargements sismiques développés dans la partie analytique. Différents types de connecteurs et épaisseurs de tablier ont été étudiés.

Les essais ont démontré que les diaphragmes faits de connecteurs de couture poinçonnés et de connecteurs à la structure soudés doivent demeurer dans le domaine élastique sous l'action des séismes. Par contre, les diaphragmes conçus à partir de connecteurs à la structure cloués et de connecteurs de couture vissés peuvent subir des déformations inélastiques tout en maintenant une résistance adéquate. Pour ce type de diaphragme, il serait possible d'utiliser un facteur relié à la ductilité, R_d, supérieur à 1.0.

D'autres études seront nécessaires pour réévaluer la demande sismique à la lumière des nouvelles informations. De plus, l'effet des joints de chevauchement devra être examiné.

ABSTRACT

At present, the procedures used for the seismic design of steel roof deck diaphragms for single-storey steel structures do not allow for inelastic deformations in the deck. In consequence, the relevant design standards require that the vertical elements of the lateral force resisting system (e.g. vertical wall bracing) be designed as the energy-dissipating element. Currently, it is not possible to consider the roof diaphragm as an energy-dissipating element due to the lack of knowledge concerning its seismic behaviour.

To address this problem, a research investigation was established at École Polytechnique de Montréal. One overall objective of this investigation was to determine the ductility related force modification factor, R_d, for each type of diaphragm. Various fasteners were considered: i.e. screws, nails and welds for deck-to-frame fasteners, screws, welds and button punches for the sidelap fasteners. A first series of tests was completed by Essa *et al.* (2001) on diaphragms subjected to monotonic and quasi-static in-plane shear loading conditions.

This thesis describes a specific research project that was aimed at evaluating the inelastic behaviour of steel diaphragms under seismic loading. The project was divided into two phases: 1) an analytical part to evaluate the seismic demand on steel roof diaphragms, and 2) an experimental part to examine the behaviour of diaphragm elements under the seismic demand evaluated in part 1.

Numerical models of steel buildings were developed using the Ruaumoko nonlinear time history analysis software. The hysteretic behaviour of diaphragms was modelled with data from existing quasi-static tests. Buildings of different dimensions were sized for Eastern and Western Canada. Moreover, the designs were made for different ductility related force modification factors, R_d, to obtain the various ductility levels in terms of

the design loads. Nonlinear analyses under historical and artificial ground motions were performed to obtain load and distortion time-histories of the single-storey buildings. From these results, loading protocols were developed for each ductility related force modification factor, R_d, considered for Eastern and Western Canada.

In total, 19 cantilever type tests were performed on a horizontal set-up of 6.10 m x 3.66 m. Various fasteners and sheet steel thicknesses were included in the test matrix. Included in this matrix were 6 monotonic tests and 13 tests under the seismic loading protocols developed in the analytical investigation.

The tests demonstrated that the diaphragms made of welded deck-to-frame fasteners and button punched sidelap fasteners should remain in the elastic range under seismic action. However, the diaphragms made of nailed deck-to-frame and screwed sidelap fasteners can sustain inelastic deformations while maintaining a sufficient in-plane shear capacity. For this type of deck assembly, it would be possible to use a ductility related factor, R_d, greater than 1.0.

Further studies are required to re-evaluate the seismic demand taking into consideration the information obtained by carrying out the seismic loading tests. In addition, the effect of overlapping joints should be examined.

CONDENSÉ EN FRANÇAIS

PROBLÉMATIQUE

Les bâtiments en acier d'un seul étage sont largement utilisés en Amérique du Nord. Ils représentent une grande proportion des bâtiments à vocation industrielle, commerciale et récréative. Dans la plupart de ces structures, le pontage métallique joue un rôle prépondérant en tant que diaphragme: le diaphragme de toit transmet les efforts latéraux de vent et séisme aux éléments de résistance aux efforts latéraux. Le diaphragme de toit est fait de feuilles de pontage métallique qui sont attachées les unes aux autres et aux éléments de structures d'acier. La Figure 1 présente un bâtiment typique en acier d'un seul étage avec le pontage métallique installé sur sa partie gauche.

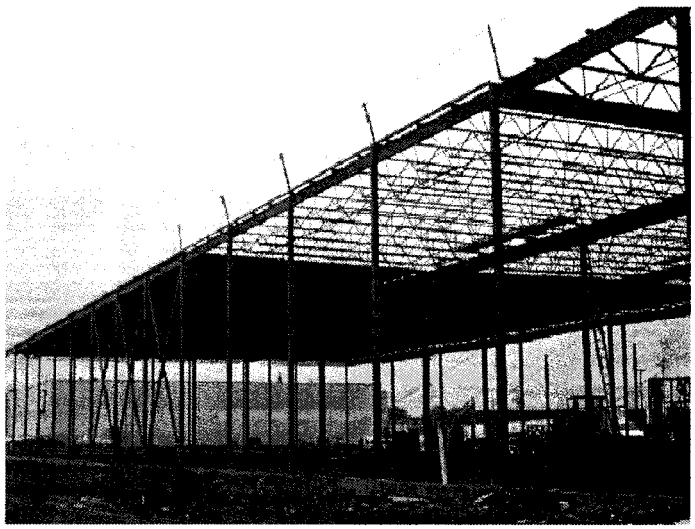

Figure 1 Structure typique en acier d'un seul étage

Plusieurs études analytiques et expérimentales portant sur le comportement des diaphragmes de toit en acier ont été faites depuis les années 1960. La plupart de ces études ont été produites sous des conditions de chargement statique et des recommandations de design ont été proposées pour de telles conditions, c'est-à-dire

quand le chargement appliqué est relativement constant, bien en dessous de la charge ultime et dans le domaine élastique (e.g.: Luttrell (SDI, 1981 et 1987), Davies and Bryan (1982), CECM (1977), CSSBI (1991)).

Le comportement typique d'un diaphragme de toit sous un chargement monotonique est présenté à la Figure 2. Il s'agit d'une courbe typique de l'effort de cisaillement par unité de longueur, S, en kN/m, versus la déformation angulaire en cisaillement, γ, en radians/1000.

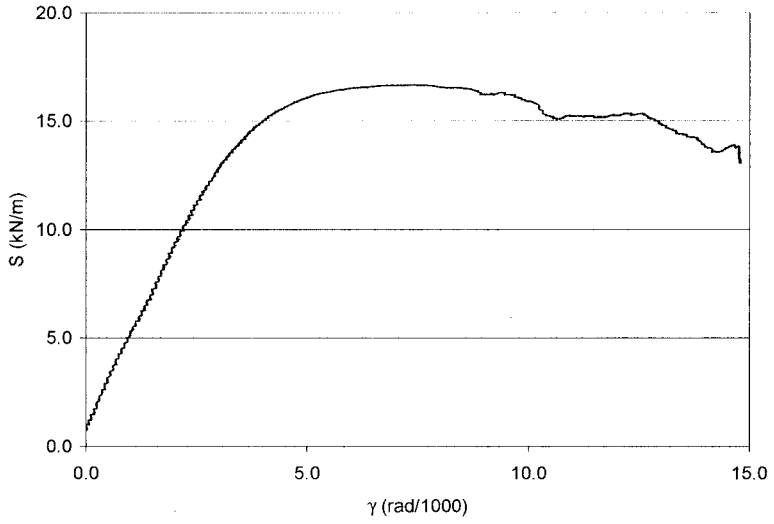

Figure 2 Comportement typique charge-déplacement d'un diaphragme sous chargement monotonique (Test 19 de cette étude)

Ce comportement peut être décrit de la façon suivante. Au départ, le comportement est essentiellement linéaire et élastique. Plus tard, certains des assemblages entrent dans le domaine inélastique ce qui se traduit par un assouplissement du diaphragme. Cet assouplissement graduel du système s'explique par le fait que les assemblages sont chargés à différents niveaux de cisaillement dus à leur localisation et leur rigidité relative. Par la suite, le diaphragme atteint sa charge maximale, lorsque la rupture

survient dans les assemblages (plus fréquent) ou par flambement du tablier en cisaillement (seulement pour les pontages à feuilles minces de longue portée). Après avoir atteint la charge maximale, la résistance du diaphragme décroît à un taux qui est fonction du type et de l'espacement des connecteurs utilisés.

Le chargement sismique en comparaison du chargement latéral statique cause une sollicitation bien différente sur un élément structural. La sollicitation sismique est de nature dynamique avec plusieurs cycles de chargement se produisant à un taux de déformation plus élevé que dans un essai monotonique habituel. De plus, si on adopte les dispositions du code national du bâtiment du Canada (CNBC) actuel (NRCC, 1995), il est possible que ces cycles de chargement se produisent à des niveaux de déformation supérieurs à celui correspondant à la charge maximale de l'essai monotonique. Enfin, parmi les diverses charges latérales susceptibles d'être appliquées aux bâtiments construits au Canada, l'effet des séismes est souvent celui qui domine et, malgré cela, aucune étude n'a été réalisée pour étudier le comportement sismique inélastique des diaphragmes métalliques.

Par conséquent, il n'existe pas, dans le CNBC ou dans le code S16.1 pour le calcul des structures d'acier (CSA, 1994), de recommandations sur la conception parasismique et le détail de construction pour des pontages métalliques qui sont susceptibles de subir de grandes sollicitations sismiques en régime inélastique. Les mêmes charges statiques équivalentes sont utilisées pour le dimensionnement du diaphragme et pour les contreventements. Ainsi, les déformations inélastiques peuvent survenir dans l'élément le plus faible : le diaphragme ou les contreventements. Étant donné que peu d'informations sont disponibles sur le sujet, le nouveau CSA-S16-2001 (CSA, 2001) et le CNBC 2004 (CANCEE, 2001) demandent à ce que le diaphragme soit protégé en lui donnant une résistance supérieure à celle des contreventements (approche de calcul par capacité avec les contreventements formant le mécanisme dissipatif). Il est nécessaire d'obtenir une meilleure compréhension du comportement sismique de ces éléments

structuraux afin de considérer l'effet du comportement non-linéaire du diaphragme sur la réponse du bâtiment en acier dans son ensemble. Ceci pourrait permettre de retenir le diaphragme comme élément dissipatif de la structure et ainsi réduire les charges sismiques de calcul pour le diaphragme et arriver à une structure plus économique.

On a démarré en 1999 un programme de recherche à l'École Polytechnique de Montréal pour mieux comprendre le comportement sismique des diaphragmes de toit en acier et pour proposer des méthodes de conception parasismique. Rogers et Tremblay (2000) ont étudié le comportement sismique inélastique de connecteurs courants à la structure et aux joints de couture pour les diaphragmes de toit en acier. Ils ont trouvé que la réponse inélastique variait de façon significative d'un type de connecteur à un autre. Compte tenu que le comportement d'un diaphragme de toit en acier dépend de ses connecteurs, il était anticipé que cette conclusion s'appliquerait aussi aux diaphragmes.

Suite à la recherche précédente, Essa *et al.* (2001) firent des tests monotoniques et cycliques de type quasi-statique sur des diaphragmes de toit en acier pleine grandeur (3.6 m x 6.1 m). Une courbe typique de la charge de cisaillement en fonction de la déformation en cisaillement pour un diaphragme de toit en acier (pontage de 38 mm de profondeur fait d'acier de 0.76 mm d'épaisseur, cloué à la structure et assemblages de couture vissés) sous un chargement cyclique quasi-statique est présenté à la Figure 3.

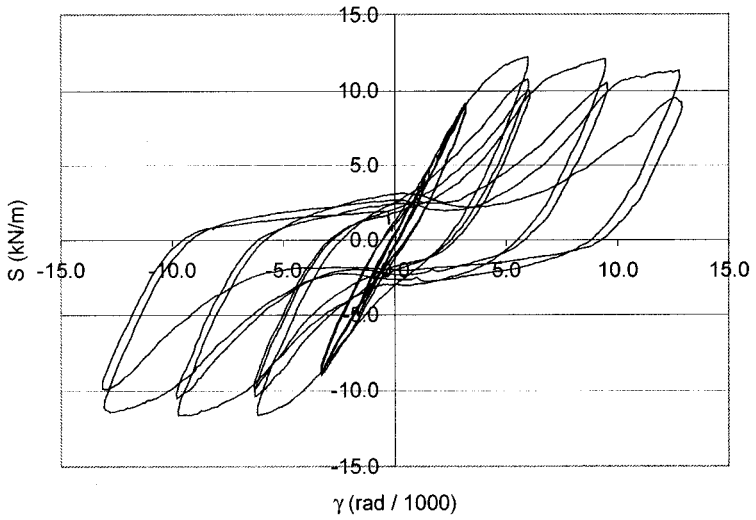

Figure 3 Comportement typique cisaillement–distortion d'un diaphragme sous chargement cyclique (provenant du test 7 (Essa *et al.*, 2001))

Dans les premiers cycles, le déplacement imposé était petit et le diaphragme est demeuré élastique. Sous des déformations plus importantes, la plastification est apparue dans les connecteurs du pontage métallique et le spécimen a commencé à se comporter de manière inélastique, avec une rigidité d'ensemble décroissante. Dans le domaine post-ultime, on observe une dégradation graduelle de la résistance en cisaillement sous les chargements cycliques qui est due aux ruptures dans les connecteurs ou au flambement local dans le pontage métallique.

Puisqu'il n'existait pas de données disponibles sur la sollicitation cyclique sismique anticipée dans les diaphragmes de toit de bâtiments réels, Essa *et al.* ont adopté un chargement simplifié, où la déformation cyclique était augmentée par incréments successifs, pour obtenir un estimé de la capacité en déformation inélastique des diaphragmes sous chargement cyclique. Cependant, il n'y avait pas de correspondance directe entre les niveaux de déformations appliqués lors de ces essais et celui auquel on peut s'attendre dans un bâtiment conçu selon les règles en vigueur au Canada. Il est de

plus possible que la sollicitation puisse varier avec le niveau de résistance du diaphragme et avec le comportement inélastique du bâtiment dans son ensemble, incluant l'effet de la flexibilité du diaphragme et ses déformations inélastiques. Afin de pouvoir porter un jugement sur la possibilité pour un bâtiment de résister aux secousses sismiques avec un diaphragme se déformant en régime inélastique, il était nécessaire d'obtenir une mesure représentative du niveau de sollicitation anticipé dans les diaphragmes de toit de bâtiments courants, puis de soumettre les diaphragmes à ce niveau de sollicitation pour étudier leur comportement.

OBJECTIFS ET PORTÉE DE LA RECHERCHE

Les objectifs de ce projet de recherche étaient 1) d'évaluer la sollicitation sismique sur les diaphragmes conçus pour entrer dans le domaine inélastique, 2) d'examiner la réponse de différents systèmes de diaphragme assujettis à cette sollicitation, et 3) de recommander des charges minimales de conception pour les diaphragmes étudiés. Cette étude était limitée à des bâtiments rectangulaires uniformes d'un seul étage, munis d'un diaphragme de toit en acier fait avec les panneaux de pontage métallique d'un modèle courant.

La sollicitation sous les tremblements de terre intra-plaques anticipés à la fois dans l'Est et l'Ouest canadien devait être évaluée. Pour l'Ouest canadien, la sollicitation sous les séismes inter-plaques de subduction Cascadia devait aussi être étudiée. Des tests devaient être complétés sous des chargements dynamiques correspondant à la sollicitation sismique véritable anticipée sous ces séismes. Des recommandations préliminaires pour la conception parasismique des diaphragmes de toit devaient ensuite être proposées, dans un format compatible avec celui adopté pour la prochaine édition (2004) du CNBC (NRCC, 2001). Ces recommandations devaient être obtenues pour les types de diaphragmes les plus prometteurs, basés sur la recherche d'Essa *et al.* Toutefois, des recommandations de conception parasismique étaient aussi requises pour

les diaphragmes communément utilisés, ceux qui, dans la pratique actuelle, sont construits à partir de soudures à l'arc et de poinçons. Finalement, un dernier objectif était de vérifier le comportement des diaphragmes connectés à la structure avec des clous Hilti, un cas où Essa *et al.* avaient observé des ruptures dans les connecteurs.

Le texte qui suit présente, en résumé, les analyses de bâtiments, le développement de protocoles de chargement et les tests sur les diaphragmes. Des recommandations pour la conception parasismique suivent et des recommandations pour les études futures sont aussi présentées.

ANALYSES DE BÂTIMENTS

Une étude analytique a été complétée dans le but d'évaluer la sollicitation sismique sur les diaphragmes de toit dans les bâtiments en acier d'un seul étage dans lesquels le diaphragme de toit est sélectionné en tant qu'élément dissipateur d'énergie. Les structures ont été conçues suivant les recommandations du prochain CNBC 2004 et le code de conception des charpentes d'acier CSA-S16-2001. On a utilisé, de façon tentative, des valeurs de 2.0 et 3.0 pour le facteur de modification des charges sismiques lié à la ductilité, R_d. L'utilisation d'une valeur plus élevée donne des charges de conception plus faibles, une résistance moins élevée pour le diaphragme et, par conséquent, des déformations inélastiques plus importantes anticipées sous un séisme important. Le choix de ces valeurs du coefficient R_d devait être validé ultérieurement en comparant les niveaux de déformation inélastique obtenus des analyses à la capacité des diaphragmes établie par Essa *et al.* dans leurs essais.

Quatre dimensions de bâtiments ont été étudiés : 15m x 30 m, 30 m x 60 m, 60 m x 120 m et 30 m x 120 m. Dans tous les cas, on a supposé un diaphragme fait avec des panneaux de pontage ayant des connecteurs de couture vissés et des connecteurs à la structure cloués. Deux sites ont été retenus qui correspondent à deux régions sismiques

différentes du Canada : l'Est canadien (Québec, QC) et l'Ouest canadien (Victoria, CB). Une fois les bâtiments conçus, on a procédé à des analyses dynamiques non linéaires pas-à-pas en utilisant le programme Ruaumoko (Carr, 2000). Pour ces analyses, on a utilisé des modèles qui pouvaient reproduire le comportement inélastique des diaphragmes de toit, tel qu'obtenu des essais de Essa *et al.* (Figure 4).

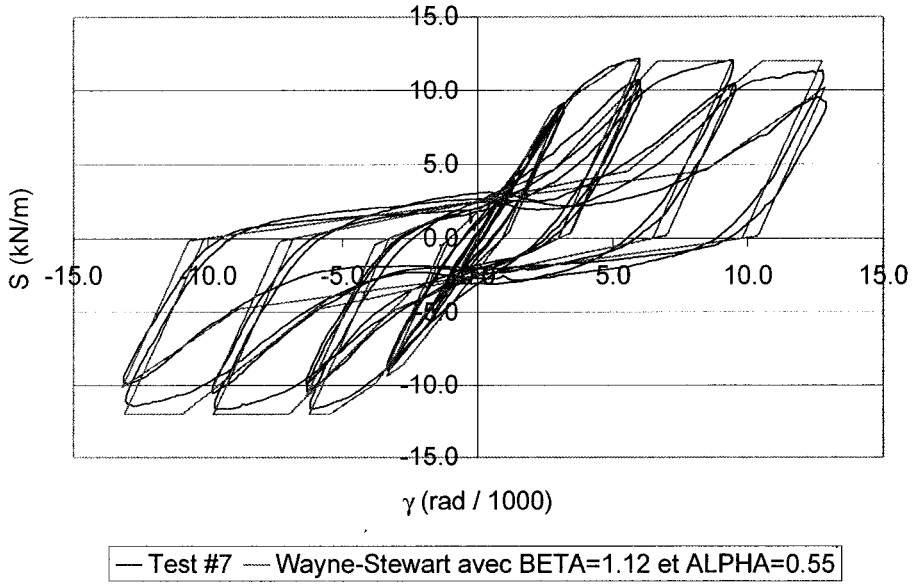

Figure 4 Comparaison du modèle d'hystérésis et du test 7 (Essa *et al.*)

Le comportement en tension-seulement des diagonales des contreventements verticaux a aussi été modélisé dans les analyses. Des historiques de mouvements de sol ont été sélectionnés pour chacun des deux sites, en fonction de la sismicité de la région, et appliqués aux modèles de bâtiment. En plus des bâtiments conçus selon le prochain CNBC 2004, on a aussi étudié le cas des bâtiments munis de diaphragmes de toit avec connecteurs de couture poinçonnés et des connecteurs à la structure soudés, conçus selon le CNBC 1995. Pour ces bâtiments, la procédure de conception du code CNBC 1995 peut donner lieu à une situation où le diaphragme de toit en acier est l'élément faible dans le système de résistance aux charges latérales. Un système de contreventement

ductile a été retenu pour les contreventements de ce bâtiment, ce qui permettait d'utiliser un facteur de modification des charges sismiques, R, égal à 3.0. Les principales découvertes de ces analyses sont présentées en deux parties : les observations pour les diaphragmes vissés-cloués conçus avec le CNBC 2004 et les résultats pour les diaphragmes poinçonnés-soudés dimensionnés avec le CNBC 1995.

Bâtiments conçus selon le CNBC 2004:

Pour tous les modèles, la déflexion dynamique maximale était plus petite que la déflexion obtenue à partir de la procédure de calcul conventionnelle, dans laquelle le bâtiment est chargé de façon uniforme avec le cisaillement à la base et les déflexions multipliées par les facteurs R_dR_o, R_o étant le facteur de modification des charges qui prend en compte la résistance réelle totale anticipée de la structure. Dans tous les cas, la déflexion latérale maximale rencontrait les critères de déformation latérale du CNBC, soit 2.5% de la hauteur de l'édifice. Les résultats ont indiqué que les bâtiments situés à Québec ont subi des déformations plus petites que ceux localisés dans l'Ouest canadien. À Québec, dû à des critères de conception autres que la résistance proprement dite, les bâtiments avaient une importante réserve de résistance et de rigidité, et la période dominante des séismes était plus courte que la période fondamentale des ouvrages, ce qui a contribué aux déformations plus faibles qui ont été obtenues.

Pour évaluer l'importance de la sollicitation sismique, on a utilisé la déformation plastique en cisaillement subie par les diaphragmes, γ_p, telle qu'illustrée sur la Figure 5.

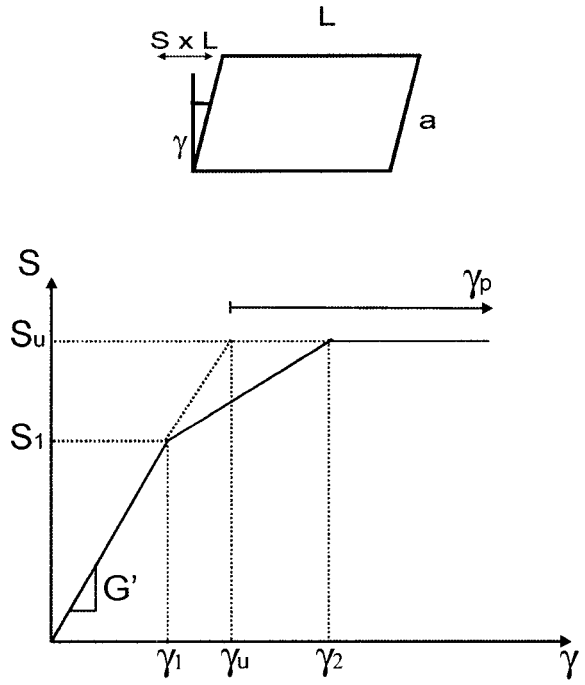

Figure 5 Paramètres de la distorsion

Sous les séismes intra-plaques, les bâtiments situés à Victoria ont subi des déformations inélastiques, γ_p, allant de 6.1 à 10.8 rad/1000 pour R_d = 2.0 et 3.0, respectivement. Généralement, les panneaux de pontage qui se sont plastifiés le plus étaient situés proches des murs de bout du bâtiment. Les niveaux de déformations inélastiques obtenus sont plus petits ou se rapprochent du niveau de déformation acceptable de 10 rad/1000 déterminé par Essa *et al.* pour des diaphragmes vissés-cloués. Ce niveau de déformation a été défini pour s'assurer que la résistance en cisaillement sous chargement cyclique restait supérieure à 80% de la résistance maximale. Les diaphragmes des bâtiments situés à Québec n'ont pas subi de déformations inélastiques. Pour Victoria, les enregistrements produits par la zone de subduction Cascadia ont produit une sollicitation moins importante que les séismes intra-plaques, mais un nombre total de cycles plus élevé. Les mouvements de sol Cascadia étaient d'une durée plus longue en comparaison des séismes intra-plaques, ce qui a donné un nombre de cycles plus grand.

Pour les trois cas, le comportement observé indique que les valeurs de R_d considérés lors de la conception étaient envisageables.

Les analyses pour les séismes intra-plaques à Victoria ont cependant démontré que les distorsions inélastiques des diaphragmes, γ_p, ne sont pas proportionnelles au facteur de modification de force sismique, R_d, utilisé dans le calcul. Par exemple, la sollicitation inélastique obtenue des analyses de bâtiments semblait augmenter plus rapidement qu'anticipé quand un facteur de modification de force sismique, R_d, de 3.0 était utilisé au lieu d'un facteur de 2.0.

Bâtiments conçus selon le CNBC 1995:

Pour les assemblages poinçonnés-soudés conçus suivant le CNBC 1995, des déformations inélastiques allant jusqu'à 9.8 rad/1000 ont été obtenues. Par contre, les tests d'Essa *et al.* ont montrés que ce type de diaphragme ne peut soutenir de déformations inélastiques. Conséquemment, des dommages importants avec perte possible de l'intégrité structurale peuvent être anticipés pour ce type de système sous un séisme majeur.

PROTOCOLES DE CHARGEMENT

Des historiques de chargement ont été développés de telle sorte que la sollicitation sismique sur les diaphragmes obtenue lors de l'étude analytique puisse être imposée sur les spécimens de tests. Une analyse statistique des historiques de déformation a été réalisée dans le but d'évaluer la sollicitation et deux protocoles de chargement ont été développés.

Pour les séismes intra-plaques, on a observé que les bâtiments situés à Victoria et conçus avec $R_d = 3.0$ ont subi la plus grande sollicitation, suivi du cas Victoria avec $R_d = 2.0$ et, finalement des bâtiments localisés à Québec et dimensionnés avec $R_d = 3.0$. La sollicitation pour Québec avec $R_d = 2.0$ était trop faible et a été ignorée. De plus, il a été observé que la sollicitation pour les diaphragmes poinçonnés-soudés (CNBC 1995) pour Victoria avec R = 3.0 était similaire à celle des diaphragmes vissés-cloués pour Victoria $R_d = 3.0$. Toutefois, pour les séismes Cascadia, la sollicitation était complètement différente de celle des séismes intra-plaques : le nombre de cycles sous les séismes Cascadia étant beaucoup plus grand que sous les séismes intra-plaques mais le niveau de déformation étant plus faible.

Une étude statistique a été complétée pour obtenir des valeurs représentatives des paramètres de la sollicitation sous les différents types de mouvement de sol : amplitude de la distorsion, nombre de cycles, etc.. À partir de ces résultats et d'une inspection visuelle des historiques de déformation des diaphragmes, deux protocoles de chargement ont été développés : le protocole de courte durée (SD) et le protocole de longue durée (LD). Ces deux historiques sont illustrées à la Figure 6. Le protocole SD est approprié pour les assemblages vissés-cloués et poinçonnés-soudés. Il comprend trois segments qui sont arrangés de façon séquentielle pour représenter la sollicitation cumulative sur la structure pour les trois conditions suivantes : à Québec avec $R_d = 3.0$, à Victoria avec $R_d = 2.0$, et à Victoria avec $R_d = 3.0$. Le protocole LD est représentatif de la sollicitation sismique des structures à Victoria conçues avec un R_d de 3.0 et assujettis aux mouvements de sol induits par les séismes inter-plaques de Cascadia. Pour les deux protocoles, l'amplitude des cycles de chargement est fonction des déformations γ_u et γ_2 qui sont propres au diaphragme soumis à l'essai (Fig. 5). On doit donc réaliser au préalable un essai monotonique pour obtenir ces paramètres. La fréquence des cycles de chargement a aussi été établie sur la base des résultats des analyses.

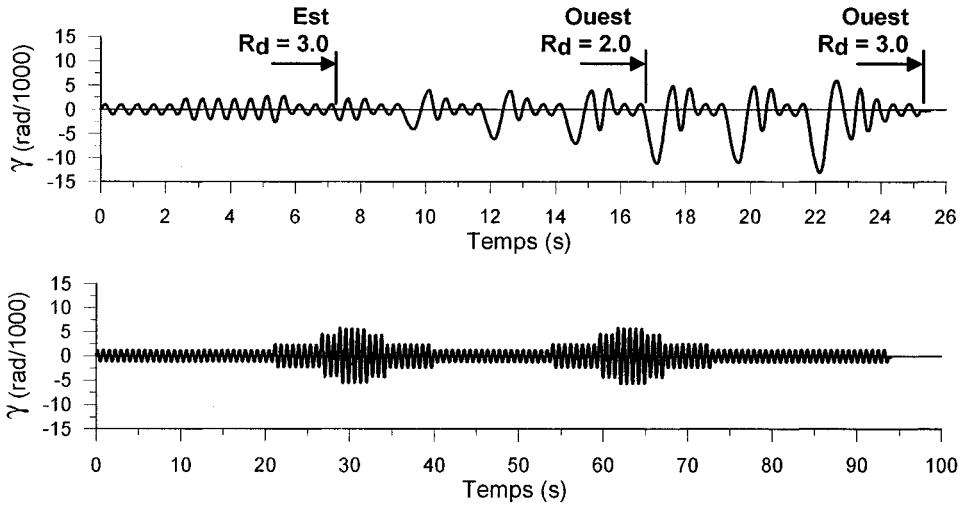

Figure 6 Protocoles de chargement SD et LD

TESTS SUR DIAPHRAGMES

Un ensemble de 19 tests pleine grandeur a été réalisé sur des spécimens de diaphragmes faits de quatre feuilles de pontage métallique de 6.1 m de longueur x 914 mm de largeur (Figure 7). Un cadre d'essais en porte-à-faux, avec joints rotulés à chaque extrémité et comprenant des membrures intermédiaires espacées de 1524 mm, a été utilisé (Figure 8). Un vérin de grande capacité (1.5 MN) a été intégré au montage dans le but d'appliquer les protocoles de chargement dynamique établis précédemment. Quatre combinaisons de connecteurs à la couture et à la structure ont été étudiés : des connecteurs de couture poinçonnés avec des connecteurs à la structure soudés, mais sans rondelles, (diaphragmes WB), des soudures de 16 mm de diamètre avec rondelle de 3 mm d'épaisseur à la fois comme connecteurs de couture et connecteurs à la structure (diaphragmes W'W), les mêmes soudures de 16 mm de diamètre avec rondelles de 3 mm d'épaisseur pour les joints de couture avec des clous Hilti X-EDNK22-THQ12 à la structure (diaphragmes NW), et des vis auto-perçantes Hilti no.12 avec les mêmes connecteurs Hilti à la structure (diaphragmes NS).

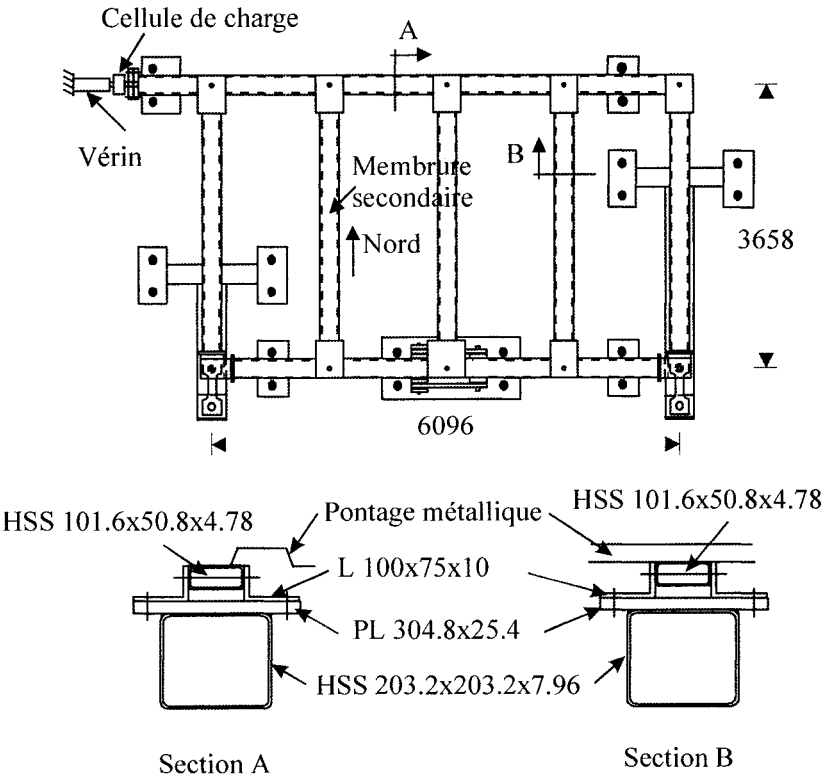

Figure 7 Schéma du cadre d'essai (Essa *et al.*)

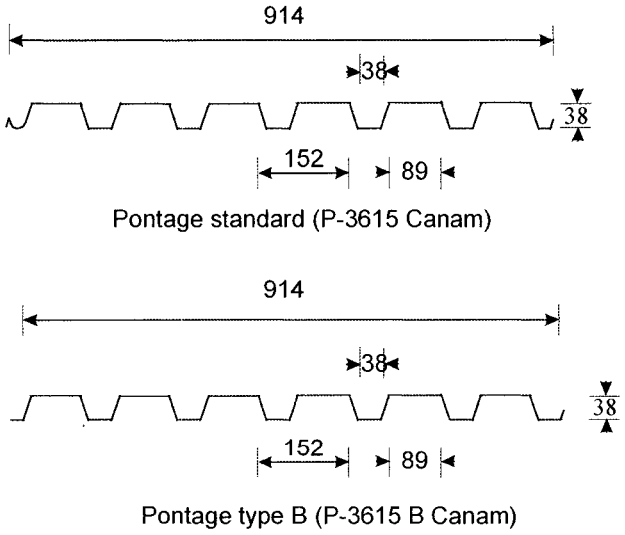

Figure 8 Profilés de pontage métallique utilisés dans les tests

Pour tous les types d'assemblages, l'épaisseur du pontage métallique était de 0.91 mm. Toutefois, des feuilles de 0.76 mm ont aussi été étudiées pour les diaphragmes NS et WB. L'espacement des connecteurs était de 305 mm dans tous les tests à l'exception de tests sur des assemblages NS pour lesquels on a aussi considéré un espacement de 152 mm. Les diaphragmes ont été soumis à des chargements monotoniques ou sismiques. Un test monotonique additionnel a été fait sur un diaphragme fait de clous Hilti comme connecteurs à la structure (diaphragmes NS). De plus, un diaphragme poinçonné-soudé a été assujetti à des cycles de faible amplitude dans le but d'évaluer la dégradation possible des propriétés structurales due à la fatigue produite par des chargements de vent précédant l'événement sismique.

La réponse des diaphragmes a été principalement influencée par le comportement des connecteurs. La Figure 9 présente le comportement charge-déformation des différents agencements de connecteurs étudiés (WB, W'W, NW et NS) sous le protocole SD. En ordonnée, l'effort de cisaillement par unité de longueur, S_U, en kN/m, normalisé par rapport à la valeur maximale mesurée dans le protocole, $S_{U,SD}$, est donné en fonction de la déformation angulaire en cisaillement, γ, en radians/1000.

Les diaphragmes poinçonnés-soudés (WB) ont démontré un comportement non-ductile et des dommages à des déformations inférieures à γ_u. Sous le protocole de chargement SD, la dégradation de la résistance a débuté dans le segment Est $R_d = 3.0$, suite à des ruptures fragiles apparues dans les soudures sur les membrures secondaires situées aux joints de couture, indiquant une capacité inélastique limitée pour ce type d'assemblages (voir Figure 10). La séparation complète des joints de couture est apparue avant la fin du segment Ouest $R_d = 2.0$.

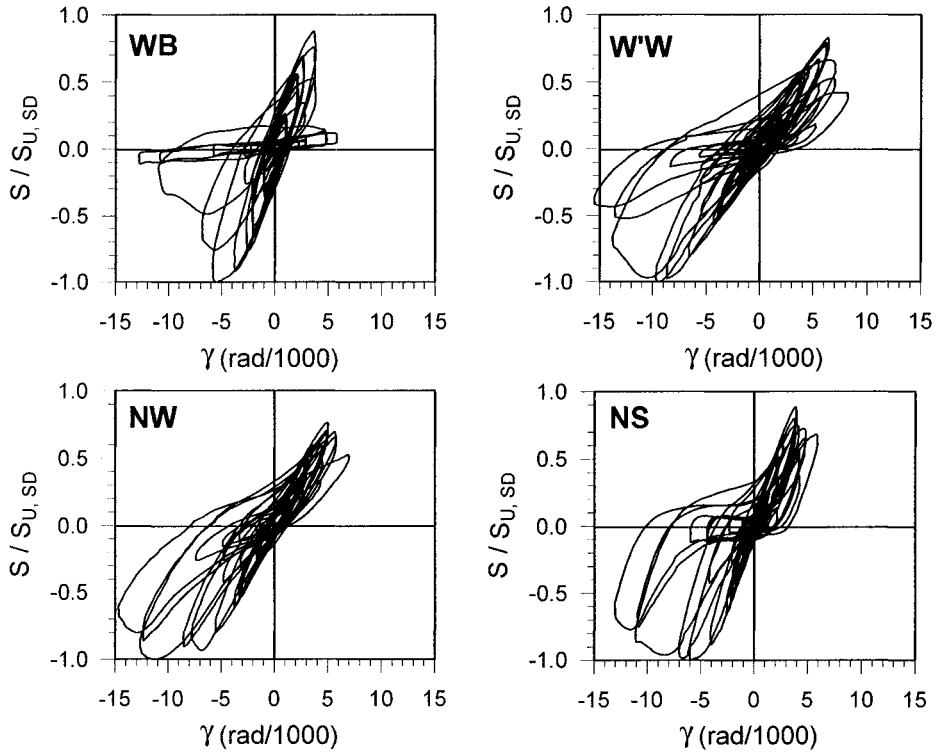

Figure 9 Comportement charge-déformation sous le protocole SD pour les systèmes WB, W'W, NW et NS

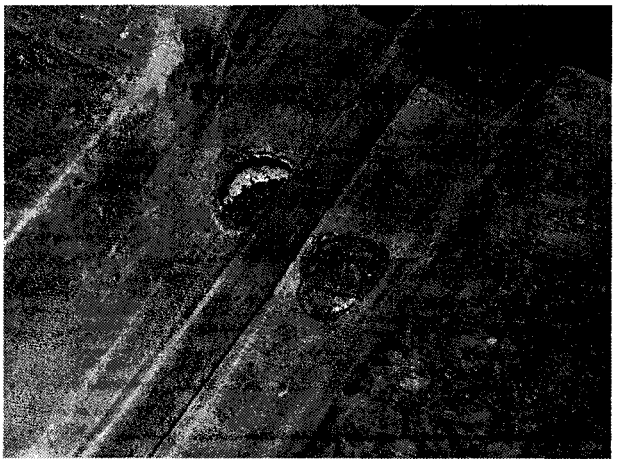

Figure 10 Rupture fragile dans une soudure aux joints de couture (diaphragme WB)

Les diaphragmes W'W ont une résistance plus grande en comparaison des autres types de diaphragmes. Toutefois, la résistance en cisaillement s'est dégradée rapidement et de façon significative une fois la charge maximale atteinte, ceci du aux ruptures des soudures aux joints de couture. Les ruptures aux joints de couture impliquent un comportement avec ductilité limitée dans lequel le joint entre la feuille de métal et la soudure est brisé et/ou du flambement local apparaît dans la feuille d'acier près des soudures. Sous le protocole de chargement SD, les connecteurs sont demeurés intacts jusqu'au segment Ouest $R_d = 2.0$ et la dégradation fut observée dans le segment Ouest $R_d = 3.0$.

Dans les tests sismiques, les systèmes NW se sont comportés comme un diaphragme fait d'une seule feuille avec des déformations inélastiques qui ne se sont développés qu'aux bouts du diaphragme. Ce comportement était ductile puisqu'au périmètre la feuille d'acier exerçait une pression diamétrale contre les clous. Toutefois, cela résultat en une grande sollicitation inélastique le long des bouts du diaphragme. Par exemple, dans le segment Ouest $R_d = 3.0$ du protocole SD, l'ovalisation des trous s'est prolongée jusque dans l'âme du pontage dans la direction perpendiculaire aux nervures (Figure 11), ce qui a résulté en une perte de l'intégrité de ces connecteurs. Ce comportement ne fut pas observé dans le test monotonique puisque les ruptures sont apparues aux joints de couture. Ce mode de rupture n'était pas aussi ductile que celui observé avec le comportement en une seule feuille puisqu'il impliquait des ruptures dans les connecteurs soudés avec rondelle. La localisation des déformations inélastiques dépend de la résistance relative des joints de couture intérieurs versus celle des joints en périphérie.

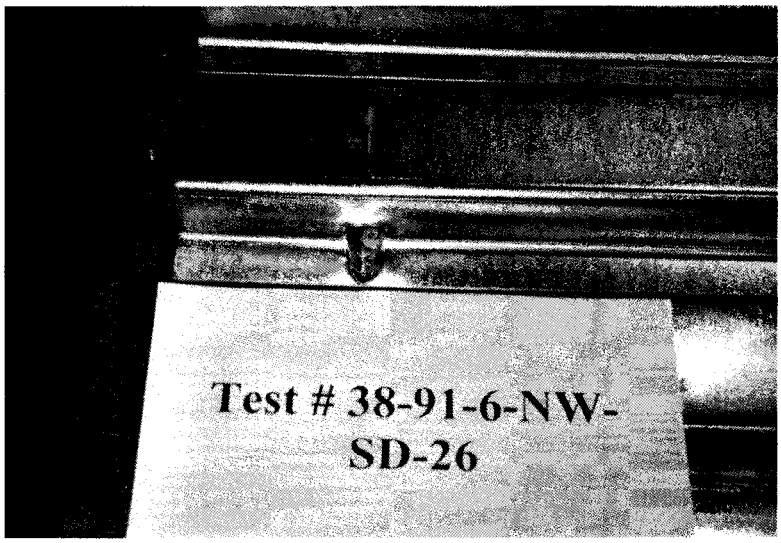

Figure 11 Ovalisation des trous aux connecteurs de bouts du diaphragme (diaphragme NW)

Les diaphragmes de type NS ont présenté un comportement ductile avec pincement (pinching). Le comportement inélastique est apparu essentiellement le long des joints de couture intérieurs, dû au mouvement de va-et-vient des vis qui s'inclinaient dans une direction puis dans l'autre et aux déformations inélastiques causées par la pression diamétrale de la feuille d'acier contre les clous situés aux poutrelles (Figure 12). Dans le segment Ouest $R_d = 3.0$ du protocole SD, ce mode de déformation a produit une réponse hystérétique avec un pincement important, c'est-à-dire une perte importante de résistance et de rigidité autour de la position non déformée.

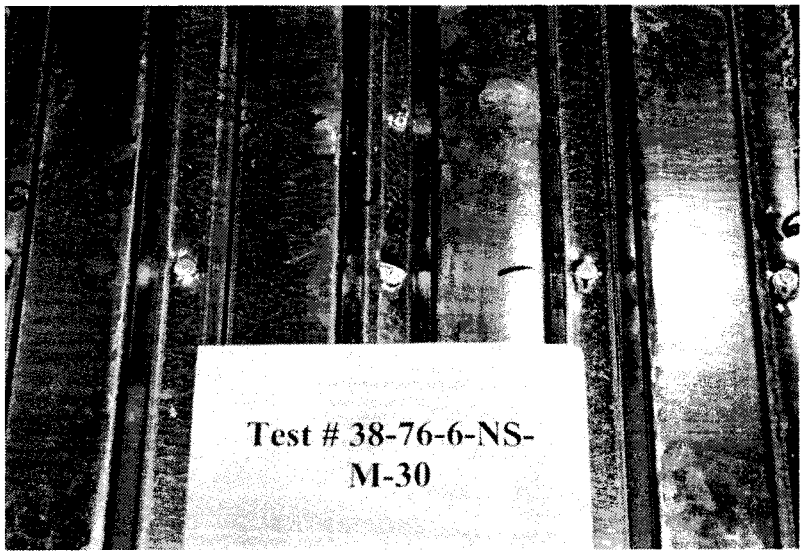

Figure 12 Déformations dans les connecteurs (diaphragmes NS)

En augmentant l'épaisseur d'acier du pontage, la résistance en cisaillement des assemblages de diaphragmes a aussi augmenté. En réduisant l'espacement des connecteurs, c'est-à-dire en augmentant le nombre de connecteurs, les déformations en gauchissement du tablier ont diminué, ce qui donna une rigidité et une résistance plus grandes mais des déformations plus précoces et importantes au niveau des joints de couture. Finalement, l'effet des séismes de type Cascadia simulé par le protocole LD était différent de celui des séismes intra-plaques reproduit par le protocole SD. Les deux types de protocole ont cependant eu un impact similaire, quoique le protocole SD ait eu un effet un peu plus important en termes de dommages et de réduction de la capacité.

Sur la base des résultats de l'étude analytique et des essais, des valeurs ont été proposées pour les facteurs de modification de force sismique reliés à la ductilité et à la surcapacité, R_d et R_o. Ces valeurs sont présentées dans la section suivante.

On avait supposé que les tests dynamiques étaient plus représentatifs de la sollicitation sismique en comparaison des tests cycliques de type quasi-statique. Toutefois, dans cette

série de tests, aucun effet dynamique significatif, tel que des vibrations hors plan entre les membrures intermédiaires ou près des connecteurs, n'a été remarqué.

RECOMMANDATIONS

Des recommandations générales ont été faites au sujet des recherches futures incluant : la nécessité de recourir à des études sur le terrain, d'améliorer les modèles analytiques et de réaliser des tests supplémentaires en laboratoire. Par la suite, des recommandations sont présentées à titre préliminaire pour la conception des diaphragmes. Ces recommandations devront être vérifiées avec de nouveaux modèles analytiques améliorés et des tests additionnels.

Études futures

Études futures sur le terrain

Des données sur les propriétés dynamiques prises sur le terrain (période, amortissement) des bâtiments de faible hauteur en acier devront être obtenues car la sollicitation sismique obtenue dans cette étude était fortement dépendante des propriétés structurales et dynamiques supposées au départ, et il est important que ces propriétés soient vérifiées.

Analyses et modèles analytiques améliorés

À partir des nouvelles données fournies par les tests réalisés dans cette étude, les modèles hystérétiques pourront être améliorés pour mieux représenter le comportement de chaque type de diaphragme et la sollicitation sismique pourrait être vérifiée avec ces nouveaux modèles. L'étude analytique pourrait aussi être poursuivie dans le but de confirmer qu'il n'y a pas de sollicitation inélastique dans les diaphragmes de toit pour l'Est canadien. Ceci pourrait permettre d'adoucir les recommandations de conception

formulées plus bas. Finalement, des analyses supplémentaires devront être complétées sur un éventail plus large de bâtiments, à la fois pour l'Est et l'Ouest canadiens, et pour s'assurer que les conclusions sont adéquates pour différents types de structures : dimensions, formes, localisation des contreventements, variation des propriétés du diaphragme sur la superficie du toit, etc. Les effets P-delta ont été négligés dans ce projet et devront être pris en compte dans ces analyses futures.

Futures études expérimentales

L'effet des éléments non-structuraux de la toiture (isolant, membrane, etc.) sur les propriétés hystérétiques des diaphragmes (rigidité, résistance, dégradation, etc.) devra être étudié. Il serait aussi souhaitable que de nouveaux types de connecteurs soient examinés dans le but d'obtenir un comportement sismique amélioré. De plus, l'influence des joints de chevauchement et des ouvertures dans les diaphragmes doit être étudiée. Finalement, l'effet de la fatigue sur les diaphragmes, tel qu'imposée par les cycles de chargement dus au vent, avant l'avènement d'un séisme important doit être étudié sous contrôle en chargement.

Recommandations préliminaires pour la conception des diaphragmes

Des recommandations préliminaires de design ont pu être formulées à partir des résultats des analyses et du comportement des diaphragmes observé dans les tests. Ces recommandations ont été développées pour l'Ouest canadien et sont applicables à la fois aux séismes intra-plaques et inter-plaques. Certaines de ces recommandations pourraient être allégées pour l'Est canadien. Toutefois ceci n'est pas considéré dans ce texte, car on croit que des études plus approfondies au sujet de la réponse de bâtiments sous les tremblements de terre de l'Est canadien devront être menées avant d'appliquer de tels allégements. De plus, ces recommandations sont valides pour les diaphragmes dans lesquels les connecteurs sont espacés à toutes les deux nervures dans la direction

perpendiculaire aux nervures, permettant ainsi un minimum de déformations en gauchissement dans le tablier. Une plus grande sollicitation inélastique est anticipée dans les connecteurs de diaphragmes avec des espacements de connecteurs plus petits. Cet aspect devra être examiné avant d'étendre l'application de ces recommandations aux assemblages avec des espacements de connecteurs réduits.

Diaphragmes poinçonnés-soudés (WB)

Il est recommandé que ce système demeure élastique sous un chargement sismique, c'est-à-dire qu'un facteur R_d = 1.0 devrait être utilisé dans les calculs. En ce qui concerne le facteur de modification de force relié à la surcapacité, nous croyons qu'un facteur $R_o = 1/\phi$ serait trop grand puisque le système n'est pas ductile et qu'une dégradation de la rigidité et de la résistance a été observée à des déformations cycliques d'une amplitude égale à γ_u. De plus, les connecteurs de couture et à la structure sont tous deux sujets à une grande variabilité de leurs propriétés, impliquant une difficile prédiction de leur comportement: résistance ultime, rigidité, etc.. Cette variabilité peut produire une concentration de la sollicitation inélastique et une rupture complète dans une portion limitée du diaphragme, ce qui résulterait en une perte de l'intégrité structurale du système de résistance aux charges latérales. Ainsi, une valeur de 1.0 est suggérée pour R_o. Avec de nouvelles études expérimentales et analytiques, le facteur R_o pourrait être augmenté si les résultats le permettent. Dans le but de mieux contrôler la sollicitation appliquée sur les diaphragmes, les tests sur ce type de diaphragme devraient être faits en contrôle de charge plutôt qu'en contrôle en déplacement.

Diaphragmes soudés avec rondelles-soudés avec rondelles (W'W)

Un facteur relié à la surcapacité, R_o, égal à $1/\phi$ peut être utilisé pour ces diaphragmes puisque les propriétés des connecteurs sont plus fiables en comparaison des connecteurs poinçonnés et soudés sans rondelle et qu'aucune rupture ne fut observée sous une déformation égale à γ_2. Cette combinaison de connecteurs est aussi acceptable pour un système où le diaphragme est l'élément dissipatif à la condition que les connecteurs de bout soient plus résistants que les joints de couture intérieurs, faisant en sorte que les déformations inélastiques soient distribuées dans les joints de couture intérieurs et ne se concentrent pas en périphérie du diaphragme. Malgré que ce système se soit bien comporté sous les déformations correspondant à $R_d = 2.0$ dans le test sismique, un facteur de modification de force relié à la ductilité, R_d, égal à 1.5 seulement est recommandé. Cette valeur prudente est suggérée puisque les déformations γ_u et γ_2 sont rapprochées pour ce diaphragme, et qu'une dégradation prononcée de la capacité en cisaillement a été observée après l'atteinte de la charge maximale, en raison du mode de rupture à ductilité limitée associé aux joints de couture soudés.

On notera que les résultats des tests sont directement reliés à la sollicitation sismique obtenue dans des analyses où on a assumé un diaphragme de type vissé-cloué. Conséquemment, il serait approprié de réviser la sollicitation sismique basée sur un nouveau modèle hystérétique adapté pour représenter le comportement des diaphragmes W'W. Dans l'ensemble, ce système démontre une très grande résistance et serait approprié dans les bâtiments situés dans les régions à forte sismicité.

Diaphragmes soudés avec rondelles-cloués (NW)

Pour ce système, on doit aussi respecter une limite rapport de la résistance des connecteurs des joints de couture et des connecteurs à la structure afin que les déformations inélastiques prennent place aux joints de couture intérieurs et non aux bords du diaphragme. Les diaphragmes NW ainsi conçus devrait se comporter d'une façon similaire aux diaphragmes W'W et, par conséquent, un facteur de modification de force relié à la ductilité, R_d, de 1.5 et un facteur relié à la surcapacité , R_o, égal à $1/\phi$ sont recommandés.

Diaphragmes vissés-cloués (NS)

Grâce à la fiabilité des connecteurs mécaniques utilisés dans ce diaphragme, un facteur de modification de force R_o égal à $1/\phi$ peut être utilisé. En tenant compte du pincement prononcé qui caractérise le comportement du système sous la sollicitation correspondant à $R_d = 3.0$, il est recommandé qu'un facteur relié à la ductilité égal à 2.0 soit utilisé pour la conception d'un diaphragme de ce type. Cette valeur pourrait être augmentée s'il peut être démontré par de futures analyses que le pincement n'a pas d'effets négatifs sur la réponse du bâtiment ou si des connecteurs de joints de couture avec un meilleur comportement inélastique sont utilisés. Encore une fois, lors de la conception, on devra fournir une résistance suffisante aux connecteurs en périphérie afin de s'assurer que les déformations inélastiques se produisent dans les joints de couture intérieurs du diaphragme.

TABLE OF CONTENTS

LIST OF TABLES

LIST OF FIGURES

LIST OF SYMBOLS

A:	Area
A_g:	Gross area of a structural element
ALPHA:	Reloading or pinch power factor
AS:	Effective shear area of the member section
AVE:	Average of peak distortions
B:	Maximum value of B_x
B_x:	Ratio at level x used to determine torsional sensitivity
B1:	Buckling on one side of nail with possible bearing deformation
B2:	Buckling on two sides of nail with possible bearing deformation
BB:	Bond failure where both sheets disconnected from weld to frame, BB1 or BB2
BB1:	Bond failure of top sheet with buckling on one side
BB2:	Bond failure of top sheet with buckling on two sides
BBF:	Bond failure with little amount of inelastic deformation
BETA:	Beta or softening factor
BF:	One of the two cases (not determined): BT or BB; BBF or DBF, bearing failure (with or without buckling) (SB, BFS, TT, B1 or B2 not identified)
BFL:	Bearing failure perpendicular to the flute (may extend into the web)
BFS:	Bearing failure (slot) without buckling
BO:	Buckling of sheet on one side of weld without weld failure
BT:	Bond failure of top sheet from bottom sheet with little amount of inelastic deformation
C:	Connector slip parameter
CSSBI:	Canadian Sheet Steel Building Institute
C_b:	Roof load parameter
C_w:	Wind exposure parameter

C_s:	Roof slope parameter
C_a:	Snow accumulation parameter
C_r:	Factored strength in compression
d:	Corrugation pitch
D:	Diaphragm width
D_n:	Warping constant
D_{nx}:	Plan dimension of the building at level x perpendicular to the direction of seismic loading considered
D_s:	Total braced length per wall
DBF:	Bond failure with buckling
DL:	Roof dead load
LL:	Roof snow and rain live load
e_x:	Distance measured perpendicular to the direction of earthquake loading between centre of mass and centre of rigidity at the level being considered
E:	Young's modulus
$E_H / (S_{U,SD} \cdot \Sigma(\Delta\gamma))$:	Cumulated hysteretic energy in segment I, II or III normalised to the maximum force measured in the SD loading protocol and cumulated absolute distortion in same time interval
$E_H / (S_{U,LD} \cdot \Sigma(\Delta\gamma))$:	Cumulative hysteretic energy in the 1st half of the loading protocol normalised to the maximum force measured in the LD loading protocol and cumulated absolute distortion in same time interval
E_H, Run2/Run1:	Ratio of the cumulative hysteretic energy in run 2 compared to run 1
E_H 2nd half/ E_H 1st half,	

E_H 5th seg./
E_H 2nd seg.,
EH2/EH1,
EH3/EH1,
EH4/EH1: Ratio of the hysteretic energy dissipated in one time interval to the energy dissipated in another time interval of same time duration and total distortion

EH1: Hysteretic energy dissipated in the first set (1) of cycles at $(\gamma_u+\gamma_2)/2$

EH2: Hysteretic energy dissipated in the second set (2) of cycles at $(\gamma_u+\gamma_2)/2$

EH3: Hysteretic energy dissipated in the third set (3) of cycles at $(\gamma_u+\gamma_2)/2$

EH4: Hysteretic energy dissipated in the fourth set (4) of cycles at $(\gamma_u+\gamma_2)/2$

F: Foundation factor

F_a: Acceleration-based site coefficient

F_v: Velocity-based site coefficient

F_y: Specified minimum yield stress

FI: Intercept force

FU: Ultimate force

FX: Spring yield force in the x-direction

FW: Fracture of weld between top and bottom sheets with limited inelastic deformation

g: Acceleration due to gravity

G: Shear modulus of member material

G': Diaphragm rigidity in shear

G' i/G' at zero displacement: Ratio of the residual stiffness at zero displacement to initial stiffness

G'_{SECANT}/
G': Ratio of G'_{SECANT} to initial G'. G'_{SECANT} is a secant stiffness, measured in the largest excursion in segment II and III (SD) or the largest excursion

	of the 2nd half (LD), from the origin to the intersection of shear-distortion curve and $0.4S_{U,SD}$.
G'_{STIFF}/G':	Ratio of G'_{STIFF} to initial G'. G'_{STIFF} represents the stiffness found when reloading of the deck occurs.
$G'_{STIFF\ ADD}$:	Stiffness found in the additional loop when reloading of the deck occurs
GAP+:	Initial slackness, positive axis
GAP-:	Initial slackness, negative axis
h_n:	Building height
h_s:	Interstorey height
I:	Earthquake importance factor of the structure, moment of inertia of diaphragm flanges (perimeter members) about centroidal axis of diaphragm, moment of inertia of section
j:	Mode j
J:	Numerical reduction coefficient for base overturning moment
k:	Effective length factor
k_{LAT}:	Lateral stiffness of the truss system
K_B:	Total lateral stiffness of the vertical bracing
K_D:	Total lateral stiffness of the diaphragm
KX:	Spring stiffness in the local x-direction
L:	Diaphragm length, length of a structural element
LD:	Long duration
Level i:	Any level of the building, i=1 for first level above the base
Level n:	That level which is uppermost in the main portion of the structure
Level x:	That level which is under design consideration
M:	Monotonic
M_v:	Factor to account for higher mode effect on base shear
n:	Number of peaks
N:	Total number of storeys above exterior grade to level n

NS:	Screw-nail design
NW:	Weld with washer-nail design
PHA:	Unscaled peak horizontal acceleration
PHV:	Peak horizontal velocity
PTRI:	Tri-linear factor beyond ultimate force
PUNL:	Unloading stiffness factor
P_W:	Pinching width
P_W/ S_U:	Ratio of the pinching width, P_W, to the maximum measured force in the SD loading protocol. P_W is calculated in the last cycle at $0.4\gamma_u$ in segment I, II and III
r:	Radius of gyration
R:	Force modification factor
R_d:	Ductility related force modification factor
R_o:	Overstrength related force modification factor
R_ϕ:	$1 / \phi$
R_y:	Factor applied to F_y to estimate the probable yield stress
R_{yield}:	Ratio of probable yield strength to minimum specified yield strength
R_{sh}:	Overstrength due to strain hardening
R_{size}:	Overstrength due to discrete member sizes
R_{mech}:	Overstrength developed when a full collapse mechanism is formed
RF:	Bi-linear factor
s:	Girth of corrugation per rib
S:	Roof snow and rain live load
$S1/ S_{U, LD}$, S2/ S1, S3/ S1, S4/ S1:	Ratio of the maximum force in one cycle at $(\gamma_u+\gamma_2)/2$ to a reference force. S1 is the maximum force in the last cycle of the 1st set of cycles at

$(\gamma_u+\gamma_2)/2$. S2 is the maximum force in the first cycle of the 2nd set of cycles at $(\gamma_u+\gamma_2)/2$. S3 is the maximum force in the last cycle of the 3rd set of cycles at $(\gamma_u+\gamma_2)/2$. S4 is the maximum force in the first cycle of the 4th set of cycles at $(\gamma_u+\gamma_2)/2$.

SB: Slight buckling around nail

SD: Short duration

SDI: Steel Deck Institute

SN: Shear failure in the nail

SU: Sheet uplifted around nail with possible bearing deformation

S_{ADD} : Maximum measured force in the additional loop

S_F: Scaling factor used

$S_i / S_{U,SD}$: Ratio of the maximum force in largest excursion in segment I, II or III to the maximum measured force in the total SD signal

$S_i / S_{U,LD}$: Ratio of the maximum force in largest excursion in 1st and 2nd halves to the maximum measured force in the total signal

S_L / S_{2L}: Ratio of the maximum force in the largest excursion in segment I, II and III to the maximum force in the 2nd largest excursion in the same time interval

S_r: Rain load

S_s: Ground snow load

S_u: Deck ultimate shear strength

S_U ,

Run2/Run1: Ratio of maximum measured force in run 2 compared to maximum force in run 1

$S_{U,SDI*}$: Deck ultimate shear strength predicted by the SDI method based on test values for connectors

$S_{U,SDI}$: Deck ultimate shear strength predicted by the SDI method

$S_{U,MON}$: Deck ultimate shear strength from monotonic test

$S_{U,SD}$:	Deck ultimate shear strength from test with a short duration (SD) loading protocol
$S_{U,LD}$:	Deck ultimate shear strength from test with a long duration (LD) loading protocol
Srequ:	Deck design force considered
S(T):	The design spectral response acceleration, expressed as a ratio to gravitational acceleration, for a period of T
S_a (T):	The 5% damped spectral response acceleration, expressed as a ratio to gravitational acceleration, for a period of T
S1:	Shear strength at γ_1
SD:	Standard deviation
t:	Base metal thickness
T:	Period in seconds
T_a:	Fundamental lateral period of vibration of the building or structure in the direction under consideration
T_f:	Tension force considered in design
T_x:	Floor torque at level x
$T_{ANALYTICAL}$:	Period evaluated by the Medhekar's formula
TT:	Tearing of top sheet at nail
U:	Factor representing level of protection based on experience = 0.6
v:	Zonal velocity ratio
V:	Lateral earthquake design force at the base of the structure as determined by the equivalent static force procedure
V_d:	Lateral earthquake design force at the base of the structure as determined by a dynamic analysis procedure
V_e:	Lateral earthquake elastic force at the base of the structure as defined by a dynamic analysis procedure
V_p:	Lateral force on a part of the structure

V_u:	Expected lateral strength of the structure
w:	Uniform load
W:	Seismic weight of the building
WB:	Button punch-weld design
WT:	Tilting of washer with partial fracture of weld
W'W:	Weld with washer-weld with washer design
WF:	One of the two cases (FW or WT)
Z:	Plastic section modulus
Z_a:	Acceleration-related seismic zone
Z_v:	Velocity-related seismic zone
α:	Ratio of the in-plane diaphragm deformation to the lateral-system absolute drift at mid-height of the structure
δ_{ave}:	Average of the displacements at the extreme points of the structure at level x
δ_{max}:	Maximum displacement of the structure at level x
Δt:	Time interval
Δ_B:	Lateral deflection of braced walls
Δ_F:	Flexural lateral deflection
Δ_S:	Shear deflection of diaphragm
Δ_{TOT}:	Total lateral deflection of the structure
Δ_{LIMIT}:	Limit criteria for the lateral deflection of the structure
ϕ:	Resistance factor, purlin effect factor on warping
γ:	Average shear strain
γ_p:	Inelastic distortion starting from γ_u
γ_u:	Shear deformation obtained from S_u/G'
γ_1:	Shear deformation where stiffness deterioration starts
γ_2:	Shear deformation where shear strength reaches its peak value

λ:	Non-dimensional slenderness parameter of the brace
Λ_j:	Frequency modification factors at mode j
ω_j:	Frequency of j^{th} mode
ν:	Poisson's ratio (ν= 0.3)
ρ:	Ratio of the wall mass to the total mass of the system

LIST OF APPENDICES

CHAPTER 1

INTRODUCTION

1.1 BACKGROUND

Single-storey steel structures are widely used in North America. They represent a large proportion of the light industrial, commercial and recreational buildings that are constructed. In most of these structures, the steel roof deck plays an important role acting as a structural diaphragm: the roof deck diaphragm brings the lateral forces due to earthquake and wind loading to the vertical lateral force resisting system. The roof diaphragm is made of corrugated steel deck units that are fastened to one another and to the supporting steel roof framing. Figure 1.1 presents a typical single-storey steel structure with roof deck installed on the left portion.

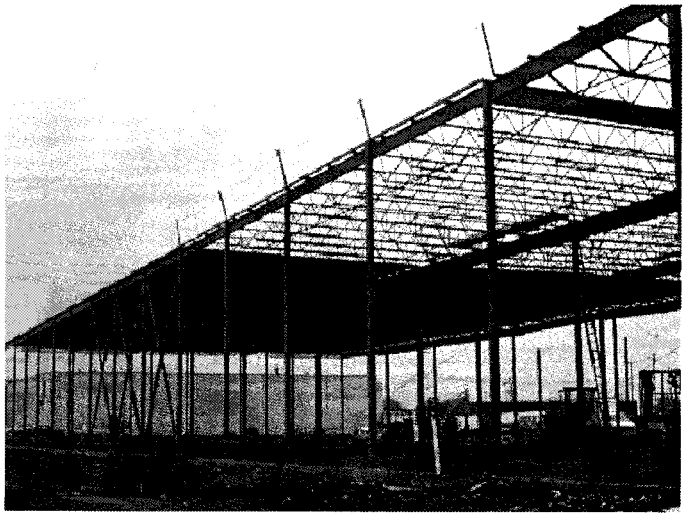

Figure 1.1 Typical single-storey steel structure

Several analytical and experimental studies that have detailed the behaviour of steel deck diaphragms have been performed since the 1960s. Most of the studies were carried out for static loading conditions, and hence design provisions were proposed for such conditions, i.e. when the applied loads remain relatively constant and well below the ultimate capacity within the elastic range (e.g.: Luttrell (SDI, 1981 and 1987), Davies and Bryan (1982), CECM (1977), CSSBI (1991).

A typical response of a steel deck diaphragm under a monotonically applied load is shown in Figure 1.2. This is a typical load per unit length (kN/m) versus deflection (γ rotation) curve.

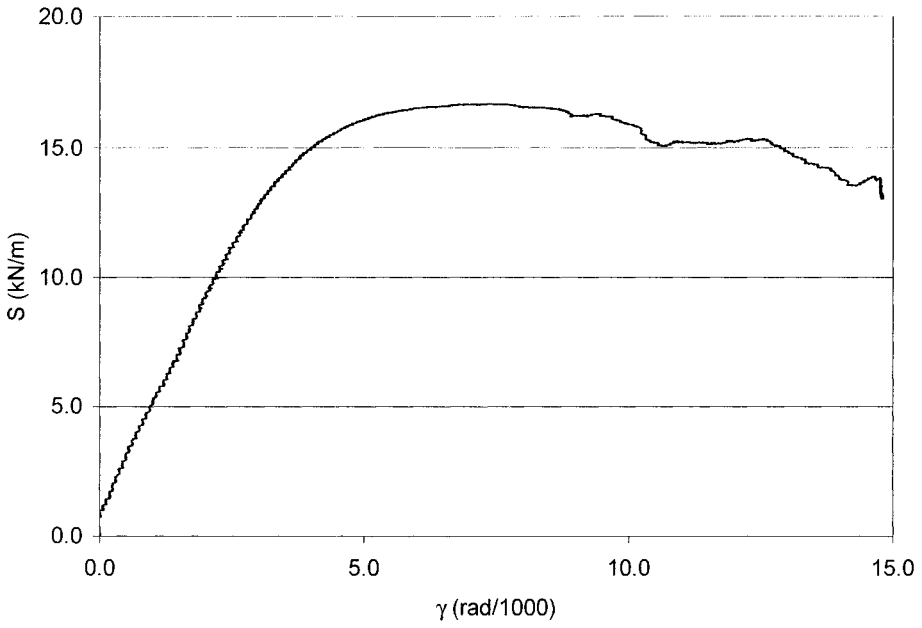

Figure 1.2 Typical load-displacement behaviour of a diaphragm under monotonic loading (Test 19 from this study)

The behaviour of a steel deck diaphragm can be described as follows. At the beginning, the behaviour is essentially linear. Later, some of the fasteners experience a nonlinear

behaviour which translates into a softening of the overall diaphragm. The gradual softening of the system is caused by the fasteners being loaded at different shear levels due to their location and relative rigidity. Later, the diaphragm reaches its peak value where failure appears most often in the fasteners or by shear buckling (for long-span thin deck). After the peak load is reached, strength degradation always occurs, the rate of degradation being dependent upon the type and spacing of fasteners used.

Seismic loading compared to lateral static loading causes a very different demand on the structural components. The seismic loading can be characterised by several cycles in the inelastic deformation range and by the higher deformation rate than in typical monotonic tests. In spite of this, the behaviour of steel deck diaphragm under seismic loading has not been explored yet in an extended manner.

There exists no guidance in the current 1995 National Building Code of Canada (NBCC) (NRCC, 1995) or in the S16.1-94 Steel Structures Design Standard (CSA, 1994) on the seismic design and detailing for steel deck that is expected to respond inelastically to large seismic excitations. This is due to the lack of knowledge on the inelastic seismic response of metal deck diaphragms. The same equivalent static design loads are used for the diaphragm and for the braced frames. Consequently, inelastic deformations might occur in the weaker component: the diaphragm or the braced frames. Considering that limited information exists on this subject, the new CSA-S16-2001 (CSA, 2001) and the proposed NBCC 2004 (CANCEE, 2001) both require the roof diaphragms to be capacity protected. It is necessary that a better understanding of the seismic behaviour of such structural members be developed. With this additional information it will be possible for the designer to consider the effects of nonlinear diaphragm behaviour on the overall structural response of the building. A possible outcome is that the design loads on the building could be reduced due to the inelastic performance of diaphragms under cyclic loads.

An experimental research program was established at École Polytechnique de Montréal to better understand the behaviour of steel roof deck diaphragms and to address their design when subject to seismic loading. Rogers and Tremblay (2000) studied the inelastic seismic response of frame and sidelap fasteners for steel roof deck diaphragms. They found that the inelastic response of fasteners varied significantly between fastener types. Considering that the performance of a steel roof deck diaphragm depends on its fasteners it was anticipated that a similar response would take place in the overall roof structure.

As an extension of this original study Essa *et al.* (2001) performed cyclic quasi-static tests on full-scale steel roof deck diaphragms. A typical load versus shear distortion response of a steel deck diaphragm (38 mm deep 0.76 mm thick deck with screw-nail design) under cyclic quasi-static applied load is shown in Figure 1.3.

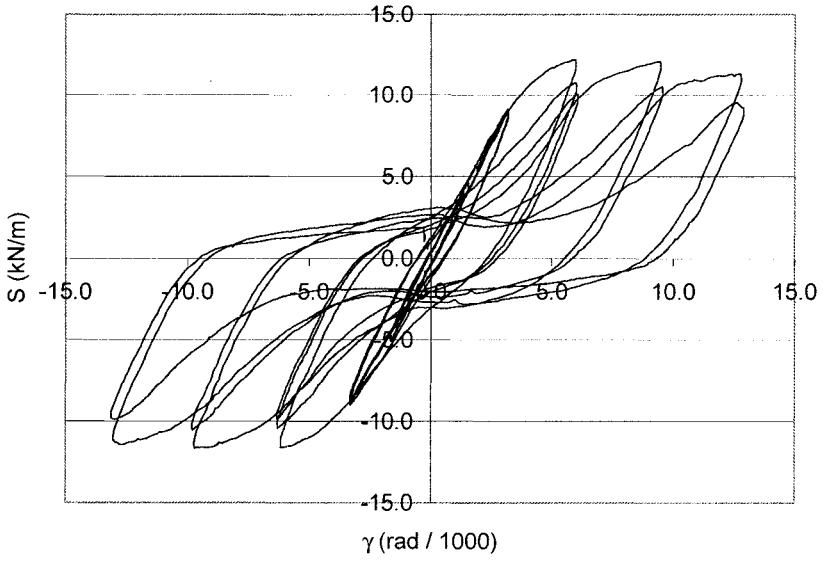

Figure 1.3 Typical shear-distortion behaviour of a diaphragm under cyclic loading (from test 7 (Essa *et al.*, 2001))

In the first cycles, the imposed displacement was small and the diaphragm remained elastic. At a certain displacement level, some yielding in the deck arose at the connections and the specimen started to show an hysteretic behaviour. At this time the most highly stressed connectors entered into the inelastic range, in effect decreasing the rigidity of the overall diaphragm. Further, in the post ultimate range a gradual deterioration in shear capacity occurred with further cyclic loading due to failure in connectors or by local buckling in the sheet steel.

A simplified stepwise incremental cyclic loading was adopted by Essa *et al.* to obtain an estimate of the inelastic deformation capacity of diaphragms under cyclic loading, as no data was available on the inelastic cyclic demand for roof diaphragms. It is possible that the demand might vary with the resistance level of the diaphragm and with the dynamic behaviour of the building as a whole, including the effect of the diaphragm flexibility and its inelastic deformations. Such information on the seismic behaviour of single-storey structures with diaphragms was not available, hence, a better knowledge of the nature of the anticipated inelastic loading was required.

1.2 OBJECTIVES AND SCOPE

The objectives of this project were 1) to evaluate the seismic demand on diaphragms designed to respond in the inelastic range, 2) to examine the response of various diaphragm designs subjected to that demand, and 3) to recommend minimum design strength levels for the diaphragms studied. This study was limited to rectangular, uniform, single-storey buildings with a metal deck diaphragm made with the most common roof deck panels.

The demand from intra-plate earthquakes expected to occur both in Eastern and Western Canada was to be assessed. For Western Canada, the demand from inter-plate

subduction earthquakes also needed to be examined. Tests were to be performed under dynamic loading that matches as closely as possible the actual demand anticipated under seismic ground motions. The minimum strength recommendations were to be expressed in a format compatible with that adopted for the proposed 2004 NBCC. These recommendations were to be obtained for the most promising diaphragm designs in terms of inelastic seismic response, based on the study by Essa *et al.* However, seismic design recommendations were also needed for the common diaphragms, which under current practice are constructed with spot weld frame connections and button punched sidelap. In addition, an aim of the project was to verify the behaviour of diaphragms connected with Hilti nails, a case for which Essa *et al.* observed shear failures in the fasteners.

1.3 METHODOLOGY

To achieve the stated objectives, a research program including two main phases was prepared and a literature review was done prior to the research.

The literature review addressed the seismic design and behaviour of buildings with flexible diaphragms. Several aspects were examined. Among them were the NBCC 2004 seismic provisions, the CSA-S16-2001 (CSA, 2001) provisions on concentrically braced frames, and the Steel Deck Institute (SDI, 1987) diaphragm design procedure. Research articles on the subject were also reviewed.

The second phase consisted of an analytical study performed on different single-storey steel frame buildings to determine the typical time history deformation demand response on roof diaphragms. The work was limited to the most common steel roof deck, i.e. a 38 mm x 914 mm deck profile made of 0.76 mm and 0.91 mm thick ASTM A653 (2002) grade 230 steel. The demand was evaluated using a nonlinear dynamic time history

analysis of typical single-storey buildings located in Victoria, BC and Quebec City, QC. The buildings were rectangular in shape with an aspect ratio of 1:2. Three building sizes were considered: 450, 1800, and 7200 m^2, and the vertical bracing was located along the exterior walls. A 30 m wide x 120 m long building with additional vertical bracing at mid-length was also studied. In all cases, a nailed-screwed diaphragm design was used. Essa *et al.* found that this system was the most promising in terms of seismic applications. A weak-diaphragm design was performed for two different lateral load resistance levels. These were determined using the NBCC 2004 provisions using two values for the ductility-related force modification factor, R_d: 2.0 and 3.0. Buildings with a button punched-welded diaphragm were also designed according to the 1995 NBCC provisions requirements to assess the demand for existing buildings. The analyses were performed with the Ruaumoko (Carr, 2000) program using sets of ground motion records from intra-plate earthquakes for both Eastern and Western Canada. Additional analyses were carried out using records representative of the subduction earthquakes anticipated along the Pacific west coast. The hysteretic response of the roof was modelled based on the test results by Essa *et al.*

Based on the analytical study, two loading protocols were developed to mimic the essential characteristics of the inelastic demand as obtained in the analyses, i.e. amplitude of plastic shear deformations, number of loading cycles and loading rates. An initial loading protocol was developed to capture the demand from both Eastern and Western intra-plate earthquakes. This protocol was also applicable for both diaphragm systems studied: button punch-weld and screw-nail designs. The second protocol was proposed to reproduce the demand from subduction earthquakes on the diaphragms designed to enter the inelastic behaviour range.

A total of 19 full-scale tests were performed on steel roof deck diaphragms with screwed, button punched, and welded with washer sidelap connectors, as well as nailed, welded and welded with washer deck-to-frame fasteners. The diaphragms were

subjected to monotonic or seismic loading. The test set-up by Essa *et al.* was adopted for use except that a dynamic high capacity actuator was incorporated to apply realistic dynamic loading. An additional test was performed on a diaphragm that was constructed with Hilti nails as the frame connectors. Furthermore a weld-button punch diaphragm was subjected to low amplitude cycles prior to applying the seismic loading protocol in order to examine possible degradation of the structural properties due to wind loading over time prior to the occurrence of an earthquake.

Based on the performance observed in tests, a minimum design strength level was proposed for each diaphragm system. This was mainly based on the deformation capacity reached before shear strength degradation developed. Other parameters were also considered such as the energy dissipation, residual strength and stiffness, pinching width.

1.4 THESIS ORGANISATION

The thesis was organised in the following manner. Chapter 2 includes the literature review of previous research. This section contains a short summary of the knowledge on the subjects of steel deck diaphragms, seismic loading, steel brace design. Chapter 3 explains the analysis of the building models and the results of the nonlinear time history analyses. Chapter 4 was included to describe the choice of the loading protocols. Chapter 5 includes a description of the experimental apparatus and the test procedures, in addition to a presentation of the laboratory results. Preliminary design implications based on the findings of this work and of previous work by Essa *et al.* are discussed. Finally, the conclusions and remarks follow in Chapter 6. Future implications of the research are also presented in this section.

CHAPTER 2

LITERATURE REVIEW

This chapter contains a literature review with a summary and discussion of the seismic provisions included in the future version of the National Building Code of Canada, NBCC 2004, and the provisions for the design of concentrically braced frames contained in the Canadian Standards Association CSA S16 Limit States Design of Steel Structures Standard (2001). Also, the Steel Deck Institute SDI (1987) method on the design of steel deck diaphragms is presented. In addition, previous studies on metal buildings with flexible diaphragms are outlined, including, experimental studies on metal deck diaphragms, work on dynamic loading protocols and analytical studies on buildings with flexible roof diaphragms.

2.1 NATIONAL BUILDING CODE OF CANADA 2004

In Canada, the National Building Code (NBCC) specifies the minimum loading to consider in a building design. The new edition is due out in 2004, and hence has not been adopted at the time of writing. However, a draft version of the future code (CANCEE, 2001) was used in this study and is presented in the text. This version will be referred to as the NBCC 2004.

2.1.1 General considerations

Different types of analysis can be used to evaluate the earthquake effects on a building. Two methods are described herein: the dynamic analysis procedure and the equivalent static force procedure. The first method is more general and can be used in all design

circumstances. The second approach is simplified in nature and can only be used for structures that meet more stringent criteria regarding building size, height, complexity, etc. The two procedures are presented in Sections 2.1.3 and 2.1.4, respectively. Both methods depend on a design spectrum for seismic loading and an importance factor, which are described in Section 2.1.2.

In NBCC 2004 (NRCC, 2001), earthquake loads (E) have to be combined with gravity dead (D) and live (L) loads using the most critical of the two following load combinations: D + E and D + 0.5L + E.

2.1.2 Design spectrum

The design seismic loading imposed on a building is based on a design spectrum which gives the maximum absolute acceleration, S_a, of an idealised single-degree-of-freedom structure for a given amount of viscous damping as a function of its period, T, and the potential for earthquakes in the area. In this section, the procedure to obtain the design spectrum is explained.

In future versions of the NBCC the locality of the building will influence its design in a more thorough fashion than the current National Building Code (NRCC, 1995). Basic spectral response acceleration values will be given for a number of cities across Canada. Spectral response acceleration values $S_a(T)$ are provided for periods T of 0.2s, 0.5s, 1.0s and 2.0s for a critical viscous damping of 5%. Each value is based on a 2% probability of exceedance in 50 years for the reference ground condition, which is a very dense soil or soft rock. The probability of exceedance is the probability that the spectral values are exceeded at a site in a given time interval. The aim of the new building code is to develop a consistent approach to seismic risk in terms of location and building

behaviour, and as such spectral ordinates form a so-called Uniform Hazard Spectrum (UHS) (Figure 2.1).

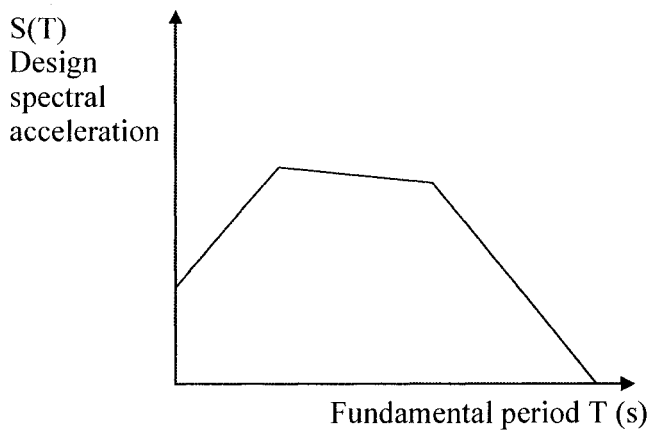

Figure 2.1 Design spectrum

The site specific UHS are given for a reference ground condition, and hence the design spectrum must be modified to account for other site conditions. The acceleration and velocity-based site coefficients, F_a and F_v, are used to modify the basic design spectrum values for the local soil conditions. F_a and F_v depend on the site class and vary with the fundamental period of the structure. Very dense soil and soft rock are considered site class C, which is the reference ground condition. Other site classes for seismic site response are defined in the Code.

F_a, the acceleration-based site coefficient, varies between 0.7 for a very hard rock and 2.1 for a soft soil. It should be mentioned that very soft soil when subjected to high seismic activity will undergo inelastic deformations, which have a tendency to diminish the spectral acceleration that is transferred to the building that is located above. In addition, F_v, the velocity-based site coefficient, varies between 0.5 for a hard rock and 2.1 for a soft soil.

The design spectrum incorporates these values, i.e. $S_a(T)$, F_a and F_v, in the determination of the design spectral acceleration values, S(T). The relevant equations are listed below, with linear interpolation being used for intermediate values of T:

$$S(T) = F_aS_a(0.2) \text{ for } T \leq 0.2s \quad (2\text{-}1)$$
$$= F_vS_a(0.5) \text{ or } F_aS_a(0.2) \text{ whichever is smaller for } T=0.5$$
$$= F_vS_a(1.0) \text{ for } T= 1.0s$$
$$= F_vS_a(2.0) \text{ for } T= 2.0s$$
$$= F_vS_a(2.0)/2 \text{ for } T \geq 4.0s$$

2.1.3 Equivalent static force procedure

The equivalent static force procedure can be used for structures that meet any of the following criteria :

a) For cases where $IF_aS_a(0.2)$ is less than 0.35
b) Regular structures that are less than 60 m in height and have fundamental periods less than 2 seconds
c) Structures with structural irregularity, Types 1, 2, 3, 4, 5, 6 or 8 that are less than 20 m in height and have a fundamental period less than 0.5 seconds. Irregularities Types 1 to 8 are related respectively to the vertical distribution of stiffness, the vertical distribution of mass, the vertical geometric irregularity, the in-plane discontinuity in the vertical lateral force-resisting element, the out-of-plane offsets, the discontinuity in capacity (weak storey), the torsional sensitivity and the non-orthogonal systems. NBCC 2004 specifies limits on each of these parameters to determine if a building is regular or irregular.

In this method, a total earthquake lateral force, V, is first computed and then distributed at each level of the building. That force is obtained by the following equations:

$$V = S(T_a)M_vIW/(R_dR_o) \geq S(2.0)M_vIW/(R_dR_o) \quad (2\text{-}2)$$

If $R_d \geq 1.5$

$$V \leq (2/3)\ S(0.2)IW/(R_dR_o)$$

The fundamental lateral period, T_a, in the direction under consideration is approximated as:

$$T_a = 0.085\ (h_n)^{3/4} \text{ for steel moment frames} \quad (2\text{-}3)$$

$$T_a = 0.075\ (h_n)^{3/4} \text{ for concrete moment frames} \quad (2\text{-}4)$$

$$T_a = 0.1\ N \text{ for other moment frames} \quad (2\text{-}5)$$

$$T_a = 0.05\ (h_n)^{3/4} \text{ for other structures} \quad (2\text{-}6)$$

N is the total number of storeys above exterior grade and h_n is the height of the building in metres.

Alternatively, the fundamental period can be determined using an established method of mechanics using a structural model, however, T_a so computed cannot be taken greater than 1.5 times the value determined from the formulas above.

M_v is a factor that accounts for higher mode effects on the base shear in tall structures. It depends on the $S_a(0.2)/ S_a(2.0)$ ratio, the type of lateral resisting systems and the value of T_a. The values of M_v are given in Table 2.1.

Table 2.1 Higher mode factor (from NBCC 2004)

$S_a(0.2)/S_a(2.0)$	Type of Lateral Resisting Systems	M_v For $T_a \leq 1.0$	M_v For $T_a \geq 2.0$
<8.0	Moment resisting frames or "coupled walls"	1.0	1.0
	Braced frames	1.0	1.0
	Walls, wall-frame systems, other systems	1.0	1.2
>8.0	Moment resisting frames or "coupled walls"	1.0	1.2
	Braced frames	1.0	1.5
	Walls, wall-frame systems, other systems	1.0	2.5

The earthquake importance factor, I, depends on the importance of a building in terms of useability after a major earthquake: 1.5 for post disaster buildings, 1.3 for schools and 1.0 for all other buildings.

R_d is a ductility related force modification factor that reflects the capability of a structure to dissipate energy through inelastic behaviour.

R_o is the overstrength related force modification factor that accounts for the predictable portion of reserve strength in a structure. R_o is taken as (Mitchell *et al.*, 2002):

$$R_o = R_\phi \cdot R_{yield} \cdot R_{sh} \cdot R_{size} \cdot R_{mech} \qquad (2\text{-}7)$$

where:

$R_\phi = 1 / \phi$; ϕ is the resistance factor used in the design;

R_{yield} = ratio of probable yield strength to minimum specified yield strength;

R_{sh} = overstrength due to strain hardening;

R_{size} = overstrength due to discrete member sizes;

R_{mech} = overstrength developed when a full collapse mechanism is formed;

R_ϕ is used in Equation 2-7 since it is considered adequate to use nominal instead of factored resistance when designing for the rare earthquake event. R_{yield} accounts for the fact that the minimum specified material strength typically underestimates the actual strength. R_{sh} takes into account the possibility of strain hardening developing in the material at the anticipated level of deformation of the structure. R_{size} accounts for the fact that building designers usually have restricted choices for sizes of members. For example, only standardised choices of sheet steel thickness are available for steel roof deck diaphragms. Finally, R_{mech} accounts for the additional resistance that can be developed before a collapse mechanism is developed in the structure.

R_d and R_o depend on the type of lateral force resisting system. The values specified in the Code for steel structures are given in Table 2.2.

Table 2.2 Seismic force resisting system (SFRS), Rd and Ro for steel structures (adapted from NBCC 2004)

Type of SFRS	R_d	R_o	RESTRICTIONS				
			Cases Where $IF_aS_a(0.2)$				Cases Where
			<0.2	≥0.2 to <0.35	≥0.35 to ≤0.75	>0.75	$IF_aS_a(1.0)$ >0.3
Steel Structures Designed and Detailed According to CSA S16-2001							
▪ Ductile moment resisting frames	5.0	1.5	NL	NL	NL	NL	NL
▪ Moderately ductile moment resisting frames	3.5	1.5	NL	NL	NL	NL	NL
▪ Limited ductility moment resisting frames	2.0	1.3	NL	NL	60	NP	NL
▪ Moderately ductile concentric braced frames							
Non-chevron braces	3.0	1.5	NL	NL	40	40	NL
Chevron braces	3.0	1.5	NL	NL	40	40	NL
Tension-only braces	3.0	1.5	NL	NL	20	20	NL
▪ Limited ductility concentric braced frames							
Non-chevron braces	2.0	1.3	NL	NL	60	60	60
Chevron braces	2.0	1.3	NL	NL	60	60	60
Tension-only braces	2.0	1.3	NL	NL	40	40	60
▪ Ductile eccentric braced frames	4.0	1.5	NL	NL	NL	NL	NL
▪ Ductile frame plate shearwall	5.0	1.6	NL	NL	NL	NL	NL
▪ Moderately ductile plate shearwall	2.0	1.5	NL	NL	60	60	60
▪ Conventional construction of moment frames, braced frames or shearwalls	1.5	1.3	NL	NL	15	15	60
▪ Other steel SFRS(s) not defined above	1.0	1.0	15	15	NP	NP	60

Notes on restrictions:

(a) NP: not permitted
(b) Numbers in table are maximum height limits in metres.
(c) NL: system is permitted and not limited in height as an SFRS. Height may be limited elsewhere in other sections of the code.
(d) The most stringent requirement governs.

In a single storey building, the entire force V is considered to act at the roof level. A procedure is proposed in the draft code to distribute lateral forces between levels in a multi-storey building.

Torsional effects must be considered in design dependent on the torsional sensitivity of the building. The torsional sensitivity is determined by calculating a coefficient B, which corresponds to the maximum value of the ratios B_x, a function of the storey displacement, computed at each level x and for each orthogonal direction with the following equation:

$$B_x=\delta_{max}/\delta_{ave} \qquad (2\text{-}8)$$

where δ_{max} is the maximum storey displacement at the extreme points of the structure at level x in the direction of the earthquake induced by the equivalent static forces acting at accidental eccentricities of $\pm 0.10D_{nx}$ from the centres of mass (C.M.) at each floor, and δ_{ave} is the average of the displacements at the extreme points of the structure at level x produced by the above forces (Figure 2.2).

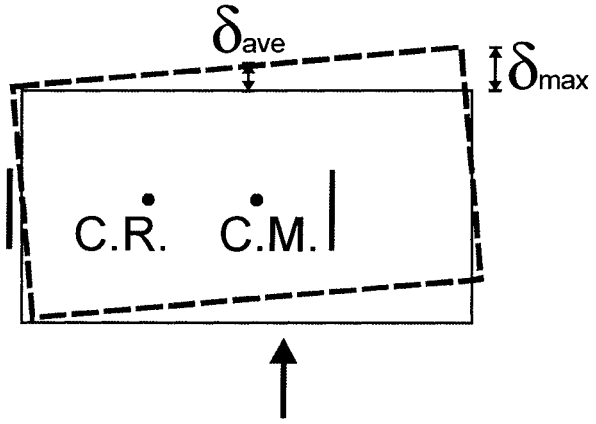

Figure 2.2 Maximum and average storey displacements

If B<1.7, torsional effects may be evaluated by applying torsional moments about a vertical axis at each level throughout the building derived for each of the following load cases considered separately:

i) $T_x = V (e_x + 0.1D_{nx})$ (2-9)

ii) $T_x = V (e_x - 0.1 D_{nx})$

For a building with B>1.7, a dynamic analysis procedure is required, as described in Section 2.1.4.

It has to be noted that this procedure for torsional effects is based on a rigid diaphragm hypothesis. In this research project, the roof deck diaphragms are flexible, and hence do not meet this assumption. In the case of a flexible diaphragm, caution has to be exercised in using the above formulas and in taking into account the torsion caused by eccentrically located mass or building stiffness. A more detailed analysis of such a structure may be needed. In all cases, analyses carried out following the equivalent static force procedure are based on the hypothesis of an elastic structure.

2.1.4 Dynamic analysis procedures:

Different approaches are available in the dynamic analysis procedure, including:

a) Linear dynamic analysis by either the modal response spectrum method or the numerical integration linear time history method

b) Nonlinear dynamic analysis method

These are standard methods developed for seismic engineering and descriptions are available in most comprehensive books covering dynamic analysis (e.g., Chopra (2000)) and hence, a detailed description has not been included in the text. Some specific requirements are, however, given in the Code which can be summarised as follows:

- The spectral acceleration values in the modal response spectrum method shall be the design spectrum, S(T), as defined in (2-1).

- The ground motion histories used in the numerical integration linear time history method shall be compatible with a response spectrum constructed from the design spectral acceleration values S(T).

- The elastic base shear, V_e, obtained from a linear dynamic analysis shall be multiplied by the importance factor I and shall be divided by R_oR_d to obtain the design base shear V_d.

- If the base shear V_d is less than 80% of the lateral earthquake force, V, V_d shall be taken as 0.8V except that for irregular structures requiring dynamic analysis V_d shall be taken as the larger of the V_d and 100% of V.

- The values of elastic storey shears, storey forces, member forces, and deflections obtained from the linear dynamic analysis shall be multiplied by V_d/V_e to determine their design values.

- The effects of accidental torsional moments acting concurrently with and due to lateral earthquake forces shall be accounted for by the following methods:

a) the static effects of torsional moments due to $(0.10D_{nx})\ F_x$ shall be combined with the effects determined by dynamic analysis.

b) if B<1.7, it is permitted to use a 3-dimensional dynamic analysis with the centres of mass shifted by a distance $-0.05D_{nx}$ and $+0.05D_{nx}$.

2.1.5 Deflections and drift limits

Lateral deflections obtained from a linear elastic analysis using the methods discussed previously and incorporating the effects of torsion shall be multiplied by R_dR_o/ I to give realistic values of anticipated deflections. The calculated deflections are from an elastic approach and since the structure is expected to go into the inelastic range the predicted elastic deflections must be increased accordingly. The largest interstorey deflection at any level shall be limited to 0.025 h_s for all buildings except schools (0.02 h_s) and post-disaster buildings (0.01 h_s).

2.1.6 Diaphragm provisions

Special provisions concerning diaphragms are explicitly required in the NBCC 2004.

- "Diaphragms and their connections shall be designed so as not to yield and the design shall account for the shape of the diaphragm, including openings and for the forces in the diaphragm due to the following cases, whichever governs."

"Forces in the diaphragm due to loads increased to reflect the lateral load capacity of the SFRS, plus forces in the diaphragm due to the transfer of forces between elements of the SFRS associated with the lateral load capacity of such elements of the SFRS associated with the lateral load capacity of such elements and accounting for discontinuities and changes in stiffness in these elements."

"A minimum force corresponding to the design base shear divided by N for the diaphragm at level x."

- "The design forces in elements need not exceed the following values:

a) the forces multiplied by $R_d R_o$ when the SFRS is designed for a value of $R_d > 2.0$.
b) the forces multiplied by 1.4 $R_d R_o$ when the SFRS is designed for a value of $R_d < 2.0$."

The 1.4 factor used when $R_d < 2.0$ gives an additional security for low ductility systems. More ductile systems do not need this security.

These provisions have a large impact on the design of a steel deck diaphragm due to the requirement that the metal roof diaphragm remain essentially elastic under the design level earthquake.

2.2 PERFORMANCE LEVEL AND ACCEPTANCE CRITERIA

The earthquake-resistant design provisions of NBCC 2004 aim to provide an acceptable level of public safety by designing a structure to prevent major failure and loss of life. Hence, the intended performance level is the life safety level. In addition, buildings under a severe earthquake should be kept from experiencing partial or total collapse. This is called the collapse-prevention level.

Acceptance criteria are proposed in FEMA 273 (BSSC, 1997) for various performance levels, i.e collapse prevention, life safety, immediate occupancy and operational levels. These criteria relate to permissible earthquake-induced forces and deformations for various elements of the building. Table 2.3 shows anticipated damage at life-safety and collapse-prevention levels.

Table 2.3 Anticipated damage at the collapse prevention and life safety level (BSSC, 1997)

Element	Collapse prevention level	Life safety level
Braced steel frame	Extensive yielding and buckling of braces. Many braces and their connections may fail.	Many braces yield or buckle but do not totally fail. Many connections may fail.
Metal deck diaphragm	Large distortion with buckling of some units and tearing of many welds and seam attachments.	Some localised failure of welded connections of deck to framing and between panels. Minor local buckling of deck.
Cladding	Severe damage to connections and cladding. Many panels loosened.	Severe distortion in connections. Distributed cracking, bending, crushing, and spalling of cladding elements. Some fracturing of cladding, but panels do not fall.

In addition, drift limits that provide an indication of the collapse prevention and life safety levels for concentrically braced frames (CBFs) are presented in Table 2.4.

Table 2.4 Indicative range of CBFs drift for collapse prevention and life-safety level (BSSC, 1997)

Collapse prevention level	Life safety level
2% transient or permanent drift	1.5% transient; 0.5% permanent

FEMA 273 (BSSC, 1997) recommends that every rehabilitated building meet as a minimum the basic safety objectives, which is realised with a two-level design check. In fact, buildings have to be designed to achieve both life safety performance level for the Basic Safety Earthquake 1 (BSE-1) demand and the collapse prevention level for the

Basic Safety Earthquake 2 (BSE-2) demand. BSE-1 earthquakes are related to an earthquake having a probability of exceedance of 10% in 50 years and BSE-2 are related to 2% in 50 years.

2.3 LATERAL-LOAD RESISTING SYSTEM -S16

Several systems can be used for steel structures, in conjunction with a diaphragm, to resist lateral seismic and wind forces: moment frames, concentrically braced frames, eccentrically braced frames, plate walls, etc. In practice, concentrically braced frames (CBFs) are typically found in single-storey steel structures and, therefore, their influence on diaphragm design has been studied in this project. In this section, design provisions included in the CSA-S16-2001 Standard and problems related to CBFs are discussed. The S16-2001 was not officially adopted at the beginning of the project and the work was done using a draft version of the Standard. In the text, the draft is referred as S16-2001.

The cyclic inelastic response of concentrically braced frames is generally poor (Bruneau *et al.*, 1998 and Tremblay, 2001). The limited energy dissipation characteristics of the bracing members, the inherent low redundancy of the system, and the likelihood of premature brace fracture under cyclic loading and brittle failure of brace connections are among the main concerns that have been raised against the use of CBFs in active seismic regions. Moreover, soft-storey response in multi-storey buildings is a major problem due to the limited capacity of the system to redistribute the inelastic demand over the height of the building.

With the aim of improving the behaviour of CBFs under seismic loading, research has been undertaken on this subject over the last 25 years as reported by Bruneau *et al.* (1998) and Tremblay (2001). S16-2001 brings new recommendations resulting from

these improvements which should result in more robust earthquake-resistant CBFs. General S16 seismic provisions are first discussed in this text, followed by the clauses related to CBFs.

2.3.1 General provisions

Capacity based design is explicitly required in S16-2001. Clause 27.1.2 requires that there shall be designated energy dissipating elements in the framing system, that all other elements of the lateral-load-resisting system shall be provided with sufficient strength such that the chosen means of energy dissipation may be achieved and structural integrity can be maintained under seismic ground motion.

For example, if the braces of a CBF are chosen as the energy-dissipation device, all other elements, in the lateral load path, including the roof diaphragm, must be strong enough in order to remain elastic under seismic ground motions. In NBCC 2004 and S16-2001, only vertical lateral resisting systems can be used as the energy-dissipation device. Thus, there is an inherent requirement that the diaphragm remain elastic under a design earthquake.

S16-2001 brings a new nomenclature into the definition of designated lateral-force resisting systems, which is also used in NBCC 2004. Designated lateral-force resisting systems for steel structures are as listed in Table 2.2 which are moment resisting frames, CBFs, eccentric braced frames, frame plate shearwalls. Only CBFs are described in this text since they are the standard lateral system for single storey steel structures. In addition, this is the system that was used in this study.

2.3.2 Moderate ductility (MD) CBFs

Through yielding of braced members, moderate ductility (MD) concentrically braced frames have the capacity to *dissipate moderate amounts of energy* (from S16-2001 (CSA, 2001)). Tension-compression, chevron and tension-only bracing systems may be included in this category if they respect code defined limits. These frames have a ductility related force modification factor, R_d, equal to 3.0.

Chevron bracing systems, in which pairs of braces that meet either above or below a beam at a single point within the middle half of the beam span are permitted, provided that the beams are continuous over their length and are designed to carry the brace induced loads after buckling of the braces has occurred.

Tension-only braced frames, in which braces are connected at beam-to-column intersections and are designed to resist, in tension, 100% of the seismic load, are also permitted for low-rise buildings.

The slenderness ratio, KL/r, of the diagonal bracing members shall not exceed 200 including tension-only bracing members. Also, specific width-thickness ratio criteria have to be respected for the bracing members. These criteria vary as a function of the brace slenderness and the seismic activity of the region in which the building is located. In an active seismic zone, when the brace slenderness ratio is less than or equal to 100, the width-thickness ratios should respect class 1 criteria or more severe restrictions. When the brace slenderness ratio is between 100 and 200, the width-thickness ratios are less stringent. A class 2 or class 1 is required depending on the cross-section shape. All other things being equal, a slender brace can have a larger width-thickness ratio compared to a non slender brace.

For built-up members in seismically active regions, certain provisions need to be respected. When buckling induces shear in stitches, the slenderness ratio of the element must be smaller than 0.5 times the slenderness ratio of the overall brace. Also, stitch connections shall be designed for a particular amount of shear. When buckling does not induce shear in stitches, the slenderness ratio of the element shall be smaller than 0.75 times the slenderness ratio of the overall brace. In any case, bolted stitches are not allowed at hinge locations.

Brace connections shall have a factored resistance to resist the probable axial tensile yield strength ($A_g R_y F_y$) and 1.2 times the probable nominal compressive resistance ($1.2C_r/\phi$) of the bracing members. R_y is equal to 1.1 and takes into account that the probable yield stress is higher than the specified minimum yield stress F_y. The product $R_y F_y$ is limited to 385 MPa. The net section fracture resistance of the brace shall also be adequate to resist this same tensile force. The tensile forces need not exceed the combined effect of the gravity load in the bracing members and the full elastic seismic loads on the bracing members with $R_d R_o=1$. In addition, brace connections, including gusset plates, shall be detailed to avoid brittle failures due to rotation of the bracing member when it buckles. In short, they should be detailed to rotate upon buckling or designed to resist $1.1ZR_y F_y$, Z being the plastic section modulus of the brace. Equally important, eccentricities should be minimised in bracing connections.

Columns, beams and connections in the lateral-load-resisting systems other than the brace connections, shall be designed to resist gravity loads together with the forces induced by the brace connection loads. Redistribution of the loads due to brace buckling shall be considered.

2.3.3 Limited ductility (Type LD) CBFs

Limited ductility (Type LD) concentrically braced frames are capable of dissipating *limited amounts of energy through yielding of bracing members* (from S16-2001 (CSA, 2001)). Tension-compression, chevron and tension-only bracing systems may be included in this category if they respect limits mentioned in the code. These frames have a ductility related force modification factor, R_d, equal to 2.0. Type LD frames have the same general design requirements as type MD frames except that in some cases these requirements are relaxed.

For tension-only bracing systems, the standard slenderness ratio limits apply (200 in compression and 300 in tension). There are no width-thickness limits for tension-only braces. In non-active seismic zones, the braces need not be more compact than Class 2. The requirements for bracing connections are waived in low-activity seismic zone if the brace slenderness ratio is greater than 100.

Other provisions not relevant to this project need to be respected for LD and MD concentrically braced frames. For example, requirements concerning the column splices, chevron braces and tension-compression CBFs are not presented in this text.

2.4 DIAPHRAGM DESIGN

In most building codes, static equivalent loads are used to simulate the forces imposed on a building due to seismic ground movement. Hence, the present diaphragm design methods are based on static loading approaches (CECM (1977), CSSBI (1991), and SDI (1987)). Only the SDI method is presented here, as it is the method used in the project. This method was used mainly due to its flexibility in terms of incorporating different fastener types. Moreover, the CSSBI method (Canadian Sheet Steel Building Institute, 1991) is from the Tri-Services Technical Manual (1982) which in the latest version (US Army Corps of Engineer (1998)) no longer contains this method but rather points to the SDI method for diaphragm design. The SDI method approach was developed mainly by Luttrell at West Virginia University as detailed in the Steel Deck Institute Diaphragm Design Manual (1981). It is important to note that the SDI method was developed for use with Imperial units, hence, modifications are required when SI units are used.

For diaphragm design, the serviceability and ultimate limit states are considered.

i) Shear resistance (Ultimate limit states)
ii) Flexural resistance (Ultimate limit states)
iii) Lateral deflection of the diaphragm (Serviceability or ultimate limit states)

The SDI method is based on a plate girder analogy. The web, which is the roof deck diaphragm, resists in-plane shear forces and the flanges, which are the framing elements around the roof perimeter, carry the flexural loads caused by lateral loading. This analogy is shown in Figure 2.3.

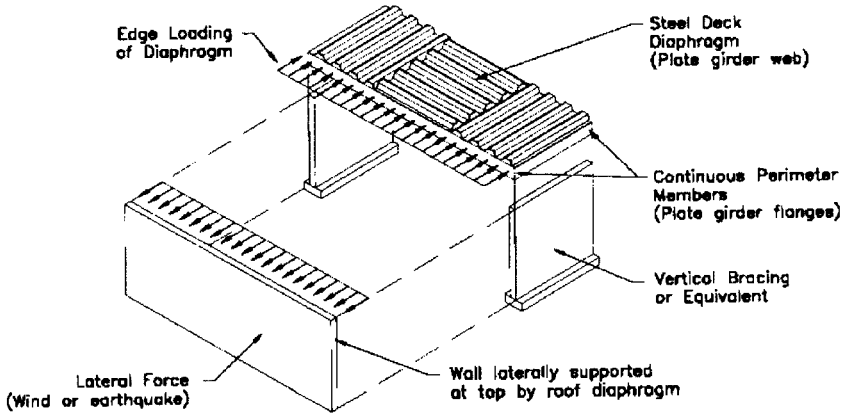

Figure 2.3 Plate girder analogy (adapted from CSSBI, 1991)

The shear resistance provided by the deck depends on the cross-sectional area, depth, profile, panel length, and inelastic limit of the deck as well as the location, type and spacing of the deck-to-frame and sidelap fasteners. Arc-spot welds with or without washers, powder-actuated nails and screws are commonly used as deck-to-frame fasteners. In the case of sidelap fasteners, button punches, stitch screws and seam welds are possible choices. An important hypothesis of the SDI method is that the orientation of the deck (flutes running parallel or perpendicular to the direction of lateral loading) does not influence the shear resistance.

Three connection related failure mechanisms are considered in the SDI method, with the strength of the diaphragm taken as the lesser of the resistance associated with the following:

a) Failure along a sidelap connector line,
b) Failure along a connector line located at the diaphragm edge,
c) Failure of a corner connector.

It is also possible for the diaphragm to buckle under shear forces over the entire roof area. A stability check is also recommended in the SDI method. Shear buckling would typically occur only for thin decks that are shallow in depth and that have closely spaced fasteners.

Flexural resistance of the roof system to lateral loads is provided by the perimeter framing members. It is assumed that axial forces in the perimeter members give rise to a resisting moment couple. The deck is not considered to carry any flexural stresses due to its limited stiffness in comparison with spandrel members.

In the working stress design approach, the SDI method prescribes the following safety factors: 2.75 for welded connections, 2.35 for mechanical connections and 2.75 for combinations of welds and mechanical connections.

The lateral deflection of the roof diaphragm is composed of a flexural and a shear component. The flexural deflection, Δ_F, depends on the moment of inertia of the diaphragm, as provided by the perimeter framing members only. Conventional beam deflection formulae can be used to evaluate Δ_F.

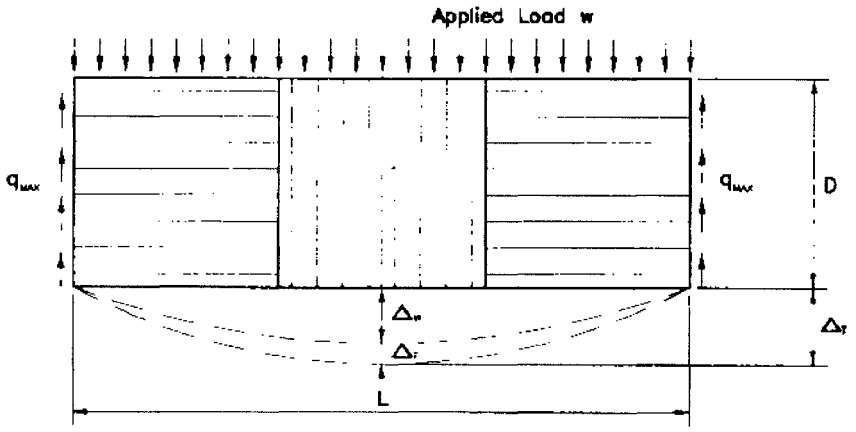

Figure 2.4 Diaphragm deflection for simple span (adapted from CSSBI, 1991)

For instance, in the case of a single span beam under uniform loading, as illustrated in Figure 2.4, the flexural deflection is given by:

$$\Delta_F = \frac{5wL^4}{384EI} \qquad (2\text{-}10)$$

where

w: uniform load = V/L

L: span of simple beam

E: Modulus of elasticity of steel

I: Moment of inertia of diaphragm flanges (perimeter members) about centroidal axis of diaphragm

The shear deflection, Δ_s, depends on the in-plane shear stiffness of the diaphragm G'. For a simple span beam under uniform load, the shear deflection is given by:

$$\Delta_s = \frac{wL^2}{8DG'} \tag{2-11}$$

G' depends on the shear deformation of the steel sheets, warping deformation of the deck profile at the sheet ends and the deformation of the deck-to-frame and sidelap fasteners. It is obtained from a monotonic loading test performed on a diaphragm and it is defined as the secant stiffness at 40% of the ultimate load. The SDI proposes a semi-empirical equation to predict G' that accounts for these three contributions:

$$G' = \frac{Et}{2(1+\nu)s/d + \phi D_n + C} \tag{2-12}$$

where

E: modulus of elasticity
t: base metal thickness
ν: Poisson's ratio (ν= 0.3)
s: girth of corrugation per rib
d: corrugation pitch
D_n : warping constant
ϕ: purlin effect factor on warping
C: connector slip parameter

This equation has been adapted from the shear deflection formula for a flat plate. A warping distortion term for the deck panel, D_n, has been added as well as a slip coefficient, C, which takes into account the flexibility of the deck side-lap and frame fasteners.

The diaphragms are classified in function of their rigidity (SDI, 1987): flexible for G' between 1.2 and 2.5 kN/mm, semi-flexible for G' between 2.5 and 17.5 kN/mm, semi-rigid for G' between 17.5 and 175 kN/mm and rigid for G' greater than 175 kN/mm.

As noted previously, the shear deflection is added to the flexural deflection to obtain the total lateral deflection of the diaphragm. The total horizontal deflection of the roof system relative to the ground must also include the deflection of the vertical lateral-force resisting elements, such as the vertical bracing, moment resisting frames, etc. It is this total roof deflection that is compared to the drift limits given by NBCC.

Principally, two types of lateral loading are considered to act on roof diaphragms: wind and seismic loads. The wind loads result from the sum of local wind pressures on the walls of the building, whereas the seismic loads are caused by inertia forces that arise mainly at the roof level due to the mass of the building components and the relative ground movement during an earthquake. Following the NBCC design requirements, both loading types are considered to act perpendicular to the principal building directions, as shown in Figure 2.4. Wind and seismic design loads are obtained according to the approaches detailed below.

For wind loading, a wind pressure with an annual exceedance of 1/30 is used to check the lateral resistance of the building, whereas the wind pressure with an annual exceedance of 1/10 is taken to check the lateral deflection. The lateral deflection is a serviceability limit state whose limit depends on the building type, whereas the strength check is an ultimate limit state.

For seismic loading, both the lateral deflection and strength checks are considered to be ultimate limit states. The lateral force and deflection are calculated with the approach discussed in Section 2.1.

The shear resistance of the deck diaphragm must be sufficient to resist both the wind and seismic loads. From the American Iron and Steel Institute (AISI) Specification (1997), the design shear strength for the Load and Resistance Factor Design (LRFD) method is found by multiplying the nominal shear strength by a resistance factor that depends on the types of loading and connectors involved. Table 2.5 lists the possible diaphragm conditions and associated resistance factors.

Table 2.5 Resistance factors for diaphragms (from AISI (1997))

ϕ	Diaphragm condition
0.60	For diaphragms for which the failure mode is that of buckling, otherwise;
0.50	For diaphragms welded to the structure subjected to earthquake loads, or subjected to load combinations which include earthquake loads.
0.55	For diaphragms welded to the structure subjected to wind loads, or subjected to load combinations which include wind loads
0.60	For diaphragms mechanically connected to the structure subjected to earthquake loads, or subjected to load combinations which include earthquake loads.
0.65	For diaphragms mechanically connected to the structure subjected to wind loads, or subjected to load combinations which include wind loads
0.65	For diaphragms connected to the structure by either mechanical fastening or welding subjected to load combinations not involving wind or earthquake loads.

With regard to resistance factors when earthquake loads are involved, FEMA 302 (BSSC, 1997) gives the same resistance factors as found in the AISI Specification (1997). A resistance factor, ϕ, equal to 0.50 is given for welded diaphragms and 0.60 for mechanically connected diaphragms.

2.5 PAST EXPERIMENTAL RESEARCH ON DIAPHRAGMS

Over the past four decades, several experimental and analytical studies have been performed regarding the behaviour of steel deck diaphragms: Nilson (1960), Bryan and El-Dakhakhni (1968), Easley and McFarland (1969), Luttrell and Ellifritt (1970), Nilson and Ammar (1974), etc. A brief summary of these studies has been provided in the Section. The more relevant studies are discussed: Luttrell (SDI, 1981), Davies and Bryan (1982), Beaulieu and Brindamour (1984), Mazzolani *et al.* (1997) and Essa *et al.* (2001).

Luttrell (SDI, 1981) carried out in-depth testing of different deck patterns and connectors. Stiffness and strength characteristics were evaluated in terms of parameters such as deck type, purlin spacing, panel length, connector arrangement and type, material properties and sheet thickness. These tests were completed under monotonic loading conditions. The SDI diaphragm design method described in the previous section is a result of these laboratory studies along with detailed analytical work.

Similarly, Davies and Bryan (1982) also conducted extensive investigations and developed a design method including the calculation of both the resistance and the flexibility of steel roof deck diaphragms, which is known as the stressed skin design approach to roof diaphragms. The European Recommendations for diaphragm design, CECM (1977), are based mainly on the work of Davies and Bryan.

In addition, at Laval University, Beaulieu and Brindamour (1984) worked on the subject of diaphragm design. Studies were completed on different calculation approaches and testing was carried out on connections for steel deck diaphragms.

Mazzolani *et al.* (1997) and DeMatteis (1998) studied the dynamic behaviour of sandwich diaphragms in simple pin-jointed steel frames. Hysteretic analytical models were developed following an experimental program. This experimental program involved tests of full-scale diaphragms under monotonic and quasi-static loading. Hysteretic models were employed in inelastic analyses with several earthquakes characterising low seismicity zones. A different structural system, walls with cladding on two sides, was investigated in these researches in comparison to the steel roof deck diaphragms studied in the present project. The cladding panels have smaller corrugations or not at all compared to steel deck. The wall cladding was also installed with self-tapping screws, scotch or bi-adhesive bands.

Essa *et al.* (2001) conducted a survey of past experimental studies on diaphragms. Table 2.6 presents a summary of this survey. The main characteristics for tests are shown: test type (cantilever or simply supported beam), deck profiles, connection types, loading types, size, etc.

Table 2.6 Past tests described in the literature (Essa *et al.*, 2001)

Reference	Test Specimen	Loading Protocol	Size	No. of Panels	No. of Purlins	Frame Corners	Instrumentation
Nilson (1960)	20 to 12 gauges	Monotonic to failure	10 ft to 30 ft span cantilevers 12 ft by 30 ft (3-span frame)	Not reported	None	Not reported	Deflections of frame corners, strains in marginal beams, and sidelap slips
Bryan and El-Dakhakhni (1968)	0.024 inch thich hat section	Not reported	10 ft by 16 ft (2-span frame)	4	1	Not reported	Not reported
Easley and McFarland (1969)	0.0191 inch to 0.0363 inch thick	Monotonic to buckling	8 ft by 9.58 ft to 15 ft by 13.58 ft cantilevers	Not reported	None	Pins	Dial gauges were used to measure the lateral deflection at one of the buckle's crest
Luttrell and Ellifritt (1970)	22 to 16 gauges	Monotonic to failure	12 ft by 16 ft to 20 ft by 16 ft cantilevers	Not reported	1 to 4	Clip angles	Deflections at the frame corners
Nilson and Ammar (1974)	Cellular	Monotonic to failure	10 ft by 12 ft cantilever	6	None	Not described	Frame corner connections and sidelap slips
Easley (1975)	0.016 inch thick hat section	Monotonic to buckling	26 in. by 34 in to 30 in. by 30 in. (diagonal loading)	Not reported	None	Pins	Shear deflection and lateral (buckling) deflection
Easley (1977)	3 ft wide panels	Monotonic to failure	15 ft by 10 ft to 15 ft by 24 ft cantilevers	5	1 to 4 girts	Pins	Frame corner deflections were measured with 0.0001 inch dial gauges
Atrek and Nilson (1980)	Cellular, open corrugated and open trapezoidal	Monotonic to failure	10 ft by 12 ft cantilevers	5 6	3 1	Not described	Not reported
Mazzolani and Labini (1983)	Not described	Monotonic and cyclic	Not reported	4	None	Double-angle	Not reported
Italsider (1984), and Sanpaolesi et al. (1983)	1.2 mm thick and 47 mm deep	Cyclic	3516 mm by 2643 mm cantilever	3	None	Double-angle	Not reported
Klingler (1986)	26 to 18 gauges	Monotonic to failure	16 ft by 20 ft	6 + a partial	2	Clip angles	Frame corner deflections
Landolfo and Mazzolani (1994)	1.2 mm thick and 47 mm deep	Monotonic to failure	4688 mm by 2643 mm cantilevers	4	None	Double-angle	Not reported
Walter (1994)	1mm thick with depth of 40 mm or 135 mm	Half a cycle	11.3 ft by 9 ft cantilevers	3	None	Pins	Sidelap slips and warping deformations
De Matteis (1998)	Sandwich panels	Monotonic and cyclic	10 ft by 8.2 ft or 3.3 ft by 8.2 ft cantilevers	1 or 3	None	Pins	Relative slip of adjacent panels, and shear deflection

Most of the tests were conducted monotonically. Hence, limited data are available on the seismic behaviour of deck diaphragms. The other tests were carried out in a cyclic fashion: Mazzolani and Labini (1983), Italsider (1984), Sanpaolesi *et al.* (1983) and De Matteis (1998). However, no test was carried out under dynamic loading, in which the energy dissipation capabilities of specimens can be evaluated.

To address this lack of knowledge concerning the seismic behaviour of steel roof deck diaphragms, a research program was established in 1999 at École Polytechnique de Montréal. The experimental and analytical studies that make up this research program are outlined in the following Sections.

Rogers and Tremblay (2000):

This study focused on connector behaviour because the overall performance of a roof diaphragm is directly related to the means by which it is interconnected, as well as connected to the structural framing. A total of 189 connection tests, including 45 sidelap (16 screw, 20 button punch, 9 weld) and 144 deck-to frame tests (47 screw, 71 powder actuated fastener, 26 weld) were performed. Monotonic, quasi-static, 0.5 Hz cyclic, 3 Hz cyclic and simulated earthquake motion loading protocols were applied to specimens. A number of methods were used to quantitatively evaluate the ability of sidelap and deck-to-frame connections to absorb energy through distortion of the sheet steel adjacent to the fastener during cyclic and simulated earthquake tests. Results showed that the type of fastener influences the ultimate capacity and ability of connection to dissipate energy.

Important recommendations could be drawn from the study. Powder actuated and screwed connections imbedded in a material thick enough to limit fastener tilting would be recommended if the plastic behaviour of deck-to-frame connections is to be depended on. In the case of welded deck-to-frame connections, washers are required in order to carry load in the inelastic range.

Bond *et al.* (2001):

This research focused on the inelastic cyclic response of deck-to-frame arc-spot welds with or without washers. Basically, the same approach as used by Rogers and Tremblay (2000) was relied on for this test series. The laboratory results show that the use of weld washers can improve the ductility, strength, and energy absorption ability of the connection when weld quality is high. However, caution is warranted because premature shear failure through the cross-section of the weld may take place when the weld metal does not fully penetrate into the frame material. Hence, the addition of weld washers may not increase the seismic resistance of the roof diaphragm to the expected levels when a lack of penetration exists. If the seismic resistance of welds with washers is to be relied on, appropriate welding protocols and washer specifications need to be developed, to ensure that the connection will behave as predicted.

Peuler (2002):

A study on the inelastic response of arc-spot welded deck-to-frame connections for steel roof deck diaphragms was performed. Two hundred and thirty five specimens were tested under monotonic, cyclic and seismic loading. Welds with or without washers were used with different electrode types, various steel deck and frame thicknesses. Test results showed that welded with washer deck-to-frame connections gave higher ultimate capacities and improved ductility compared to welded connections without washer. Test data and a welding procedure from Peuler (2002) were used in the present research.

Essa *et al.* (2001):

A series of 18 full-scale diaphragm tests were conducted under monotonic and quasi-static cyclic loading conditions. The main objective of the series of tests was to evaluate

the extent of ductile behaviour in diaphragms; principally, to ascertain the effect of different deck-to-frame and sidelap connectors on overall performance. A testing apparatus was constructed to test diaphragms of 3.66 m by 6.10 m. This apparatus was also used for this research project and is described in Chapter 5.

Essa *et al.* concluded that the diaphragms with welded deck-to-frame connections have limited ductility. Screwed sidelap fasteners with nailed or welded-with-washer deck-to-frame connectors showed higher ability to maintain their capacity under inelastic cyclic loading. It was also determined that an equivalent viscous damping ratio of 5% is appropriate for use in the dynamic analysis of steel deck diaphragm structures.

Summary:

Over the last 40 years, extensive research has been conducted on steel diaphragms. Luttrell (SDI, 1981) carried out in-depth testing of different deck patterns and connectors. These studies have led to the development of the SDI method, which was used in this project for strength and stiffness predictions. De Matteis (1998) did an experimental evaluation of sandwich wall diaphragms and developed an analytical model from the experimental results. A similar approach for steel roof diaphragms was used in the present project. From Rogers and Tremblay (2000), Bond *et al.* (2001) and Peuler (2002), test data on connectors were obtained. These values were used for diaphragm strength and stiffness predictions. Principally, this research was the continuation of Essa *et al.* (2001) project. Test results from cyclic tests were studied to develop the hysteretic analytical model. The most promising deck connectors recommended by Essa *et al.* were tested under dynamic loading.

2.6 DYNAMIC LOADING PROTOCOLS

The effect of an earthquake on a structure strongly depends on the characteristics of the ground motions, which exhibit various frequency contents, amplitudes, durations, etc. The loading and the ductility/ strength demand on the components of a structure are also influenced by the configuration and dynamic characteristics of the building frame. Hence, dynamic loading protocols are typically developed for each component of a steel structure that is subjected to earthquake forces. Researchers specify dynamic loading protocols in order to create a demand on test specimens that includes the target parameters involved in the ductile behaviour of the component: peak ductility demand, number and amplitude of inelastic excursions, amount and rate of energy dissipation, etc. No loading protocol has yet been suggested for low-rise buildings with flexible roof diaphragms. However, standardised quasi-static loading histories have been proposed, such as the ATC-24 (ATC, 1992) or FEMA-350 (SAC Joint Venture, 2000).

ATC (1992):

Guidelines for the cyclic seismic testing of components of steel structures have been developed and detailed in the ATC-24 document. These guidelines were drafted because it was recognised that difficulties arose in the interpretation of the results from previous laboratory experiments, and hence, a common approach to seismic testing was necessary. Information is provided on how to choose load-time histories and how to present test results and other aspects of experimentation. Recommendations are written specifically for experiments with slow cyclic (quasi-static) load application. "Slow cyclic" means that the load or deformation cycles are imposed on a test specimen in a slow, controlled and predetermined manner; where dynamic effects including the rate of deformation are not considered. Strength, stiffness, deformation capacities, cyclic

hardening or softening, deterioration behaviour at large deformations, etc, of structural elements can be determined if ATC-24 guidelines are followed. The guidelines may also be used with some restrictions for high-cyclic load application. With regard to the loading protocol, FEMA-350 is similar to ATC-24.

ATC-24 and FEMA-350 have been developed for California earthquakes and, as mentioned, do not allow for the examination of dynamic effects. For Canada, the demand is expected to vary depending upon the location of the buildings as the characteristics of the anticipated seismic ground motions vary across the country. Tremblay and Atkinson (2001), Tremblay and Lacerte (2002) and Bouatay (2001) showed that the building response varies in Canada. These studies are summarised herein.

Tremblay and Atkinson (2001) performed nonlinear dynamic analyses on bi-linear single-degree-of-freedom models with various ductility levels and damage indicators. The aim of the study was to compare the damage potential of ground motions for cities with moderate seismicity levels in eastern (Montreal) and western (Vancouver) North America. Damage potential was investigated by comparing R factors required to prevent structural failure. In addition, the extent of damage experienced by code-designed structures with fixed R values was studied. The study demonstrated that the required R factors vary from one structural system to another. For buildings in which peak deformations govern, higher R factors could be used in the East in comparison to the West. In addition, the required R factors increase linearly with the structural period. It was found that the current approach in which the UHS is divided by R factors that vary only with the structural system fails to provide a uniform level of protection against structural damage. Accounting for the period dependence on the R factors for the lower vulnerability, for eastern sites, of structures that collapse under large inelastic excursions could improve the uniformity in the level of protection.

Tremblay and Lacerte (2002) completed an analytical study with the objective of choosing accelerograms that are representative of the seismic activity in Quebec and Victoria, sites located in the Eastern and Western regions of Canada. For Victoria, 14 ground motions were selected: 6 historical and 8 simulated. For Quebec, 10 ground motions were chosen: 6 historical and 4 simulated. The response spectra of these ground motions were scaled to match the design spectrum of the proposed NBCC 2004.

Bouatay (2001) established various dynamic loading protocols for steel braced frames through an analytical study. Buildings of 2, 4 and 8 storeys in Quebec, Qc, and Victoria, B.C., were studied under varied seismic ground motions. Software was also developed to facilitate statistical studies of the dynamic nonlinear time history analyses results. Several demand parameters were analysed, of which the peak ductility demand, the number and amplitude of inelastic excursions, the amount and rate of energy dissipation, and the cumulative damage. Four different loading protocols were proposed to cover the various types of ground motions: eastern intra-plate, western intra-plate, near-field motions with pulses and Cascadia subduction events.

In the three above mentioned studies, a significant difference was found in the response of the structures subjected to intra-plate earthquakes in the East and the West, with typically much lower demand in the East. In addition, it was observed that the demand under Cascadia earthquakes was also different: longer in duration with a larger number of loading cycles.

These guidelines and studies were not used directly in the study. However, a similar approach to Bouatay (2001) was used to evaluate the demand. ATC-24 guidelines were not used in the loading protocol development.

2.7 ANALYTICAL STUDIES OF BUILDINGS WITH FLEXIBLE DIAPHRAGMS

Currently, the seismic design of buildings is typically performed using an equivalent static lateral force procedure similar to the one described previously. In such an approach, the dynamic effects of earthquakes on the structure are approximated by applying a static horizontal load at the centre of mass of the building. This procedure is based on the assumption that the roof diaphragm is infinitely stiff. In reality, the steel roof deck diaphragm is most often flexible in shear, and furthermore it has been shown that this in-plane flexibility may influence markedly the dynamic behaviour of the structure. In this section, a summary of several analytical studies of the dynamic response of buildings with flexible metal roof deck diaphragms is presented.

At École Polytechnique de Montréal, several analytical studies of buildings with flexible diaphragms have been carried out; including research by Tremblay and Stiemer (1996), Bérair (1999), and Nedisan (2002). These investigations form part of the overall research program at École Polytechnique on the behaviour of single storey steel structures with steel roof deck diaphragms. Likewise, Medhekar and Kennedy (1999) at the University of Alberta have worked on a seismic study of single storey steel structures.

Tremblay and Stiemer (1996) examined the nonlinear response of 36 rectangular single-storey steel buildings under seismic demand. The lateral-resisting system of the buildings was composed of a flexible steel roof deck diaphragm and concentrically braced frames. Historical seismic ground motions were used for the analytical time history analyses. In the computer model the diaphragm was assigned to have an infinite strength, and hence it remained elastic in all cases. As a result, hysteretic capability of the roof diaphragm was neglected. The results indicated that the fundamental period of

the structures, the maximum drift, the forces and deformations in the roof deck diaphragm, and the ductility demand were inadequately predicted with existing design provisions. For example, the in-plane forces and deformations based on a linear static analysis were different than those obtained from time history dynamic analyses. In fact, dynamic effects should be taken into account in design. A parabolic shape for the shear diagram is more realistic than the linear distribution obtained when assuming the seismic load is uniformly and statically applied along the length of the building.

This behaviour was also recognised in the FEMA 1997 provisions which require that a parabolic distribution be used. The total lateral force on the diaphragm, V_p, rather than being considered to be of uniform intensity of V_p/L, is distributed in a parabolic manner with an ordinate of $1.5V_p/L$ at mid-span, where L is the span of the diaphragm (Figure 2.5). The resulting variation in shear is cubic. Figure 2.5 also shows the plausible force distribution in a flexible diaphragm.

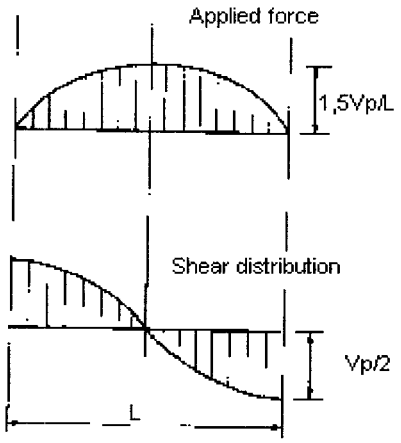

Figure 2.5 Plausible force distribution in a flexible diaphragm (adapted from FEMA 273 (BSSC, 1997))

A similar study has been produced by Medhekar and Kennedy (1999) in which the seismic performance of single-storey steel buildings was evaluated. Analytical models of

the buildings were developed. The seismic response of the models was assessed by means of a linear static analysis, a response spectrum analysis, a nonlinear static or "pushover" analysis, and nonlinear dynamic time history analyses.

The results showed that current design procedures provide a reasonable estimate of the drift and brace ductility demand, but do not ensure that ductility is restricted to the braces. Moreover, in moderate and high seismic zones, the roof diaphragm responded inelastically. Currently, in design, the diaphragm is considered to behave elastically.

In the analytical model, the inelastic behaviour was taken into account by a rigid-plastic link inserted between the CBFs and the roof diaphragm. This link transferred the shear force from the diaphragm end to the CBFs. The maximum force in this link depended on the strength of the CBF and the diaphragm. The idealised rigid-plastic link did not represent the actual behaviour of the diaphragm, as the diaphragm behaviour depends on the fasteners used (nails, welds, etc).

Moreover, Medhekar (1997) developed an expression to estimate the fundamental period of the single storey steel structure. Tremblay and Berair (1999) adapted the expression to obtain Equation 2-13.

$$T = 2\pi\sqrt{\frac{(K_B + K_D)}{K_B K_D}\frac{W}{g}} \qquad (2\text{-}13)$$

and

$$K_D = \frac{\pi^2}{\frac{L^3}{\pi^2 EI} + \frac{L}{G'D}} \qquad (2\text{-}14)$$

where

K_B = total lateral stiffness of the vertical bracing
K_D = total lateral stiffness of the diaphragm
W = seismic weight of the building
g = acceleration due to gravity
G' = diaphragm stiffness
D and L are plan dimensions of the building

Shake-table tests were performed at École Polytechnique de Montréal in which a scale low-rise steel building model with a flexible roof diaphragm was subjected to seismic ground motions (Bérair, 1999). The experimental results showed that the simplified formula developed by Medhekar (1997), described previously, for estimating the natural period of the structures can be used. Test results tended to confirm the previous analytical studies for the distribution of forces in the roof.

Nedisan (2002):

Tremblay *et al.* (2002) based on Nedisan's thesis (2002) investigated the behaviour of single-storey steel structures with flexible roof diaphragms as designed according to NBCC 2004. A strong diaphragm design was used and the actual period of the structure was considered to determine V, not the 1.5 T_a. It was found that the behaviour was acceptable in terms of drift, ductility, etc but the structures were much more flexible than with the previous NBCC 1995 or when using the formula for T_a.

In addition, Nedisan (2002) studied the SDI method and its limits of application for steel roof deck diaphragms. It was shown that the existing method does not take into account the possibility of non-simultaneous connector failure, a characteristic that has been observed in laboratory tests of full diaphragms. Nedisan also observed that the method is

appropriate when failure of connectors occur at the same time, hence, ductile connectors should be used to attain this objective.

Outside Canada, studies have been realised on the analysis of flexible roof diaphragms that are not related directly to steel roof deck diaphragms. However, information on the general behaviour of flexible diaphragms may be relevant to this investigation.

Tena-Colunga and Abrams (1996) analysed three existing buildings subjected to the 1989 Loma Prieta earthquake. These buildings had previously been instrumented and it was possible to gather information on their seismic response. It was found that the results from an analytical model agreed with on-site measurements. When subjected to the real earthquake, the structure of the buildings remained in the elastic range, as was also shown by the analytical study. Results indicated that diaphragm and shear-wall accelerations can increase with the flexibility of the diaphragm.

Fleischman and Farrow (2001) developed analytical models that capture the diaphragm flexibility of structures with long-floor spans and perimeter lateral-systems. Modal and time history analyses were performed to determine the effect of diaphragm flexibility and diaphragm inelastic behaviour on the overall dynamic behaviour of these structures. The study involved multi-storey precast concrete structures. However, some findings can be related to this project.

Of particular interest in that research is the relation that is proposed between the frequencies of a rigid diaphragm system and a related flexible diaphragm system. The resisting lateral system can be represented by a 2 degree-of-freedom system.

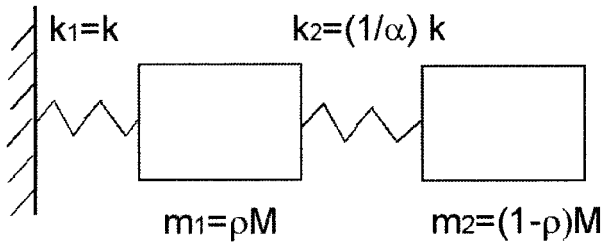

Figure 2.6 Two-DOF system

k_1 and k_2 are the lateral rigidity of the vertical lateral force resisting system and the diaphragm, respectively. m_1 and m_2 are the masses related to the walls and the roof. The flexibility ratio, α, is defined as the ratio of the in-plane diaphragm deformation to the lateral-system absolute drift at mid-height of the structure. It provides an average measure of the flexibility of the diaphragm for multi-storey structures. In the model, M represents the total mass of the system, ρ is the ratio of the wall mass to the total mass of the system, and k is the rigidity of the vertical lateral-force resisting system.

When $\alpha \to 0$, $k_2 \to \infty$, the diaphragm is rigid and the system responds at a single frequency:

$$w_{rig} = \sqrt{\frac{k}{W/g}} \tag{2-15}$$

If the diaphragm has some flexibility ($\alpha \neq 0$), the frequencies of the system are given by:

$$\varpi_j = \Lambda_j(\alpha, \rho)\varpi_{rig} \tag{2-16}$$

$$\Lambda_j(\alpha,\rho)=\sqrt{\frac{1-\rho+\frac{1}{\alpha}+(-1)^j\sqrt{\left(1-\rho+\frac{1}{\alpha}\right)^2-4\rho(1-\rho)\frac{1}{\alpha}}}{2\rho(1-\rho)}} \qquad (2\text{-}17)$$

Λ_j (α, ρ) are frequency modification factors. The subscript j indicates the mode (j = 1 and 2) in the plane of the diaphragm. (Personal correspondence with Farrow, University of Notre Dame).

Figure 2.7 shows the variation of the frequency modification factor Λ_j (α, ρ) in the first mode (j=1) as a function of diaphragm flexibility.

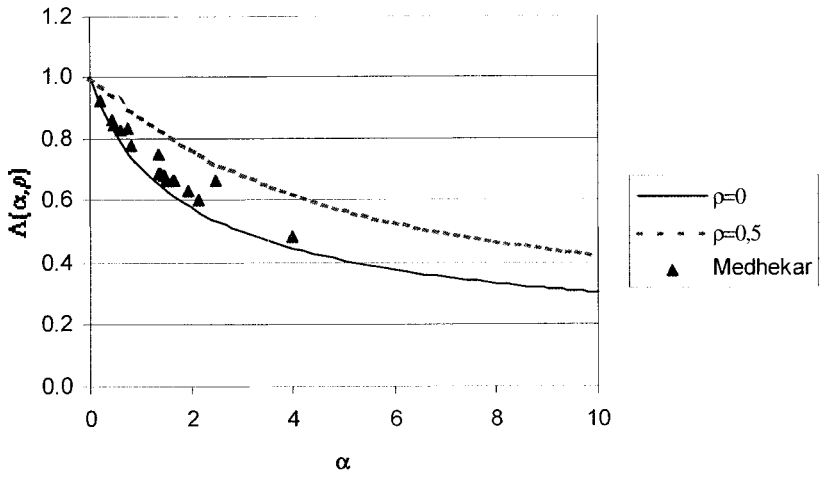

Figure 2.7 Frequency modification factor, Λ, as a function of α for ρ= 0,0 and 0,5 (fundamental mode j=1)

In the first mode, the frequency modification factor $\Lambda(\alpha,\rho)$ tends to diminish when the diaphragm flexibility is increased. In general terms, the natural period of the structure increases with an increase of the diaphragm flexibility.

In addition, results from Medhekar's (1997) formula are presented in the figure for comparison of the different prototype buildings designed by Nedisan (2002). Results from Medhekar's formula show a good correlation with Fleishman and Farrow's approach. Overall, the Medhekar's study showed that diaphragm flexibility can lead to unexpected force and drift patterns.

Ju and Lin (1999) investigated the difference between the rigid-floor and flexible-floor analyses of moment frame buildings with and without shear walls. The study was restricted to elastic models. Results showed that in buildings without shear walls the diaphragm flexibility had little effect on the response. On the other hand, for buildings with shear walls, the diaphragm flexibility had an important influence on the results and a formula has been developed by the authors to evaluate the error made when neglecting diaphragm flexibility in the calculations of column forces.

The error formula is presented herein. The following procedure can be used to evaluate the error in column forces. First, a displacement difference ratio has to be calculated.

Step 1: The floor is assumed to be a simply supported beam subjected to a uniform load.

Step 2: The approximate averaged lateral displacements of the rigid-floor analysis are assumed as follows:

$$\Delta_{rigid} = \Delta_w \qquad (2\text{-}18)$$

Δ_{rigid} represents the approximate averaged lateral displacement of the floor under the rigid-floor assumption. Δ_w is the lateral displacement of the shear walls.

$$\Delta_{flexible} = \Delta_w + \Delta_f/2 \qquad (2\text{-}19)$$

$\Delta_{flexible}$ represents the averaged lateral displacement of the floor under the flexible-floor assumption. Δ_f is the lateral displacement at the centre of the simply supported roof diaphragm.

The displacement difference ratio is defined as:

$$R = \frac{\Delta_{flexible} - \Delta_{rigid}}{\Delta_{flexible}} \qquad (2\text{-}20)$$

From R, the error can be evaluated with the following equation:

$$Error\% = 81.53R + 3.8 \qquad (2\text{-}21)$$

If R is under 0.2, the error of the rigid-floor analysis is smaller than 20%. In some cases, the designer may consider this error to be acceptable.

Ju and Lin (1999) studied moment frame buildings with flexible or rigid diaphragms with or without shear walls. They found that in buildings with shear walls the influence of the flexibility of the diaphragm may be important and should be considered in analysis. The structures investigated by Ju and Lin were different than those of this study since they were made of moment frames. Hence, the error formula is not applicable to our buildings.

Summary:

Overall, this review of the analytical work brought these main elements. Tremblay and Stiemer (1996) evaluated the effect of the diaphragm flexibility on single storey steel structures. They found that the dynamic effects, increased by the flexibility of the

diaphragm, were not taken into account by the conventional method for predicting forces (uniform distribution of lateral loads). FEMA-273 (BSSC, 1997) recommended a new approach with a parabolic distribution of lateral forces that takes into account the dynamic effects. Also, Medhekar and Kennedy (1999) investigated the behaviour of single storey steel structures. Medhekar (1997) developed an analytical formula for the building period that takes into account the flexibility of the braced bents and the roof diaphragm. Bérair (1999) demonstrated by an experimental program that the Medhekar's formula was adequate. This formula was used in the present project to evaluate building periods. Fleischman and Farrow (2001) developed an analytical method that capture the diaphragm flexibility of structures with long-floor spans and perimeter lateral-systems. As explained previously, results from Medhekar's formula show a good correlation with Fleishman and Farrow's approach.

CHAPTER 3

BUILDING ANALYSES

3.1 INTRODUCTION

The first objective of this study was to obtain a better knowledge of the anticipated inelastic seismic demand on metal roof deck diaphragms, for single storey buildings in which the diaphragm is selected as the energy dissipating element. Sections 3.2 to 3.4 describe the design and the analysis of the building structures with a weak-diaphragm design that were sized using the NBCC 2004 provisions. The design of the structures, the nonlinear dynamic analytical model that was adopted and the selection of the ground motion ensembles are respectively presented in these three sections. Section 3.5 presents the design and the modelling of the buildings designed according to the NBCC 1995 provisions. The results of the nonlinear dynamic analyses performed on all the building structures are given and discussed in Section 3.6. The development of the loading protocols that were used in the experimental program is presented in Chapter 4.

3.2 BUILDING GEOMETRY AND DESIGN

3.2.1 General assumptions

Single-storey structures with concentrically braced frames and metal roof deck diaphragms were considered in this study (Figure 3.1). The buildings that were studied were rectangular and symmetrical in plan with an aspect ratio of 1:2 with braced bays in the external walls (except for the double configuration structure). Figure 3.2 presents a plan view of one of the building considered (medium size).

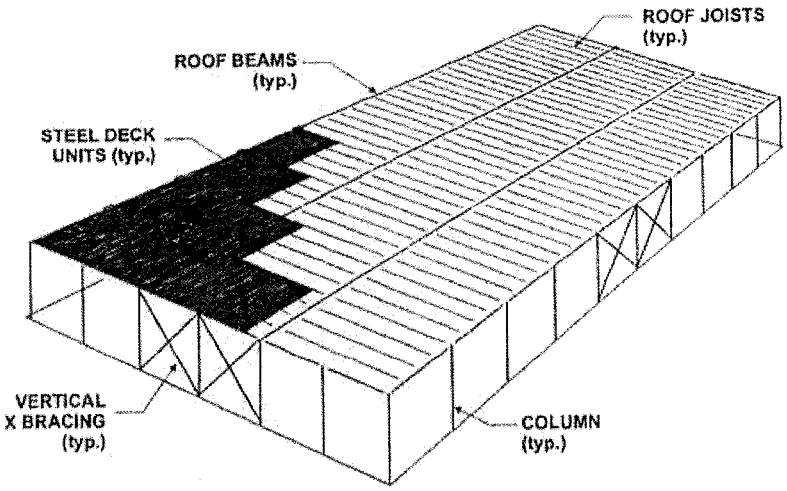

Figure 3.1 Typical single-storey steel building

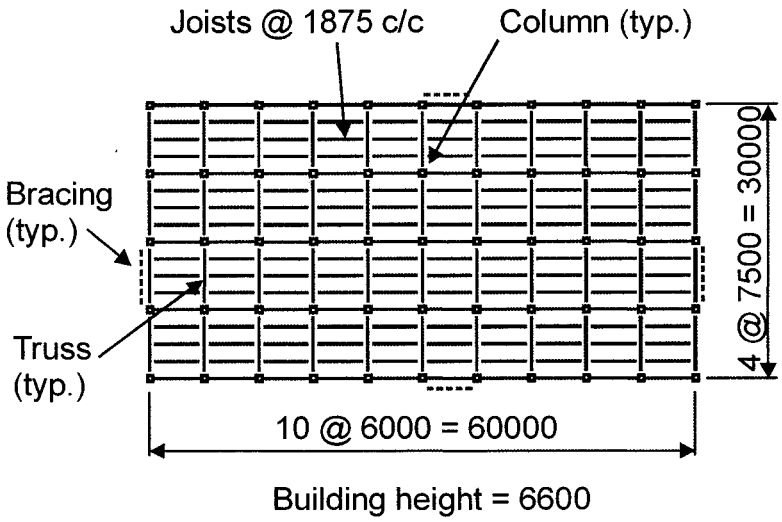

Figure 3.2 Plan view of the medium size building

The aim of the study was to evaluate the demand on metal roof deck diaphragms when they are selected as the weak link in the lateral load resisting components of the structure. The selection of the deck profile (38 mm x 914 mm) and fasteners (nailed-screwed) were based on findings by Essa *et al.* (2001). The structures were designed

according to a draft versions of NBCC 2004 (CANCEE, 2001) and CSA-S16-2001 (CSA, 2001) with the exception that the roof diaphragm was selected as the ductile energy dissipating element. Both standards were presented in the literature review. In the 2004 Code and in S16-2001 it will be required that the building be designed according to the capacity design principles. As such, an element in the lateral load carrying path is chosen to be the energy-dissipating device and all other structural members are designed so as not to yield. Hence, for the buildings included in this study the CBFs (tension-only braces), perimeter beams and other members along the lateral force path were designed to remain elastic.

Table 3.1 presents the dimensions of the buildings that were considered, including a double span diaphragm configuration. The purpose of this additional configuration was to investigate the effect of having an internal vertical brace element on the diaphragm behaviour. Essentially, this 120 m long building is composed of two medium size structures joined at their ends.

Table 3.1 Sizes of buildings studied

	Small	Medium	Large	Double
Width (m)	15	30	60	30
Length (m)	30	60	120	120
Height (m)	5.4	6.6	9.0	6.6
D_s (m)	7.5	7.5	15.0	7.5

All columns were spaced at 6.0 m along the length of the building and 7.5 m along the width. Tension-only cross braces were used on each of the four sides of the buildings: one 7.5 m braced bay per wall for the small and medium buildings and one 15.0 m braced bay per wall for the large building. In the case of the double building, one 7.5 m braced bay per exterior wall was used and the interior CBF located at the building mid-

length was designed to be twice as strong and stiff as the perimeter wall CBFs. In Table 3.1, the parameter D_s is the total braced length per wall. The buildings were loaded in their short direction so the effect of the flexible diaphragm would be most evident.

Two Canadian sites with different seismicity were considered: Victoria, B.C., situated in the Pacific Northwest and Quebec, Qc, representative of Eastern North America. These two seismic zones had to be studied since crustal earthquakes occurring in Eastern North America produce ground motions that are richer in high frequency than those anticipated along the Pacific coast. The properties of the buildings considered in this study are given in Table 3.2.

Buildings in Quebec were only designed with $R_d = 3.0$ values. Analyses were performed for buildings in Quebec with $R_d = 3.0$ where no inelastic demand, or very limited, was observed. Hence, it was felt that there was no need to study structures in Quebec for $R_d = 2.0$.

Table 3.2 Summary of building designs

Design		Screw- nail connector pattern - NBCC 2004					
		Victoria Rd=3.0			Victoria Rd=2.0		
		Small (15x30)	Medium (30x60)	Large (60x120)	Small (15x30)	Medium (30x60)	Large (60x120)
Width	(m)	15	30	60	15	30	60
Length	(m)	30	60	120	30	60	120
Height	(m)	5.4	6.6	9.0	5.4	6.6	9.0
D_s	(m)	7.5	7.5	15.0	7.5	7.5	15.0
DL	(kPa)	1.0	1.0	1.0	1.0	1.0	1.0
LL	(kPa)	1.0	1.0	1.0	1.0	1.0	1.0
W	(kN)	563	2250	9000	563	2250	9000
T (for design)	(s)	0.266	0.309	0.390	0.266	0.309	0.390
S	(g)	1.079	1.000	0.851	1.079	1.000	0.851
V	(kN)	89.8	359.3	1437.1	134.7	538.9	2155.7
P3615 B deck, sidelap fastener screws #10, deck-to-frame fastener Hilti nails ENP2-21-L-15							
S requ	(kN/m)	2.99	5.99	11.98	4.49	8.98	17.96
Type		0.76-938-3/7	0.76-625-7/7	0.91-225-7/7	0.76-938-3/7	0.76-210-4/7	0.91-125-7/7
Su	(kN/m)	5.87	10.00	20.00	7.50	15.00	30.00
G'	(kN/mm)	2.15	11.85	19.62	2.28	4.57	23.10
Braces							
Type		T/O	T/O	T/O	T/O	T/O	T/O
T_f diag	(kN)	120	440	1539	152	659	2309
Dimensions	(mm)	PL6.4x70	PL12.7x128	PL38.1x210	PL6.4x90	PL19x128	PL38.1x225
A_g diag	(mm^2)	444	1628	8000	565	2442	8552
K_B	(kN/mm)	12.7	36.7	134.5	16.1	55.1	143.8
Perimeter beams							
Section		W150x22	W150x22	W200x46	W150x22	W150x22	W200x46
A beam	(mm^2)	2850	2850	5820	2850	2850	5820
EI	(kN-mm^2)	6.413E+13	2.565E+14	2.095E+15	6.413E+13	2.565E+14	2.095E+15
Deflection							
Δ_B	(mm)	7.09	9.78	10.68	8.37	9.78	14.99
Δ_F	(mm)	0.49	3.94	15.43	0.74	5.91	23.15
Δ_S	(mm)	10.44	7.58	18.31	14.77	29.48	23.33
RdRo Δ_{TOT}	(mm)	90.3	106.7	222.6	79.8	150.9	205.3
Δ limit	(mm)	135	165	225	135	165	225
K_D	(kN/mm)	10.14	38.84	53.21	10.73	18.87	58.01
$T_{ANALYTICAL}$	(s)	0.63	0.69	0.97	0.59	0.80	0.94

Table 3.2 Summary of building designs (continued)

Design		Screw- nail connector pattern - NBCC 2004				B.Punch-welds -NBCC 95	
			Quebec Rd=3.0		Victoria Rd=3.0	Victoria R=3.0	
		Small (15x30)	Medium (30x60)	Large (60x120)	Double (30x120)	Small (15x30)	Medium (30x60)
Width	(m)	15	30	60	30	15	30
Length	(m)	30	60	120	120	30	60
Height	(m)	5.4	6.6	9.0	6.6	5.4	6.6
D_s	(m)	7.5	7.5	15.0	7.5	7.5	7.5
DL	(kPa)	1.0	1.0	1.0	1.0	1.0	1.0
LL	(kPa)	3.14	3.14	3.14	1.0	1.0	1.0
W	(kN)	803	3213	12852	4500	563	2250
T (for design)	(s)	0.266	0.309	0.390	0.309	0.177	0.217
S	(g)	0.426	0.382	0.299	1.000	4.200	4.200
V	(kN)	52.7	210.9	766.2	718.6	113.4	453.6
P3615 B deck, sidelap fastener screws #10, deck-to-frame fastener Hilti nails ENP2-21-L15 or P3615 Std deck, sidelap fastener button punch, deck-to-frame fastener welds 16 mm diameter							
S requ	(kN/m)	1.76	3.51	6.39	5.99	3.78	7.56
Type		0.76-938-3/7	0.76-938-4/7	0.76-625-7/7	0.76-625-7/7	0.76-625-4/7	0.76-175-7/7
Su	(kN/m)	5.87	5.87	10.66	10.00	6.30	12.60
G'	(kN/mm)	2.15	3.58	12.40	11.85	3.52	10.94
Braces							
Type		T/O	T/O	T/O	T/O	T/C	T/C
T_f diag	(kN)	120	258	821	440	N/A	N/A
Dimensions	(mm)	PL6.4x70	PL12.7x75	PL12.7x65	PL12.7x128	HSS127x6.4	HSS127x6.4
A_g diag	(mm^2)	444	956	3040	1628	2960	2960
K_B	(kN/mm)	12.7	21.6	51.1	36.7	168.7	133.6
Note: Victoria double span Rd=3.0 has a CBF at mid-length. This CBF has twice the area and force as end wall CBFs. Values presented here are for the end wall CBFs.							
Perimeter beams							
Section		W150x22	W150x22	W200x27	W150x22	W150x22	W150x22
A beam	(mm^2)	2850	2850	3390	2850	2850	2850
EI	(kN-mm^2)	6.413E+13	2.565E+14	1.220E+15	2.565E+14	6.413E+13	2.565E+14
Deflection							
Δ_B	(mm)	4.16	9.78	14.99	9.78	0.67	3.4
Δ_F	(mm)	0.29	2.31	14.13	3.94	0.62	4.97
Δ_S	(mm)	6.13	14.73	15.45	7.58	8.05	10.37
RdRo Δ_{TOT}	(mm)	53.0	134.4	223.3	106.7	28.0	56.2
Δ limit	(mm)	135	165	225	165	108	132
K_D	(kN/mm)	10.14	15.33	32.39	N/A	16.16	36.81
$T_{ANALYTICAL}$	(s)	0.76	1.20	1.62	N/A	0.39	0.56

For all buildings, a typical roof dead load (DL) value for single-storey buildings was selected (1.0 kPa). The snow and rain live loads (LL) considered for each site are presented in Table 3.3. The live loads were calculated with the approach of NBCC 1995 since the approach of NBCC 2004 was not published at time of investigation.

$$S = KS_S + S_r \tag{3-1}$$

In this equation, S_s and S_r represent the ground snow load and the rain load, respectively. The coefficient K is the product of four parameters.

$$K = C_b C_w C_S C_a \tag{3-2}$$

where C_b is the roof load parameter, a fixed value equal to 0.80, C_w is the wind exposure parameter and is taken equal to 1.0 for buildings that are protected from wind, C_s is the roof slope parameter taken equal to 1.0 in the case of a flat roof, and C_a is taken as 1.0 if no snow pile-up is considered. In consequence, K was equal to 0.80.

Table 3.3 Live loads for Victoria and Quebec

	Victoria	Quebec
S_s (kPa)	1.0	3.3
S_r (kPa)	0.2	0.5
LL (kPa)	1.00	3.14

3.2.2 Base shear calculation

Considering that the analyses were carried out for loading in the short direction of the buildings the fundamental period and, in addition, the design of all structural elements

corresponded to the base shear in this direction. Wind loading and accidental torsion resulting from eccentric building mass were neglected in the design.

The design base shear, V, was obtained from these equations:

$$V = S(T_a)M_vIW/(R_dR_o) \geq S(2.0)M_vIW/(R_dR_o) \qquad (3\text{-}3)$$

If $R_d \geq 1.5$

$$V \leq (2/3)\, S(0.2)IW/(R_dR_o)$$

The seismic weight of the buildings, W, consisted of the dead load per area (DL) and 25% of the live load (LL) multiplied by the roof area. The wall weights were neglected in the evaluation of W, because in general, the walls represent a negligible proportion of the total weight in single-storey steel structures.

The fundamental lateral period, T_a, is used in the base shear evaluation. For braced frames, the period is evaluated as equal to $0.05\ (h_n)^{3/4}$, where h_n is the height of the building in metres. The code allows for the period to be evaluated by other methods of mechanics, however, for braced frames, T_a shall not be taken greater than 1.5 times the value determined from the preceding formula. An evaluation of the period based on an analytical model was used in this project and is presented later in the text. It was assumed, based on past design experience, that the period evaluated from the analytical formula would give higher values than 1.5 times $0.05\ (h_n)^{3/4}$,therefore, this limiting period was used in the building design.

The 5% damped spectral response acceleration values, S_a (T), for the reference ground condition for Victoria and Quebec are presented in Table 3.4. These values were

obtained from the Uniform Hazard Spectra (UHS) and were derived for a uniform probability of exceedance of 2% in 50 years (Adams *et al.*, 1999).

Table 3.4 S_a values

T (s)	S_a 2% in 50 years (g)	
	Victoria	Quebec
0.2	1.20	0.59
0.5	0.83	0.29
1.0	0.38	0.14
2.0	0.19	0.05

The structures were assumed to be located on Site Class B (rock), in which the shear wave velocity is between 760 and 1500 m/s. Ground motions used in the analytical study were obtained from stations located on rock soil (between Soil Class A and C), hence, Class B was deemed the most appropriate site class type. The design spectra were adapted to this type of soil through the use of the appropriate site coefficient F_a and F_v values for Victoria and Quebec from NBCC 2004 (Table 3.5).

Table 3.5 Site coefficients for Site Class B (rock)

	Victoria	Quebec
F_a	1.00	0.84
F_v	0.78	0.64

The design spectral acceleration values, S(T), were determined with the following formulas. Intermediate values of T were calculated using linear interpolation.

$S(T) = F_a S_a(0.2)$ for $T \leq 0.2s$ (3-4)

$= F_v S_a(0.5)$ or $F_a S_a(0.2)$ whichever is smaller for $T=0.5$

$= F_v S_a(1.0)$ for $T= 1.0s$

$= F_v S_a(2.0)$ for $T= 2.0s$

$= F_v S_a(2.0)/2$ for $T \geq 4.0s$

Table 3.6 presents the S(T) values adjusted with site coefficients at T= 0.2, 0.5, 1.0, 2.0 and 4.0 seconds.

Table 3.6 Design spectral acceleration values, S(T)

T (s)	S(T) (g)	
	Victoria	Quebec
0.2	1.20	0.49
0.5	0.65	0.19
1.0	0.30	0.09
2.0	0.15	0.03
4.0	0.07	0.02

The factor to account for higher mode effect on base shear, M_v, was set equal to 1.0 because this characteristic normally only affects multi-storey buildings and the importance factor of the structure, I, was assumed equal to 1.0.

The deck diaphragm was chosen as the energy-dissipating system. In consequence, R_o and R_d values needed to be representative of the nonlinear behaviour of the roof deck.

No R_d values were available at the time of design as no R_d values are specified in NBCC 2004 because that code prescribes a strong diaphragm design. Therefore, arbitrary values were to be selected which could be deemed appropriate for ductile steel roof diaphragms. The range of R_d in NBCC 2004 is from 1.0 for very brittle systems to 5.0

for very ductile systems. Based on tests by Essa *et al.*, it was deemed that the nail-screw diaphragm design would exhibit a moderate ductility and it was decided to examine the behaviour of structures designed with R_d = 2.0 and 3.0. The appropriateness of these numbers would need to be validated based on the amplitude of the inelastic demand obtained from the analysis and the experimental program.

A number of parameters are considered in the evaluation of the overstrength related force modification factor, R_o, as shown in the following equation.

$$R_o = R_\phi \; R_{yield} \; R_{sh} \; R_{size} \; R_{mech} \qquad (3\text{-}5)$$

R_ϕ depends on the resistance factor used in the design of the energy-dissipating element. With regard to resistance factors for diaphragm design under earthquake loads, FEMA 302 (BSSC, 1997) and AISI (1997) prescribe a ϕ value equal to 0.60 for mechanically connected roof systems, hence,

$$R_\phi = 1 / \phi = 1/0.6 = 1.67 \qquad (3\text{-}6)$$

The nominal capacity will be considered in the analytical model of the structures and, hence, R_{yield} = 1.0 was to be specified for consistency. Tests by Essa *et al.* showed that steel deck roof diaphragms do not exhibit any strain hardening after the peak load is reached. Thus, R_{sh} = 1.0 was adopted. The overstrength due to discrete member sizes, R_{size}, was assumed equal to 1.0 because the diaphragm strength was chosen to closely match the required strength. The parameter R_{mech} was also set to 1.0 as the lateral load resisting system of the buildings studied is not redundant and that no increase in lateral resistance is expected after the ultimate resistance of the roof diaphragm is reached.

The lateral earthquake design force at the base of the structure was calculated based on these design variables.

The base shear value, V, found from these equations should not be mistaken as the maximum force that the system could sustain under the design earthquake. Since capacity based design is required, and the diaphragm has been chosen as the weak element in the lateral load path, the roof diaphragm will sustain a force equal to its ultimate strength or the elastic base shear if lower.

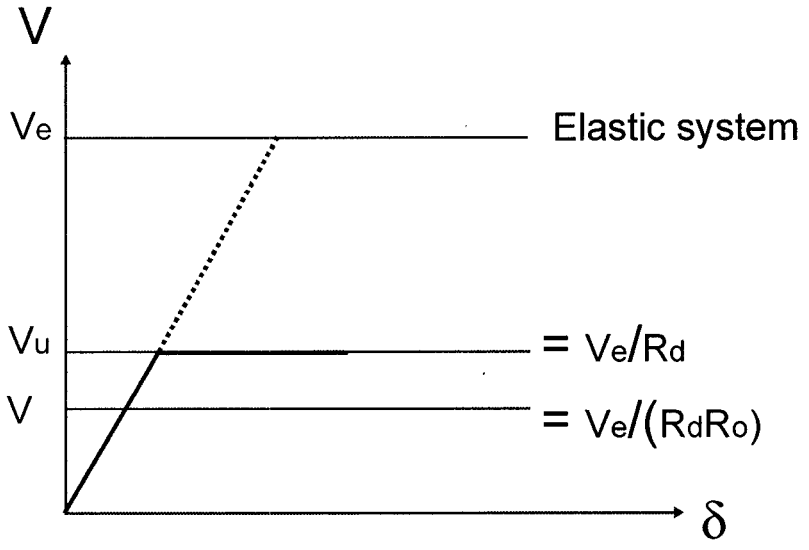

Figure 3.3 Force levels considered in design

The design force, V, was obtained from the approach described previously. The factored resistance of the diaphragm, ϕV_u, was matched to the design force knowing that the overstrength factors will come into play. Hence, the system ended up with an expected shear strength of the deck V_u. The elastic force, V_e, is the load that would be considered if the system was to remain elastic under the design level seismic event (Figure 3.3).

$$V_u = \frac{V_e}{R_d} \tag{3-7}$$

$$V = \frac{V_e}{R_d \cdot R_o} \tag{3-8}$$

The design V values are presented in Table 3.2.

3.2.3 Deck

Canam steel profile deck sheets (P3615) conforming to ASTM A653 SS Grade 230 steel (ASTM, 2002) were considered in the evaluation of the diaphragm properties. The deck sheets were 38 mm deep, 914 mm wide by 7500 mm long (Figure 3.4). The intermediate supports were located at 1875 mm c/c, thus the panels consisted of four spans. Deck-to-frame connections were made with Hilti nails (ENP2-21-L15), and the sidelap connections were designed having #10 screws.

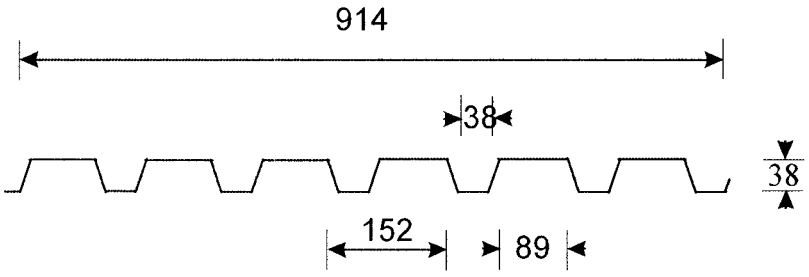

B-deck (P-3615 B Canam)

Figure 3.4 Deck panel dimensions considered in design

The SDI procedure was used to assess the ultimate strength, S_u, and stiffness, G', of the roof diaphragm. Nominal values for the steel deck material properties were used in the SDI predictions.

As explained in the previous section, it was intended to find a design with a factored strength, ϕS_u, that matched the design force considered, Srequ. Due to the capacity design approach, if an overstrength was present in the diaphragm, all the other elements would have to be increased in size, thus increasing the building cost. In two cases (Small building R_d= 3.0 for Victoria and Quebec), the ultimate nominal shear strength was greater than the target value in design (Srequ * R_ϕ). For all other cases, the factored shear strength of the deck was equal to the effect of the design base shear (Srequ).

The same design was used over the entire roof area, i.e. the connector spacing, sheet steel thickness, etc, were not varied. For each building design, different connector spacings were considered, as listed in Table 3.2. Nomenclature was used to describe the deck assembly, for example the term 0.76-938-3/7 refers to a 0.76 mm nominal sheet steel thickness, 938 mm is the sidelap connector spacing and 3/7 indicates that the deck-to-frame connectors are installed in 3 of 7 corrugations for each panel. In some cases, the sidelap connector spacings were not realistic but gave designs that matched the strength required. For example, in most situations the sidelap connections are placed at a maximum of 305 mm hence the 938 mm spacing is unusually large.

For the screw-nail designs, based on the SDI categories according to G', the diaphragms were considered flexible for small R_d=3.0 and R_d=2.0 buildings in Victoria and small R_d=3.0 building in Quebec. For medium R_d=3.0 and R_d=2.0 and double R_d=3.0 buildings in Victoria, medium and large R_d=3.0 in Quebec, the diaphragms were semi-flexible. For large R_d=3.0 and R_d=2.0 buildings in Victoria, the diaphragms were

considered semi-rigid. Besides, for button punch-weld designs, the diaphragms were semi-flexible.

3.2.4 Bracing

Since a weak diaphragm/strong brace design was adopted, the braces were to remain elastic under the design earthquake and the S16-2001 detailing requirements for the braces (minimum brace slenderness, etc) need not be applied. Therefore, a tension-only X bracing system was selected as it is the most economical for low-rise applications. Flat bars from steel conforming to CSA G40.21- 300W grade material (CSA, 1992) were used. The braces were capacity protected by sizing them for lateral loads corresponding to 1.10 times the ultimate capacity of the roof diaphragms, S_u. The 1.1 factor is only there to protect against variability in strength that could be exhibited by the diaphragm. The cross-section of the brace was chosen that its factored tension capacity, T_r, equal exactly the factored tension force, T_f, where $T_r = \phi A_g F_y$ and $T_f = 1.1 S_u D / \cos\theta$.

ϕ : resistance factor for CBFs = 0.90
A_g: total gross area of one flat bar (mm^2)
F_y: flat bar specified minimum yield stress (MPa) = 0.300 kN/ mm^2
θ: inclination of the brace with respect to horizontal
S_u: deck ultimate nominal shear strength (kN/m)
D: width of the building (m)

The calculated values of S_u, T_f and A_g are given in Table 3.1. The total lateral stiffness of the vertical bracings is also given in the table. For all structures, K_B is equal to $2 E A_g \cos^3\theta / D_S$ except for the double building for which $K_B = 4 E A_g \cos^3\theta / D_S$.

3.2.5 Perimeter beams

Flexural resistance of the roof diaphragm when considering lateral loads is provided by the perimeter framing members. It is assumed in design that the axial forces in the perimeter members give rise to a resisting moment couple.

The perimeter beams at the roof level also had to be designed according to the capacity design requirements. A schematic plan view of a typical building illustrates the nature of the forces that must be carried by the perimeter beams (Figure 3.5). The buildings were designed with the common assumption of a uniform loading giving a linear variation of the shear force.

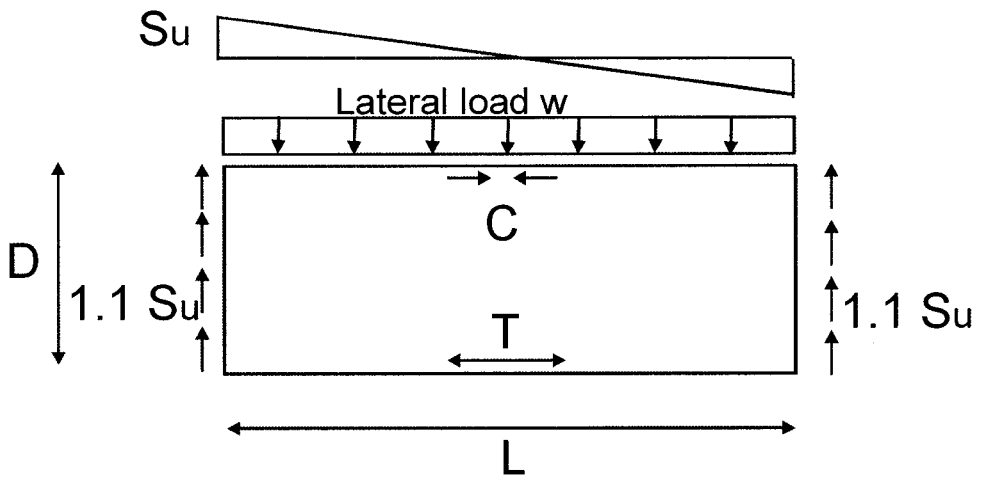

Figure 3.5 Forces to consider on perimeter beams

The building should sustain the moment, M, obtained when the ultimate nominal shear strength of the deck, S_u, is reached at the end walls times 1.1, a factor that accounts for the inherent variability in resistance. The axial forces, C and T, were found by dividing the moment M by the lever arm, D. The uniform applied load is represented by w.

$$w = \frac{1.1 \cdot Su \cdot D}{L/2} \tag{3-9}$$

$$M = \frac{w.L^2}{8} \tag{3-10}$$

$$C = T = M / D \tag{3-11}$$

The perimeter beams had to sustain gravity and axial loads according to the NBCC 2004 (NRCC, 2001) load combinations (D+0.5L+E). The steel material conformed to G40.21-300W (CSA, 1992).

3.2.6 Lateral deflection criteria and period check

In design, the lateral deflection of the building must be determined to be within the code allowed value. The formula and method used for this calculation were explained in the literature review (Sections 2.1.3 and 2.1.5). A uniform load was assumed to exist over the length of the building.

The flexural deflection of the roof diaphragm, Δ_F, as well as its shear deflection, Δ_S, were obtained from the following equations:

$$\Delta_F = \frac{5wL^4}{384EI} \tag{3-12}$$

$$\Delta_S = \frac{wL^2}{8DG'} \tag{3-13}$$

G' is the shear stiffness of the metal roof deck obtained from the SDI method.

The total lateral deflection of the structure is made up of the sum of the diaphragm shear and flexural displacements as well as the lateral deflection of the CBFs, Δ_B, which are all multiplied by R_dR_o.

This total lateral deflection was compared to the lateral deflection criteria, Δlimit, equal to $0.025h_s$.

If the design was not sufficient with respect to the deflection criteria, the element sizes were increased, in the following order. The brace cross-sectional area was increased first, since it represented a small increase in the cost for a significant gain in the braced bent stiffness. Second, the perimeter beam size was increased. Third, the deck stiffness was improved with a new design. However, any modification to the deck type and connection pattern produced an increase in the diaphragm strength, and hence, due to the capacity design requirements, all other elements in the lateral load carrying path would require rechecking and possible resizing to match the elevated strength requirements.

In the buildings designed for this project, two buildings had to be stiffened to respect the lateral deflection requirements. For the large $R_d = 3.0$ building in Victoria, the gross area of the brace section was increased from 2850 mm^2 to 4000 mm^2. The period decreased from 1.03 sec to 0.97 sec after the increase in stiffness, which is not significant. For the large $R_d = 3.0$ building in Quebec, a W200x27 perimeter beam section was used to respect the lateral deflection. A smaller section may have been used if the lateral deflection did not govern the design. However, this did not have a significant effect on the period. With the W200x27 ($A_g = 3390$ mm^2) section, the period was equal to 1.62 sec whereas, if a W150x22 section ($A_g = 2850$ mm^2) was used (however the section

could not respect strength requirements), the analytical period would have been equal to 1.66 sec.

The period of the building was calculated with the analytical formula from Medhekar (1997), which is discussed in the literature review.

$$T = 2\pi\sqrt{\frac{(K_B + K_D)}{K_B K_D}\frac{W}{g}} \tag{3-14}$$

and

$$K_D = \frac{\pi^2}{\frac{L^3}{\pi^2 EI} + \frac{L}{G'D}} \tag{3-15}$$

where

K_b = total lateral stiffness of the vertical bracing
K_d = total lateral stiffness of the diaphragm
W = seismic weight of the building
g = acceleration due to gravity

The period based on the analytical formula was evaluated and compared to the period used in the design of the building. As noted previously, the period used in the design was calculated with the code formula, $T_a = 0.05\ (h_n)^{3/4}$ and then multiplied by 1.5. The calculated period for all structures was much longer than the design period. This was in line with the findings of previous studies (Tremblay and Stiemer (1996), Tremblay *et al.* (2002), Medhekar (1997), etc.). The difference was generally more important when lower seismic loads were used. The period values from the analytical formula confirmed

that the periods used in the design of the different buildings were conservative (Table 3.20).

Fleischman and Farrow (2001) developed analytical models that capture the diaphragm flexibility of structures with long-floor spans and perimeter lateral-systems. They have suggested a parameter α that represents the ratio of the lateral stiffness of the perimeter lateral system to the lateral stiffness of the diaphragm. Table 3.7 presents the α values for the buildings with screw-nail designs of this study.

Table 3.7 α values for buildings with screw-nail designs (NBCC 2004)

Victoria $R_d = 3.0$			Victoria $R_d = 2.0$			Quebec $R_d = 3.0$		
Small	Medium	Large	Small	Medium	Large	Small	Medium	Large
1.25	0.94	2.53	1.50	2.92	2.48	1.25	1.41	1.58

Except in one case, all α values are greater than 1.0 which means that the lateral stiffness of the diaphragm is smaller than the lateral stiffness of the perimeter lateral system.

3.3 ANALYTICAL MODEL

3.3.1 General

Nonlinear time step analyses were performed using the Ruaumoko program 2D version March 15th 2000 developed by Carr (2000). The model was made of different elements for deck, perimeter beams, interior members, the lateral inertia of joists and beams, braces and columns. A view of the model that was used can be seen in Figure 3.6.

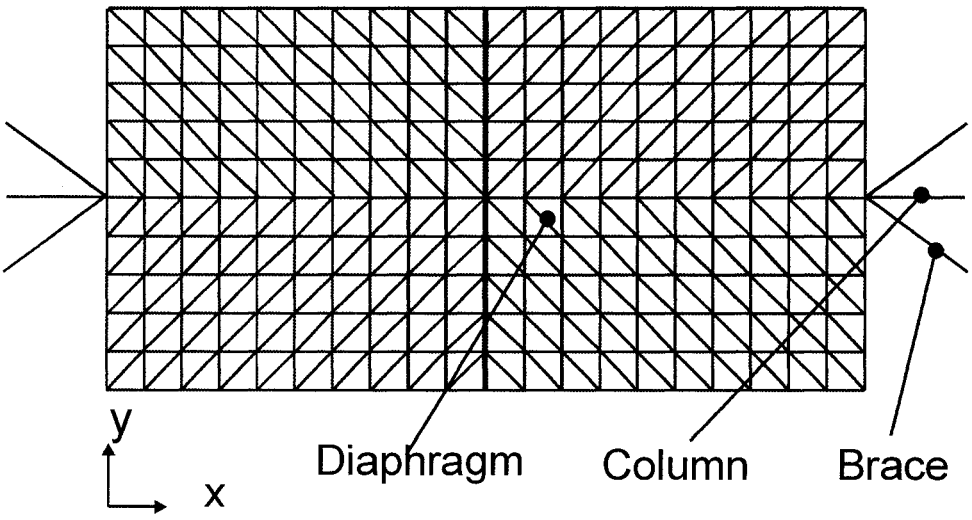

Figure 3.6 Plan view of the building model

A 2D model simulating 3D conditions was used. Bérair (1999) and Nedisan (2002) used a similar model except that they specified elastic membrane elements for the diaphragm. A Newmark constant average acceleration scheme with a time step of 0.001 seconds was incorporated into the model, and P-delta effects were neglected. Rayleigh damping equal to 5% of critical damping in the first two modes was assumed based on the diaphragm test results from Essa *et al.* (2001).

Only the roof weight was considered in the mass matrix of the model. The weight was equal to 100% of the dead load and 25% of the live load.

The deck elements were made of springs with hysteretic capacities. Perimeter beams used linear spring elements as well as the columns. The braces were made of nonlinear spring elements modelling the buckling in compression and yielding in tension. The lateral inertia of joists and beams was modelled by frame type elements. This is discussed in the following section. Table 3.8 presents a summary of the model properties used in Ruaumoko.

Table 3.8 Summary of model properties

Parameters used in Ruaumoko

		Screw- nail connector pattern - NBCC 2004					
		Victoria Rd=3.0			Victoria Rd=2.0		
		Small (15x30)	Medium (30x60)	Large (60x120)	Small (15x30)	Medium (30x60)	Large (60x120)
Deck members							
Spring member - Wayne-Stewart hysteresis							
Length	(m)	2.121	4.243	8.485	2.121	4.243	8.485
FU	(kN)	12.5	42.4	169.7	15.9	63.6	254.6
FX	(kN)	9.0	30.4	121.7	11.4	45.6	182.6
FI	(kN)	2.6	8.8	35.3	3.3	13.2	53.0
KX	(kN/m)	4300	23700	39240	4560	9140	46200
RF		0.40	0.40	0.40	0.40	0.40	0.40
PTRI		0.001	0.001	0.001	0.001	0.001	0.001
PUNL		1.30	1.30	1.30	1.30	1.30	1.30
GAP+	(m)	0	0	0	0	0	0
GAP-	(m)	0	0	0	0	0	0
BETA		1.12	1.12	1.12	1.12	1.12	1.12
ALPHA		0.55	0.55	0.55	0.55	0.55	0.55
Perimeter beams							
Spring member - Elastic							
Length	(m)	1.5	3.0	6.0	1.5	3.0	6.0
KX	(kN/m)	380000	190000	194000	380000	190000	194000
Interior members (Horizontal and vertical)							
Spring member - Elastic							
Length	(m)	1.5	3.0	6.0	1.5	3.0	6.0
KX	(kN/m)	43000	235000	100000	45500	90000	470000
Joist lateral inertia members							
Frame member - Elastic							
Length	(m)	1.5	3.0	N/A	1.5	3.0	N/A
E	(kN/m2)	2.00E+08	2.00E+08	N/A	2.00E+08	2.00E+08	N/A
G	(kN/m2)	7.70E+07	7.70E+07	N/A	7.70E+07	7.70E+07	N/A
A	(m2)	1.383E-02	1.383E-02	N/A	1.383E-02	1.383E-02	N/A
AS	(m2)	0	0	N/A	0	0	N/A
I	(m4)	1.321E-05	1.945E-05	N/A	1.321E-05	1.945E-05	N/A
Braces							
Spring member - Bi-linear with slackness hysteresis							
Length	(m)	9.242	9.990	17.493	9.242	9.990	17.493
KX	(kN/m)	9609	32593	91466	12222	48889	97778
RF		0.001	0.001	0.001	0.001	0.001	0.001
FX+	(kN)	133.2	488.4	2400.0	169.4	732.6	2565.6
FX-	(kN)	-0.001	-0.001	-0.001	-0.001	-0.001	-0.001
Columns							
Spring member - Elastic							
Length	(m)	5.4	6.6	9.0	5.4	6.6	9.0
KX	(kN/m)	1000000	1000000	1000000	1000000	1000000	1000000

Table 3.8 Summary of model properties (continued)

Parameters used in Ruaumoko

		Screw- nail connector pattern - NBCC 2004				B.Punch-welds -NBCC 95	
		Quebec Rd=3.0			Victoria Rd=3.0	Victoria R=3.0	
		Small (15x30)	Medium (30x60)	Large (60x120)	Double (30x120)	Small (15x30)	Medium (30x60)
Deck members							
Spring member - Wayne-Stewart hysteresis							
Length	(m)	2.121	4.243	8.485	4.243	2.121	4.243
FU	(kN)	12.5	24.9	90.5	42.4	13.4	54.3
FX	(kN)	9.0	17.9	64.9	30.4	7.1	28.9
FI	(kN)	2.6	5.2	18.8	8.8	0.9	3.6
KX	(kN/m)	4300	7160	24800	23700	7040	21880
RF		0.40	0.40	0.40	0.40	0.90	0.90
PTRI		0.001	0.001	0.001	0.001	0.001	0.001
PUNL		1.30	1.30	1.30	1.30	1.10	1.10
GAP+	(m)	0	0	0	0	0	0
GAP-	(m)	0	0	0	0	0	0
BETA		1.12	1.12	1.12	1.12	1.30	1.30
ALPHA		0.55	0.55	0.55	0.55	0.40	0.40
Perimeter beams							
Spring member - Elastic							
Length	(m)	1.5	3.0	6.0	3.0	1.5	3.0
KX	(kN/m)	380000	190000	113000	190000	380000	190000
Interior members (Horizontal and vertical)							
Spring member - Elastic							
Length	(m)	1.5	3.0	6.0	3.0	1.5	3.0
KX	(kN/m)	43000	72000	80000	235000	69500	218000
Joist lateral inertia members							
Frame member - Elastic							
Length	(m)	1.5	3.0	N/A	3.0	1.5	3.0
E	(kN/m2)	2.00E+08	2.00E+08	N/A	2.00E+08	2.00E+08	2.00E+08
G	(kN/m2)	7.70E+07	7.70E+07	N/A	7.70E+07	7.70E+07	7.70E+07
A	(m2)	1.383E-02	1.383E-02	N/A	1.383E-02	1.383E-02	1.383E-02
AS	(m2)	0	0	N/A	0	0	0
I	(m4)	1.321E-05	1.945E-05	N/A	1.945E-05	1.321E-05	1.945E-05
Braces							
Spring member		**Bi-linear with slackness hysteresis**				**Elastic linear**	
Length	(m)	9.242	9.990	17.493	9.990	9.242	9.990
KX	(kN/m)	9609	19138	34757	32593	64057	59256
RF		0.001	0.001	0.001	0.001	N/A	N/A
FX+	(kN)	133.2	286.8	912.0	488.4	N/A	N/A
FX-	(kN)	-0.001	-0.001	-0.001	-0.001	N/A	N/A
Note: Victoria double span Rd=3.0 has a CBF at mid-length. This CBF has twice the area and force as end wall CBFs. Values presented here are for end wall CBFs.							
Columns							
Spring member - Elastic							
Length	(m)	5.4	6.6	9.0	6.6	5.4	6.6
KX	(kN/m)	1000000	1000000	1000000	1000000	1000000	1000000

3.3.2 Convention on the distortion parameters

The nonlinear behaviour of the deck diaphragm under cyclic loading was to be reproduced in the model. The hysteretic response from test No. 7 by Essa *et al.* (2001) was used as a reference to define the main characteristics of the diaphragm studied. This hysteresis is presented in Figure 3.7. The test was performed on a 0.76 mm thick 38 mm deep deck profile with nail-screws, i.e., a diaphragm system similar to that assumed for the building studied herein.

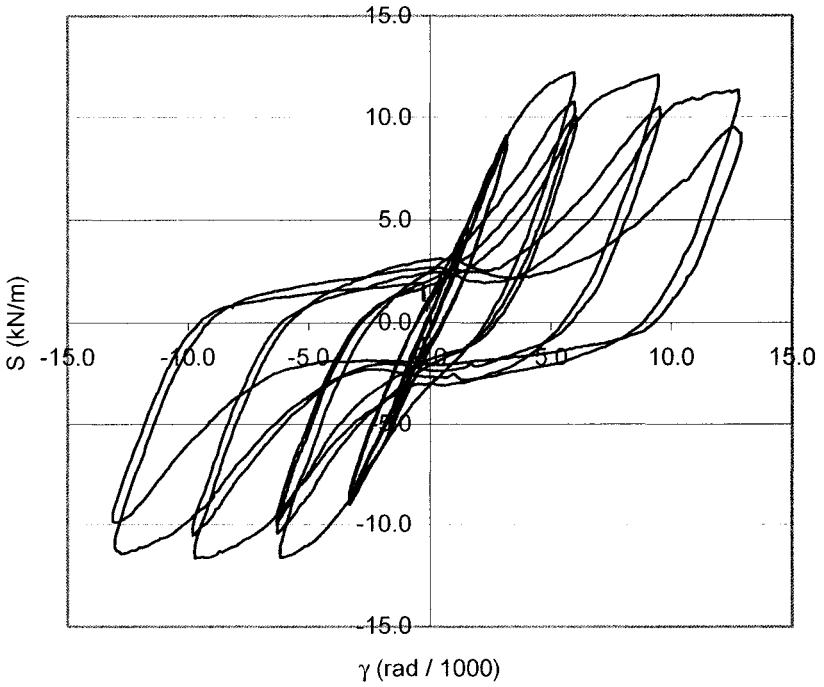

Figure 3.7 Shear-distortion curve from test 7 (Essa *et al.*, 2001)

In the linear range of shear deformations, the shear strain of a diaphragm, γ, and the applied shear force per unit length, S, are related: $\gamma = S/ G'$, where G' is the diaphragm shear stiffness. This shear stiffness is influenced by the deck profile and fastener type

and pattern as presented in the literature review (Section 2.4). As shown in Figure 3.7, the measured response of a diaphragm is more complex and simplifications had to be made to represent this behaviour, and hence a simplified load-deformation response was used for modelling purposes. Figure 3.8 shows the simplified load-deformation response and parameters that were adopted to characterise the response of diaphragms under monotonic loading up to failure. The same basic parameters were then used for modelling the response under cyclic loading in Section 3.3.3 and to develop the loading protocols.

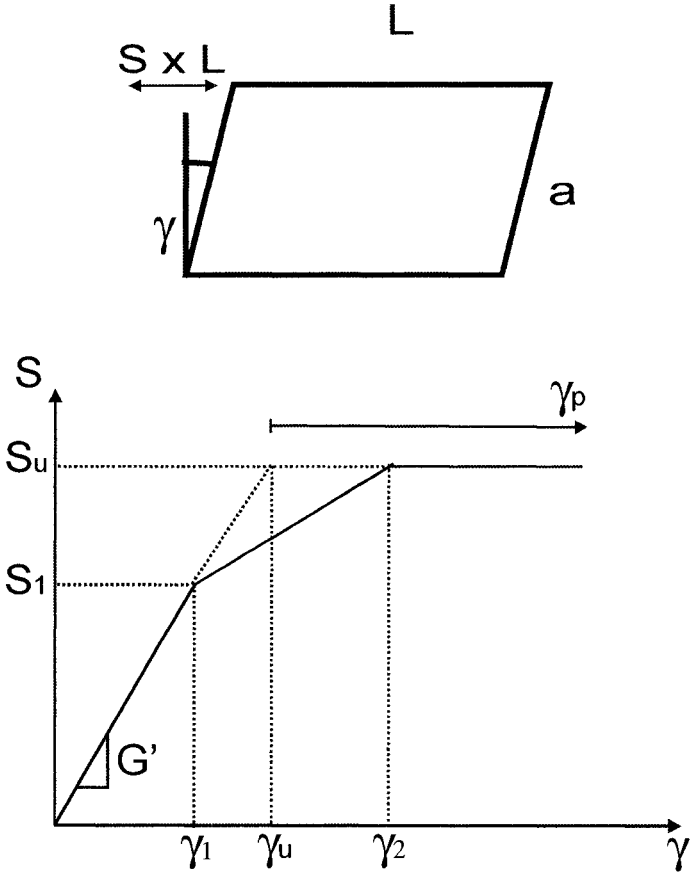

Figure 3.8 Distortion parameters

γ_u is the shear deformation obtained from S_u/G': S_u being the ultimate shear force and G' the shear stiffness. In a test situation, when a deflection of γ_u is reached the diaphragm typically has not reached its maximum shear capacity. In most cases additional shear deflection, up to the point γ_2, was necessary to allow the shear force to attain its maximum.

It was found from test curves (Essa *et al.*, 2001) that the stiffness of the diaphragm degrades at a certain distortion level γ_1, which is smaller than γ_u. The related shear force, S_1, can be observed in Figure 3.8. At this point, the onset of inelastic deformation in the fasteners results in the decrease in stiffness, as reported by Essa *et al.*.

In the elastic range, the deck distortion is due to three components: warping, sheet distortion and the flexibility of the deck-to-frame and sidelap fasteners. In the inelastic range, the load reaches a maximum value, and the plastic deformation of the diaphragm is due mainly to the deformations in the fasteners.

The distortion in the inelastic range, γ_p, starting from γ_u, is an indicator of the damage in the deck. Essa *et al.* (2001) found that it is an absolute value which depends on the deck connectors used, and hence there is no need to rely on a normalised value.

Inelastic distortion starts at a shear deflection of γ_1, after which a progressive decrease in the system rigidity and a reliance on the inelastic performance of some fasteners takes place. The gradual softening of the system is caused by the fasteners being loaded at different shear levels due to their location and relative rigidity. At γ_2, the system reaches a purely inelastic level and can no longer carry increasing shear loads. Due to these considerations, γ_u was used as a compromise in the development of loading protocols between γ_1 and γ_2.

3.3.3 Deck model

Truss elements were used to model the load-deformation response of the roof diaphragms. Figure 3.9 shows the analogy between a diaphragm and the truss model used for the roof.

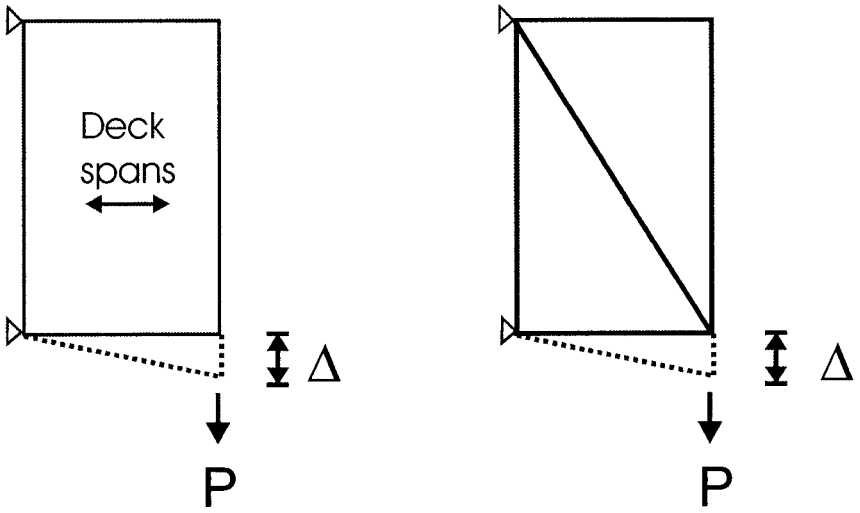

Figure 3.9 Diaphragm and truss

In the Ruaumoko model, spring members (Figure 3.10) were used for the roof deck instead of plate elements. A quadrilateral plate element was available in the program, however, it possessed at the time of writing only linear elastic capabilities. A more advanced element that could account for the nonlinear aspects of the diaphragm behaviour was needed. The width of the square deck units varied with the building sizes: 1.5 x 1.5 m for the small building, 3.0 x 3.0 m for the medium and the double, and 6.0 x 6.0 m for the large.

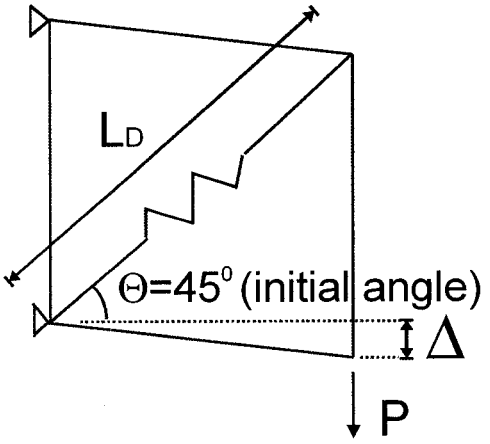

Figure 3.10 Deck spring unit model

The shear deformation behaviour of a deck panel could be replicated through the axial deformation of the diagonal member in the deck spring element. The diagonal axial stiffness, KX, was chosen to match the stiffness G' of the deck, assuming that the perimeter springs were infinitely rigid. Relationships between the following properties exist for the spring element; k_{LAT} is the lateral stiffness of the truss system in the direction of P, E is the Young's modulus of the bar, A is the area of the bar and KX is the axial stiffness of the diagonal.

$$k_{LAT} = \frac{EA}{L_D}\cos^2 45^0 \tag{3-16}$$

$$k_{LAT} = \frac{P}{\Delta} \tag{3-17}$$

$$G' = \frac{P}{\Delta} \tag{3-18}$$

The matching area of the diagonal, A, is given by:

$$A = \frac{G' L_d}{E \cos^2 45^0} \tag{3-19}$$

$$KX = \frac{EA}{L_d} \tag{3-20}$$

$$KX = 2.0 \cdot G' \tag{3-21}$$

Hence, the axial stiffness of the diagonal member is 2 times G'.

As shown in Figure 3.6, the diagonal braces were oriented in such a way that they were symmetrically located in both the x and y directions.

Essa *et al.* (2001) were able to show that deck panels under cyclic in-plane shear loading develop an hysteretic load versus displacement behaviour. The hysteresis from test 7 (Figure 3.7) was utilised to develop the deck spring element used in the analyses carried out for this investigation.

Among the hysteresis models that have been made available in Ruaumoko, the Wayne-Stewart hysteresis (Stewart, 1987) model was able to best represent the deck panel cyclic behaviour (Figure 3.11). This was due to the fact that pinching was present in the model. This general rule was initially developed to represent timber framed structural walls sheathed in plywood nailed to the framework. The model allows for initial slackness as well as subsequent degradation of the stiffness.

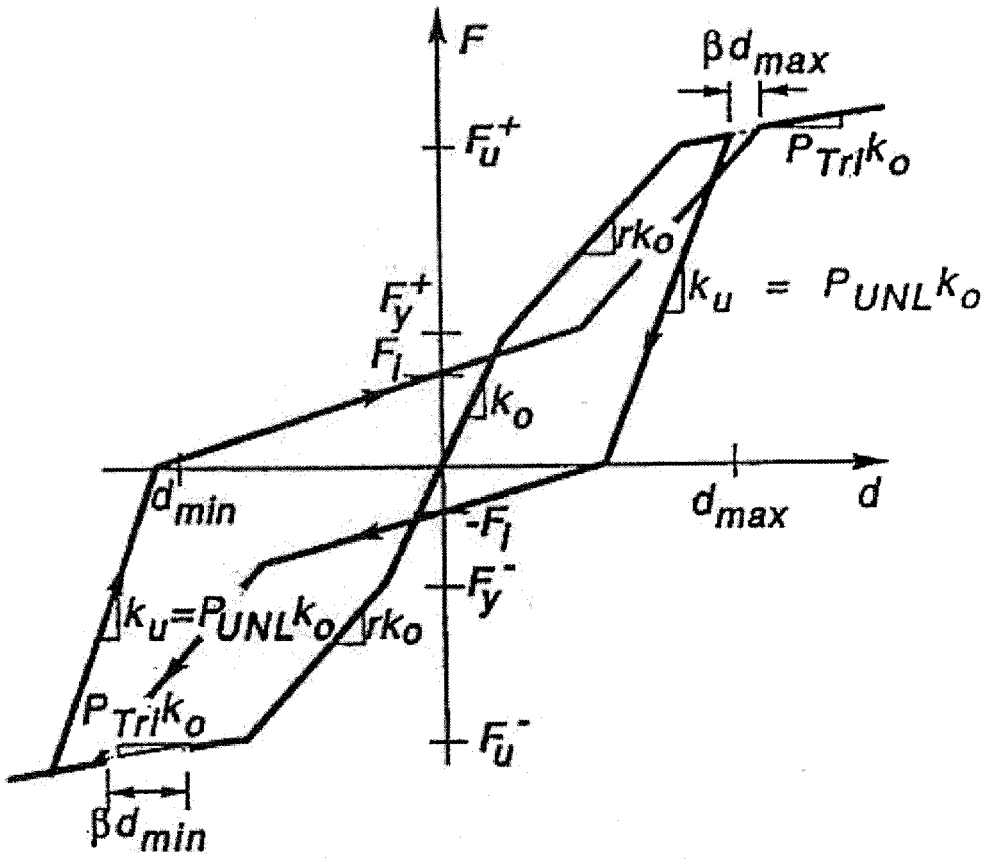

Figure 3.11 Wayne-Stewart hysteresis model (Carr, 2000)

The following parameters were used for the spring member and the Wayne-Stewart hysteresis.

Table 3.9 Spring member parameters

ITYPE =1	No interaction between X, Y or theta Z components
IHYST = 9	Wayne-Stewart hysteresis rule
ILOS = 0	No strength degradation
IDAMG =0	No damage indices computed
KX	Spring stiffness in the local x-direction
KY	Spring stiffness in the local y –direction (not used)
GJ	Rotational stiffness of the member section (not used)
WGT	Weight of the member (not used)
RF	Bi-linear factor (r in Figure 3.11)
FX+	Positive spring yield force in the x-direction
FX-	Negative spring yield force in the x-direction

Table 3.10 Wayne Stewart hysteresis parameters

FU	Ultimate force
FI	Intercept force
PTRI =0.001	Tri-linear factor beyond ultimate force
PUNL	Unloading stiffness factor
GAP+ = 0.0	Initial slackness, positive axis
GAP- =0.0	Initial slackness, negative axis
BETA	Beta or softening factor
ALPHA	Reloading or pinch power factor
LOOP = 0	Loop as defined

The FU values were found from the SDI predictions for ultimate shear strength, S_u. The initial load versus displacement curve from test 7 (Essa *et al.*, 2001) was studied and the following parameters were obtained: FX, the equivalent of S1, was determined to be equal to 72% of FU, which is related to S_u. FI, the intercept force was set equal to 20%

of FU. The ratio γ_2/γ_1 was taken equal to 1.42. RF, the ratio of the second to first slope stiffness, was determined to be equal to 0.40. PUNL was given a value of 1.30.

The BETA and ALPHA factors are very useful in fine tuning the model hysteresis in order that it follows the test results. BETA gives the softening of the stiffness with each cycle. ALPHA is used to obtain the point at which the deck element attains a higher stiffness in the reloading portion of the load versus deflection hysteresis.

A parametric study was performed to find appropriate ALPHA and BETA factors in an attempt to match the hysteresis from test 7 (Essa *et al.*, 2001). Factors equal to 1.12 for BETA and 0.55 for ALPHA were selected from the results of this study. Based on these values a close approximation of the test load versus deflection behaviour could be provided, as shown in Figure 3.12.

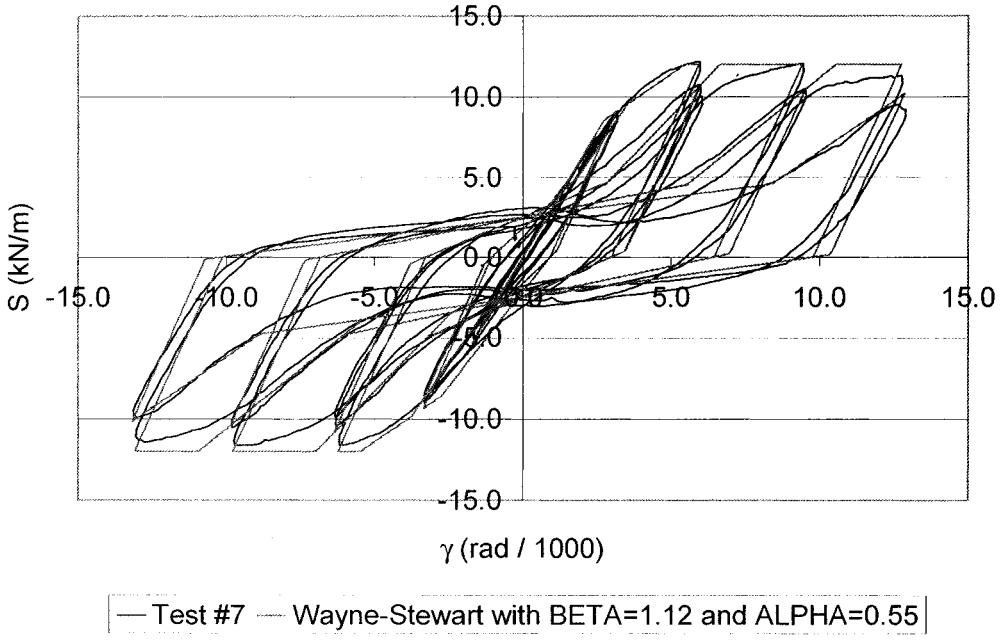

Figure 3.12 Wayne-Stewart hysteresis compared to test 7 (Essa *et al.*, 2001)

3.3.4 Perimeter beam members

Along the perimeter of the building, spring members have been used to represent the spandrel beam members that deform axially when the structure is loaded laterally. Their axial stiffness, KX, was chosen as equal to EA_{beam} divided by the beam length.

3.3.5 Interior members (horizontal and vertical)

As mentioned, horizontal and vertical spring elements were used in conjunction with the diagonal spring element to produce the truss model (see Figure 3.10). It was initially planned to specify infinite stiffness for both horizontal and vertical spring elements, so that the truss model of the roof diaphragm model deforms in shear with the desired shear stiffness. In the vertical direction (Y), it was then decided to constraint the vertical DOF to the node at the same X location at the centreline of the building so that the stiffness of the vertical spring became irrelevant and these elements were given the same stiffness as the horizontal members. In the horizontal direction (X), specifying infinite stiffness for the spring elements resulted in a diaphragm that had no flexural deformation mode, which was incorrect. Specifying a very small stiffness and relying only on the perimeter beams to provide the flexural stiffness to the diaphragm resulted in an unstable model.

A compromise regarding the stiffness of the horizontal members had to be adopted. The horizontal members needed to be stiff enough to represent the G' of the deck elements, with an error to be evaluated, but flexible enough to allow deformation due to flexure. In what follows, the source of the error is presented.

The lateral deformation of the deck unit can be related to that found for tension-only CBFs. In the case where an infinitely stiff column is used, the lateral deformation of the frame bent is due to the axial elongation of the diagonal member. However, the axial

shortening of a non-infinitely stiff column under lateral loads will increase the lateral deformation of the system. In the deck spring unit, the column can be related to the horizontal member and the brace to the diagonal spring member.

The axial stiffness of the horizontal members was adjusted to match an error of 5% in the evaluation of the lateral deformation compared to an infinitely stiff member hypothesis. It has to be mentioned that the error was calculated based on one element only.

$$Error = \frac{G'_{THEO} - G'_{MODEL}}{G'_{THEO}} \tag{3-22}$$

where:

G'_{MODEL}: G' with the non-infinite stiffness for horizontal members
G'_{THEO}: G' with infinitely stiff horizontal members

This procedure was used successfully for the two smaller buildings: small and medium. The period obtained from the Ruaumoko model and the analytical formula from Medhekar were similar as the error in the period was kept below 5%. However, in the large buildings (60 m x 120 m), it was found that by choosing an axial stiffness in the fashion noted above, the stiffness of the building and its period were modified as the error in the period increased above 5%. In these cases, the axial stiffness of the horizontal members was chosen to obtain a period from the building model that matched the analytical period from Medhekar's formula.

3.3.6 Joist and beam lateral inertia

It was expected that the beams and joists supporting the steel deck in a real building would carry some of the diaphragm shear force if the shear deformations in the diaphragm was to vary over the length of the joists or beams. This is because the deck panels are continuously attached to the joists and beams and non uniform shear deformations in the deck would produce weak axis bending of the beams and joists. It was decided to include this behaviour in the roof diaphragm model as it could influence the redistribution of the inelastic shear deformations in the diaphragm under cyclic loading.

It was assumed that the joists were spaced at 1875 mm. From the building width, the number of steel joists was found. It was assumed that the joist top chords were all made of two angles L51x51x4.8. with a gap of 20 mm. The lateral inertia from steel joist top chords was added to the lateral inertia of the 2 perimeter beams to obtain the total lateral inertia. To model the lateral inertia of the joists and beams, frame type elements were installed at the centreline of the building (Figure 3.13).

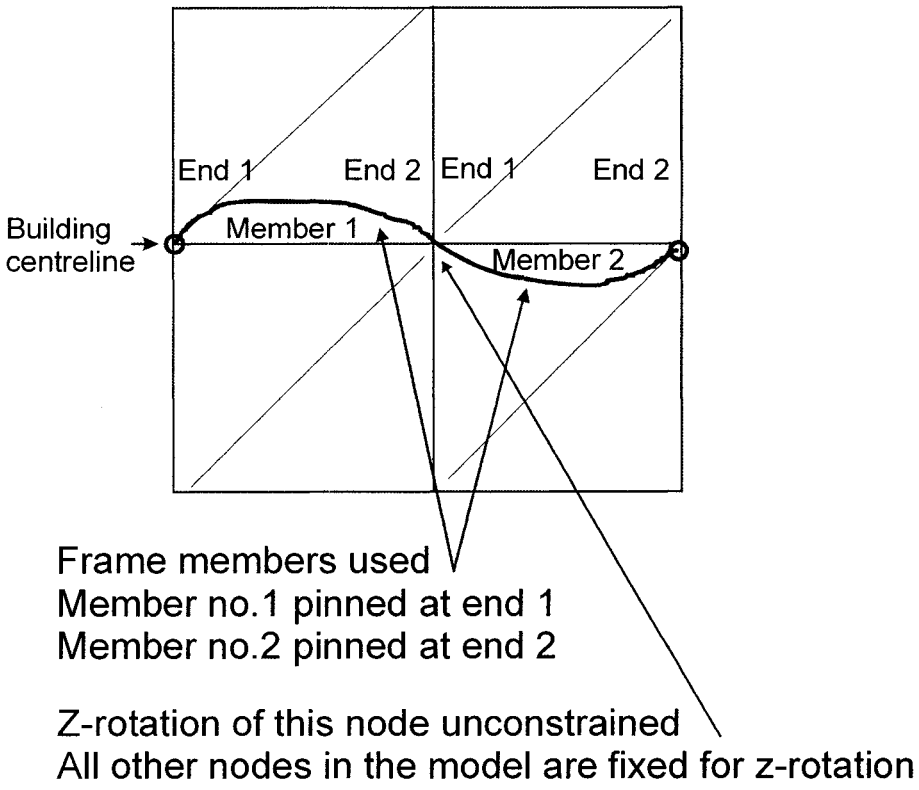

Figure 3.13 Model for joists and beams lateral inertia

Table 3.11 Frame member parameters

ITYPE =1	One component beam member
IPIN =1 or 2	=1 End 1 pinned (internally) to the joint =2 End 2 pinned (internally) to the joint
ICOND = 0	No initial loads
IHYST =0	No hysteresis
E	Young's modulus of the member material
G	Shear modulus of member material
A	Cross-sectional area of the member section
AS = 0	Effective shear area of the member section
I	Moment of inertia of section
WGT = 0	No weight considered

In the model, the lateral inertia frame members spanned over two deck units. In the buildings, the joist and perimeter beam spans were equal to 7.5 m for all building sizes.

Hence, the effect of the joists and beams lateral inertia could not work for spans higher than 7.5 m. The lateral inertia members were not modelled for the large building in which the deck elements were 6.0 m long, since two deck elements were giving a larger span than 7.5 m.

3.3.7 Bracing members

Spring elements were used to model the brace members. Since bracing members were designed as tension-only, the capacity of these elements in compression was close to 0. Bracing members develop an hysteretic behaviour that can be idealised by using the bi-linear with slackness hysteresis from Ruaumoko (see Figure 3.14). The braces were placed in the plane of the deck.

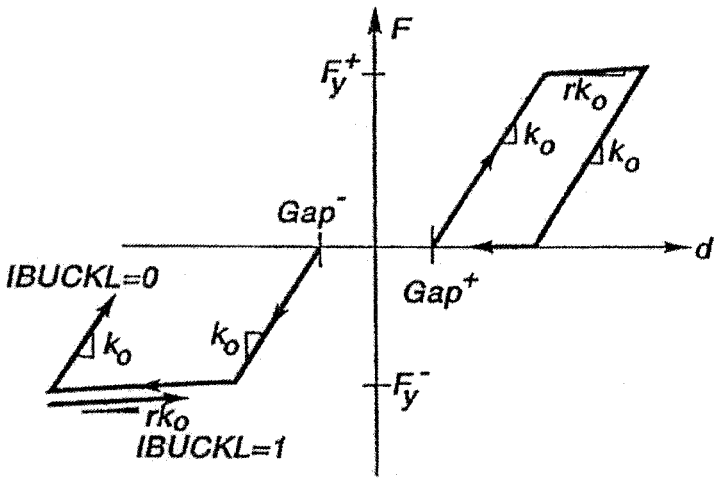

Figure 3.14 Bi-linear with slackness hysteresis (Carr, 2000)

In the following tables, the parameters used for the spring members and the hysteretic model are described.

Table 3.12 Spring member parameters for braces

ITYPE =1	No interaction between X, Y or theta Z components
IHYST = 5	Bi-linear with slackness hysteresis
ILOS = 0	No strength degradation
IDAMG =0	No damage indices computed
KX	Spring stiffness in the local x-direction
KY	Spring stiffness in the local y –direction (not used)
GJ	Rotational stiffness of the member section (not used)
WGT	Weight of the member (not used)
RF	Bi-linear factor (r in Figure 3.14)
FX+	Positive spring yield force in the x-direction
FX-	Negative spring yield force in the x-direction. This value was set to -0.001 to represent the negligible resistance of the bracing member in compression.

Table 3.13 Bi-linear with slackness hysteresis for braces

GAP+= 0.0	Initial slackness, positive direction
GAP- = 0.0	Initial slackness, negative direction
IMODE= 1	Bi-linear elastic buckling in compression

3.3.8 Column members

An elastic spring member was used to represent the column member in the tension-only braced frames. An axial stiffness of 1000000 kN/m was incorporated in the model, hence, the lateral deflection of CBFs due to the axial deformation of the column members was negligible.

3.4 GROUND MOTION RECORDS

Crustal earthquakes occurring in Eastern North America produce ground motions that are richer in high frequency than those anticipated along the Pacific coast (Tremblay and Atkinson (2001)). In addition, sites in the Pacific Northwest are exposed to the potential for great (M >8) earthquakes on active plate boundaries. The two sites selected, Victoria B.C and Quebec Qc, are located in each of the two regions and Victoria is exposed to the effects of the large plate boundary earthquakes.

A set of representative ground motions for each site was needed. For the crustal and sub-crustal earthquakes, two dominant magnitude-hypocentral distance scenarios were considered for each site (Table 3.14): one for the short period range and one for the long period range. In addition, the Cascadia scenario was considered for Victoria.

Table 3.14 Ground motion scenarios

Site	Short period	Long period	Cascadia
Victoria	M = 6.5 at r = 30 km	M = 7.2 at r = 70 km	M= 8.5
Quebec	M = 6.0 at r = 30 km	M = 7.0 at r = 70 km	

Table 3.15 lists the ground motions considered for each site, which were named A, B, C up to P for simplicity.

Table 3.15 Selected ground motion time histories

	Event	Magn.	R (km)	Station	Comp	PHA (g)	PHV (m/s)	S_F
Victoria								
A	Apr. 24, 1984 Morgan Hill	M_S 6.1	38	San Ysidro, Gilroy #6	90°	0.29	0.37	1.00
B	Jan. 17, 1994 Northridge	M_W 6.7	44	Castaic, Old Ridge Rd	90°	0.57	0.52	0.70
C	Apr. 13, 1949 West.Wash.	M_W 7.1	76	Olympia, Test Lab	86°	0.28	0.17	1.40
D	Oct. 18, 1989 Loma Prieta	M_W 7.0	100	Presidio	90°	0.20	0.34	1.30
G	Jan. 17, 1994 Northridge	M_W 6.7	44	Castaic, Old Ridge Rd	0°	0.51	0.53	0.60
H	Oct. 18, 1989 Loma Prieta	M_W 7.0	54	Stanford Univ.	0°	0.29	0.28	1.00
E	Simul. Cascadia (Trial #2)	M_W 8.5	120			0.09	0.24	2.20
F	Simul. Cascadia (Trial #3)	M_W 8.5	120			0.11	0.21	2.20
Quebec								
M	Simulated (Trial #1)	M_W 6.0	30			0.43	0.17	0.70
N	Simulated (Trial #1)	M_W 7.0	70			0.30	0.15	0.70
O	Dec. 23, 1985 Nahanni	M_S 6.5	24	Battlement Creek	270°	0.19	0.06	2.10
P	Nov. 25, 1988 Saguenay	M_S 5.7	97	La Malbaie	63°	0.12	0.04	2.00

An ensemble of 8 ground motions was used for Victoria, B.C. Six ground motions were chosen for the two crustal event scenarios. Two artificial ground motions were chosen for the M8.5 earthquakes occurring along the Cascadia subduction zone. For Quebec City, four ground motions were considered. The ensemble included two simulated ground motions in view of the limited database of records for eastern North America. Except for two records, the ground motions considered were selected and used by Tremblay and Lacerte (2002). The G and H ground motions for Victoria were suggested by Atkinson (Private communication with Atkinson ,2001).

The analyses were not performed for all buildings and all earthquakes. G and H records were added afterwards for the West to confirm the range of ductility obtained with the first four crustal earthquakes (A to D). For the NBCC 2004 models, only the small and medium R_d = 3.0 buildings in Victoria were analysed under the G and H ground motions. Those were the buildings which were found to experience the largest inelastic demand.

All ground motions were scaled to match the NBCC 2004 design spectra over the applicable period range, short period or long period, depending on the magnitude-hypocentral distance scenario considered. The ground monitoring sites where these earthquake records were obtained were located on rock soil (between Soil Class A and C), hence Class B was deemed to be the most appropriate Site Class type. The scale factors were found by comparing the ground motion spectra with the design spectra adapted to the type of soil, with the according site coefficients, F_a and F_v. For the Cascadia ground motions, scaling was performed with respect to 84^{th} percentile spectral ordinates determined for that specific hazard (Adams et al., 1999). The characteristics of the records including unscaled peak acceleration, PHA, and peak velocity, PHV, as well as the scaling factor used, S_F, are given in Table 3.15. Figure 3.15 present two comparisons of design spectra with ground motion spectra (scaled and unscaled) for Victoria. Figure 3.16 displays two cases for Quebec.

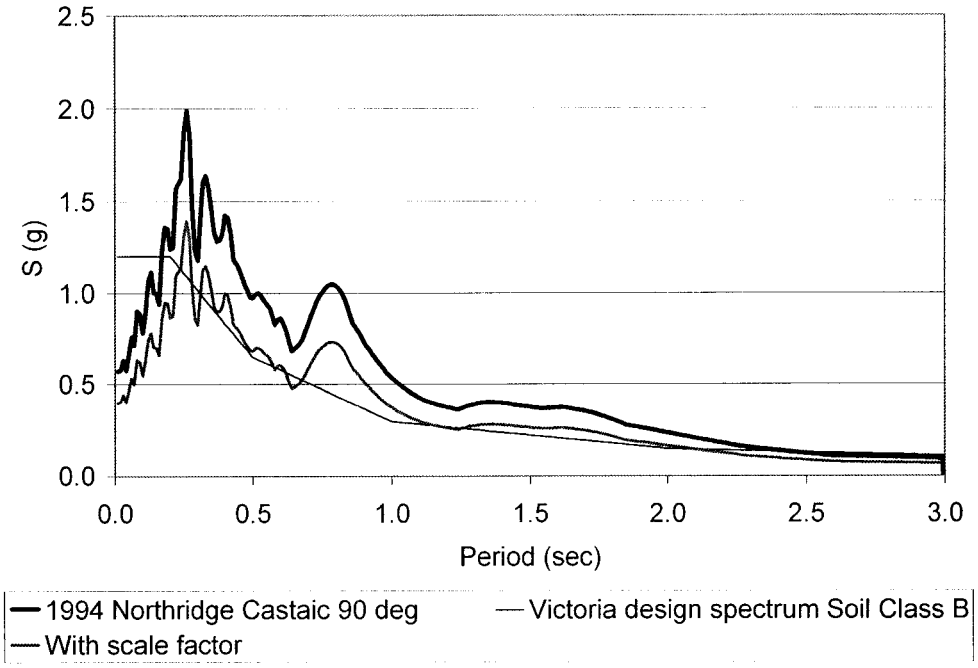

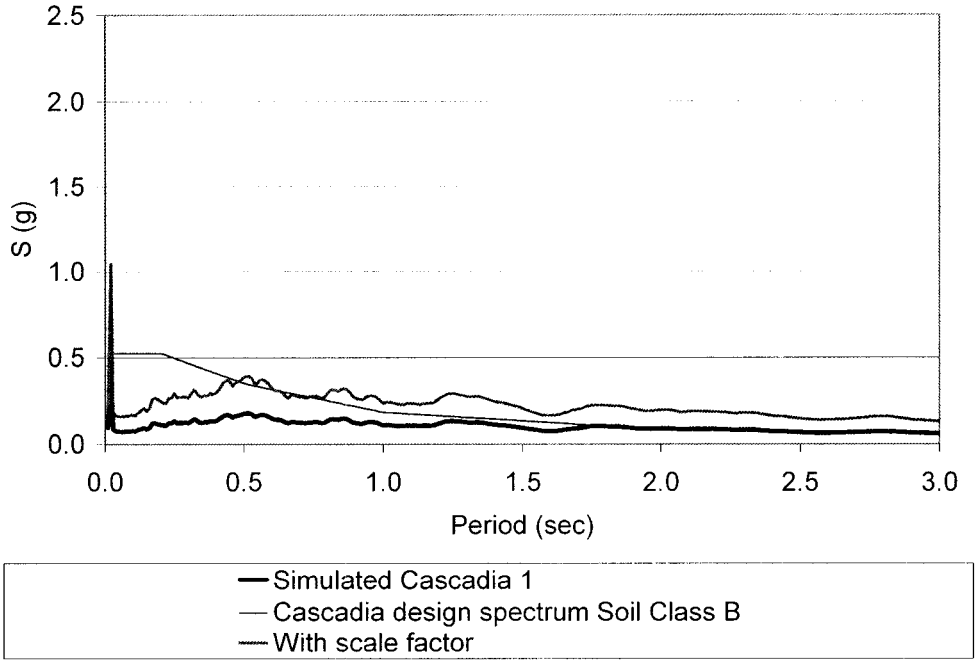

Figure 3.15 Design and ground motion response spectra for Victoria

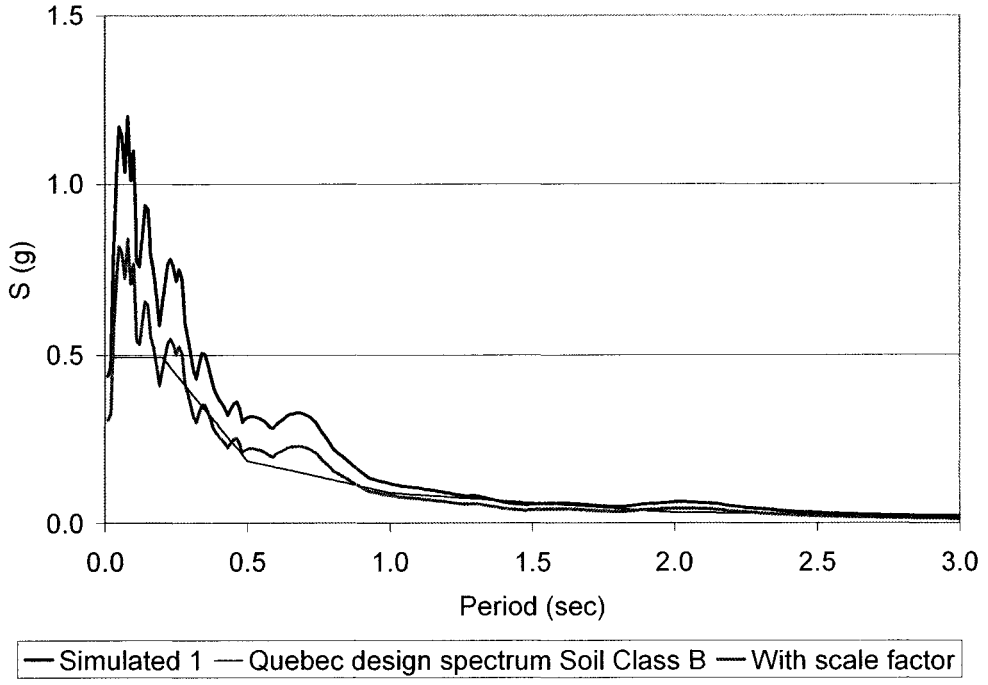

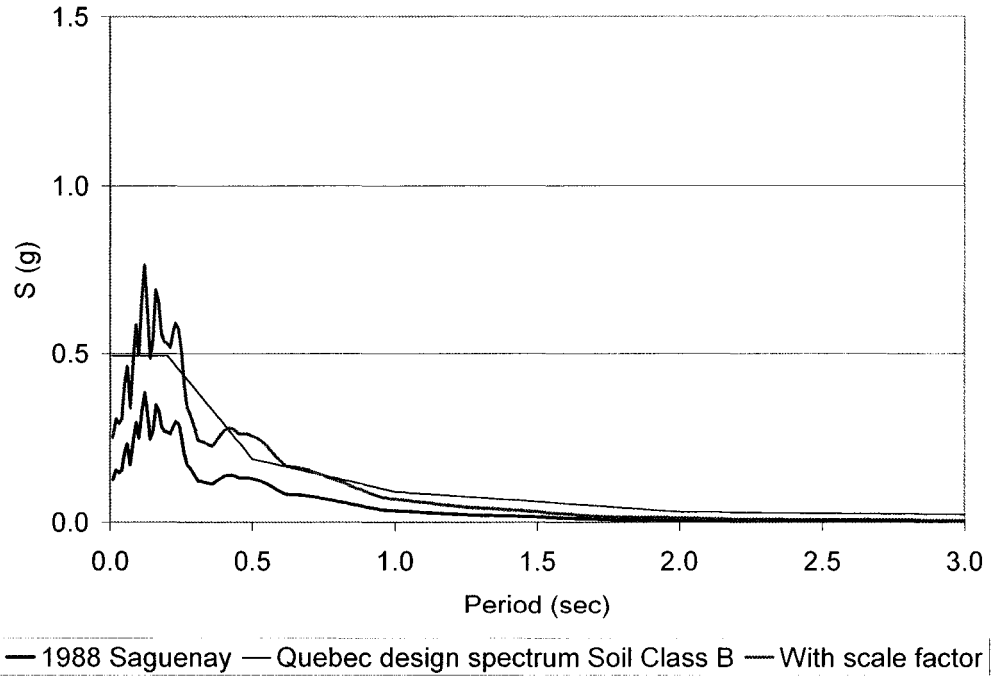

Figure 3.16 Design and ground motion response spectra for Quebec

3.5 NBCC 1995 DESIGN WITH BUTTON PUNCH-WELD DECK ASSEMBLIES

Building models with button punch-weld deck assemblies were designed and analysed for Victoria. The designs were selected according to the NBCC 1995 (NRCC, 1995). Tension-compression CBFs were used with a force reduction factor R of 3.0. The intent of these analyses was to investigate the present situation in which a building designed according to NBCC 1995, where no capacity design requirements are prescribed, has an accidentally weak diaphragm. In other words, the fragile diaphragm would be the weak link in the lateral load carrying system.

3.5.1 Building designs

As mentioned, NBCC 1995 was used in the building design. Only the main remarks regarding the design are presented in the text. The reader is referred to the code for a comprehensive description of the requirements.

The base shear, V, was calculated with the following approach:

For Victoria: $Z_a = 6$, $Z_v = 5$ and $v = 0.30$.

The elastic base shear was:

$$Ve = vSIFW \tag{3-23}$$

The period was found from the basic formula:

$$T = 0.09\frac{h_n}{D_s^{1/2}} \tag{3-24}$$

where h_n is the building height and D_s the width of the CBF. The period, T, was used to find the seismic response coefficient, S. The importance factor, I, and the foundation factor, F, were both equal to 1.0. The seismic weight, W, was obtained by taking the dead load, DL, and 25% of the live load, LL.

$$V = \left(\frac{Ve}{R}\right)U \tag{3-25}$$

The force reduction factor, R, was equal to 3.0 since ductile CBFs were used. U is a calibration factor that is equal to 0.6.

It is possible to use other methods of mechanics to find a period T and a corresponding S value. However, the elastic base shear, V_e, has to remain greater than 80% of the V_e calculated from the standard approach. Since the buildings considered in the study had much larger periods ($T_{ANALYTICAL}$) when calculated using the formula from Medhekar, 80% of V_e was considered in the design. In Table 3.2, the listed V values take into account the 0.80 factor.

No capacity design requirements are prescribed in NBCC 1995. Hence, all the elements are designed to be stronger than the force produced by the base shear V.

CBFs were designed as tension-compression elements in which square HSS were used. Ductile CBFs (R=3.0) requirements were respected. The bracing members needed to have a slenderness ratio, L/r, less than $1900/(F_y)^{0.5}$. The width thickness ratio of the HSS members needed to be smaller than $330/(F_y)^{0.5}$. The factored compressive resistance of a brace was equal to C_r, obtained from the standard formula, multiplied with a reduction

factor $(1+0.35\lambda)$, λ being the non-dimensional slenderness parameter of the brace. Due to these requirements, the CBF capacities were considerably higher than the base shear effects.

For deck elements, the button punch-weld deck assembly was used. Welds with a nominal diameter of 16 mm were used in the SDI predictions with a resistance factor of 0.6 for deck strength. The deck was not capacity protected, i.e., it was designed for the base shear, V, irrespective of the actual strength of the bracing members.

The design had to respect a deflection of $0.02h_s$. In addition, the period was calculated based on Medhekar's formula to check if the V force used in the design was conservative. The results of the design are presented in Table 3.2.

As presented for screw-nail designs with NBCC 2004, the α parameter from Fleischman and Farrow (2001) are presented for buildings with button punch-weld deck assemblies (See Table 3.7).

Table 3.16 α values for buildings with button punch-weld designs (NBCC 1995)

Victoria R = 3.0	
Small	Medium
10.44	3.63

The α values show clearly that the brace stiffness is much greater than the diaphragm stiffness.

3.5.2 Analytical model

The analytical model used for the design with screw-nail deck assemblies was discussed in Section 3.3. The model used for the button punch-weld scenario was slightly different, and hence its characteristics are discussed in this Section.

The brace elements were linear elastic. It was assumed that because of their high strength compared to the deck, they would not enter into the inelastic range. The parameters for the deck elements had to be modified to reflect the hysteretic behaviour of the diaphragm with a button punch-weld connection pattern. Test 2 from Essa *et al.* (2001) was used to determine these parameters. Figure 3.17 presents the model used for button punch deck assemblies and the test 2 curve. The FU values were found from the SDI predictions for ultimate shear strength, S_u. FX was determined to be equal to 53% of FU. FI, the intercept force was set equal to 7% of FU. The ratio γ_2/γ_1 was taken equal to 1.05. A value of 0.90 was chosen for RF, the ratio of the second to first slope stiffness. PUNL was equal to 1.10. BETA was equal to 1.30 and ALPHA to 0.40. The model properties are given in Table 3.8.

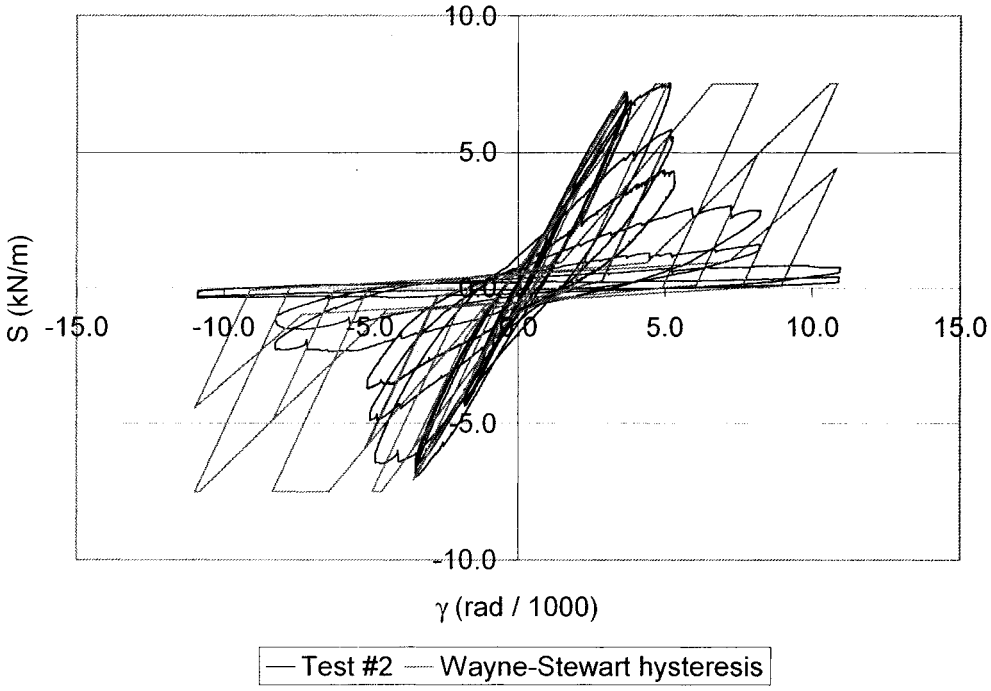

Figure 3.17 Wayne-Stewart hysteresis for button punch-weld design compared to test 2 (Essa *et al.*, 2001)

Figure 3.17 shows that the behaviour of the model used for the button punch-weld deck assemblies reproduces well the experimental results except for the strength degradation. Attempts were made to model the strength degradation but the Ruaumoko program did not give good results when including this feature. Therefore, it was decided to proceed without this behaviour.

Only 3 ground motion records (A,G and H) were used for the NBCC 1995 analyses as only a comparison with NBCC 2004 was needed. The ground motions with the scale factor presented in Section 3.4 were used for the button punch diaphragm analyses.

3.6 ANALYSIS RESULTS

Analyses were performed with the building models and the ground motions described in the previous Sections. The results from these analyses are presented and commented on in this section. At first, the general behaviour of the model is discussed. Second, the deck panel behaviour is more thoroughly studied.

Figure 3.19 shows the time history of the scaled ground motion B as well as the time history of key response parameters for the medium size building located in Victoria and designed with NBCC 2004 and R_d= 3.0. The first response parameter is the lateral deformation at the mid-length of the diaphragm and along the end walls. The second parameter is the weak axis bending moment acting at mid-span of the beam element representing the joists at the mid-length of the diaphragm. Member no. 637 is the first lateral inertia member on the left end side of the building model (See Figure 3.18). The third parameter is the shear force per unit length in the diaphragm along the end walls, as obtained after transformation from the axial force acting in the diagonal truss element 511 of the roof diaphragm model. Member 511 is the diagonal spring element located just beside member no. 637. The response shown for that particular case is representative of the structures with a screwed-nailed weak-diaphragm design.

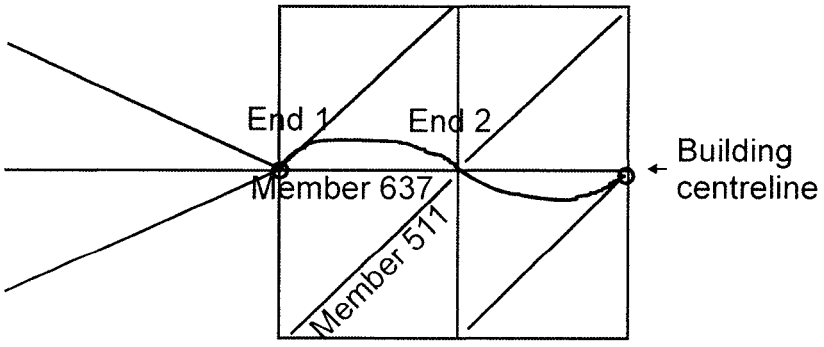

Figure 3.18 Members no.637 and 511

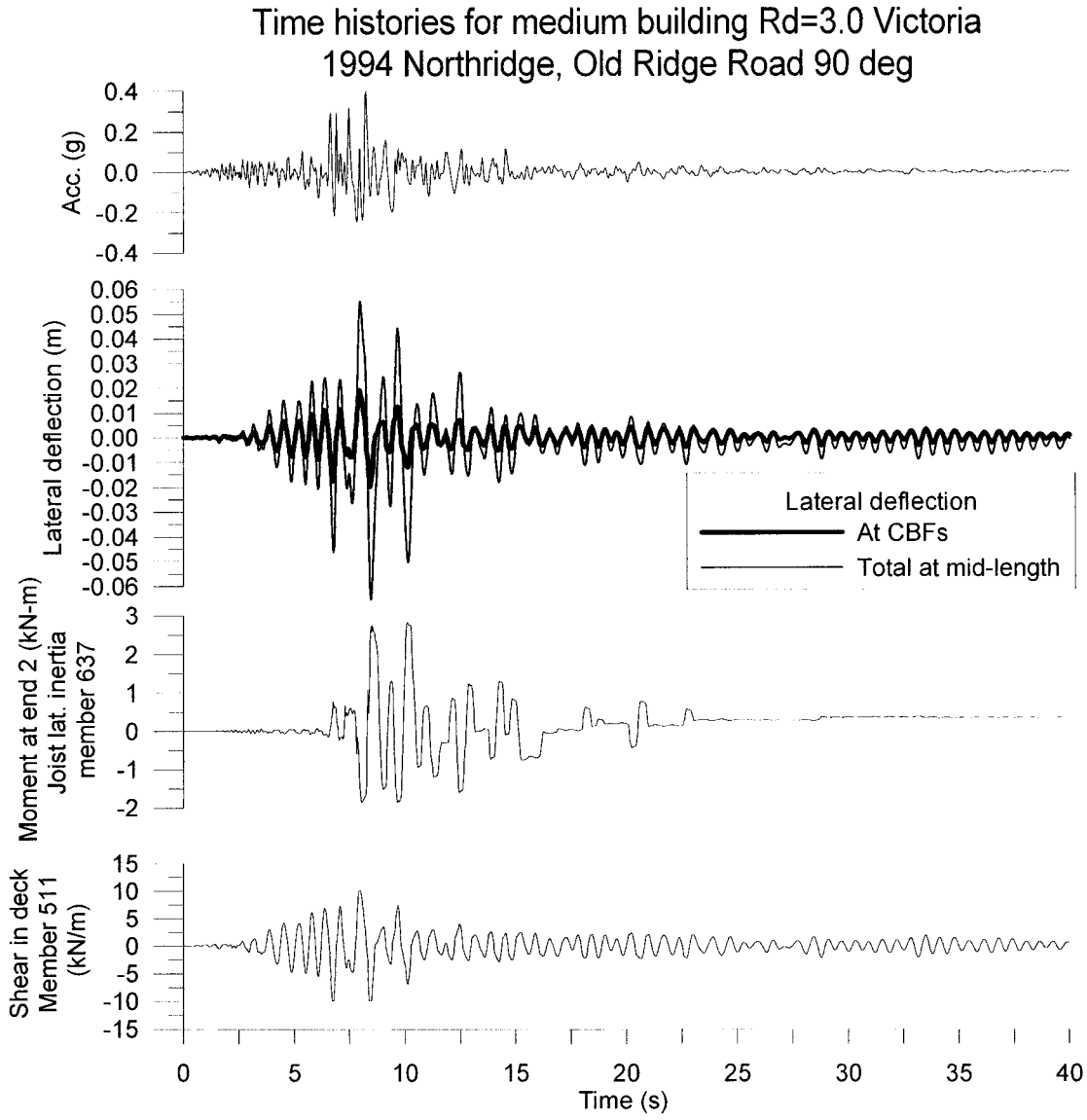

Figure 3.19 Time histories for medium building Rd=3.0 Victoria for ground motion B

The drift is much larger at the centre than along the walls, as a result of the flexibility of the diaphragm. Both deformations are in phase, which indicates a first mode response. The large cycles also occurred at a period of approximately 0.7 s, which corresponds to the first mode period for that building ($T_{ANALYTICAL}$ = 0.69 s and T_{MODEL} = 0.67 s). The storey peak drift along the walls was equal to 20 mm whereas the peak total deformation

at mid-length of the diaphragm reached 65 mm. The drift at mid-span remained below 0.025 h_s for that structure.

The shear transmitted through the lateral inertia members was small. Shear in that member is equal to the moment divided by 3.0 m. The shear flow is obtained by dividing by the building width (30 m). This gives a shear flow equal to approximately 3 kN-m / 3.0 m / 30 m = 0.03 kN/m, compared to that acting in the diaphragm, which is approximately equal to 10 kN/m. The inertia of the lateral inertia member was set equal to the sum of the inertia of all joist top chords and of the two perimeter beams. The shear in the roof diaphragm is often very small after inelastic action has developed (pinching, etc.) and the role of the joists might not have been negligible when this occurred. Thus, it is possible that the joists may have influenced somewhat the distribution of shear forces and deformations in the roof diaphragm after inelastic action developed. It would be required to compare the building response (shear deformation in deck) with and without these members included in the model to prove that their influence is negligible. This could be investigated in future studies.

Figure 3.20 presents the shear-distortion curve for the element 511. S and γ on the figure were obtained by transformation of the axial load-deformation response of the element. The distortion in deck element 511 went into the inelastic range. The maximum inelastic distortion, γ_p, was equal to 3.89 rad/1000. This was considered to be a level of inelastic distortion that a deck element could sustain without major strength degradation based on test results from Essa *et al.* (2001).

It was also possible to monitor the roof deck panels during the nonlinear analyses and observe the extent of yielding during the applied seismic event, as shown in Figure 3.21.

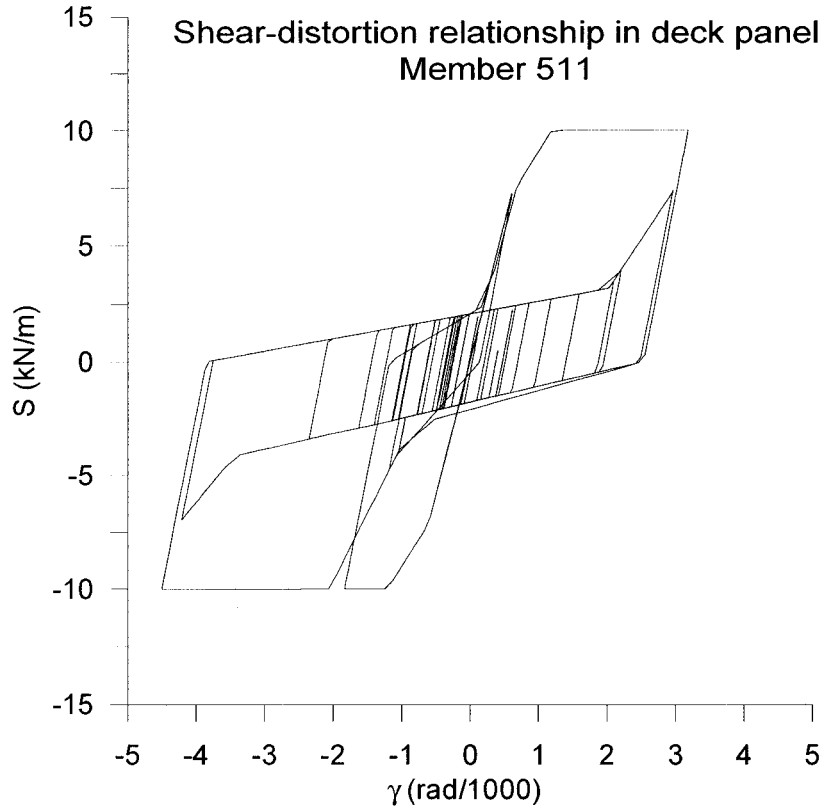

Figure 3.20 Shear-distortion curve in deck element member 511

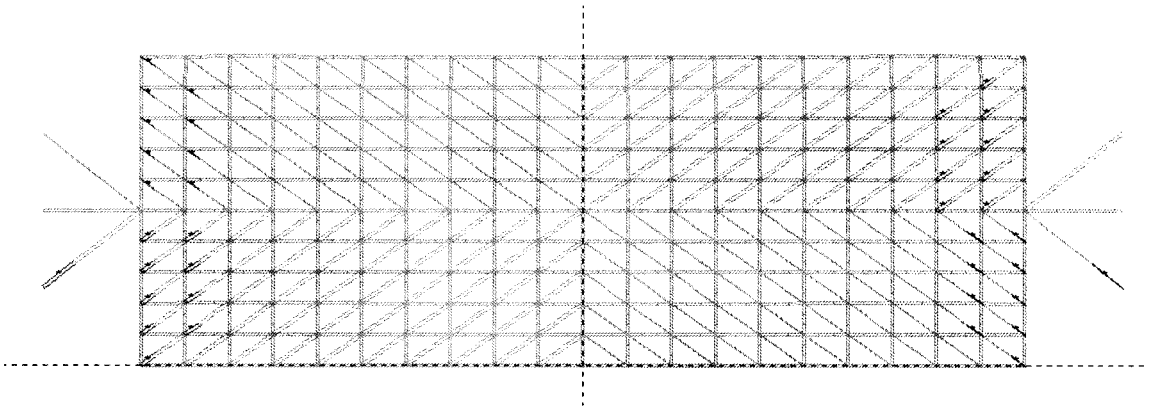

Figure 3.21 Panels that yielded for Victoria medium Rd=3.0 under ground motion B

This Figure illustrates the panels that have yielded at a certain time in the medium size building for Victoria R_d=3.0 under ground motion B. The panels that had reached the inelastic range are marked by an asterisk. The roof panels that yielded were located adjacent to the end walls since the shear was greater at the diaphragm ends. This was observed generally in other analyses with inelastic distortions. It is important to note that the number of panels that yielded during each run depended on the characteristics of the applied ground motion. In Figure 3.21, two of the wall braces are marked by an asterisk. In fact, they are in compression buckling at a very low load.

Representative deck distortion time histories for the different nonlinear analyses are provided in Figure 3.22 to Figure 3.26. The deck distortions presented are for the deck elements that experienced the largest deformations in each analysis. The γ_u value has also been shown for each time history in Figure 3.22 to Figure 3.26. The response varies according to various parameters: site, R_d factor, size of buildings, etc. Figure 3.22 presents time histories for the small, medium and large buildings in Victoria with R_d=3.0. The inelastic distortions tend to decrease when the building size increases. The shape of the cycles are narrower for the small size buildings as the period is shorter. Figure 3.23 shows the time histories for the same buildings as in Figure 3.22 but under Cascadia ground motions. The number of cycles under Cascadia earthquakes is much greater than under intra-plate earthquakes. Figure 3.24 displays time histories for medium size building in Victoria with R_d=2.0. The amplitude of the cycles is lower in comparison to the building designed with R_d =3.0. Figure 3.25 and Figure 3.26 display time histories for the medium and large size R_d =3.0 buildings in Quebec. All distortions are kept below or near γ_u for the Quebec ground motions.

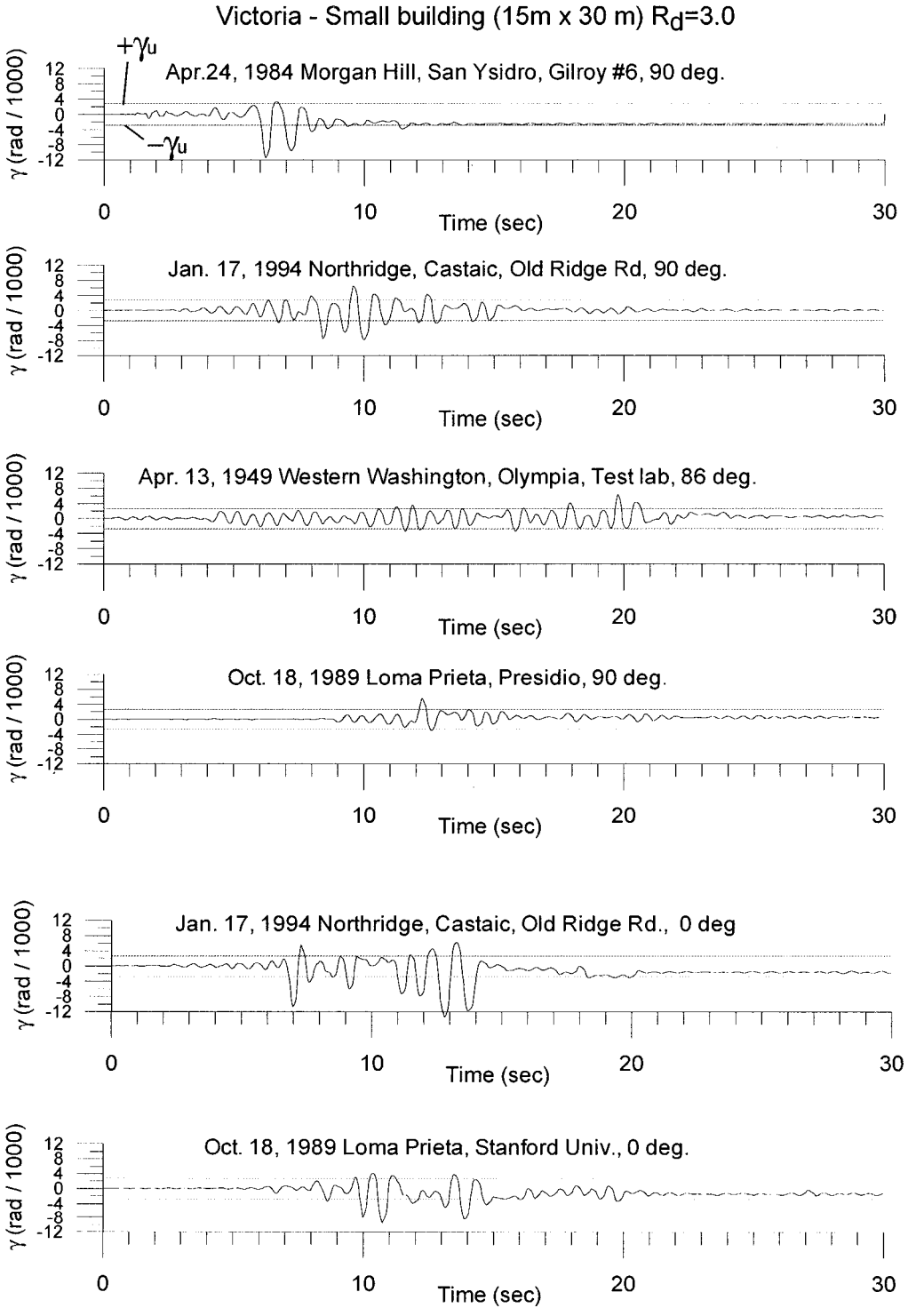

Figure 3.22 Deck panel distortion time histories for Victoria Rd=3.0

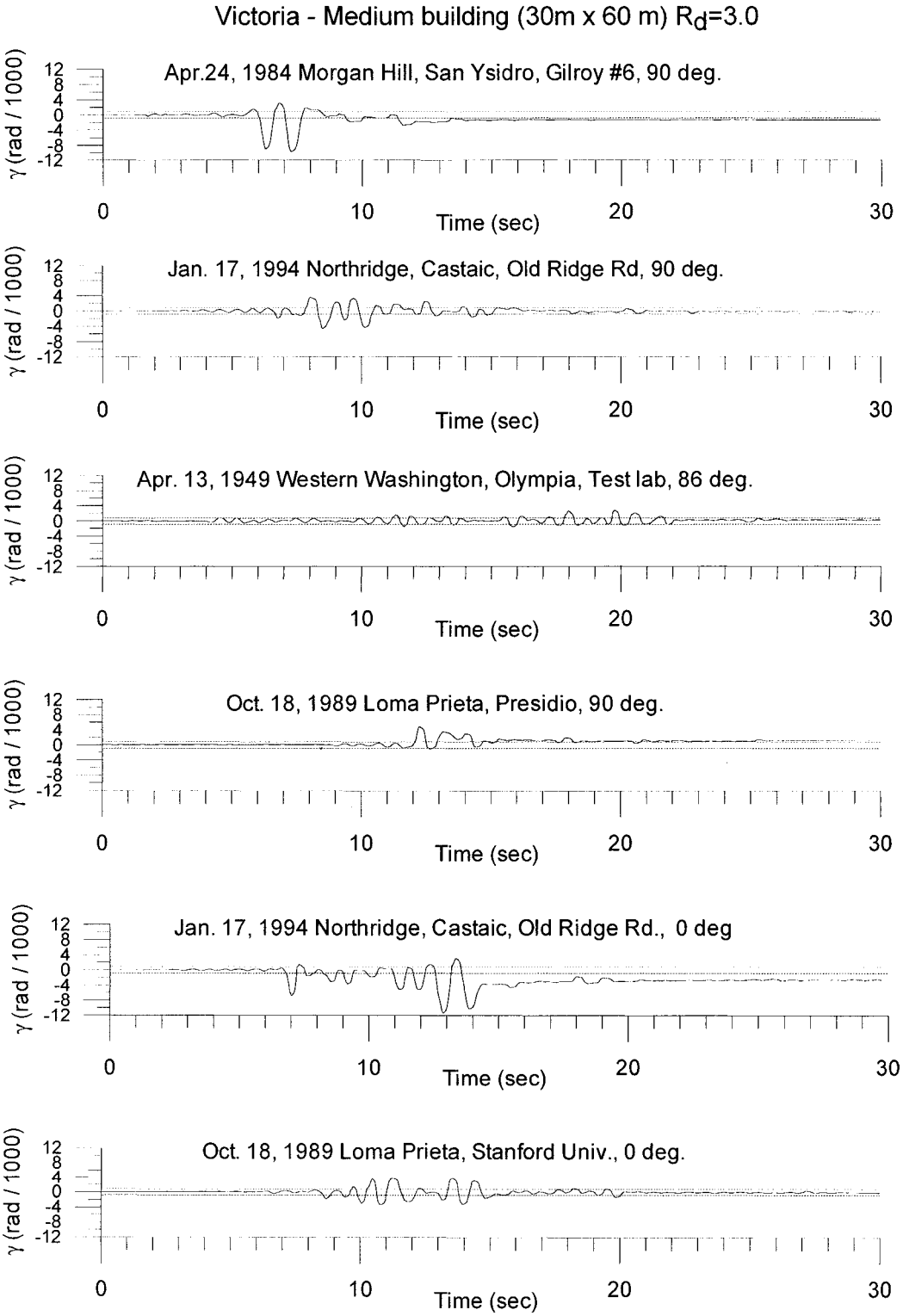

Figure 3.22 Deck panel distortion time histories for Victoria Rd=3.0 (continued)

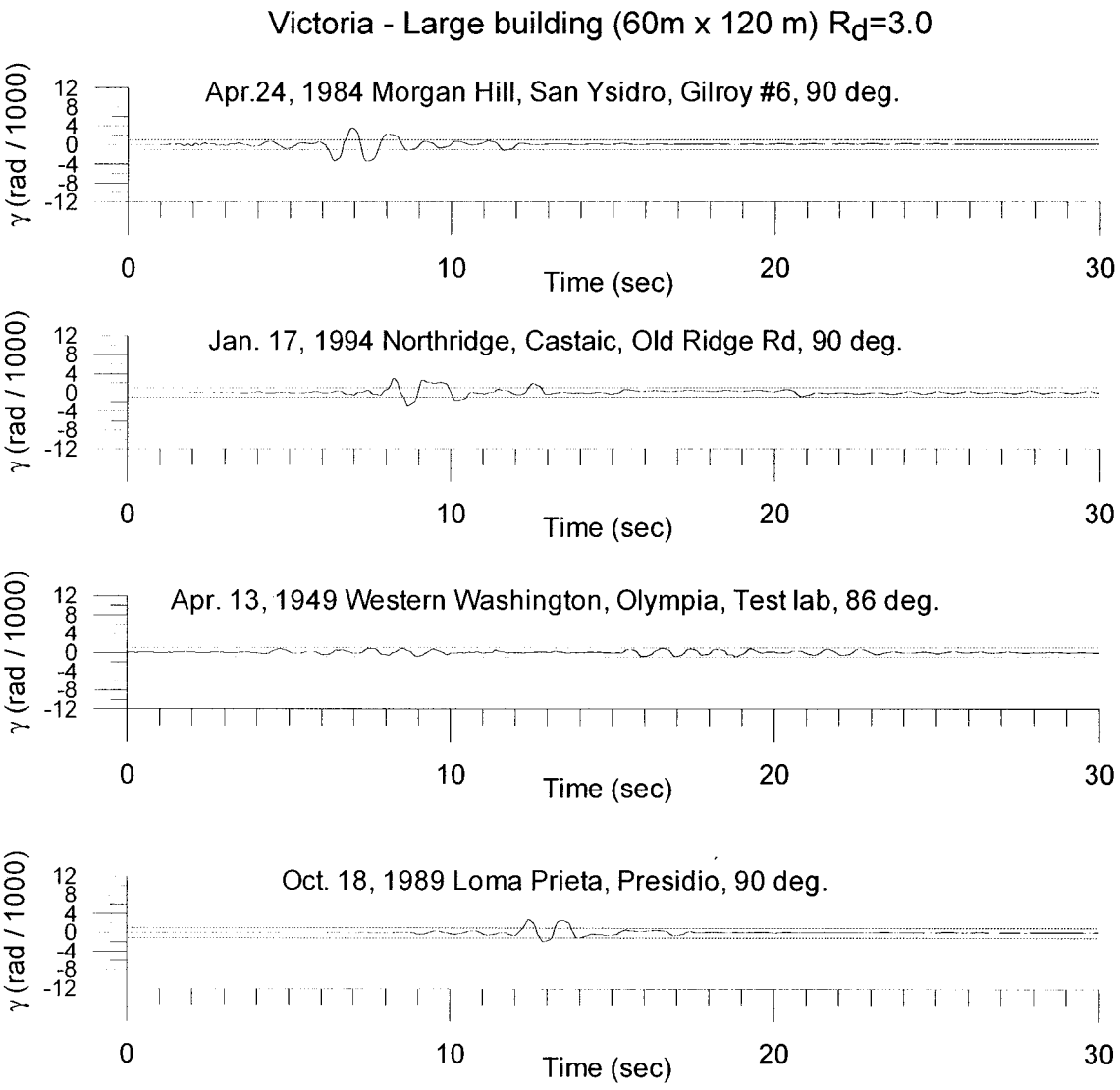

Figure 3.22 Deck panel distortion time histories for Victoria Rd=3.0 (continued)

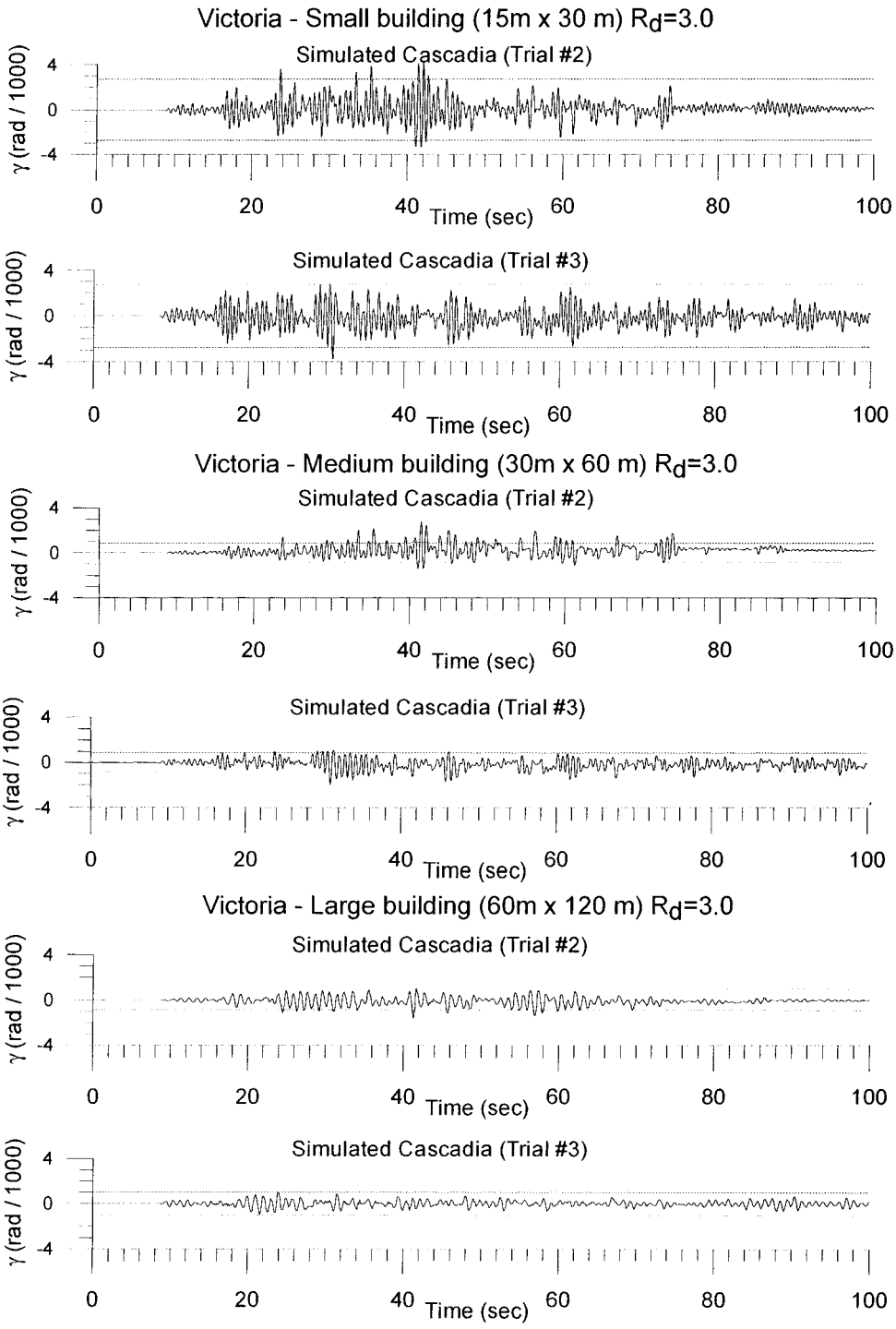

Figure 3.23 Deck panel distortion time histories for Victoria Rd=3.0 under Cascadia ground motions

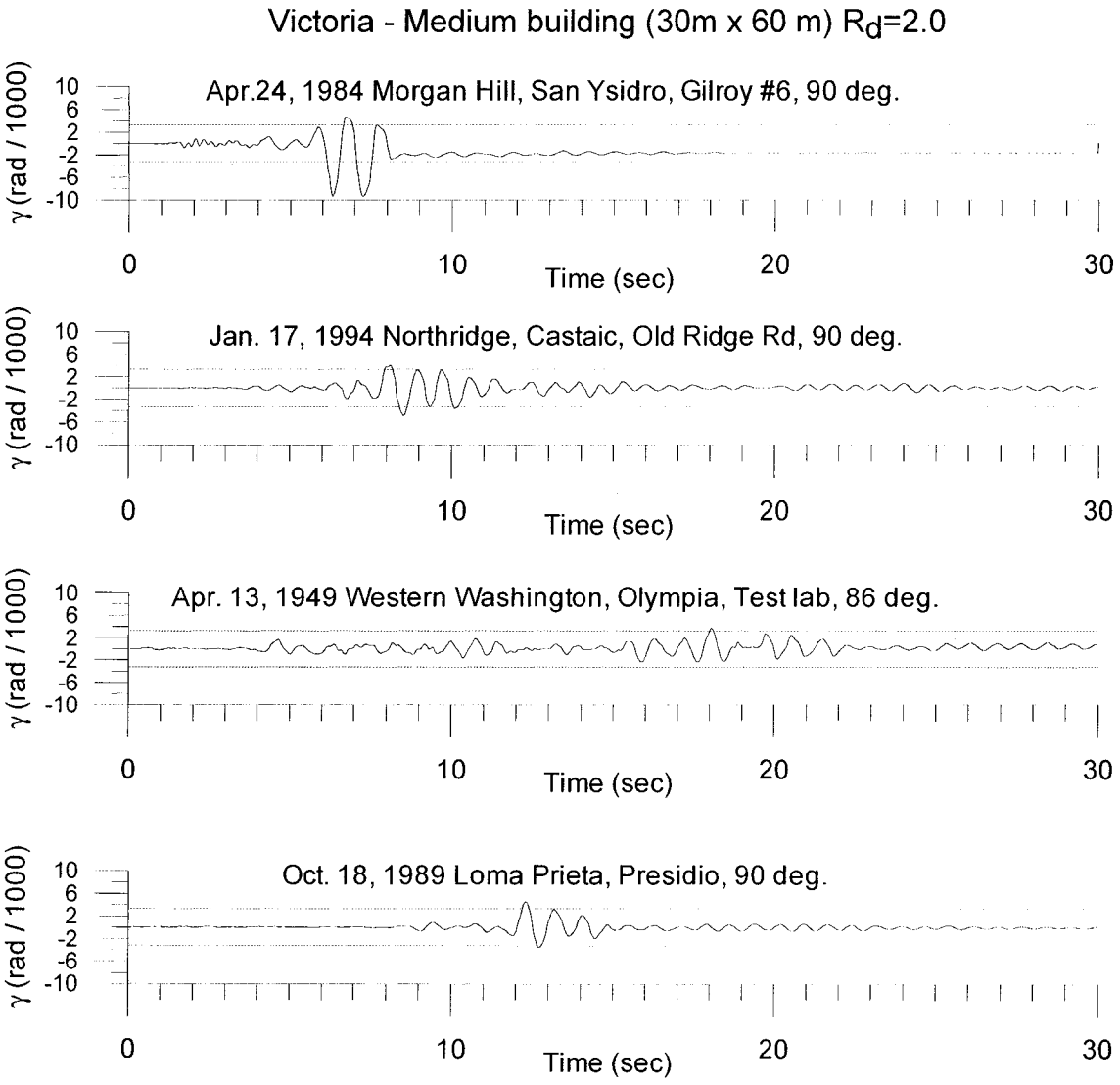

Figure 3.24 Deck panel distortion time histories for Victoria Rd=2.0

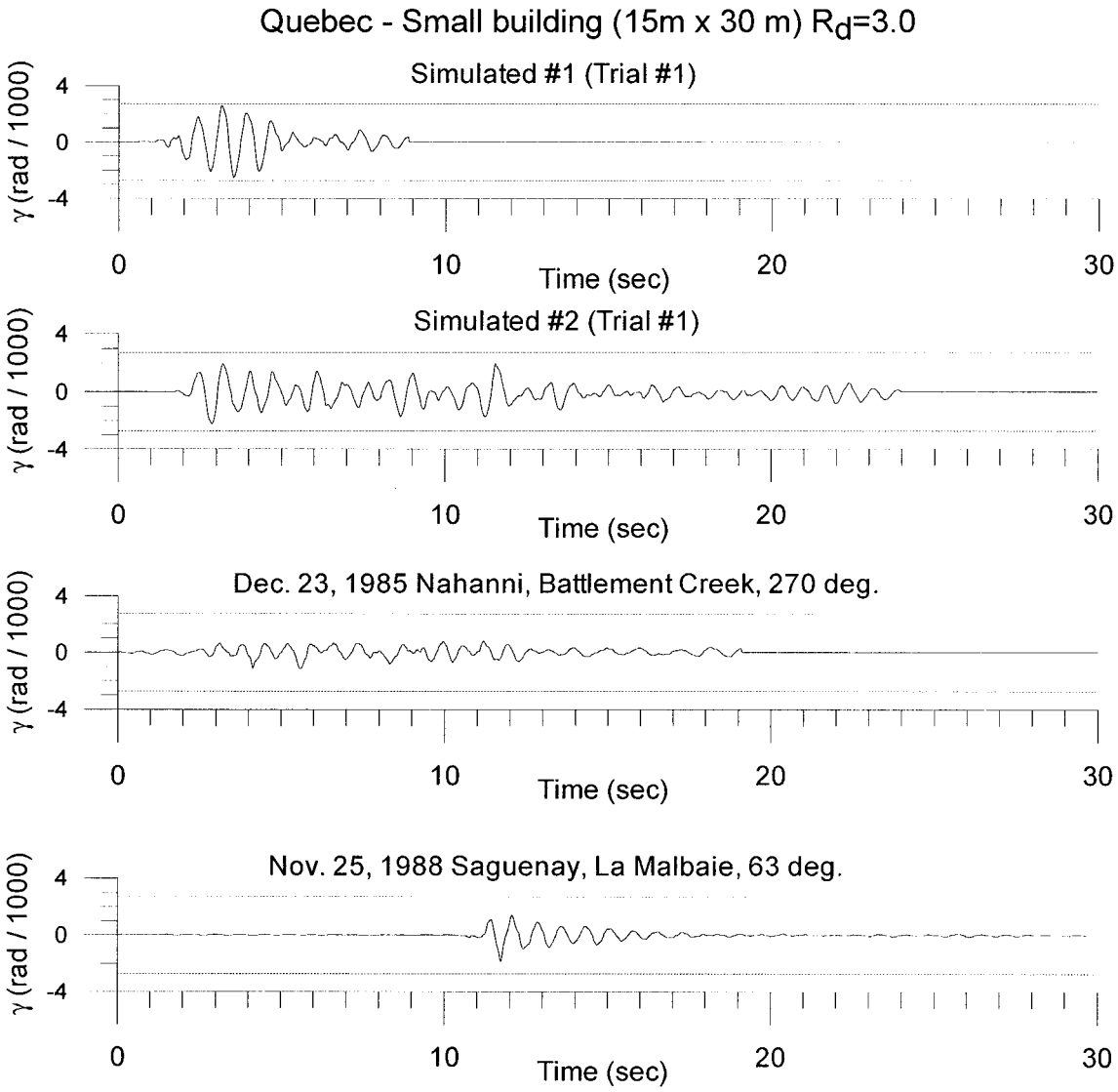

Figure 3.25 Deck panel distortion time histories for Quebec Rd=3.0

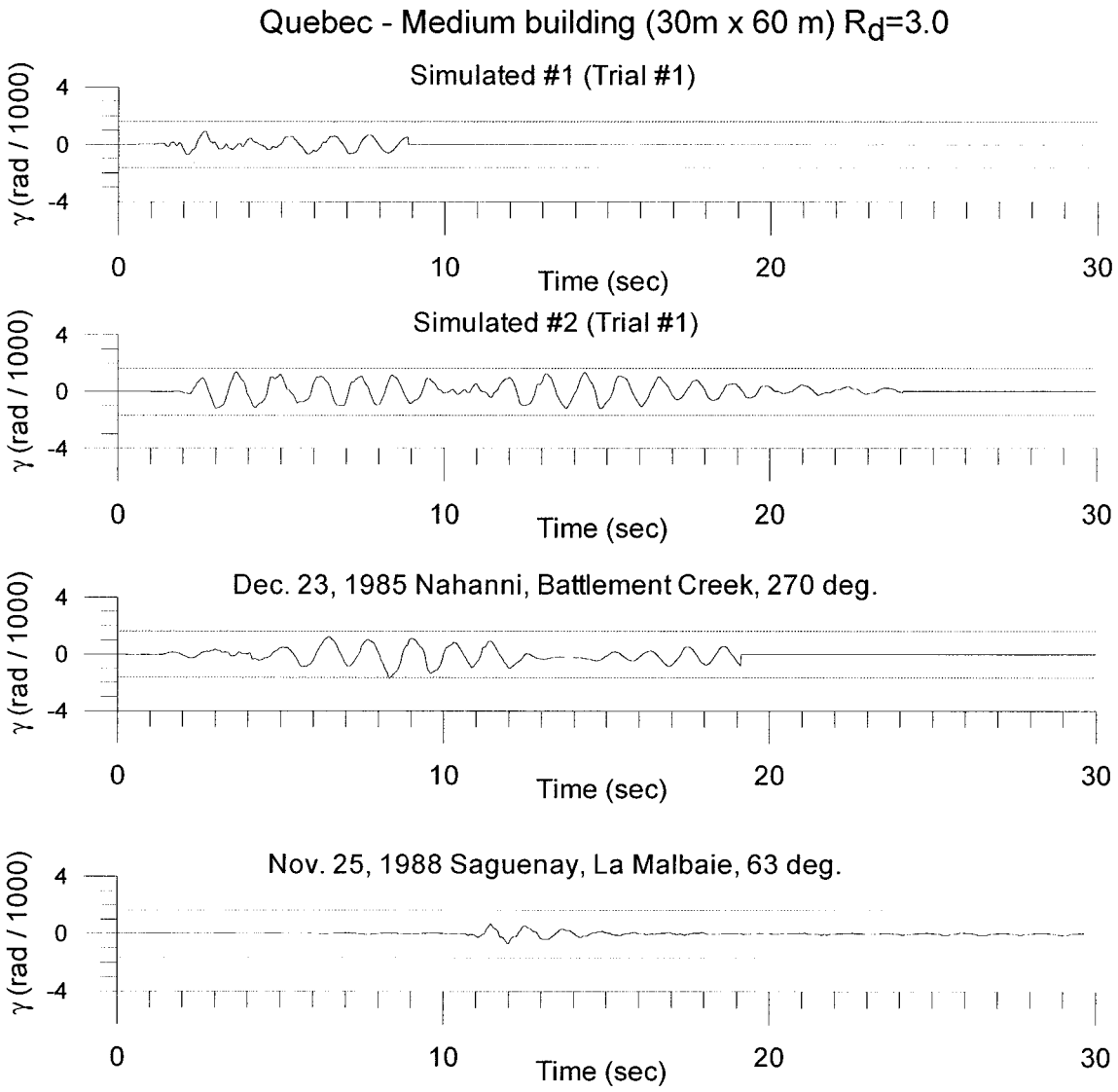

Figure 3.26 Deck panel distortion time histories for Quebec Rd=3.0

The peak response parameters for all cases studied are presented, where the results for screw-nail designs with NBCC 2004 are given together with results for the button punch-weld designs with NBCC 1995. In Table 3.17, the peak lateral deflections (Δ_{dyn}) for each analysis using the Ruaumoko software are presented. In addition, a comparison of the peak dynamic lateral deflection with the deflection found from the conventional design approach ($\Delta_{dyn}/\Delta_{conv}$) is given. For all models, the peak dynamic deflection was

smaller than the deflection found from the conventional method, in which the building is uniformly loaded with the base shear force and the deflection multiplied by R_dR_o. Also, the peak lateral deflection is compared to the lateral drift requirements ($\Delta_{dyn}/\Delta_{limit}$). All models had a maximum lateral deflection that respected the lateral drift requirements ($0.025h_s$). It has to be mentioned that the ratios $\Delta_{dyn}/\Delta_{conv}$ and $\Delta_{dyn}/\Delta_{limit}$ were calculated with the maximum value of Δ_{dyn} for each model. For the NBCC 1995 buildings, the peak dynamic lateral deflection is greater than the deflection found from the conventional method, as well the lateral deflection respected the lateral drift requirement ($0.020h_s$).

Table 3.18 provides a listing of the maximum inelastic distortion, γ_p, for each analysis. As discussed, the inelastic distortion is the parameter that has been chosen to evaluate the inelastic demand in the deck assemblies. For the screw-nail designs, nearly all maximum inelastic distortions were below 10 rad/1000, which is within the acceptable range as determined by Essa *et al.* (2001) for this type of diaphragm construction. The allowable range was defined to ensure that the strength level of the diaphragm under cyclic loading does not degrade below 80% of the peak load. Two exceptions were noted, small and medium buildings with R_d=3.0 in Victoria under ground motion G, with γ_p values of 10.76 and 10.55 rad/1000. The demand was higher in these two cases because the ground motion scaled spectrum was higher than the design spectrum. For structures designed with R_d = 3.0, γ_p under crustal earthquakes varies from 0 to 10.76 rad/1000 for Victoria and between 0 and 0.25 rad/1000 for the Quebec site. For Victoria, the peak plastic deformation under the Cascadia earthquakes was generally smaller than the demand from the crustal earthquakes, varying from 0.05 to 1.85 rad/1000. For the NBCC 1995 designs, the inelastic distortions varied from 1.22 to 9.75 rad/1000 for Victoria.

The anticipated inelastic distortions for R_d= 2.0 and 3.0 are presented in Figure 3.27.

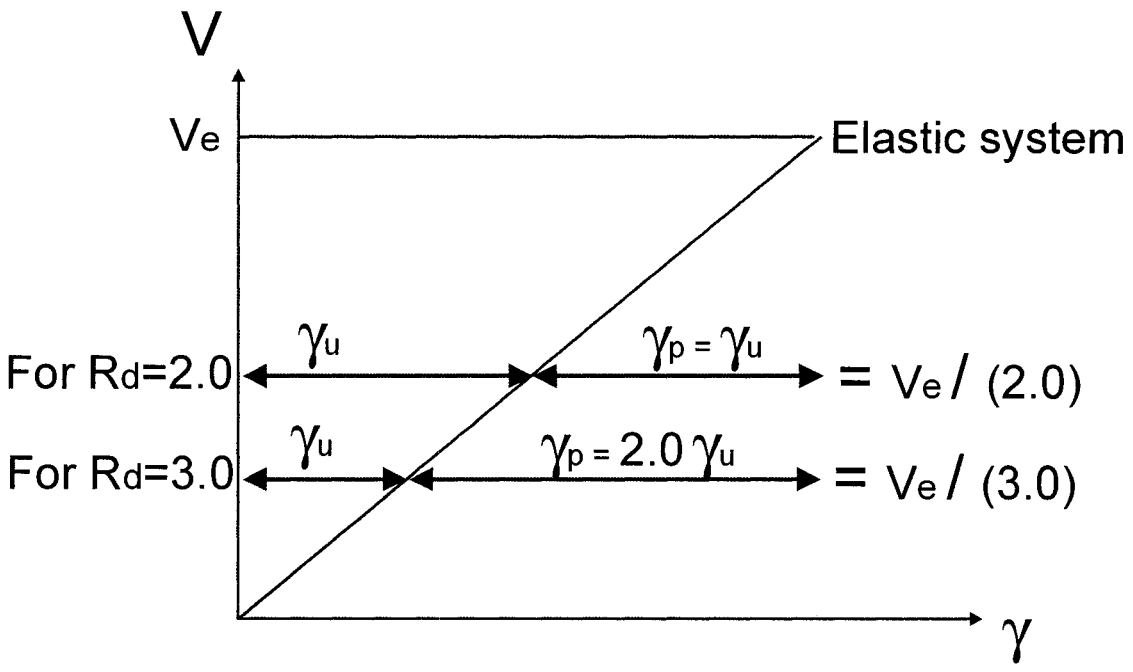

Figure 3.27 Anticipated inelastic distortions for Rd= 2.0 and 3.0

As shown in Figure 3.27, according to the equal displacement principle, it was expected that γ_p would equal γ_u for R_d=2.0 buildings, whereas a γ_p of 2.0 γ_u was anticipated for the R_d = 3.0 structures. Table 3.19 presents the peak values of the ratio γ_p/γ_u obtained from the analyses. For Victoria, the results showed that the γ_p values are greater for R_d=3.0 than those for R_d = 2.0. The values for Victoria R_d = 2.0 were close to 1.0. For Victoria R_d = 3.0, the mean γ_p / γ_u values for each model were between 1.13 and 5.19, hence, they were more or less centred around 2.0. For Quebec, little to no inelastic distortion was observed to have taken place in the diaphragm, which is different from the anticipated behaviour for an R_d factor of 3.0. For NBCC 1995 models, the ratios γ_p/γ_u were between 0.68 and 8.34.

	Screw-nail connector pattern										Button punch-weld	
	Victoria Rd=3.0			Victoria Rd=2.0			Quebec Rd=3.0			Victoria Rd=3.0	Victoria R=3 NBCC 95	
	Small (15x30)	Medium (30x60)	Large (60x120)	Small (15x30)	Medium (30x60)	Large (60x120)	Small (15x30)	Medium (30x60)	Large (60x120)	Double (30x120)	Small (15x30)	Medium (30x60)
Dynamic deflection (Δ dyn) in mm												
Ground motions												
A	65.6	86.8	122.7	58.6	124.2	129.1	N/A	N/A	N/A	83.2	20.0	48.6
B	59.7	65.6	102.1	57.9	111.8	116.5	N/A	N/A	N/A	64.1	N/A	N/A
C	58.8	51.9	71.2	62.6	80.8	78.8	N/A	N/A	N/A	N/A	N/A	N/A
D	48.0	59.6	107.0	52.1	95.0	99.8	N/A	N/A	N/A	N/A	N/A	N/A
E	44.2	49.8	84.2	38.2	51.8	68.3	N/A	N/A	N/A	47.3	N/A	N/A
F	42.6	43.7	71.1	37.9	47.3	56.6	N/A	N/A	N/A	N/A	N/A	N/A
G	75.3	93.0	N/A	N/A	N/A	N/A	N/A	N/A	N/A	N/A	38.0	86.1
H	62.0	53.1	N/A	N/A	N/A	N/A	N/A	N/A	N/A	N/A	30.0	56.0
M	N/A	N/A	N/A	N/A	N/A	N/A	31.2	26.7	28.7	N/A	N/A	N/A
N	N/A	N/A	N/A	N/A	N/A	N/A	29.4	41.8	43.4	N/A	N/A	N/A
O	N/A	N/A	N/A	N/A	N/A	N/A	16.5	41.2	71.8	N/A	N/A	N/A
P	N/A	N/A	N/A	N/A	N/A	N/A	21.9	21.6	21.9	N/A	N/A	N/A
Maximum	75.3	93.0	122.7	62.6	124.2	129.1	31.2	41.8	71.8	83.2	38.0	86.1
Minimum	42.6	43.7	71.1	37.9	47.3	56.6	16.5	21.6	21.9	47.3	20.0	48.6
Mean	57.0	62.9	93.1	51.2	85.2	91.5	24.8	32.8	41.5	64.9	29.3	63.6
Std deviation	11.3	17.9	20.9	10.7	31.3	28.4	6.8	10.2	22.1	18.0	8.5	19.9
Deflection from conventional method												
Δ conv (mm)	90.3	106.7	222.6	79.8	150.9	205.3	53.0	134.4	223.3	106.7	28.0	56.2
Δ dyn/ Δ conv	0.83	0.87	0.55	0.78	0.82	0.63	0.59	0.31	0.32	0.78	1.36	1.53
Deflection limit check												
Criteria	0.025hs	0.025hs	0.025hs	0.025hs	0.025hs	0.025hs	0.025hs	0.025hs	0.025hs	0.025hs	0.020hs	0.020hs
Δ limit (mm)	135	165	225	135	165	225	135	165	225	165	108	132
Δ dyn/ Δ limit	0.56	0.56	0.55	0.46	0.75	0.57	0.23	0.25	0.32	0.50	0.35	0.65

Table 3.17 Deflection at mid-length of building

Table 3.18 Maximum inelastic distortion in deck panels, γ_p (rad/1000)

Ground motions	Screw-nail connector pattern									Button punch-weld	
	Victoria Rd=3.0			Victoria Rd=2.0			Quebec Rd=3.0			Victoria Rd=3.0 Double	Victoria R=3 NBCC 95
	Small (15x30)	Medium (30x60)	Large (60x120)	Small (15x30)	Medium (30x60)	Large (60x120)	Small (15x30)	Medium (30x60)	Large (60x120)	(30x120)	Small (15x30)	Medium (30x60)
A	8.76	8.86	2.47	4.79	6.07	2.53	N/A	N/A	N/A	7.55	1.22	4.00
B	5.13	3.89	1.96	2.80	1.57	1.57	N/A	N/A	N/A	5.06	N/A	N/A
C	3.59	1.91	0.01	4.14	0.46	0.40	N/A	N/A	N/A	N/A	N/A	N/A
D	2.72	3.99	1.85	2.24	1.21	0.88	N/A	N/A	N/A	N/A	N/A	N/A
E	1.54	1.85	0.55	0.15	0.00	0.00	N/A	N/A	N/A	3.48	N/A	N/A
F	1.01	1.18	0.05	0.00	0.00	0.00	N/A	N/A	N/A	N/A	N/A	N/A
G	10.76	10.55	N/A	N/A	N/A	N/A	N/A	N/A	N/A	N/A	7.18	9.75
H	6.71	2.84	N/A	N/A	N/A	N/A	N/A	N/A	N/A	N/A	4.78	3.39
M	N/A	N/A	N/A	N/A	N/A	N/A	0.00	0.00	0.00	N/A	N/A	N/A
N	N/A	N/A	N/A	N/A	N/A	N/A	0.00	0.00	0.00	N/A	N/A	N/A
O	N/A	N/A	N/A	N/A	N/A	N/A	0.00	0.07	0.25	N/A	N/A	N/A
P	N/A	N/A	N/A	N/A	N/A	N/A	0.00	0.00	0.00	N/A	N/A	N/A
Maximum	10.76	10.55	2.47	4.79	6.07	2.53	0.00	0.07	0.25	7.55	7.18	9.75
Minimum	1.01	1.18	0.01	0.00	0.00	0.00	0.00	0.00	0.00	3.48	1.22	3.39
Mean	5.03	4.38	1.15	2.35	1.55	0.90	0.00	0.02	0.06	5.36	4.40	5.71
Std deviation	3.73	3.50	0.94	1.82	1.75	0.82	0.00	0.02	0.07	2.58	2.36	2.99

Table 3.19 Ratio of the inelastic distortion, γ_p, over γ_u

Ground motions	Screw-nail connector pattern									Button punch-weld	
	Victoria Rd=3.0			Victoria Rd=2.0			Quebec Rd=3.0		Victoria Rd=3.0	Victoria R=3 NBCC 95	
	Small (15x30)	Medium (30x60)	Large (60x120)	Small (15x30)	Medium (30x60)	Large (60x120)	Small (15x30)	Medium (30x60)	Large (60x120)	Double (30x120)	Small (15x30)	Medium (30x60)
A	3.21	10.50	2.43	1.46	1.85	1.95	N/A	N/A	N/A	8.94	0.68	3.42
B	1.88	4.61	1.92	0.85	0.48	1.21	N/A	N/A	N/A	5.99	N/A	N/A
C	1.32	2.27	0.01	1.26	0.14	0.31	N/A	N/A	N/A	N/A	N/A	N/A
D	1.00	4.73	1.81	0.68	0.37	0.68	N/A	N/A	N/A	N/A	N/A	N/A
E	0.56	2.20	0.54	0.04	N/A	N/A	N/A	N/A	N/A	4.12	N/A	N/A
F	0.37	1.39	0.05	N/A	N/A	N/A	N/A	N/A	N/A	N/A	N/A	N/A
G	3.94	12.50	N/A	N/A	N/A	N/A	N/A	N/A	N/A	N/A	4.01	8.34
H	2.46	3.36	N/A	N/A	N/A	N/A	N/A	N/A	N/A	N/A	2.67	2.90
M	N/A	N/A	N/A	N/A	N/A	N/A	0.00	0.00	0.00	N/A	N/A	N/A
N	N/A	N/A	N/A	N/A	N/A	N/A	0.00	0.00	0.00	N/A	N/A	N/A
O	N/A	N/A	N/A	N/A	N/A	N/A	0.00	0.04	0.29	N/A	N/A	N/A
P	N/A	N/A	N/A	N/A	N/A	N/A	0.00	0.00	0.00	N/A	N/A	N/A
Mean	1.84	5.19	1.13	0.86	0.71	1.04	0.00	0.01	0.07	6.35	2.46	4.88
Maximum	3.94	12.50	2.43	1.46	1.85	1.95	0.00	0.04	0.29	8.94	4.01	8.34
Minimum	0.37	1.39	0.01	0.04	0.14	0.31	0.00	0.00	0.00	4.12	0.68	2.90
Std deviation	1.36	4.15	0.92	0.55	0.53	0.63	0.00	0.01	0.08	3.05	1.32	2.55

The drift and the maximum inelastic distortion, γ_p, are the two main parameters that permit a conclusion to be drawn on the performance of a diaphragm. Hence, these parameters are discussed in the following text.

With regard to the lateral drift of the buildings, the values were all lower than the limit, which suggests that buildings designed with the procedure adopted, i.e. NBCC 2004 seismic load with a weak diaphragm, would perform adequately according to requirements for drift. The results also indicate that the buildings in Quebec would generally experience smaller deformations than for Victoria. The NBCC 2004 method to predict inelastic drifts (multiplying by R_d R_o the drift under V) was found to be conservative in all cases, particularly in Quebec.

Remarks are made on the obtained inelastic distortions with respect to a number of different parameters.

Effect of the site and type of ground motion:

Table 3.20 presents different evaluations of the building period in seconds and the relationship with the spectral values that explains to some extent the difference in the demand with the site and type of ground motions.

Table 3.20 Spectral values for UHS and ground motions

	Screw-nail connector pattern									Button punch-weld	
	Victoria Rd=3.0			Victoria Rd=2.0			Quebec Rd=3.0			Victoria R=3 NBCC 95	
	Small (15x30)	Medium (30x60)	Large (60x120)	Small (15x30)	Medium (30x60)	Large (60x120)	Small (15x30)	Medium (30x60)	Large (60x120)	Small (15x30)	Medium (30x60)
T=1.5Ta	0.27	0.31	0.39	0.27	0.31	0.39	0.27	0.31	0.39	0.18	0.22
$T_{analytical}$	0.63	0.69	0.97	0.59	0.80	0.94	0.76	1.20	1.62	0.39	0.56
$S_{UHS}(T_{anal})$ / S (1.5Ta)	0.52	0.51	0.37	0.54	0.44	0.40	0.32	0.20	0.18	0.90	0.60
$S_{UHS}(T_{anal})/ S_{ground\ motion}(T_{anal})$											
Short period	0.97	0.87	0.65	1.02	0.63	0.65	0.97	0.93	0.78	5.73	2.79
Long period	0.99	1.05	0.96	0.99	0.97	0.99	0.89	1.07	1.33	3.94	3.53
Cascadia	1.64	1.59	1.27	1.59	1.50	1.37	N/A	N/A	N/A	N/A	N/A

Short period:	Ground motions A, B and G for Victoria, M and O for Quebec
Long period:	Ground motions C, D and H for Victoria, N and P for Quebec
Cascadia:	Ground motions E and F

	Victoria Rd=3.0			Victoria Rd=2.0			Quebec Rd=3.0			Victoria Rd=3.0	Victoria R=3 NBCC 95	
	Small (15x30)	Medium (30x60)	Large (60x120)	Small (15x30)	Medium (30x60)	Large (60x120)	Small (15x30)	Medium (30x60)	Large (60x120)	Double (30x120)	Small (15x30)	Medium (30x60)
T=1.5Ta	0.27	0.31	0.39	0.27	0.31	0.39	0.27	0.31	0.39	0.31	0.18	0.22
$T_{analytical}$	0.63	0.69	0.97	0.59	0.80	0.94	0.76	1.20	1.62	N/A	0.39	0.56
$S_{UHS}(T_{anal})$ / S (1.5Ta)	0.52	0.51	0.37	0.54	0.44	0.40	0.32	0.20	0.18	N/A	0.90	0.60
$S_{UHS}(T_{anal})/ S_{ground\ motion}(T_{anal})$												
Short period	0.97	0.87	0.65	1.02	0.63	0.65	0.97	0.93	0.78	N/A	5.73	2.79
Long period	0.99	1.05	0.96	0.99	0.97	0.99	0.89	1.07	1.33	N/A	3.94	3.53
Cascadia	1.64	1.59	1.27	1.59	1.50	1.37	N/A	N/A	N/A	N/A	N/A	N/A

The fundamental period of the building, $T_{ANALYTICAL}$, from Medhekar's formula was not equal to the period used in the design procedure. The period used in the design of the buildings was equal to $1.5T_a$, T_a being the formula given in the code. In all cases, $T_{ANALYTICAL}$ was longer than the design period since Medhekar's formula takes into account the flexibility of the system, whereas the other formula does not. For example, for the medium size building with R_d=3.0 in Victoria, the design period ($1.5T_a$) was equal to 0.31 s compared to a fundamental period equal to 0.69 s. In addition, the ratios of the UHS spectral values for the fundamental period to the UHS spectral value of the design period (S_{UHS} (T_{ANAL})/ S_{UHS} (1.5Ta)) are presented. The values show that the spectral values at the design period are greater than at the analytical period. For Victoria, the ratios vary from 0.37 to 0.54. For Quebec, the ratio are smaller than for Victoria as the values vary from 0.18 to 0.32. Besides, the ratio of the UHS spectral values at the fundamental period to the spectral values of the ground motions at the same period (S_{UHS} (T_{ANAL})/ S ground motion (T_{ANAL})) are given. The values presented are average of ratios for 3 ensembles of ground motions: short period (A, B, G for Victoria, M and O for Quebec), long period (C, D and H for Victoria, N and P for Quebec) and Cascadia (E and F). For intra-plate ground motions in Victoria, the ratios vary between 0.63 and 1.05. These ratios are larger for Cascadia earthquakes, varying from 1.27 to 1.64. However, these values are computed with the Victoria UHS and not with the spectrum related to the Cascadia hazard. If the latter was used, the ratios would vary from 0.77 to 0.90. It must be noted that the scaling factors for Cascadia ground motions (E and F) were chosen by matching the ground motion spectra with the Cascadia spectrum, not the Victoria UHS. For Quebec, the ratios vary between 0.78 and 1.33. For the NBCC 1995 designs, the ratios ($S_{UHS}(T_{ANAL})$/ S_{UHS}(1.5Ta)) vary between 0.60 and 0.90. The ratios $S_{UHS}(T_{ANAL})$/ S ground motion (T_{ANAL}) are much greater than for NBCC 2004 since they vary between 2.79 and 5.73.

The buildings located in Quebec exhibited a very low or no inelastic demand in the roof deck. In contrast the demand on the structures in Victoria that were designed with the same R_d factor was much higher. In the case of Quebec City, the ratio of S values for $T_{ANALYTICAL}$ normalised to the design period was smaller than that determined for Victoria. The design period was much shorter than that obtained from the analytical equation, which caused the calculated equivalent static seismic forces to be much larger than the loads experienced during the nonlinear computer runs. Hence, the buildings had a significant strength in reserve, and hence the diaphragm did not enter into the inelastic range.

For Victoria, intra-plate earthquakes (A, B, C, D, G, H) created much greater demand than Cascadia earthquakes (E, F). For intra-plate ground motions, the maximum γ_p values were in the range of 10.0–11.0 rad/1000 for small and medium buildings with an R_d=3.0 factor, which can be compared with values between 1.0-2.0 rad/1000 under Cascadia ground motions. This may be attributed to the fact that Cascadia ground motions had lower spectral values at the fundamental period in comparison to the intra-plate ground motions. For instance, for the Victoria R_d=3.0 medium building, the ratio $S_{UHS}(T_{ANAL})$/ S ground motion (T_{ANAL}) was greater for Cascadia (1.59) in comparison to the short period records (0.87) and the long period records (1.05). It has to be mentioned that the buildings subjected to the Cascadia ground motions were subjected to a larger number of cycles than under intra-plate ground motions as shown in Figure 3.23. Cascadia ground motions were of much longer duration than intra-plate records and, as discussed in Chapter 4, the number of loading cycles was much greater. For the medium size building with R_d=3.0 in Victoria, the most demanded deck panel experienced around 50 cycles in average under intra-plate earthquakes in comparison to 240 under Cascadia ground motions. The detrimental effect of such a large number of inelastic cycles can be such that the condition under Cascadia earthquakes could be more critical

than under intra-plate earthquakes and that it would be worth verifying that situation in tests.

Effect of R_d:

Force modification factors of R_d equal to 2.0 and 3.0 were used in the analyses. As anticipated, for Victoria, the results showed that the γ_p values are greater for R_d=3.0 than those for R_d = 2.0 (see Table 3.18). With regard to the γ_p / γ_u ratios, the ratios were also higher for R_d = 3.0 in comparison to R_d = 2.0 (see Table 3.19). The values for Victoria R_d=2.0 were close to 1.0. For Victoria R_d = 3.0, the mean γ_p / γ_u value for each model was between 1.13 and 5.19, hence, they were more or less centred around 2.0. However, values of 10.5 and 12.5 were obtained for the medium size building with R_d = 3.0 in Victoria under ground motions A and G. The γ_u was very small for the medium building (0.84 rad/1000) in comparison to other designs and it is possible that this explains the higher ratios. However, this does not fit with the assumptions made previously in Figure 3.27. It seems that γ_p is not proportional to R_d, as expected (much higher values of γ_p with R_d = 3.0 than with R_d = 2.0). This may be attributed to the hysteretic model involving pinching used with screw-nail designs. The inelastic demand seems to grow very rapidly when R_d increases from 2.0 to 3.0.

Effect of building dimensions:

For Victoria R_d= 3.0 under intra-plate earthquakes, the small and medium buildings exhibited comparable inelastic distortion demand in the diaphragm members. The large size building had a much lower inelastic demand. For Victoria R_d= 3.0 under Cascadia earthquakes, the small and medium buildings again had comparable demand. Again, the large building experienced less of an inelastic demand. For Victoria with R_d= 2.0, the observations were similar. However, in this case, the medium building was subjected to

less of an inelastic demand in the diaphragm than the small building for Cascadia earthquakes. The fact that the large buildings experienced lesser inelastic demand in comparison to smaller ones may be explained by the fact that the ratios of the spectral value at the fundamental period to the spectral value at the design period were smaller for the larger buildings. The double building experienced similar inelastic distortion in comparison to the medium $R_d = 3.0$ building.

Effect of the period:

The ground motions used for the analyses have varied spectra compared to the Uniform Hazard Spectra. An attempt has been made to match the UHS by scaling the ground motion records, however, it is possible that for a certain period, for example the fundamental period of the building, the scaled values may be different from the UHS values.

The results suggested that the lateral drift requirements would be respected for a building designed with the procedure adopted, i.e. NBCC 2004 seismic load with a weak diaphragm. The results also indicate that the buildings in Quebec would generally experience smaller deformations than for Victoria. In addition, the NBCC 2004 method to predict inelastic drifts was found to be conservative.

In terms of ductility demand, the performance is adequate with $R_d = 3.0$ except that the ductility demand in some cases was found to be near the limit of 10.0 rad/1000 and considering the limited number of cases studied (in terms of E/Q records and building geometries), the ductility demand might exceed the capacity of the system in some other cases.

For button punch-weld designs with NBCC 1995, the performance is inadequate. The results are from an hysteresis model that did not reproduce the test results (shape of

hysteresis, strength degradation). Nevertheless, based on Essa *et al.* (2001) tests, this study clearly shows that the demand will very likely exceed by far the deformation capacity for that system and that extensive damage, even loss of structural integrity, can be anticipated. Again, this should be verified by tests in which a realistic estimate of the anticipated demand is applied.

CHAPTER 4

CHOICE OF LOADING PROTOCOLS

In this chapter, the choice of loading protocols for the seismic testing of the steel deck diaphragm specimens is presented. The loading protocols were used for the dynamic testing of full-scale diaphragms, discussed in Chapter 5. The loading histories were developed such that the diaphragm demand obtained from the analytical investigation of this project (Chapter 3) would be imposed on the deck panel test specimens.

Chapter 4 begins with a discussion of the parameters considered for the development of the loading protocols. This is followed by a statistical analysis of the analytical results, which was performed to evaluate a representative demand to be used in testing. Finally, the established loading protocols are described.

4.1 GENERAL REMARKS

A representative loading protocol for testing structural components in the laboratory must reflect as closely as possible the demand anticipated in the field for that component in the actual building structure. The behaviour and deterioration of diaphragms subjected to seismic loading, as described previously, is used in the development of the loading protocols.

Inelastic response for mechanical frame fasteners like nails is mainly governed by bearing and tearing of the steel sheet material. This phenomenon was observed by Essa *et al.* (2001). Therefore, damage only occurs when contact develop between the sheet and the connector, i.e., in cycles where the imposed deformation is larger than in

previous cycles. Therefore, the key parameter that was selected to quantify the damage to the diaphragms studied is the absolute value of the peak plastic deformation, γ_p, reached during the ground motion. The absolute value was chosen as the direction has no effect on the damage imposed on the deck. In addition, the maximum value reached over the diaphragm area in each analysis was retained.

Although the peak value of γ_p represents the key measure of the damage to diaphragms, the inelastic response of diaphragms during a particular seismic ground motion is likely to also depend on the whole deformation history that is imposed during the ground motion (see Figure 4.2). For instance, failure that may develop in some of the fasteners at a given deformation level during an earthquake can influence the force or displacement demand on the remaining fasteners for the rest of the ground motion. If a deck panel distorts on one side, the connection creates a hole along the movement of the connector (see Figure 4.1). On one hand, this hole means a loss of stiffness when the connector is in the middle of the hole. However, when the connector hits one side of the hole, the stiffness of the connector increases. This explains the increase of the diaphragm stiffness at large displacements. If the displacement range is in the intermediate zone where the connectors are in the middle of their slot, there is not much damage. As said, damage deterioration occurs at the peaks. Therefore, it was believed that the loading protocol had to reproduce the deformation history typically observed in the buildings studied. Parameters such as the number and amplitude of all inelastic cycles experienced by diaphragms were therefore also examined. The maximum in the positive range and minimum in the negative range are considered as peaks (Max and min in Figure 4.2). In addition, the rate of deformation was also studied in order to impose strain rates in the tests that would mimic those imposed during real earthquakes.

Figure 4.1 Schematic view of a slot in steel sheet

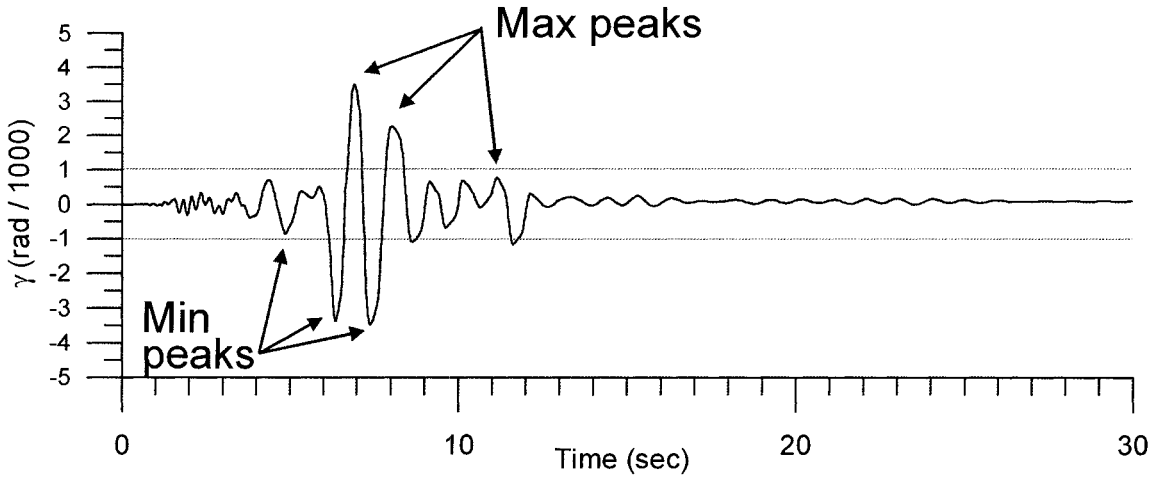

Figure 4.2 Typical deck panel distortion time history

4.2 STATISTICAL ANALYSIS OF THE RESULTS

In order to establish loading protocols for the diaphragm test specimens, a statistical analysis based on the remarks made in the previous section was performed. The number of peaks (pseudo-cycles) in different displacement ranges, which are based on the γ_u and γ_2 shear distortion limits, was evaluated. In the elastic range, the limits were determined using γ_u, whereas in the inelastic range fixed distortion values were relied on. This approach was used because strength and stiffness deterioration depends largely on the distortion amplitude attained during seismic loading and the number of cycles at these amplitudes. Table 4.1 presents the ranges of deformation amplitudes that were selected to characterise the diaphragm deformation response. These include elastic cycles (below γ_u) as well as inelastic cycles (beyond γ_u).

Table 4.1 Distortion ranges considered

1st	$0.2\,\gamma_u \leq \gamma < 0.6\,\gamma_u$
2nd	$0.6\,\gamma_u \leq \gamma < 1.0\,\gamma_u$
3rd	$\gamma_u \leq \gamma < \gamma_2$
4th	$4.0 \leq \gamma < 8.0$ rad/1000
5th	$\gamma \geq 8.0$ rad/1000

The intervals chosen cover the whole range of observed deformations. In addition, the number of ranges was found to be sufficient to capture with adequate accuracy the various amplitude cycles that were obtained in the analyses. Cycles below 0.2 γ_u were deemed not to produce any damage and were therefore neglected. The amplitude of 0.6 γ_u corresponds to the demand under factored loads (resistance factor = 0.6 for mechanical fasteners) and that value was retained as a range limit. The deformation equal to 1.0 γ_u corresponds to the theoretical deformation where S reaches S_u, assuming elastic response. This value is likely to be commonly used as a reference in design and it was deemed appropriate to characterise the number of cycles between 0.6 and 1.0 γ_u. The deformation γ_2 corresponds to the actual deformation at peak load and it was also found of interest to distinguish between the cycles at γ_u and those beyond which inelastic deformations really take place. For the cycles with inelastic deformation, γ value were used instead of a multiple of γ_u. This choice was made because in Chapter 3, no relationships between γ_p / γ_u and R_d were found, thus it was not possible to express γ_p as a function of γ_p / γ_u. As shown, two intervals were selected for the inelastic deformation cycles. Although ranges of γ were used to count the peaks of inelastic cycles in that section, the γ values were transformed into γ_p (by removing γ_u of the deck diaphragm studied) when developing the loading protocols, γ_p being a more direct measure of damage as described earlier. This is discussed in the next section.

Except for the M, N, O and P ground motions, the deck distortion time histories were not considered in their entirety. In fact, the results of the nonlinear analyses at the beginning and end of the seismic records were not processed because they were not considered relevant. Table 4.2 shows the time intervals considered for each ground motion.

Table 4.2 Time intervals processed

Ground motions	Time interval	
	Start (sec)	End (sec)
A	0	12
B	0	30
C	4	23
D	8	22
E	0	100
F	0	100
G	2	19
H	6	20

Table 4.3 presents the statistical analysis performed for the medium size building designed with R_d= 3.0 in Victoria with the screwed-nailed connection pattern. For each distortion range in each direction, the number of peaks, n, the average amplitude of the peak distortions in rad/1000, AVE, and the standard deviation of the amplitude of the peaks in rad/1000, SD, are presented. The same procedure was followed for the other buildings studied and the results are presented in Appendix A.

Table 4.3 Statistical analysis for medium building Rd=3.0 in Victoria

Characteristics of the deck distortion

Victoria Rd=3
Medium building (30 m x 60 m)
Screw- Nail connector pattern
gamma u= 0.84 rad/1000

N.B.: Ave.and SD are deck distortions in rad/1000

E/Q			0.2-0.6 gamma u	0.6-1.0 gamma u	1.0-1.42 gamma u	1.198-4.0 rad/1000	4.0 - 8.0 rad/1000	> 8.0 rad/1000	Total
A	Positive	n	3	1	0	7	0	0	11
		Ave.	0.23	0.52	N/A	1.64	N/A	N/A	
		SD	0.06	N/A	N/A	0.65	N/A	N/A	
	Negative	n	7	3	3	6	0	2	21
		Ave.	-0.39	-0.61	-0.92	-2.28	N/A	-9.34	
		SD	0.09	0.08	0.06	0.46	N/A	0.50	
B	Positive	n	8	5	1	6	0	0	20
		Ave.	0.37	0.65	0.91	2.33	N/A	N/A	
		SD	0.06	0.06	N/A	0.83	N/A	N/A	
	Negative	n	29	6	5	5	2	0	47
		Ave.	-0.32	-0.66	-1.13	-1.78	-4.56	N/A	
		SD	0.09	0.14	0.06	0.45	0.24	N/A	
C	Positive	n	10	8	6	5	0	0	29
		Ave.	0.29	0.68	1.09	1.99	N/A	N/A	
		SD	0.11	0.08	0.09	0.62	N/A	N/A	
	Negative	n	8	5	5	5	0	0	23
		Ave.	-0.37	-0.68	-0.94	-1.35	N/A	N/A	
		SD	0.10	0.10	0.09	0.15	N/A	N/A	
D	Positive	n	4	6	11	12	1	0	34
		Ave.	0.39	0.66	1.07	1.71	4.80	N/A	
		SD	0.09	0.13	0.09	0.70	N/A	N/A	
	Negative	n	4	5	2	0	0	0	11
		Ave.	-0.33	-0.61	-1.00	N/A	N/A	N/A	
		SD	0.11	0.08	0.21	N/A	N/A	N/A	
G	Positive	n	6	7	2	3	0	0	18
		Ave.	0.27	0.56	0.90	1.91	N/A	N/A	
		SD	0.07	0.04	0.02	0.91	N/A	N/A	
	Negative	n	4	0	0	29	4	2	39
		Ave.	-0.22	N/A	N/A	-3.21	-5.44	-10.82	
		SD	0.06	N/A	N/A	0.61	0.86	0.76	
H	Positive	n	7	2	3	5	0	0	17
		Ave.	0.30	0.69	0.96	3.04	N/A	N/A	
		SD	0.11	0.07	0.07	0.96	N/A	N/A	
	Negative	n	5	2	2	9	0	0	18
		Ave.	-0.38	-0.57	-0.87	-2.28	N/A	N/A	
		SD	0.10	0.01	0.02	0.77	N/A	N/A	

Comparison

0.2 gamma u	0.17 rad/1000
0.6 gamma u	0.51 rad/1000
1.0 gamma u	0.84 rad/1000
1.42 gamma u	1.20 rad/1000

As shown, there were considerable variations in the results obtained from one building or from one ground motion to the next, and careful interpretation was needed to come up

with a simplified, yet realistic, estimate of the demand for each combination of R_d and type of ground motion. For the number of peaks in each deformation interval, a range or a unique number was determined which was deemed representative of the maximum number of peaks observed for all buildings sizes and ground motions. This was done for each combination of R_d-ground motion type, as well as for the buildings and ground motion used for the NBCC 1995 buildings. For each deformation interval, a reference deformation was selected, which corresponded to the average deformation of the interval. In that process, the γ value were transformed into γ_p for the cycles with $\gamma > \gamma_u$, as discussed earlier.

For button punch-weld design analysis, the number of peaks, n, was affected by an oscillation, at a relatively high frequency, of the output deck distortion from the Ruaumoko analyses. Hence, the number of peaks would be significantly overestimated if a filtering technique had not been used. The author chose to neglect the peaks which were not relevant, based on the following criteria. If between two peaks the distortion diminished by 20%, both peaks were considered in the statistical evaluation of deck distortion. If the drop was less than 20% only the first peak was considered. The analysis of the time history results was subjective and the final number of peak distortion values can only be considered as approximate.

Table 4.4 presents the values that were deemed representative of the demand for the screw-nail design with NBCC 2004. In the table, the distortion level that was reached most often is presented first, followed by those with a decreased demand, except for the Cascadia earthquake results which are listed separately (see Table 4.5). The buildings located in Victoria with R_d= 3.0 experienced the greatest demand, followed by Victoria R_d= 2.0 and Quebec with R_d= 3.0. Δt is defined as the approximate time interval between two peaks in the same range (positive or negative).

Table 4.4 Demand characteristics for NBCC 2004 designs under intra-plate earthquakes

Site and R_d factor	Number of cycles	Distortion level	Δt (sec)
Victoria R_d= 3.0	8-15	0.4 γ_u	0.6-0.7
	5 –10	0.8 γ_u	0.6-0.7
	1	0.95 γ_u	
	4	$(\gamma_u + \gamma_2)/2$	
	3	γ_p= 3.0 – 4.0 rad/1000	
	2	γ_p = 8.0 rad/1000	
	1	γ_p = 10.0 rad/1000	
Victoria R_d= 2.0	8-15	0.4 γ_u	0.6-0.7
	5 –10	0.8 γ_u	0.6-0.7
	1	0.95 γ_u	
	3	γ_p = 3.0 –4.0 rad/1000	
Quebec R_d= 3.0	10-15	0.4 γ_u	1.0
	5	0.75 γ_u	1.0
	1	0.95 γ_u	

Δt is presented only for cycles of lower amplitudes. The cycles of larger amplitudes were separated between peaks of smaller amplitudes hence it was felt that Δt was not relevant for larger peaks.

Cascadia ground motions produced a different demand on the models. A larger number of cycles was present in Cascadia time histories in comparison to other ground motions. In addition, the shapes of the distortion time histories were different. The reader is

invited to look at the deck distortion time histories in Chapter 3 to observe this behaviour.

Table 4.5 Demand characteristics for NBCC 2004 designs under Cascadia earthquakes

Site and R_d factor	Number of cycles	Distortion level	Δt (sec)
Cascadia R_d=3.0	80	0.4 γ_u	0.6-0.7
	30	0.8 γ_u	0.6-0.7
	10	$(\gamma_u + \gamma_2)/2$	0.6-0.7
	10	2 γ_u	0.6-0.7

The demand for the button punch-weld designs is presented in Table 4.6. As noted previously, analyses of this structure were carried out to determine the demand on buildings designed under NBCC 1995 with an accidentally weak diaphragm.

Table 4.6 Demand characteristics for NBCC 1995 designs

Site and R factor	Number of cycles	Distortion level	Δt (sec)
Victoria R= 3.0	5-10	0.4 γ_u	
	5	0.8 γ_u	
	2	γ_p=1.0–3.0 rad/1000	
	3	γ_p=3.0–4.0 rad/1000	
	1	γ_p = 8.0 rad/1000	

From Table 4.6 and Table 4.4, we can see that the demand (number of cycles in each displacement range and maximum distortion) for the button punch-weld deck assemblies for Victoria with R= 3.0 was similar to the screw-nail connection case for Victoria R_d= 3.0. Hence, the demand for these two cases was considered similar.

4.3 CHOICE OF LOADING PROTOCOLS

Based on the representative values found in Section 4.2, two loading protocols were developed that are illustrated in Figure 4.3: a) short duration (SD) loading protocol; b) long duration (LD) loading protocol. For the LD protocol, only half of the displacement history is shown, that is the signal shown is repeated twice and the total duration is 93.6 s. As indicated, both signals in Figure 4.3 were produced assuming γ_u = 1 rad/1000. The amplitude of the signal for a particular diaphragm varies as it is a function of γ_u, a parameter that can vary from one diaphragm to another.

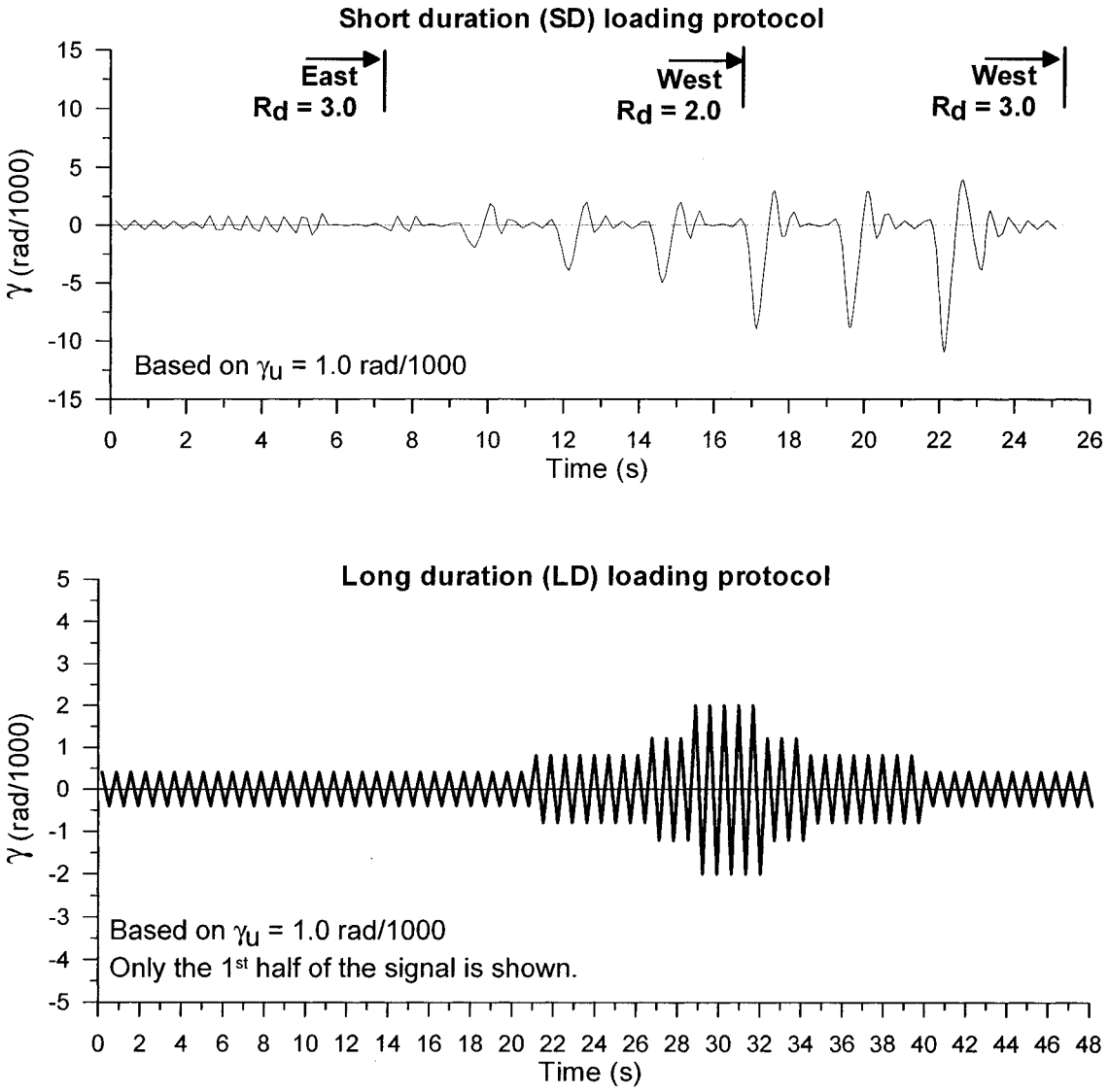

Figure 4.3 SD and LD loading protocols

For the screw-nail connection pattern, it was possible to create the short duration (SD) loading protocol that covered R_d= 2.0 and R_d= 3.0 buildings for Eastern and Western Canada ground motions. Table 4.7 presents the peak distortions for the SD loading protocol. The peak distortions in the protocol were chosen to match the demand from Table 4.4. The demand for East R_d= 3.0 is located in the first 7.12 seconds. 8 peaks of $0.4\gamma_u$, 5 peaks of $0.8\gamma_u$ and 1 peak of γ_u were chosen to match the demand. The demand

for West R_d= 2.0 goes from 0 s to 16.38 s. In this time interval, 16 peaks of $0.4\gamma_u$, 9 peaks of $0.8\gamma_u$, 1 peak of γ_u and 1 peak of $(\gamma_u + \gamma_2)/2$ were used. In addition, 1 peak of $(\gamma_u + 1)$, $(\gamma_u + 3)$ and $(\gamma_u + 4)$ were chosen to match the inelastic demand. The total signal covered the demand for West R_d = 3.0. 22 peaks of $0.4\gamma_u$, 10 peaks of $0.8\gamma_u$, 1 peak of γ_u, 4 peaks of $(\gamma_u + \gamma_2)/2$ were considered. The inelastic demand was covered by 1 peak of $(\gamma_u + 1)$, $(\gamma_u + 3)$, $(\gamma_u + 4)$, 2 peaks of $(\gamma_u + 8)$ and 1 peak of $(\gamma_u + 10)$. Only peaks in the negative ranges are discussed here. The peaks in the positive range are lower in amplitude due to the asymmetry of the signal.

In Chapter 3 (Fig. 3.22, 3.24 to 3.26), the largest cycles were generally observed at mid-length of the ground motion duration. The sequence was re-arranged so that the amplitude of the cycles was continually increasing with time. This way, it was possible to apply the demand for the NBCC 1995, followed by the additional cycles required to reproduce the demand for West R_d = 3.0. The behaviour for the three conditions could be studied by applying only one signal. Each of the three phases finished and started with cycles at 0.4 γ_u, so that the variation in stiffness could be assessed for each phase and compared to the initial stiffness, G'. G' is defined as the secant stiffness at 0.4Su, thus 0.4 γ_u if linear assumption is made. It has been found from visual inspection of distortion time histories that the deck distortion tended to be more or less centred. However, the largest peaks did tend to occur in the negative direction. Accordingly, the loading protocol reflected these observations. The frequency of the loading was chosen to match the frequency found in the statistical analysis. The signal duration was considered similar to the duration of the ground motions considered.

The Cascadia ground motions differed substantially in terms of behaviour, and hence needed to be considered apart. For this reason the long duration (LD) loading protocol was created. The peak distortions of the LD loading protocol are given in Table 4.8. The following imposed distortions were chosen to match the demand from Table 4.5: 80

peaks of $0.4\gamma_u$, 32 peaks of $0.8\gamma_u$, 12 peaks of $(\gamma_u + \gamma_2)/2$ and 10 peaks of $2\gamma_u$. These imposed distortions were both applied in the positive and negative ranges reflecting the relative symmetry in the deck panel distortion time histories. A constant time step between each peak in the same range (positive or negative) was used (0.70 seconds). This timing was observed in deck distortion time histories for the building analyses. In addition, the loading protocol reflected that typically there were two zones of large intensity ground shaking during the Cascadia type earthquakes.

Table 4.7 Peak distortions for the short duration (SD) loading protocol

Time (s)	0.125	0.375	0.625	0.875	1.125	1.375	1.625
γ (rad/1000)	0.4 γ_u	-0.4 γ_u	0.4 γ_u	-0.4 γ_u	0.4 γ_u	-0.4 γ_u	0.4 γ_u
Time (s)	1.875	2.125	2.375	2.625	2.875	3.125	3.375
γ (rad/1000)	-0.4 γ_u	0.4 γ_u	-0.4 γ_u	0.8 γ_u	-0.8 γ_u	0.8 γ_u	-0.8 γ_u
Time (s)	3.625	3.875	4.125	4.375	4.625	4.875	5.125
γ (rad/1000)	0.8 γ_u	-0.8 γ_u	0.8 γ_u	-0.8 γ_u	0.8 γ_u	-0.8 γ_u	γ_u
Time (s)	5.375	5.625	5.875	6.125	6.375	6.625	6.875
γ (rad/1000)	-γ_u	γ_u	-0.4 γ_u	0.4 γ_u	-0.4 γ_u	0.4 γ_u	-0.4 γ_u
Time (s)	7.125	7.375	7.625	7.875	8.125	8.375	8.625
γ (rad/1000)	0.4 γ_u	-0.8 γ_u	0.8 γ_u	-0.8 γ_u	0.8 γ_u	-0.4 γ_u	0.4 γ_u
Time (s)	8.875	9.125	9.625	10.125	10.375	10.625	10.875
γ (rad/1000)	-0.4 γ_u	0.4 γ_u	-(γ_u +1)	(γ_u +1)	-0.8 γ_u	0.8 γ_u	-0.4 γ_u
Time (s)	11.125	11.375	11.625	12.125	12.625	12.875	13.125
γ (rad/1000)	0.4 γ_u	-0.4 γ_u	0.4 γ_u	-(γ_u +3)	(γ_u +1)	-0.8 γ_u	0.8 γ_u
Time (s)	13.375	13.625	13.875	14.125	14.625	15.125	15.375
γ (rad/1000)	-0.4 γ_u	0.4 γ_u	-0.4 γ_u	0.4 γ_u	-(γ_u +4)	(γ_u +1)	-(γ_u+ γ_2)/2
Time (s)	15.625	15.875	16.125	16.375	16.625	17.125	17.625
γ (rad/1000)	(γ_u+ γ_2)/2	-0.4 γ_u	0.4 γ_u	-0.4 γ_u	0.4 γ_u	-(γ_u +8)	(γ_u +2)
Time (s)	17.875	18.125	18.375	18.625	18.875	19.125	19.625
γ (rad/1000)	-(γ_u+ γ_2)/2	(γ_u+ γ_2)/2	-0.4 γ_u	0.4 γ_u	-0.4 γ_u	0.4 γ_u	-(γ_u +8)
Time (s)	20.125	20.375	20.625	20.875	21.125	21.375	21.625
γ (rad/1000)	(γ_u +2)	-(γ_u+ γ_2)/2	(γ_u+ γ_2)/2	-0.4 γ_u	0.4 γ_u	-0.4 γ_u	0.4 γ_u
Time (s)	22.125	22.625	23.125	23.375	23.625	23.875	24.125
γ (rad/1000)	-(γ_u +10)	(γ_u +3)	-(γ_u +3)	(γ_u+ γ_2)/2	-(γ_u+ γ_2)/2	0.8 γ_u	-0.8 γ_u
Time (s)	24.375	24.625	24.875	25.125			
γ (rad/1000)	0.4 γ_u	-0.4 γ_u	0.4 γ_u	-0.4 γ_u			

Table 4.8 Peak distortions for the long duration (LD) loading protocol (for 1st half only)

Time (s)	γ (rad/1000)
0.175	0.4 γ_u
0.525	-0.4 γ_u
0.875	0.4 γ_u
1.225	-0.4 γ_u
Inc.= +0.350	0.4 γ_u
Inc.= +0.350	-0.4 γ_u
21.175	0.8 γ_u
21.525	-0.8 γ_u
Inc.= +0.350	0.8 γ_u
Inc.= +0.350	-0.8 γ_u
26.775	$(\gamma_u + \gamma_2)/2$
27.125	$-(\gamma_u + \gamma_2)/2$
Inc.= +0.350	$(\gamma_u + \gamma_2)/2$
Inc.= +0.350	$-(\gamma_u + \gamma_2)/2$
28.875	2.0 γ_u
29.225	-2.0 γ_u
Inc.= +0.350	2.0 γ_u
Inc.= +0.350	-2.0 γ_u
32.375	$(\gamma_u + \gamma_2)/2$
32.725	$-(\gamma_u + \gamma_2)/2$
Inc.= +0.350	$(\gamma_u + \gamma_2)/2$
Inc.= +0.350	$-(\gamma_u + \gamma_2)/2$
34.475	0.8 γ_u
34.825	-0.8 γ_u
Inc.= +0.350	0.8 γ_u
Inc.= +0.350	-0.8 γ_u
40.075	0.4 γ_u
40.425	-0.4 γ_u
Inc.= +0.350	0.4 γ_u
Inc.= +0.350	-0.4 γ_u

Inc.: Increment of time at each peak. + means add this increment to find the time values at peak.

CHAPTER 5

DIAPHRAGM EXPERIMENTS

The first objective of this research project was to obtain a better knowledge of the anticipated inelastic seismic demand on metal roof deck diaphragms. This was described in Chapters 3 and 4, which included the analytical models and the choice of loading protocols for the experiments. The second objective of the project was to evaluate the response of such diaphragms to seismic activity. Tests of full-scale diaphragms were performed at Ecole Polytechnique to observe and categorise their behaviour. This chapter contains a description and discussion of the laboratory test program, including: set-up, specimen and loading protocol selection, test results and observations.

5.1 TEST SET-UP AND INSTRUMENTATION

Diaphragm tests were performed using a horizontal cantilevered test set-up (3.66 m x 6.10 m) on which steel deck was laid. All tests used 3 intermediate joists and four 914 mm wide steel deck roof panels. The test set-up was developed and used by Essa *et al.* (2001). A full discussion of the test set-up and complete drawings are given in the report by Essa *et al.*.

The test set-up is presented in Figure 5.1 and Figure 5.2. The perimeter members and purlins were made of HSS 203.2 x 203.2 x 7.95 sections. Above these main members, smaller rectangular HSS 101.6 x 50.8 x 4.78 sections were installed. The steel deck was attached to these smaller HSS sections, which were assumed to represent a joist top chord, given their 4.78 mm wall thickness.

Since the installation of welded or nailed connections would damage the smaller HSS framing members, it was decided not to fasten at locations where previous connections were made. Subsequent deck specimens were positioned at 4 different locations over the width of the 101.6 mm wide HSS sections. In addition, 2 lines of connections could be made by sliding the deck by one inch along the length of the frame. Also, the HSS could be turned upside down and the other side of the tubes could be used as the connecting surface. In total, 16 tests could be installed with one set of tubes.

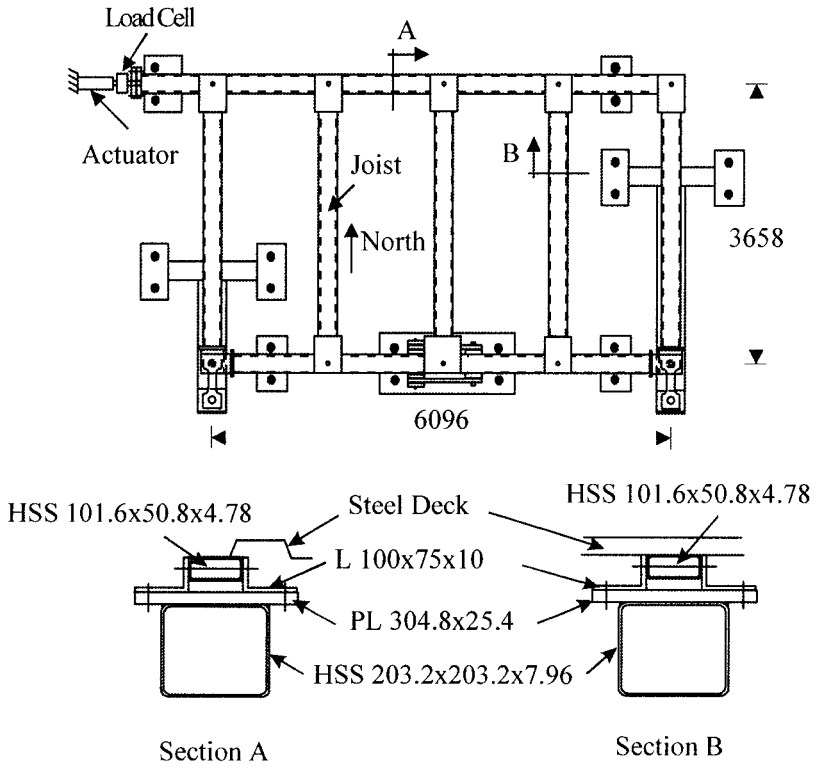

Figure 5.1 Schematic of test set-up (Essa *et al.*, 2001)

The diaphragm experiments were intended to measure the shear forces in the diaphragm. Pinned connections were then used at the junction of the main members, as shown in Figure 5.3 for the South-East corner. The friction at the joints was reduced by introducing 1.6 mm thick teflon sheets lubricated with silicon grease.

Load was applied by a 1500 kN capacity MDT actuator with dynamic capability, which was anchored to the strong floor at one end and fixed to a longitudinal test frame member at the other. Control of the actuator was provided by an MTS Flextest GT system with a 2 kHz frequency closed loop displacement transducer corrected shear distortion protocol. That is, the shear displacement imposed on the test diaphragm was controlled by means of the movements measured by transducers located around the frame. A 222 kN secondary load cell was installed between the actuator and test frame (Figure 5.4).

The dynamic nature of the short and long duration loading protocols created inertia forces due to the mass of the test frame. To evaluate the inertia effects, a 1C Sensor accelerometer (model no. 3140-002) was installed on the main load cell attached to the actuator (see Figure 5.4). The accelerometer could accurately measure acceleration up to ± 2 g and frequency from 0 to 100 Hz. The effect of inertia on the recorded shear forces is further discussed in Section 5.6.

Horizontal restraints of the frame in the N-S and E-W directions were provided by means of special steel elements exhibiting a reduced section segment forming a dog bone shape (Figure 5.5). These elements were instrumented with strain gauges in order to measure the reaction developed at the horizontal supports. The readings from the dog bones were calibrated in a testing machine prior to installation in the diaphragm test frame. The forces measured from the dog bones during diaphragm testing were compared to the applied force from the actuator to verify that the load was applied and measured correctly. Essa *et al.* (2001) present a discussion on the calibration of the dog bones and the static equilibrium check of loads and reactions for the diaphragm test frame.

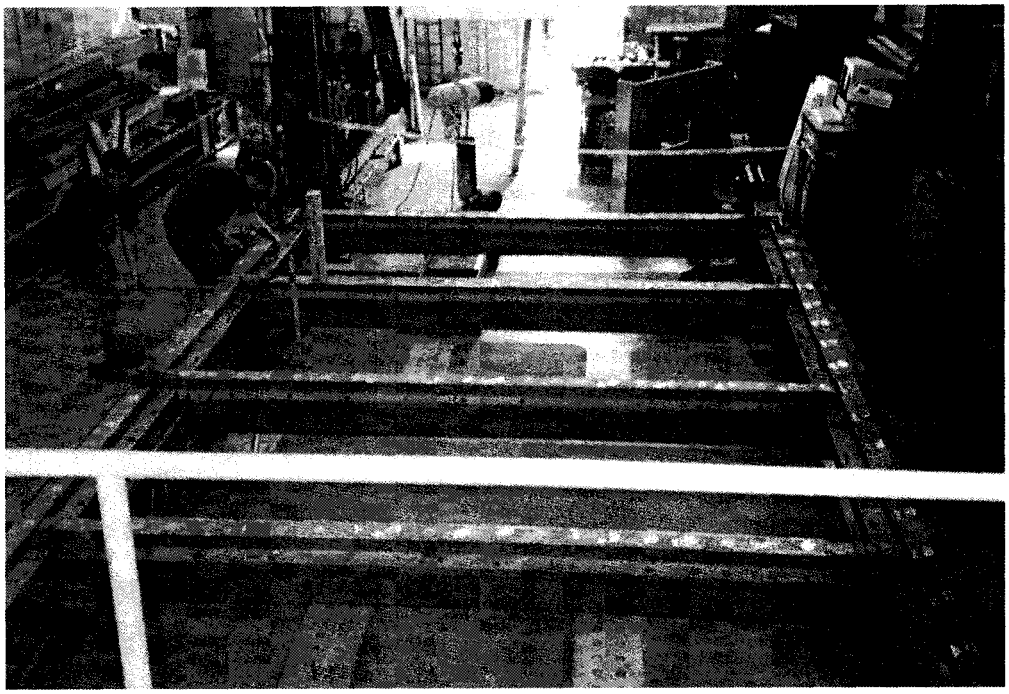

Figure 5.2 Test set-up (Essa *et al.*, 2001)

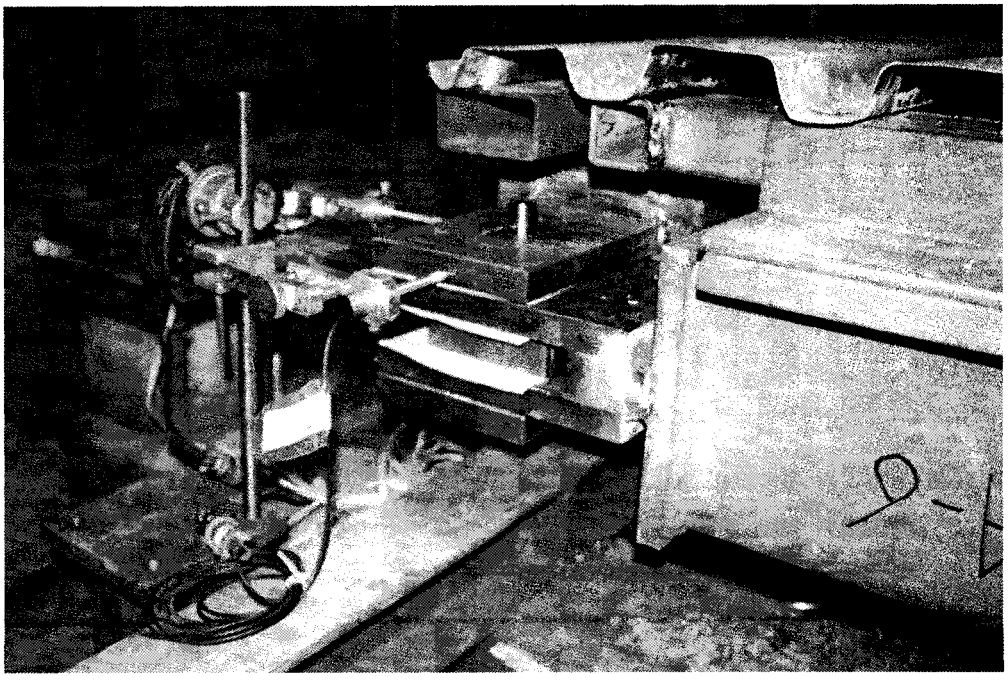

Figure 5.3 Details at South-East corner (Essa *et al.*, 2001)

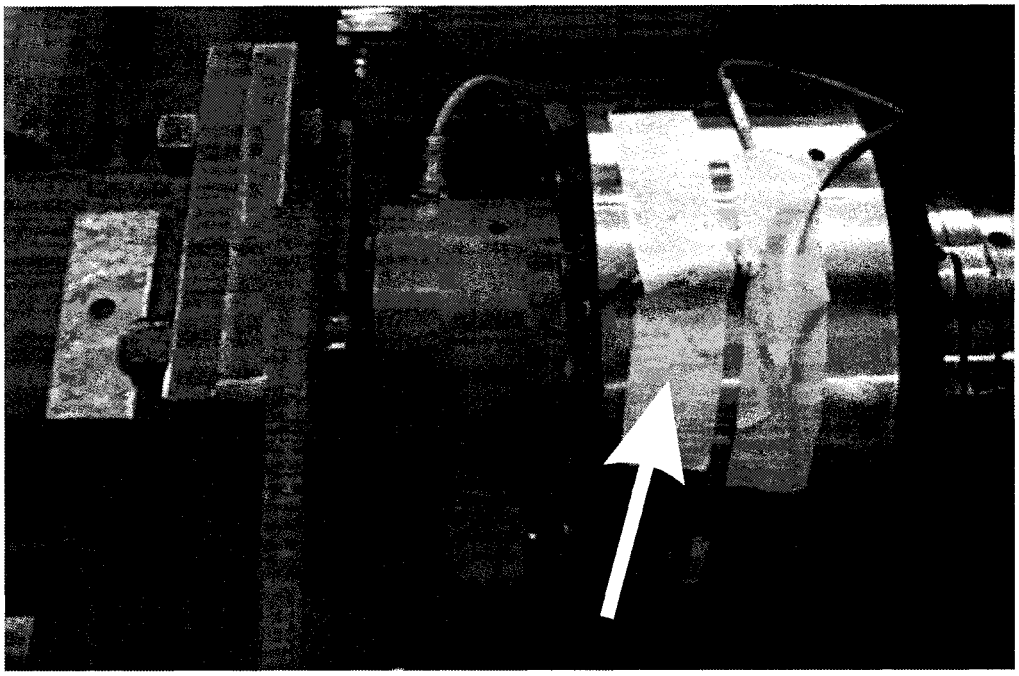

Figure 5.4 Secondary 222 kN load cell (blue) with main load cell and attached accelerometer

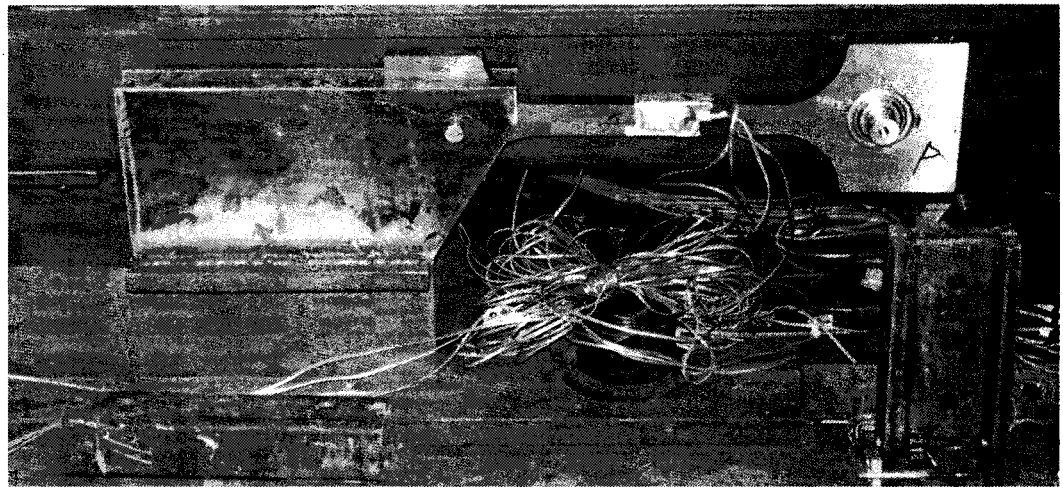

Figure 5.5 Dog-bone assembly restraining the frame in the East-West direction (Essa et al., 2001)

It was necessary to restrain the frame against movements at supports. Figure 5.6 and Figure 5.7 show the connection details used in restraining the frame in the North-South

direction. A W460 x 52 section was attached at two ends to the strong floor. An L-shape member, built of a horizontal and a vertical HSS 8"x 6" x ½", was connected to the W460 x 52. On top of the vertical HSS, a 50.8 mm (2") thick plate was welded. A 38.1 mm (1.5") diameter pin was inserted in a hole in the thick plate and then welded. The dog-bone was fitted on the 38.1 mm pin at one end and at the other end to a 25.4 mm (1") pin fixed to the test frame.

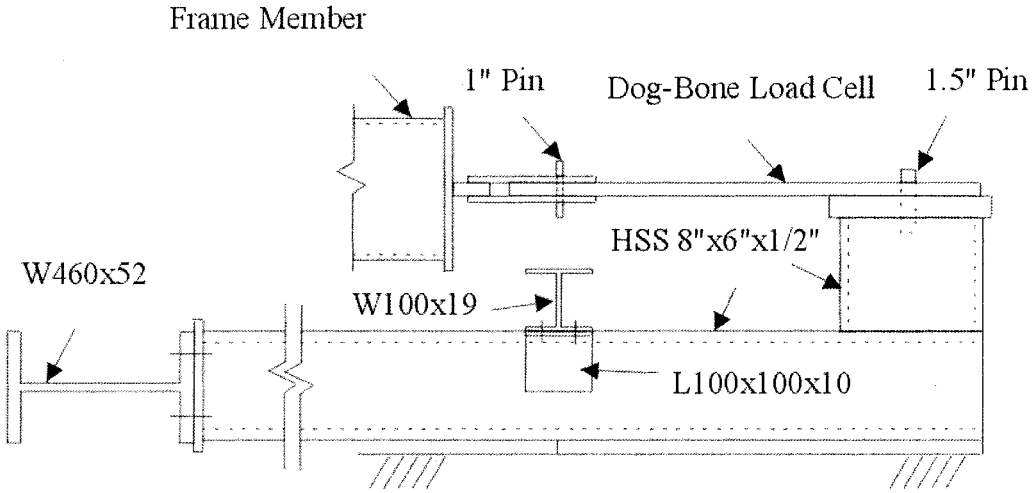

Figure 5.6 Details of restraining the test frame in the North-South direction (Essa *et al.*, 2001)

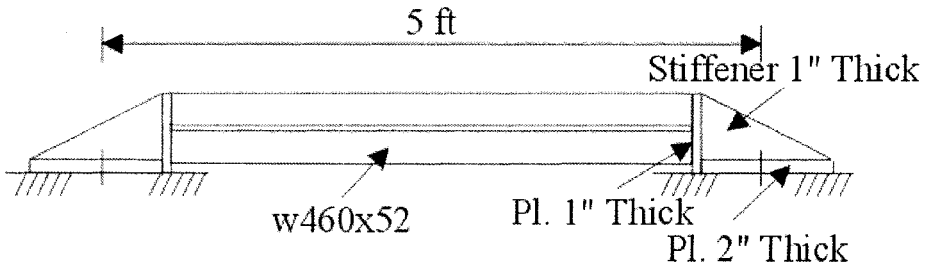

Figure 5.7 Details of anchoring the W460x52 member for the North-South restraint (Essa *et al.*, 2001)

In the East-West direction, a different detail was used to support the test frame (Figure 5.5, Figure 5.8 and Figure 5.9). At the South end of the test set-up, two dog-bones were

placed symmetrically along the frame member. On the East end of the dog-bones, a 38.1 mm (1.5") pin was used to connect the dog-bones to the frame members. On the West end, two 25.4 mm (1") thick plates were placed beside each dog bone. A 25.4 mm (1") diameter pin was inserted connecting the two dog-bones and the 25.4 mm thick plates. These four 25.4 mm plates were connected to a 25.4 mm (1") plate welded to a horizontal W360x57. The W360 x 57 was welded to a 25.4 mm (1") thick base plate that was anchored by four bolts to the strong floor.

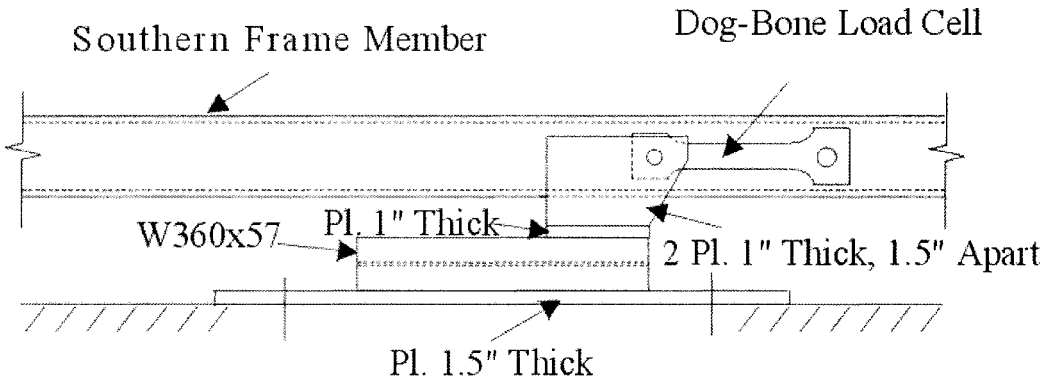

Figure 5.8 Details of supporting the Southern frame member in the East-West direction (Essa *et al.*, 2001)

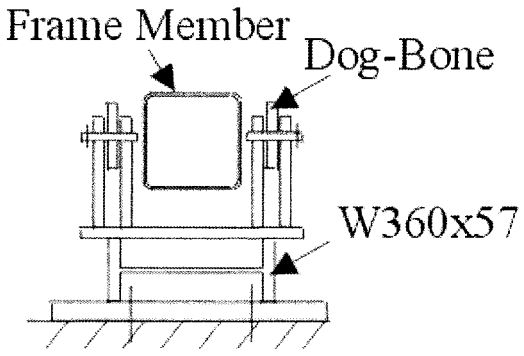

Figure 5.9 Side view of the East-West restraint assembly (Essa *et al.*, 2001)

In addition, the test set-up had to be restrained against vertical movement. Figure 5.10 presents the typical vertical restraint assembly, where two angles were attached to the

sides of the HSS 203.2 x 203.2 x 7.95 frame members. The horizontal legs of the angles were placed underneath a seat plate. The seat plate was welded to a short W shape column that was fixed to the strong floor. Greased teflon sheets were placed between the seat plate and HSS to reduce the frictional forces at supports.

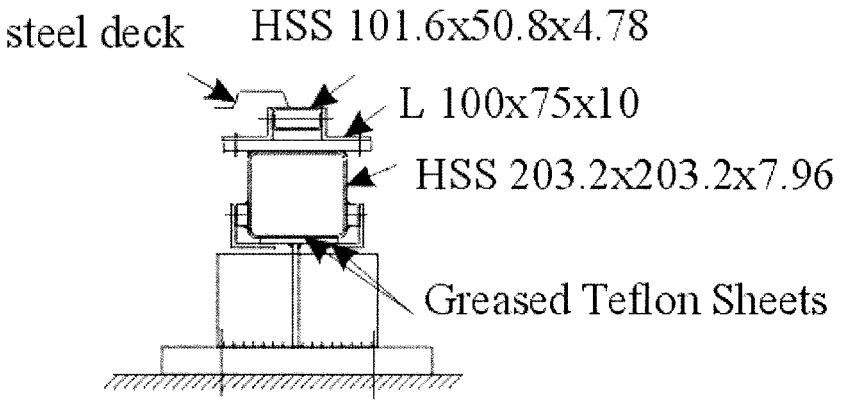

Figure 5.10 Details of vertical supports (Essa *et al.*, 2001)

To evaluate the importance of friction, a cyclic test was performed with the bare frame. The friction forces (1 kN maximum) due to the pin corner and purlin connections and seat plates were deemed to be negligible, and hence the recorded test results were not adjusted to take the frame friction into account.

As shown in Figure 5.11, the frame deflection was measured at five locations: A to E. At the North-East corner, the East-West deflection (A) was measured using a linear potentiometer with a 150 mm range. At the South-East and South-West corners, deflections along both main frame directions (B to E) were measured using LVDT's with a ± 5 mm stroke.

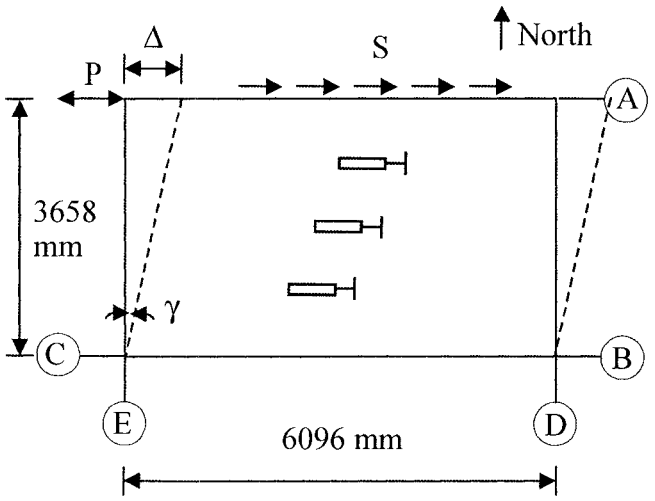

Figure 5.11 Measured displacements to monitor support movements (adapted from Essa *et al.*, 2001)

The displacements at the South-East and South-West corners were related to the support movements. They were used to correct the East-West displacements, A, and to determine the true diaphragm deflections according to the following formula:

$$\Delta = A - \frac{B+C}{2} - (E-D)\frac{3658}{6096} \qquad (5\text{-}1)$$

Due to the small dimensions of the test set-up and the rigidity of the framing members, the bending deformations were negligible. Equation 5-1 was introduced in the control loop of the actuator so that the control during the dynamic tests was performed on the corrected diaphragm deflection, not the gross deflection.

In this project, the distortion, γ, was used to assess the shear deformation level of the diaphragm. Therefore, the corrected displacement, Δ, in metres was transformed to obtain the distortion γ in radians: $\gamma = \Delta/3.658$. Also, the shear flow, S, was used to represent the force in the system. In consequence, the force at the load cell, P, in kN was converted to shear in kN/m by the following formula: S= P/6.096.

The slip at deck-to-frame and sidelap connections was measured using displacement transducers with ±15 mm or ±25 mm stroke. Along the North and South sides of the set-up, the LVDTs were attached to the frame members to measure slip between the frame and the deck panels (see Figure 5.12). At sidelap locations two independent LVDTs on either side of the sidelap were mounted on the frame below the deck, with an angle fixed under the deck to support the tip of the measuring devices. In this fashion the movement of each deck panel was measured and the slip could be calculated from the relative difference between the two readings. This approach was reliable since the LVDTs were fixed to a stable element and were not subject to errors caused by distortion of the deck panels. In addition, two independent measurements of slip of each panel with respect to the frame were made.

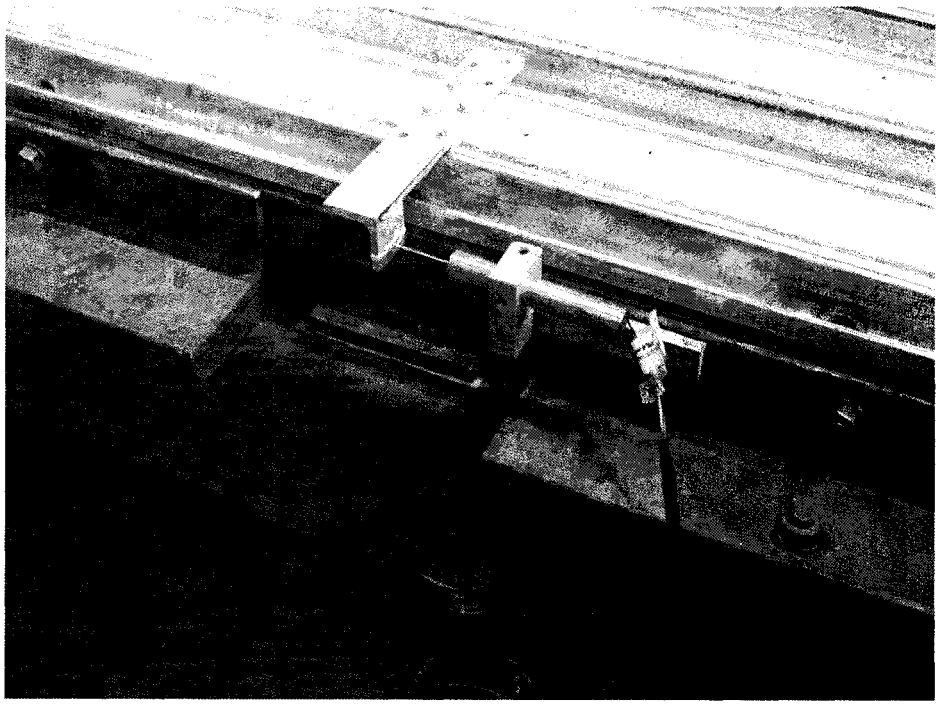

Figure 5.12 Measuring deck-to-frame slip

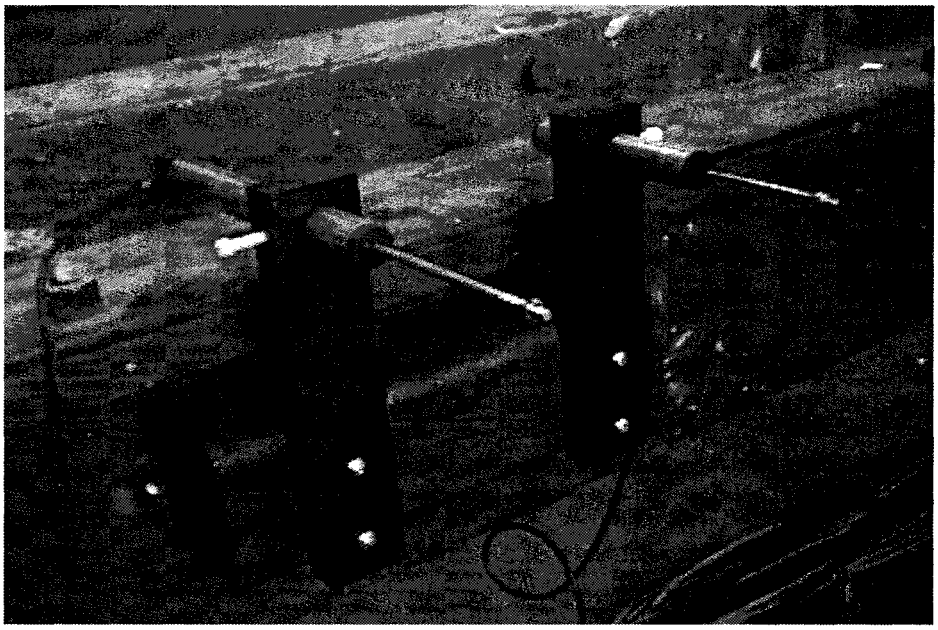

Figure 5.13 Measuring sidelap slips using LVDTs attached to frame

5.2 CHOICE OF TEST SPECIMENS AND LOADING PROTOCOLS

A diaphragm test series had been carried out by Essa *et al.* (2001) prior to this investigation. A total of 18 diaphragm tests had been performed in which nine combinations of deck-to-frame and sidelap connections were used. Diaphragms were subjected to monotonic and quasi-static cyclic loading as indicated in Table 5.1.

The sidelap fasteners were either button punched, screwed or welded whereas the deck-to-frame fasteners were welded, screwed or welded with washer. In all tests, the fastener arrangement was kept the same, with a 305 mm c/c spacing for sidelap and deck-to-frame connections.

Table 5.1 Test series carried out by Essa *et al.* (2001)

Test	Sidelap [1]	Frame [1]	Deck profile	Loading protocol
38-76-6-WB-M-1	b. p.	welded[2]	P3615 0.76 mm	Monotonic
38-76-6-WB-Q-2	b. p.	welded[2]	P3615 0.76 mm	Quasi-static
38-76-6-SS-M-3	screwed	screwed	P3615 B 0.76 mm	Monotonic
38-76-6-NS-M-4	screwed	nailed (H)	P3615 B 0.76 mm	Monotonic
38-76-6-NS-M-5	screwed	nailed (B)	P3615 B 0.76 mm	Monotonic
38-76-6-SS-Q-6	screwed	screwed	P3615 B 0.76 mm	Quasi-static
38-76-6-NS-Q-7	screwed	nailed (H)	P3615 B 0.76 mm	Quasi-static
38-76-6-NS-Q-8	screwed	nailed (B)	P3615 B 0.76 mm	Quasi-static
38-76-6-WW-M-9	welded[4]	welded[2]	P3615 0.76 mm	Monotonic
38-76-6-W'W-M-10	welded[4]	w. w. washer[3]	P3615 0.76 mm	Monotonic
38-76-6-WS-M-11	screwed	welded[2]	P3615 B 0.76 mm	Monotonic
38-76-6-WW-Q-12	welded[4]	welded[2]	P3615 0.76 mm	Quasi-static
38-76-6-W'W-Q-13	welded[4]	w. w. washer[3]	P3615 0.76 mm	Quasi-static
38-76-6-WS-Q-14	screwed	welded[2]	P3615 B 0.76 mm	Quasi-static
38-76-6-W'S-M-15	screwed	w. w. washer[3]	P3615 B 0.76 mm	Monotonic
38-76-6-W'S-Q-16	screwed	w. w. washer[3]	P3615 B 0.76 mm	Quasi-static
38-91-6-NS-M-17	screwed	nailed (H)	P3615 B 0.91mm	Monotonic
38-91-6-NS-Q-18	screwed	nailed (H)	P3615 B 0.91mm	Quasi-static

Notes:
(1): Nailed connections with Hilti (H) X-EDNK22-THQ12 and Buildex (B) BX-12 fasteners for nailed connections, 12-24x7/8'' fasteners for screwed structural connections, and 12-14x7/8'' fasteners for screwed sidelap connections.
(2): Welded frame connections were made with 19 mm diameter arc spot welds.
(3): Mix of welds and welded with washer frame connections.
(4): Welded sidelap connections were made with 35 mm long welds.

In all tests, intermediate rib galvanised sheets with a nominal depth of 38 mm were used. The steel deck conformed to ASTM Standard A653 (2002) with zinc thicknesses corresponding to the Z275 designation. Tests were performed with 0.76 mm nominal thickness deck except 2 tests with 0.91 mm. Two types of intermediate rib deck profiles were used: standard (interlock) and B-deck (nestable) (see Figure 5.14). The edge profile used depended on the type of sidelap fastener chosen. For example, button punched

sidelap connections were used with standard deck whereas screwed sidelap connections required B-deck panels.

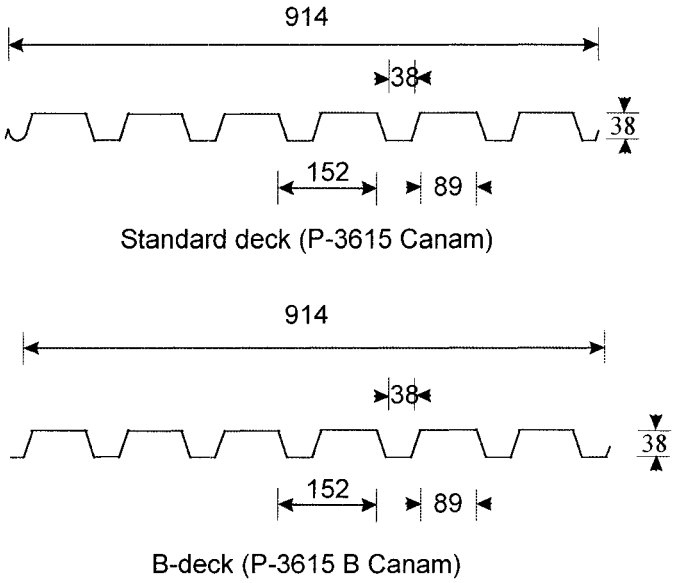

Figure 5.14 Deck profiles (adapted from Essa *et al.*, 2001)

The diaphragm tests by Essa *et al.* showed that ductile inelastic diaphragm behaviour under seismic loading could be achievable provided that proper fastener systems were used. The most promising systems were made of welded-with-washer, nailed or screwed deck-to-frame connections in combination with screwed sidelap connections. Button punched sidelap fasteners performed poorly and are of a questionable reliability. Limited ductility and inability to sustain cyclic loading were observed when using welded deck-to-frame fasteners.

Based on findings from Essa *et al.* and the evaluated anticipated seismic demand (Chapter 3), a new test series was proposed and carried out (see Table 5.2). Test specimens were subjected either to monotonic, short duration or long duration loading

protocols. The basis of the simulated seismic SD and LD loading protocols is discussed in Chapter 4.

Table 5.2 Test series list

Test	Sidelap	Frame	Deck profile	Loading protocol
38-91-6-NS-M-19	Screwed	nailed (H) [1]	P3615B 0.91 mm	Monotonic
38-76-6-WB-SD-20	b. p.	welded [2]	P3615 0.76 mm	Short duration
38-91-6-WB-SD-21	b. p.	welded [2]	P3615 0.91 mm	Short duration
38-91-6-W'W-M-22	w.w.w.[3]	w.w. washer [4]	P3615B 0.91 mm	Monotonic
38-91-6-W'W-SD-23	w.w.w.[3]	w.w. washer [4]	P3615B 0.91 mm	Short duration
38-91-6-W'W-LD-24	w.w.w.[3]	w.w. washer [4]	P3615B 0.91 mm	Long duration
38-91-6-NW-M-25	w.w.w.[3]	nailed (H) [5]	P3615B 0.91 mm	Monotonic
38-91-6-NW-SD-26	w.w.w.[3]	nailed (H) [5]	P3615B 0.91 mm	Short duration
38-91-6-NW-LD-27	w.w.w.[3]	nailed (H) [5]	P3615B 0.91 mm	Long duration
38-76-6-NS-SD-28	Screwed	nailed (H) [1]	P3615B 0.76 mm	Short duration
38-76-6-NS-LD-29	Screwed	nailed (H) [1]	P3615B 0.76 mm	Long duration
38-76-6-NS-M-30[6]	Screwed	nailed (H) [1]	P3615B 0.76 mm	Monotonic
38-76-6-NS-SD-31[6]	Screwed	nailed (H) [1]	P3615B 0.76 mm	Short duration
38-91-6-NS-M-32[6]	Screwed	nailed (H) [1]	P3615B 0.91 mm	Monotonic
38-91-6-NS-SD-33[6]	Screwed	nailed (H) [1]	P3615B 0.91 mm	Short duration
38-91-6-NS-SD-34	Screwed	nailed (H) [1]	P3615B 0.91 mm	Short duration
38-91-6-NS-LD-35	Screwed	nailed (H) [1]	P3615B 0.91 mm	Long duration
38-76-6-WB-SD-36	b. p.	welded [2]	P3615 0.76 mm	Cyclic + Short dur.[7]
38-91-6-WB-M-37	b.p.	welded [2]	P3615 0.91 mm	Monotonic

Notes:
(1): Used Hilti (H) X-EDNK22-THQ12 fastener for nailed frame connections and 12-14x7/8'' fastener for screwed sidelap connections.
(2): Welded frame connections were made with 16 mm diameter arc spot welds.
(3): Welded sidelap connections with washers.
(4): Welded frame connections with washers.
(5): Used Hilti (H) X-EDNK22-THQ12 fastener for nailed frame connections
(6): All fasteners spaced at 152 mm o/c in both directions, spacing in all other tests equal to 305 mm.
(7): 200 cycles at 0.4 γ_u and 2 cycles at 0.6 γ_u prior to short duration loading protocol

The test designation nomenclature, developed by Essa *et al.*, was adapted for this test series. The tests were designated according to panel depth (in mm), sheet thickness (76= 0.76 mm), diaphragm length (in m, to the nearest metre), deck-to-frame (W for welded, W' for welded with washer, N for powder actuated nails, S for screwed) and sidelap (B for button punched, S for screwed and W for welded) connection types, loading protocol (M for monotonic, SD for short duration and LD for long duration protocols) and the test number (sequential).

The tests in Table 5.2 have been presented in chronological order. Test specimens can also be grouped as shown in Table 5.3 according to the connection patterns.

Table 5.3 Test groups

Test no.	Sidelap	Frame	Fastener spacing (mm)	Nominal thickness (mm)	Related tests from Essa *et al.*
37, 21	button punched	welded	305-305	0.91	
20, 36	button punched	welded	305-305	0.76	1, 2
22, 23, 24	welded with washer	welded with washer	305-305	0.91	
25, 26, 27	welded with washer	nailed (H)	305-305	0.91	
19, 34, 35	screwed	nailed (H)	305-305	0.91	17, 18
28, 29	screwed	nailed (H)	305-305	0.76	4, 7
32, 33	screwed	nailed (H)	152-152	0.91	
30, 31	screwed	nailed (H)	152-152	0.76	

Seismic dynamic tests were carried out instead of slow cyclic quasi-static tests. In the latter, it is difficult to evaluate the energy dissipation capabilities of specimens. The energy dissipation is related to the mode and propagation of failures, which may change depending on the rate of deformation. In addition, it was anticipated that out-of-plane displacements would be amplified under dynamic loading.

Button punched-welded assemblies were investigated in tests 20 and 21. Because Essa *et al.* observed very poor behaviour under quasi-static loading for this system, it was of interest to see how button punched-welded assemblies would behave under real earthquake demand. In addition, it was important to include these specimens in the test protocol because the system is currently very common in practice, mainly because it is easy and cost effective to install. Test 37 was performed since no monotonic test was available for the 0.91 mm nominal thickness deck. Test 36 was carried out to investigate the effect of prior wind loading on subsequent seismic loading. The specimen was subjected to 200 reversed cycles at 0.4 γ_u and 2 cycles at 0.6 γ_u prior to the short duration (SD) loading protocol. The 0.4 γ_u corresponds to the service wind loads and 0.6 γ_u corresponds to the factored wind load level.

Tests 22, 23 and 24 involved a new design with welded with washer sidelap connections intended for high seismic zones. The thicker 0.91 mm steel deck panels were selected because the use of this deck gauge was deemed to be more realistic for regions of high seismic loads. No information was available on the performance of welded sidelap connections with a B-deck profile, and hence a test program was developed and performed to compare the feasibility and the behaviour of three different types of welded sidelap connections for that deck profile. This program and the results that were obtained are presented in Appendix D. Based on this study, the connection made using a circular weld with a washer was selected for the diaphragm tests.

In tests 25, 26 and 27, the behaviour of nailed frame connections used with the welded with washer sidelap connections was investigated. To improve robustness of the system, 0.91 mm thick deck panels were used.

Since the screw-nail deck assemblies offered a promising hysteretic behaviour and are commonly used in industry, it was decided to perform a number of tests with this

system. Test 19 was carried out to repeat monotonic test 17 from Essa *et al.* with 0.91 mm thick deck panels. Shear failures of the nails had occurred in test 17, a behaviour that was not expected nor desirable. A new specimen constructed in the same manner, except that screws from a different lot number were installed, was included in the series of test to determine the response of this type of system when nail failure did not occur. Further information was obtained with tests 34 and 35, which were nominally identical to test 19, although they were subjected to the seismic loading protocols. Tests 28 and 29 were added to the scope of the investigation to evaluate the seismic response of the 0.76 mm nail-screw deck panels. The monotonic version of this deck assembly had been tested by Essa *et al.*. In order to observe the effect of using a 152 mm c/c connector spacing on the 0.91 mm thick deck panels tests 32 and 33 were planned and carried out. For similar reasons tests 30 and 31, with the thinner 0.76 mm thick deck panels, also formed part of the research project.

For diaphragm assemblies that were subjected to the short duration (SD) loading protocol, the test specimens were subjected to the full protocol in two separate runs. The intent of the 2nd run was to provide information such that the residual capacity of the diaphragm, that which would be required under a seismic aftershock, could be evaluated.

In tests where the long duration (LD) loading protocol was implemented, only 1 seismic run was performed. The long duration (LD) protocol was representative of the demand under a Cascadia type subduction earthquake. Due to the low probability of an aftershock of an intensity similar to the main event, it was deemed that a 2nd run would not be relevant. Instead, the specimen was subjected to a slow single reversed cyclic test, called *additional loop*, to assess its residual capacity. The diaphragm was pushed in the positive direction until its maximum shear capacity was attained. The loading was then reversed to obtain the maximum negative strength (Figure 5.15).

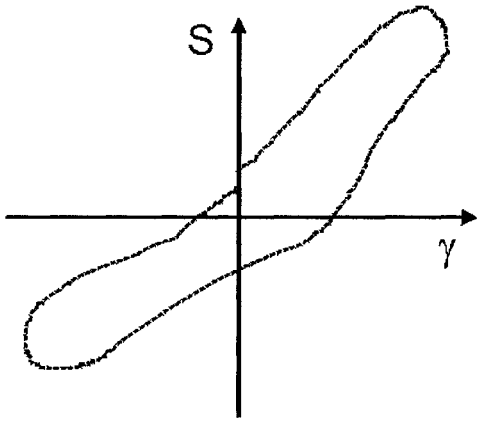

Figure 5.15 Additional loop following LD loading protocols

The fastener identification system developed by Essa *et al.* and shown in Figure 5.16 was also used in this study. This numbering system is valid for fasteners spaced at 305 mm apart. The same system was also used in tests where the fasteners were spaced at 152 mm o/c. The additional fasteners were then designated using the same identification as the connector immediately to the North-East except that that the symbol ' was added to the number. For instance, the first connector to the East of connector A1 is designated A1' and the first connector to the South of A1 is A'1.

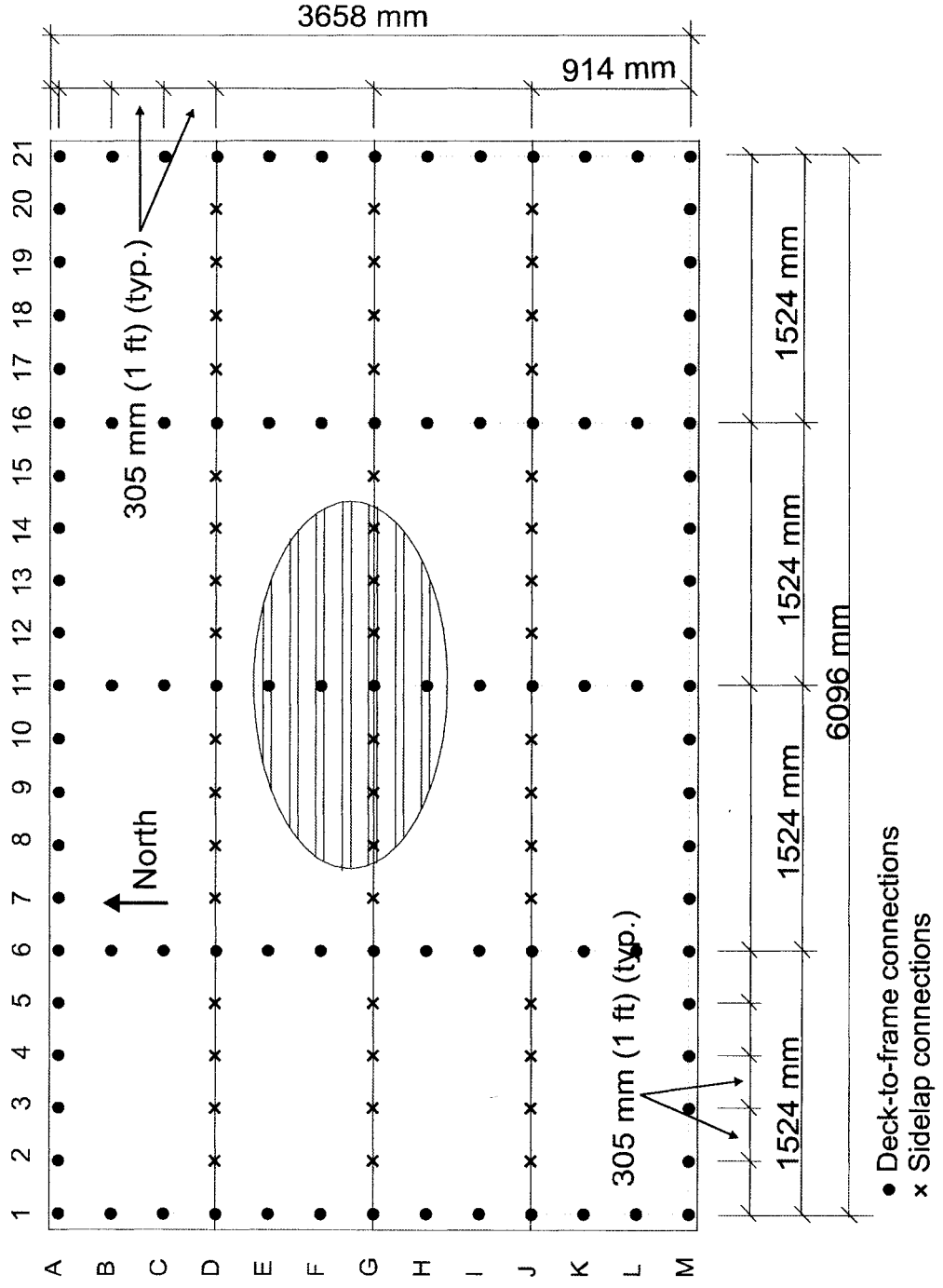

Figure 5.16 Layout of deck-to-frame and sidelap connections (305 mm c/c spacing)

Deck-to-frame welds without washer (16 mm nominal diameter) were fabricated with an E6011 2.5 mm diameter electrode with a current of 100 Amp. Welded with washer deck-to-frame connections were also used. The standard bolt washer had a 35 mm outer diameter, a 14 mm inner diameter and a 2.5 mm thickness. The welding procedure was taken from Peuler (2002). An E6011 3.2 mm electrode was used under weld current of 110 A. Welded with washer connections were also used as sidelap connections. The same bolt washer was used but the weld procedure was different. The welder would start the weld at the centre of the washer and penetrate through the two layers of sheet steel. The electrode was then moved in a circular fashion around the inner diameter of the washer so that the two sheets and washer would become connected. An E6010 3.2 mm diameter electrode was used with a direct current setting of 115 Amp. For both welded with washer connections (sidelap and frame), but particularly for sidelap, it was important to have good contact between the parts to be welded together.

Hilti powder-actuated EDNK- 22- THQ-12 fasteners were used for the deck-to-frame connections. The nails were made of modified AISI 1070 austempered steel and were zinc plated (Hilti, 2001). They were installed using the Hilti DX A41 SM tool at the mid-level setting with 6.8/ 11M Hilti #5 short red cartridges.

Screwed sidelaps were composed of Hilti screws S-MD 12- 14 x 1 HHWH Stitch (product number: #00312010 (Hilti, (2001)). The nail featured a length of 25 mm, a thread length of 19 mm, a socket recess of 8 mm, a diameter of 5.4 mm and a coarse thread. The hexagonal washer head provided a bearing surface for the driving sockets.

5.3 STEEL DECK MATERIAL PROPERTIES

Z275 galvanised grade 230 structural quality ASTM A653 (2002) sheet steel was specified for the standard and B-deck profiles used in the test series. Each combination of thickness and profile was obtained from a different coil of steel, hence, it was necessary to determine the material properties from tension coupon tests. Three coupons per material type were prepared and tested according to the requirements of ASTM A370 (2002). Tension coupon tests are presented in Appendix B and the results are summarised in Table 5.4. The standard deck profile sheets made with 0.76 mm thick steel were fabricated from the same steel as the specimens tested by Essa *et al.* (2001). The properties measured by Essa *et al.* were then used herein. In all cases, the measured properties met the minimum values specified for grade 230 ASTM A653 steel: F_y = 230 MPa, F_u = 310 MPa, elongation in 50 mm = 20%.

Table 5.4 Sheet steel material properties

	Base metal thickness (mm)	Fy (MPa)	Fu (MPa)	E (MPa)	50 mm gauge Elongation %
Standard 0.91mm	0.86	285	368	198000	31
Standard 0.76 mm[(1)]	0.71	301	373	197000	31
B-deck, 0.91 mm	0.88	319	394	210000	24
B-deck, 0.76 mm	0.70	248	327	204000	32

(1): Properties for 0.76 mm standard deck taken from Essa *et al.* (2001)

5.4 CONNECTION PROPERTIES

Table 5.5 and Table 5.6 present the resistance and stiffness values for the sidelap and deck-to-frame connections used in the test series. Test results are from Rogers and Tremblay (2000) except for the welded with washer connections. Values for welded with washer deck-to-frame connections are from Peuler (2002), and values for sidelap connections are from the sidelap study presented in Appendix D. The SDI and CSSBI strength and stiffness prediction values, based on the measured base metal thickness and material properties (Section 5.3), are shown for comparison.

Table 5.5 Strength and stiffness of deck-to-frame connections used in diaphragm tests

	Strength (kN)			Stiffness (kN/mm)	
	Test	SDI	CSSBI	Test	SDI
Welds (0.91 mm)	15.0	10.5	6.93	31.8	28.0
Welds (0.76 mm)	11.0	8.84	5.72	25.5	25.5
Welds with washers (0.91 mm) (1)	20.8	21.8	-	115.4	28.5
Hilti nails (0.91 mm)	7.46	7.98 (2)	-	23.9	26.5 (2)
Hilti nails (0.76 mm)	6.41	6.67 (2)	-	23.2	24.0 (2)

(1) : Test values for welded with washer connections with 0.91 mm sheet steel thickness from Peuler (2002).

(2): SDI values are from the manufacturer's catalogue (Hilti (2001)) for the 20 and 22 gauge material (0.91 mm and 0.76 mm thickness). The connection properties found in the catalogue are given for nominal sheet values and therefore not based on the measured material properties. For comparison, the strength and stiffness for the ENP2-21-L15 fastener calculated with the measured properties and the SDI equations for the 0.91 mm nominal thickness, are 8.11 kN and 26.1 kN/mm, respectively. In the case of the 0.76 mm sheet steel, the strength is equal to 6.66 kN and the stiffness to 23.3 kN/mm.

Table 5.6 Strength and stiffness of sidelap connections used in diaphragm tests

	Strength (kN)			Stiffness (kN/mm)	
	Test	SDI	CSSBI	Test	SDI
Button punch (0.91 mm)	1.54	1.22	0.54	0.71	1.07
Button punch (0.76 mm)	0.78	0.83	0.45	0.35	0.98
Welds with washers (0.91 mm) (1)	8.00	-	-	4.00	-
Screws #12 (0.91 mm) (2)	3.06	3.74	-	2.26	10.9
Screws #12 (0.76 mm) (2)	2.37	2.98	-	1.35	9.69

(1): Test results are from sidelap tests. See Appendix D.
(2): Screws 12 – 14 x 1" are used in diaphragm tests. However, test results for 10 – 14 x 7/8" screw are presented. SDI and CSSBI values based on #12 screws.

For the welded with washer deck-to-frame connections, the stiffness measured in tests was much higher than the SDI prediction. This is believed that there was a large influence of the apparatus in the test results. With regard to the sidelap connection stiffness, it must be noted that the test values were lower than the SDI predictions. The test set-up used by Rogers and Tremblay (2000), which is presented in the AISI Cold-Formed Steel Design Manual (1996) results in a measured shear stiffness that includes both the deformation characteristics of the connection as well as the surrounding web and flange elements. Due to the short dimensions of the test specimens, and the loading that was eccentric to the centreline of the sidelap connectors, the set-up produced a level of distortion that was not consistent with that which was observed in the full diaphragm tests. Hence, the test obtained shear stiffness values are conservative (lower) than what would be expected in a full length diaphragm panel sidelap.

5.5 CHOICE OF LOADING REFERENCES

Loading protocols were developed based on the seismic demand estimated from the results of the analytical study carried out for various building sizes using different earthquake records (See Chapter 3). Chapter 4 presents the short duration (SD) and long duration (LD) loading protocols, which depend on the diaphragm shear-distortion loading references: γ_u and γ_2 . Figure 5.17 shows the loading references on a typical shear-distortion curve measured for a monotonic test of a steel deck diaphragm.

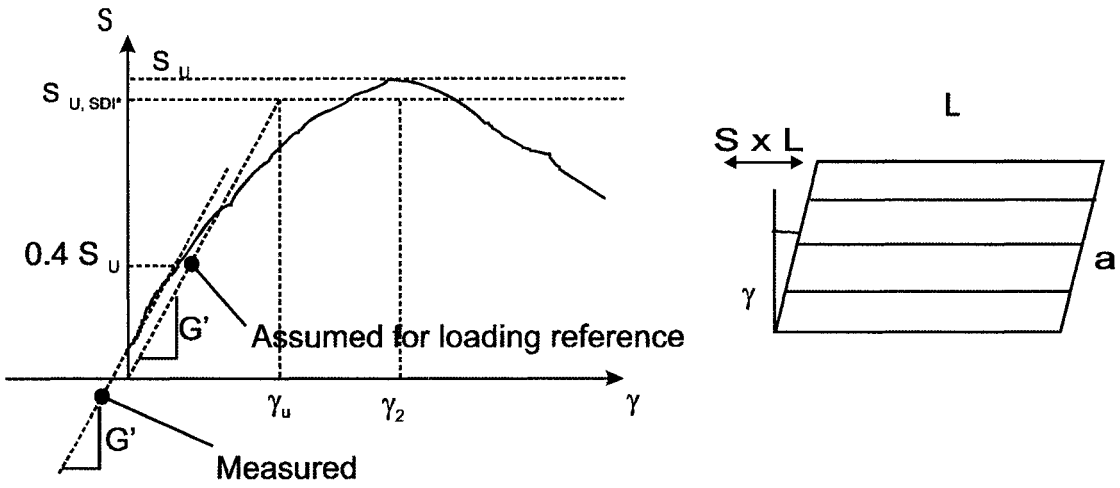

Figure 5.17 Schematic representation of loading references

The loading reference, γ_u, is the distortion level found when dividing the predicted ultimate nominal load, $S_{U,\ SDI*}$, by the measured shear stiffness G'. $S_{U,\ SDI*}$ is the predicted ultimate load based on the SDI equations together with the connection properties from tests (see section 5.4). G' is the secant shear stiffness of the steel deck diaphragm based on monotonic tests or on cyclic tests run at low amplitude. G' was determined by extending the load-deformation curve to the left of the y-axis to simulate a situation where there would be no friction or restraint at low load in the system. The

shear stiffness was defined as the slope of the line that connected the x-axis intercept and the 40% maximum measured force level on the shear-distortion curve. γ represents the true diaphragm distortion. As discussed in section 5.1, the measured displacements were corrected for support movements.

The loading reference, γ_2, is the distortion at which the peak load was reached during the monotonic diaphragm test. The following table displays the values used in the evaluation of distortion loading references.

Table 5.7 Loading references used in tests

Test	Parameters used in the evaluation of the loading references used in tests		Loading references used in tests	
	$S_{U, SDI}$ * (kN / m)	G' (kN / mm)	γ_u (rad / 1000)	γ_2 (rad / 1000)
21	11.5	4.05	2.84	2.98
20, 36	11.4	2.14	5.33	5.60
23, 24	29.6	4.86	6.08	8.64
26, 27	21.2	4.51	4.69	6.67
34, 35	13.5	4.18	3.23	6.60
28, 29	11.1	3.12	3.55	5.04
33	24.9	20.3	1.22	5.50
31	20.2	12.7	1.59	3.70

For tests 21, 23 and 24, the $S_{U, SDI*}$ values were not evaluated properly, due to an improper choice of connection resistance. In addition, the evaluation of secant stiffness was performed in a slightly different manner from the target approach described above. In consequence, there are discrepancies in the evaluation of the loading reference, γ_u. Table 5.8 displays the target values that should have been used for testing. For each test, a ratio of the value that was used with regards to the target value has been listed.

Table 5.8 Target values for loading references

Test	$S_{U, SDI}$ * (kN/m)	G' (kN/mm)	Target γ_u (rad / 1000)	Used γ_u (rad / 1000)	Ratio Used/ Target
21	16.9	3.32	5.09	2.84	0.56
20, 36	11.4	2.14	5.33	5.33	1.00
23, 24	36.6	4.54	8.06	6.08	0.75
26, 27	21.2	4.33	4.90	4.69	0.96
34, 35	13.5	4.13	3.27	3.23	0.99
28, 29	11.1	3.12	3.55	3.55	1.00
33	24.9	18.3	1.36	1.22	0.90
31	20.2	13.5	1.50	1.59	1.06

The values for γ_2 were evaluated correctly in all cases, except for test 21. A value of 2.98 was used, compared to an appropriate value of 5.50 rad/1000, because the monotonic test results were not available at the time the loading protocol was established. A γ_2 / γ_u ratio equal to 1.05 was assumed, which was based on the 0.76 mm thick sheet steel monotonic diaphragm test curves. A monotonic test was performed subsequent to the dynamic test (21), from which it was realised that the evaluation of γ_2 was based on an incorrect value for γ_u. It was shown however, that the ratio of γ_2 / γ_u = 1.05 was correct, given the results of the monotonic test performed afterward.

In tests 21, 23 and 24, the specimens were not sufficiently displaced into the inelastic range since the loading reference values, γ_u and γ_2, that were used were smaller than what was subsequently determined to be adequate. It is assumed that the other tests were adequately loaded since the error in the γ_u value was kept below 10%.

The use of these loading references had varied impacts on the results obtained from the tests depending on the loading protocol that was implemented. Figure 5.18 presents the used and target loading protocols for tests 21 and 23 and Figure 5.19 for test 24.

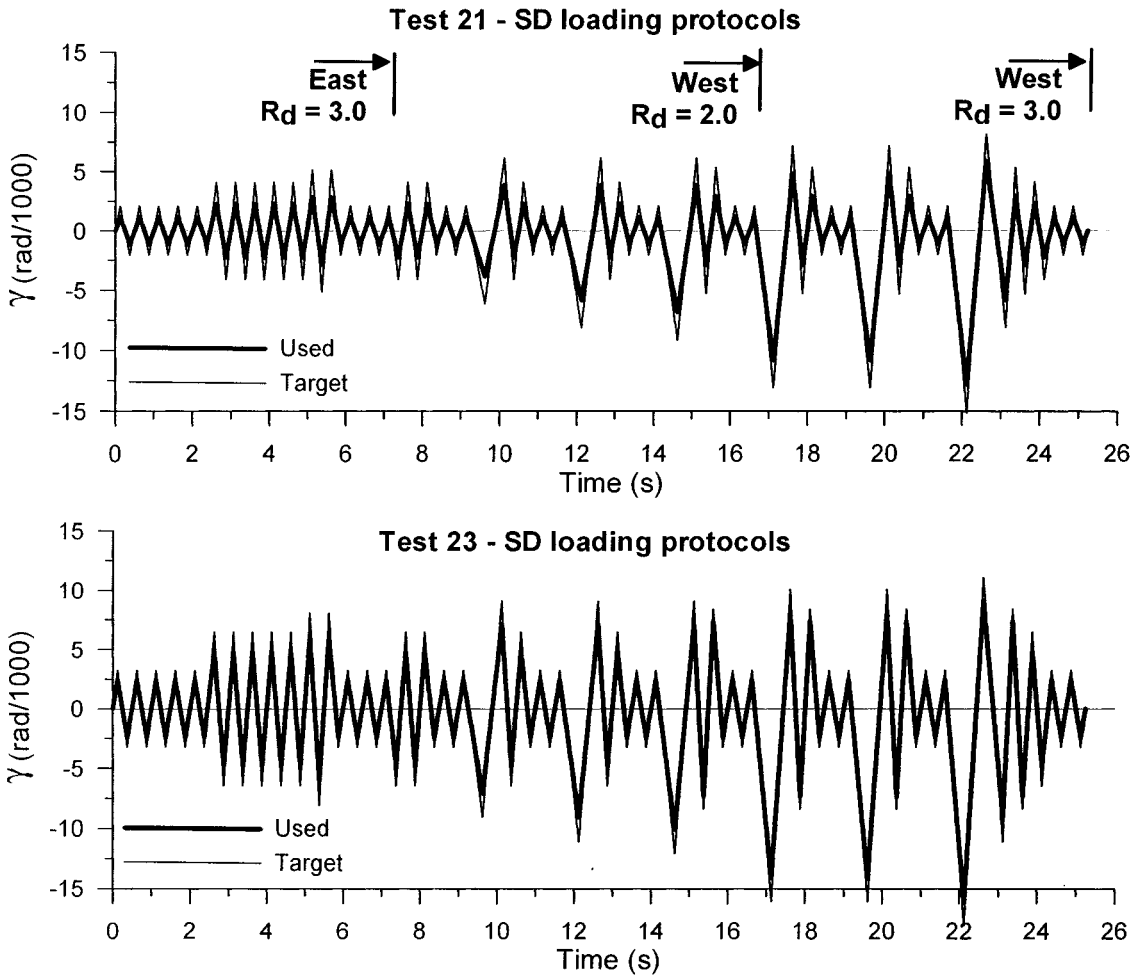

Figure 5.18 Used and target loading protocols for tests 21 and 23

For the SD loading protocols, the error in γ_u had a varied impact on the imposed peak distortion values. The amplitude of all cycles below or equal to γ_u was directly proportional to the loading reference γ_u , which was the case for all cycles in the East R_d = 3.0 loading protocol. In consequence, the relative error in the imposed peak distortion values was equal to the relative error in γ_u. For the West R_d = 2.0 and R_d = 3.0 protocols, the largest peaks were equal to γ_u plus a fixed plastic distortion. Table 5.9 presents the relative error in the largest peak values throughout the SD loading protocol.

Table 5.9 Relative error on imposed peak values for distortion (Tests 21 and 23)

Time (sec)	Distortion peak value	Relative error (%)	
		Test 21	Test 23
5.375	γ_u	45	24
9.625	$\gamma_u + 1$	37	22
12.125	$\gamma_u + 3$	28	18
14.625	$\gamma_u + 4$	25	16
17.125	$\gamma_u + 8$	17	12
19.625	$\gamma_u + 8$	17	12
22.125	$\gamma_u + 10$	15	11

For the largest peaks, due to the increasing fixed plastic distortion, the error in the imposed peak values tends to decrease with increased amplitude. The error in γ_2 was considered to be minor since only 8 peaks, depended on this loading reference.

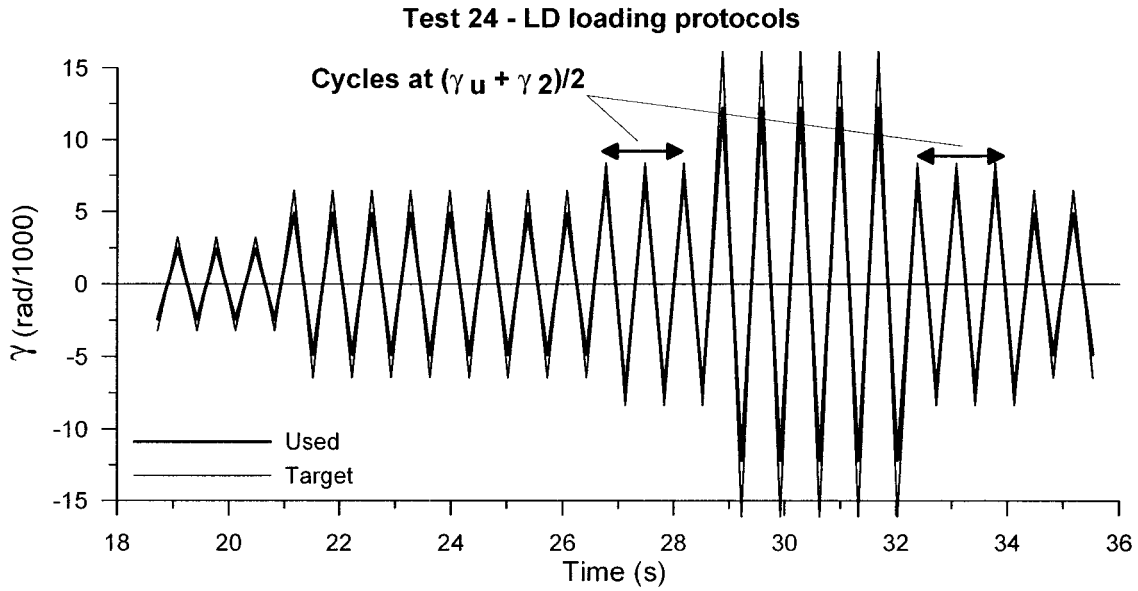

Note: Only the time interval from t = 18 to 36 seconds is presented.

Figure 5.19 Used and target loading protocols for test 24

For the LD loading protocols, the imposed peak distortions were in direct proportion to γ_u, except for the pre-peak and post-peak cycles where the effect of γ_u and γ_2 were combined. For test 24, the relative error for peaks in direct proportion to γ_u was equal to 24% whereas the relative error for peaks at $(\gamma_u + \gamma_2)/2$ was equal to 12%.

5.6 SIGNAL TREATMENT AND REMOVAL OF INERTIA FORCES

During the dynamic tests, the force measured by the load cell included inertia forces due to the mass of the test frame. To obtain the real forces that were subjected to the deck panels it was necessary to remove these inertia forces. For each dynamic test loading protocol, a dummy test was performed without any diaphragm specimen. At each time step of data acquisition, the force measured by the load cell was divided by the acceleration measured by the accelerometer mounted on the load cell, giving an effective

mass for the test frame. The average effective mass from these tests was equal to 18.6 kN/g.

The effective mass determined with the method presented above was compared to another value. Since all of the frame connections were pinned, the acceleration profile would be linear over the width of the test set-up (see Figure 5.20). Hence, the effective mass is approximately half of the total bare frame mass. This value was evaluated as equal to 18.8 kN/g, which confirmed the value determined through the use of the load and acceleration data. Figure 5.1, which presents the bare frame test set-up, was used to determine the effective mass for this alternative method.

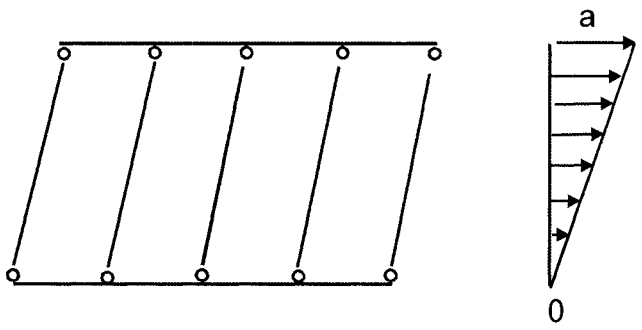

Figure 5.20 Acceleration shape

Using the evaluated effective mass and multiplying it by the measured acceleration obtained during the testing of the SD and LD diaphragm specimens, inertia forces were obtained. These inertia forces were then removed from the forces measured by the actuator's load cell to obtain the true force in the deck panels.

It must be mentioned that the measured acceleration and load cell signals both contained high frequency motions due to the local friction and impact phenomena that occurred in the frame during the dynamic tests. The two signals were therefore filtered to isolate the main signals. In all cases, the chosen low-pass filter was set to 3 Hz for the acceleration

and 10 Hz for the load cell recording. Figure 5.21 illustrates this filtering process for Test 29.

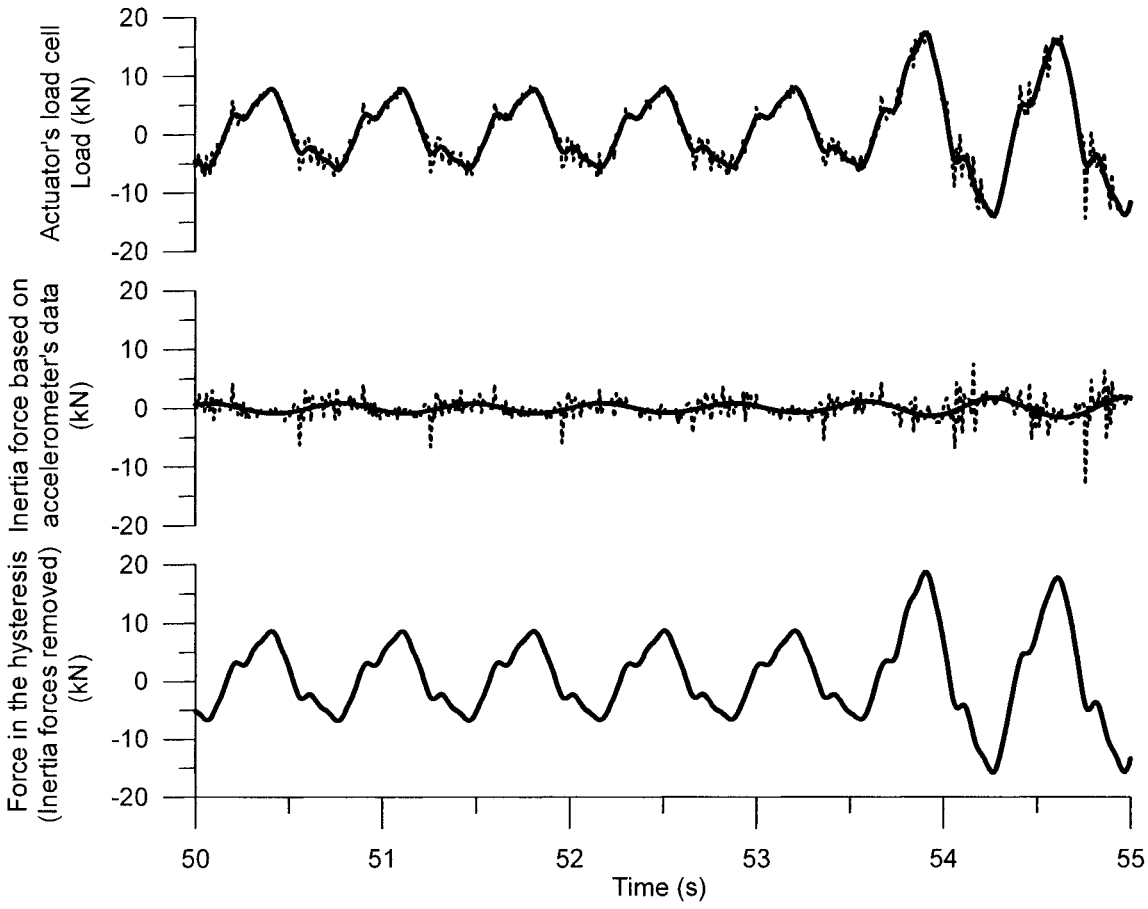

Figure 5.21 Signal treatment and removal of inertia forces in test 29

5.7 MAIN TEST RESULTS

In this section, the main results, i.e. ultimate loads and stiffnesses, are presented and compared with predicted values. In the following section, the specimen behaviour, i.e. failure modes and test curves, are shown and discussed. A data analysis follows in Section 5.9, which was undertaken to obtain quantitative values of the hysteretic behaviour.

The ultimate loads and initial stiffnesses for all tests are presented in Table 5.10. The method implemented to determine the initial stiffness varied depending on the type of loading. In monotonic tests, the secant stiffness at $0.4S_u$ was used based on the approach described in section 5.5. For tests with SD and LD loading protocols, a linear regression was performed in the first cycle at $0.4\gamma_u$ at the beginning of the signal. Only the linear part of the shear-distortion curve was considered.

In addition, test-to-SDI predicted ratios are given in Table 5.10 for ultimate loads and stiffnesses. The SDI (1987) method was summarised in the literature review. Two sets of test-to-predicted values are given in each table. Test/SDI ratios are based on the SDI formulas with nominal values for materials and connection properties, in other words, the value a designer would use. Test/SDI* values are based on SDI equations with connection properties from tests. Results from test 36 were not included in the statistical analysis since the specimen was subjected to prior cycling (200 cycles at 0.4 γ_u and 2 cycles at 0.6 γ_u). Table 5.11 and Table 5.12 display the predicted strengths and stiffnesses of connections based on nominal deck properties. The test values are added for comparison.

Table 5.10 Test values for ultimate load and stiffness and comparison with SDI predictions

Test	Date of testing	Test values		Test to predicted			
		Su kN/m	G' kN/mm	Su Test/SDI*	Su Test/SDI	G' Test/SDI*	G' Test/SDI
38-91-6-WB-M-37	03/20/2002	12.6	3.32	0.75	1.09	0.80	0.72
38-91-6-WB-SD-21	02/15/2002	13.8	3.16	0.82	1.19	0.76	0.68
38-76-6-WB-SD-20	02/13/2002	9.81	2.44	0.86	1.07	0.88	0.74
38-76-6-WB-SD-36a(1)	03/19/2002	5.80	2.40	0.51	0.63	0.87	0.73
38-76-6-WB-SD-36b(1)		5.69	0.94	0.50	0.62	0.34	0.28
Mean (2)				0.81	1.11	0.81	0.71
C.o.V. (2)				0.07	0.06	0.08	0.04
38-91-6-W'W-M-22	02/20/2002	32.1	4.54	0.88	N/A	0.81	N/A
38-91-6-W'W-SD-23	02/22/2002	34.6	4.60	0.95	N/A	0.82	N/A
38-91-6-W'W-LD-24	02/27/2002	33.2	4.36	0.91	N/A	0.78	N/A
Mean				0.91		0.80	
C.o.V.				0.04		0.03	
38-91-6-NW-M-25	03/01/2002	22.5	4.33	1.06	N/A	0.91	N/A
38-91-6-NW-SD-26	03/04/2002	26.5	4.09	1.25	N/A	0.86	N/A
38-91-6-NW-LD-27	03/18/2002	26.2	3.64	1.24	N/A	0.76	N/A
Mean				1.18		0.84	
C.o.V.				0.09		0.09	
38-91-6-NS-M-19	02/08/2002	16.7	4.13	1.24	1.07	0.91	0.75
38-91-6-NS-SD-34	03/14/2002	17.0	4.01	1.26	1.09	0.89	0.73
38-91-6-NS-LD-35	03/15/2002	17.3	3.90	1.28	1.11	0.86	0.71
38-76-6-NS-SD-28	03/06/2002	14.1	2.45	1.27	1.08	0.87	0.65
38-76-6-NS-LD-29	03/07/2002	13.6	2.39	1.23	1.05	0.85	0.64
Mean				1.25	1.08	0.88	0.70
C.o.V.				0.02	0.02	0.03	0.07
38-91-6-NS-M-32	03/13/2002	34.4	18.3	1.38	1.19	1.27	0.88
38-91-6-NS-SD-33	03/14/2002	35.2	18.4	1.41	1.21	1.28	0.88
38-76-6-NS-M-30	03/08/2002	23.4	13.5	1.16	0.97	1.30	0.84
38-76-6-NS-SD-31	03/12/2002	26.5	15.0	1.31	1.10	1.44	0.93
Mean				1.32	1.12	1.32	0.88
C.o.V.				0.09	0.10	0.06	0.04

(1): Cycles at 0.4 γ_u and 0.6 γ_u were performed prior to the SD loading protocol.
a refers to the cyclic part, b to the SD loading protocol.
(2): Test 36 results are not included in the mean and C.o.V.

Table 5.11 Predicted strength and stiffness of deck-to-frame connections based on nominal deck properties

	Strength (kN)			Stiffness (kN/mm)	
	Test	SDI	CSSBI	Test	SDI
Welds (0.91 mm)	15.0	9.29	7.33	31.8	28.8
Welds (0.76 mm)	11.0	7.84	6.12	25.5	26.3
Welds with washers (0.91 mm) [1]	20.8	22.6	-	115.4	28.8
Hilti nails (0.91 mm)	7.46	7.98	-	23.9	26.5
Hilti nails (0.76 mm)	6.41	6.67	-	23.2	24.0

(1) : Test values for welded with washer connections with 0.91 mm sheet steel thickness from Peuler (2002).

Table 5.12 Predicted strength and stiffness of sidelap connections based on nominal deck properties

	Strength (kN)			Stiffness (kN/mm)	
	Test	SDI	CSSBI	Test	SDI
Button punch (0.91 mm)	1.54	1.37	0.57	0.71	1.10
Button punch (0.76 mm)	0.78	0.96	0.48	0.35	1.01
Welds with washers (0.91 mm) [1]	8.00	-	-	4.00	-
Screws #12 (0.91 mm) [2]	3.06	3.87	-	2.26	11.1
Screws #12 (0.76 mm) [2]	2.37	3.23	-	1.35	10.1

(1): Test results are from sidelap tests. See Appendix D.
(2): Screws 12 – 14 x 1" are used in diaphragm tests. However, test results for 10 – 14 x 7/8" screw are presented. SDI and CSSBI values based on #12 screws.

The SDI predictions are dependent on the fastener properties incorporated in the calculation. If connection properties that reflect the behaviour of the actual diaphragm connections are used, then the SDI method should provide accurate predictions of the overall diaphragm shear capacity and stiffness if the design method assumptions are respected. This problem was studied by Nedisan (2002), where it was found that the SDI method cannot be used to predict the strength and stiffness of deck assemblies in which the relative stiffness between the deck-to-frame and sidelap connectors is higher than 10. Also, the SDI method assumes that all connectors at the edge of a panel fail at the same time, which based on observations of full-scale diaphragm tests is not true in all cases. It

is necessary for the fasteners to possess a certain amount of ductility to meet this assumption. Making a general conclusion on the accuracy of the SDI method is beyond the scope of this text. In consequence, only general comments are made on the test-to-predicted ratios. It must be noted that in all deck families the scatter of measured results was low, indicated by the coefficient of variation which was kept below 0.10.

For simplification, the abbreviations for the deck assembly types from the test nomenclature (Section 5.2) (WB, W'W, NW and NS) are used in the following comments.

For the S_u test/ SDI* comparisons, the WB system had a ratio of 0.81, as the test values were below the SDI* predictions. The NS designs gave ratios of 1.25 and 1.32, as the test values were above the predicted ones. On another hand, W'W and NW gave ratios equal to 0.91 and 1.18, respectively.

For the S_u test/ SDI ratios, the WB designs gave a mean equal to 1.11, whereas NS designs gave means equal to 1.08 and 1.12. In this case, the test-to-predicted values between deck assembly families are closer, compared to the SDI* method.

For stiffness test values, there was a discrepancy between the approach used in this project and the SDI assumptions. On one hand, the shear stiffness used in the project was defined as the slope of the line that connected the x-axis intercept and the 40% maximum measured force level on the shear-distortion curve. On another hand, the stiffness computed with the SDI method corresponds to a secant stiffness at $0.4S_u$ that starts from the origin (0,0). The approach used in the project for G' values described in a better way the overall behaviour of the specimen, in comparison to the SDI approach, which is more suited to deflection predictions under service loads. The ratio of the secant stiffness (SDI method) and the stiffness obtained with the method used in this project was computed for all specimens. In all cases, the ratio was greater than 1.0 with

an average of 1.17 and a coefficient of variation of 0.11. For deck assemblies with welds with washer at sidelap (W'W and NW), the G' values measured according to the two methods were similar.

For the G' test/SDI* ratios, all assemblies with 305 mm c/c (WB, W'W, NW and NS) gave ratios between 0.80 and 0.88. However, the NS system with a 152 mm c/c spacing gave a ratio equal to 1.32. With the secant method from SDI, the ratio would have increased, and for 305 mm c/c they would have been closer to 1.0.

For the G' test/SDI ratios, WB and NS systems with a 305 mm c/c spacing gave ratios equal to 0.71 and 0.70, respectively. However, the NS system with a 152 mm c/c spacing gave a ratio equal to 0.88.

The following discussion is limited to each individual type of deck assembly.

For the WB deck assemblies, the test/SDI* ratios for strength were always lower than test/SDI values. This was explained by the higher test values for welds used in SDI* in comparison with the SDI predictions for welds used in SDI. Besides, it should be mentioned that the welds used at sidelap purlin intersections were weaker compared to other welds, due to the oval shape of the standard deck profile at these locations. The SDI method considers that all welds have the same properties, which is not the case with the standard deck profile.

For the W'W deck assemblies, the difference between test results and the SDI* predictions could be attributed to the choice of strengths and stiffnesses for the welded with washer sidelap connections. As discussed in Appendix D and Section 5.4, there was considerable variation in the stiffness of the welded with washer sidelap connection that was measured in the connection tests. It is possible that the value used for the calculation of SDI* (Table 5.6) did not correspond to that in the full diaphragm assembly. In

addition, the stiffnesses of the sidelap and deck-to-frame connections are considerably different (around 4.0 kN/mm compared to 28.8 kN/mm), a condition where the SDI method cannot be used to accurately predict the diaphragm stiffness (Nedisan, 2002).

In the NW designs, failures were observed in connections on the test frame perimeter. However, the SDI* predictions for strengths were governed by the failure of fasteners at panel corners. This failure mode was not observed in the tests involving NW designs, hence it is possible that the SDI method was not applicable.

In the NS systems with 152 mm c/c spacing, the screws had more of an impact on the diaphragm behaviour. As explained later, the screws in the NS systems played a relatively more important role when the fastener spacing was reduced from 305 mm to 152 mm. This is because the behaviour of NS diaphragms is mainly governed by the sidelap response and only screws were added along the sidelaps. Considering that the measured stiffness of screw sidelap connections was a function of both the fastener and web stiffness of the test specimen an increase in the difference between the measured and predicted overall diaphragm stiffness was obtained compared to the 305 mm c/c designs. Overall, the SDI strength predictions based on nominal values approached more closely the test results. This can be attributed to the fact that the governing failure mode in the SDI and SDI* strength predictions was the failure for the corner fasteners and that failure mode was not observed in the tests.

Table 5.13 presents the test-to-predicted values using the CSSBI (1991) method. CSSBI values are only available for the WB deck system and only these tests are presented in the table. Since the CSSBI method provides allowable load shear strengths, the results were multiplied by a safety factor of 2.5 to obtain ultimate values. Again, test-to-CSSBI ratios are given for nominal connection properties (CSSBI), and in addition for connection test results (CSSBI*).

Table 5.13 Test values for ultimate load and stiffness and comparison with CSSBI predictions

Test	Date of testing	Test values		Test to predicted			
		Su	G'	Su	Su	G'	G'
		kN/m	kN/mm	Test/CSSBI*	Test/CSSBI	Test/CSSBI*	Test/CSSBI
38-91-6-WB-M-37	03/20/2002	12.6	3.32	0.45	0.76	0.94	0.79
38-91-6-WB-SD-21	02/15/2002	13.8	3.16	0.49	0.83	0.89	0.75
38-76-6-WB-SD-20	02/13/2002	9.81	2.44	0.61	0.87	1.15	0.94
38-76-6-WB-SD-36a(1)	03/19/2002	5.80	2.40	0.36	0.51	1.13	0.92
38-76-6-WB-SD-36b(1)		5.69	0.94	0.36	0.50	0.44	0.36
Mean (2)				0.52	0.82	0.99	0.83
C.o.V. (2)				0.17	0.07	0.14	0.12

(1): Cycles at 0.4 γ_u and 0.6 γ_u were performed prior to the SD loading protocol.
a refers to the cyclic part, b to the SD loading protocol.
(2): Test 36 results are not included in the mean and C.o.V.

The S_u test/CSSBI* ratio was equal to 0.52 compared to 0.82 with the CSSBI standard approach. For stiffnesses comparison, CSSBI* gave a ratio equal to 0.99 compared to 0.83 with the CSSBI standard approach. These results confirm that the test values for connections (welds and button punches) are not to be used with the CSSBI method for strength prediction.

Also, it was interesting to compare results from this phase of the diaphragm investigation to results from Essa *et al.* (2001) for test specimens that had similar characteristics. Table 5.14 presents results for the following tests from Essa *et al.*. Tests 1 and 2 involved a button punched-welded connection pattern with 0.76 mm deck thickness. Tests 4 and 7 used nailed-screwed connections with 0.76 mm deck thickness and tests 17 and 18 involved 0.91 mm deck thickness. It should be noted that test 19, which was carried out for the current investigation, was a rerun of test 17 by Essa *et al.*, in which shear failures in the nails were observed.

Table 5.14 Test results from Essa *et al.* (2001) compared to related tests in phase 2

Test	Date of testing	Test values		Test to predicted			
		Su kN/m	G' kN/mm	Su Test/SDI*	Su Test/SDI	G' Test/SDI*	G' Test/SDI
38-91-6-WB-M-37	03/20/2002	12.6	3.32	0.75	1.09	0.80	0.72
38-91-6-WB-SD-21	02/15/2002	13.8	3.16	0.82	1.19	0.76	0.68
38-76-6-WB-M-1	Essa (2001)	8.05	2.14	0.71	0.87	0.78	0.65
38-76-6-WB-Q-2	Essa (2001)	7.53	2.14	0.66	0.82	0.78	0.65
38-76-6-WB-SD-20	02/13/2002	9.81	2.44	0.86	1.07	0.88	0.74
Mean				0.76	1.01	0.80	0.69
C.o.V.				0.11	0.15	0.06	0.06
38-91-6-NS-M-17	Essa (2001)	14.6	4.22	1.08	0.94	0.93	0.77
38-91-6-NS-Q-18	Essa (2001)	15.6	4.76	1.16	1.00	1.05	0.87
38-91-6-NS-M-19	02/08/2002	16.7	4.13	1.24	1.07	0.91	0.75
38-91-6-NS-SD-34	03/14/2002	17.0	4.01	1.26	1.09	0.89	0.73
38-91-6-NS-LD-35	03/15/2002	17.3	3.90	1.28	1.11	0.86	0.71
38-76-6-NS-M-4	Essa (2001)	12.3	3.12	1.11	0.95	0.96	0.83
38-76-6-NS-Q-7	Essa (2001)	12.2	2.87	1.10	0.94	0.88	0.77
38-76-6-NS-SD-28	03/06/2002	14.1	2.45	1.27	1.08	0.87	0.65
38-76-6-NS-LD-29	03/07/2002	13.6	2.39	1.23	1.05	0.85	0.64
Mean				1.19	1.02	0.91	0.75
C.o.V.				0.07	0.07	0.07	0.10

Test values from Essa *et al.* (2001) are always lower compared to values from this test series. No general explanation for this situation could be found. However, test results from Essa *et al.* are compared with this test series in the next section, when the behaviour of test specimens is presented and commented.

5.8 SPECIMEN BEHAVIOUR

In this section, the test result curves and behaviour are presented. The failure modes for sidelap and deck-to-frame fasteners are commented on and pictures have been added for completeness. Tables are included which contain a description of each test specimen along with a listing of damage observed after testing.

Depending on the type of loading involved, the test curve contents vary. For monotonic tests, the shear-distortion curve and sidelap slip are shown. For the SD and LD loading protocols, the distortion time history is shown together with measured forces, dissipated energy and sidelap slip. Also, shear-distortion curves are presented for each portion of the overall loading protocol.

5.8.1 Button punch - weld design

5.8.1.1 Tests 37 and 21

Tests 37 and 21 were performed with button punched sidelap connections and welded structural fasteners, which were both spaced at 305 mm c/c. Decks with a standard profile (P3615) and a nominal thickness of 0.91 mm were used. Sheets were welded to the frame members on both sides of each sidelap line. Test 37 was monotonic and test 21 was performed with a short duration (SD) loading protocol.

Table 5.15 presents a description of test specimen properties for tests 37 and 21. Sheet steel properties i.e., supplier and coil number, and properties from tension coupon tests are given. In addition, the type and spacing of fasteners are shown, as well as the average measured properties of the installed fasteners together with comments on the quality of the connections.

Test 37

Test curves for strength and sidelap slip in terms of distortion are presented in Figure 5.23. In addition, the observed damage is shown in Table 5.16. The coordinate system that was used in the table of observed damage was presented in Figure 5.16. A nomenclature of failure modes was defined for each fastener type with abbreviations used for simplicity. The nomenclature of failure mode types is presented together with the observed damage table.

The main failure modes observed in the project, i.e. buckling, bearing, bond failure, shear failure and tearing are defined here. The nomenclature used combinations of these failure modes to reflect what was observed in the tests. Buckling is considered as an out-of-plane deformation in the sheet steel, normally due to compression. Bearing happens when the fastener pushes into the sheet steel and, thus, elongates the hole in the sheet as well as piles the steel in front of the fastener. A bond failure occurs on the tension side of the sheet-to-weld metal connection. This failure is located in the heat-affected region around the weld. Shear failure occurs when the fastener fractures instead of the surrounding sheet steel, as observed in a limited number of nailed connections. Tearing is found when the sheet steel is pulled apart locally.

The maximum measured load of 12.6 kN/m occurred at a distortion of 5.5 rad/1000. No yielding plateau was observed. At peak load, muffled noises attributed to weld failures

were heard and strength degradation happened thereafter. At 8.0 rad/1000, the deck specimen strength went below 80% of the maximum measured load.

Because the deck-to-frame connection along the frame edges was much stiffer and stronger than the deck sidelap connection, the axis of zero deformation across the width of the outermost deck sheets was located near the frame edge and, hence, relatively larger slip developed along sidelaps 1-2 and 3-4. Shear deformation in the middle deck panels was symmetrical, leading to smaller slip along sidelap 2-3. The exterior panels at the North and South edges were connected by welds to the frame, whereas the sidelap joints were connected by a combination of welded and button punched connections. The button punched connections are weaker and more flexible compared to the welded connections. Welds have been measured to be approximately 50 times stiffer than button punches (Rogers and Tremblay, 2000).

Strength degradation may be explained by the failure of connections at the sidelap locations during the loading protocol. As said, two types of connections were found at sidelap lines: uniformly distributed button punches and welds located at purlins. Due to their higher stiffness, the welds tended to sustain a much larger share of the transferred load. As observed in Rogers and Tremblay (2000), the welded frame connections failed suddenly at displacements between 2 and 5 mm. Failure developed early in these welds due to their limited ductility. It often took place by fracture of the heat affected deck material with no associated bearing deformation in the adjacent sheet steel. Two cases were observed in tests: BT and BB. BT is a bond failure of the top sheet from the bottom sheet whereas BB is a failure of both sheets from the weld to frame. These failures occurred because of the low quality deck-to-frame welds associated with standard deck at one edge (with round-shaped flute) of each panel. As the slip and force time histories demonstrate, the strength degradation started when the sidelap slip, or connection deformation, reached around 2 mm and continued as the slip increased.

Figure 5.24 presents a BT failure mode. At 3 locations at sidelaps, bond failure where both sheets disconnected from weld (BB) were noticed. Button punched sidelap connections remained together except at line 2-3 where the sidelap was disengaged over half of its length (see Figure 5.25). Slips at the North and South ends were minimal. Only one connection (A1) on these lines failed.

Buckling of the sheet on one side of weld without weld failure (BO) was observed at 14 locations (Figure 5.26). However, in some instances, the premature failure of puddle welds, where no sheet distortion was observed, took place because of a separation between the weld perimeter and the steel panel. Figure 5.27 displays this failure mode (BBF). Deck to purlin welds not located at sidelaps were generally of better quality because the bottom flange of the deck was flat, providing good contact between the deck and the frame. Hence, compression buckling was observed for those welds and these connections were able to sustain load over greater displacements than those at sidelaps. However, since they were not located at the critical sidelap and purlin locations, their improved performance did not have a substantial effect on the overall diaphragm behaviour: overall strength degradation developed after weld failure took place at sidelaps, even if welds not at sidelap were still sound.

Test 21

Test 21 was performed under a short duration (SD) loading protocol. The maximum measured load was equal to 13.8 kN/m. As explained in Section 5.5, the amplitude of the imposed displacement on that specimen was too low in view of its actual strength and stiffness properties, the selected value for γ_u being equal to 0.56 times the required value. Figure 5.28 presents the test curves and Table 5.17 the observed damage after run 1.

Under the East R_d = 3.0 loading protocol, the test specimen developed a stable elliptical hysteretic behaviour without degradation. It was an ideal behaviour since the diaphragm could develop its strength and dissipate energy. This good behaviour is attributed to the fact that the specimen was loaded only to 0.56 γ_u in the large cycles of East R_d = 3.0. The target γ_u, 5.09 rad/1000, and the maximum measured force were reached in the second peak of West R_d = 2.0 (γ_u+3 rad/1000). In the following peak, of an amplitude of γ_u+4 rad/1000, the specimen degraded and the remaining force reached 76% of Su. In the first large displacement cycle of West R_d = 3.0, the specimen capacity had reduced to 0.11 S_u and, at completion of the test, the capacity left was negligible.

As in Test 37, slip essentially developed in sidelaps 1-2, 2-3 and 3-4. For this specimen, however, the slips were equally distributed along the three sidelap lines. Slip was initiated under the West R_d = 2.0 portion of the loading but increased significantly during the West R_d = 3.0 segment. In the first large cycle in that last portion (at t $\cong$ 17 s), the cumulated slip at sidelap resulted in a shear deformation of 8.76 rad/1000, which corresponds to 80 % of the applied distortion. In that last large amplitude cycle (at t $\cong$ 22 s), 86 % of the applied distortion translated into slip. This suggests that most of the damage developed in the sidelap joints.

As discussed in test 37, strength degradation may be explained by the failure of connections at the sidelap locations during the loading protocol. Figure 5.22 presents the slip time history for sidelap 1,2 together with the measured load in the test specimen. The strength degradation started when the sidelap slip, or connection deformation, reached around 2 mm and continued when the slip increased. The failure of welded connections at sidelaps occurred in this deformation range, and explain the degradation noticed in the test. Figure 5.29 shows one of the two typical failure modes involved (BT and BF). Remarks on these failure modes are as found for test 37. Figure 5.30 gives an

example of the DBF failure mode, which is a bond failure with buckling. This failure mode occurred at welds located in the interior of deck panels.

The maximum measured load in test 37 of, 12.6 kN/m, was smaller than that in test 21, 13.8 kN/m. This may be attributed to the size of the sidelap purlin welds, which were smaller in test 37. The average length for slotted welds was 18.0 mm for test 37 compared to 20.0 mm in test 21 (see Table 5.15). Although past tests on welded deck-to-frame fasteners (Rogers and Tremblay (2000), Bond *et al.* (2001) and Peuler (2002)) did not indicate a clear correlation between the strength of welds and the applied strain rate, it is deemed that for this test, dynamic loading may have led to the observed greater resistance. However, this would need to be confirmed through additional tests.

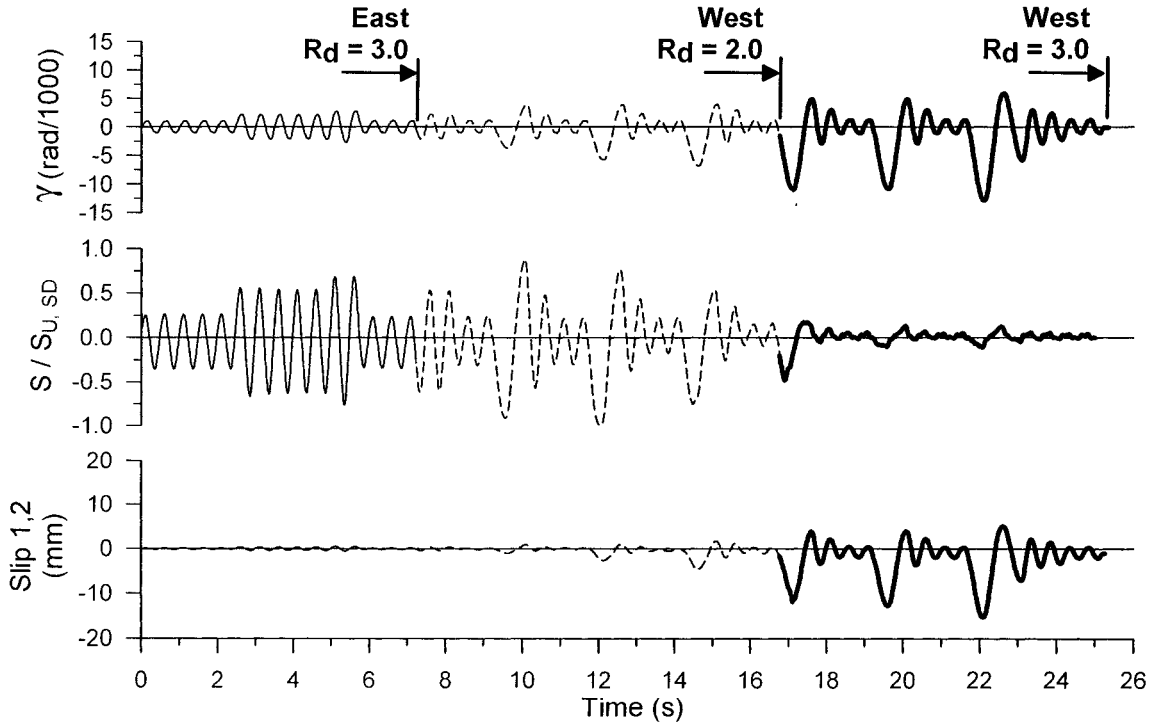

Figure 5.22 Slip at sidelap 1,2 compared with the measured load, Test 21

Table 5.15 Test specimen description (Tests 37 and 21)

Steel properties:	
Supplier and coil number	Canam P-3615 standard deck 0.91 mm Coil supplier: unknown Coil number: unknown Deck panels from Essa *et al.* (2001) order.
Base metal thickness (mm)	0.86
Fy test (MPa)	285
Fu test (MPa)	368
E (MPa)	198000
50 mm gauge % elongation	31 %
Fasteners:	
Type and spacing for sidelap fasteners	Button punch Spacing: 305 mm c/c
Type and spacing for deck-to-frame fasteners	Puddle weld 16 mm nominal diameter Electrode E6011 2.5 mm diameter 100 Amp Spacing: 305 mm c/c
Comments on quality of fasteners:	
Test 37	Weld dimensions: Round welds Diameter: Average: 16.6 mm C.o.V.: 0.03 Slotted welds at sidelap and purlin junctions Length: Average: 18.0 mm C.o.V.: 0.00 Width: Average: 10.0 mm C.o.V.: 0.00 Weld quality deemed appropriate. However, it was difficult to obtain a high percent connectivity at sidelaps because of the round shape of deck profile.
Test 21	Weld dimensions: Round welds Diameter: Average: 16.1 mm C.o.V.: 0.06 Slotted welds at sidelap and purlin junctions Length: Average: 20.0 mm C.o.V.: 0.25 Width: Average: 10.0 mm C.o.V.: 0.00 Weld quality deemed appropriate. However, it was difficult to obtain a high percent connectivity at sidelaps because of the round shape of deck profile.

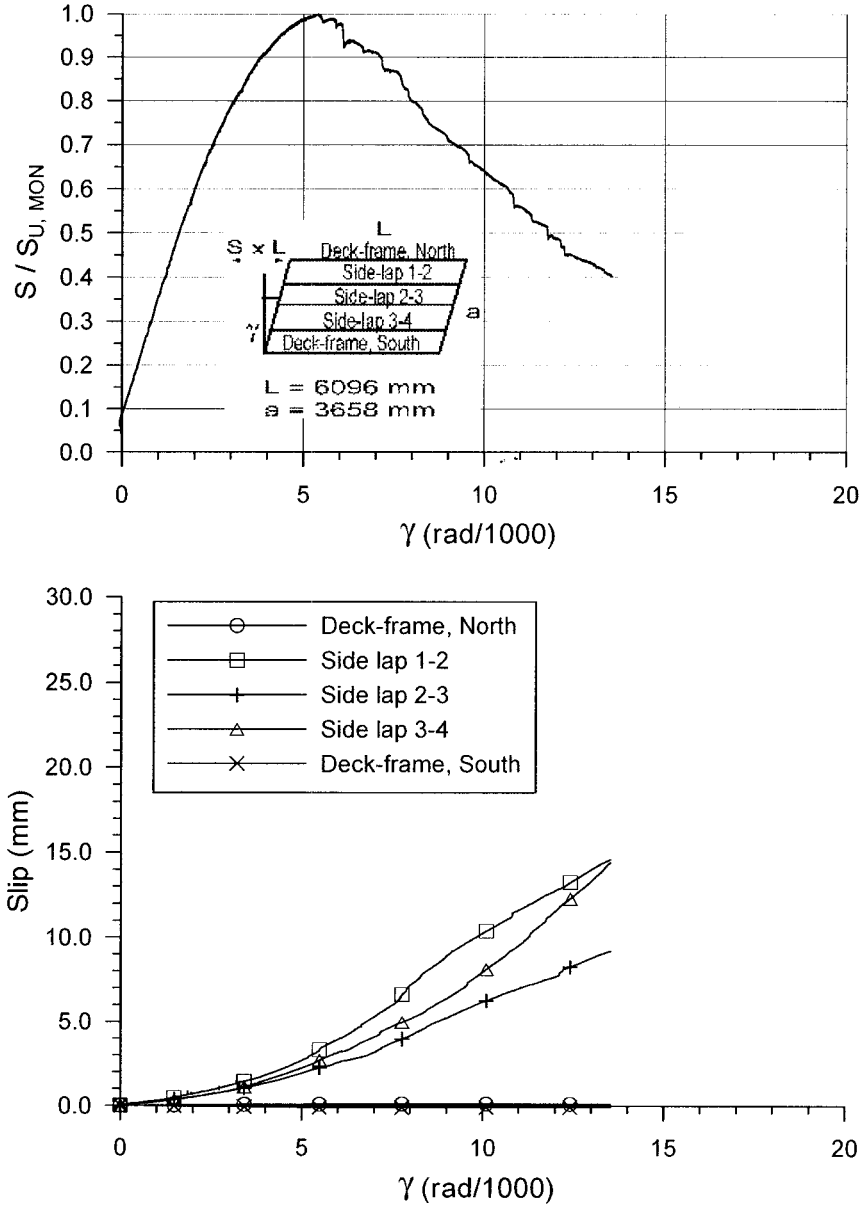

Test No. 37
P3615 - 0.91 mm
Sidelap fasteners : Button punched @ 305 Frame fasteners : Welds 16 mm @ 305
$S_{u,SDI*}$ = 16.9 kN/m $S_{u,MON}$ = 12.6 kN/m

Figure 5.23 Test no.37 results

	1	2	3	4	5	6	7	8	9	10	11	12	13	14	15	16	17	18	19	20	21
A	BF																				
B																					
C	BO					BO					BO					BO					BO
D	BO					BT					BF					BB					BT
E						BO					BO					BO					BF
F	BO																				
G	BO															BT					BT
H						BO															BBF
I	BO															DBF					
J	BB					BT					BB					BT					BT
K	BO					BF					DBF					BBF					DBF
L						DBF					BF					BF					BBF
M																					

Table 5.16 Observed damage (Test 37)

Comments: Sidelap G was disengaged over half of its length.

Nomenclature of failure modes (button punch - weld pattern)

Welded connections at sidelap
BT: Bond failure of top sheet from bottom sheet with little amount of inelastic deformation
BB: Bond failure where both sheets disconnected from weld to frame
BF: One of the two cases mentioned above (not determined)

Welded connections (not at sidelap)
BBF: Bond failure with little amount of inelastic deformation
DBF: Bond failure with buckling
BF: One of the two cases mentioned above (not determined)

For both types of weld
BO: Buckling of sheet on one side of weld without weld failure

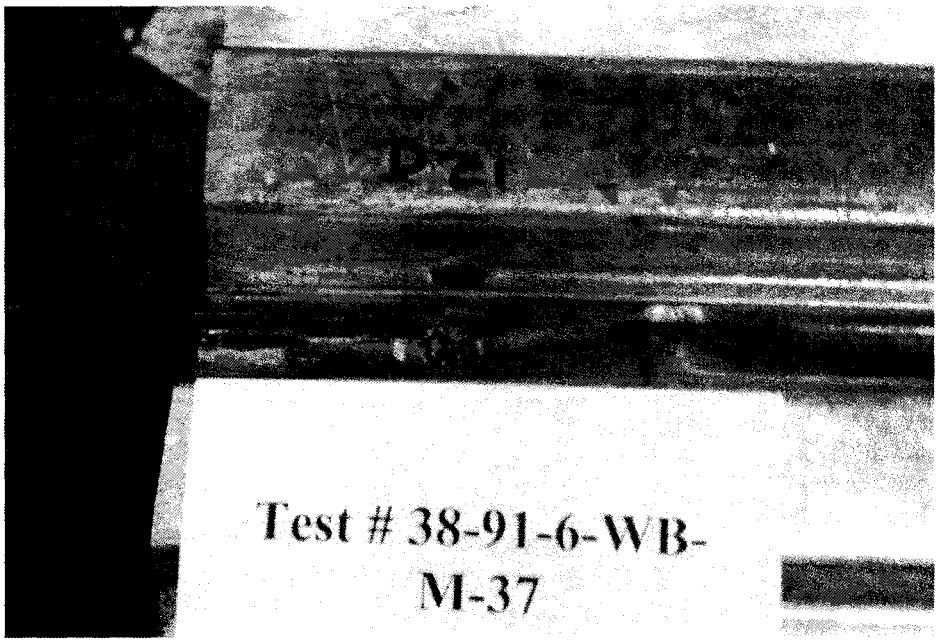

Figure 5.24 BT failure mode at D21, Test 37

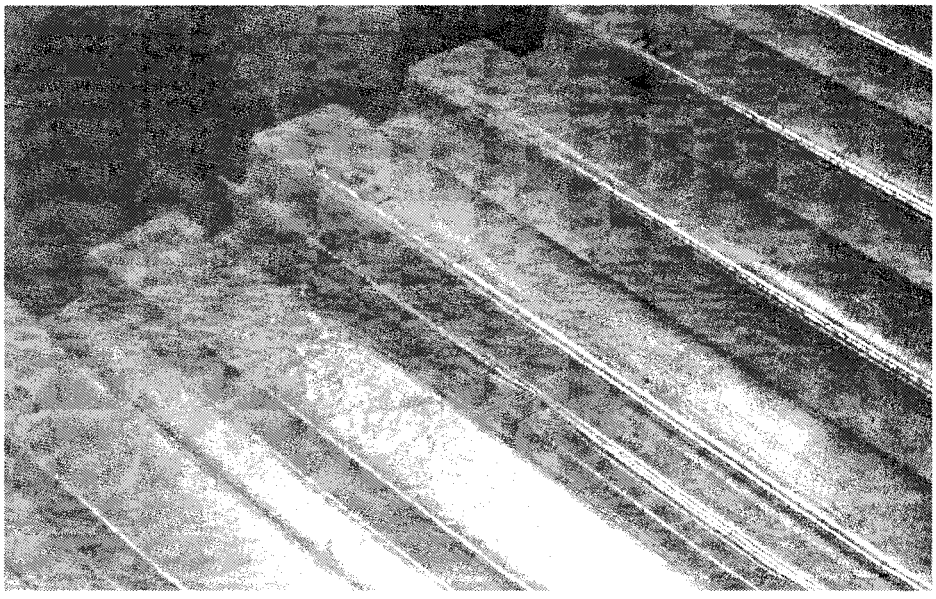

Figure 5.25 Sidelap 2-3 disengaged, Test 37

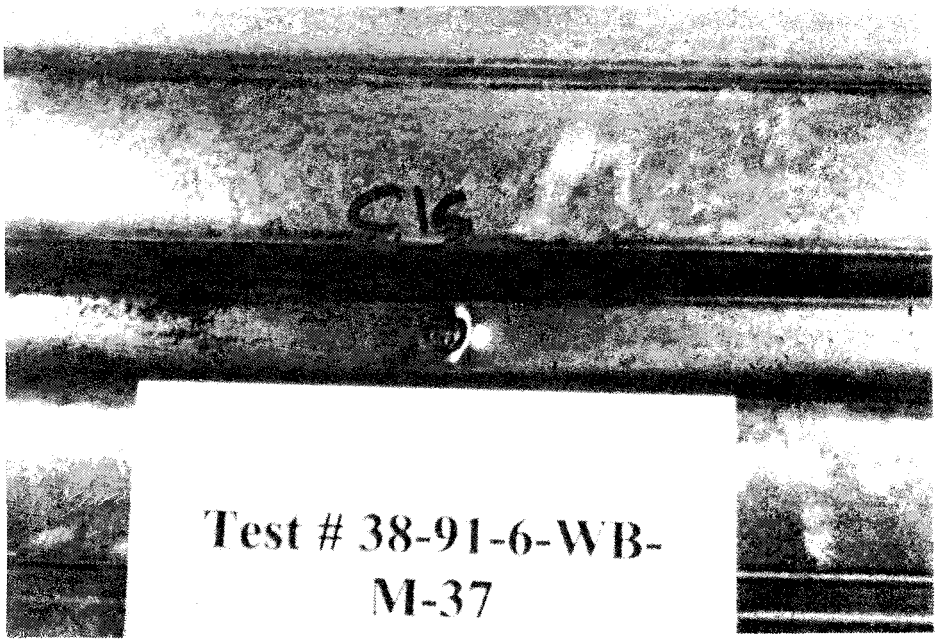

Figure 5.26 BO failure mode at C16, Test 37

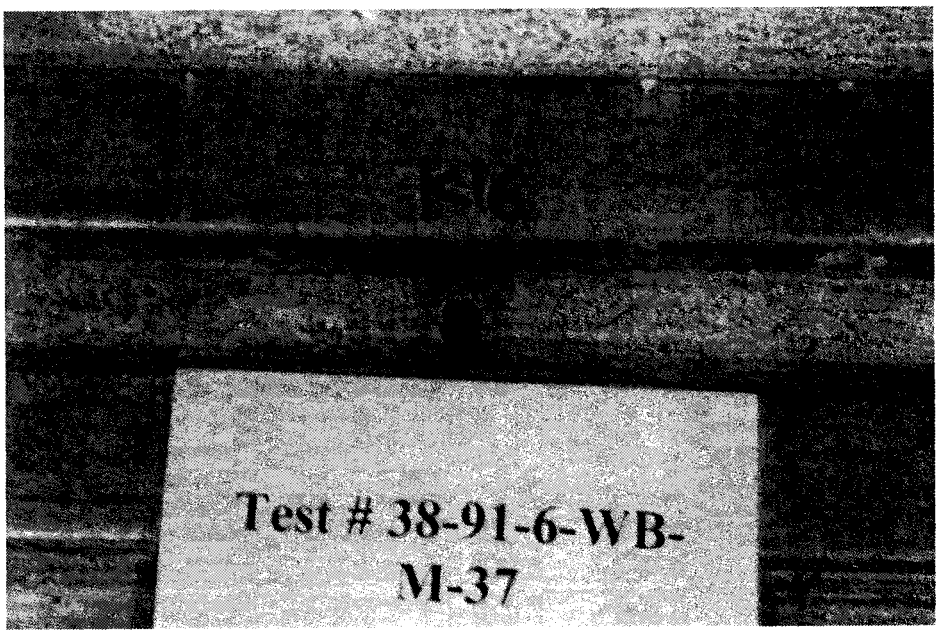

Figure 5.27 BBF failure mode at K16, Test 37

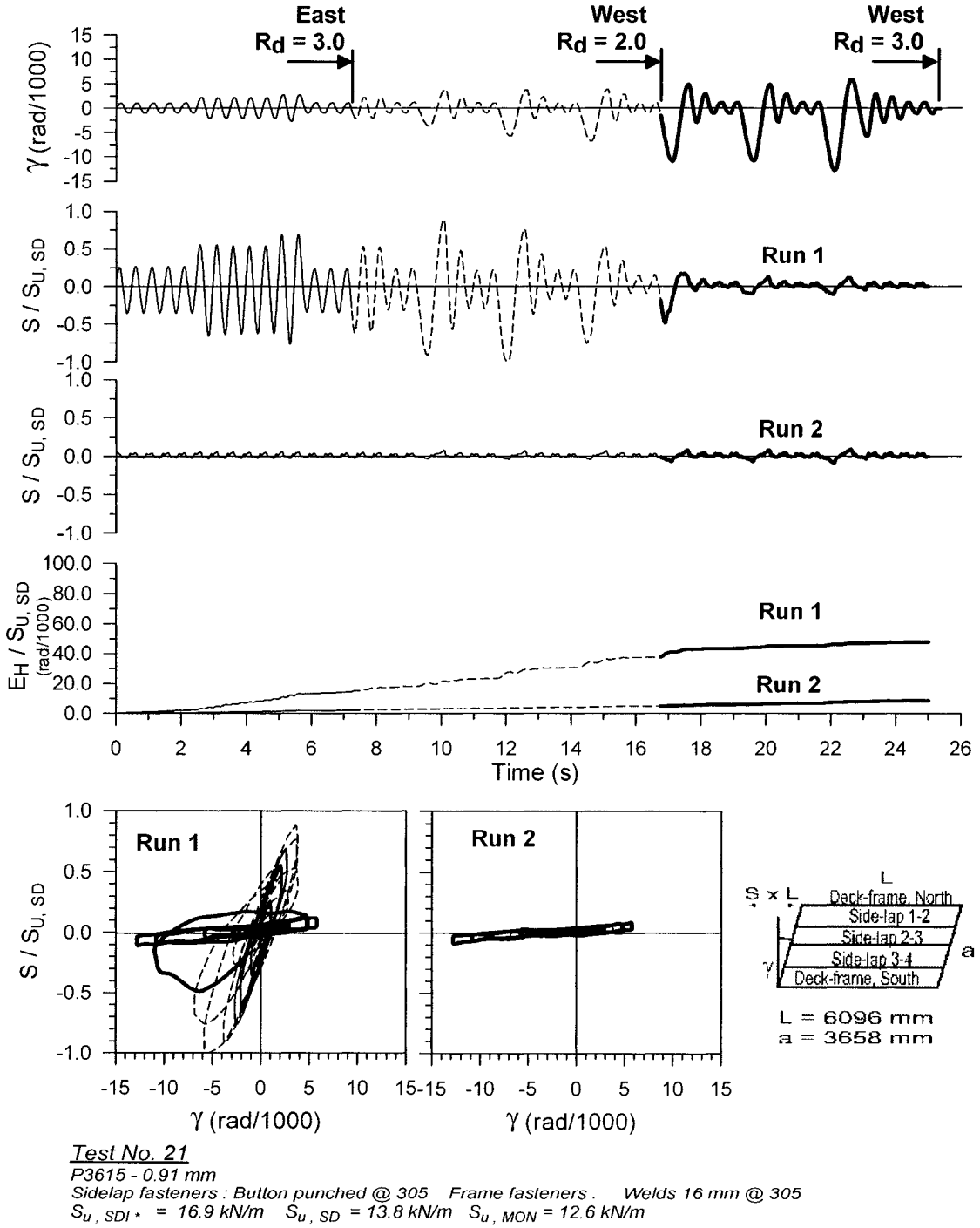

Test No. 21
P3615 - 0.91 mm
Sidelap fasteners : Button punched @ 305 Frame fasteners : Welds 16 mm @ 305
$S_{u,SDI*}$ = 16.9 kN/m $S_{u,SD}$ = 13.8 kN/m $S_{u,MON}$ = 12.6 kN/m

Figure 5.28 Test no.21 results

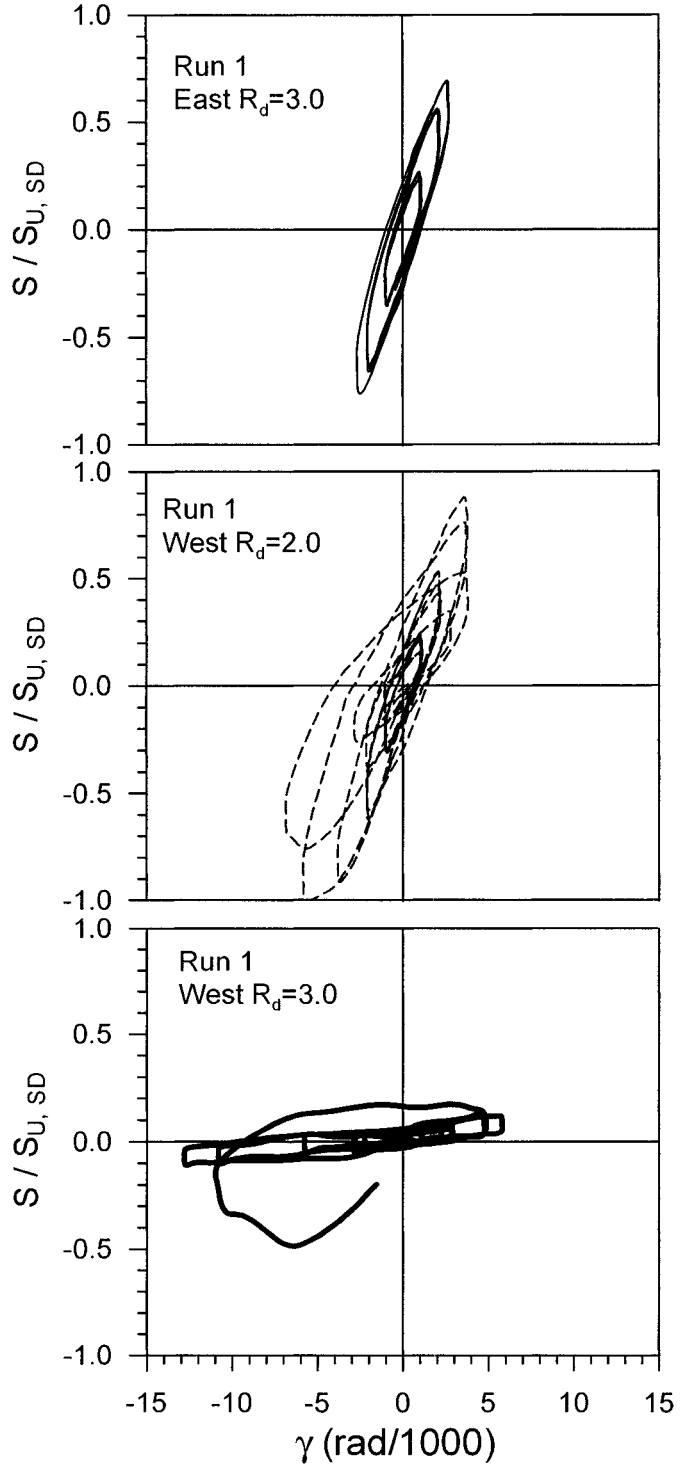

Test No. 21

P3615 - 0.91 mm
Sidelap fasteners :
Button punched @ 305
Frame fasteners :
Welds 16 mm @ 305

$S_{u, SDI*}$ = *16.9 kN/m*
$S_{u, SD}$ = *13.8 kN/m*
$S_{u, MON}$ = *12.6 kN/m*

Figure 5.28 Test no.21 results (continued)

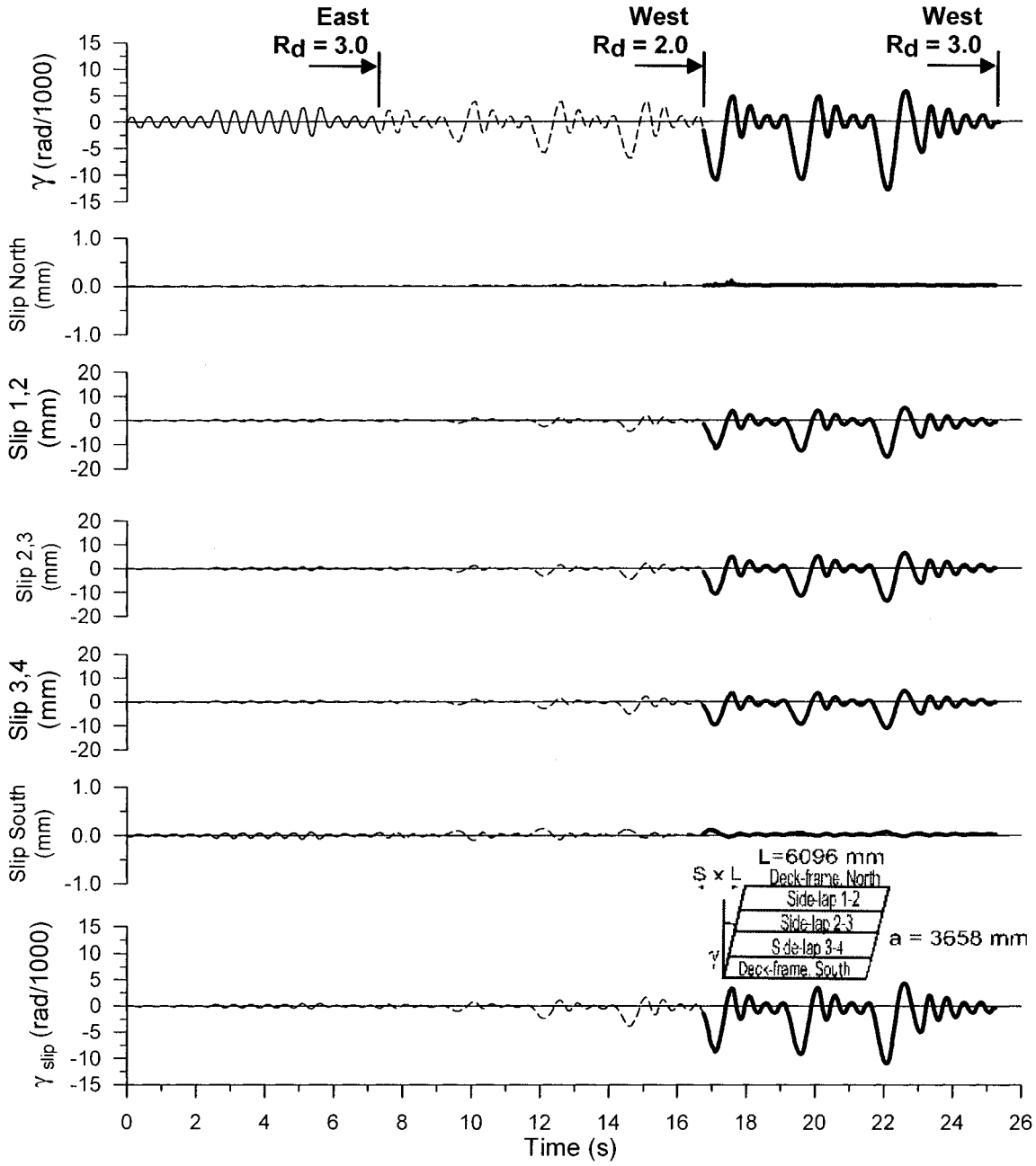

Test No. 21- Run 1
P3615 - 0.91 mm
Sidelap fasteners : Button punched @ 305 Frame fasteners : Welds 16 mm @ 305
$S_{u,SDI}$ = 16.9 kN/m $S_{u,SD}$ = 13.8 kN/m $S_{u,MON}$ = 12.6 kN/m

Figure 5.28 Test no.21 results (continued)

Table 5.17 Observed damage after run 1 (Test 21)

	1	2	3	4	5	6	7	8	9	10	11	12	13	14	15	16	17	18	19	20	21
A																					
B	BO										BO										DBF
C	DBF					DBF					DBF					DBF					DBF
D	BF										BF					BF					BF
E	BO										BO					DBF					
F						BO					DBF										DBF
G	BF					BT					BF					BT					
H	DBF					DBF					DBF					DBF					BBF
I	DBF															BO					
J	BT					BF					BF					BT					BF
K	BBF					DBF					DBF					DBF					BBF
L	BO															DBF					
M																					

Nomenclature of failure modes (button punch - weld pattern)

Welded connections at sidelap
BT: Bond failure of top sheet from bottom sheet with little amount of inelastic deformation
BB: Bond failure where both sheets disconnected from weld to frame
BF: One of the two cases mentioned above (not determined)

Welded connections (not at sidelap)
BBF: Bond failure with little amount of inelastic deformation
DBF: Bond failure with buckling
BF: One of the two cases mentioned above (not determined)

For both types of weld
BO: Buckling of sheet on one side of weld without weld failure

Figure 5.29 BT failure mode , Test 21

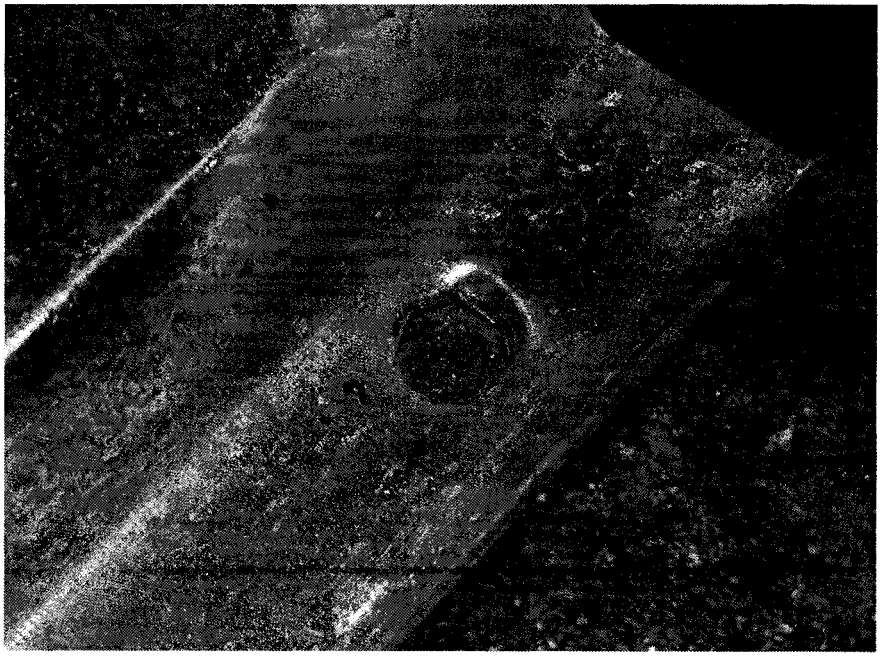

Figure 5.30 DBF failure mode, Test 21

5.8.1.2 Tests 20 and 36

Test specimens 20 and 36 were constructed of 0.76 mm standard deck and connected with button punched sidelap and welded deck-to-frame fasteners. The sheets were welded to the frame members on both sides of each sidelap line. In both tests, a short duration (SD) loading protocol was used, however, 202 elastic cycles of approximately $0.50\gamma_u$ were applied to specimen 36 prior to the SD loading protocol. The aim of these cycles was to investigate, in a preliminary fashion, the effect of wind fatigue loading at the service level. Test 1 from Essa *et al.* (2001) was utilised as the matching monotonic test. A description of test specimen 20 and 36 is presented in Table 5.18.

Test 20

Test curves for test 20 are presented in Figure 5.32 whereas the observed damage is shown in Table 5.19. The maximum measured load was equal to 9.81 kN/m, which is higher than the maximum measured load in tests 1 and 2 by Essa *et al.* (2001): 8.05 kN/m and 7.53 kN/m. In tests 1 and 2, button punches were found to be too high with respect to the male part of the connection, leading to poor connectivity at the sidelaps. This problem did not occur in this test series, which may explain the observed higher capacity.

In Figure 5.32, the slip at sidelap 3,4 is not presented after t = 17 s because LVDT #8 at that location was rendered out-of-service beyond that time. For the same reason, the distortion due to slip at sidelap (γ_{slip}) was removed for the same time interval. Nevertheless, it can be seen that the behaviour of that specimen is nearly identical to that of test 21, with most of the diaphragm shear distortion taking place in the intermediate sidelaps under West $R_d = 2.0$ and West $R_d = 3.0$.

Strength degradation occurred under the East R_d =3.0 loading protocol in cycles at $0.8\gamma_u$. The maximum measured load was found in the first cycle at $0.8\gamma_u$. and the forces measured in peaks at γ_u were smaller– contrary to what would be expected. It is possible that the imposed $0.8\gamma_u$ value was close to the real γ_u of the system. The measured shear stiffness, G', was equal to 2.44 kN/mm, which is different from the G', 2.14 kN/mm obtained in test 1 (Essa *et al.*, 2001), which was used to evaluate the target γ_u The specimen may have been pushed too far with regards to its real γ_u. This cannot be verified since no monotonic test was carried out with the same test specimen. Under the West R_d = 2.0 segment, the strength degraded to such a degree that negligible shear resistance was available at end of this time interval.

In test 20, the strength degradation began earlier compared to test 21. This is attributed to the wrong evaluation of loading references in test 21, which was discussed in Section 5.5. The behaviour in test 20 is deemed more relevant to what would occur during a design level earthquake than the behaviour obtained in test 21 because the loading reference was more appropriate.

Similar to the behaviour observed in tests 37 and 21, strength degradation in test 20 was caused by the failure of welded connections at the sidelap purlin locations. Figure 5.31 shows the time histories for strength and slip at sidelap 1,2. Again, the strength degradation became more pronounced when the sidelap failed as a whole

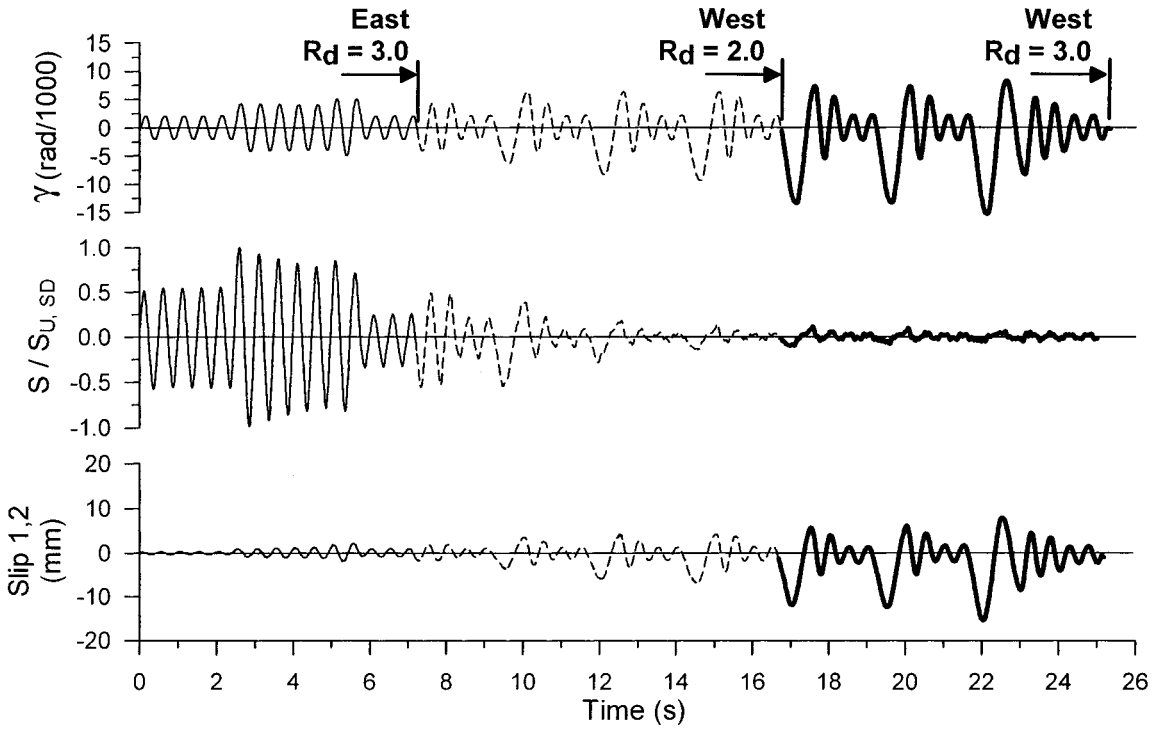

Figure 5.31 Slip at sidelap 1,2 compared with the measured load, Test 20

Failure modes observed in tests 37 and 21 were also encountered in test 20. Figure 5.33 shows bond failure with buckling (DBF). Figure 5.34 displays a weld with buckling on one side (BO).

Test 36

As explained previously, test 36 involved elastic cycling prior to the SD loading protocol. Two hundred cycles at $0.4\gamma_u$ and two cycles at $0.6\gamma_u$ were applied. The aim of these cycles was to investigate the effect of repeated service loads on the subsequent seismic resistance of the diaphragm.

Figure 5.35 presents the test result curves. Two pages cover the elastic cycling prior to the SD loading protocol. On the first page, the distortion time history together with

measured forces and dissipated energy are presented. In addition, a shear-distortion curve is shown. On the second page, shear-distortion curves for 5 cycles (1^{st}, 50^{th}, 100^{th}, 150^{th} and 200^{th}) are displayed. The test curves for the SD loading protocol follow. Table 5.20 shows the observed damage after the 202 elastic cycles whereas Table 5.21 gives the observed damage after run 1 of the SD loading protocol.

The maximum force in the cyclic portion of the loading protocol, 5.80 kN/m, was measured in the first cycle. Afterwards, strength degradation started and the maximum force in the last cycle at $0.4\gamma_u$ was equal to 3.67 kN/m giving a 37% drop in capacity. In the following two cycles that were imposed at $0.6\gamma_u$, the maximum force was equal to 5.14 kN/m, which is smaller than the maximum measured force in the initial cycles at $0.4\gamma_u$. If there had been no strength degradation, a force equal to 8.70 kN/m would have been anticipated based on the maximum force in the first cycle.

As stated, the maximum measured load in the cycles at $0.4\gamma_u$ was equal to 5.80 kN/m, which was greater than 3.92 kN/m, the value corresponding to 0.4 S_u of Test 20 assuming elastic response and that the strength of both specimens were the same. This discrepancy can be explained by the evaluation of γ_u used in the loading protocol. As discussed in Section 5.5, the loading reference γ_u was based on $S_{u,\ SDI*}$ and a secant stiffness G'. In fact, γ_u was equal to the ratio of $S_{u,\ SDI*}$ to G'. $S_{u,\ SDI*}$ was supposed to be equal to 11.4 kN/m which is larger than the measured force from test 20. The ratio between $S_{u,\ SDI*}$ and S_u from test 20 was equal to 1.17. In addition, the assumed G' was equal to 2.14 kN/mm which was smaller than the measured G' in test 36, 2.40 kN/m. The ratio between the measured and the assumed stiffness G' was equal to 1.12. These two factors worked together to increase the γ_u used in the loading protocol in comparison with the real γ_u of the deck specimen. Taking both ratios 1.17 and 1.12 and multiplying them with the expected $0.4S_u$ gives $0.52S_u$, which is not far from the measured $0.59S_u$.

At the end of the 202 fatigue cycles, failures were observed in a number of connections. At sidelap purlin welds, the BT failure mode (see Figure 5.36) was observed at 67% of locations, whereas the BB failure mode was found at 13% of locations. Bond failure at welded deck-to-frame connections inside deck panels (BF) was noticed at 6 locations. Overall, the cycles in the elastic range caused a significant number of connections to fail prior to the implementation of the SD loading protocol.

This fatigue test was intended to investigate the effect of wind load on deck diaphragms. Winds induce pressures and loads on the structure and this situation would have been more realistically reproduced if a load controlled cyclic tests had been performed in lieu of a displacement controlled test. Under load control, it can be expected that more significant damage would have been imposed on the diaphragm. Hence, in future studies, it is suggested that wind fatigue testing be performed with a load controlled protocol.

Following the low amplitude cycles, the short duration (SD) loading protocol was applied. The maximum measured load, 5.69 kN/m, occurred in the first cycle at $0.8\gamma_u$. This was smaller than the maximum measured force in the elastic cycles that were applied prior to the SD loading protocol. In addition, this value is smaller than the maximum force recorded for test 20, i.e., 9.80 kN/m. Hence, the imposed fatigue cycling had a large impact on the strength of the deck specimen that was available to resist the seismic loading. Under the SD loading protocol the specimen in test 36 behaved in a similar fashion to that observed for test 20. For comparison, the S/S_u curve from test 20 was imposed on the test 36 curve. Under the East R_d =3.0 segment, the strength in test 36 was approximately half of the strength in test 20, again due to the prior fatigue test (see Figure 5.35). However, under the West R_d = 2.0 and the West R_d = 3.0 segments, the S/S_u curve in test 36 tended to meet the curve from test 20. In the first peak in West

R_d = 2.0, the force was about 84% of what was measured for the same peak in test 20. Overall, the 202 cycles had the same effect as the East R_d = 3.0 segment.

Slip at the North and South edges was minimal, however, slips as large as 20 mm were measured at interior sidelaps. Furthermore, all interior sidelaps were completely separated at the end of the test. Failure modes from test 20 were also observed in test 36. Figure 5.37 displays a BT failure mode after run 1 of the SD loading protocol.

The 202 elastic cycles had a large influence on strength degradation, where the maximum measured force in test 36 was equal to 5.80 kN/m compared to 9.81 kN/m in test 20. However, the fatigue demand on the deck specimen under service loads was not evaluated thoroughly and further study is recommended.

Table 5.18 Test specimen description (Tests 20 and 36)

Steel properties:	
Supplier and coil number	Canam P-3615 standard deck 0.76 mm Coil supplier: unknown Coil number: unknown Deck panels from Essa et al. (2001) order.
Base metal thickness (mm)	0.71
Fy test (MPa)	301
Fu test (MPa)	373
E (MPa)	197000
50 mm gauge% elongation	31 %
Fasteners:	
Type and spacing for sidelap fasteners	Button punch Spacing: 305 mm c/c
Type and spacing for deck-to-frame fasteners	Puddle weld 16 mm nominal diameter Electrode E6011 2.5 mm diameter 100 Amp Spacing: 305 mm c/c
Comments on quality of fasteners:	
Test 20	Weld dimensions: Round welds Diameter: Average: 16.1 mm C.o.V.: 0.04 Slotted welds at sidelap and purlin junctions Length: Average: 22.5 mm C.o.V.: 0.12 Width: Average: 10.0 mm C.o.V.: 0.00 Weld quality deemed appropriate. However, it was difficult to obtain a high percent connectivity at sidelaps because of the round shape of deck profile.
Test 36	Weld dimensions: Round welds Diameter: Average: 16.5 mm C.o.V.: 0.08 Slotted welds at sidelap and purlin junctions Length: Average: 15.3 mm C.o.V.: 0.05 Width: Average: 10.0 mm C.o.V.: 0.00 Weld quality deemed appropriate. However, it was difficult to obtain a high percent connectivity at sidelaps because of the round shape of deck profile.

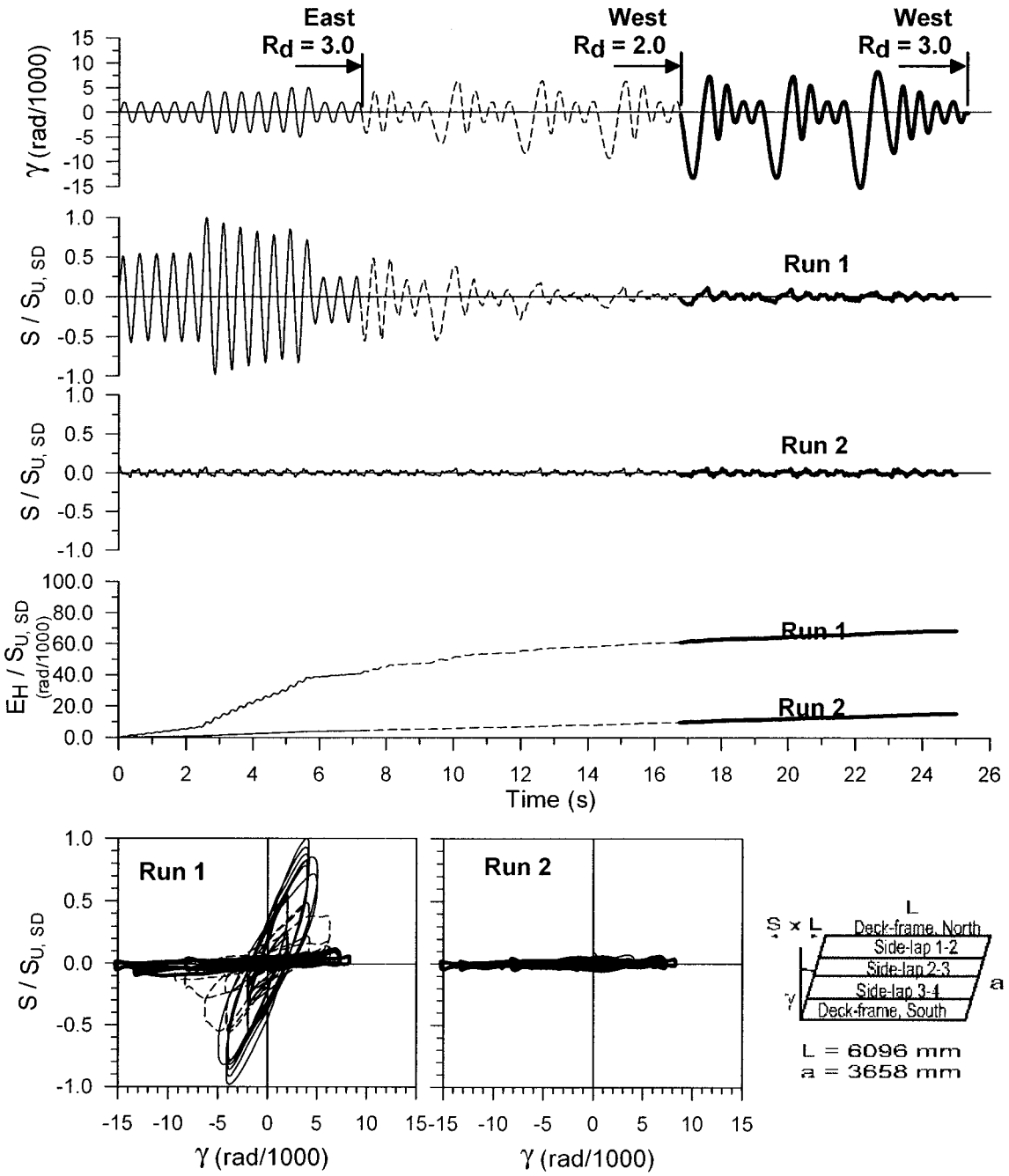

Test No. 20
P3615 - 0.76 mm
Sidelap fasteners : Button punched @ 305 Frame fasteners : Welds 16 mm @ 305
$S_{u,SDI*}$ = 11.4 kN/m $S_{u,SD}$ = 9.81 kN/m $S_{u,MON}$ = 8.05 kN/m

Figure 5.32 Test no. 20 results

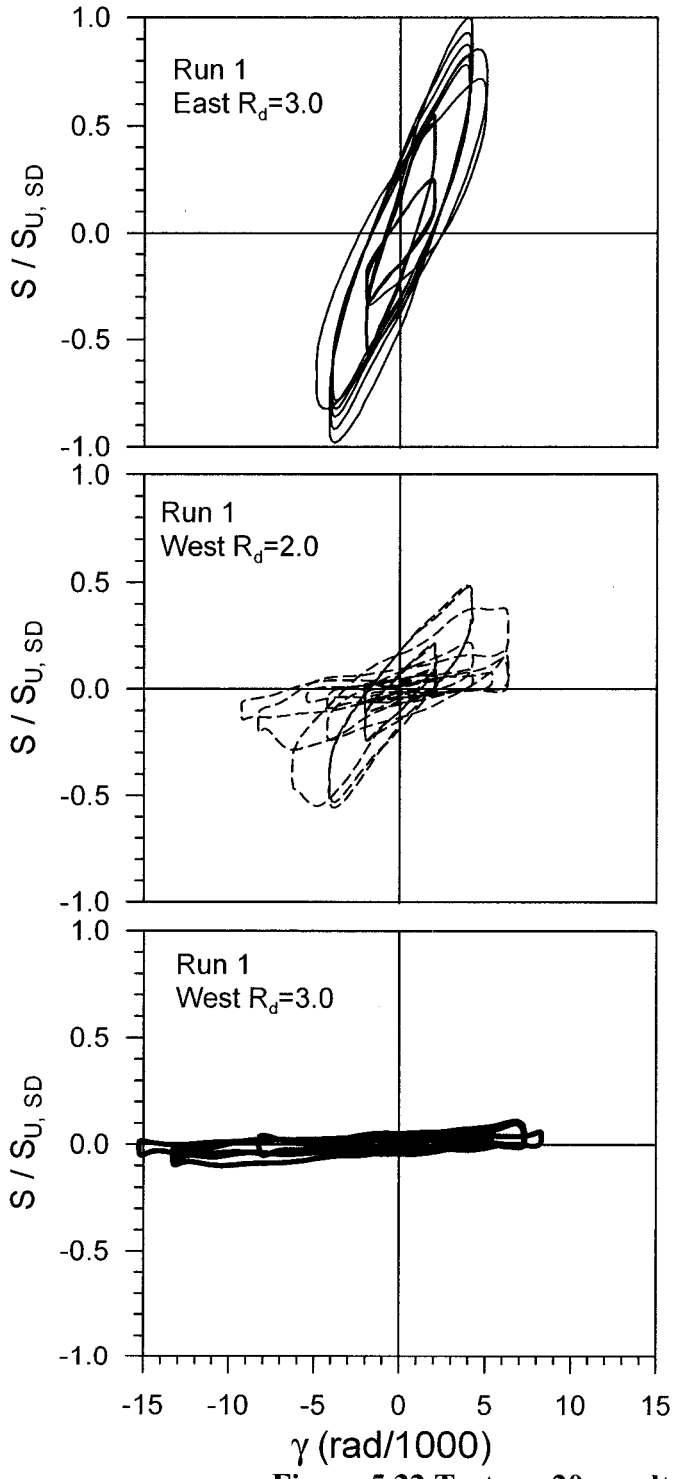

Test No. 20

P3615 - 0.76 mm
Sidelap fasteners :
Button punched @ 305
Frame fasteners :
Welds 16 mm @ 305

$S_{u, SDI*}$ = 11.4 kN/m
$S_{u, SD}$ = 9.81 kN/m
$S_{u, MON}$ = 8.05 kN/m

Figure 5.32 Test no. 20 results (continued)

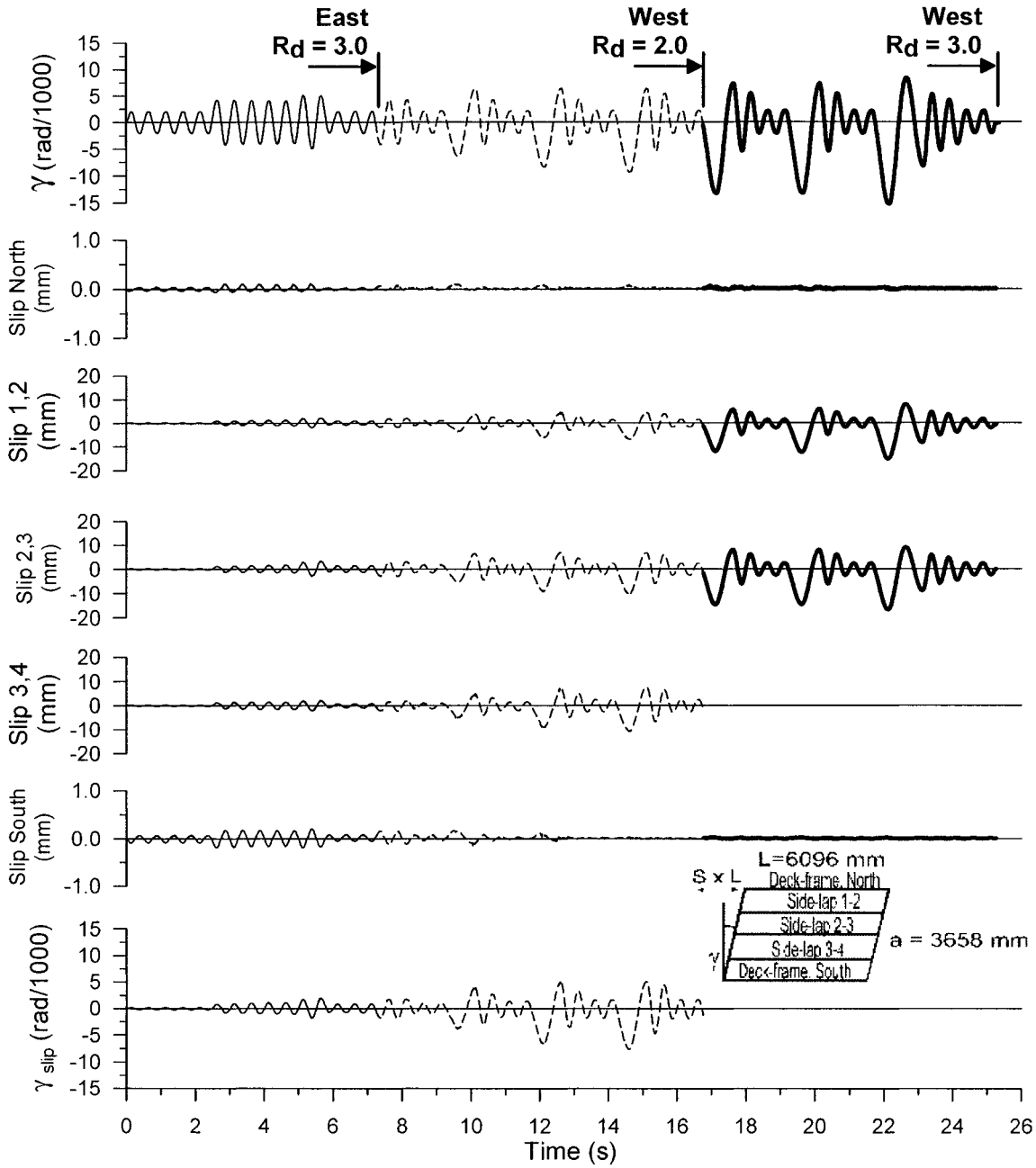

Test No. 20- Run 1
P3615 - 0.76 mm
Sidelap fasteners : Button punched @ 305 Frame fasteners : Welds 16 mm @ 305
$S_{u,SDI*}$ = 11.4 kN/m $S_{u,SD}$ = 9.81 kN/m $S_{u,MON}$ = 8.05 kN/m

Figure 5.32 Test no. 20 results (continued)

Table 5.19 Observed damage after run 1 (Test 20)

	1	2	3	4	5	6	7	8	9	10	11	12	13	14	15	16	17	18	19	20	21
A																					
B	DBF										BO					BO					DBF
C	DBF					DBF					DBF					DBF					DBF
D	BF					BF					BF					BF					BF
E																					
F	DBF					DBF					DBF					DBF					DBF
G	BF					BF					BF					BF					BF
H	DBF					DBF					BBF					DBF					DBF
I																					
J	BF					BF					BF					BF					BF
K	BBF					DBF					DBF					BBF					DBF
L	DBF					DBF					DBF					DBF					DBF
M																					

Nomenclature of failure modes (button punch - weld pattern)

Welded connections at sidelap
BT: Bond failure of top sheet from bottom sheet with little amount of inelastic deformation
BB: Bond failure where both sheets disconnected from weld to frame
BF: One of the two cases mentioned above (not determined)

Welded connections (not at sidelap)
BBF: Bond failure with little amount of inelastic deformation
DBF: Bond failure with buckling
BF: One of the two cases mentioned above (not determined)

For both types of weld
BO: Buckling of sheet on one side of weld without weld failure

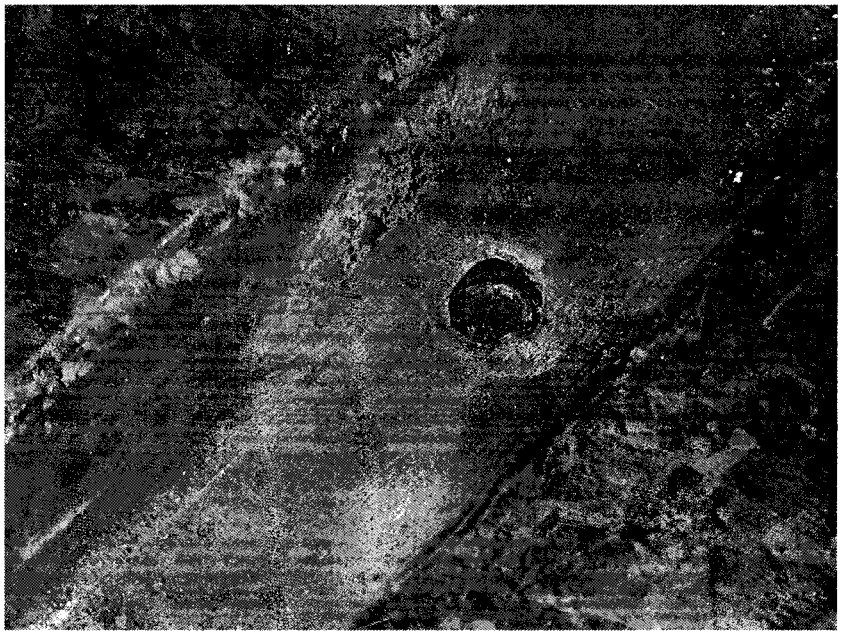

Figure 5.33 DBF failure mode, Test 20

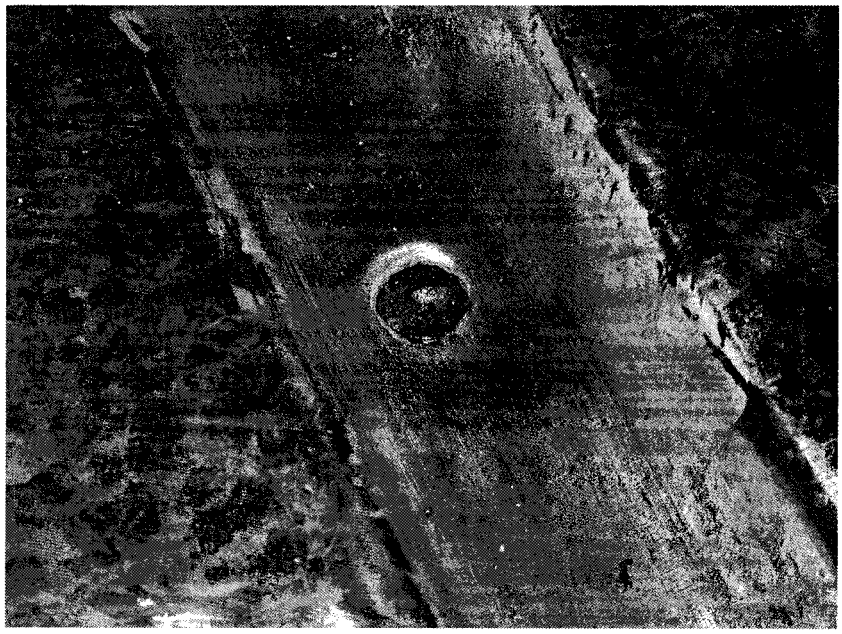

Figure 5.34 BO failure mode, Test 20

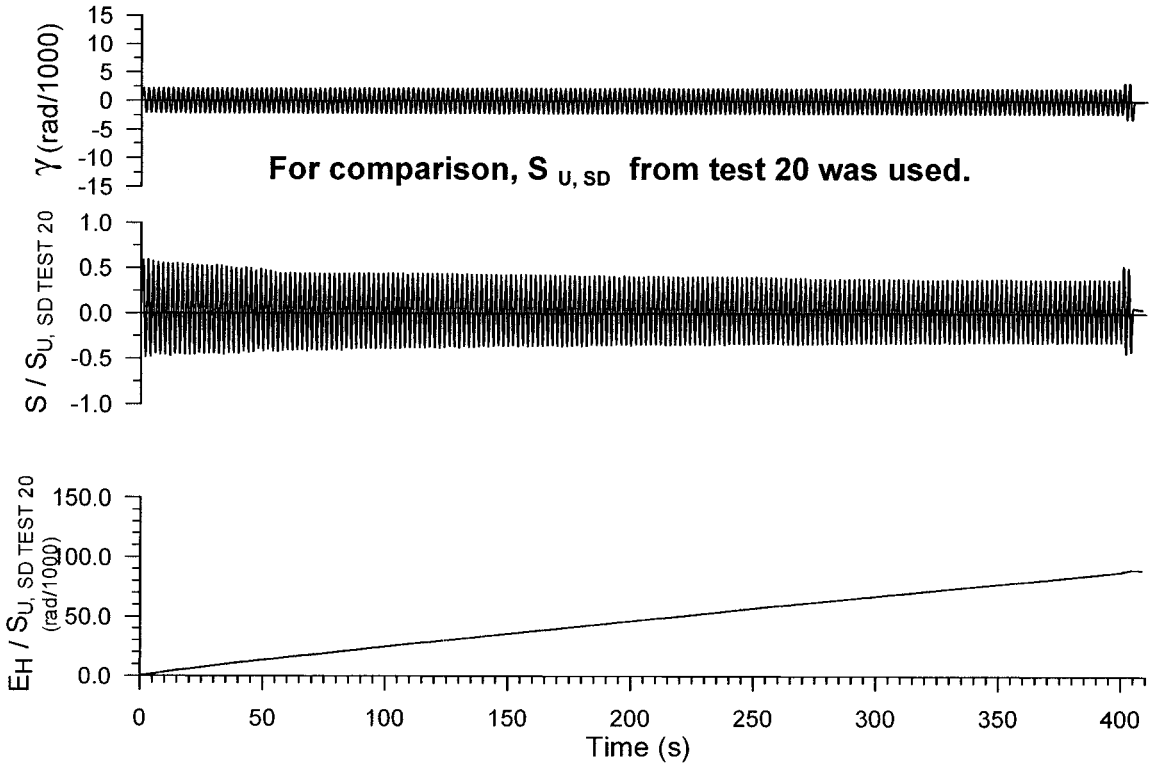

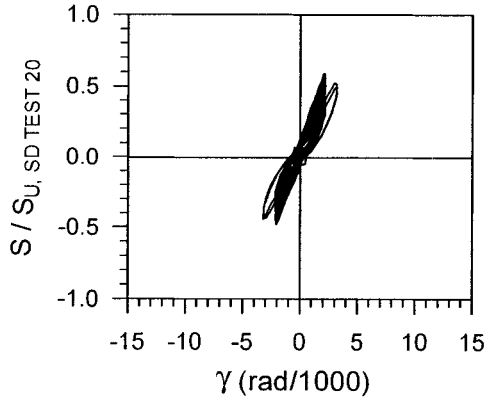

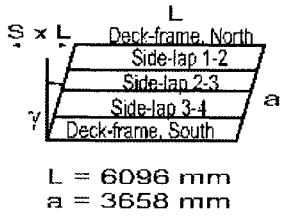

Test No. 36- Cycles prior to SD protocol
P3615 - 0.76 mm
Sidelap fasteners : Button punch @ 305 Frame fasteners : Welds 16 mm @ 305
$S_{u,\ SDI*}$ = 11.4 kN/m $S_{u,\ SD\ TEST\ 36}$ = 5.80 kN/m $S_{u,\ SD\ TEST\ 20}$ = 9.81 kN/m $S_{u,\ MON}$ = 8.05 kN/m

Figure 5.35 Test no.36 results

For comparison, $S_{U, SD}$ from test 20 was used.

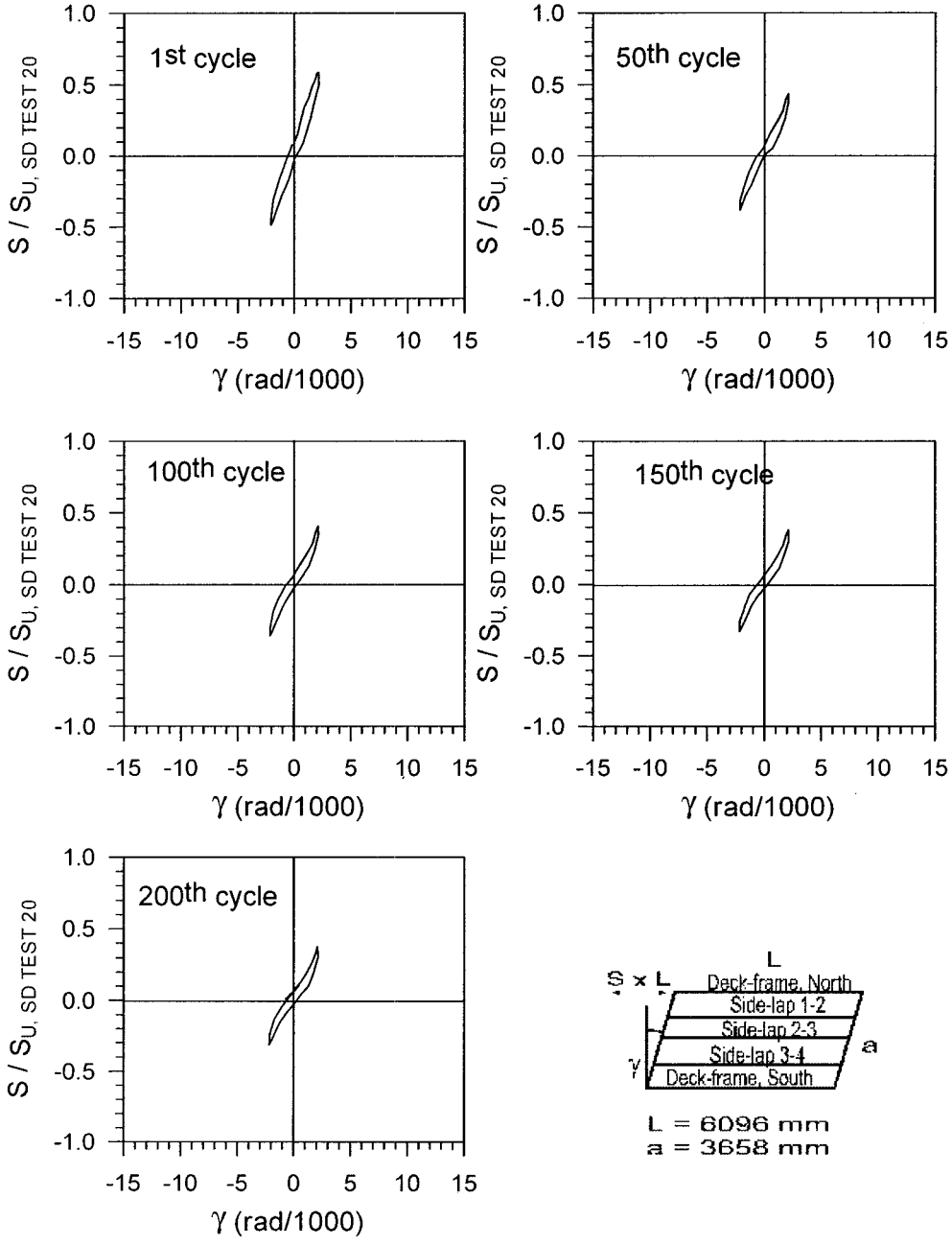

Test No. 36- Cycles prior to SD protocol

P3615 - 0.76 mm

Sidelap fasteners : Button punch @ 305 Frame fasteners : Welds 16 mm @ 305

$S_{u, SDI*}$ = 11.4 kN/m $S_{u, SD\ TEST\ 36}$ = 5.80 kN/m $S_{u, SD\ TEST\ 20}$ = 9.81 kN/m $S_{u, MON}$ = 8.05 kN/m

Figure 5.35 Test no.36 results (continued)

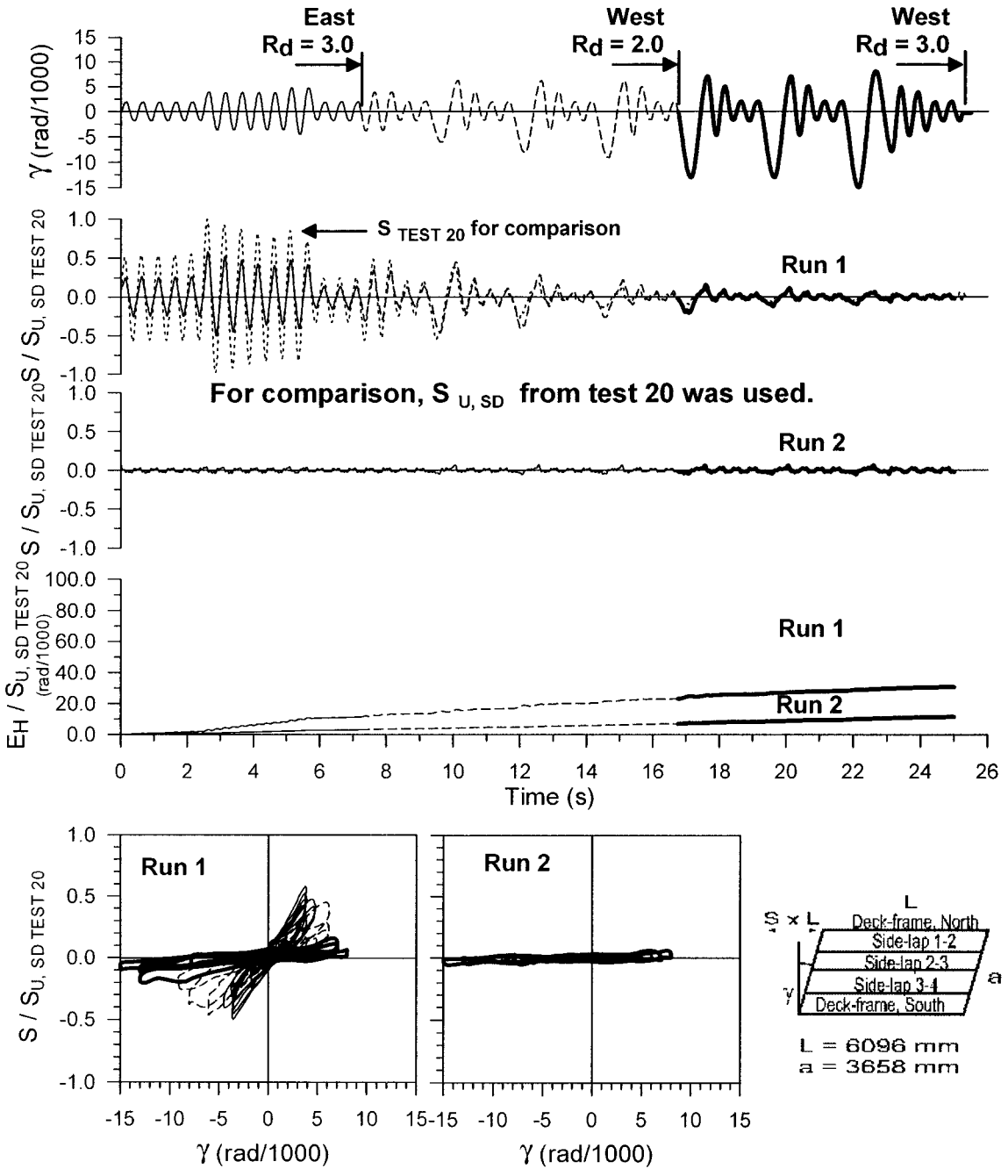

Test No. 36
P3615 - 0.76 mm
Sidelap fasteners : Button punch @ 305 Frame fasteners : Welds 16 mm @ 305
$S_{u,\,SDI*}$ = 11.4 kN/m $S_{u,\,SD\,TEST\,36}$ = 5.80 kN/m $S_{u,\,SD\,TEST\,20}$ = 9.81 kN/m $S_{u,\,MON}$ = 8.05 kN/m

Figure 5.35 Test no.36 results (continued)

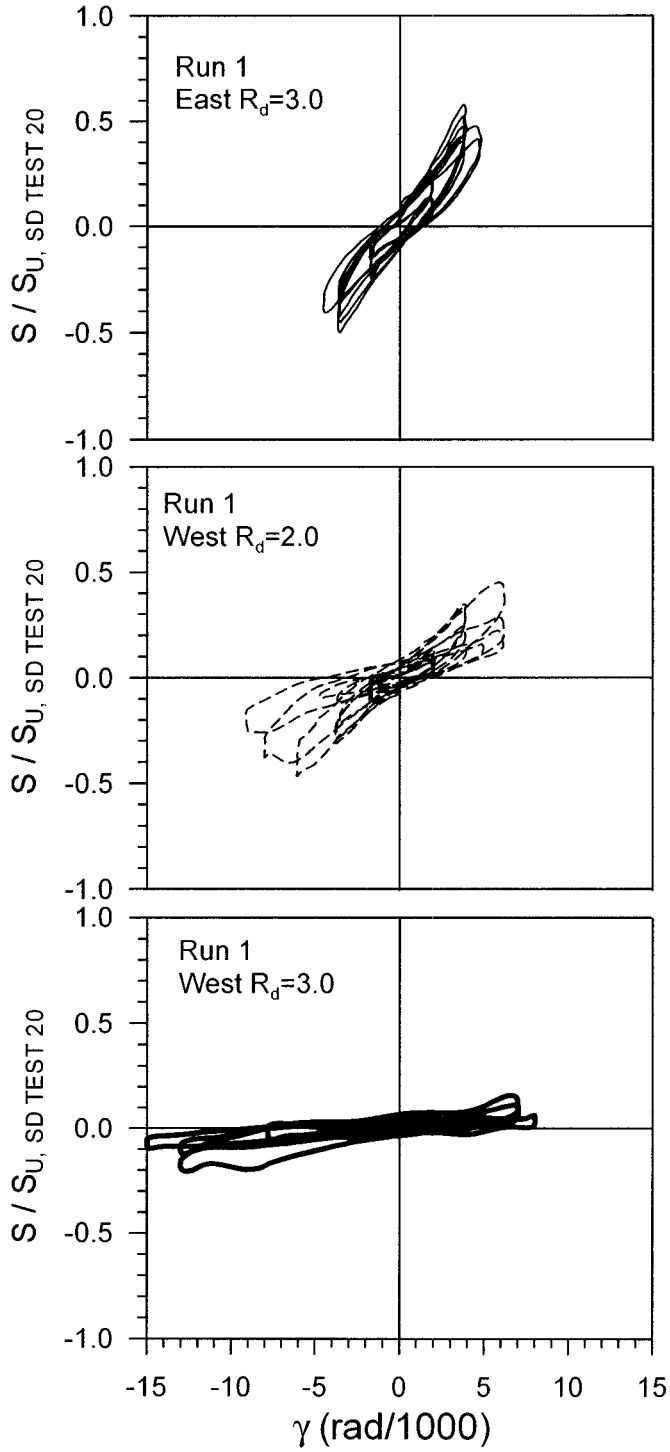

Test No. 36

P3615 - 0.76 mm
Sidelap fasteners :
Button punched @ 305
Frame fasteners :
Welds 16 mm @ 305

$S_{u, SDI*}$ = *11.4 kN/m*
$S_{u, SD TEST 36}$ = *5.80 kN/m*
$S_{u, SD TEST 20}$ = *9.81 kN/m*
$S_{u, MON}$ = *8.05 kN/m*

For comparison, $S_{U, SD}$ from test 20 was used.

Figure 5.35 Test no.36 results (continued)

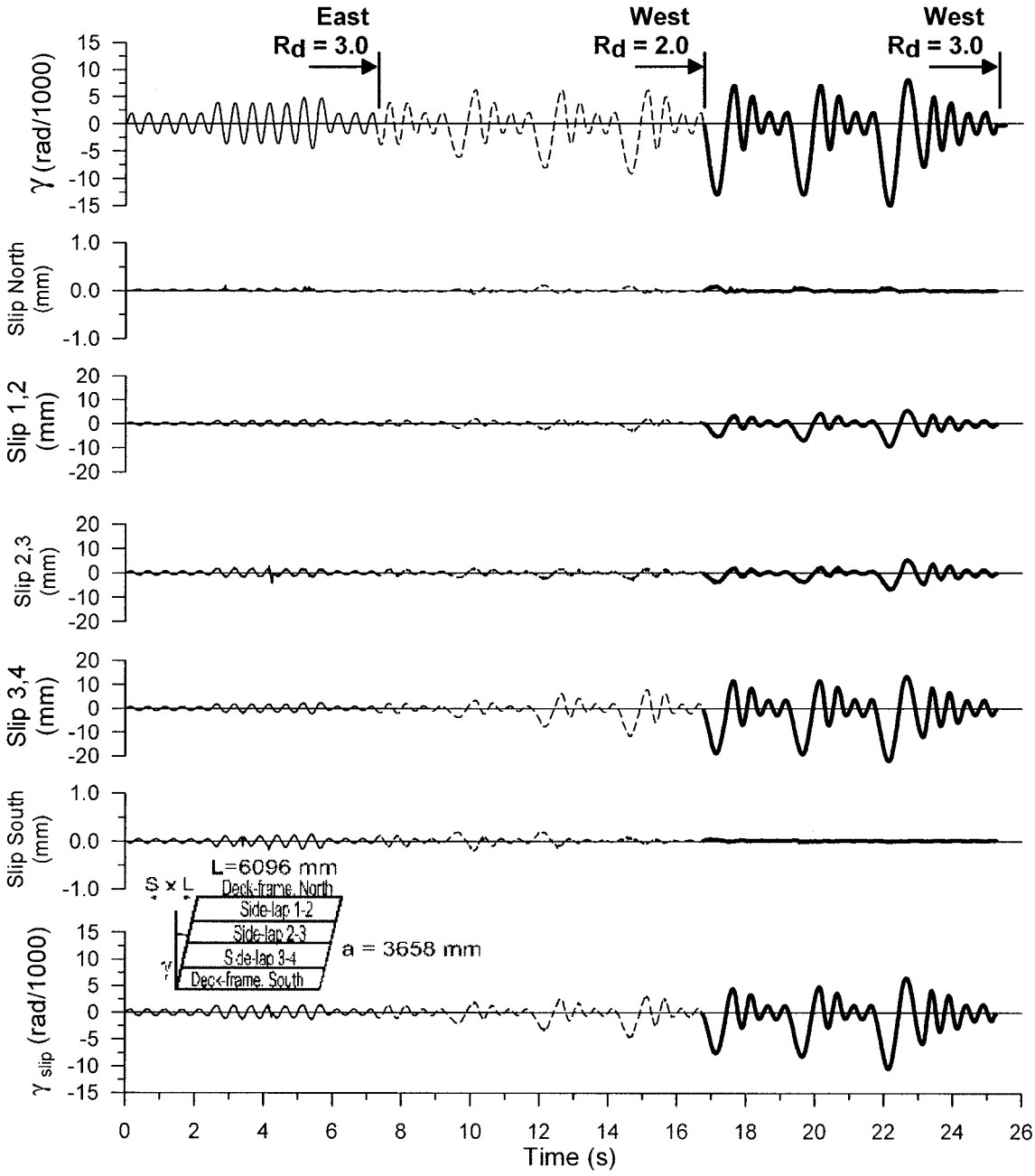

Test No. 36- Run 1
P3615 - 0.76 mm
Sidelap fasteners : Button punched @ 305 Frame fasteners : Welds 16 mm @ 305
$S_{u,\,SDI*}$ = 11.4 kN/m $S_{u,\,SD\,TEST\,36}$ = 5.80 kN/m $S_{u,\,SD\,TEST\,20}$ = 9.81 kN/m $S_{u,\,MON}$ = 8.05 kN/m

Figure 5.35 Test no.36 results (continued)

Table 5.20 Observed damage (Test 36 after 202 elastic cycles)

	1	2	3	4	5	6	7	8	9	10	11	12	13	14	15	16	17	18	19	20	21
A																					BF
B	BF																				
C	BF																				
D	BF					BT					BT					BT					
E																					
F																					
G	BT					BT					BT					BT					BB
H	BF																				
I						BF															
J	BT										BT					BT					BT
K																					BF
L																					
M																					

Nomenclature of failure modes (button punch - weld pattern)

Welded connections at sidelap
BT: Bond failure of top sheet from bottom sheet with little amount of inelastic deformation
BB: Bond failure where both sheets disconnected from weld to frame
BF: One of the two cases mentioned above (not determined)

Welded connections (not at sidelap)
BBF: Bond failure with little amount of inelastic deformation
DBF: Bond failure with buckling
BF: One of the two cases mentioned above (not determined)

For both types of weld
BO: Buckling of sheet on one side of weld without weld failure

	1	2	3	4	5	6	7	8	9	10	11	12	13	14	15	16	17	18	19	20	21
A																					
B	BF																				BF
C	BF										BF					BF					BF
D	BB					BB					BB					BB					BB
E	BF																				BF
F	BF					BF					BF					BF					BF
G	BT					BB					BB					BB					BB
H	BF																				BF
I	BF					BF					BF					BF					BF
J	BB					BB					BB					BB					BB
K	BF					BF										BF					BF
L	BF					BF					BF					BF					BF
M																					

Comments: Sidelaps D and G uplifted between 16 and 21, and, 1 and 6. Line J uplifted on the whole length.

Nomenclature of failure modes (button punch - weld pattern)

Welded connections at sidelap
BT: Bond failure of top sheet from bottom sheet with little amount of inelastic deformation
BB: Bond failure where both sheets disconnected from weld to frame
BF: One of the two cases mentioned above (not determined)

Welded connections (not at sidelap)
BBF: Bond failure with little amount of inelastic deformation
DBF: Bond failure with buckling
BF: One of the two cases mentioned above (not determined)

For both types of weld
BO: Buckling of sheet on one side of weld without weld failure

Table 5.21 Observed damage (Test 36 after run 1 of SD)

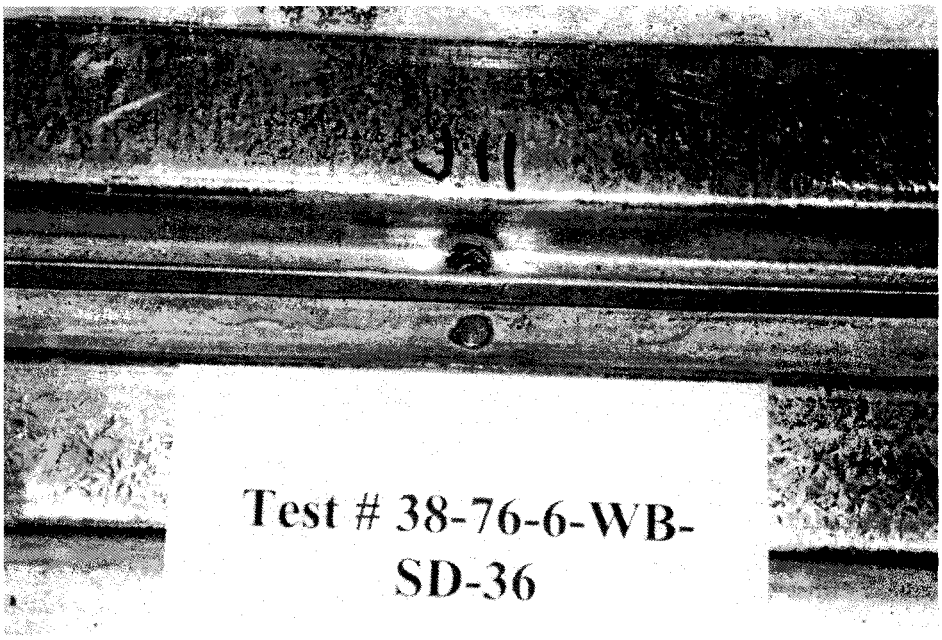

Figure 5.36 BT failure mode at J11 after 202 elastic cycles, Test 36

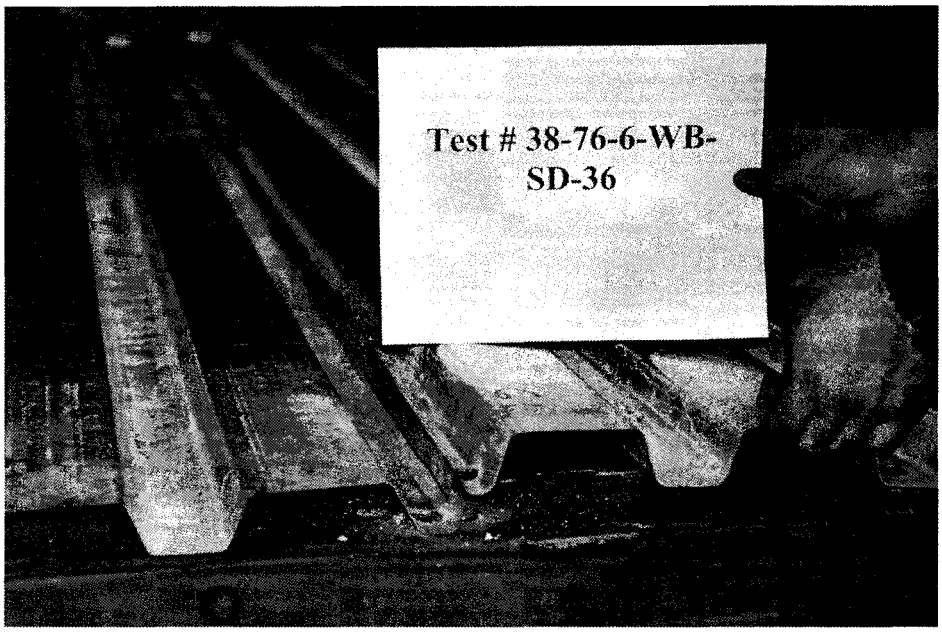

Figure 5.37 BT failure mode at G1 after run 1 of SD, Test 36

5.8.2 Weld with washer-weld with washer design

5.8.2.1 Tests 22, 23 and 24

Tests 22, 23 and 24 were conducted with 0.91 mm thick sheets and welded with washer sidelap and frame connections. Welded with washer sidelaps necessitated the use of B-deck profile sheets. Test 22 underwent a monotonic loading whereas test 23 was subjected to a short duration (SD) loading protocol and test 24 to a long duration (LD) loading protocol. Table 5.22 presents the description of specimens for tests 22, 23 and 24.

Test 22

The applied load vs. distortion curve remained nearly linear up to peak (Figure 5.39). The maximum measured load was equal to 32.1 kN/m and was found at a distortion of 8.5 rad/1000. No ductile behaviour was developed as a steep degradation in load capacity occurred. In fact, the strength reached $0.8S_u$ at 12 rad/1000. This deck assembly was much stronger in comparison to the button punch-weld deck assembly. For example, test 37 which used 0.91 mm thick deck with button punch-weld connections exhibited a maximum load of 12.6 kN/m.

One can see from Figure 5.39 that strength degradation was mainly governed by the sidelap slip behaviour. Up to 6.5 rad/1000, interior slips were kept below 1 mm, whereas deck-to-frame slips at the North and South edges were negligible. At this point, the slips at the North edge increased and became greater than the slips at two of the interior sidelaps (1,2 and 2,3). At 8.5 rad/1000, the slips at North edge and sidelap 3,4 became pronounced and strength degradation of the diaphragm started. Later, the distortion at sidelap 3,4 became greater than the slip at North edge.

This sidelap slip behaviour, where the North edge experienced large deformations, was not common. It may be attributed to the poor connectivity at this location, because only half of the washer sat on the deck sheet, and hence, the remaining portion was not effective in transferring forces. Figure 5.40 displays BB1, the failure mode that was found in 85% of the connections at North edge of the test diaphragm. BB1 is a bond failure of sheet with buckling on one side. This mode of failure was not observed at the South edge because of the improved connectivity at this location, where the washer sat entirely on the sheet steel (Figure 5.41). In addition, the inclined lip of the B-deck profile stiffened the deck giving a much better connection than that possible at the North edge.

As shown in Figure 5.38, the sidelap slips were not symmetric over the width of the test specimen. This was due to the "softer" connections along the North edge. The neutral axis in panel 1 tended to move toward the interior edge of the panel when the slip increased at the North edge, thus protecting sidelap 1,2 from undergoing large displacements. Because of the stiffer connections at the South edge, panel 4 was more rigid, compared to panels 2 and 3, and, therefore, sidelap 3,4 underwent the largest displacement along the edges of the interior panels.

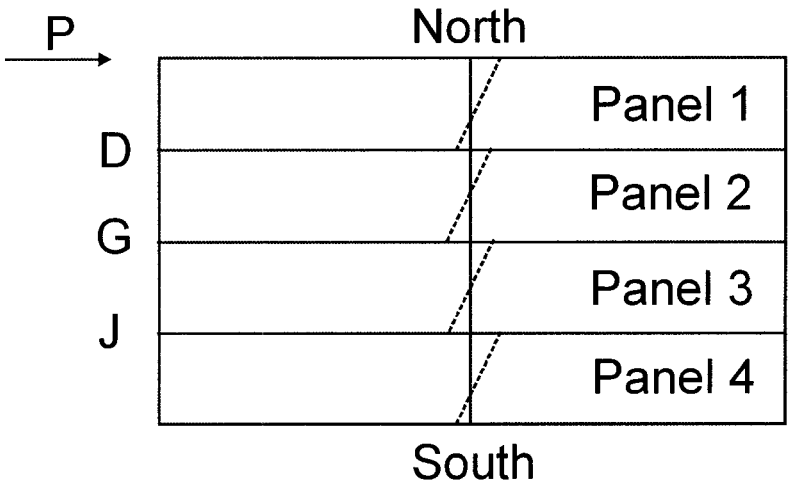

Figure 5.38 Slip distributions in different panels

At interior sidelaps (not including the welds at purlins), fracture of the weld between the top and bottom sheets with limited inelastic deformation (FW) was typical when weld quality was poor (Figure 5.42). Away from the purlin locations and where weld quality was adequate, it was common for the sheet steel around the connection to buckle on the compression side and fail on the tension side (BB1), which resulted in a higher connection capacity (Figure 5.43). Due to the robustness of the welded with washer connection, high force transfer occurred at some places and buckled the top flange beside the connector (see Figure 5.44). In addition, because of large forces associated with a high quality weld, the deck panel sustained significant out-of-plane deformations as demonstrated in Figure 5.45. The failure modes that occurred away from connections, such as that shown in Figure 5.45, are not shown in Table 5.23.

For sidelap connections located at purlins, bond failure of the top sheet with buckling (BB) occurred at 12 of 15 locations. Photographs of this failure mode are not available, although the buckling pattern is similar to that shown for sidelaps away from purlins (Figure 5.43). A figure for the deck-to-frame case is presented in the discussion on the cyclic test results (See Figure 5.48).

Test 23

In tests 23 and 24, there was an error in the evaluation of the loading references γ_u and γ_2, as discussed in Section 5.5. The displacement imposed on specimens 23 and 24 was too small as γ_u used to define the amplitude of the loading protocol corresponded only to 75% of the value associated with the actual properties of the specimens. Figure 5.46 presents the test curves for test 23 and Table 5.24 lists the observed damage after run 1.

The maximum measured load was equal to 34.6 kN/m, which is greater than the value of 32.1 kN/m which was measured in the monotonic test 22. Under the East $R_d = 3.0$ and the West $R_d = 2.0$ loading protocols where the displacement amplitude was below 10 rad/1000, the test specimen performed in an ideal manner, whereby the system developed a stable elliptical load vs. displacement behaviour (Figure 5.46). The real γ_u and γ_2 distortions, which are close for this type of deck assembly (around 10 rad/1000), were reached in the last two peaks of West $R_d = 2.0$. In the first peak of West $R_d = 3.0$, the system passed γ_2 and strength degradation occurred in a similar fashion to monotonic test 22. Substantial strength degradation was observed under the West $R_d = 3.0$ segment, considering that the load at peak displacement went below 50% of the maximum measured force. In run 2, the maximum measured load was approximately 34% of the maximum measured load in run 1.

Sidelap slips were negligible before the 16 second point. Afterwards, slips started at all locations except at the South edge. Meanwhile, the diaphragm shear strength degraded as occurred for test 22, which again is attributed to the failure of sidelaps. As observed in test 22, sidelap 3,4 underwent larger displacements compared to the other interior sidelap lines.

At the North edge, large slips happened due to poor connectivity at this location, which is similar to the behaviour observed in test 22. Figure 5.47 displays this common North edge failure mode, in which the weld with washer connections have buckles on both sides (BB2). The cyclic nature of the loading in test 23 resulted in compression and tension stresses alternating between sides of the connection, and hence explains the presence of buckles on both sides of connections. At the South edge, negligible slips were measured and no failure was observed due to the more robust connection.

At interior sidelaps, the failure modes observed in test 22 were also encountered in test 23. For instance, the separation of the top sheet from the bottom sheet (FW) occurred at 26 of 48 locations. In addition, the failure mode involving bond failure with buckles beside the washer was observed. In this case, buckles occurred on each side of the washer due to the cyclic loading (BB2). This failure mode happened at sidelap connections both between and at purlins. Also, a different failure mode was observed at 9 locations, where the washer was tilted with partial fracture of weld. The WT failure mode is a combination of two different failure modes. In the first case, the deck panel at connections distorted in such a manner that the washer tilted from the horizontal plane (see Figure 5.50). The washer was attached to the top sheet, however the weld to bottom sheets may have failed. In the second case, the washer was skewed between the top sheet and bottom sheet. This was caused by the washer pushing against the top sheet creating a fold or buckle in the adjacent steel. This fold resulted in the washer moving upward and, therefore, a lifting off of the washer from its weld at the bottom sheet. The same failure mode occurred in test 25 (See Figure 5.57). Moreover, local buckling in the top flange of the deck occurred at some locations because of a large force transfer in the vicinity of the connection (see Figure 5.50). At sidelaps, it was deemed the failure of weld to frame at purlins on the East and West ends was prevented by inelastic distortion (warping) in the deck panels (see Figure 5.51 and Figure 5.52). This underlined the high strength of the welded with washer deck-to-frame fasteners.

An interesting feature of test 23 was its strength drop under the West R_d = 3.0 loading protocol, where a degradation of approximately 50% was measured. This strength drop may be attributed to the failure of welded with washer sidelap connections, away from and at purlins. For the deck-to-frame fasteners, the sheet steel around the welds failed in tension. This was observed from test films. Under the West R_d = 3.0 loading sequence, the sheet had already buckled and elongated for a few cycles which caused a weakening of the steel. In consequence, the sheet failed in tearing leaving the load to be carried only on one side by bearing. Test results from Peuler (2002) showed that a drop in shear strength of approximately 50% follows the failure in tension of the sheet steel in welded with washer deck-to-frame connections (bond failure). Also, this failure mode was found in welds away from purlins along with the FW and WT modes. The FW failure mode is a bond failure with limited inelastic deformation, in which the post-ultimate fastener capacity is zero. For the WT failure mode, considerable inelastic distortion occurred, which most likely led to a significant drop in capacity.

Test 24

Test 24 was subjected to a long duration (LD) loading protocol. As in test 23, the loading references used in the loading protocol were smaller than what they should have been due to an error in their evaluation. The maximum measured load was equal to 33.2 kN/m, which is close to result from test 22 (monotonic): 32.1 kN/m. Test result curves are shown in Figure 5.53 and a table of observed damage for test 24 is shown in Table 5.25. Due to the lack of an adequate hydraulic oil supply to the actuator, the loading system did not reach the intended peak distortion at $2\gamma_u$, 12.2 rad/1000, since the maximum measured distortion was equal to 10.4 rad/1000. Moreover, this value was reached only in the first cycle at $2\gamma_u$ and smaller values were obtained in the following cycles. This behaviour occurred in both 1st half and 2nd half time intervals of the LD signal. If the system had been pushed to the intended distortion of 12.2 rad/1000, which

is close to the real γ_2 , the maximum measured force, 33.2 kN/m, may have been closer to the maximum measured force from test 23, 34.6 kN/m. Pinching and strength degradation occurred in the first half of the signal and this tended to increase in the second half.

Sidelap slips remained below 3 mm in first half of signal whereas in the second half, sidelap slips tended to increase. As observed in test 22 and 23, sidelap 3,4 sustained a larger displacement (7 mm) compared to other interior sidelap lines. The North edge experienced a maximum slip of about 4 mm, whereas negligible slips were measured at South edge.

Observed damages tended to reflect the measured deformations at sidelaps. Similar to tests 22 and 23, deck-to-frame connections at the North edge experienced large displacements and, hence, were damaged (see Figure 5.54). No damage was observed at the South edge. At interior sidelaps, 29 of 48 connections away from purlins were intact at the end of the loading protocol, a smaller proportion than in tests 22 and 23, which can be explained by a lower level in the imposed distortion. Other connections away from purlins displayed the FW, BB1 and BB2 failure modes. Twelve of fifteen connections at purlins and sidelap junctions showed the BB1 or BB2 failure modes where buckles appeared. Again, buckling in the top flange of the deck near the connectors occurred due to high force transfer (see Figure 5.55).

Table 5.22 Test specimen description (Tests 22, 23 and 24)

Steel properties:	
Supplier and coil number	Canam P-3615 B-deck 0.91 mm Coil supplier: Sorevco Coil number: 147624
Base metal thickness (mm)	0.88
Fy test (MPa)	319
Fu test (MPa)	394
E (MPa)	210000
50 mm gauge % elongation	24 %
Fasteners:	
Sidelap fasteners	Weld with washer Washer dimensions Outer diameter: 35 mm Inner diameter: 14 mm Thickness: 2.5 mm Electrode E6010 3.2 mm diameter 115Amp DC+ Spacing: 305 mm c/c
Deck-to-frame fasteners	Weld with washer Washer dimensions Outer diameter: 35 mm Inner diameter: 14 mm Thickness: 2.5 mm Electrode E6011 3.2 mm diameter 100 Amp Spacing: 305 mm c/c
Comments on quality of fasteners:	
Test 22	Weld connectivity 75% approx. on average. At sidelaps G between 1 and 6 and J between 16 and 21, there was a gap between sheets and weld connectivity was poor (less than 50%).
Test 23	Weld connectivity 75% approx. on average. At sidelaps G between 1 and 6 and J between 16 and 21, there was a gap between sheets and weld connectivity was poor (less than 50%).
Test 24	Weld connectivity 75% approx. on average. At sidelaps G between 6 and 10 and J between 12 and 16, there was a gap between sheets and weld connectivity was poor (less than 50%).

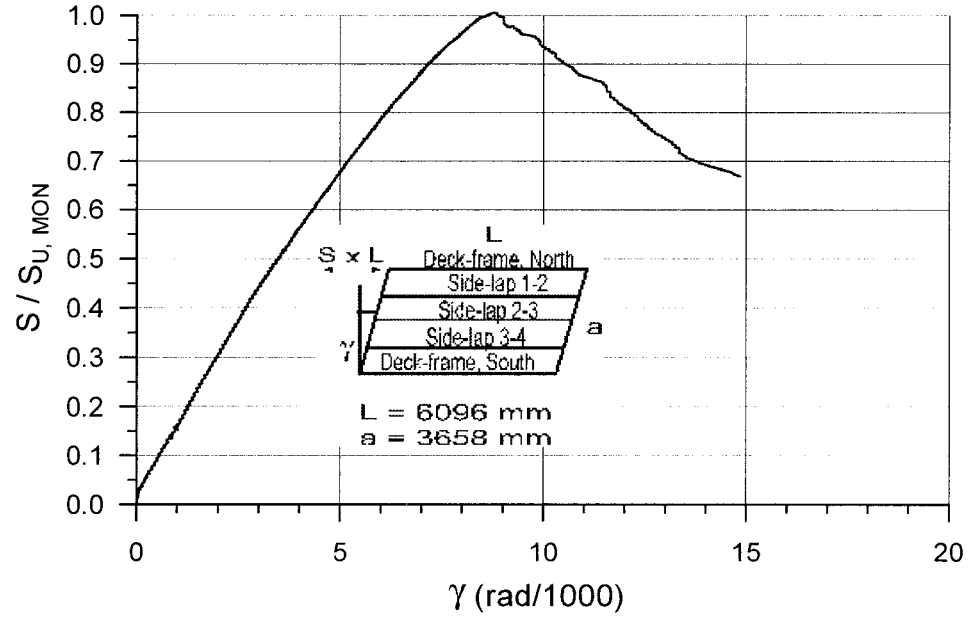

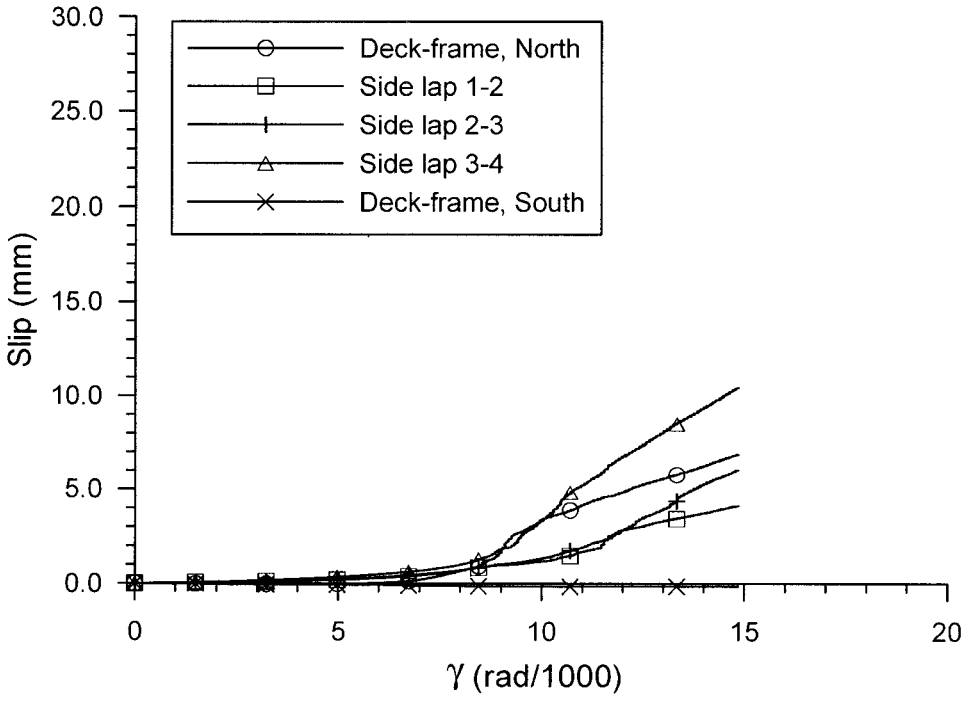

Test No. 22
P3615 B - 0.91 mm
Sidelap fasteners : Welds with washer @ 305 Frame fasteners : Welds with washer @ 305
$S_{u,SDI*}$ = 36.6 kN/m $S_{u,MON}$ = 32.1 kN/m

Figure 5.39 Test no.22 results

	1	2	3	4	5	6	7	8	9	10	11	12	13	14	15	16	17	18	19	20	21
A				BB1	BB1	BB1	BB1	BB1	BB1	BB1	BB1	BB1	BB1	BB1	BB1	BB1	BB1	BB1	BB1	BB1	BB1
B	BB					BB					BB										BB
C																BB					
D		WF	WF	WF	WF	BB	WF	WF	WF	WF	BB	WF	WF	WF	WF	BB	WF	WF	WF	WF	BB
E	BB																				
F																					
G	BB	WF	WF	WF	WF	BB	WF	WF	WF	WF	BB	WF	WF	WF	WF		WF	WF	WF	WF	BB
H	BB					BB					BB										
I																BB					
J		BB	BB	BB	BB	BB	BB	BB	BB	BB	BB	WF	WF	WF	WF	BB	BB	BB	BB	BB	BB
K	BB					BB					BB					BB					BB
L						BB					BB										
M																					

Table 5.23 Observed damage (Test 22)

Nomenclature of failure modes (weld with washer - weld with washer pattern)

Welded with washer connections at sidelap (not to frame)
FW: Fracture of weld between top and bottom sheets with limited inelastic deformation
WT: Tilting of washer with partial fracture of weld
WF: One of the two cases mentioned above (FW or WT)
BB1: Bond failure of top sheet with buckling on one side
BB2: Bond failure of top sheet with buckling on two sides
BB: Bond failure of top sheet with buckling (BB1 or BB2 not identified)

Welded with washer deck-to-frame connections
BB1: Bond failure of sheet with buckling on one side
BB2: Bond failure of sheet with buckling on two sides
BB: Bond failure of top sheet with buckling (BB1 or BB2 not identified)

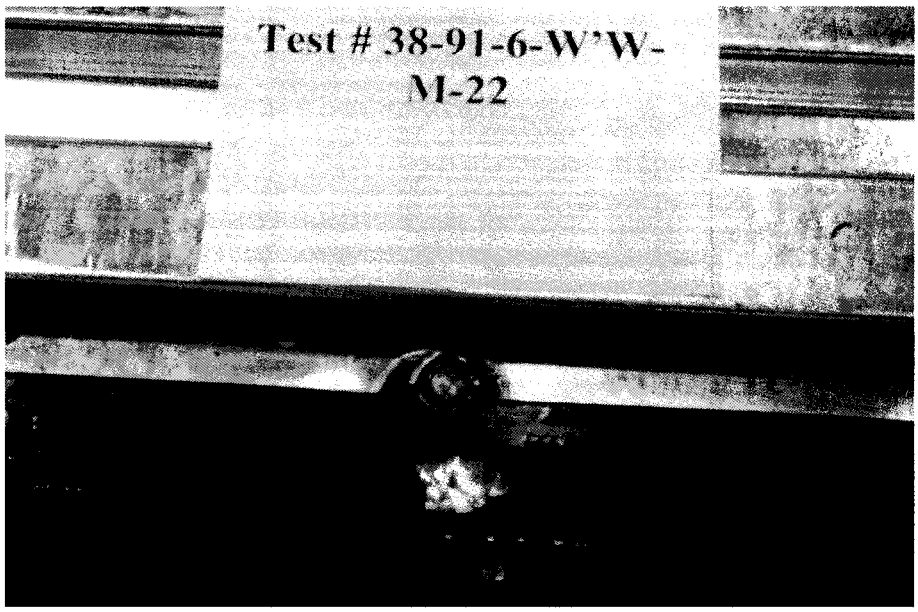

Figure 5.40 BB1 failure mode at North end, Test 22

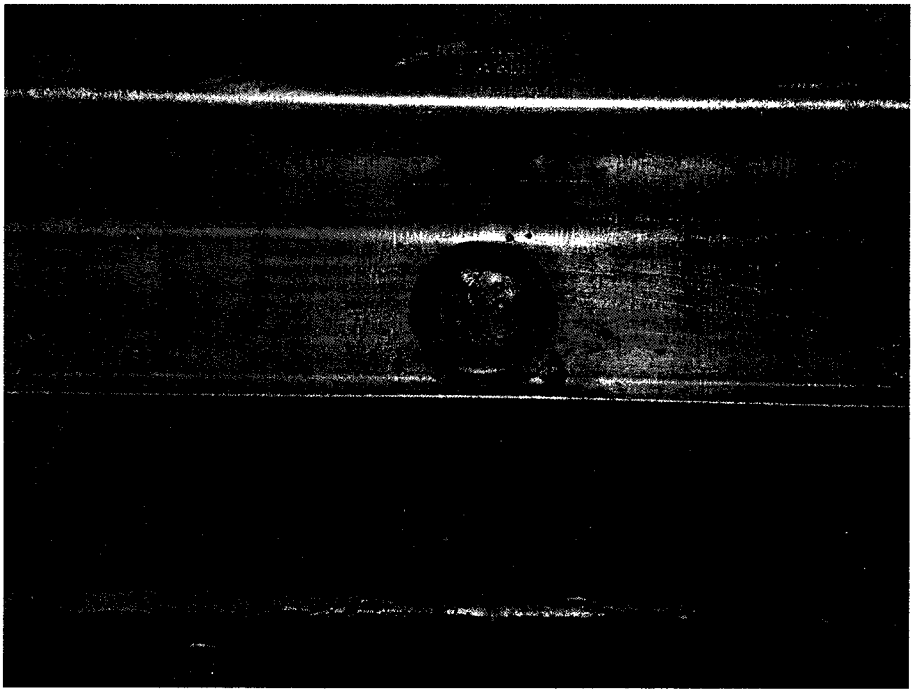

Figure 5.41 No observed damage at South end, Test 22

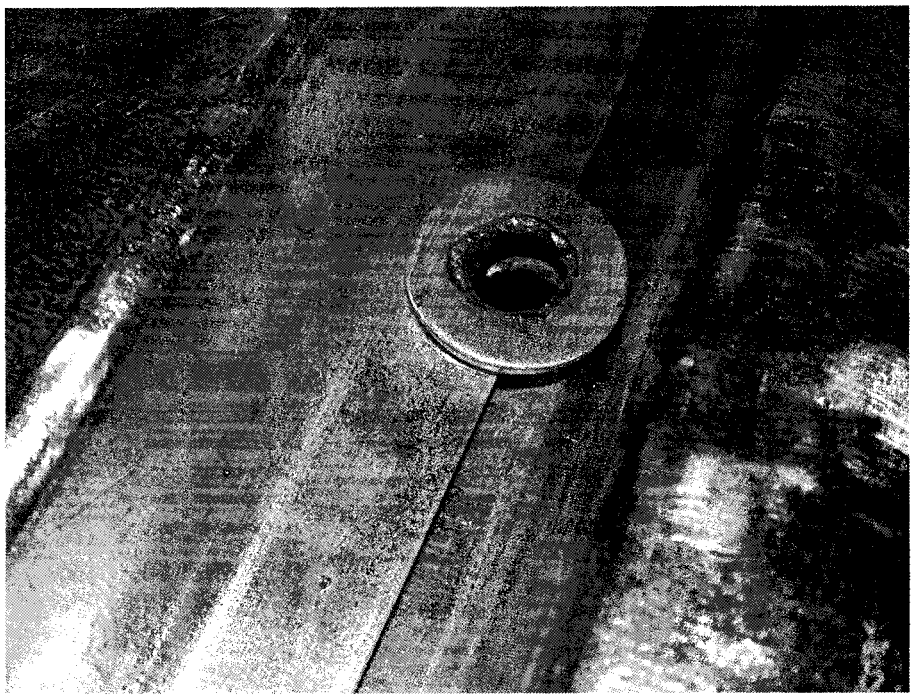

Figure 5.42 FW failure mode, Test 22

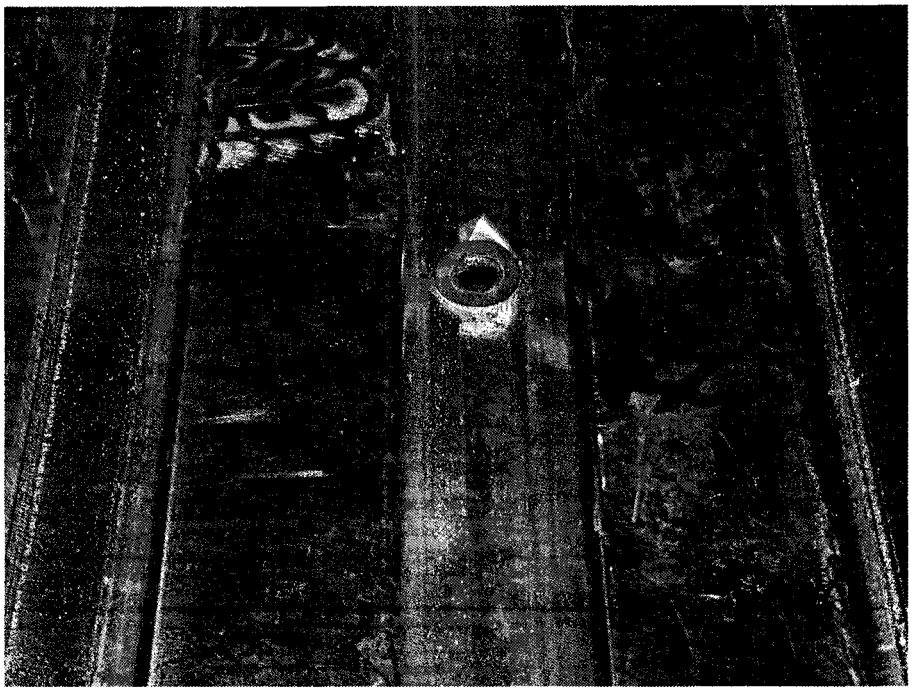

Figure 5.43 BB1 failure mode at welded w. washer sidelap connection, Test 22

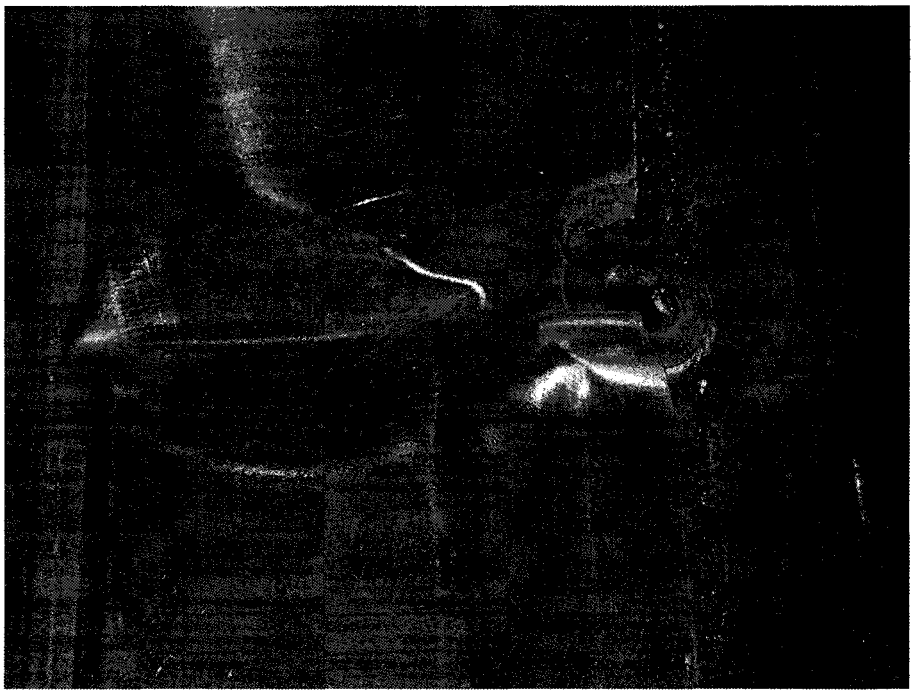

Figure 5.44 Buckling in top flange beside connector, Test 22

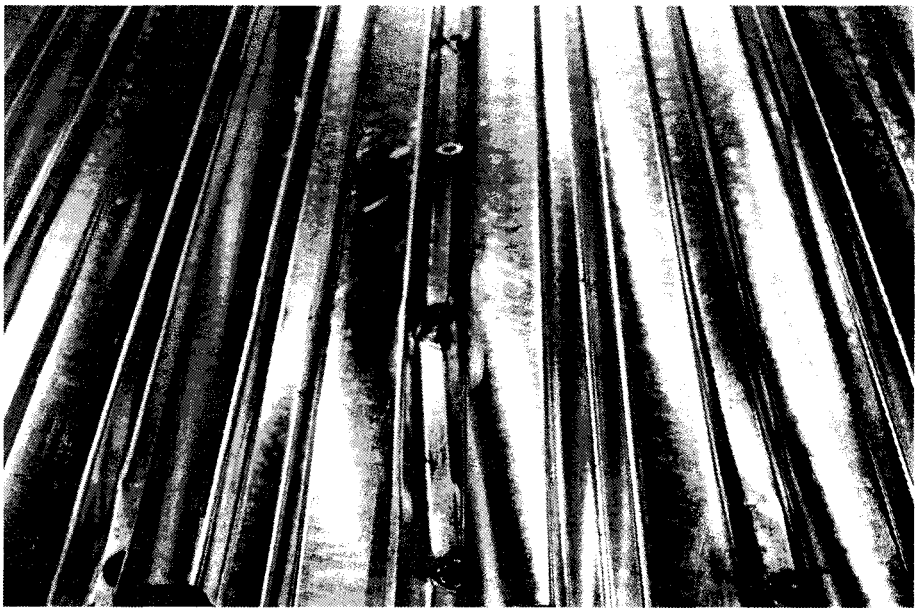

Figure 5.45 Deck distortion near sidelap, Test 22

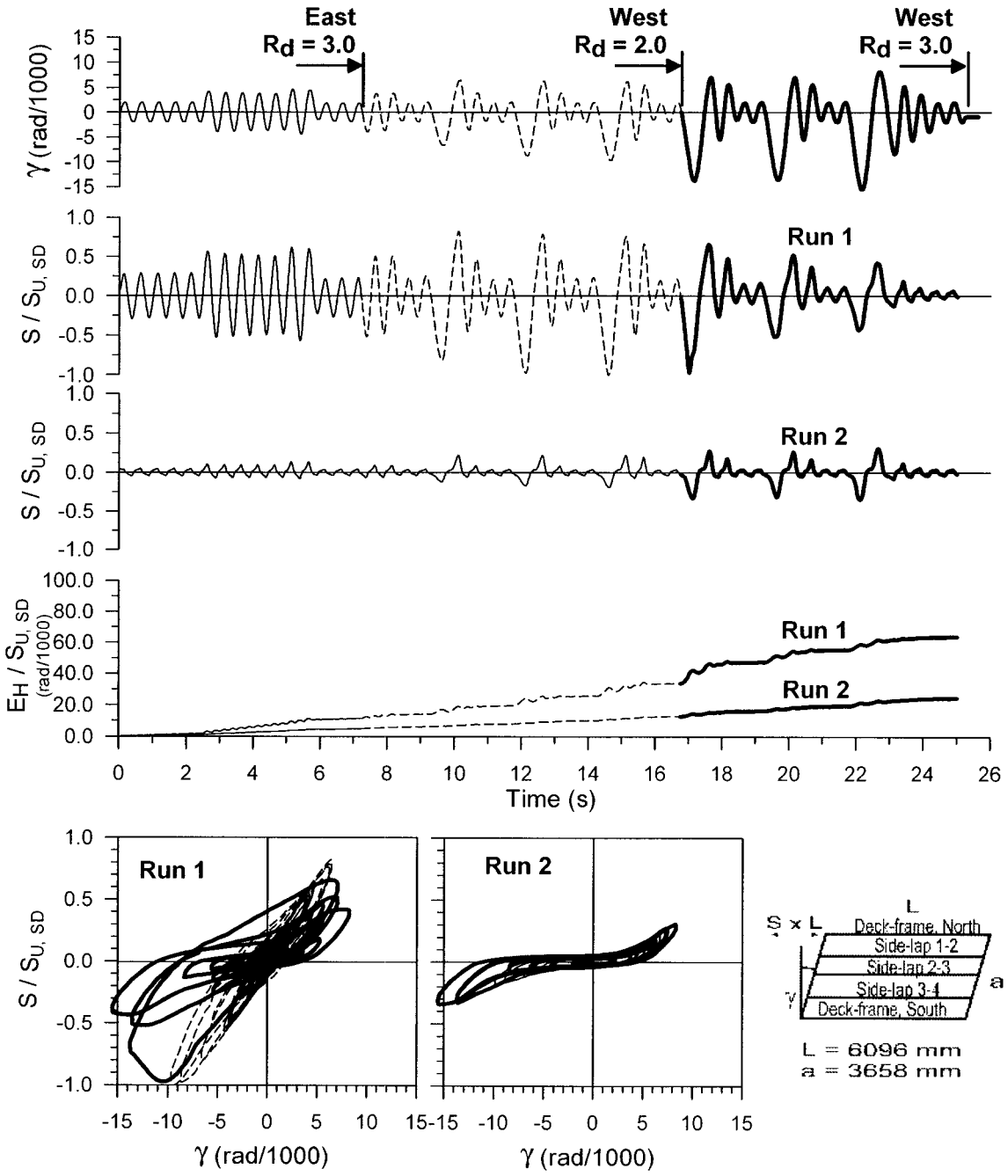

Test No. 23
P3615 B - 0.91 mm
Sidelap fasteners : Welds with washer @ 305 Frame fasteners : Welds with washer @ 305
$S_{u,SDI*}$ = 36.6 kN/m $S_{u,SD}$ = 34.6 kN/m $S_{u,MON}$ = 32.1 kN/m

Figure 5.46 Test no.23 results

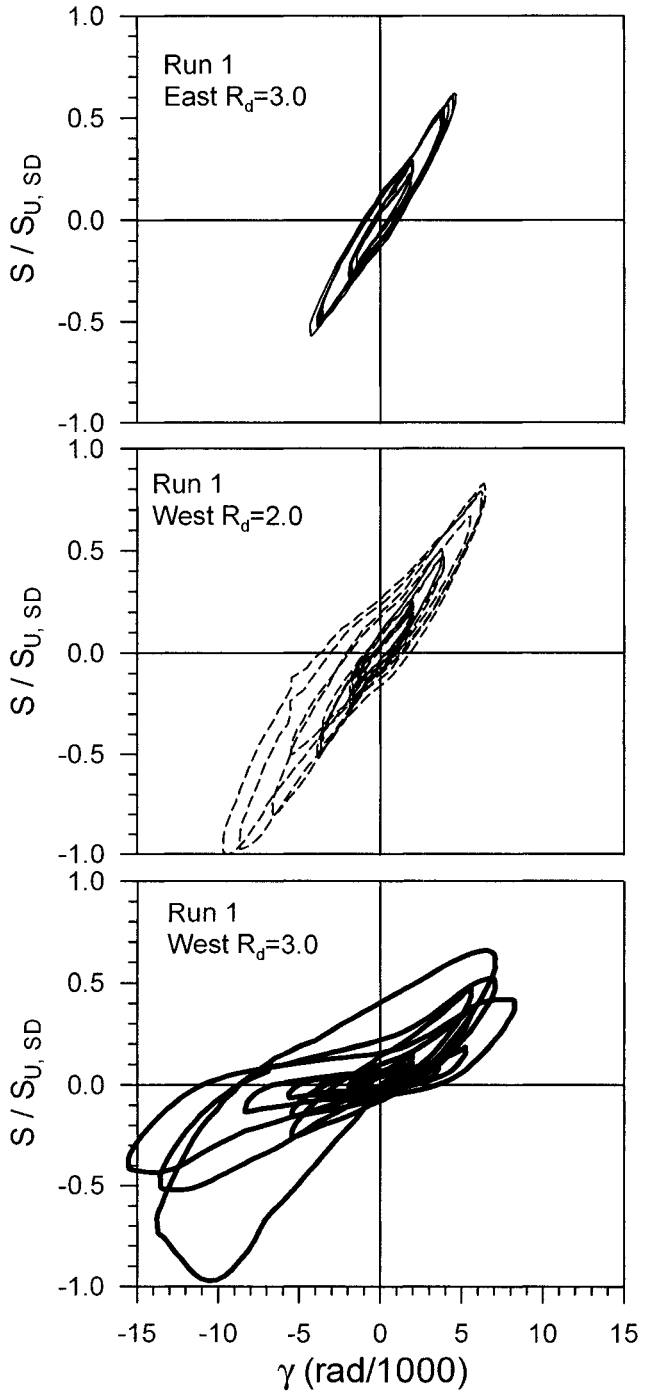

Test No. 23

P3615 B - 0.91 mm
Sidelap fasteners :
Welds with washer @ 305
Frame fasteners :
Welds with washer @ 305

$S_{u, SDI*}$ = 36.6 kN/m
$S_{u, SD}$ = 34.6 kN/m
$S_{u, MON}$ = 32.1 kN/m

Figure 5.46 Test no.23 results (continued)

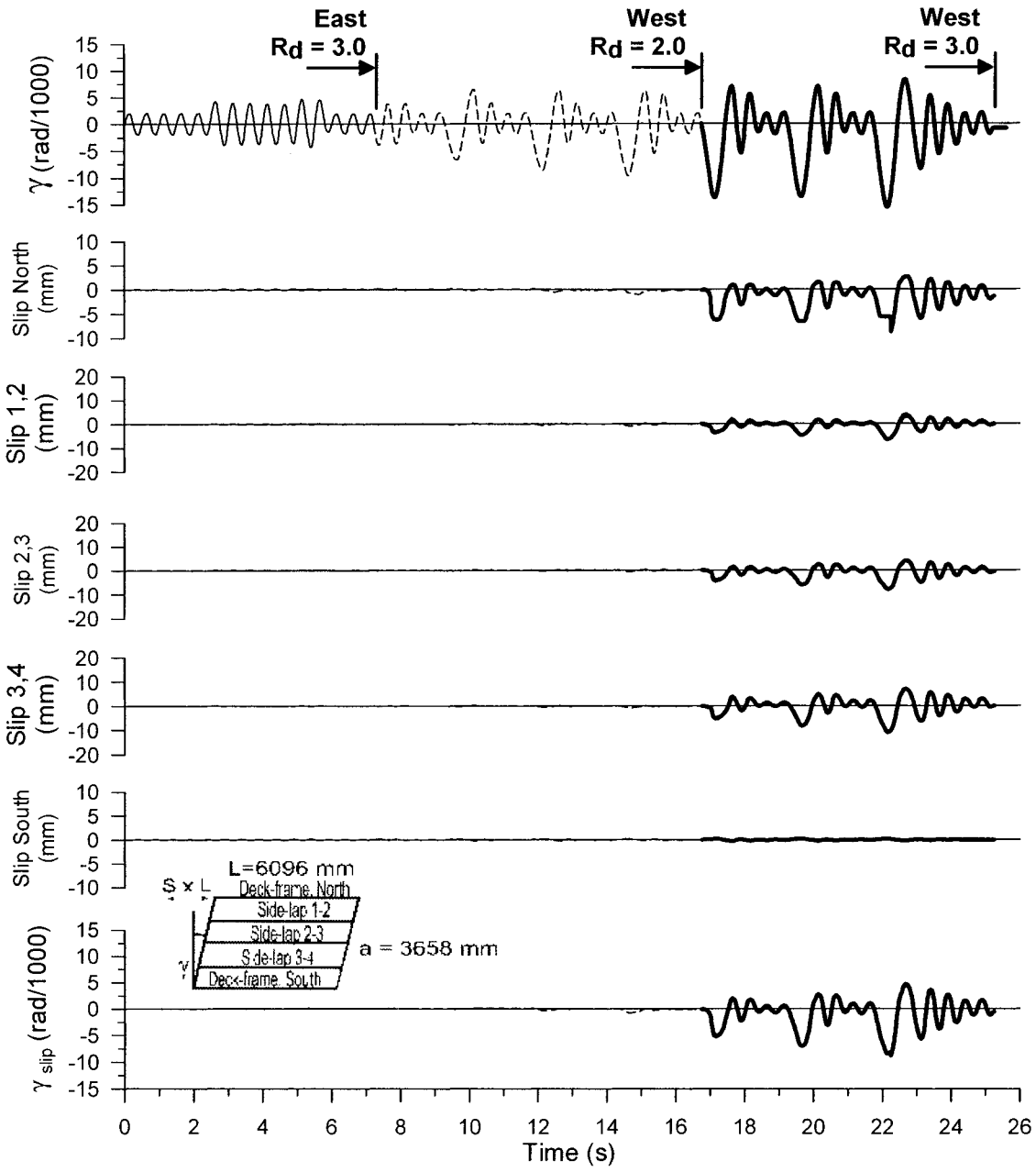

Test No. 23- Run 1
P3615 B - 0.91 mm
Sidelap fasteners : Welds with washer @ 305 Frame fasteners : Welds with washer @ 305
$S_{u,SDI*}$ = 36.6 kN/m $S_{u,SD}$ = 34.6 kN/m $S_{u,MON}$ = 32.1 kN/m

Figure 5.46 Test no.23 results (continued)

	1	2	3	4	5	6	7	8	9	10	11	12	13	14	15	16	17	18	19	20	21
A	BB2	BB2	BB2	BB2	BB2	BB2	BB2	BB2	BB2	BB2	BB2	BB2	BB2	BB2	BB2	BB2	BB2	BB2	BB2	BB2	BB2
B	BB					BB					BB					BB					BB
C																					
D	B1	FW	FW	BB2	BB2	BB2	FW	FW	FW	FW	BB2	WT	WT	FW	FW	BB2	WT	WT	FW	FW	
E						BB										BB					
F											BB										
G		FW	FW	FW	FW	BB2	FW	FW	FW	BB2	BB2	BB2	BB2	BB2	FW	BB2	BB2	BB2	FW	BB2	
H	BB					BB					BB					BB					
I																					
J		BB2	BB2	WT	WT	BB2	WT	WT	WT	BB2	BB2	BB2	FW	FW	FW	BB2	FW	FW	FW	FW	
K	BB					BB					BB					BB					BB
L																					
M																					

Table 5.24 Observed damage after run 1 (Test 23)

Nomenclature of failure modes (weld with washer - weld with washer pattern)

Welded with washer connections at sidelap (not to frame)
FW: Fracture of weld between top and bottom sheets with limited inelastic deformation
WT: Tilting of washer with partial fracture of weld
WF: One of the two cases mentioned above (FW or WT)
BB1: Bond failure of top sheet with buckling on one side
BB2: Bond failure of top sheet with buckling on two sides
BB: Bond failure of top sheet with buckling (BB1 or BB2 not identified)

Welded with washer deck-to-frame connections
BB1: Bond failure of sheet with buckling on one side
BB2: Bond failure of sheet with buckling on two sides
BB: Bond failure of top sheet with buckling (BB1 or BB2 not identified)

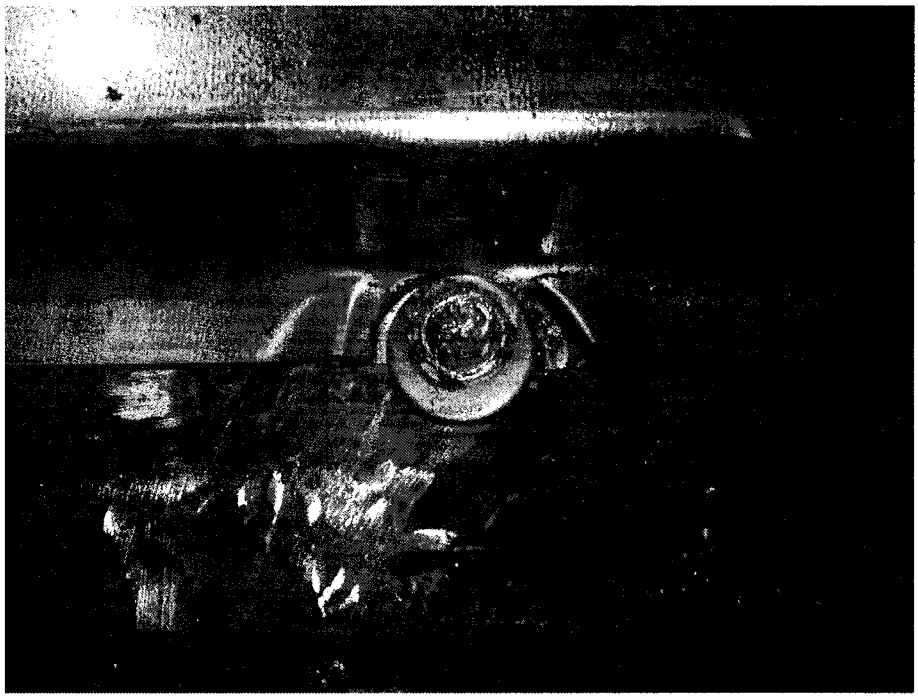

Figure 5.47 BB2 failure mode at North end, Test 23

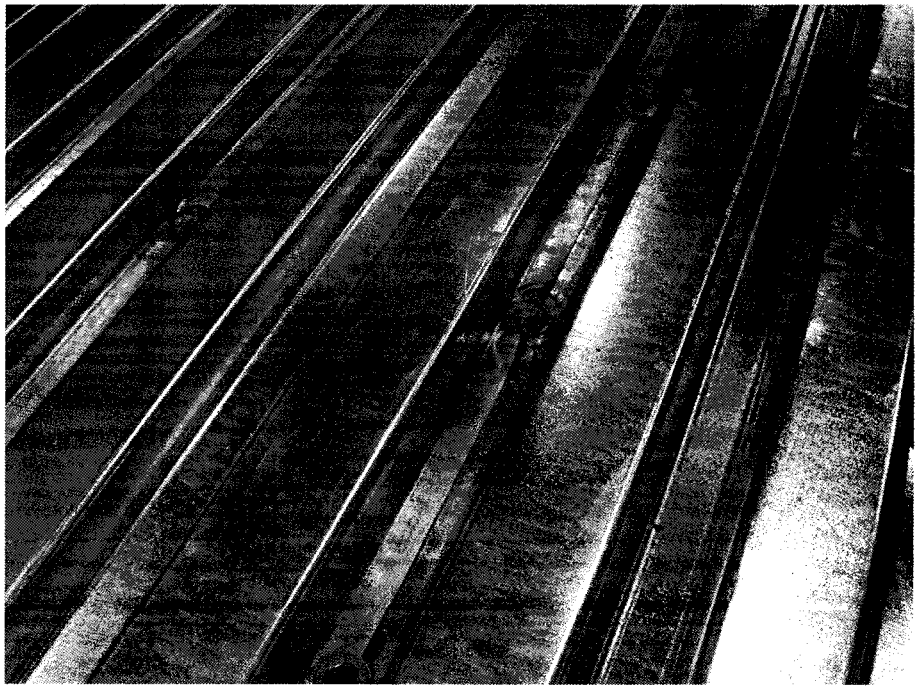

Figure 5.48 BB2 failure mode at purlin and sidelap intersection, Test 23

Figure 5.49 BB2 failure mode at weld inside deck panel, Test 23

Figure 5.50 WT failure mode with buckling in steel deck top flange, Test 23

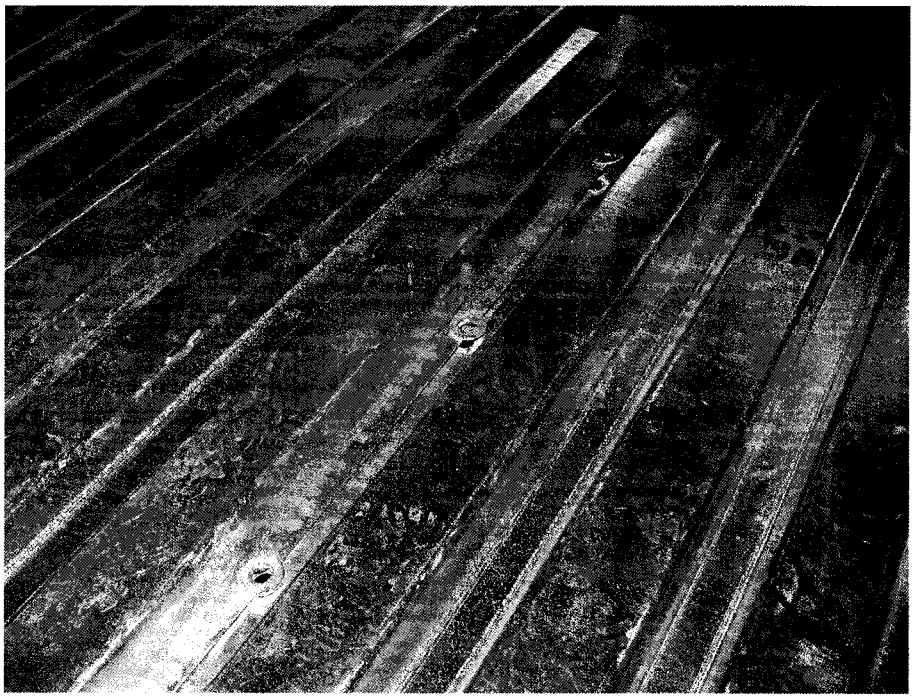

Figure 5.51 Buckling in top sheet preventing failure of weld to frame, Test 23

Figure 5.52 Buckling in top sheet preventing failure of weld to frame, Test 23

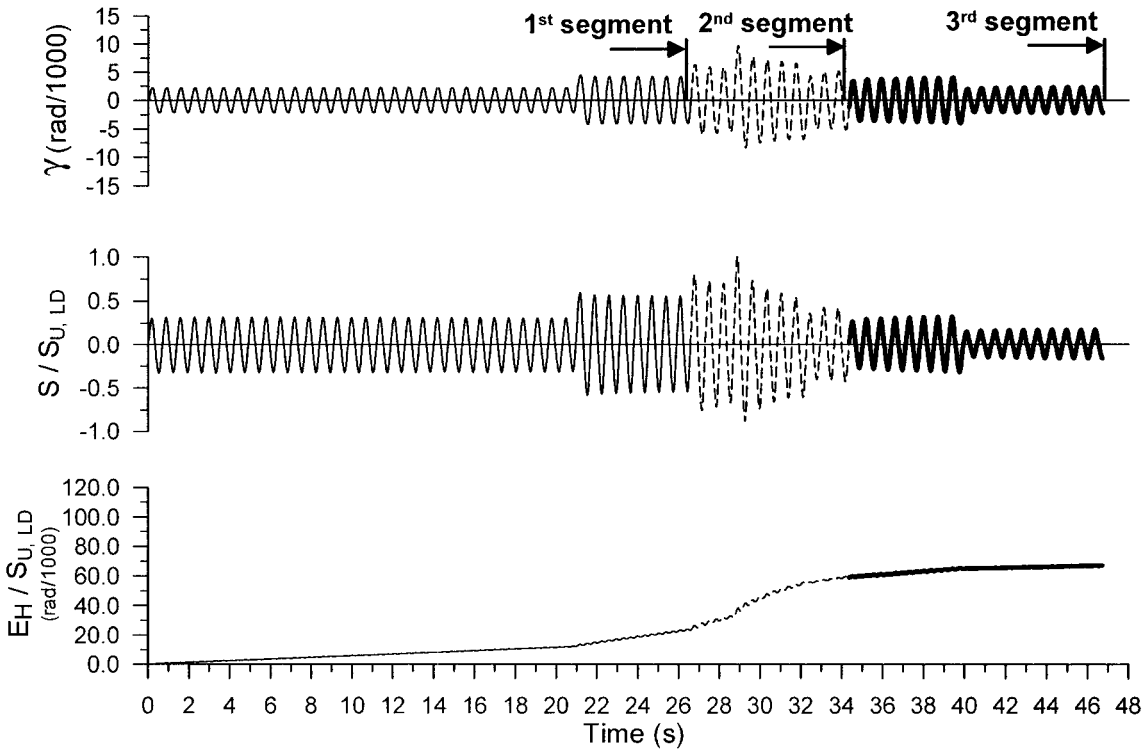

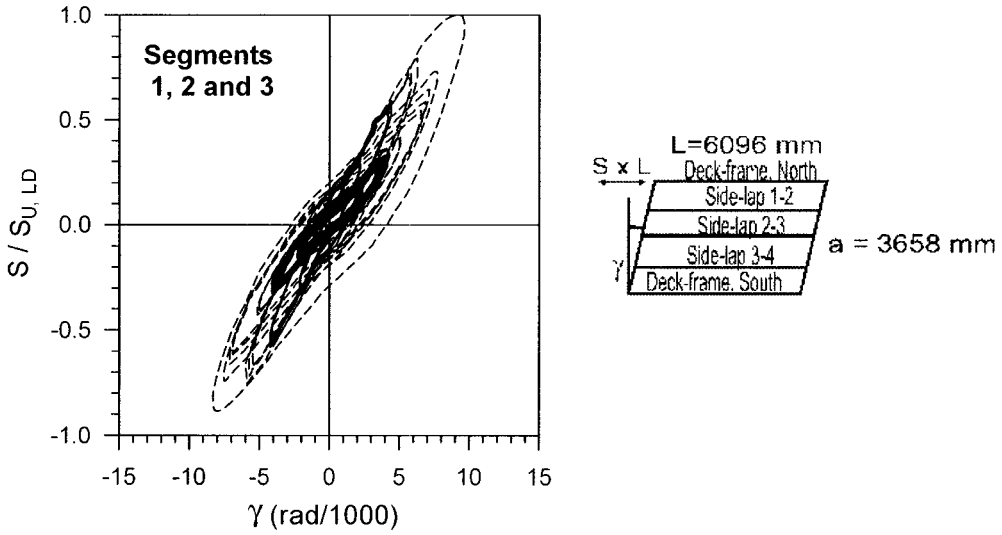

Test No. 24
P3615 B - 0.91 mm
Sidelap fasteners : Welds with washer @ 305 Frame fasteners : Welds with washer @ 305
$S_{u,SDI}$ = 36.6 kN/m $S_{u,LD}$ = 33.2 kN/m $S_{u,MON}$ = 32.1 kN/m

Figure 5.53 Test no.24 results

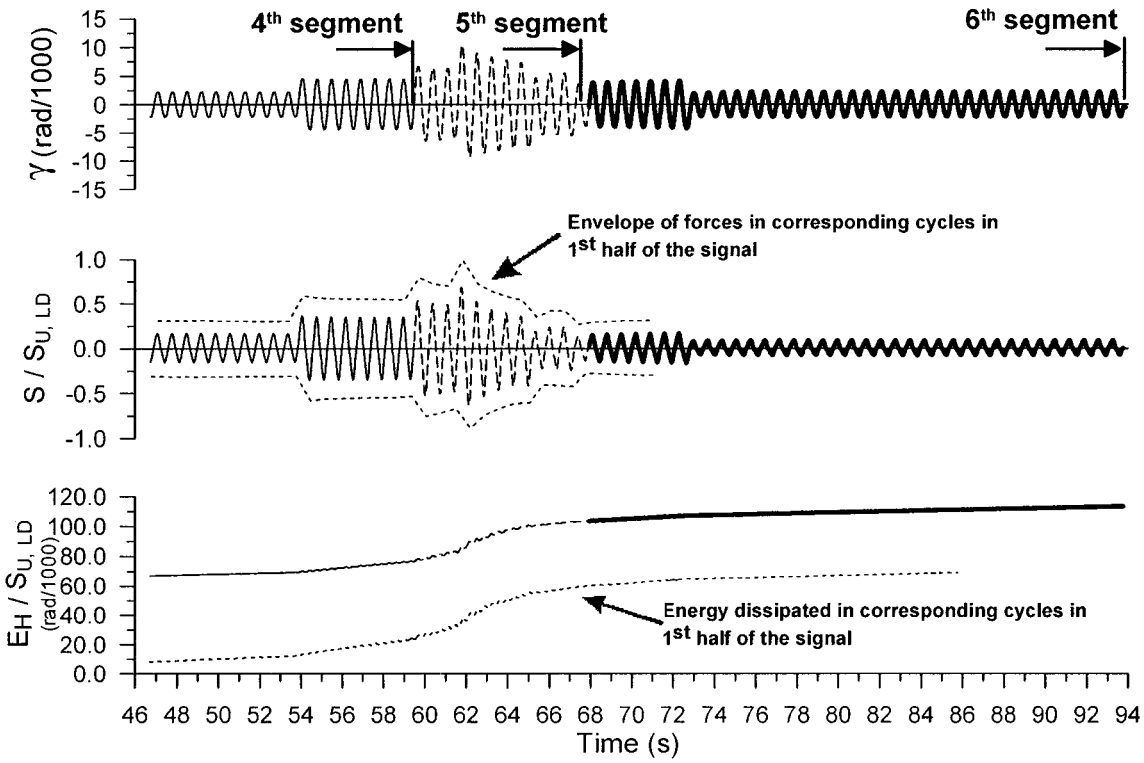

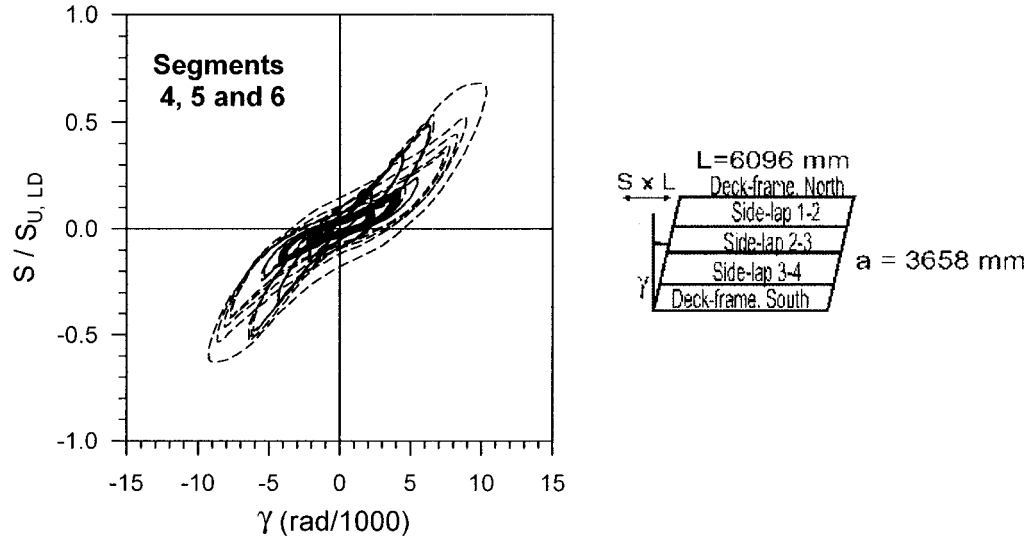

Test No. 24
P3615 B - 0.91 mm
Sidelap fasteners : Welds with washer @ 305 Frame fasteners : Welds with washer @ 305
$S_{u,SDI*}$ = 36.6 kN/m $S_{u,LD}$ = 33.2 kN/m $S_{u,MON}$ = 32.1 kN/m

Figure 5.53 Test no.24 results (continued)

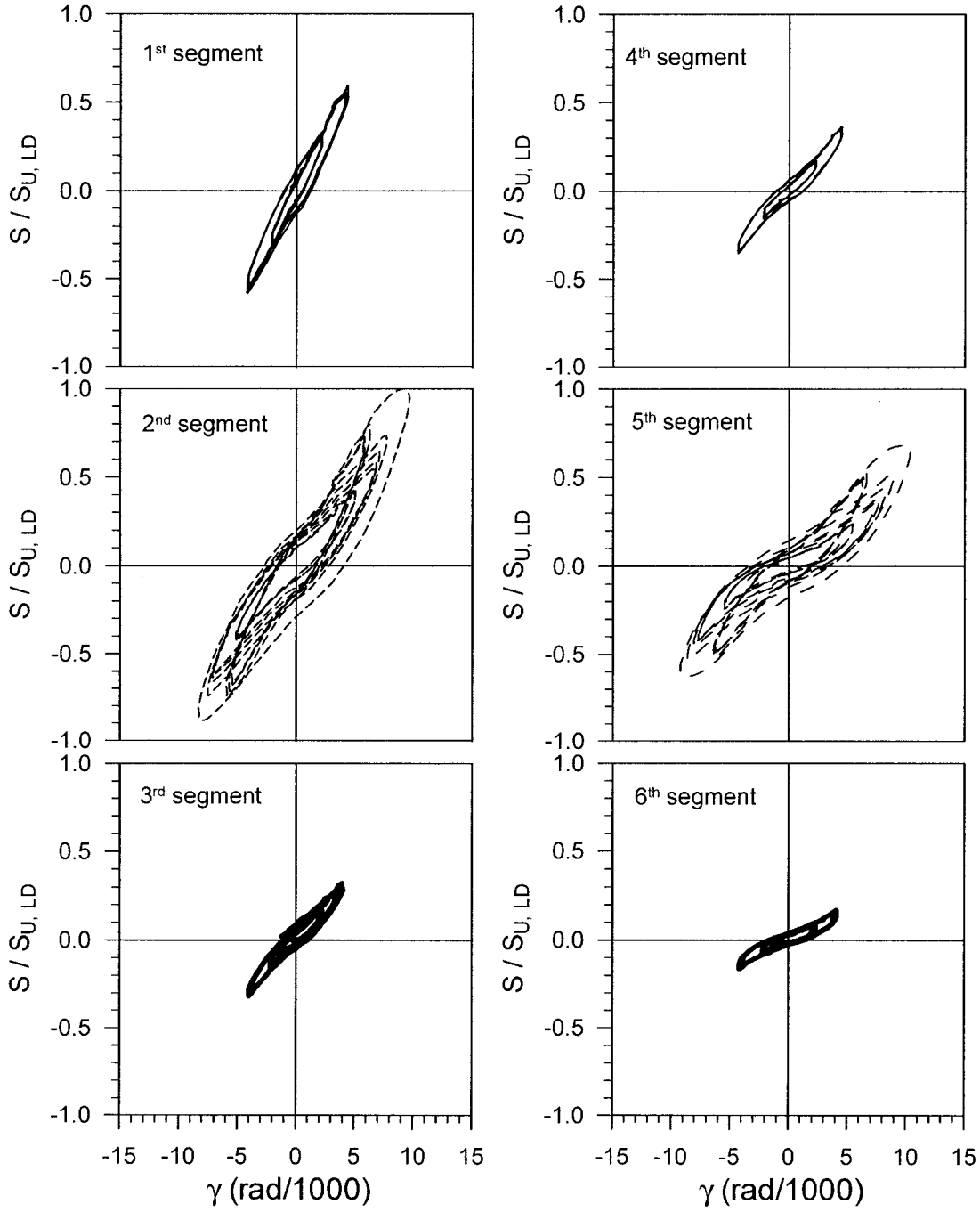

Test No. 24
P3615 B - 0.91 mm
Sidelap fasteners : Welds with washer @ 305 Frame fasteners : Welds with washer @ 305
$S_{u,SDI*}$ = 36.6 kN/m $S_{u,LD}$ = 33.2 kN/m $S_{u,MON}$ = 32.1 kN/m

Figure 5.53 Test no.24 results (continued)

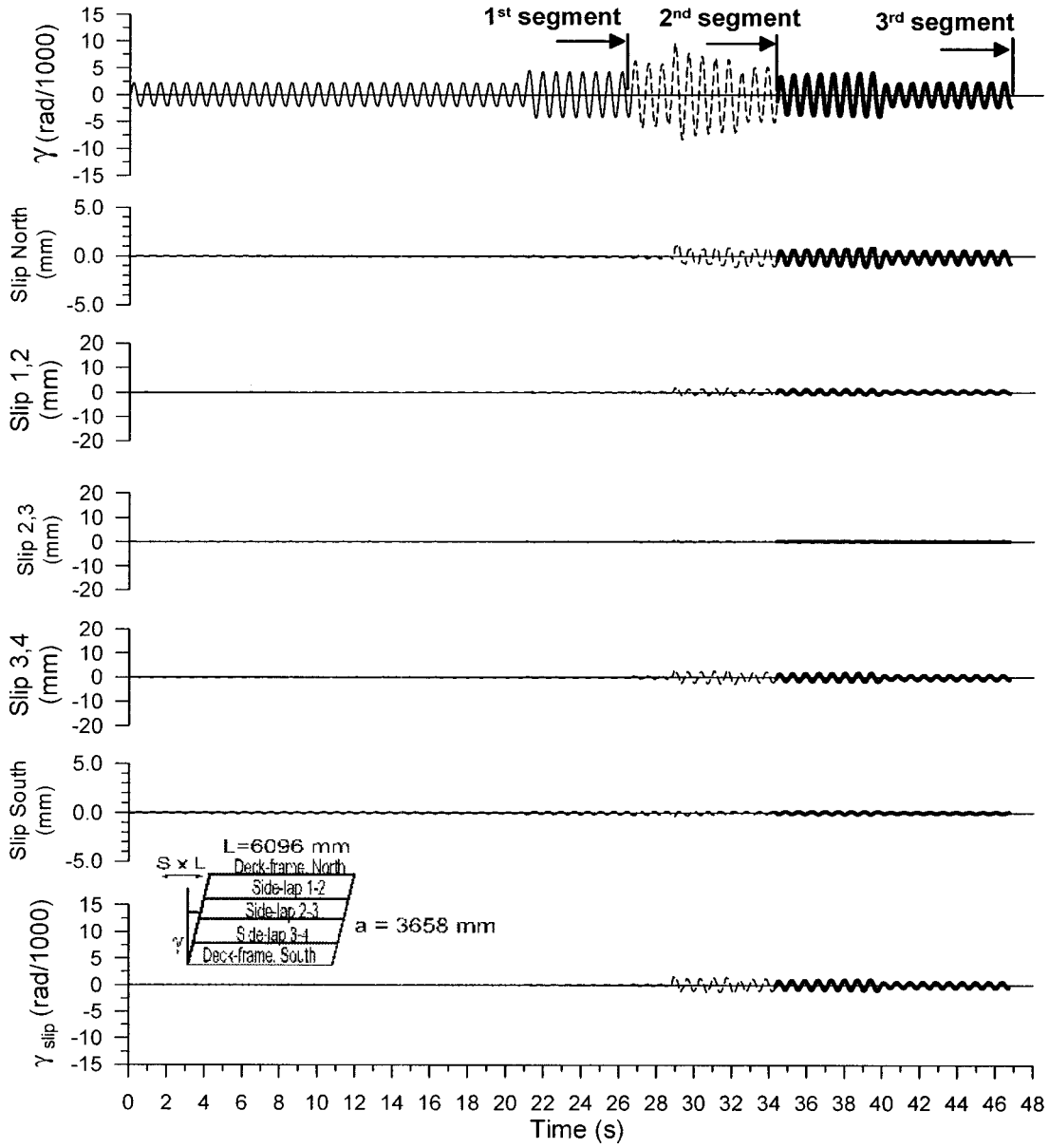

Test No. 24
P3615 B- 0.91 mm
Sidelap fasteners : Welds with washer @ 305 Frame fasteners : Welds with washer @ 305
$S_{u,SDI*}$ = 36.6 kN/m $S_{u,LD}$ = 33.2 kN/m $S_{u,MON}$ = 32.1 kN/m

Figure 5.53 Test no.24 results (continued)

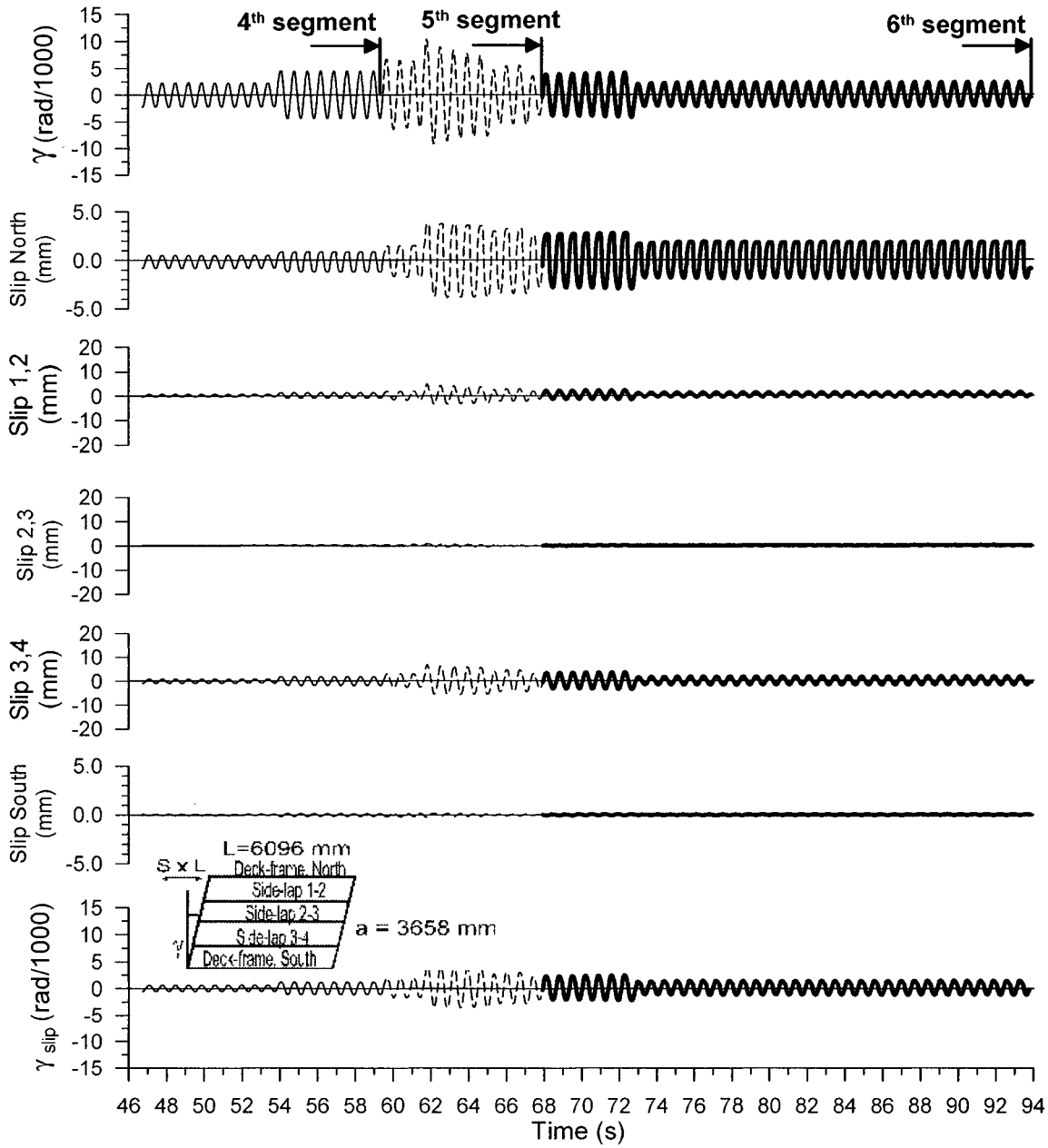

Test No. 24
P3615 B - 0.91 mm
Sidelap fasteners : Welds with washer @ 305 Frame fasteners : Welds with washer @ 305
$S_{u,SDI}$ = 36.6 kN/m $S_{u,LD}$ = 33.2 kN/m $S_{u,MON}$ = 32.1 kN/m

Figure 5.53 Test no.24 results (continued)

	1	2	3	4	5	6	7	8	9	10	11	12	13	14	15	16	17	18	19	20	21
A	BB2	BB2	BB2	BB2	BB2	BB2	BB2	BB2	BB2	BB2	BB2	BB2	BB2	BB2	BB2	BB2	BB2	BB2	BB2	BB2	BB2
B																					
C																					
D	BB1						BB2	BB2	BB2	BB2	BB2					BB	FW	FW	FW	FW	BB2
E																					
F																					
G	BB1								BB1	BB1		BB2				BB1					BB1
H																					
I																					
J	BB1			BB2	BB1	BB2	FW	FW	FW	FW	BB2	BB1				BB2		BB1			BB2
K	BB2					BB2					BB2					BB2					BB2
L																					
M																					

Table 5.25 Observed damage (Test 24)

Nomenclature of failure modes (weld with washer - weld with washer pattern)

Welded with washer connections at sidelap (not to frame)
FW: Fracture of weld between top and bottom sheets with limited inelastic deformation
WT: Tilting of washer with partial fracture of weld
WF: One of the two cases mentioned above (FW or WT)
BB1: Bond failure of top sheet with buckling on one side
BB2: Bond failure of top sheet with buckling on two sides
BB: Bond failure of top sheet with buckling (BB1 or BB2 not identified)

Welded with washer deck-to-frame connections
BB1: Bond failure of sheet with buckling on one side
BB2: Bond failure of sheet with buckling on two sides
BB: Bond failure of top sheet with buckling (BB1 or BB2 not identified)

Figure 5.54 BB2 failure mode at North end, Test 24

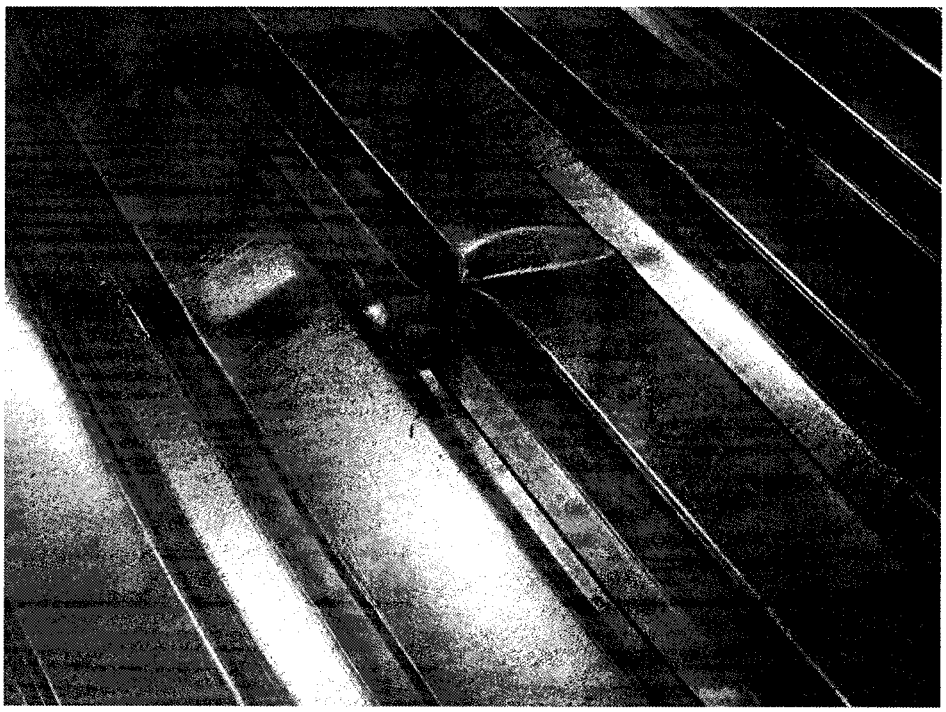

Figure 5.55 Buckling in deck top flange, Test 24

5.8.3 Weld with washer-nail design

5.8.3.1 Tests 25, 26 and 27

Tests 25, 26 and 27 were carried out using B-deck profile sheets with welded with washer sidelap and nailed deck-to-frame connections. The sidelap fasteners at purlins were nails. 0.91 mm thick steel sheets were used. Test 25 was subjected to a monotonic loading. Tests 26 and 27 sustained the short duration (SD) and long duration (LD) loading protocols, respectively.

Table 5.26 presents the description of specimens for tests 25, 26 and 27. It is mentioned in the table that the quality of welds in test 27 was better compared to the quality of welds in tests 25 and 26. For this type of sidelap with welds with washer, it was difficult to maintain a good contact between the two sheets, between the purlins, during the welding operation. The sheets had some initial differential flexural curvature which was accentuated by the weight of the welder. In order to improve the quality of the connection (for test 27), a second technician pushed down on the top sheet while the welder was performing the welding.

Test 25

The maximum measured load was equal to 22.5 kN/m and took place at approximately 7 rad/1000. At peak load, shear failure (SN) of a single nail took place and a sudden drop in resistance followed. A second nail shear failure occurred and another drop in strength was observed. The saw-tooth shape of the shear-distortion curve at peak load may be attributed to these nail failures that took place at H1 and J1 (Figure 5.56). The author does not know which failure took place first. The author heard nail failures and observed sudden drop in resistance after. The failures were observed later. The nail located at H1 had to be replaced prior testing since it did not respect the maximum stand-off. The nail

stand-off is defined as the distance from the top of nail to top of sheet steel. It is possible that the new nail was not properly installed. For instance, it could have been placed in a location where the thickness of the supporting HSS had been reduced by previous buffering of the steel surface. Although the sequence of failures is unknown, it is possible that the nail at position J1 became overloaded after failure of the nail at H1. J1 is at a critical location since it is the junction of exterior line 1 and sidelap 3,4. In this deck design, the force demand on the nail fasteners was very high because of the higher strength of the sidelap fasteners used. For instance, J1 was located at the junction of exterior line 1 and sidelap 3,4. Therefore, it was subjected to a shear force acting in both directions. Assuming the shear flow was uniformly distributed among the fasteners, the resultant shear in J1 was equal to 9.7 kN just prior to the second load drop (S = 22.5 kN/m at that time), which is in excess of the shear capacity of this nail (7.46 kN, Table 5.5). Likely, warping effects and load redistribution between the fasteners have permitted J1 to survive up to that point. Nevertheless, considering the nail was also subject to vertical upward force due to out-of-plane deformations of the deck, it would be logical that failure took place in J1 after some additional load had to be picked up when nail H1 failed. It is believed that the top part of the load deformation curve for this test was truncated by these two nail failures. Had no failure occurred in nail H1, it can be assumed that the diaphragm could have supported a slightly higher load, closer to the results from tests 26 and 27.

Up to 8.5 rad/1000, the North and South edges had larger slips than the interior sidelaps. At this distortion level, the slip at sidelap 1,2 became the largest while the degradation of the diaphragm shear strength started. At approximately 11 rad/1000, the slip at sidelap 2,3 increased, whereas sidelap 3,4 did not slip substantially during the test. This failure may be explained by poorer welds at this location. As noted for the other diaphragm tests, strength degradation may be attributed to sidelap slip.

All of the connections between purlins at sidelaps 1-2 and 2-3 failed. The 3 failure modes observed in tests 22, 23 and 24 for this type of connections were observed. One case consisted of the fracture of the weld between the top and bottom sheets with limited inelastic deformations (FW). The second case, BB1, is a bond failure of the top sheet with buckling on one side. The third case occurs when the washer tilts from the horizontal plane (WT) with partial fracture of weld (Figure 5.57).

Once the sidelap connections between purlins had failed the connections at purlins sustained a greater share of the load. Bearing failures with slots forming in the sheet steel (BFS) were observed at these locations. In some cases, the slot was so long that it reached the sheet edge. This failure mode was considered in the TT case (see Figure 5.58). At 2 locations (D1 and G1), buckling of sheet steel (B1) due to the nail pushing inside deck web was observed (see Figure 5.59).

Unlike sidelaps 1,2 and 2,3, sidelap 3,4 remained integral until the end of test. Hence, the extent of damage was limited as only 8 of 16 fasteners failed, all under the BB1 failure mode. This sidelap may have been stronger because at J3 two welded fasteners were made instead of one. After the first weld was completed, it was judged that the weld was not acceptable so a second adjacent weld was installed. No damage was observed at the North and South edges.

Test 26

The maximum measured load in test 26 was equal to 26.5 kN/m which is 18% higher than in test 25. Under the East R_d = 3.0 loading protocol, the specimen developed a stable elliptical behaviour. In the West R_d = 2.0 segment, modest stiffness degradation occured without strength degradation and, in the West R_d = 3.0 segment, strength degradation and pinching were observed (Figure 5.60).

Test results suggest that the specimen acted in a single-sheet mode response. In fact, interior sidelaps experienced negligible slips, except sidelap 2,3 in West R_d = 3.0, whereas deck-to-frame slips were significant. Slips at the North and South edges were measured suggesting that a large proportion of the slip distortion was obtained from slip at these locations.

Observed damage confirmed the single sheet mode response. The extent of damage at sidelap connections away from purlins was moderate since only 2 complete failures of connections (D2 and G15) were observed. The BB2 failure mode, not a complete failure since the washer bears against the buckles, was seen at all other locations. The extent of buckles was not severe suggesting that the displacements were not extensive.

Damages were concentrated mainly at purlins on line 16 and 21. Bearing failures perpendicular to the flute (BFL) were seen at 8 of 13 locations on line 21 and 3 locations on line 16. The openings in sheet steel were longer on line 21, approximately 35 mm, compared to line 16, approximately 20 mm (Figure 5.61). This failure mode where large displacements occured at nailed locations in the North-South directions at set-up edges confirmed the single-sheet mode behaviour. Also, slight buckling around the nail (SB) was observed at 2 locations (E16 and F16) (Figure 5.62). The connections at sidelap-purlin intersections D1 and J1 experienced the TT failure mode. The top sheet disconnected from the nailed connection since the slot due to bearing failure extended to the sheet edge. The failure pattern was not symmetric, which may have resulted from a lack of symmetry in the loading. No damage was observed at North and South sides of diaphragm (lines A and M).

The single-sheet mode behaviour may have been caused because the North and South edges possessed a smaller shear resistance compared to the interior sidelap lines. At the North and South edges, nail fasteners were used at all locations whereas at interior lines a combination of welded with washer and nailed connections were installed. At all lines,

the spacing between connectors was kept the same (305 mm c/c). The nail strength is approximatley 7.46 kN for a 0.91 mm thick sheet, as shown in Table 5.5. The critical mode of failure is the bearing of the nail against the sheet steel, for which a yield plateau is developed. The strength of a weld with washer at sidelap is approximately 8.0 kN, which is close to the strength of a nailed connection. However, due to the high variability in weld quality, the weld strength can be much lower (around 4 kN). In any case, the strengths of sidelap and deck-to-frame lines were close. If the North and South lines are weaker, a single-sheet mode behaviour is obtained as observed in test 26. When the interior sidelaps are weaker, the sidelaps fail and the single-sheet mode behaviour is not produced, as observed in test 25.

The stiffness and strength degradation of the specimen may be attributed to the BFL failures at lines 16 and 21. Once the nail movements produced a large hole in the deck, the sheet was able to move vertically thus, bearing of the nail against the sheet steel did not occur at many locations. This caused a weakening in the deck in the North-South direction and, therefore, a weakening of the overall diaphragm specimen.

Test 27

Test result curves are shown in Figure 5.63 and Table 5.29 presents the observed damage after the LD signal. The maximum load encountered in test 27 was equal to 26.2 kN/m, which is close to the result from test 26, 26.5 kN/m. Pinching and the greatest degradation in shear strength was observed in the first set of peaks at $2\gamma_u$. The maximum measured force in the 2nd half of the load protocol was in the range of 70% of the value in 1st half. This may be attributed to the large amount of pinching in the load vs. displacement behaviour. Energy dissipating capacity was similar in both halves of the loading protocol.

As seen in test 26, the deck specimen behaved in a single-sheet mode. There was no slip at interior sidelaps while large displacements occurred at North and South edges. A small proportion of the total deck distortion was caused by the slips (approximately 25%). Contrary to what happened in test 26, no slip was observed at interior sidelaps. This may be explained by the smaller distortion amplitudes in test 27.

Failure at sidelap connections between purlins was not observed. Slight buckling of the sheet steel around the nail (SB) was observed at the North and South edges (see Figure 5.64). This failure mode was also observed at 19 of 22 locations at purlins on lines 6 and 16, whereas no failure was seen on line 11. In some cases, the extent of sheet buckling for the SB failure mode was minimal. In tests 25 and 26, it is possible that the same level of deformation took place but was neglected in the recording of post test damage. The higher number of SB failures in test 27 does not imply that these connections were displaced or deteriorated to a larger extent that what took place in tests 25 and 26.

In addition, the following failure modes, observed in test 26, were noticed in test 27. The BFL failure mode, a bearing failure perpendicular to the flute, occurred on line 21 at 4 locations (see Figure 5.65). On line 21, 5 of 11 connections experienced slight buckling around the nail (SB). In addition, two connections on line 1 (K1 and L1) experienced this behaviour. Sheet uplift around the nail was observed (SU) at 8 of 11 locations on line 1 and 2 of 11 on line 21 (see Figure 5.66). The SU failure mode was not considered as a failure mode in tests 25 and 26. Contrary to what is found in tables of observed damage for tests 25 and 26, this failure mode may have occured in these tests.

Tests 26 and 27 acted in a single-sheet mode under their respective loading protocol. Test 25 behaved in a similar fashion at the beginning of the load protocol, however the failure at one sidelap changed the overall behaviour. This failure may be explained by welds of poor quality along the sidelap in question. If more connections had been added along the North and South edges, the failure could have been forced through the sidelaps

in all of these tests. With this approach, the sidelap joints would be the weak link in the system, resulting in their failure prior to slippage along the North and South edges.

A single-sheet response is possible in a real building because the deck is connected to the beams along the end walls in the same manner as the North and South ends in the test frame. All other sidelap connections in a building would be like the interior sidelaps in the frame. This means that during an earthquake, inelastic deformation would only develop in the sidelap located at the ends of the building, creating excessive deformation demand along these sidelaps and, likely, loss of structural integrity. With the weld with washer-nail design, in the direction perpendicular to the flute of the deck profile, the nailed connections lost their bearing capacity when the slot extended into the web or when the panel moved upward, thus creating a strength and stiffness degradation. Overall, it is preferable to distribute the inelastic demand among all interior sidelaps. For this reason, a deck system with nails to frame connections and welds with washer at interior sidelaps should be sized so that the interior sidelaps are the weak link in the system.

Table 5.26 Test specimen description (Tests 25, 26 and 27)

Steel properties:	
Supplier and coil number	Canam P-3615 B deck 0.91 mm Coil supplier: Sorevco Coil number: 147624
Base metal thickness (mm)	0.88
Fy test (MPa)	319
Fu test (MPa)	394
E (MPa)	210000
50 mm gauge % elongation	24 %
Fasteners:	
Sidelap fasteners	Weld with washer Washer dimensions Outer diameter: 35 mm Inner diameter: 14 mm Thickness: 2.5 mm Electrode E6010 3.2 mm diameter 115Amp DC+ Spacing: 305 mm c/c
Deck-to-frame fasteners	Hilti nail X-EDNK-22 THQ 12M Lot number: 413923 (Tests 25 and 26), 448446 (Test 27) Spacing: 305 mm c/c
Comments on quality of fasteners:	
Test 25	Nail stand-off: Total Ave.: 7.1 mm C.o.V.: 0.23 At sidelaps Ave.: 6.5 mm C.o.V.: 0.13 Other than sidelaps Ave.: 7.2 mm C.o.V.: 0.24 3 nails (A1, H1, M2) were not properly installed at first and were replaced. Weld connectivity 70% approx. on average. At sidelaps D (D2 to D4), J13 and J19, there was a gap between sheets and weld connectivity was poor (less than 50%). Weld at J3 was very poor so a second weld was performed beside the first weld (double weld).
Test 26	Nail stand-off: Total Ave.: 6.0 mm C.o.V.: 0.19 At sidelaps Ave.: 6.7 mm C.o.V.: 0.15 Other than sidelaps Ave.: 5.9 mm C.o.V.: 0.19 No problem with nail installation. Weld connectivity 70% approx. on average. At sidelaps D between 16 and 20 and J between 1 and 6, there was a gap between sheets and weld connectivity was poor (less than 50%).
Test 27	Nail stand-off: Total Ave.: 7.4 mm C.o.V.: 0.10 At sidelaps Ave.: 7.8 mm C.o.V.: 0.07 Other than sidelaps Ave.: 7.3 mm C.o.V.: 0.11 No problem with nail installation. Weld connectivity 85% approx. On average.

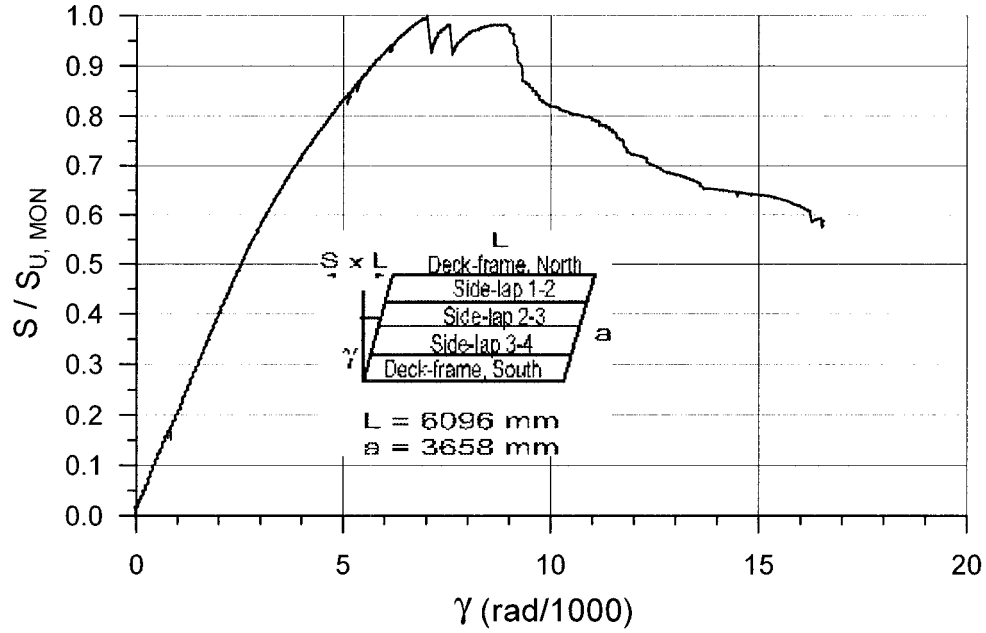

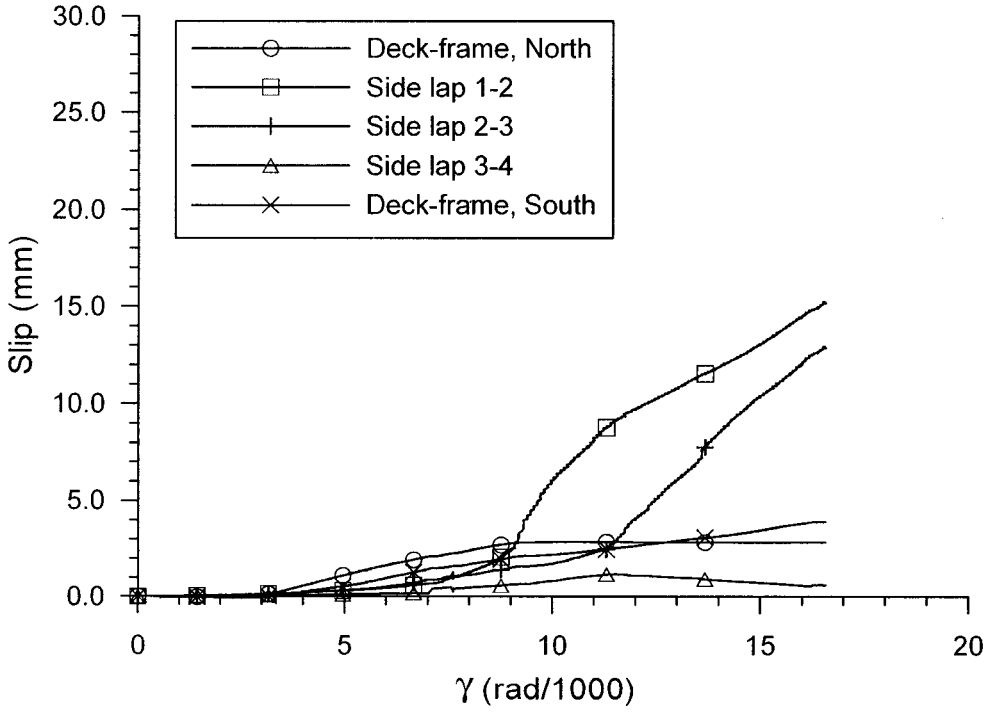

Test No. 25
P3615 B - 0.91 mm
Sidelap fasteners : Welded with washer @ 305 Frame fasteners : Hilti nails @ 305
$S_{u,SDI*}$ = 21.2 kN/m $S_{u,MON}$ = 22.5 kN/m

Figure 5.56 Test no.25 results

	1	2	3	4	5	6	7	8	9	10	11	12	13	14	15	16	17	18	19	20	21
A																					
B																					
C	BFS					BFS										BFS					
D	B1	WF	WF	WF	WF	BFS	WF	WF	WF	WF	BFS	WF	WF	WT	WF		WF	WF	WF	WT	
E																					
F																					
G	B1	WF	WF	WF	WF	BFS	WF	WF	WF	WF	BFS	WF	WF	WF	WF	BFS	WF	WF	WF	WF	TT
H	SN					BFS					BFS					BFS					BFS
I																					BFS
J	SN											BB1	BB1	BB1	BB1		BB1	BB1	BB1	BB1	TT
K																					
L																					
M																					

Table 5.27 Observed damage (test 25)

Nomenclature of failure modes (weld with washer - nail pattern)

Welded with washer connections at sidelap (not to frame)
FW: Fracture of weld between top and bottom sheets with limited inelastic deformation
WT: Tilting of washer with partial fracture of weld
WF: One of the two cases mentioned above (FW or WT)
BB1: Bond failure of top sheet with buckling on one side
BB2: Bond failure of top sheet with buckling on two sides
BB: Bond failure of top sheet with buckling (BB1 or BB2 not identified)

Nailed deck-to-frame connections
SN: Shear failure in the nail
SB: Slight buckling around nail
BFS: Bearing failure (slot) without buckling
BFL: Bearing failure perpendicular to the flute (may extend into the web)
SU: Sheet uplifted around nail with possible bearing deformation
TT: Tearing of top sheet at nail
Two failure modes are combined in TT: a) tearing due to bearing near edge b) bearing failure with slot that reach the sheet edge
B1: Buckling on one side of nail with possible bearing deformation
B2: Buckling on two sides of nail with possible bearing deformation
BF: Bearing failure (with or without buckling). (SB, BFS, TT, B1 or B2 not identified)

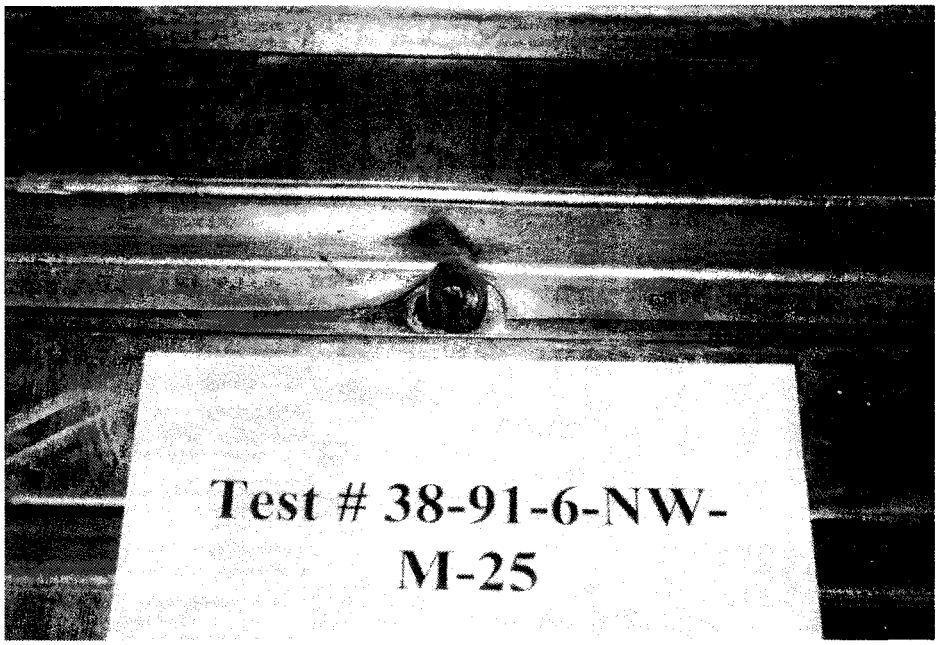

Figure 5.57 WT failure mode, Test 25

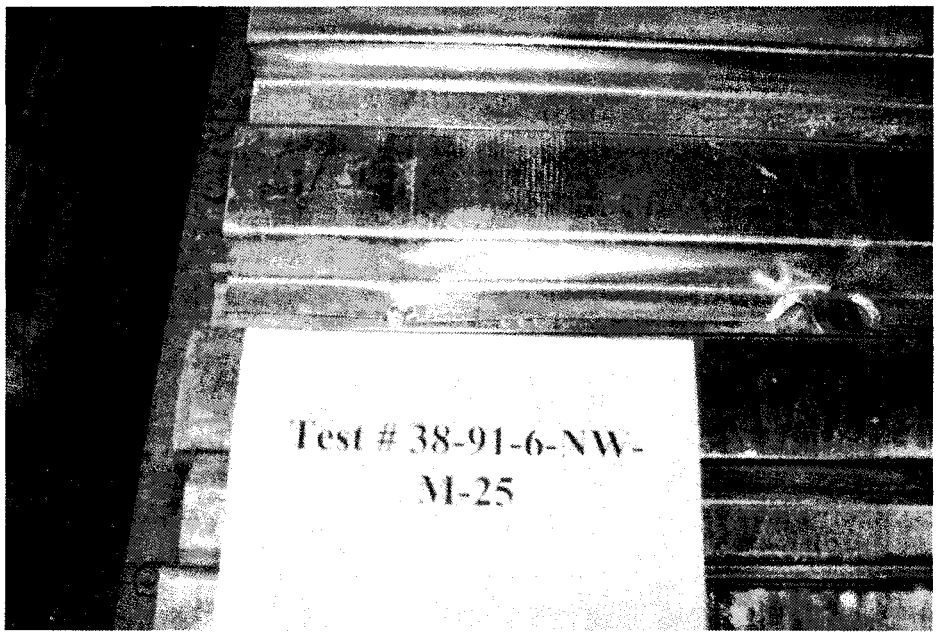

Figure 5.58 TT failure mode at nail and BB1 failure mode at welded w. washer connection, Test 25

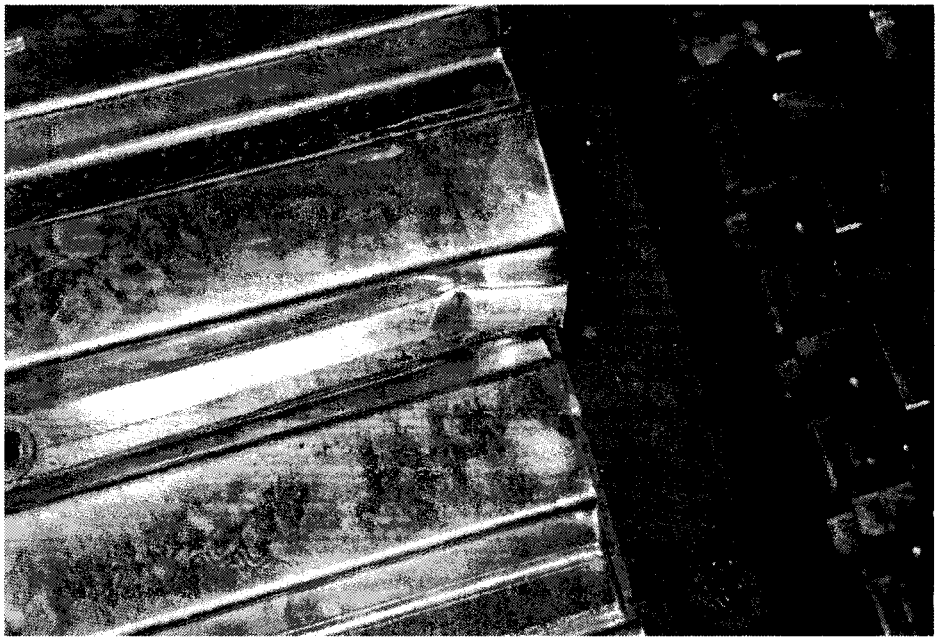

Figure 5.59 B1 failure mode at nailed connection, Test 25

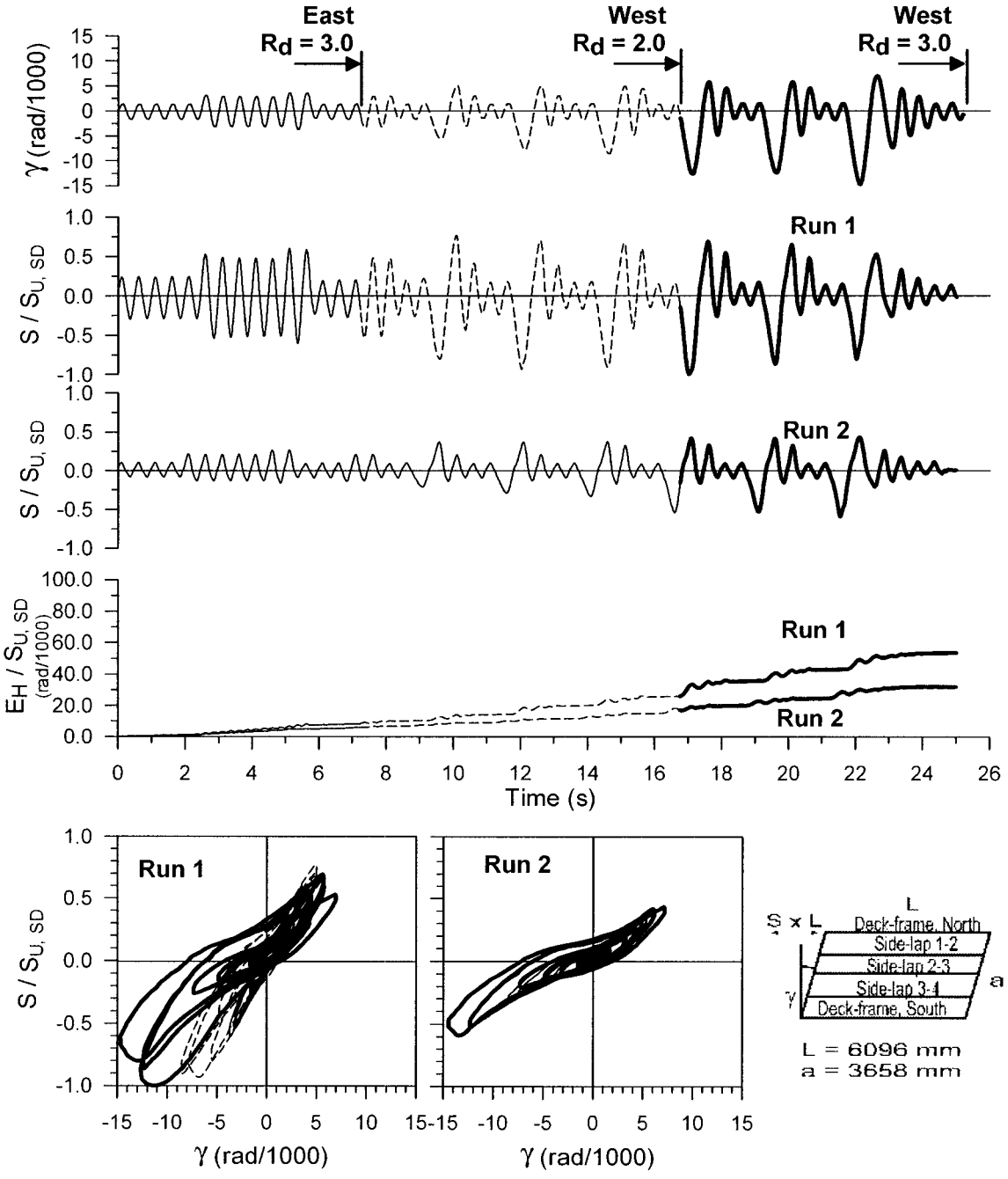

Test No. 26
P3615 B - 0.91 mm
Sidelap fasteners : Welds with washer @ 305 Frame fasteners : Hilti nails @ 305
$S_{u,SDI*}$ = 21.2 kN/m $S_{u,SD}$ = 26.5 kN/m $S_{u,MON}$ = 22.5 kN/m

Figure 5.60 Test no.26 results

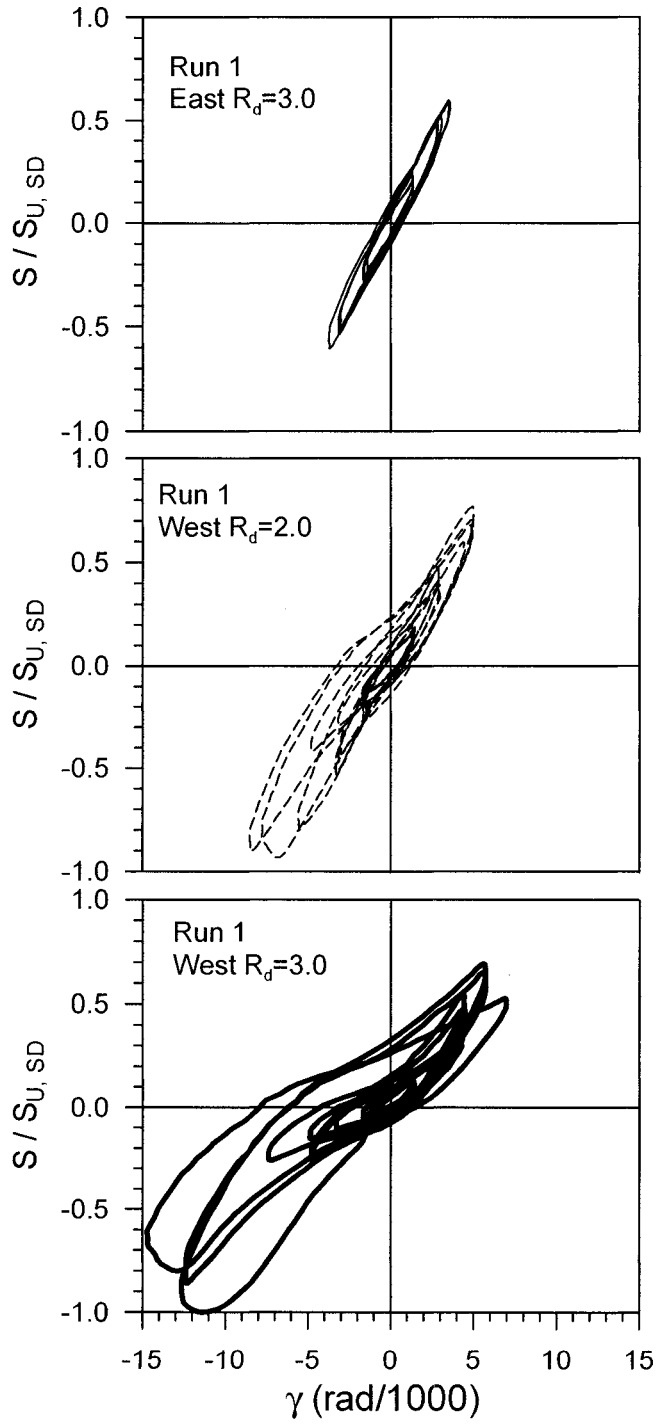

Test No. 26

P3615 B - 0.91 mm
Sidelap fasteners :
Welds with washer @ 305
Frame fasteners :
Hilti nails @ 305

$S_{u, SDI*}$ = *21.2 kN/m*
$S_{u, SD}$ = *26.5 kN/m*
$S_{u, MON}$ = *22.5 kN/m*

Figure 5.60 Test no.26 results (continued)

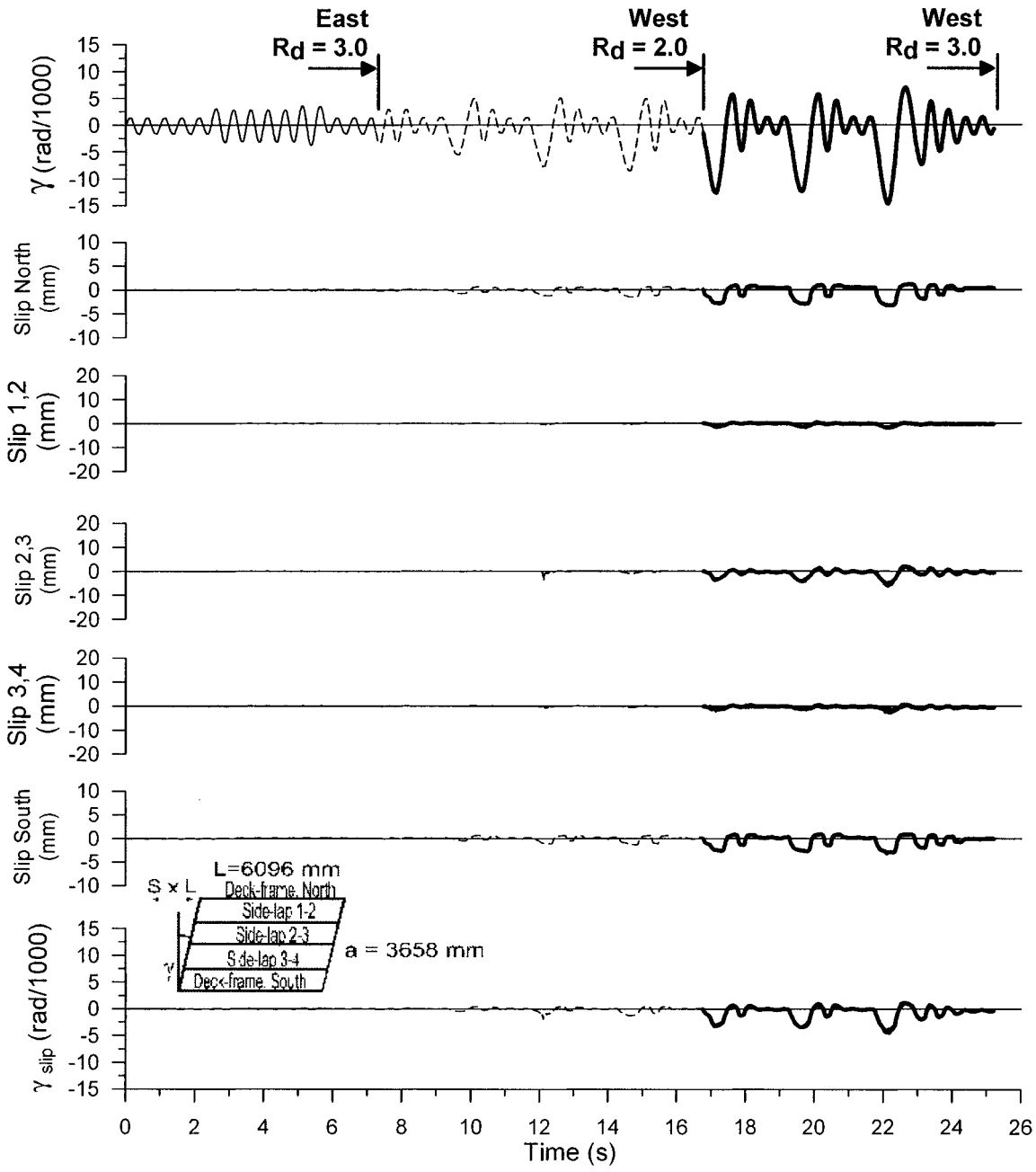

Test No. 26- Run 1

P3615 B - 0.91 mm

Sidelap fasteners : Welds with washer @ 305 Frame fasteners : Hilti nails @ 305

$S_{u,SDI*}$ = 21.2 kN/m $S_{u,SD}$ = 26.5 kN/m $S_{u,MON}$ = 22.5 kN/m

Figure 5.60 Test no.26 results (continued)

	1	2	3	4	5	6	7	8	9	10	11	12	13	14	15	16	17	18	19	20	21
A																					
B																					
C																					BFL
D	TT	FW	BB2	BB2	BB2		BB2	BB2	BB2	BB2		BB2	BB2	BB2	BB2		BB2	BB2	BB2	BB2	
E																SB					BFL
F																SB					BFL
G		BB2	BB2	BB2	BB2		BB2	BB2	BB2	BB2		BB2	BB2	BB2	FW		BB2	BB2	BB2	BB2	BFL
H																BFL					BFL
I																BFL					BFL
J	TT	BB2	BB2	BB2	BB2		BB2	BB2	BB2	BB2		BB2	BB2	BB2	BB2		BB2	BB2	BB2	BB2	BFL
K																BFL					BFL
L																					
M																					

Table 5.28 Observed damage after run 1 (Test 26)

Nomenclature of failure modes (weld with washer - nail pattern)

Welded with washer connections at sidelap (not to frame)
FW: Fracture of weld between top and bottom sheets with limited inelastic deformation
WT: Tilting of washer with partial fracture of weld
WF: One of the two cases mentioned above (FW or WT)
BB1: Bond failure of top sheet with buckling on one side
BB2: Bond failure of top sheet with buckling on two sides
BB: Bond failure of top sheet with buckling (BB1 or BB2 not identified)

Nailed deck-to-frame connections
SN: Shear failure in the nail
SB: Slight buckling around nail
BFS: Bearing failure (slot) without buckling
BFL: Bearing failure perpendicular to the flute (may extend into the web)
SU: Sheet uplifted around nail with possible bearing deformation
TT: Tearing of top sheet at nail
Two failure modes are combined in TT: a) tearing due to bearing near edge b) bearing failure with slot that reach the sheet edge
B1: Buckling on one side of nail with possible bearing deformation
B2: Buckling on two sides of nail with possible bearing deformation
BF: Bearing failure (with or without buckling). (SB, BFS, TT, B1 or B2 not identified)

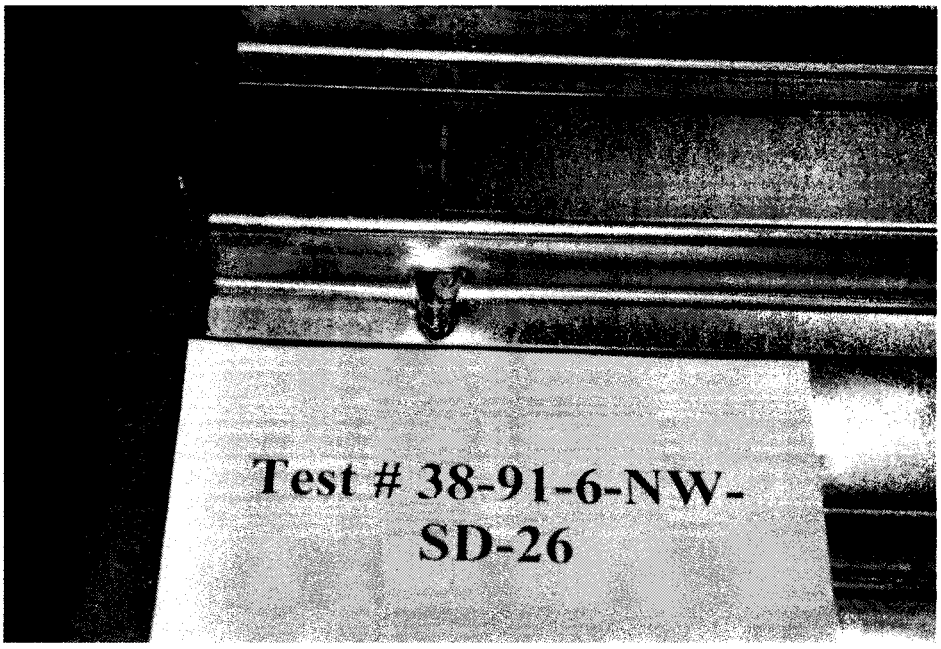

Figure 5.61 BFL failure mode at nailed connection C21, Test 26

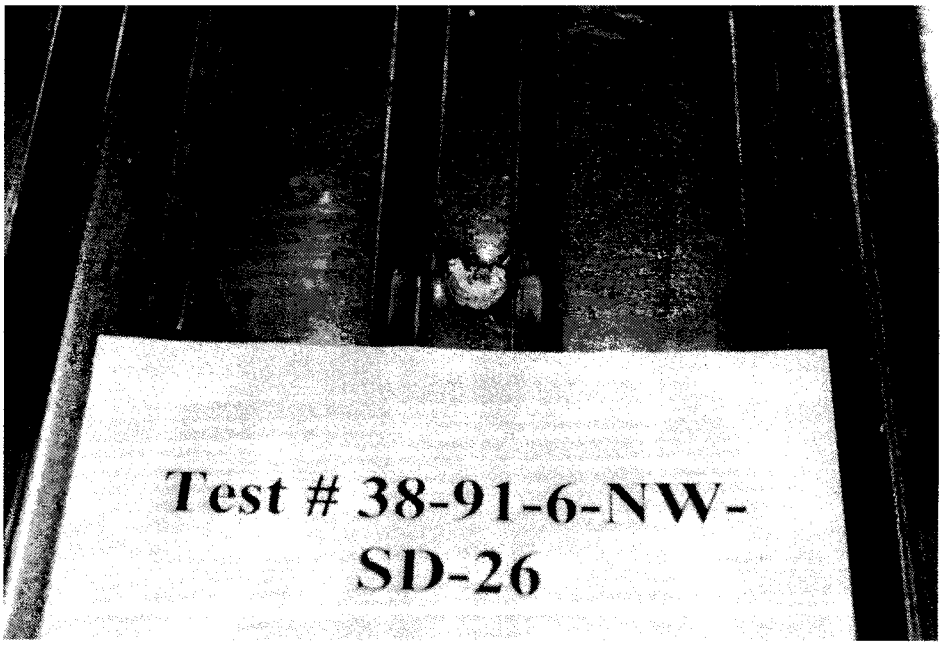

Figure 5.62 SB failure mode at nail E16, Test 26

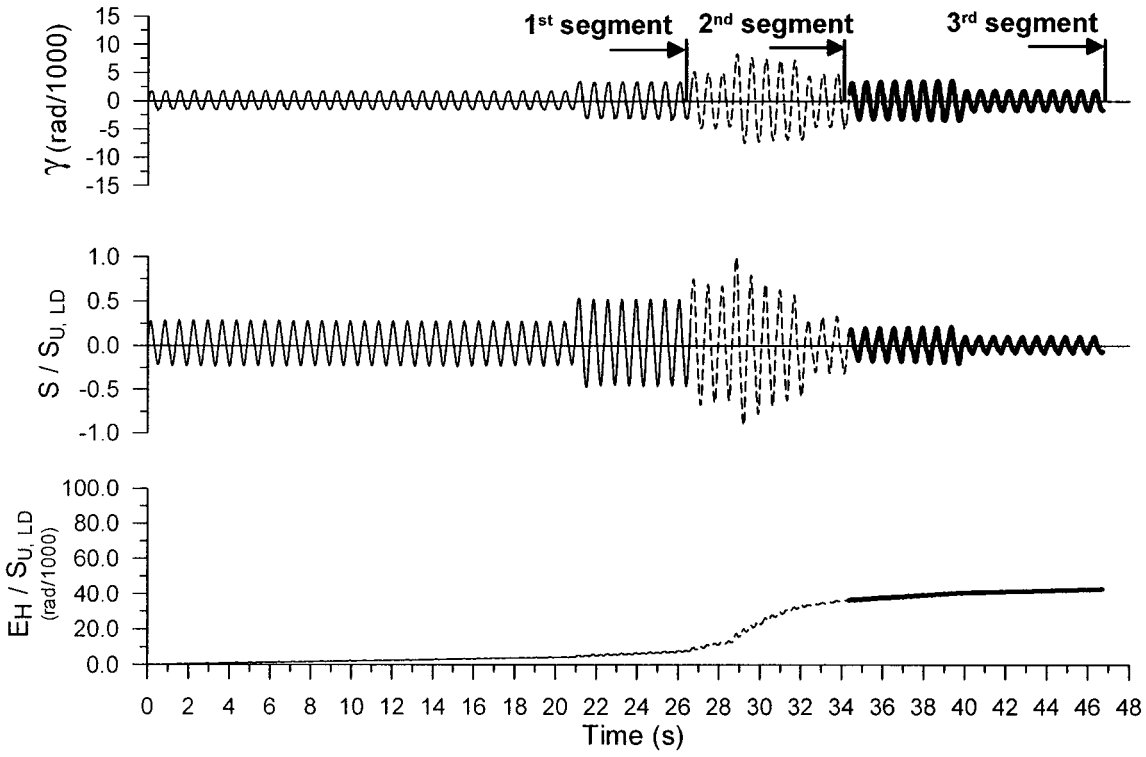

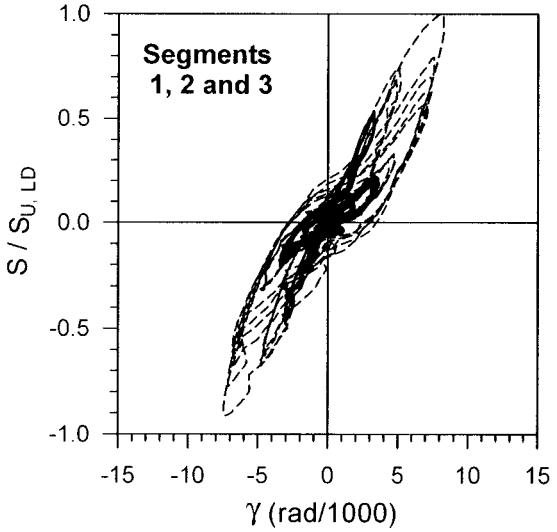

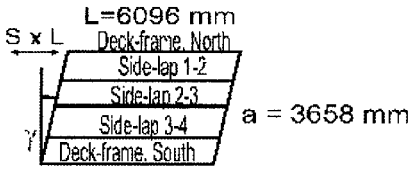

Test No. 27
P3615 B - 0.91 mm
Sidelap fasteners : Welds with washer @ 305 Frame fasteners : Hilti nails @ 305
$S_{u,SDI}$ = 21.2 kN/m $S_{u,LD}$ = 26.2 kN/m $S_{u,MON}$ = 22.5 kN/m

Figure 5.63 Test no.27 results

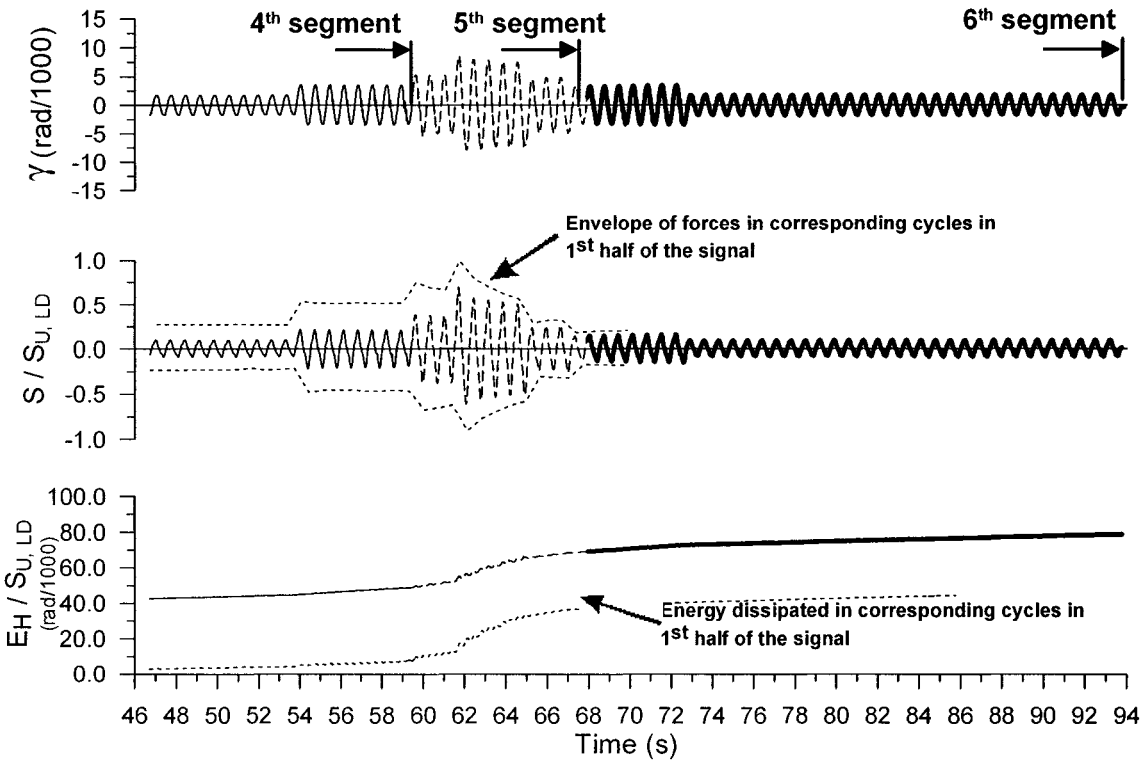

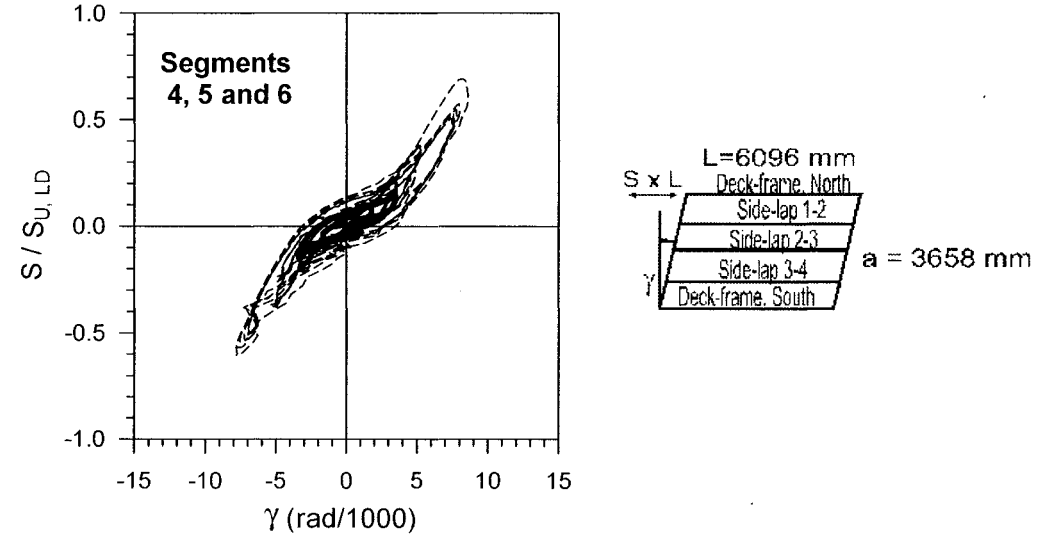

Test No. 27
P3615 B - 0.91 mm
Sidelap fasteners : Welds with washer @ 305 Frame fasteners : Hilti nails @ 305
$S_{u,SDI*}$ = 21.2 kN/m $S_{u,LD}$ = 26.2 kN/m $S_{u,MON}$ = 22.5 kN/m

Figure 5.63 Test no.27 results (continued)

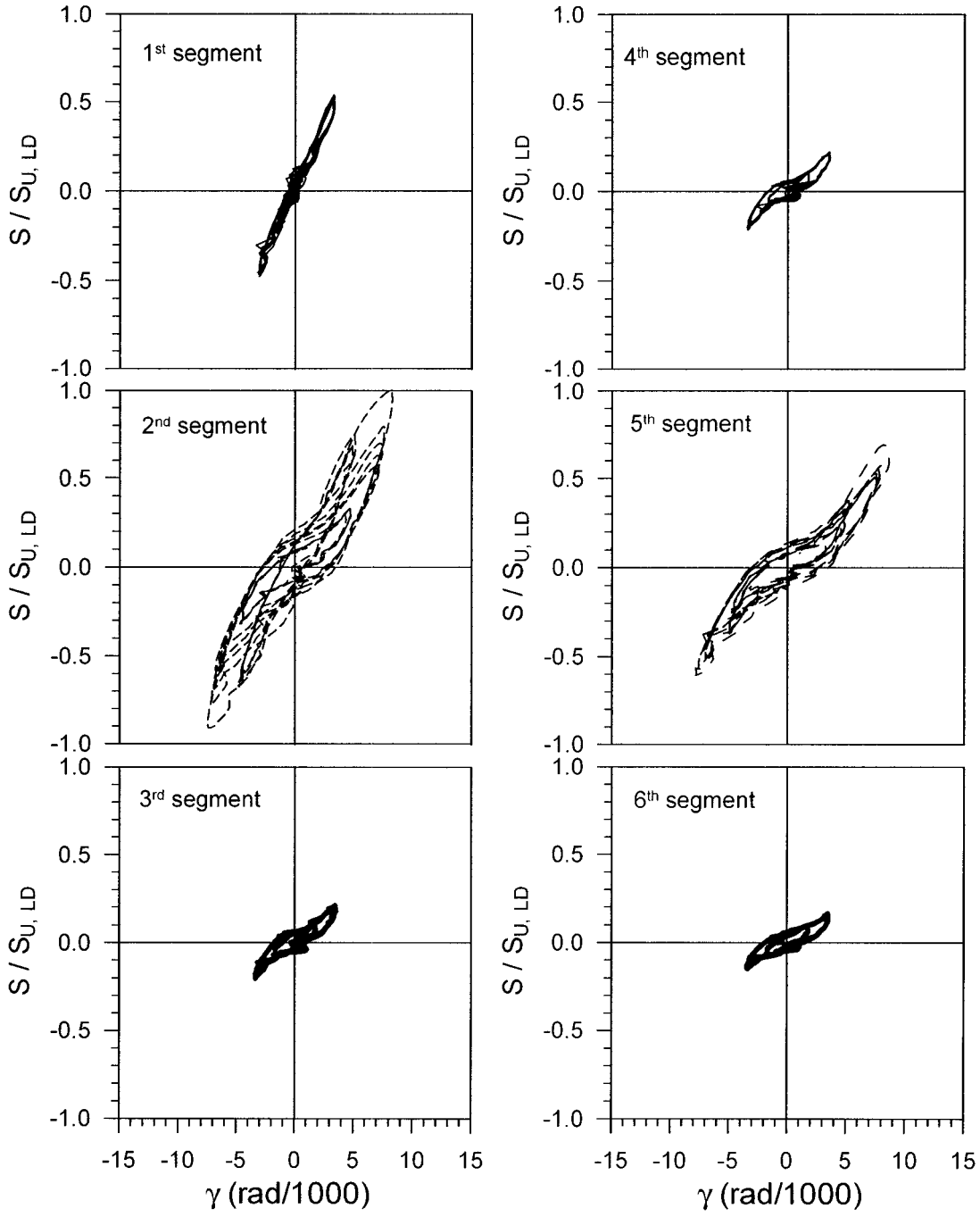

Test No. 27
P3615 B - 0.91 mm
Sidelap fasteners : Welds with washer @ 305 Frame fasteners : Hilti nails @ 305
$S_{u,SDI*}$ = 21.2 kN/m $S_{u,LD}$ = 26.2 kN/m $S_{u,MON}$ = 22.5 kN/m

Figure 5.63 Test no.27 results (continued)

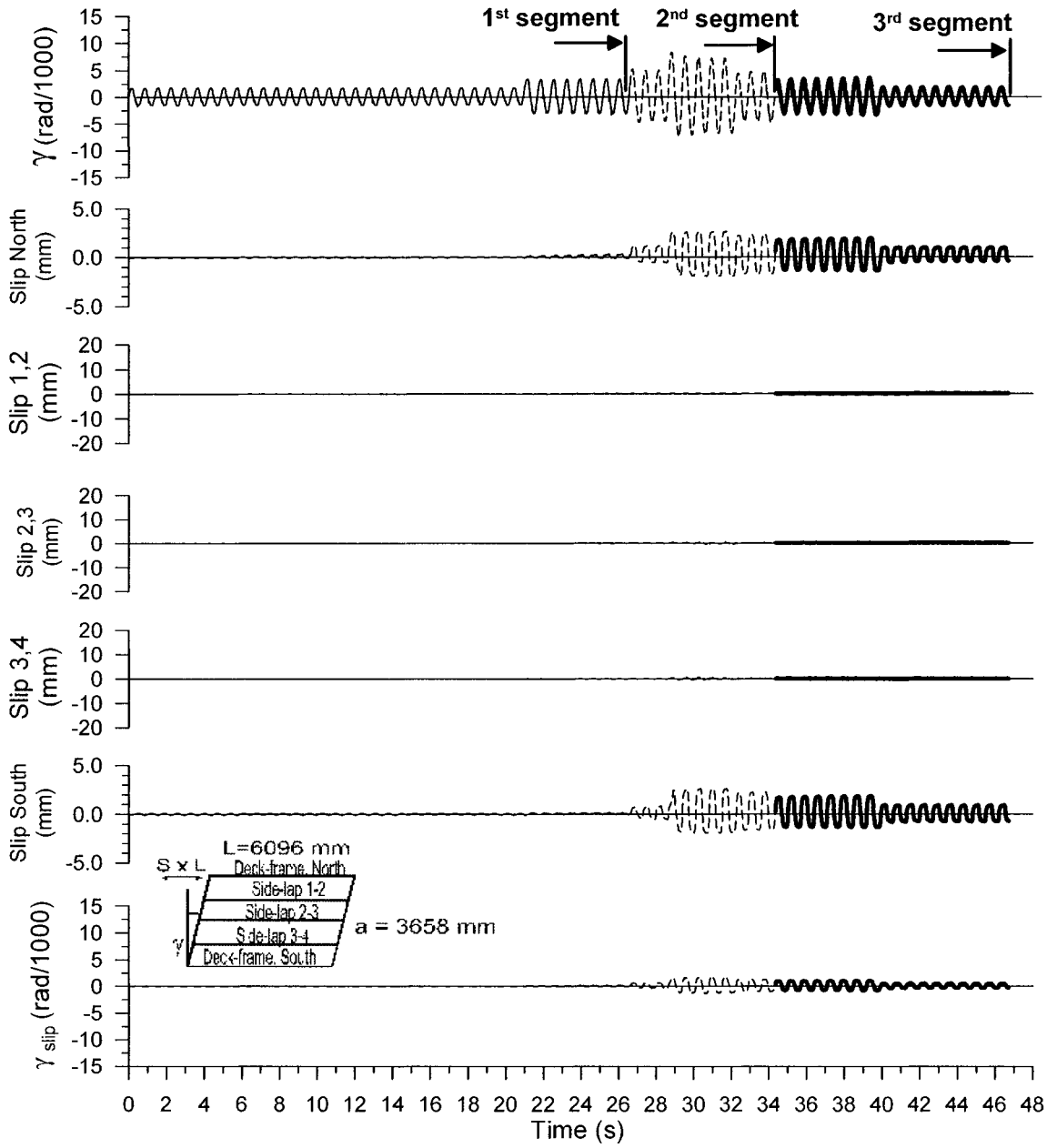

Test No. 27
P3615 B - 0.91 mm
Sidelap fasteners : Welds with washer @ 305 Frame fasteners : Hilti nails @ 305
$S_{u,SDI}$ = *21.2 kN/m* $S_{u,LD}$ = *26.2 kN/m* $S_{u,MON}$ = *22.5 kN/m*

Figure 5.63 Test no.27 results (continued)

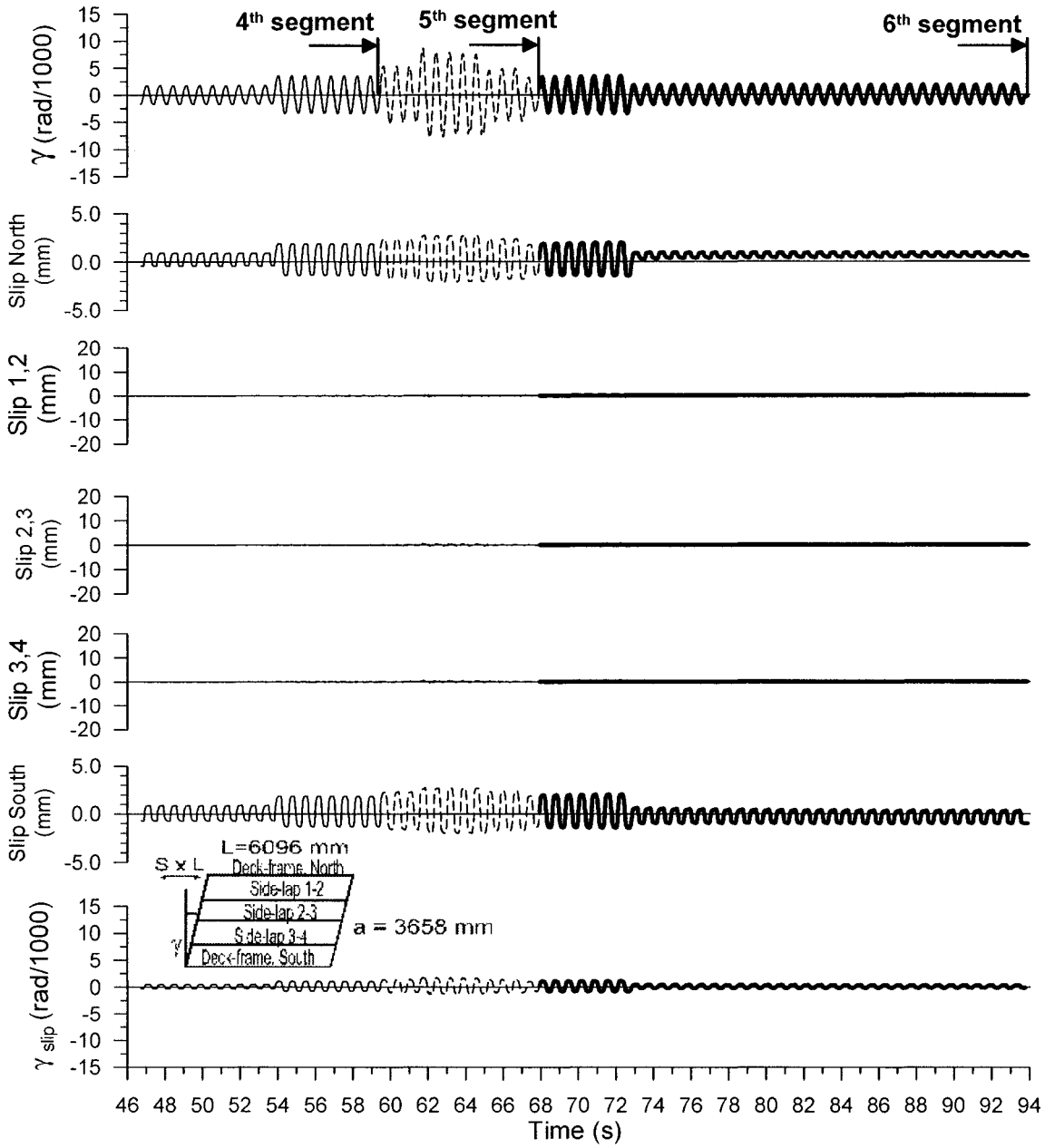

Test No. 27
P3615 B - 0.91 mm
Sidelap fasteners : Welds with washer @ 305 Frame fasteners : Hilti nails @ 305
$S_{u,SDI}$ = *21.2 kN/m* $S_{u,LD}$ = *26.2 kN/m* $S_{u,MON}$ = *22.5 kN/m*

Figure 5.63 Test no.27 results (continued)

	1	2	3	4	5	6	7	8	9	10	11	12	13	14	15	16	17	18	19	20	21
A	SB	SB	SB	SB	SB	SB	SB	SB	SB	SB	SB	SB	SB	SB	SB	SB	SB	SB	SB	SB	BFS
B	SU																				SB
C	SU					SB										SB					BFL
D	SU															SB					SU
E	SU					SB										SB					BFL
F	SU					SB										SB					BFL
G	SU					SB										SB					SB
H	SU					SB										SB					BFL
I	SU					SB										SB					SB
J						SB										SB					SU
K	SB					SB										SB					SB
L	SB					SB										SB					SB
M	SB	SB	SB	SB	SB	SB	SB	SB	SB	SB	SB	SB	SB	SB	SB	SB	SB	SB	SB	SB	SB

Table 5.29 Observed damage (Test 27)

Nomenclature of failure modes (weld with washer - nail pattern)

Welded with washer connections at sidelap (not to frame)
FW: Fracture of weld between top and bottom sheets with limited inelastic deformation
WT: Tilting of washer with partial fracture of weld
WF: One of the two cases mentioned above (FW or WT)
BB1: Bond failure of top sheet with buckling on one side
BB2: Bond failure of top sheet with buckling on two sides
BB: Bond failure of top sheet with buckling (BB1 or BB2 not identified)

Nailed deck-to-frame connections
SN: Shear failure in the nail
SB: Slight buckling around nail
BFS: Bearing failure (slot) without buckling
BFL: Bearing failure perpendicular to the flute (may extend into the web)
SU: Sheet uplifted around nail with possible bearing deformation
TT: Tearing of top sheet at nail
Two failure modes are combined in TT: a) tearing due to bearing near edge b) bearing failure with slot that reach the sheet edge
B1: Buckling on one side of nail with possible bearing deformation
B2: Buckling on two sides of nail with possible bearing deformation
BF: Bearing failure (with or without buckling). (SB, BFS, TT, B1 or B2 not identified)

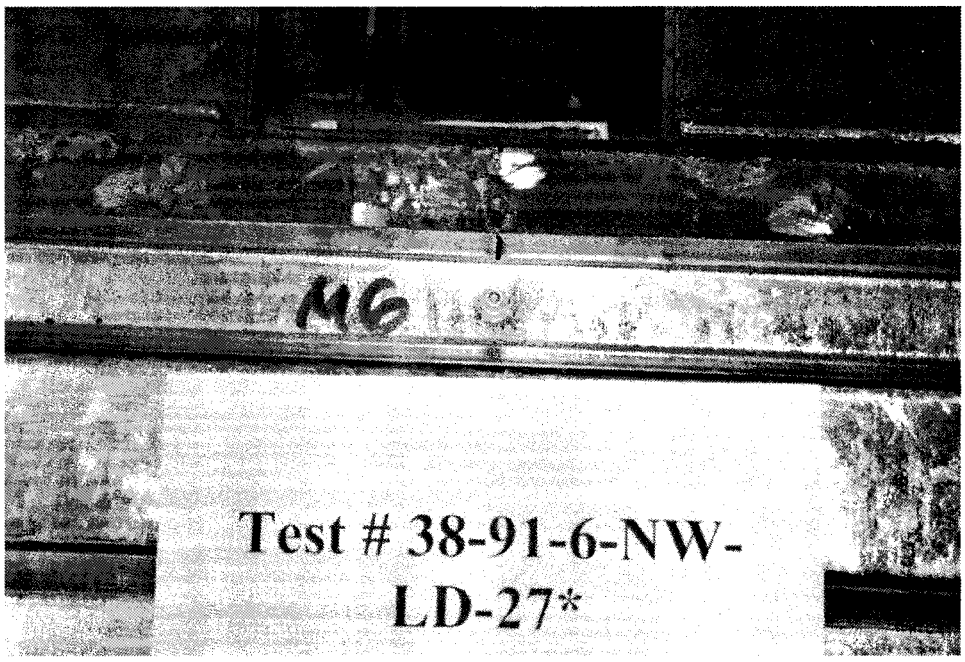

Figure 5.64 SB failure mode at South end (M6), Test 27

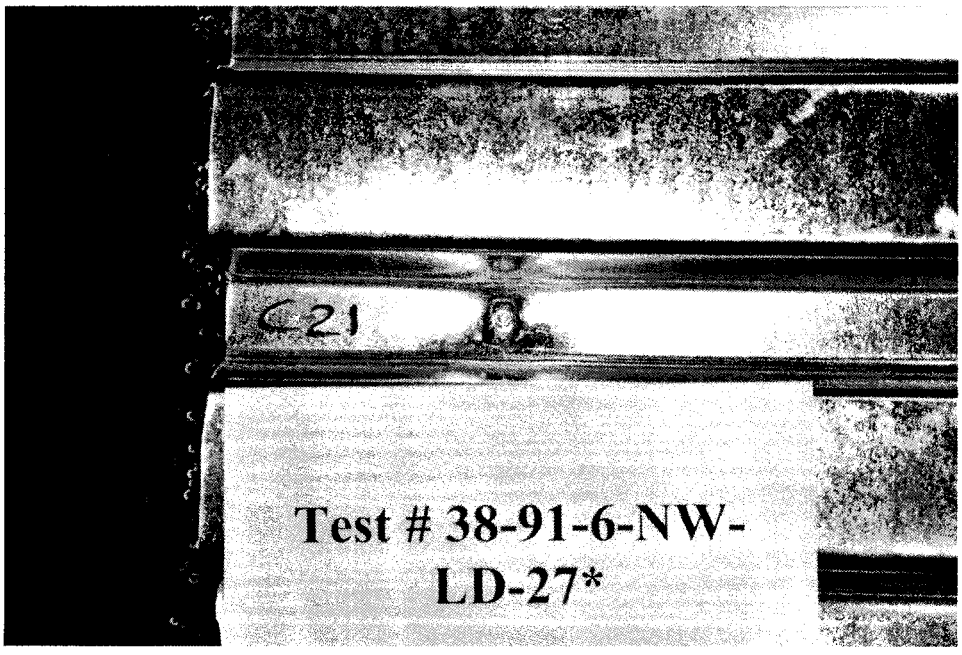

Figure 5.65 BFL failure mode at nail C21, Test 27

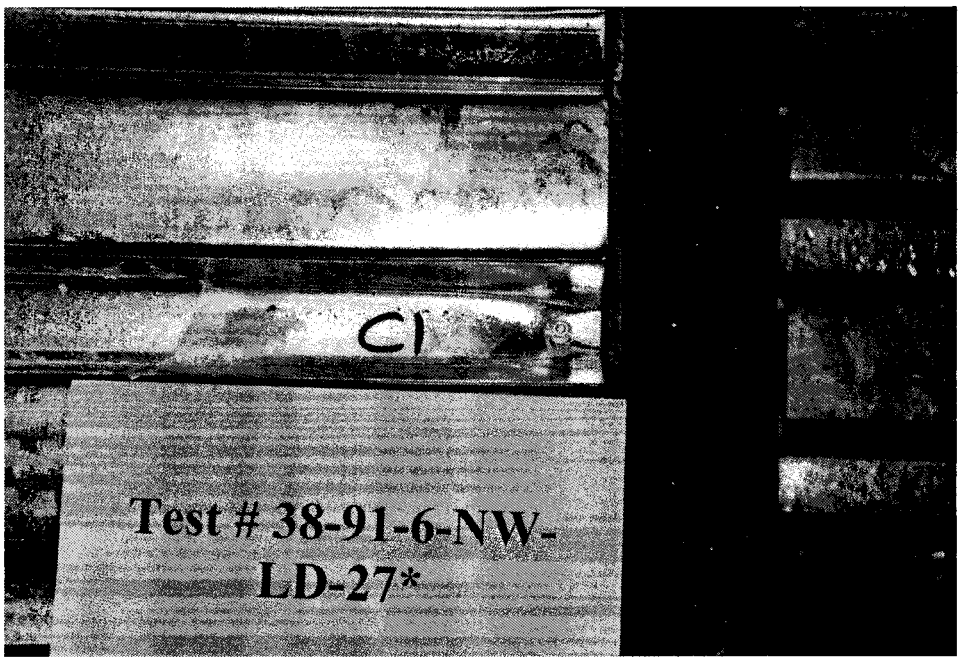

Figure 5.66 SU failure mode at nail C1, Test 27

5.8.4 Screw–nail design

5.8.4.1 Tests 19, 34 and 35

Tests 19 (monotonic), 34 (short duration, SD) and 35 (long duration, LD) were conducted with screwed sidelap connections and Hilti nailed frame fasteners. B-deck profile panels of 0.91 mm thickness were used. The connection spacing was 305 mm for both sidelap and deck-to-frame fasteners. The description of specimens for tests 19, 34 and 35 is presented in Table 5.30. Test result curves are presented in Figure 5.69, Figure 5.72 and Figure 5.73 and the observed damage in Table 5.31, Table 5.32 and Table 5.33.

Test 19

Test 17 (monotonic) performed by Essa *et al.* (2001) was nominally identical to test 19. In test 17, unexpected shear failures in the nails occurred prior to reaching the maximum

load. This behaviour was not desirable because shear failure in nails are fragile and may compromise the desired ductile behaviour in the diaphragm. The aim of repeating test 17 (test 19) was to provide further information with regards to the behaviour of deck assemblies with Hilti nails and to check the adequacy of the nail type. Slip at sidelap was not measured in that test.

In test 19, no shear failure occurred in the nails. The maximum measured load was equal to 16.7 kN/m at a shear angle of 7 rad/1000. Up to 3 rad/1000 ($\cong 0.7\ S_u$), the increase in strength was linear. Beyond this point, the stiffness gradually decreased up to peak load. This softening may be attributed to tilting of the screws at the sidelaps. Tilting of the nailed connections did not occur. Beyond the peak load, the screws were tilted (Figure 5.71) while the nails bore against sheet steel (Figure 5.70). Strength degradation then occurred in a gradual manner, the deck being capable of maintaining a capacity greater to $0.8S_u$ up to 15 rad/1000.

Overall, test 19 performed better than test 17 by Essa *et al.* (2001). Nail failure did not take place, and the maximum measured shear load in test 19, 16.7 kN/m, was greater than in test 17, 14.6 kN/m. Other tests conducted by Essa *et al.* (2001) revealed that the screw-nail connection pattern with proper installation and materials could produce a ductile diaphragm behaviour, as was confirmed by the results of Test 19.

Test 34

Test 34 was subjected to a short duration (SD) loading protocol. The maximum measured load was equal to 17.0 kN/m, which is close to the result from monotonic test 19, 16.7 kN/m. The shear-distortion curve remained linear under the East $R_d = 3.0$ loading protocol. In the West $R_d = 2.0$ segment, pinching occurred and the specimen, for cycles of equal amplitude, lost strength. Note that the loading references used, γ_u and γ_2,

were close to the real γ_u and γ_2 values imposed during the test. Therefore, the system was pushed to the real γ_u during the East R_d=3.0 loading protocol and no strength degradation was observed. Similarly, in the second peak of the West R_d = 2.0 segment, the system reached the real γ_2 and the maximum shear strength was attained. However, the diaphragm was still capable of developing 75% of its ultimate strength during the largest amplitude cycle of run 1.

Interior sidelaps experienced similar slip time histories, however, sidelap 1,2 and 3,4 sustained larger deformations compared to sidelap 2,3. This behaviour was observed in other tests. The edge connections on the North and South sides are stiffer than the intermediate sidelap connections.

At test end, it was observed that the screws were loose. However, the sidelap sheets were still connected and no gap was found between the overlapping edges of the sheets. No damage was observed on along the North and South edges, however slips smaller than 2 mm were recorded at these locations. Bearing failure (BF), a general case made of different failure modes, occurred at 40 purlin locations. The available information was not sufficient to assess the precise failure mode. Buckling on one side of nail (B1) was observed at 3 locations (D21, G21 and J21). The nail located at J16 failed in shear (SN) and the embedded part disconnected from the framing member. This may be attributed to improper installation of the nail, which had been placed after an initial fastener was inserted and removed. The failure pattern tended to be related to the slip deformation at sidelaps. In Figure 5.67, the slip distribution in different panel is shown.

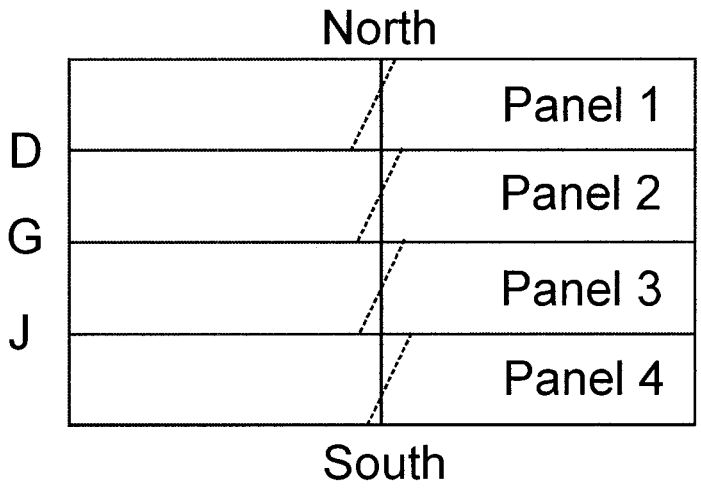

Figure 5.67 Slip distribution in different panels, Test 34

The fasteners located at sidelap lines D, G and J experienced the larger deformations, whereas the fasteners in the middle of deck panels were less deformed. The observed damage reflected this behaviour since all of the fasteners at sidelap lines failed, whereas fewer failures were found in the middle of panels.

The deformations at 3 interior sidelaps can be related to the pinching developed in the test specimen. In the East R_d = 3.0 segment, when the specimen remained elastic, the sidelap slips were negligible. Under the West R_d = 2.0 segment, sidelap slips started but were kept small and, therefore, a low level of pinching was attained. In West R_d = 3.0, the pinching was at its larger extent while sidelap slips reached their peak values. In the West R_d = 3.0 segment, the behaviour was governed by the case where 4 sheets acted separately and the sidelap slip, γ_{slip}, represented a major component in the total system distortion, γ. Figure 5.68 presents the relationship between the imposed inelastic deformation, γ_p, and the pinching behaviour. Once inelastic distortions were imposed on the diaphragm, pinching behaviour developed in which the deck exhibits a reduced capacity, with virtually no stiffness, near the zero deformation position after application of large amplitude cycles. The pinching is related to tilting of screws and bearing against

sidelap nail at purlins. In Figure 5.68, it is possible to compare the imposed inelastic distortions and the pinching for the two last cycles in the West R_d=3.0 segment. The 2nd and 3rd largest peaks in West R_d= 3.0 are presented. The 2nd peak had an imposed inelastic distortion, γ_p, equal to 8.0 rad/1000 and the 3rd peak a value of 10.0 rad/1000.

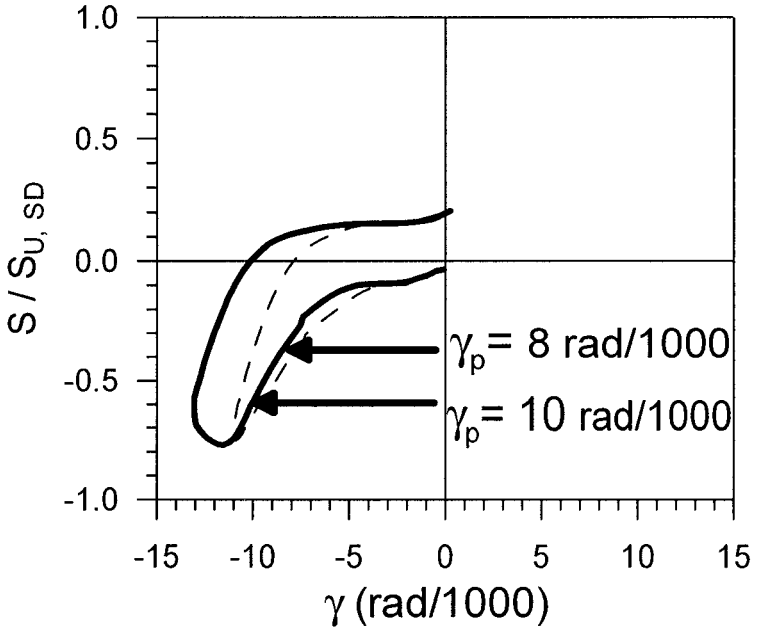

Figure 5.68 Effect of the inelastic distortions on pinching

Test 35

In test 35, the maximum recorded load was equal to 17.3 kN/m which is close to the results from tests 19 and 34. Strength degradation was observed in the 1st half of the loading protocol. In the cycles before and following the large peaks at $2\gamma_u$, one can see that strength degradation occurred. In the 2nd half of the loading protocol one can see that the measured forces at large distortion were closer to the results from the 1st half compared to the forces at low distortion amplitudes (Figure 5.73). This was attributed to the large amount of pinching in the final half of the loading protocol.

Interior sidelap slips were kept below 5 mm, which was much smaller than measured for test 34, 12 mm. Deformations below 1 mm were measured at the North and South edges. The lesser extent of damage in test 35 tended to confirm the lower distortion imposed on the specimen. Interior sidelaps were intact except that sidelap screws had become slack. No damage was observed at along the North and South edges. Also, no shear failure occurred in nails. Only the B1 and SB failure modes were found. Figure 5.74 presents a nail where buckles developed on one side (B1) and Figure 5.75 a nail with slight buckling (SB).

Tests 17 and 18 from Essa *et al.* (2001), which were nominally identical in construction to specimens 19, 34 and 35, developed smaller maximum measured forces. Test 17 was the weakest (load value), which may be attributed to the shear failure in nails. For test 18, the difference in shear capacity was less significant and may be attributed to the inherent variability in resistance.

Table 5.30 Test specimen description (Tests 19, 34 and 35)

Steel properties:	
Supplier and coil number	Canam P-3615 B-deck 0.91 mm Coil supplier: Sorevco Coil number: 147624
Base metal thickness (mm)	0.88
Fy test (MPa)	319
Fu test (MPa)	394
E (MPa)	210000
50 mm gauge % elongation	24 %
Fasteners:	
Sidelap fasteners	Screw 12- 14 x 1 HWH#1 FP Lot number: 9901-0019 Spacing: 305 mm c/c
Deck-to-frame fasteners	Hilti nail X-EDNK-22 THQ 12M Lot number: 413923 (test 19), 413920 (tests 34 and 35) Spacing: 305 mm c/c
Comments on quality of fasteners:	
Test 19	Nail stand-off: Total Ave.: 7.7 mm C.o.V.: 0.15 At sidelaps Ave.: 8.2 mm C.o.V.: 0.13 Except sidelaps Ave.: 7.7 mm C.o.V.: 0.15 The nail at B16 was removed and replaced. Nails D16 and G6 were located only 5 mm from the sheet edge.
Test 34	Nail stand-off: Total Ave.: 7.0 mm C.o.V.: 0.13 At sidelaps Ave.: 8.1 mm C.o.V.: 0.15 Except sidelaps Ave.: 6.8 mm C.o.V.: 0.10 4 nails (J6, J16, L21 and M1) were not properly installed at first and were replaced.
Test 35	Nail stand-off: Total Ave.: 6.9 mm C.o.V.: 0.17 At sidelaps Ave.: 7.3 mm C.o.V.: 0.10 Except sidelaps Ave.: 6.9 mm C.o.V.: 0.18 4 nails were higher than 10.5 mm (see Appendix E). However, they were not replaced.

N.B.: In test 19, the deck panels were placed in the opposite direction compared to all other tests. In consequence, the large lip was located along the North edge.

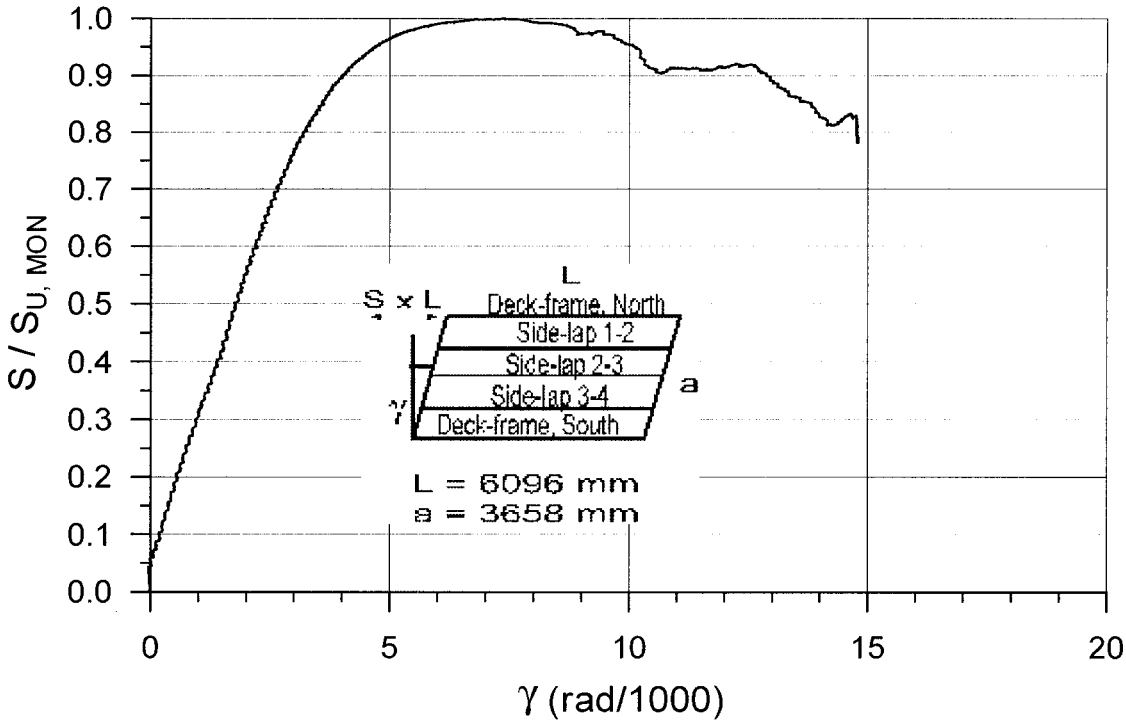

Test No. 19
P3615 B - 0.91 mm
Sidelap fasteners : Screws @ 305 Frame fasteners : Hilti nails @ 305
$S_{u,\,SDI*}$ = *13.5 kN/m* $S_{u,\,MON}$ = *16.7 kN/m*

Figure 5.69 Test no.19 results

	1	2	3	4	5	6	7	8	9	10	11	12	13	14	15	16	17	18	19	20	21
A																					
B																					
C	BF					BF					BF					BF					BF
D	BF					BF					BF					BF					
E																					
F																					
G	BF					BF					BF					BF					BF
H																					
I																					
J	BF					BF					BF					BF					BF
K	BF					BF					BF					BF					BF
L																					
M																					

Table 5.31 Observed damage (Test 19)

Nomenclature of failure modes (screw-nail pattern)

Nailed deck-to-frame connections

SN: Shear failure in the nail
SB: Slight buckling around nail
BFS: Bearing failure (slot) without buckling
BFL: Bearing failure perpendicular to the flute (may extend into the web)
SU: Sheet uplifted around nail with possible bearing deformation
TT: Tearing of top sheet at nail
Two failure modes are combined in TT: a) tearing due to bearing near edge b) bearing failure with slot that reach the sheet edge
B1: Buckling on one side of nail with possible bearing deformation
B2: Buckling on two sides of nail with possible bearing deformation
BF: Bearing failure (with or without buckling). (SB, BFS, TT, B1 or B2 not identified)

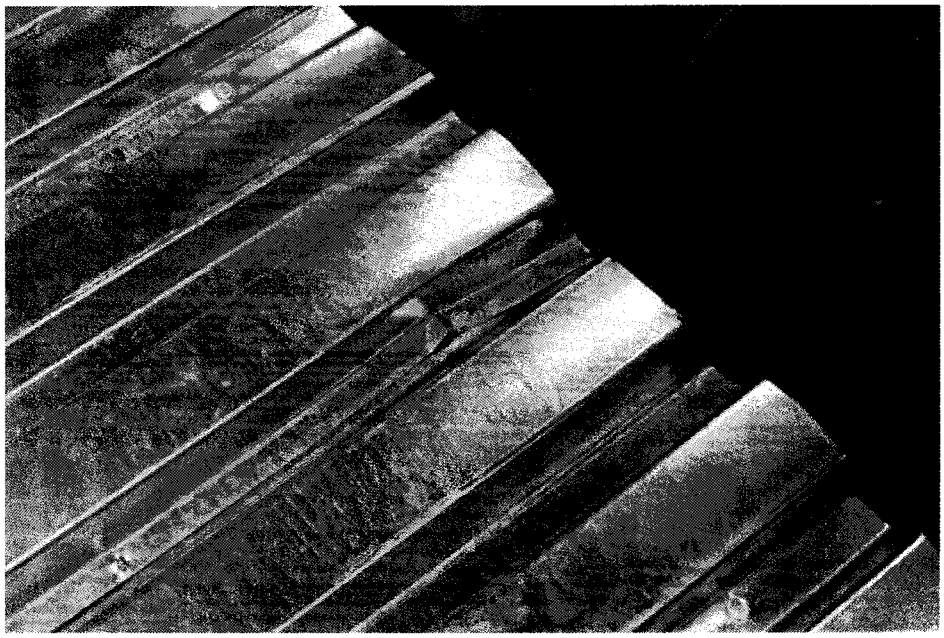

Figure 5.70 B1 failure mode, Test 19

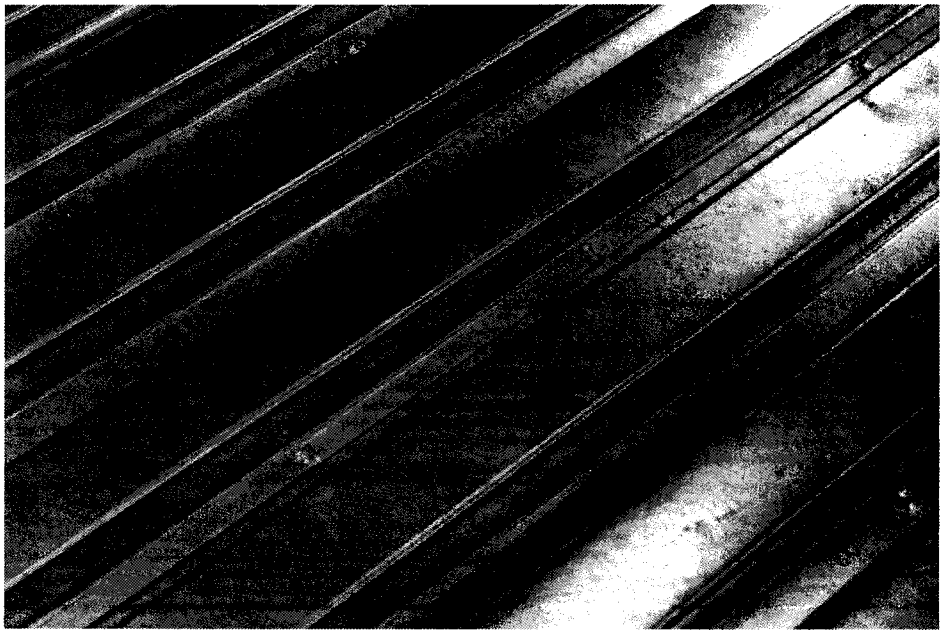

Figure 5.71 Tilted screws at sidelap, Test 19

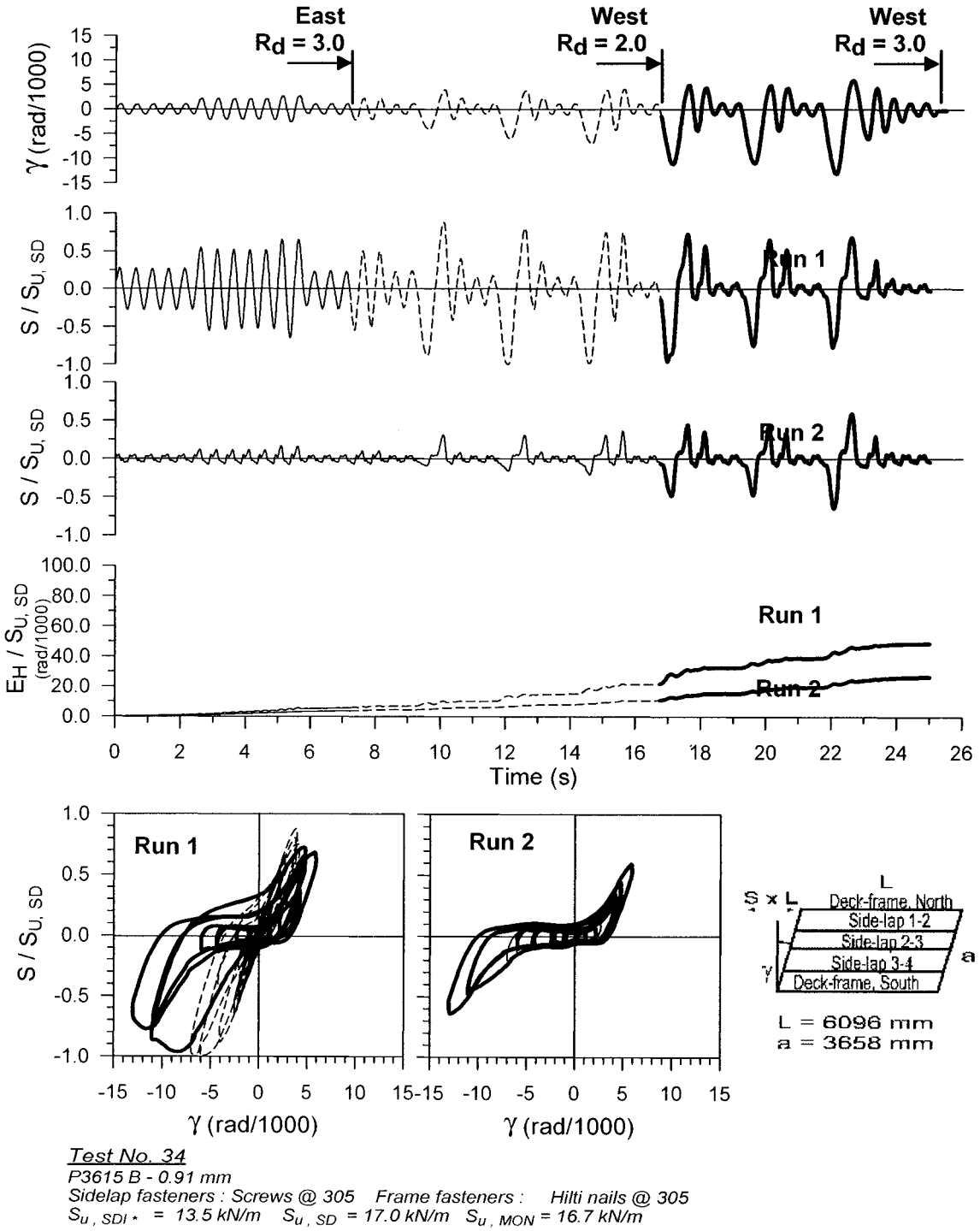

Figure 5.72 Test no.34 results

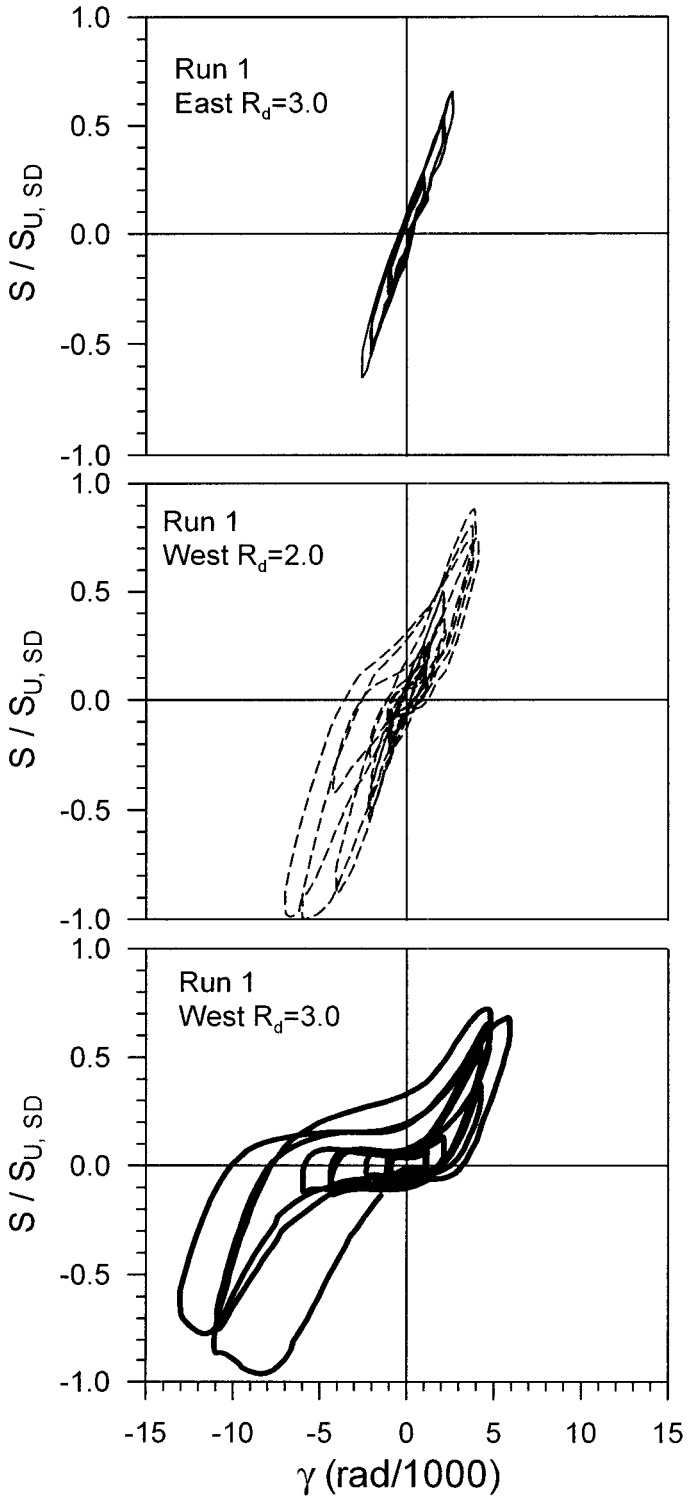

Test No. 34

P3615 B - 0.91 mm
Sidelap fasteners :
Screws @ 305
Frame fasteners :
Hilti nails @ 305

$S_{u, SDI*}$ = 13.5 kN/m
$S_{u, SD}$ = 17.0 kN/m
$S_{u, MON}$ = 16.7 kN/m

Figure 5.72 Test no.34 results (continued)

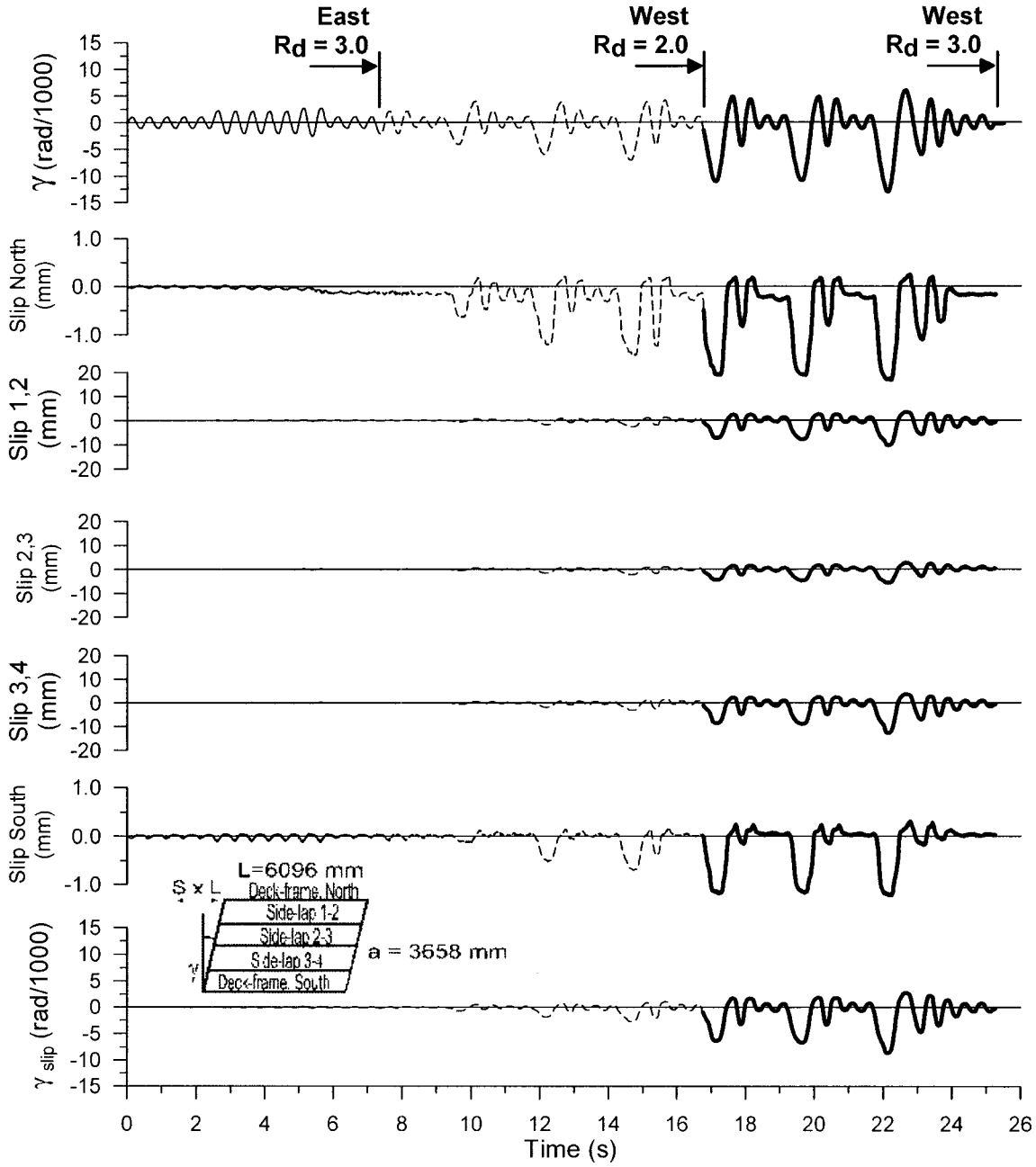

Test No. 34- Run 1
P3615 B - 0.91 mm
Sidelap fasteners : Screws @ 305 Frame fasteners : Hilti nails @ 305
$S_{u,SDI*}$ = 13.5 kN/m $S_{u,SD}$ = 17.0 kN/m $S_{u,MON}$ = 16.7 kN/m

Figure 5.72 Test no.34 results (continued)

Table 5.32 Observed damage after run 1 (Test 34)

	1	2	3	4	5	6	7	8	9	10	11	12	13	14	15	16	17	18	19	20	21
A																					
B																					BF
C	BF					BF					BF					BF					BF
D	BF					BF					BF					BF					B1
E						BF					BF					BF					BF
F						BF					BF					BF					BF
G	BF					BF					BF					BF					B1
H						BF															BF
I						BF					BF					BF					BF
J	BF					BF					BF					SN					B1
K	BF					BF					BF					BF					BF
L	BF					BF										BF					BF
M																					

Nomenclature of failure modes (screw-nail pattern)

Nailed deck-to-frame connections

SN: Shear failure in the nail

SB: Slight buckling around nail

BFS: Bearing failure (slot) without buckling

BFL: Bearing failure perpendicular to the flute (may extend into the web)

SU: Sheet uplifted around nail with possible bearing deformation

TT: Tearing of top sheet at nail
Two failure modes are combined in TT: a) tearing due to bearing near edge b) bearing failure with slot that reach the sheet edge

B1: Buckling on one side of nail with possible bearing deformation

B2: Buckling on two sides of nail with possible bearing deformation

BF: Bearing failure (with or without buckling). (SB, BFS, TT, B1 or B2 not identified)

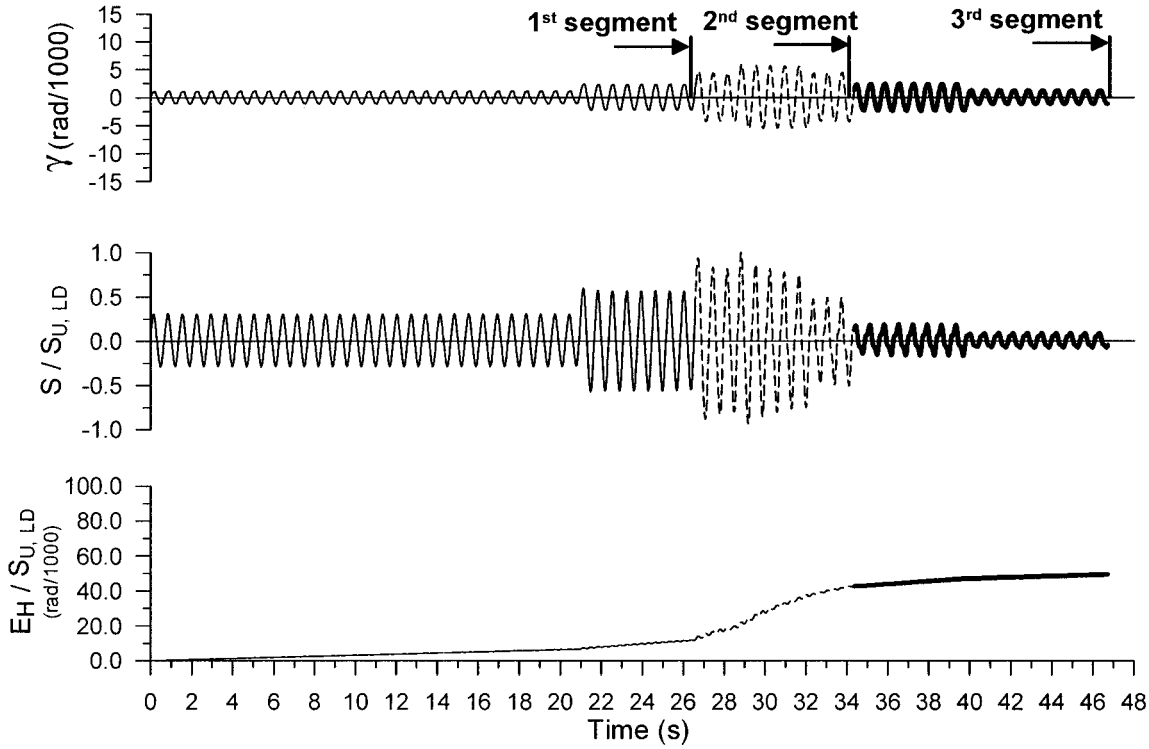

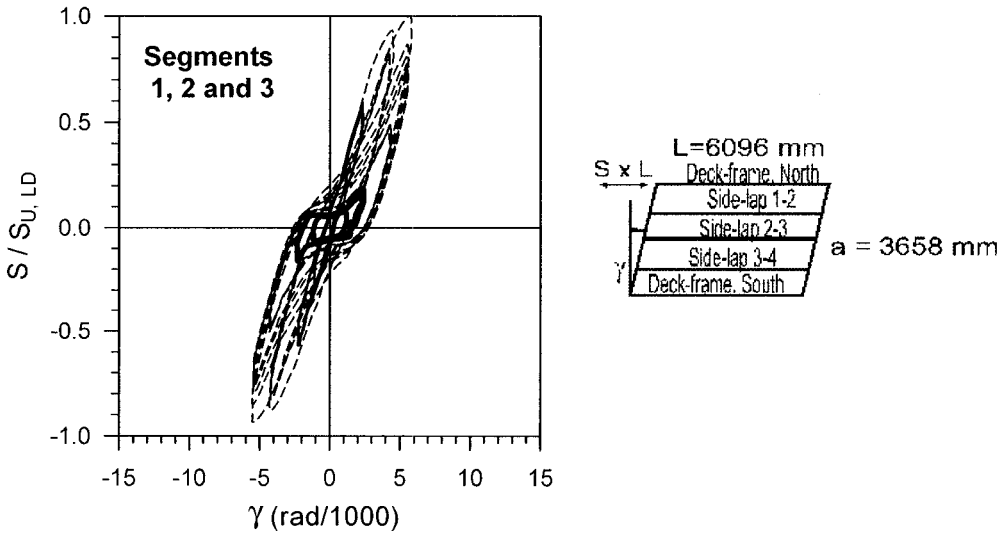

Test No. 35
P3615 B - 0.91 mm
Sidelap fasteners : Screws @ 305 Frame fasteners : Hilti nails @ 305
$S_{u,SDI*}$ = 13.5 kN/m $S_{u,LD}$ = 17.3 kN/m $S_{u,MON}$ = 16.7 kN/m

Figure 5.73 Test no.35 results

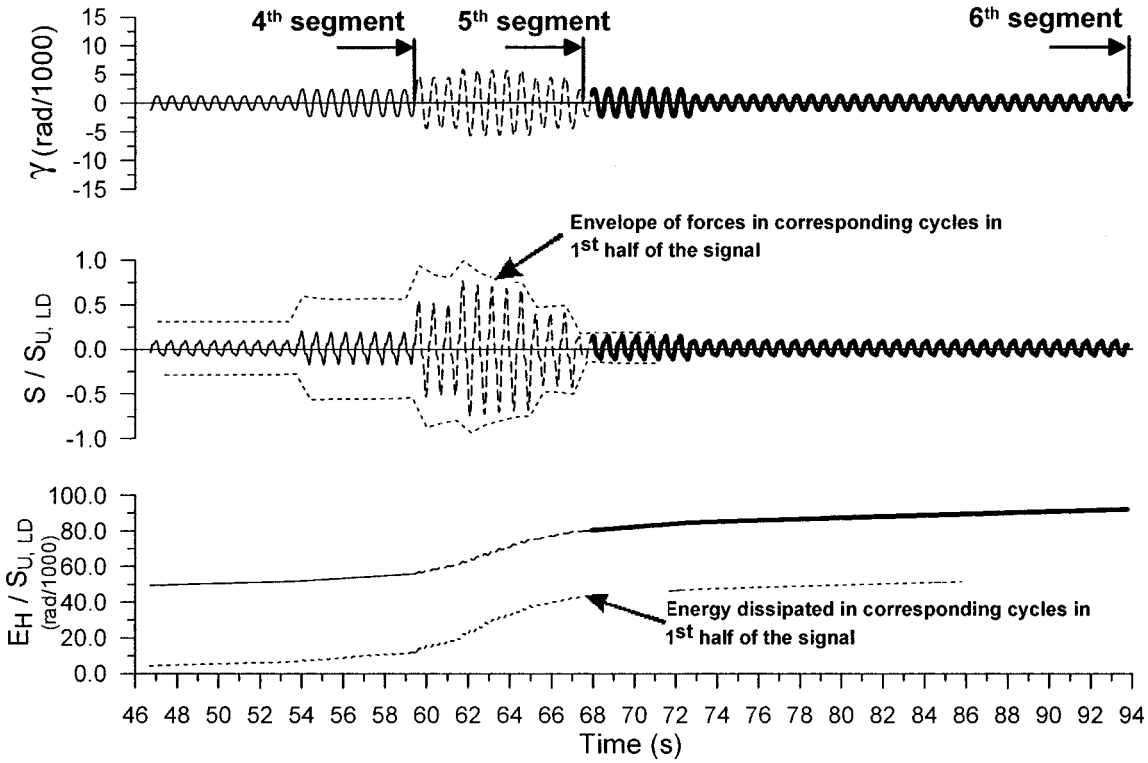

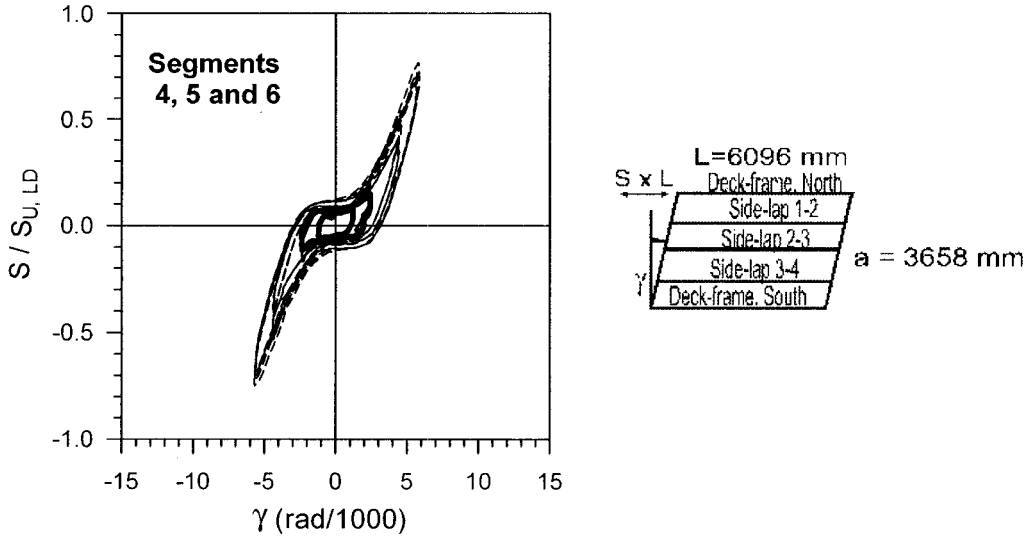

Test No. 35
P3615 B - 0.91 mm
Sidelap fasteners : Screws @ 305 Frame fasteners : Hilti nails @ 305
$S_{u,SDI*}$ = 13.5 kN/m $S_{u,LD}$ = 17.3 kN/m $S_{u,MON}$ = 16.7 kN/m

Figure 5.73 Test no.35 results (continued)

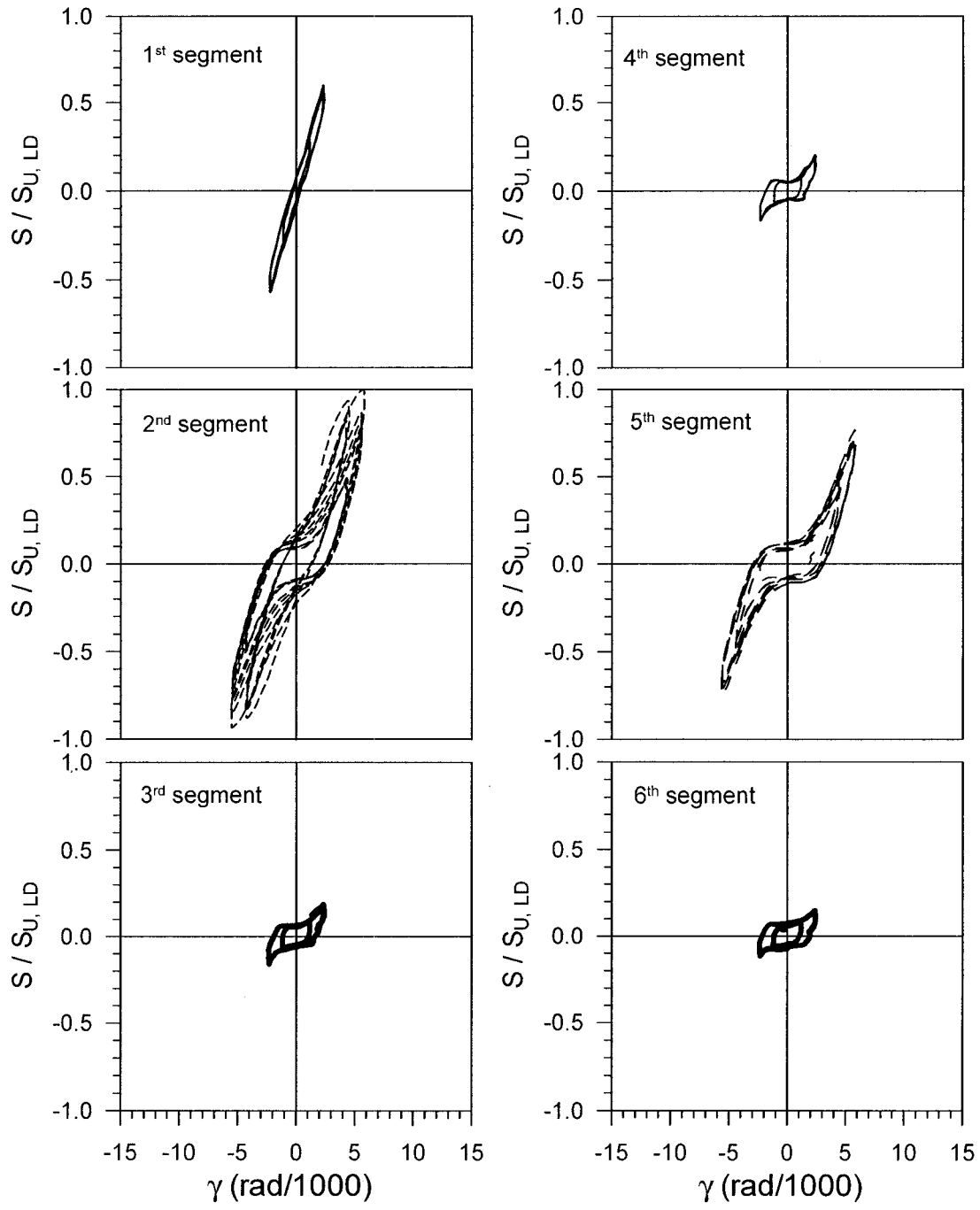

Test No. 35
P3615 B - 0.91 mm
Sidelap fasteners : Screws @ 305 Frame fasteners : Hilti nails @ 305
$S_{u,SDI*}$ = 13.5 kN/m $S_{u,LD}$ = 17.3 kN/m $S_{u,MON}$ = 16.7 kN/m

Figure 5.73 Test no.35 results (continued)

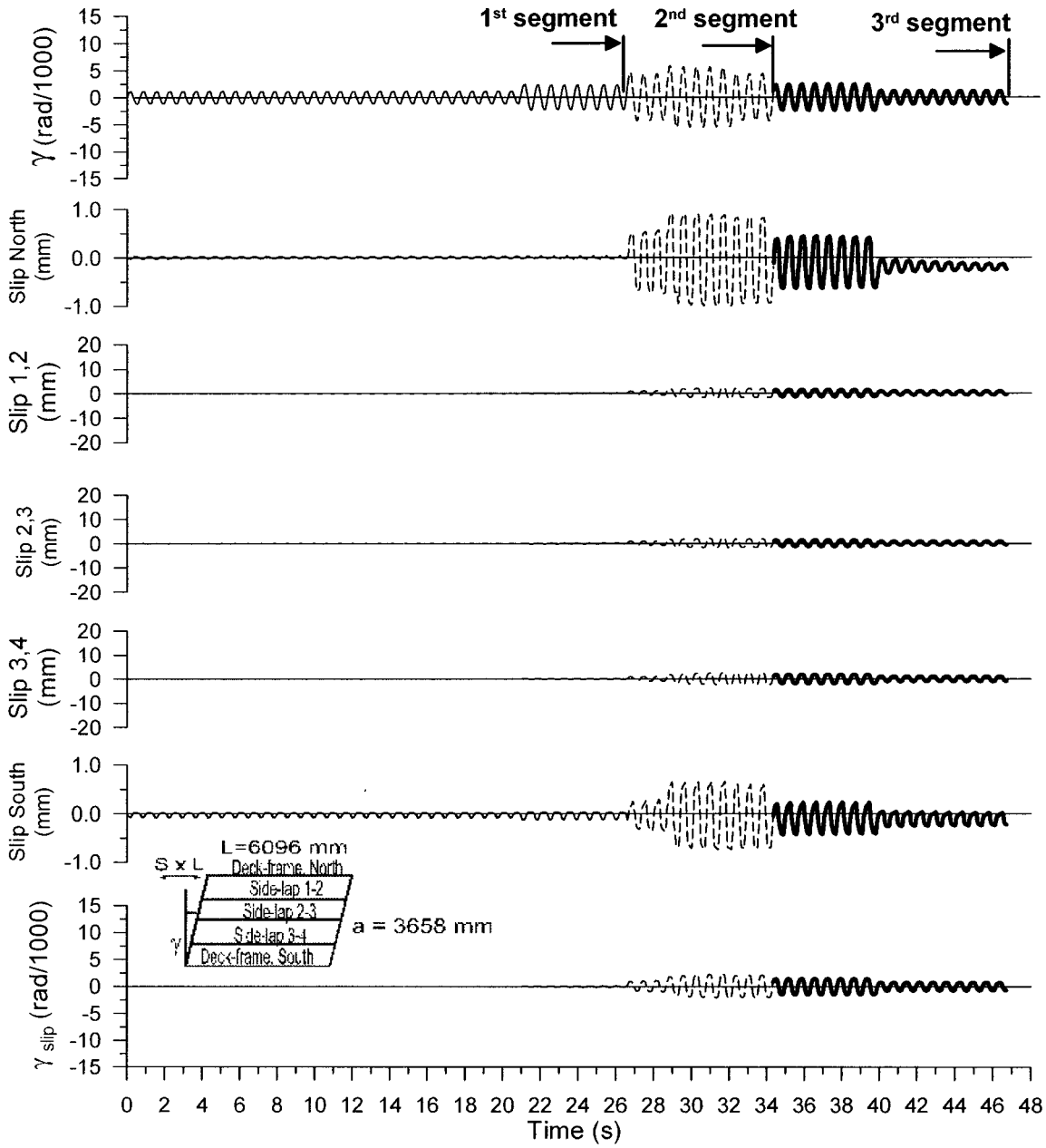

Test No. 35
P3615 B - 0.91 mm
Sidelap fasteners : Screws @ 305 Frame fasteners : Hilti nails @ 305
$S_{u,SDI}$ = *13.5 kN/m* $S_{u,LD}$ = *17.3 kN/m* $S_{u,MON}$ = *16.7 kN/m*

Figure 5.73 Test no.35 results (continued)

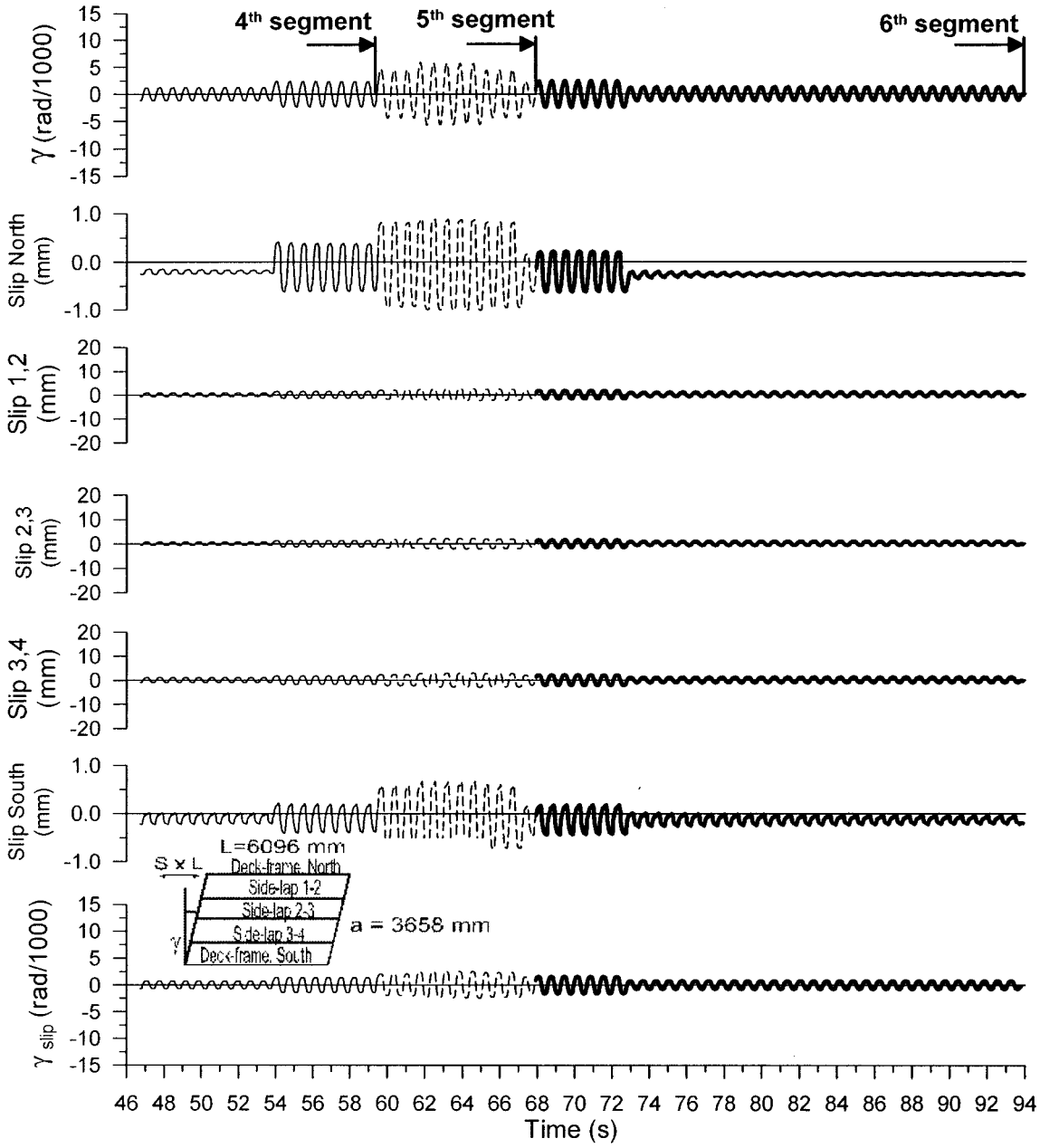

Test No. 35
P3615 B - 0.91 mm
Sidelap fasteners : Screws @ 305 Frame fasteners : Hilti nails @ 305
$S_{u,SDI}$ = *13.5 kN/m* $S_{u,LD}$ = *17.3 kN/m* $S_{u,MON}$ = *16.7 kN/m*

Figure 5.73 Test no.35 results (continued)

Table 5.33 Observed damage (Test 35)

	1	2	3	4	5	6	7	8	9	10	11	12	13	14	15	16	17	18	19	20	21
A																					
B																					
C	SB					SB										SB					
D	B1					SB					SB					SB					B1
E																					SB
F	SB					SB					SB										SB
G	B1					SB															B1
H						SB															SB
I	SB					SB										SB					SB
J	B1					SB					SB					SB					SB
K						SB										SB					SB
L																					SB
M																					

Nomenclature of failure modes (screw-nail pattern)

Nailed deck-to-frame connections

SN: Shear failure in the nail

SB: Slight buckling around nail

BFS: Bearing failure (slot) without buckling

BFL: Bearing failure perpendicular to the flute (may extend into the web)

SU: Sheet uplifted around nail with possible bearing deformation

TT: Tearing of top sheet at nail

Two failure modes are combined in TT: a) tearing due to bearing near edge b) bearing failure with slot that reach the sheet edge

B1: Buckling on one side of nail with possible bearing deformation

B2: Buckling on two sides of nail with possible bearing deformation

BF: Bearing failure (with or without buckling). (SB, BFS, TT, B1 or B2 not identified)

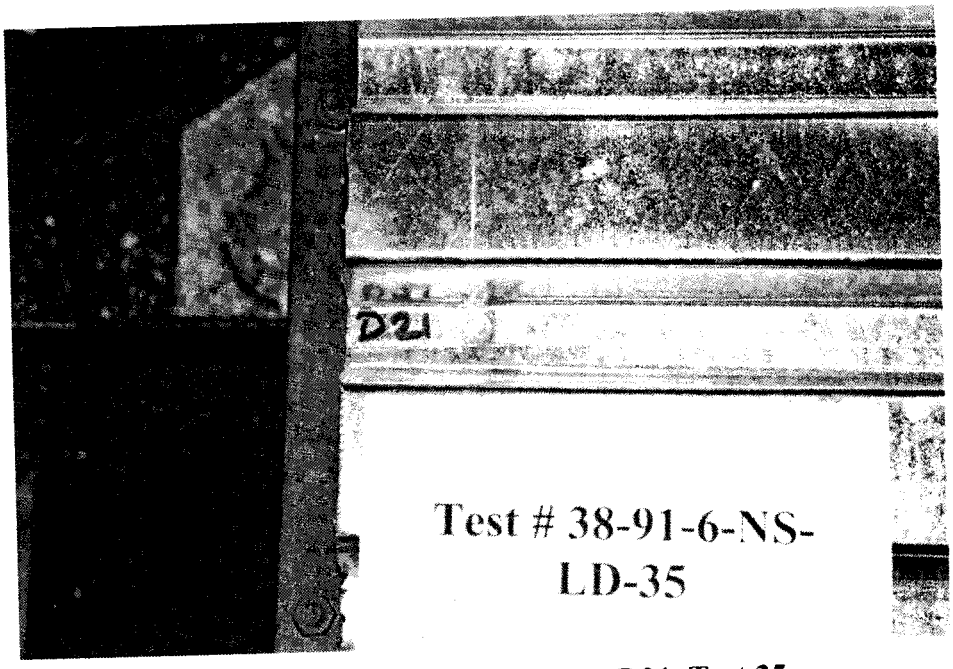

Figure 5.74 B1 failure mode at D21, Test 35

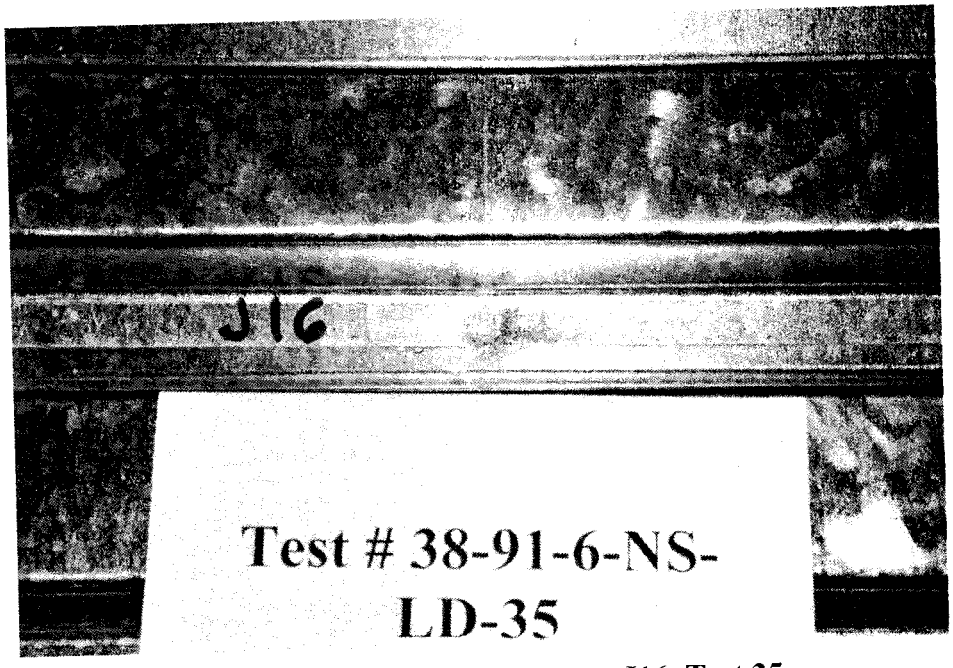

Figure 5.75 SB failure mode at J16, Test 35

5.8.4.2 Tests 28 and 29

In tests 28 and 29, 0.76 mm thick B-deck panels were used with screwed sidelaps and Hilti frame nails. Tests 4 (monotonic) and 7 (quasi-static) from Essa *et al.* (2001) were constructed with the same characteristics. Table 5.34 presents the description of specimens 28 and 29. Test result curves are shown in Figure 5.76 and Figure 5.81. The observed damage is given in Table 5.35 and Table 5.36.

Test 28

The behaviour of specimen 28 (0.76 mm) was very similar to that of specimen 34 (0.91 mm), as can be observed by comparing shear distortion curves and sidelap slip curves obtained in both tests. Again, strength and stiffness deterioration may be explained by the sidelap slip behaviour. The deck specimen remained elastic under the East $R_d = 3.0$ loading protocol. Under the West $R_d = 2.0$ segment, sidelap slip started while pinching appeared in the system. In the West $R_d = 3.0$ segment, large pinching was observed as the sidelap slips reached their maximum values (approximately 9 mm). No large deformation happened at the North and South edges (1.5 mm maximum).

At sidelaps, there was a gap between the screw head and top sheet and an additional gap between the two deck sheets (Figure 5.77). The screw uplift average value was equal to 12.0 mm. The screw uplift is defined as the distance from the top of screw to the top of bottom sheet.

The following failure modes were observed. Buckling on one side of the nail (B1) occurred at 7 locations, all on lines 1 and 21 (Figure 5.78). At purlin sidelap junctions, buckling on two sides of the nail (B2) was observed at 7 of 9 locations (see Figure 5.79). At the other purlin sidelap junctions (2 locations), the TT failure mode was found. This

failure mode was not observed in test 34, yet the loading references used were similar. This may be attributed to the thinner sheet steel used in test 28. Another failure mode, where sheet steel buckles around the nail (SB) take place, was observed at each purlin, 20 locations in total (see Figure 5.80).

Test 29

Under the long duration (LD) loading protocols, test 29 (0.76 mm thickness) and 35 (0.91 mm thickness) behaved in the same fashion. The strength and sidelap slip time histories and observed damage were similar (Figure 5.81 and Figure 5.73). In test 29, the maximum recorded load was 13.6 kN/m which is close to what was measured in test 28, 14.1 kN/m. No shear failure occurred in nails. Most of the stiffness deterioration happened during the 1st half of the loading protocol when the specimen was subjected to its first set of peaks at $2\gamma_u$.

Sidelap slip time histories were similar. The maximum measured slip was small (about 4 mm). Deformations below 1 mm were measured along the North and South edges. Distortion due to sidelap slips remained small in comparison with the total distortion. This suggests that the 3 sheets acted more or less as one piece. The level of displacement required to break the sheet interdependency was not attained.

Observed damage tended to reflect the low level of displacement in the specimen. Failure modes from test 35 were observed in test 29. Screws were uplifted, but these uplifts were kept smaller (8.3 mm) compared to test 28 (12.0 mm). Buckling on one side of nail (B1) was seen at all sidelap edges (6 locations in total) (Figure 5.82). In addition, thirteen fasteners fell under the BF category.

In tests 28 and 29, the maximum recorded loads (14.1 and 13.6 kN/m) were greater than the load measured in test 4, 12.3 kN/m, and test 7, 12.2 kN/m from Essa *et al.* (2001). Steel deck used in tests 28 and 29 had t = 0.70 mm, F_y = 248 MPa, and F_u = 327 MPa whereas Essa's *et al.* steel deck (tests 4 and 7) was stronger: t = 0.75 mm, F_y = 321 MPa, and F_u = 366 MPa. The differences in recorded loads are not explained, however the material properties were not deemed the cause.

Table 5.34 Test specimen description (Tests 28 and 29)

Steel properties:	
Supplier and coil number	Canam P-3615 B deck 0.76 mm Coil supplier: Stelco Coil number: 658104
Base metal thickness (mm)	0.70
Fy test (MPa)	248
Fu test (MPa)	327
E (MPa)	204000
50 mm gauge % elongation	32 %
Fasteners:	
Sidelap fasteners	Screw 12- 14 x 1 HWH#1 FP Lot number: 9901-0019 Spacing: 305 mm c/c
Deck-to-frame fasteners	Hilti nail X-EDNK-22 THQ 12M Lot number: 413923 Spacing: 305 mm c/c
Comments on quality of fasteners:	
Test 28	Nail stand-off: Total Ave.: 5.6 mm C.o.V.: 0.16 At sidelaps Ave.: 5.9 mm C.o.V.: 0.15 Other than sidelaps Ave.: 5.5 mm C.o.V.: 0.16 2 nails (G1 and K21) were not properly installed at first and were replaced.
Test 29	Nail stand-off: Total Ave.: 6.3 mm C.o.V.: 0.16 At sidelaps Ave.: 6.4 mm C.o.V.: 0.07 Other than sidelaps Ave.: 6.3 mm C.o.V.: 0.17 The nail at A21 was not properly installed at first and was replaced

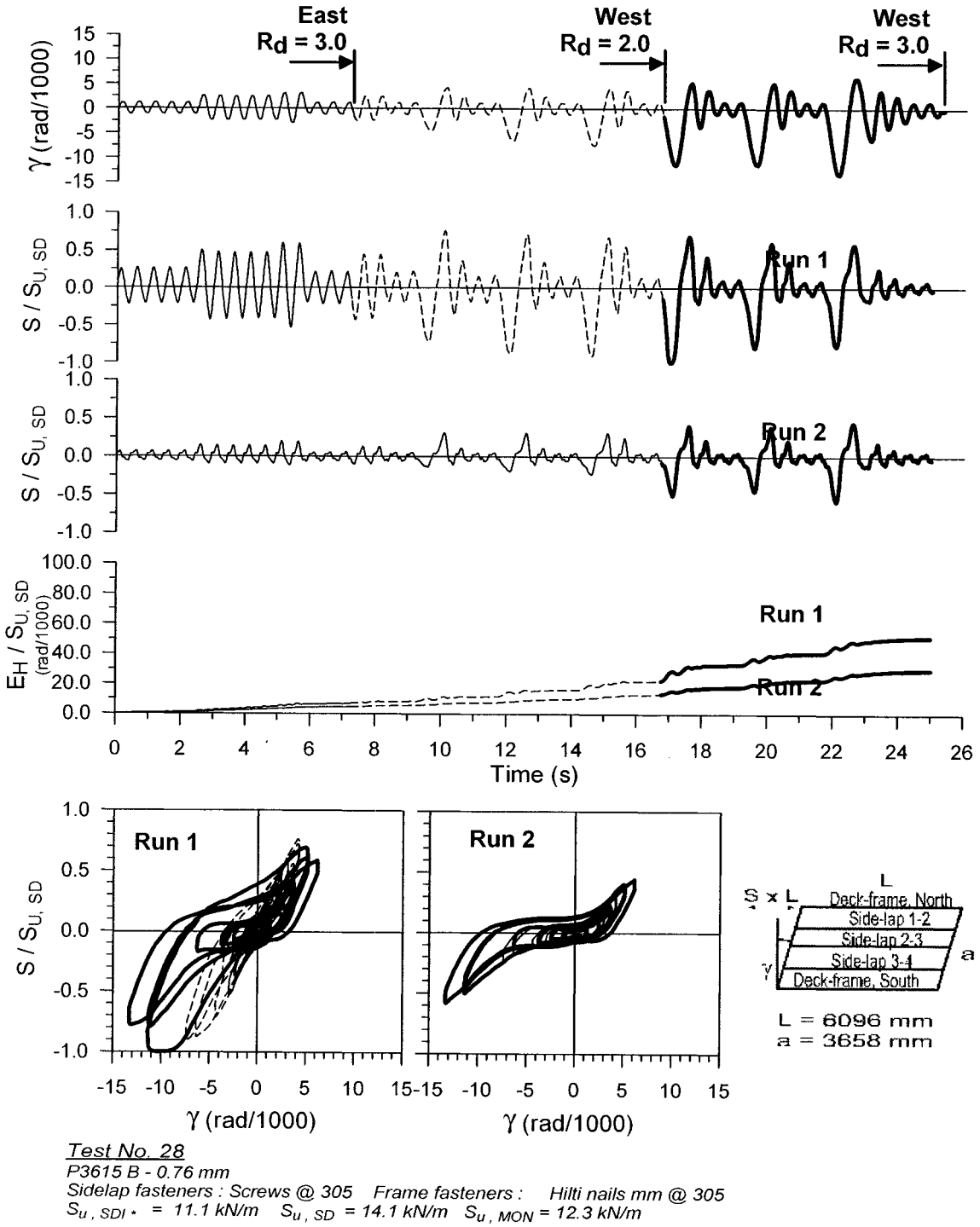

Test No. 28
P3615 B - 0.76 mm
Sidelap fasteners : Screws @ 305 Frame fasteners : Hilti nails mm @ 305
$S_{u,SDI*}$ = 11.1 kN/m $S_{u,SD}$ = 14.1 kN/m $S_{u,MON}$ = 12.3 kN/m

Figure 5.76 Test no.28 results

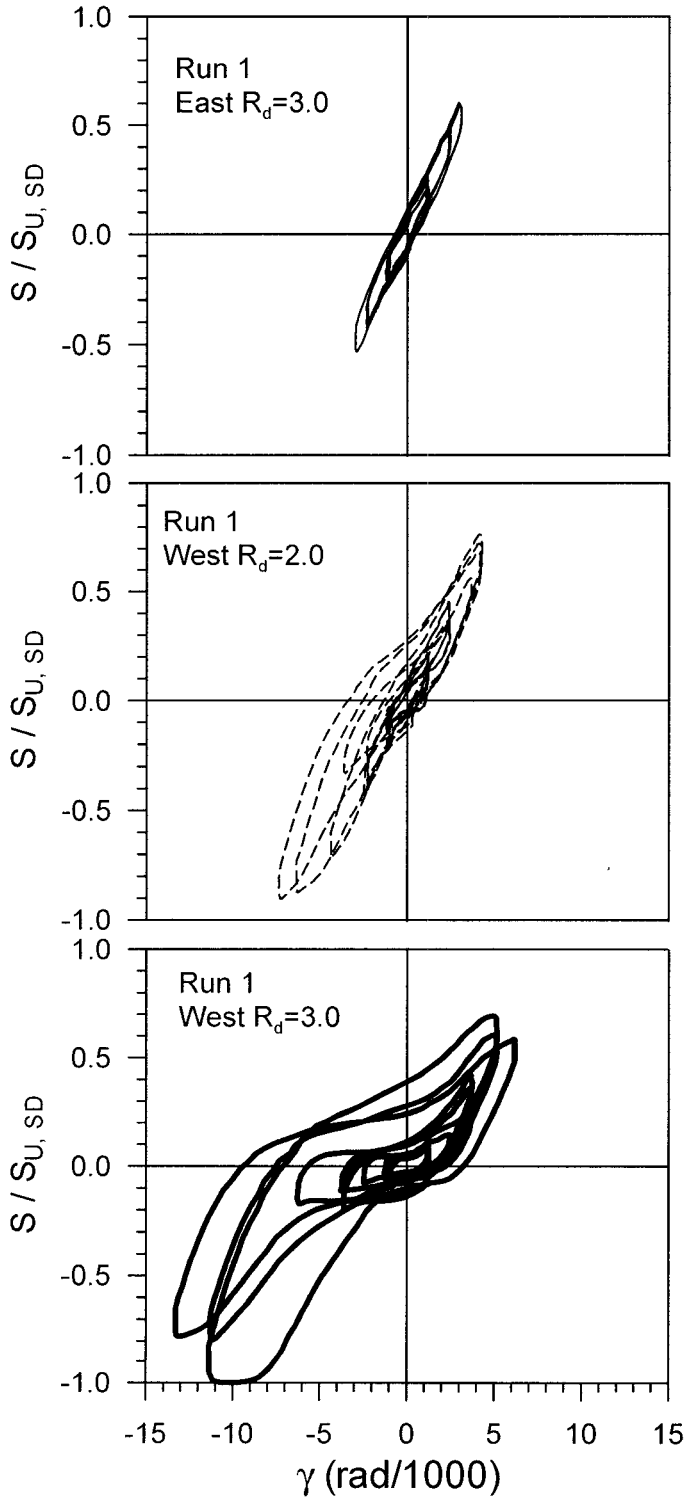

Test No. 28

P3615 B - 0.76 mm
Sidelap fasteners :
Screws @ 305
Frame fasteners :
Hilti nails @ 305

$S_{u, SDI*}$ = 11.1 kN/m
$S_{u, SD}$ = 14.1 kN/m
$S_{u, MON}$ = 12.3 kN/m

Figure 5.76 Test no.28 results (continued)

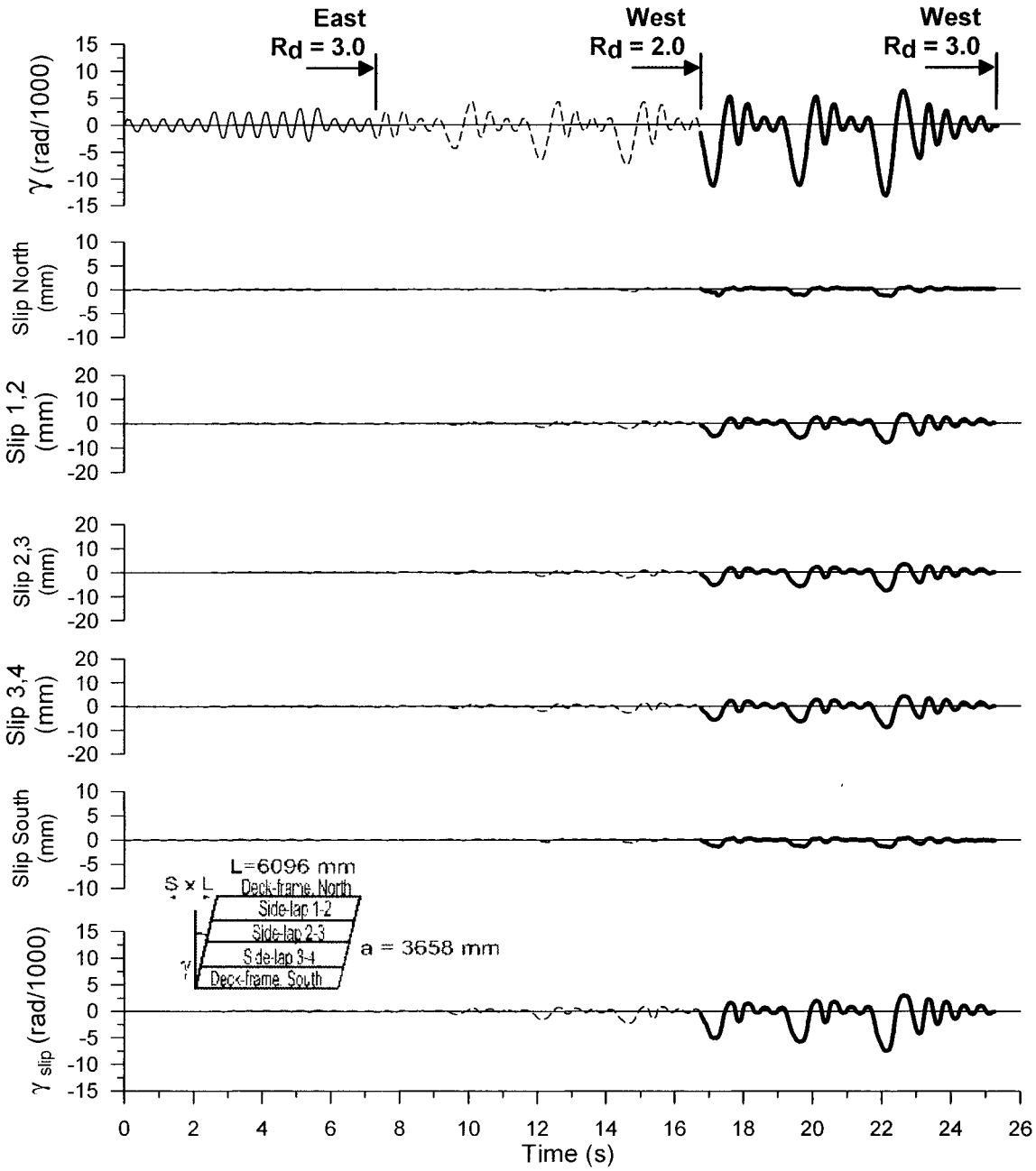

Test No. 28- Run 1
P3615 B - 0.76 mm
Sidelap fasteners : Screws @ 305 Frame fasteners : Hilti nails mm @ 305
$S_{u,SDI}$ = 11.1 kN/m $S_{u,SD}$ = 14.1 kN/m $S_{u,MON}$ = 12.3 kN/m

Figure 5.76 Test no.28 results (continued)

Table 5.35 Observed damage after 1st run (Test 28)

	1	2	3	4	5	6	7	8	9	10	11	12	13	14	15	16	17	18	19	20	21
A																					
B																					
C						SB					SB					SB					SB
D	B1					B2					B2					B2					B1
E						SB										SB					B1
F						SB					SB					SB					SB
G	B1					B2					B2					B2					B1
H						SB					SB					SB					
I											SB					SB					
J	B1					B2					TT					TT					B1
K	SB					SB										SB					SB
L																SB					
M																					

Nomenclature of failure modes (screw-nail pattern)

Nailed deck-to-frame connections

SN: Shear failure in the nail

SB: Slight buckling around nail

BFS: Bearing failure (slot) without buckling

BFL: Bearing failure perpendicular to the flute (may extend into the web)

SU: Sheet uplifted around nail with possible bearing deformation

TT: Tearing of top sheet at nail

Two failure modes are combined in TT: a) tearing due to bearing near edge b) bearing failure with slot that reach the sheet edge

B1: Buckling on one side of nail with possible bearing deformation

B2: Buckling on two sides of nail with possible bearing deformation

BF: Bearing failure (with or without buckling). (SB, BFS, TT, B1 or B2 not identified)

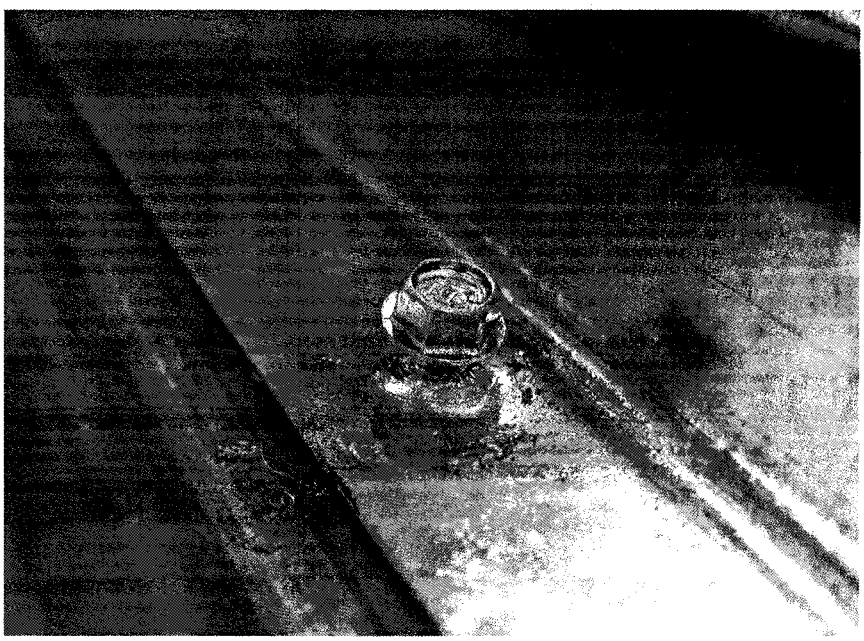

Figure 5.77 Sidelap screw uplifted, Test 28

Figure 5.78 B1 failure mode at G21, Test 28

Figure 5.79 B2 failure mode at J6, Test 28

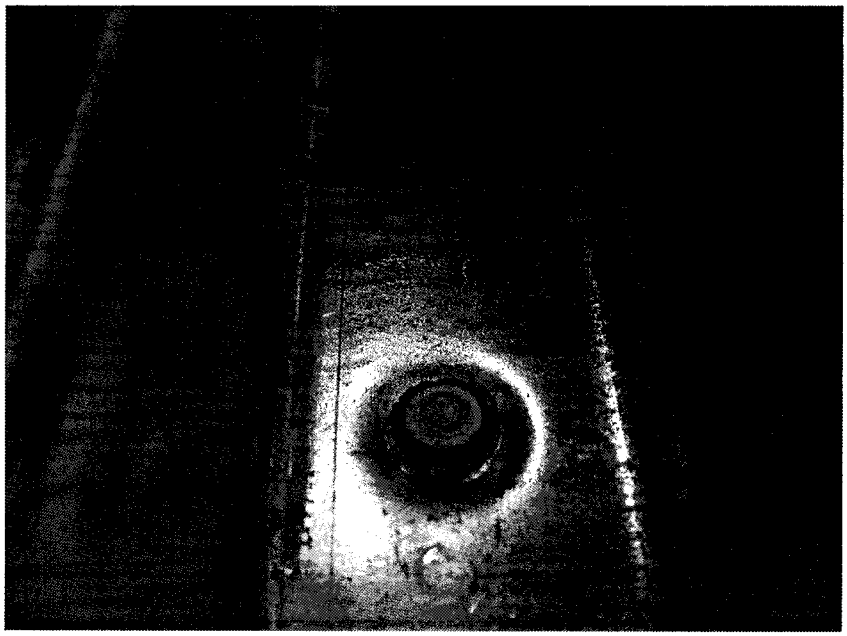

Figure 5.80 SB failure mode at I11, Test 28

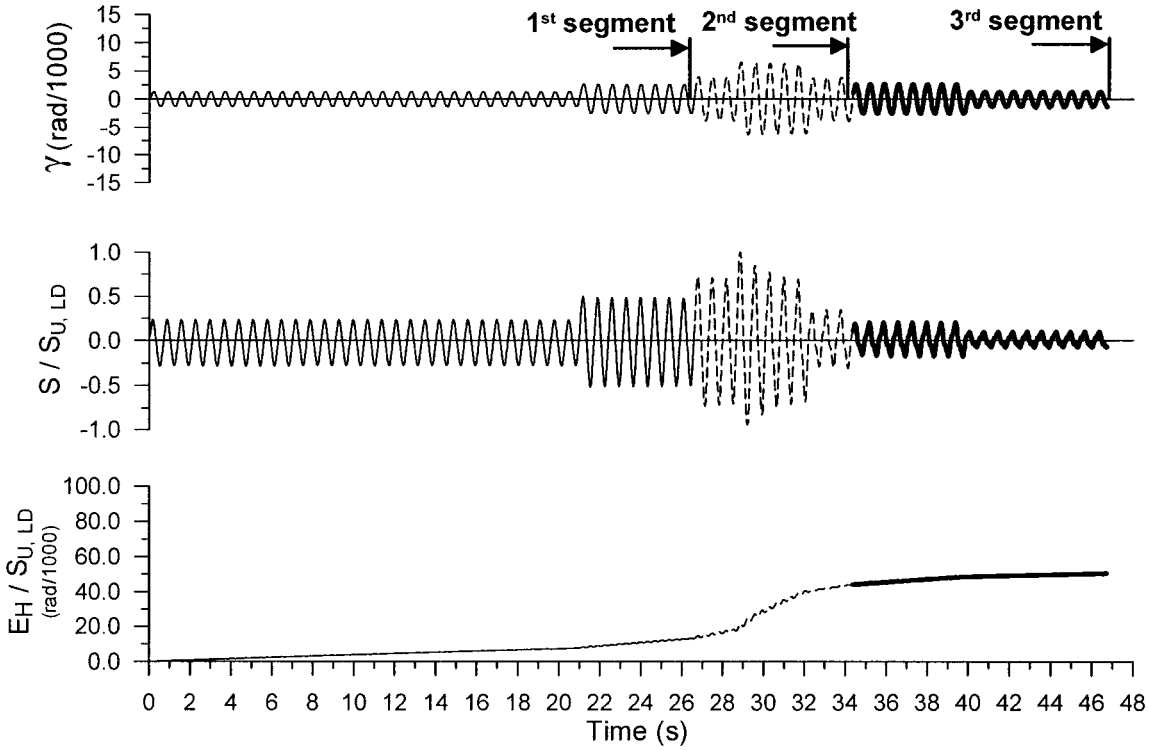

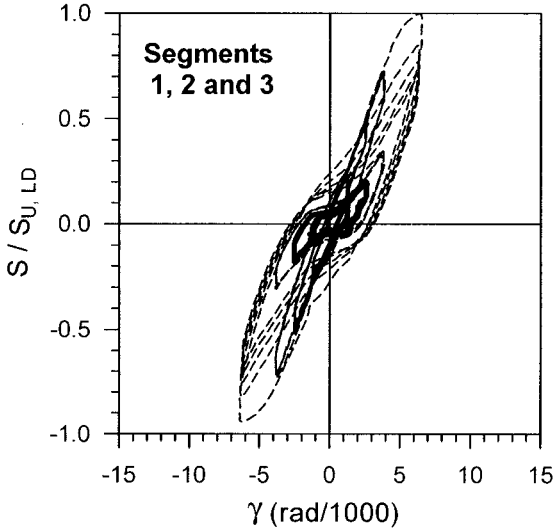

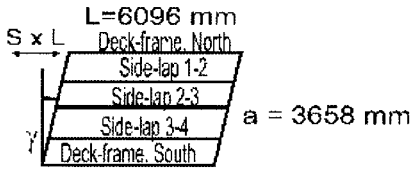

Test No. 29
P3615 B - 0.76 mm
Sidelap fasteners : Screws @ 305 Frame fasteners : Hilti nails @ 305
$S_{u,SDI*}$ = 11.1 kN/m $S_{u,LD}$ = 13.6 kN/m $S_{u,MON}$ = 12.3 kN/m

Figure 5.81 Test no.29 results

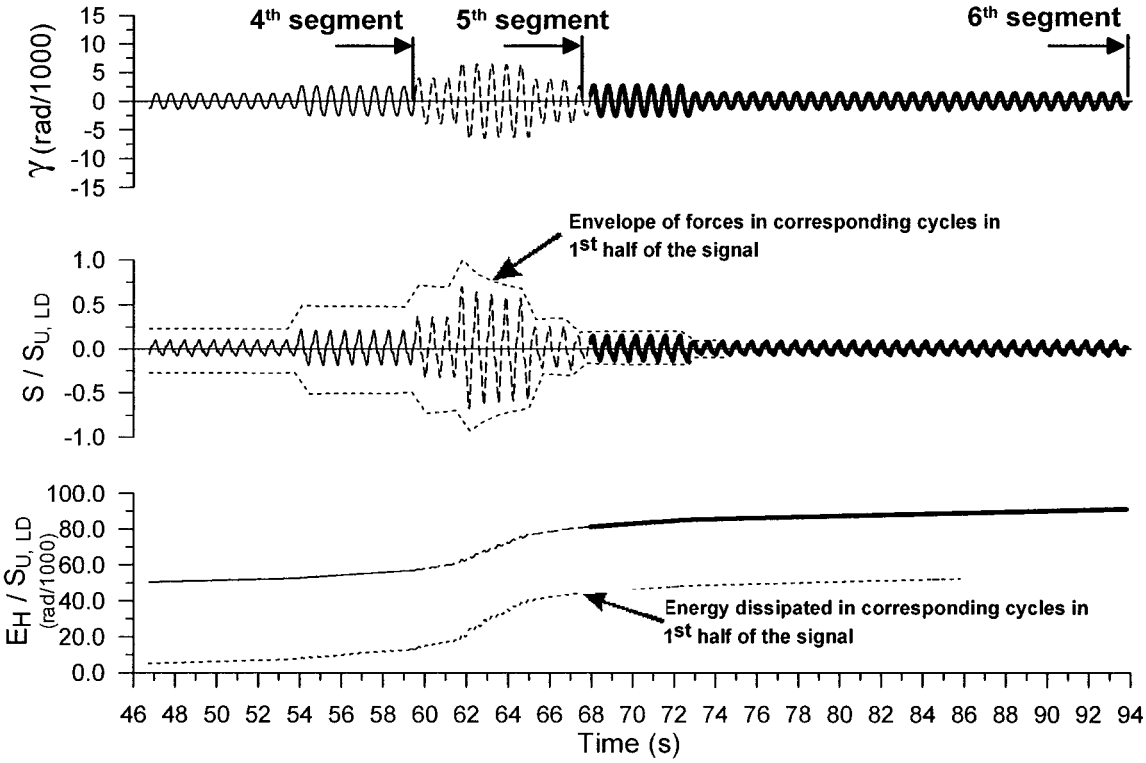

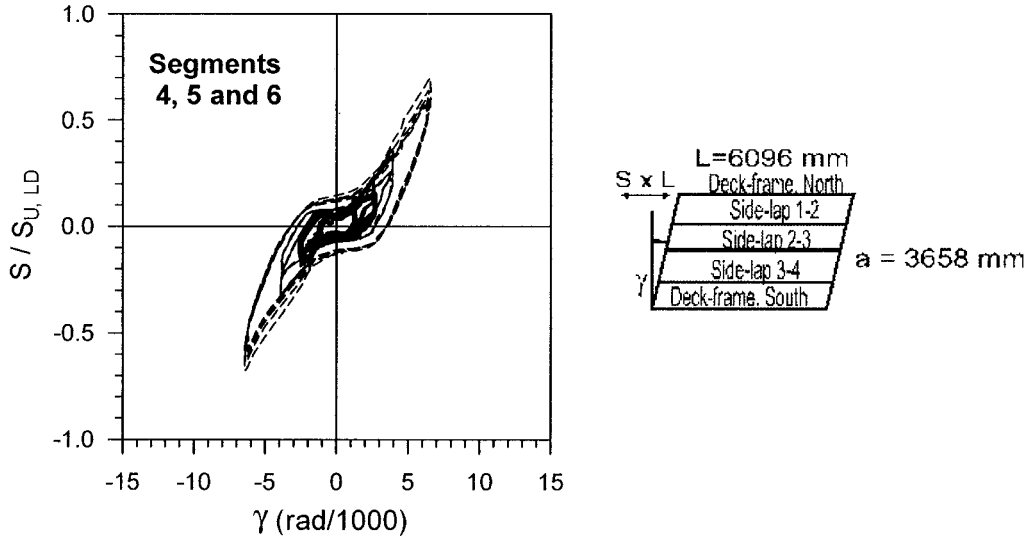

Test No. 29
P3615 B - 0.76 mm
Sidelap fasteners : Screws @ 305 Frame fasteners : Hilti nails @ 305
$S_{u,SDI*}$ = 11.1 kN/m $S_{u,LD}$ = 13.6 kN/m $S_{u,MON}$ = 12.3 kN/m

Figure 5.81 Test no.29 results (continued)

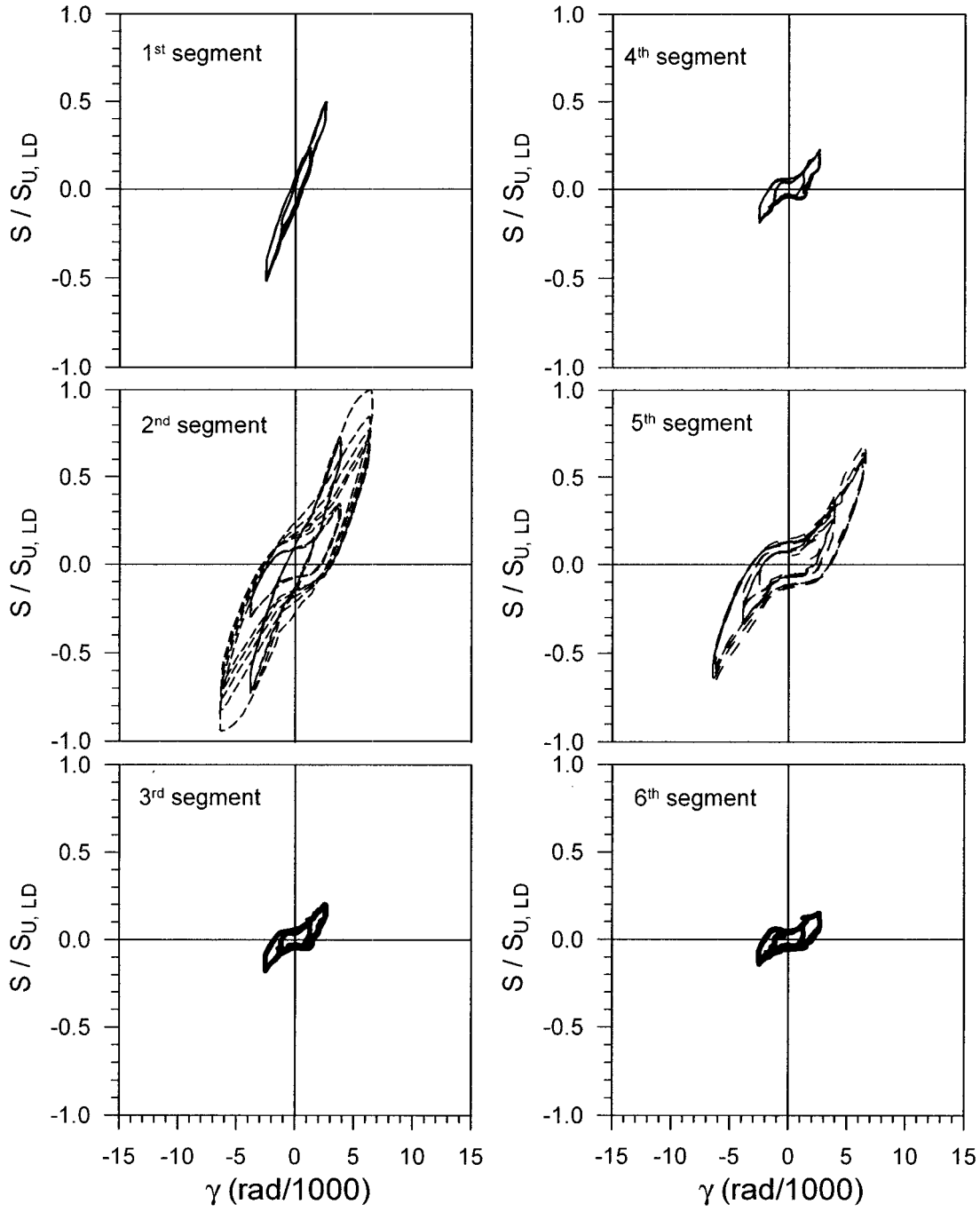

Test No. 29
P3615 B - 0.76 mm
Sidelap fasteners : Screws @ 305 Frame fasteners : Hilti nails @ 305
$S_{u,SDI*}$ = 11.1 kN/m $S_{u,LD}$ = 13.6 kN/m $S_{u,MON}$ = 12.3 kN/m

Figure 5.81 Test no.29 results (continued)

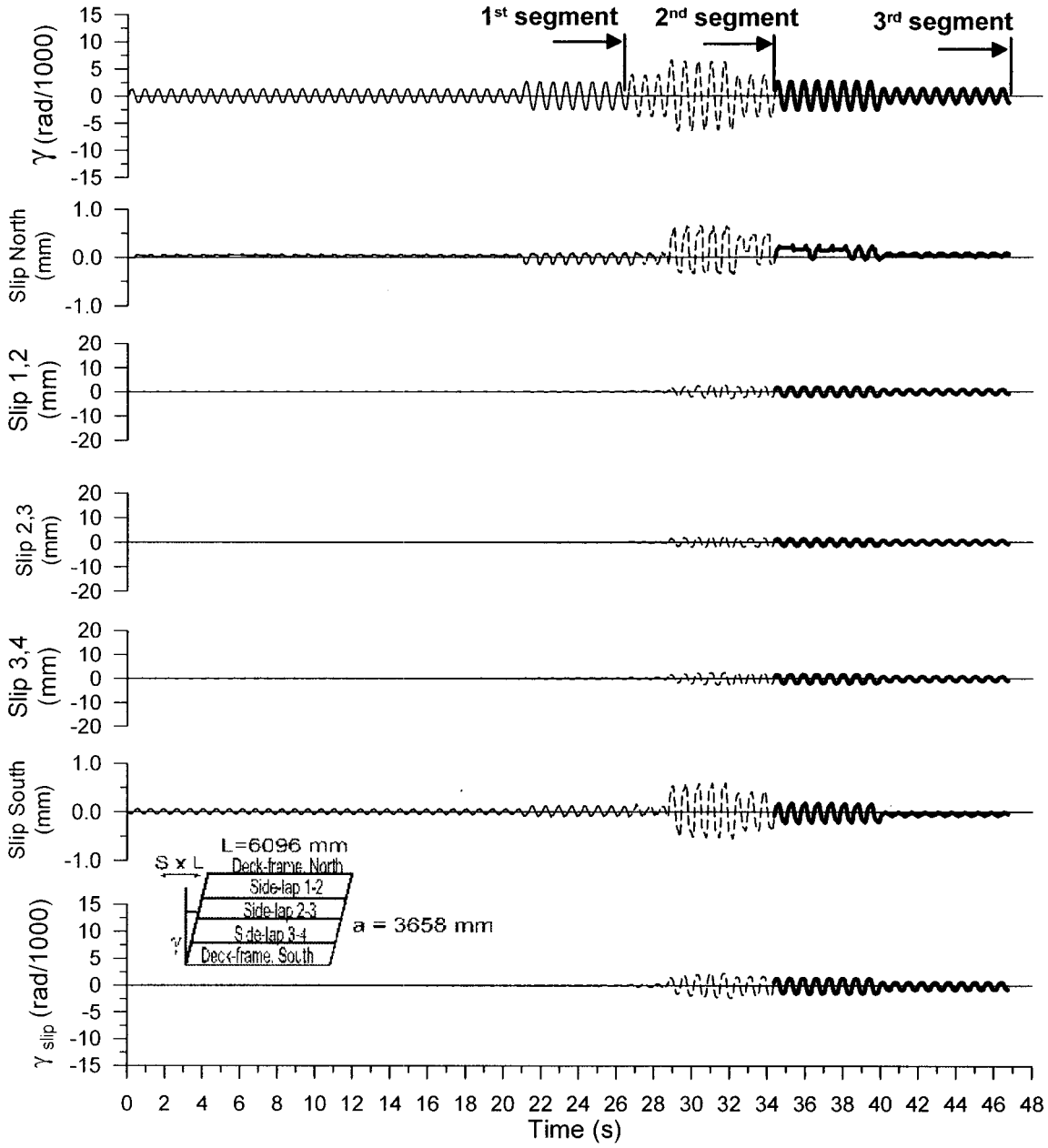

Test No. 29
P3615 B - 0.76 mm
Sidelap fasteners : Screws @ 305 Frame fasteners : Hilti nails @ 305
$S_{u,SDI}$ = *11.1 kN/m* $S_{u,LD}$ = *13.6 kN/m* $S_{u,MON}$ = *12.3 kN/m*

Figure 5.81 Test no.29 results (continued)

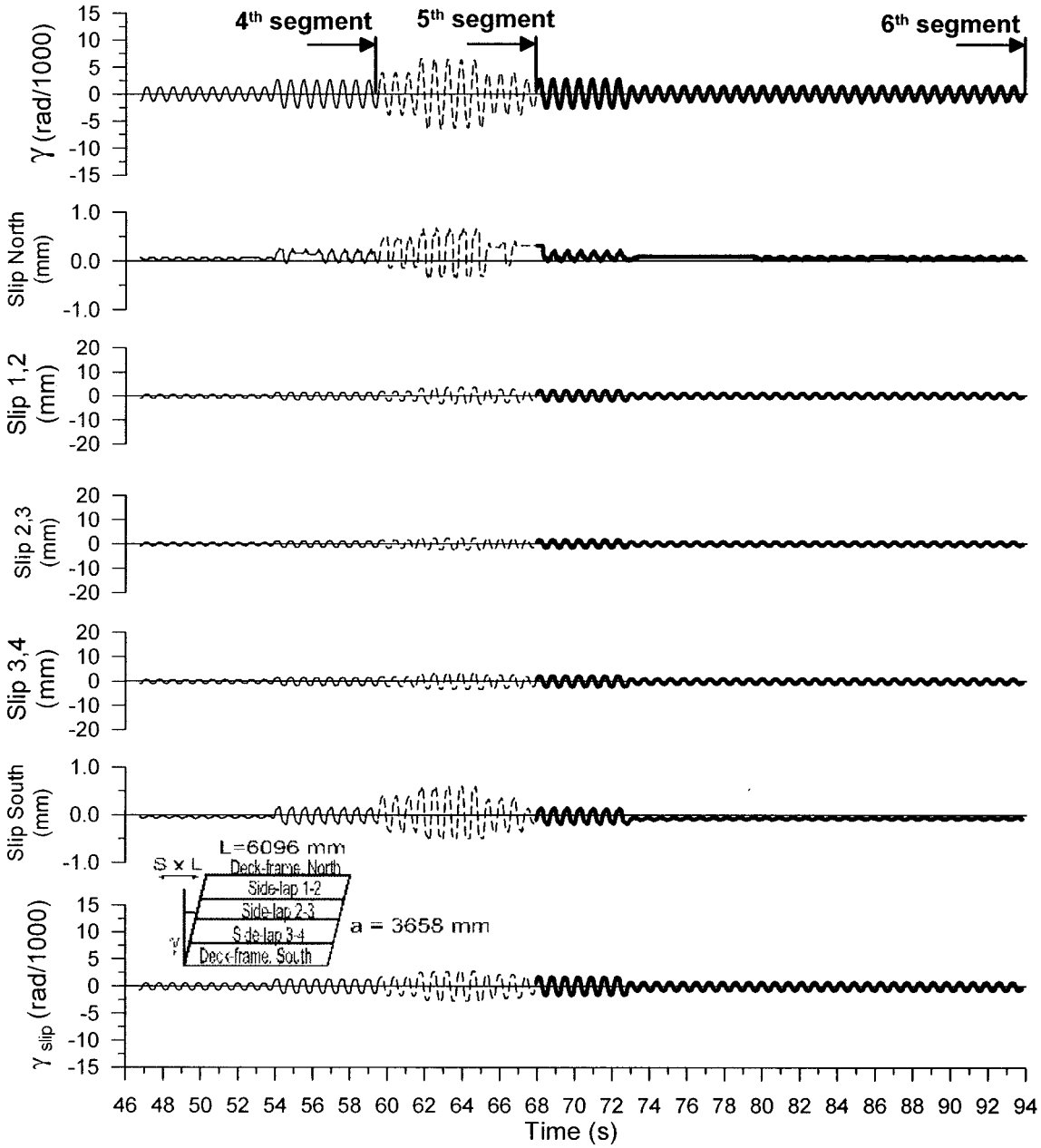

Test No. 29
P3615 B - 0.76 mm
Sidelap fasteners : Screwed @ 305 Frame fasteners : Hilti nails @ 305
$S_{u,SDI}$ = *11.1 kN/m* $S_{u,LD}$ = *13.6 kN/m* $S_{u,MON}$ = *12.3 kN/m*

Figure 5.81 Test no.29 results (continued)

	1	2	3	4	5	6	7	8	9	10	11	12	13	14	15	16	17	18	19	20	21
A																					
B																					
C						BF										BF					
D	B1					BF					BF					BF					B1
E						BF															
F						BF															
G	B1					BF					BF					SB					B1
H																					
I																					
J	B1					B2					BF					B2					B1
K						BF					BF					BF					
L																					
M																					

Table 5.36 Observed damage (Test 29)

Nomenclature of failure modes (screw-nail pattern)

Nailed deck-to-frame connections

SN: Shear failure in the nail
SB: Slight buckling around nail
BFS: Bearing failure (slot) without buckling
BFL: Bearing failure perpendicular to the flute (may extend into the web)
SU: Sheet uplifted around nail with possible bearing deformation
TT: Tearing of top sheet at nail
Two failure modes are combined in TT: a) tearing due to bearing near edge b) bearing failure with slot that reach the sheet edge
B1: Buckling on one side of nail with possible bearing deformation
B2: Buckling on two sides of nail with possible bearing deformation
BF: Bearing failure (with or without buckling). (SB, BFS, TT, B1 or B2 not identified)

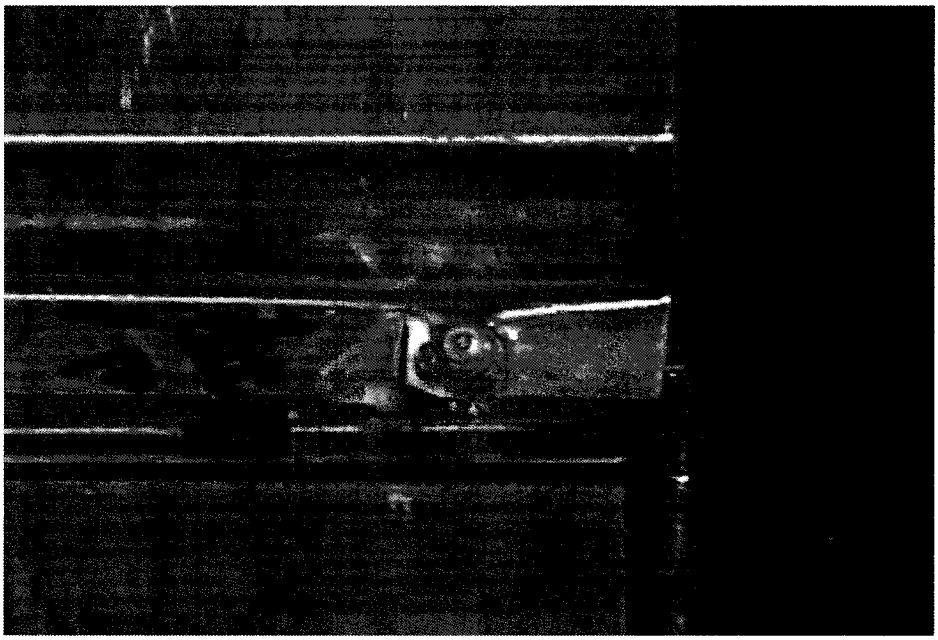

Figure 5.82 B1 failure mode at J1, Test 29

5.8.4.3 Tests 32 and 33

Unlike the tests presented above, the deck-to-frame and sidelap fasteners were spaced at 152 mm c/c in tests 32 (monotonic) and 33 (short duration loading protocol). B-deck profile sheets (0.91 mm thick) with screwed sidelap and nailed deck-to-frame connections were used. Table 5.37 presents the description of test specimens for tests 32 and 33. Figure 5.83 and Figure 5.87 present the test result curves for tests 32 and 33, and Table 5.38 and Table 5.39 the observed damage.

Test 32

In Figure 5.83, the normalised shear–distortion curve from test 19 was added to the curve from test 32 for comparison. Test 19 possessed the same characteristics as test 32 except that fasteners were spaced at 305 mm c/c instead of 152 mm c/c.

The maximum measured load in test 32 was equal to 34.4 kN/m at a corresponding displacement of 7 rad/1000. A 2 rad/1000 long plateau was observed. At 11 rad/1000, the specimen strength went below 80% of its maximum load. Roughly, the shear strength in test 32 was about 2 times the strength in test 19 whereas the stiffness was 4 times higher.

As in other tests with the screw-nail connection pattern, the strength and stiffness variation may be attributed to the sidelap slips. The shape of the shear-distortion curve was similar to that from test 19 with the 3 main differences explained below.

First, in the loading part, the load-deformation response of test 32 is characterised by two straight line segments as opposed to only one in test 19. In test 32, the stiffness changed abruptly around 1 rad/1000 ($\cong 0.5\ S_u$) when slips at interior sidelaps started. Although sidelap slips were not measured in test 19, it is possible that slips at interior sidelaps started earlier in test 32 because that diaphragm was more rigid due to the larger number of deck-to-frame connections preventing the warping. In consequence, the deformations likely tended to develop earlier in the more flexible sidelap joints. This explains why the slope changed at $0.5\ S_u$ in test 32 whereas the behaviour of test 19 was linear up to $0.7\ S_u$.

Second, when the strength drop occurred after the yielding plateau, it happened at a much faster rate than in test 32. This was explained by the connection properties and their relative proportion at sidelaps. The sidelaps in test 32 included 36 screws and 5 nailed deck-to-frame connections compared to 16 screws and, again, 5 nailed deck-to-frame connections in test 19. The behaviour in test 32 was influenced by the greater number of screws. From Rogers and Tremblay (2000), it is known that the screw connection typically exhibits a quick strength degradation once the peak shear value is reached, whereas the nailed connection develops a yielding plateau. For the deck

specimen, after the peak load, the sidelap screws were tilted and their strengths diminished whereas the nails kept almost the same load capacities. It was assumed that because of the screw tilting at peak load, the system could not develop a larger resistance and the load started to decrease with an increase in distortion. Regardless of the sidelap spacing pattern, there are only 5 deck-to-frame connections, and hence the strength degradation is more extensive when the relative proportion of screws is higher. Due to the number of connections and their relative importance in the specimen, test 32 could develop a larger force when all screws develop their maximum strengths. However, once the ability of the screws to carry shear load started to diminish, the overall capacity of the specimen degraded at a faster rate.

Third, if total shear distortion is compared, test 32 showed a faster strength degradation. In test 32, the strength went below $0.8S_u$ at 11 rad/1000 whereas in test 19 it happened at 15 rad/1000. However, if the inelastic distortions, γ_p, are compared, the values are relatively the same: 10 rad/1000 in test 32 compared to 11 rad/1000 in test 19. Due to the higher stiffness in test 32, the sidelap slip started earlier and, hence, the screw tilting began and initiated the stiffness degradation. This can be seen in the round shape of the shear-distortion curve (Figure 5.83). However, the ability of the screws to sustain a load while tilting is not affected by the spacing of the connectors.

Sidelaps 1,2 and 3,4 experienced similar slip time histories under the applied displacements. Line 2,3 slipped less than the 2 other interior lines. This behaviour was observed in other tests. The edge connections on the North and South sides are stiffer than the intermediate sidelap connections. The exterior panels at the North and South edges were connected entirely by nails to the frame, whereas the sidelap joints were connected by a combination of nails and screws. Nailed deck-to-frame connections are stiffer compared to screwed sidelap connections, and hence the exterior panels are of a greater rigidity.

Shear failure of the fasteners did not take place. Failure modes from test 19 were observed in test 32. Screw tilting was observed, along with buckling on one side of the nailed connections (B1) and bearing failure with slot (BFS). Figure 5.84 and Figure 5.85 present B1 and BFS failure modes. Figure 5.86 shows nail J11, located at a sidelap line, where the sheet buckled on one side (B1) of the connection and an adjacent nail with the B1 failure mode.

Test 33

Test 33 was subjected to a short duration (SD) loading protocol. The maximum measured force was equal to 35.2 kN/m, which is close to the result from test 32, 34.4 kN/m. The hysteretic behaviour in test 33 was similar to the behaviour observed in previously described tests with the screw-nail connection pattern. Until the West R_d = 3.0 segment, the system had no important deterioration. However, in the last portion of the loading protocol, a large amount of pinching occurred and the system lost strength at large deformations.

In test 33, however, the hysteretic shape was closer to what is expected for a nailed connection, for which the hysteresis is more severely pinched and is thinner in the reloading part. This was attributed to the higher number of fasteners with the 152 mm c/c spacing: the warping deformation of the deck was diminished so the elastic sheet deformation effects on the hysteretic curve tended to decrease. It must be noted that the sidelaps sustained very similar slip deformations in tests 33 and 34. In the West R_d= 2.0 and West R_d= 3.0 segments of the SD loading protocol, the imposed distortion peaks are equal to γ_u plus an additional fixed inelastic distortion (γ_u + 1 rad/1000, γ_u + 3 rad/1000, γ_u + 4 rad/1000, etc.). Because the sidelap slip is directly related to the inelastic distortion, the slip deformations in both tests were therefore very close, the only one

difference being that the value of γ_u in test 33 was 10% lower than the required value (Table 5.8).

All interior sidelaps in test 33 experienced the similar slips. At test end, the screws were tilted but sidelaps were still attached. In addition, no damage was observed on lines A and M and no shear failure occurred in nails. Failure modes observed in test 32 were observed in test 33. Slight buckling around the nails was seen (see Figure 5.88). Buckling on one side of the nail (B1) occurred at all sidelap ends (Figure 5.89). The folding was attributed to the weak lip of the top sheet, which does not have sufficient size or stiffness to develop the full connection capacity.

Table 5.37 Test specimen description (Tests 32 and 33)

Steel properties:	
Supplier and coil number	Canam P-3615 B deck 0.91 mm Coil supplier: Sorevco Coil number: 147624
Base metal thickness (mm)	0.88
Fy test (MPa)	319
Fu test (MPa)	394
E (MPa)	210000
50 mm gauge % elongation	24 %
Fasteners:	
Sidelap fasteners	Screw 12- 14 x 1 HWH#1 FP Lot number: 9901-0019 Spacing: 152 mm c/c
Deck-to-frame fasteners	Hilti nail X-EDNK-22 THQ 12M Lot number: 413920 Spacing: 152 mm c/c
Comments on quality of fasteners:	
Test 32	Nail stand-off: Total Ave.: 6.4 mm C.o.V.: 0.34 At sidelaps Ave.: 7.7 mm C.o.V.: 0.40 Other than sidelaps Ave.: 6.3 mm C.o.V.: 0.34 No problem with nail installation.
Test 33	Nail stand-off: Total Ave.: 6.6 mm C.o.V.: 0.34 At sidelaps Ave.: 7.3 mm C.o.V.: 0.39 Other than sidelaps Ave.: 6.6 mm C.o.V.: 0.34 2 nails were not properly installed and were replaced (K'21 and J6).

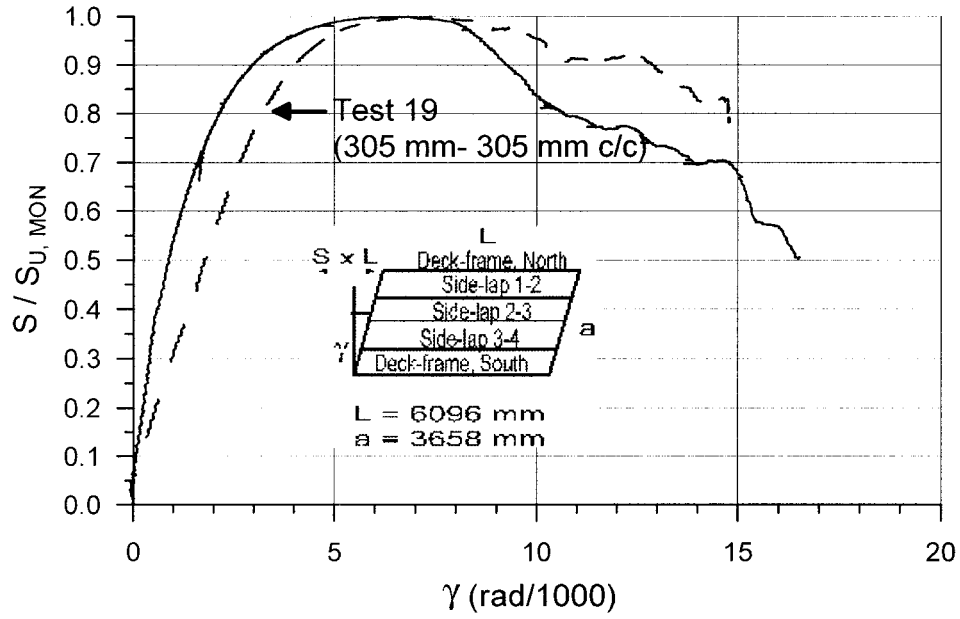

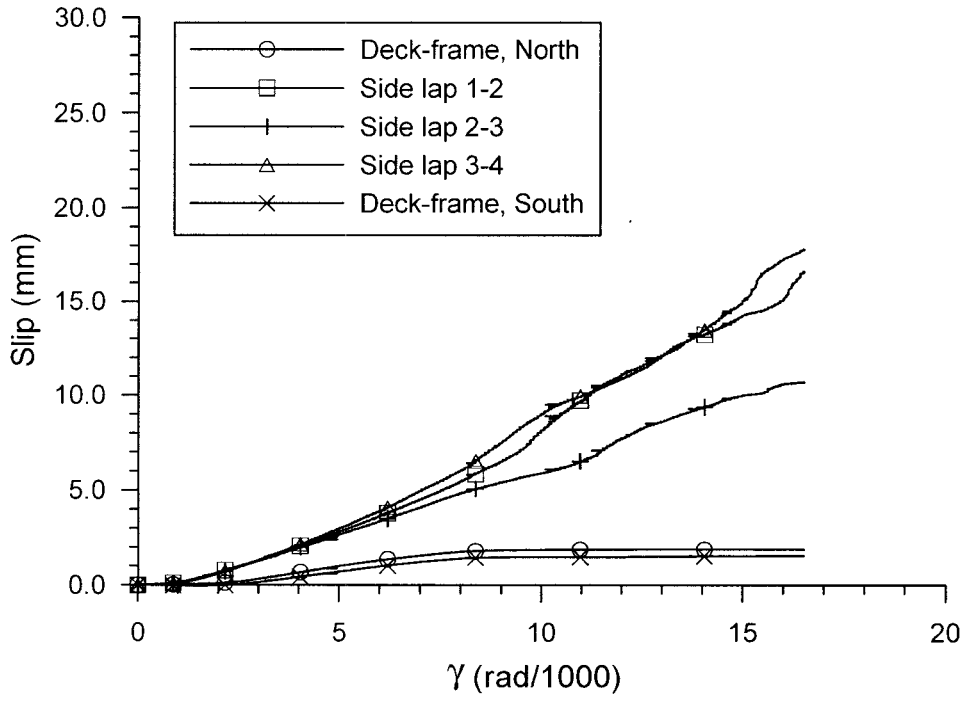

Test No. 32
P3615 B - 0.91 mm
Sidelap fasteners : Screws @ 152 Frame fasteners : Hilti nails @ 152
$S_{u,SDI}$ = 24.9 kN/m $S_{u,MON}$ = 34.4 kN/m

Figure 5.83 Test no.32 results

Table 5.38 Observed damage (Test 32)

	1	1'	2	2'	3	3'	4	4'	5	5'	6	6'	7	7'	8	8'	9	9'	10	10'	11	11'	12	12'	13	13'	14	14'	15	15'	16	16'	17	17'	18	18'	19	19'	20	20'	21
A																																								
A'																																								BF
B																																							BF
B'																																							BF
C	B1																				BF																		BFS
C'	BFS										BFS										BFS									BFS									BFS
D	B1										B1										B1									B1									B2
D'	BFS										BF										BF									BF									BFS
E	BF										BF																												BF
E'																																							
F																																							
F'																																							
G	B1										B1										B1									BFS									
G'											B1										BF									BF									
H																														BF									
H'																																							
I																																							
I'											B1																			BF									
J	B1										B1										B1									B1									BFS
J'	BFS										B1										B1									BFS									B1
K	BFS										BFS										B1									BFS									B1
K'																														B1									BF
L																																							BF
L'																																							BF
M																																							

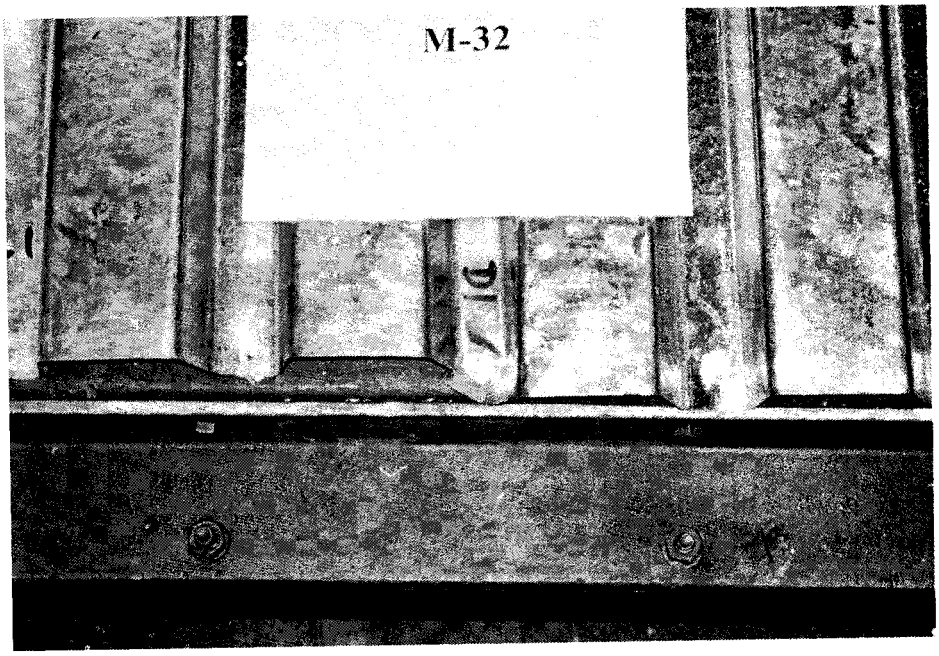

Figure 5.84 B1 failure mode at D1 and BFS at C'1 and D'1, Test 32

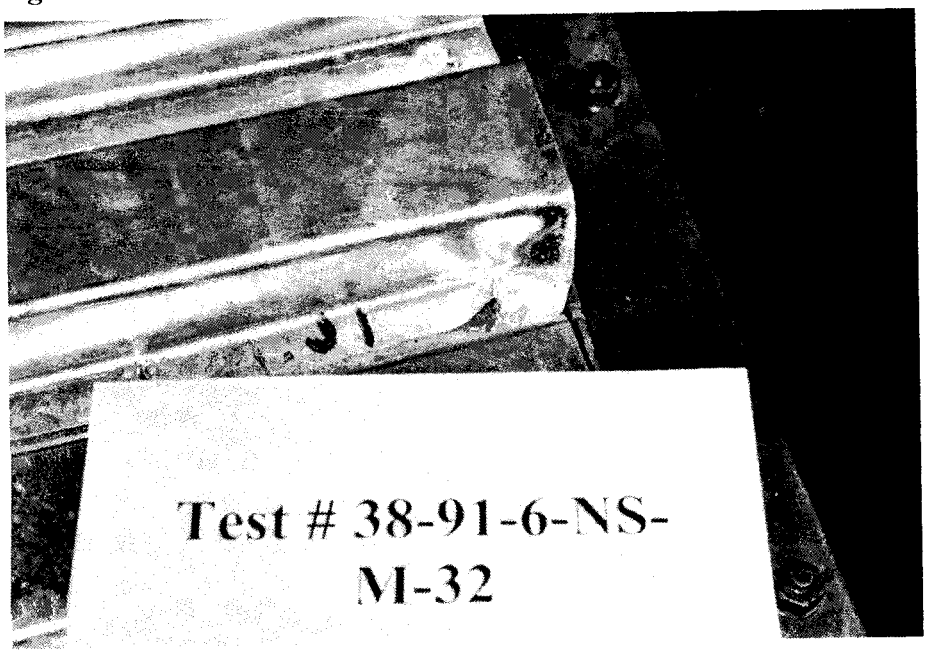

Figure 5.85 B1 failure mode at J1 and BFS at J'1, Test 32

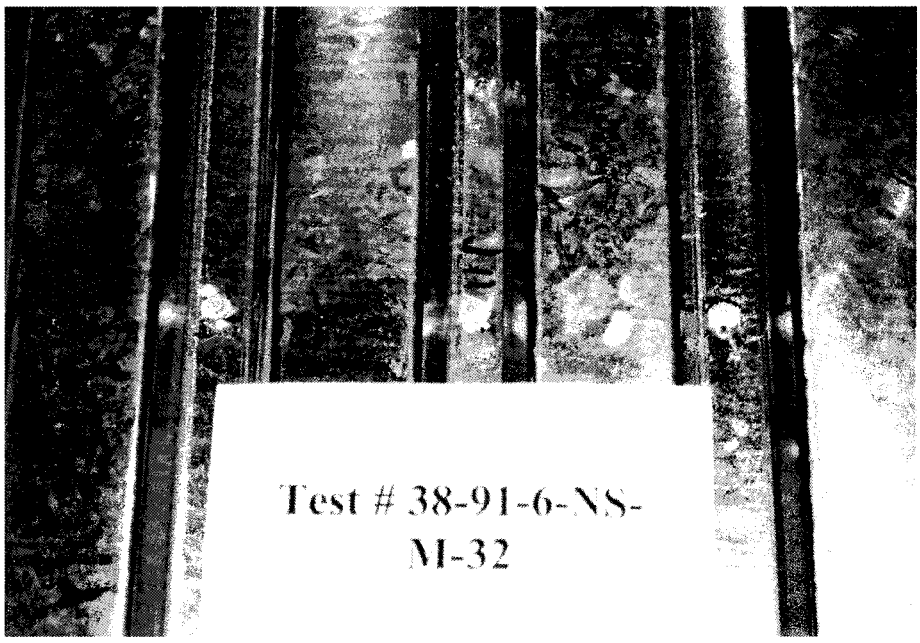

Figure 5.86 B1 failure mode at J11 and J'11, Test 32

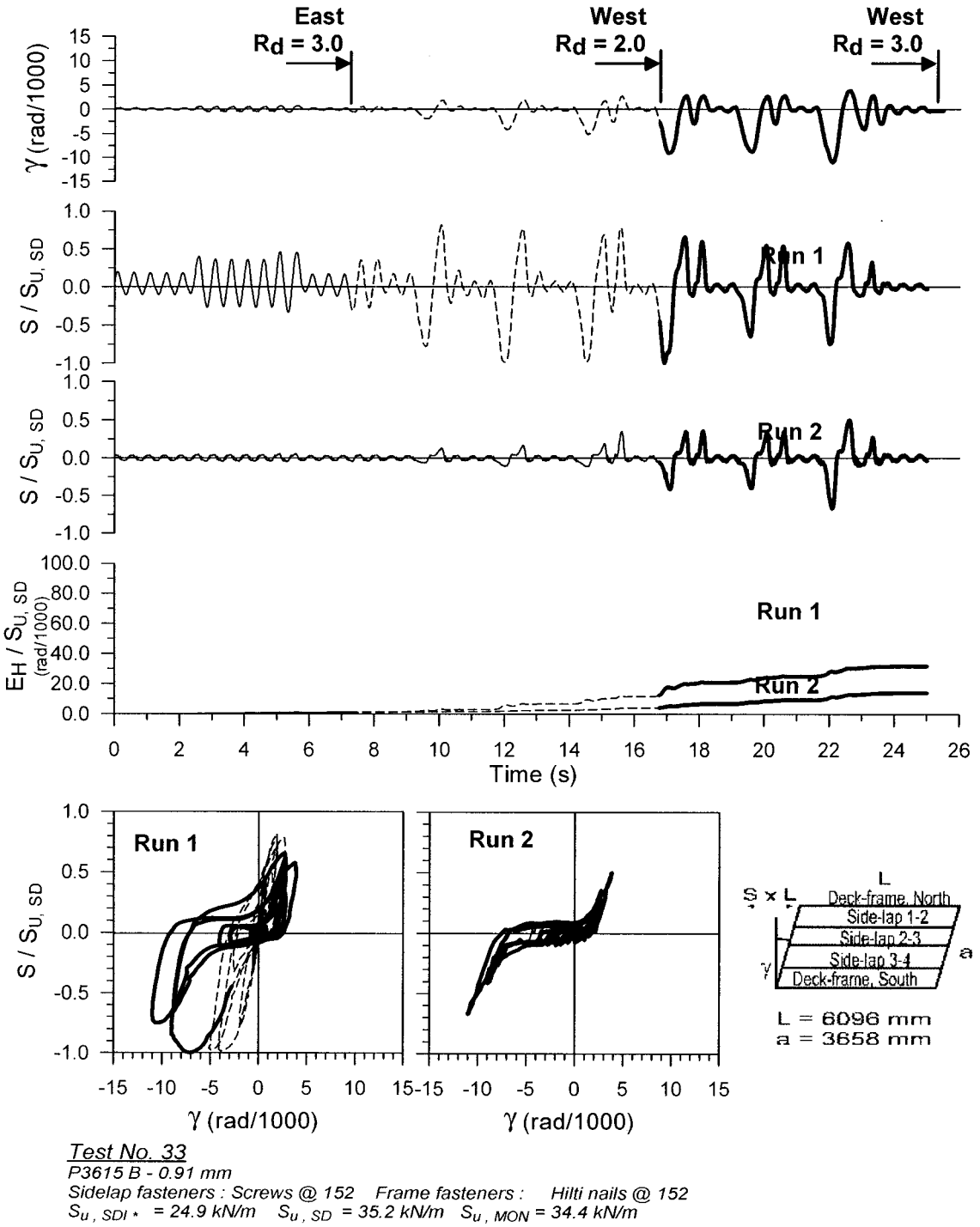

Test No. 33
P3615 B - 0.91 mm
Sidelap fasteners : Screws @ 152 Frame fasteners : Hilti nails @ 152
$S_{u,SDI*}$ = 24.9 kN/m $S_{u,SD}$ = 35.2 kN/m $S_{u,MON}$ = 34.4 kN/m

Figure 5.87 Test no.33 results

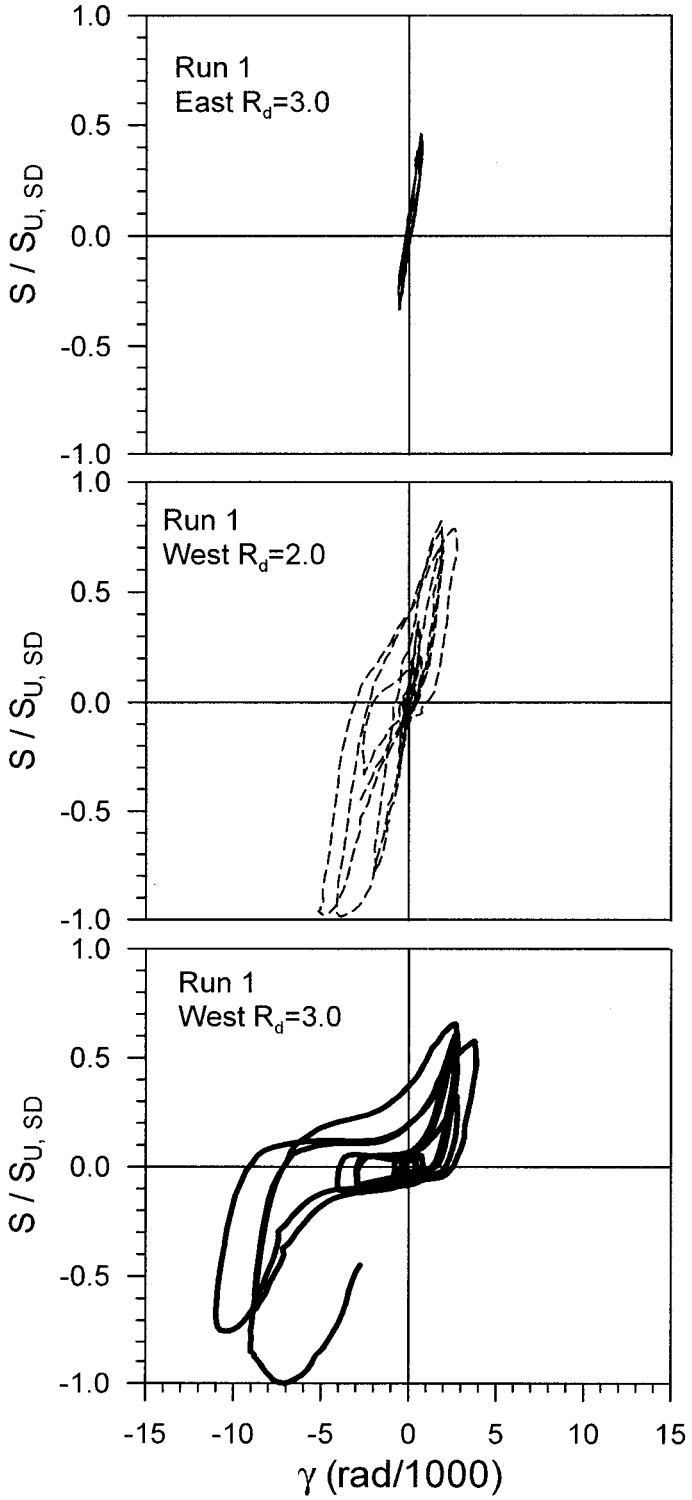

Test No. 33

P3615 B - 0.91 mm
Sidelap fasteners :
Screws @ 152
Frame fasteners :
Hilti nails @ 152

$S_{u, SDI*}$ = 24.9 kN/m
$S_{u, SD}$ = 35.2 kN/m
$S_{u, MON}$ = 34.4 kN/m

Figure 5.87 Test no.33 results (continued)

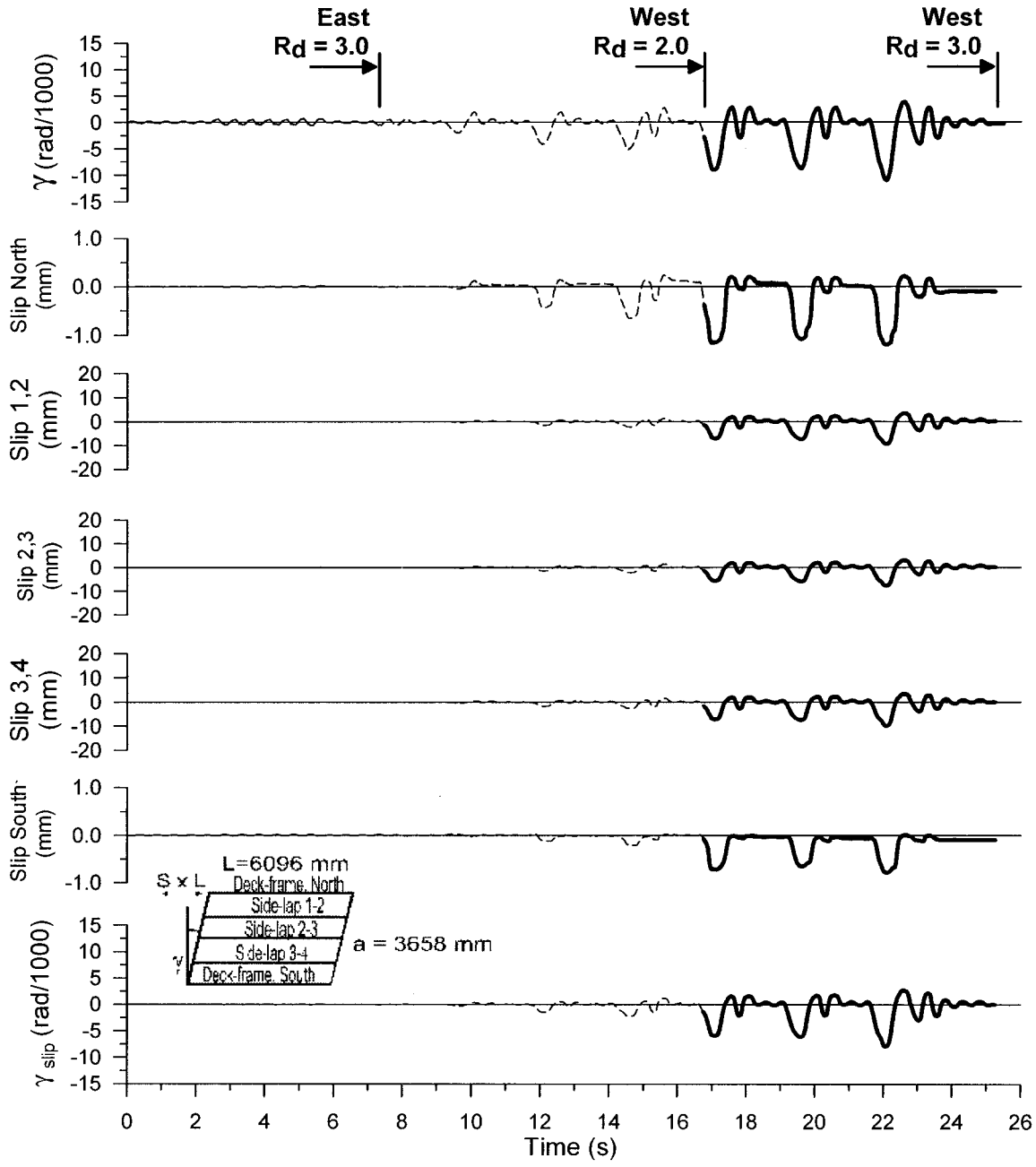

Test No. 33- Run 1
P3615 B - 0.91 mm
Sidelap fasteners : Screws @ 152 Frame fasteners : Hilti nails @ 152
$S_{u,SDI*}$ = 24.9 kN/m $S_{u,SD}$ = 35.2 kN/m $S_{u,MON}$ = 34.4 kN/m

Figure 5.87 Test no.33 results (continued)

Table 5.39 Observed damage after run 1 (Test 33)

	1	1'	2	2'	3	3'	4	4'	5	5'	6	6'	7	7'	8	8'	9	9'	10	10'	11	11'	12	12'	13	13'	14	14'	15	15'	16	16'	17	17'	18	18'	19	19'	20	20'	21
A																																								
A'																																								
B																																								
B'																																								
C	BF										BF										BF								BF										BF
C'	BF										BF										SB								BF										BF
D	B1										BF										SB								BF										B1
D'	BF										BF										SB								BF										
E																																								
E'																																								
F																																								BF
F'	BF										BF										BF								BF										BF
G	B1										BF										BF								BF										B1
G'	BF										BF										BF								BF										BF
H																													BF										
H'																																								
I																																	BF							BF
I'											BF										BF												BF							BF
J	B1										BF										BF										BF									B1
J'	BF										BF										BF										BF									BF
K	BF																				BF										BF									BF
K'	BF																																							
L																																								
L'																																								
M																																								

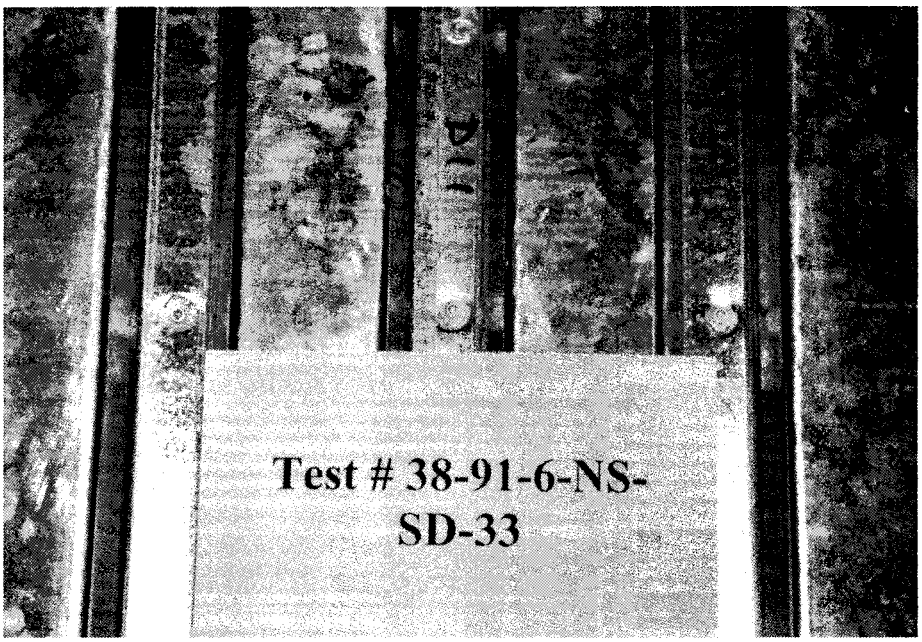

Figure 5.88 SB failure mode at D11, Test 33

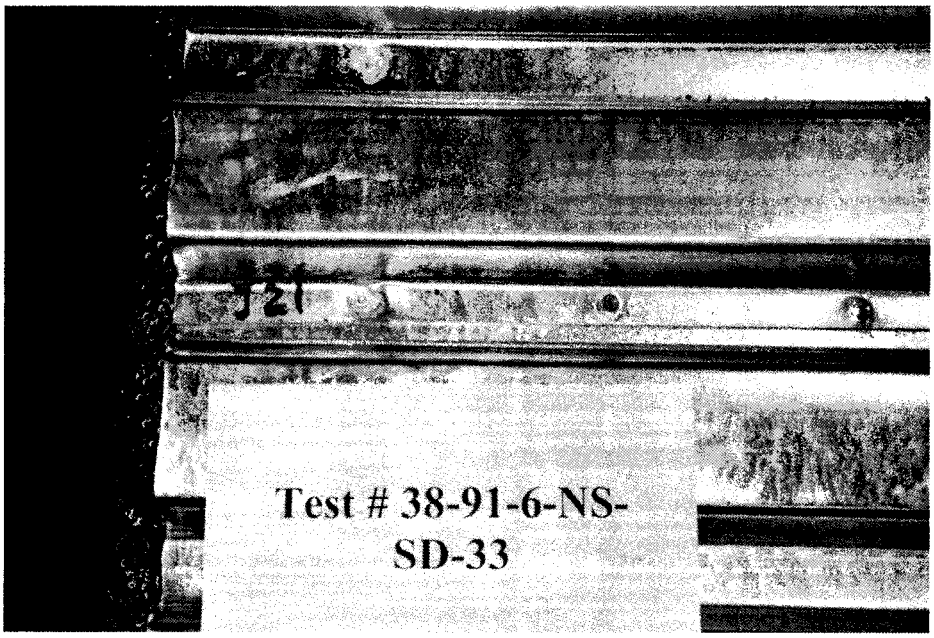

Figure 5.89 B1 failure mode at J21, Test 33

5.8.4.4 Tests 30 and 31

Tests 30 and 31 were assembled with the same connections and spacing (152 mm c/c) as tests 32 and 33. The only difference involved the use of a 0.76 mm thick deck. Tests 30 and 31 were performed using screwed sidelap and Hilti nailed deck-to-frame connections and B-deck profile. Test 30 was monotonic and test 31 was subjected to a short duration (SD) loading protocol. Table 5.40 presents description of specimen for tests 30 and 31. Figure 5.90 and Figure 5.95 display the test result curves for tests 30 and 31, and Table 5.41 and Table 5.42 the observed damage after the tests.

Test 30

The behaviour in test 30 was similar to that of test 32. The maximum measured load in test 30 was 23.4 kN/m at a corresponding distortion of 4 rad/1000. Until a distortion of 13 rad/1000 was reached, the measured load remained above 80% of its maximum. In tests 30 and 32, the sidelap slip and hence, the variation in stiffness, started at approximately 1 rad/1000 and the corresponding load level for test 30 was $0.6S_u$ (14.0 kN/m) whereas in test 32 sidelap slip commenced at $0.4S_u$ (13.8 kN/m). Up to the peak load, interior sidelaps experienced similar slips. Later, slips at sidelaps 1,2 and 3,4 increased faster than sidelap 2,3. As explained in test 32, this was due to the higher rigidity of edge connections compared to interior sidelaps. At test end, the screws were uplifted (See Figure 5.91). Tearing of the top sheet (TT) was observed at 8 locations (See Figure 5.92). Bearing failures with slot (BFS) were also noticed. Figure 5.93 presents 2 failure modes: TT and BFS. Figure 5.94 presents a B1 failure.

Test 31

The maximum load in test 31 was equal to 26.5 kN/m, which is 13% greater than in test 30 (23.4 kN/m). The hysteretic behaviour in test 31 was similar to that observed in test 33 with a 0.91 mm thick steel, with substantial pinching in the West $R_d = 3.0$ segment of the loading protocol. Similar slip deformation time histories developed at the three sidelaps and screws were fallen out at the end of the test. At most locations, there was a gap between the screw head and the top sheet and another gap between the two sheets. This was expected as the maximum sidelap slip reached about 10 mm. There was no damage at North and South ends. Figure 5.96 shows an example of a B2 failure mode whereas Figure 5.97 presents a B1 failure mode.

Table 5.40 Test specimen description (Tests 30 and 31)

Steel properties:	
Supplier and coil number	Canam P-3615 B deck 0.76 mm Coil supplier: Stelco Coil number: 658104
Base metal thickness (mm)	0.70
Fy test (MPa)	248
Fu test (MPa)	327
E (MPa)	204000
50 mm gauge % elongation	32 %
Fasteners:	
Sidelap fasteners	Screw 12- 14 x 1 HWH#1 FP Lot number: 9901-0019 Spacing: 152 mm c/c
Deck-to-frame fasteners	Hilti nail X-EDNK-22 THQ 12M Lot number: 413923 Spacing: 152 mm c/c
Comments on quality of fasteners:	
Test 30	Nail stand-off: Total Ave.: 6.0 mm C.o.V.: 0.35 At sidelaps Ave.: 6.5 mm C.o.V.: 0.40 Other than sidelaps Ave.: 6.0 mm C.o.V.: 0.34 No problem with nail installation.
Test 31	Nail stand-off: Total Ave.: 6.0 mm C.o.V.: 0.36 At sidelaps Ave.: 6.2 mm C.o.V.: 0.40 Except sidelaps Ave.: 5.9 mm C.o.V.: 0.35 No problem with nail installation.

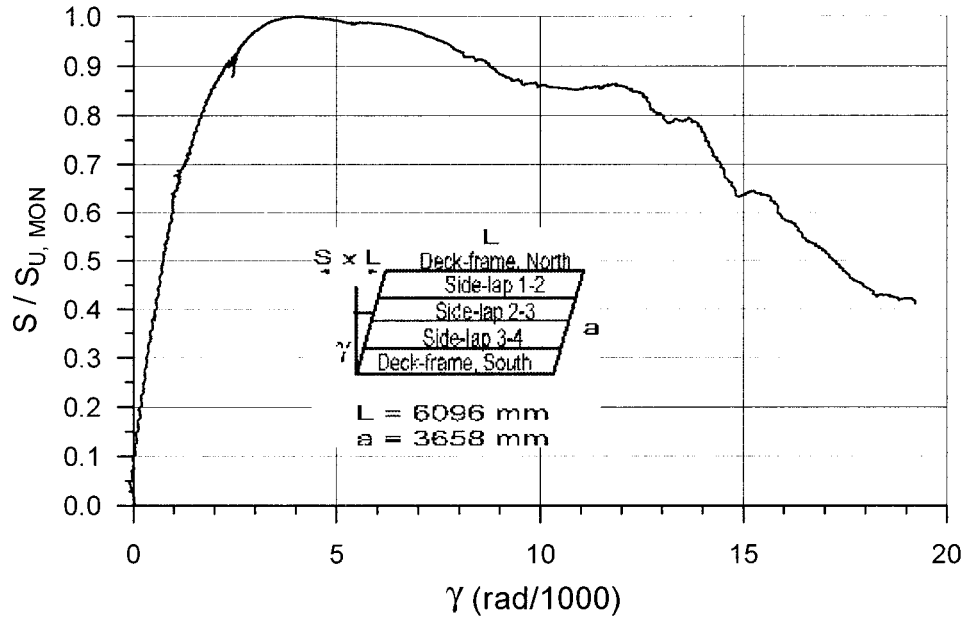

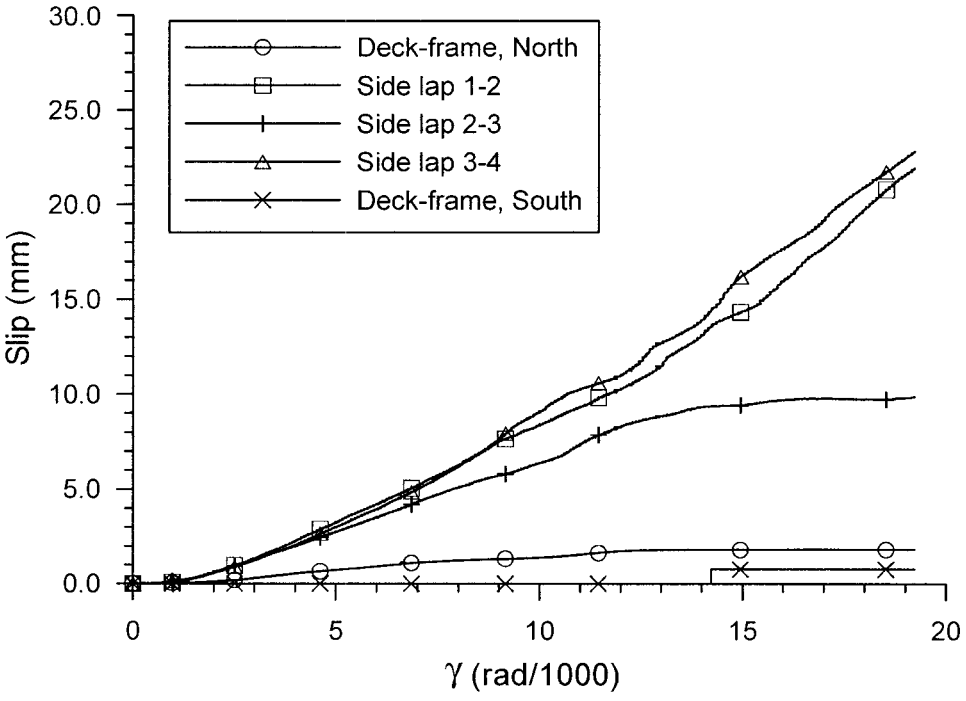

Test No. 30
P3615 B - 0.76 mm
Sidelap fasteners : Screws @ 152 Frame fasteners : Hilti nails @ 152
$S_{u,SDI*}$ = 20.2 kN/m $S_{u,MON}$ = 23.4 kN/m

Figure 5.90 Test no.30 results

Table 5.41 Observed damage (Test 30)

	1	1'	2	2'	3	3'	4	4'	5	5'	6	6'	7	7'	8	8'	9	9'	10	10'	11	11'	12	12'	13	13'	14	14'	15	15'	16	16'	17	17'	18	18'	19	19'	20	20'	21
A																																								
A'	B1																																							
B	B1										B1																													BFS
B'	B1										B1										B1										B1									B1
C	BFS										B1										B1										B1									B1
C'	BFS										BFS										BFS										BFS									BFS
D	B1										TT										TT										TT									TT
D'	BFS										B1										BFS										BFS									BFS
E	B1										B1										BFS										B1									BFS
E'	B1										B1																				B1									
F											B1										B1										B1									B1
F'											B1										B1										B1									B1
G	B1										B1										B1										B1									B1
G'																															B1									
H																															B1									
H'											B1																				B1									
I	BFS										B1										B1										B1									B1
I'	B1										BFS										BFS										BFS									B1
J	B1										TT										TT										TT									TT
J'	BFS										BFS										BFS										BFS									BFS
K	BFS										BFS										BFS										BFS									BFS
K'											B1										BFS										BFS									BFS
L											SB										B1										SB									B1
L'																																								
M																																								

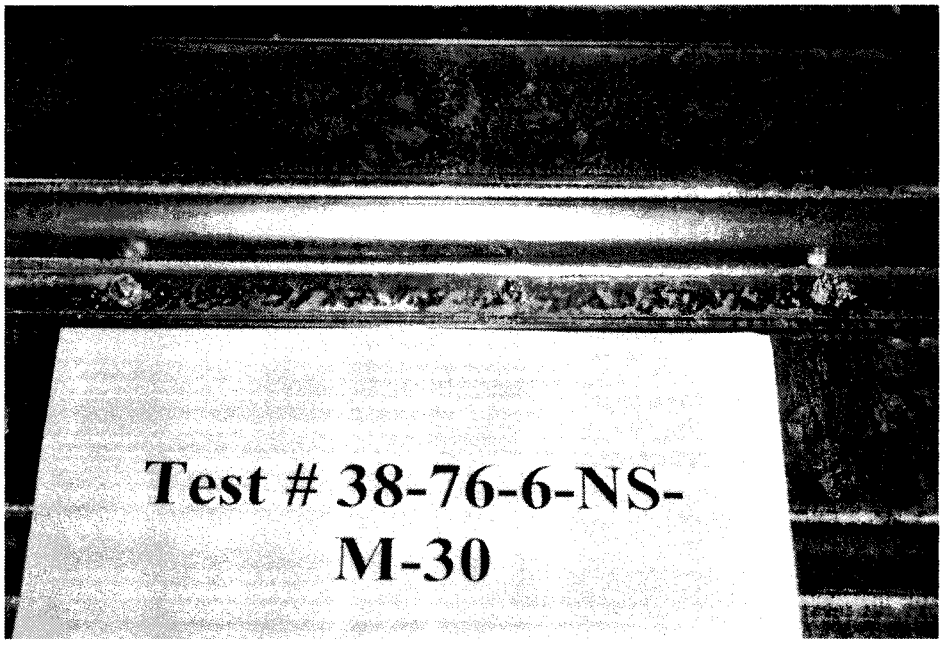

Figure 5.91 Screw tilting and uplifting, Test 30

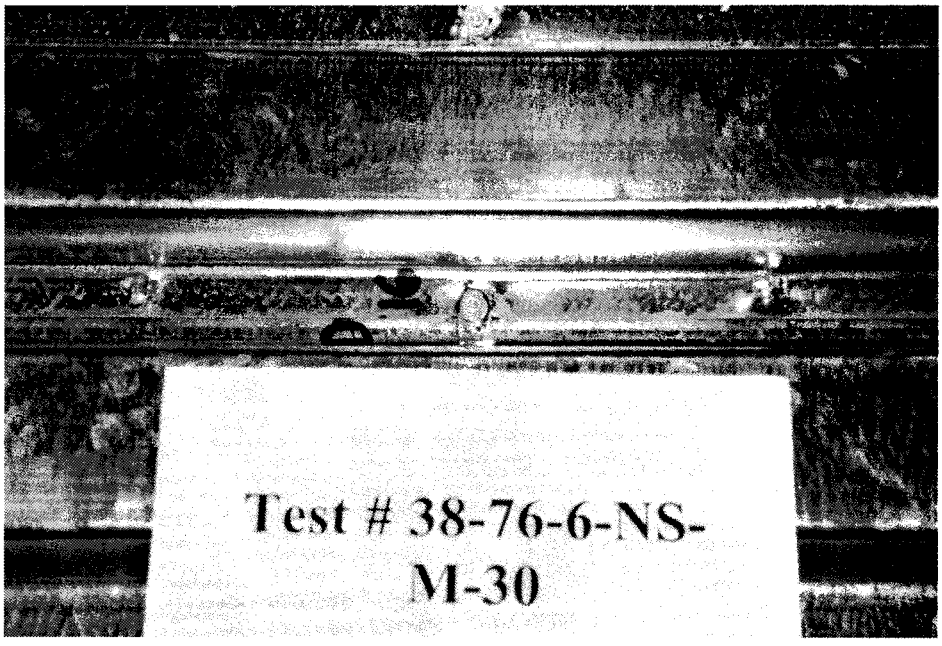

Figure 5.92 TT failure mode at D16, Test 30

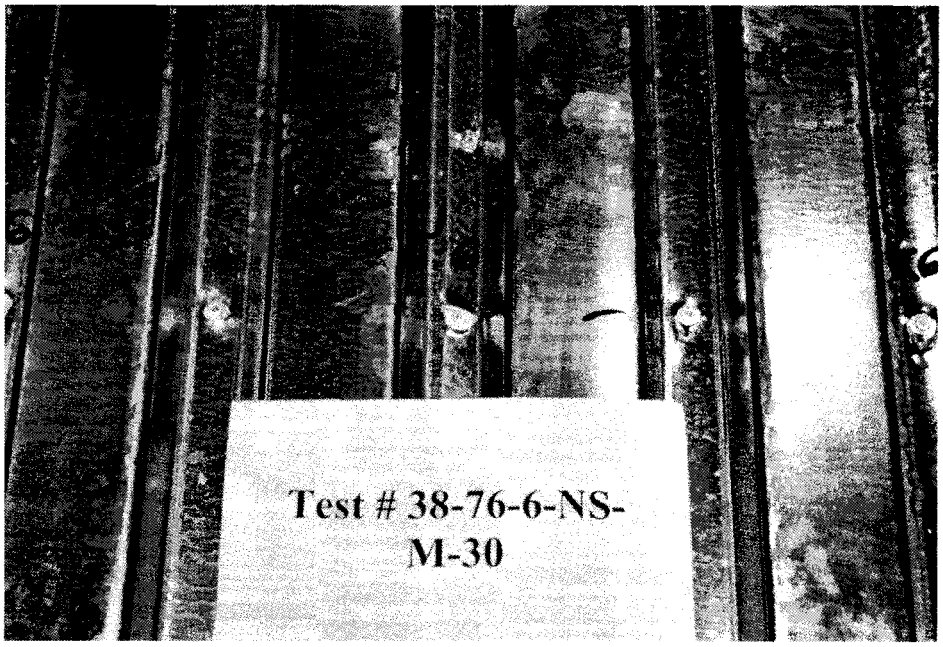

Figure 5.93 TT failure mode at J6 and BFS at I'6, J'6, Test 30

Figure 5.94 B1 failure mode at J1, Test 30

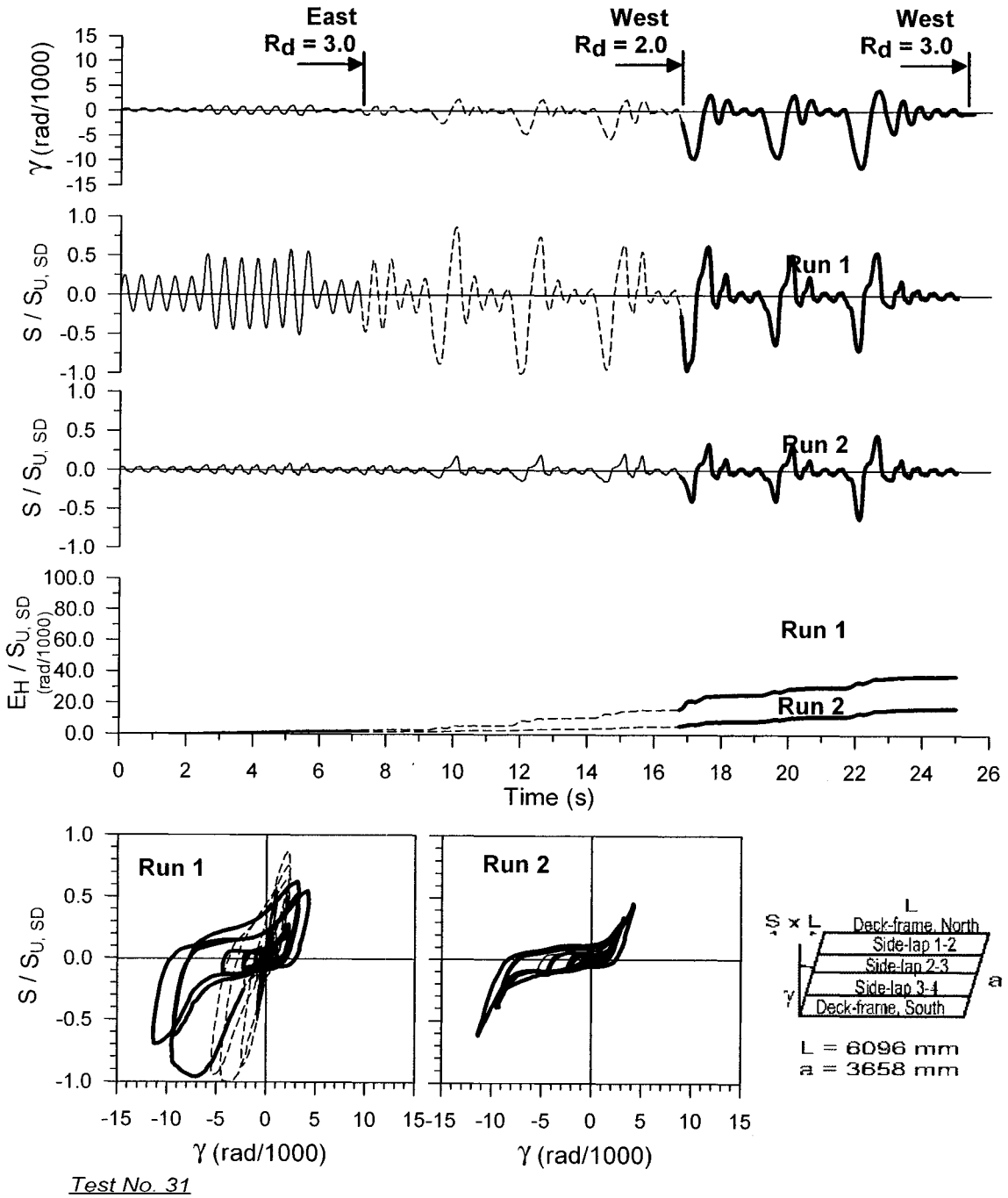

Test No. 31
P3615 B - 0.76 mm
Sidelap fasteners : Screws @ 152 Frame fasteners : Hilti nails @ 152
$S_{u,SDI}$ = *20.2 kN/m* $S_{u,SD}$ = *26.6 kN/m* $S_{u,MON}$ = *23.4 kN/m*

Figure 5.95 Test no.31 results

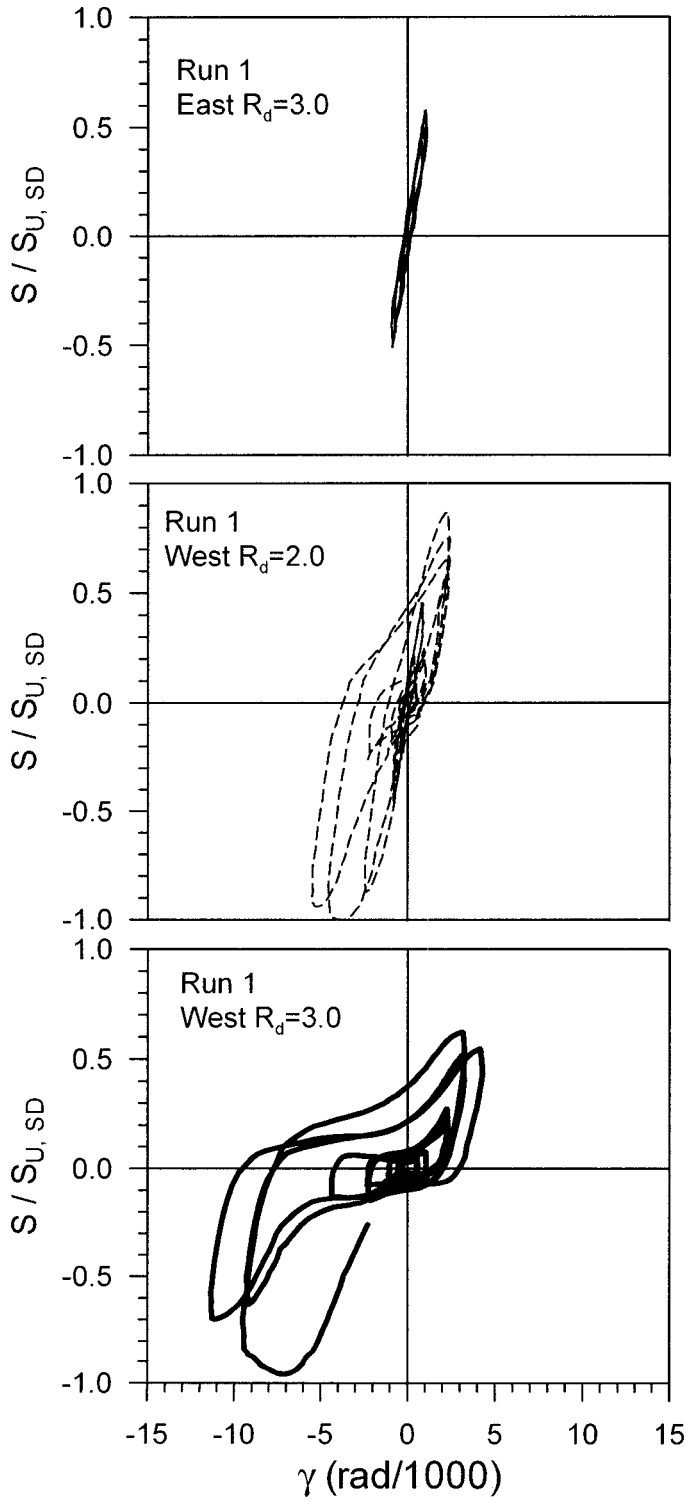

Test No. 31

P3615 B - 0.76 mm
Sidelap fasteners :
Screws @ 152
Frame fasteners :
Hilti nails @ 152

$S_{u, SDI*}$ = 20.2 kN/m
$S_{u, SD}$ = 26.6 kN/m
$S_{u, MON}$ = 23.4 kN/m

Figure 5.95 Test no.31 results (continued)

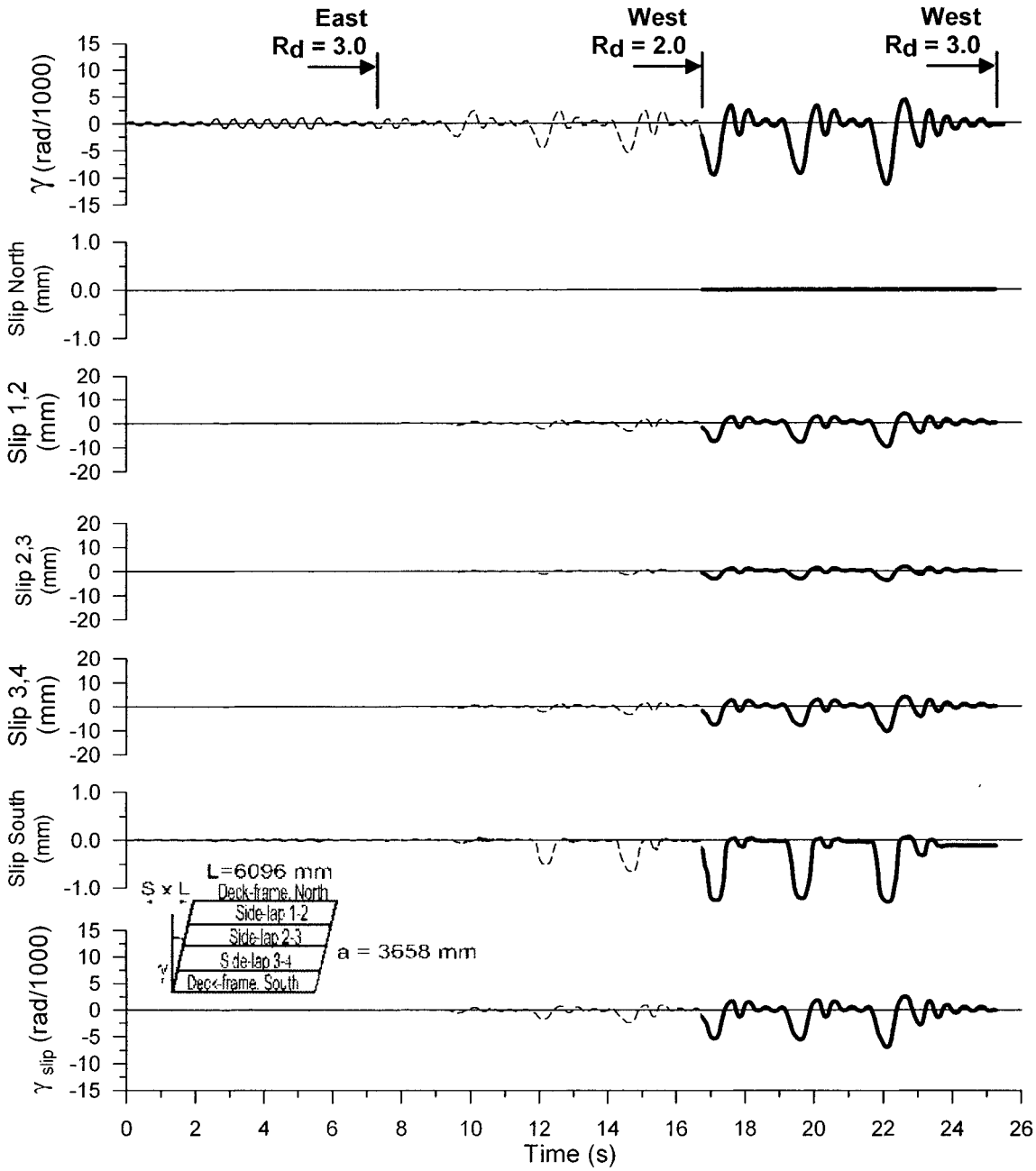

Test No. 31- Run 1
P3615 B - 0.76 mm
Sidelap fasteners : Screws @ 152 Frame fasteners : Hilti nails @ 152
$S_{u,SDI*}$ = 20.2 kN/m $S_{u,SD}$ = 26.6 kN/m $S_{u,MON}$ = 23.4 kN/m

Figure 5.95 Test no.31 results (continued)

Table 5.42 Observed damage (Test 31)

	1	1'	2	2'	3	3'	4	4'	5	5'	6	6'	7	7'	8	8'	9	9'	10	10'	11	11'	12	12'	13	13'	14	14'	15	15'	16	16'	17	17'	18	18'	19	19'	20	20'	21
A																																								B1
A'											BF																													BF
B																																								BF
B'																																								BF
C	BF										BF										BF								BF										BF
C'	BF										BF										B2								BF										BF
D	B1										BF										B2								BF										B1
D'	BF										BF										B2								BF										BF
E	BF																												BF										BF
E'																																								BF
F	BF										BF																				BF									BF
F'	BF										BF										BF								BF										BF
G	B1										BF										BF								BF										B1
G'	BF										BF										BF								BF										BF
H	BF																												BF										BF
H'																													BF										BF
I	BF																												BF										BF
I'											SB										BF								B2										BF
J	B2										B2										BF								B2										B1
J'	BF										SB										BF								B2										BF
K	BF										BF										BF								B2										BF
K'																																								BF
L																															BF									
L'																															BF									
M																																								

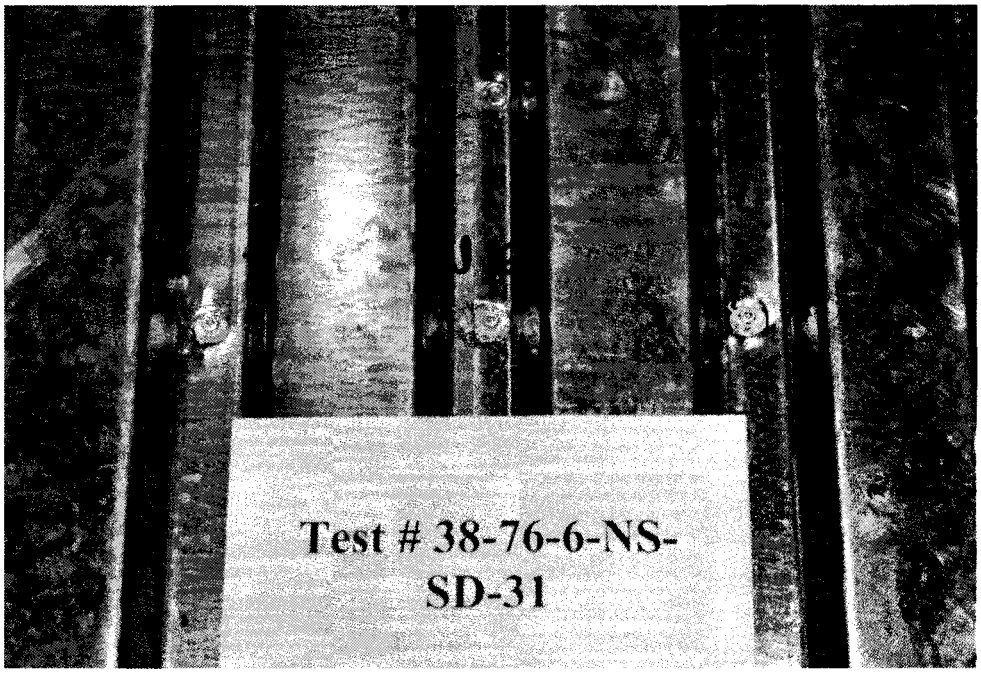

Figure 5.96 B2 failure mode at J16, Test 31

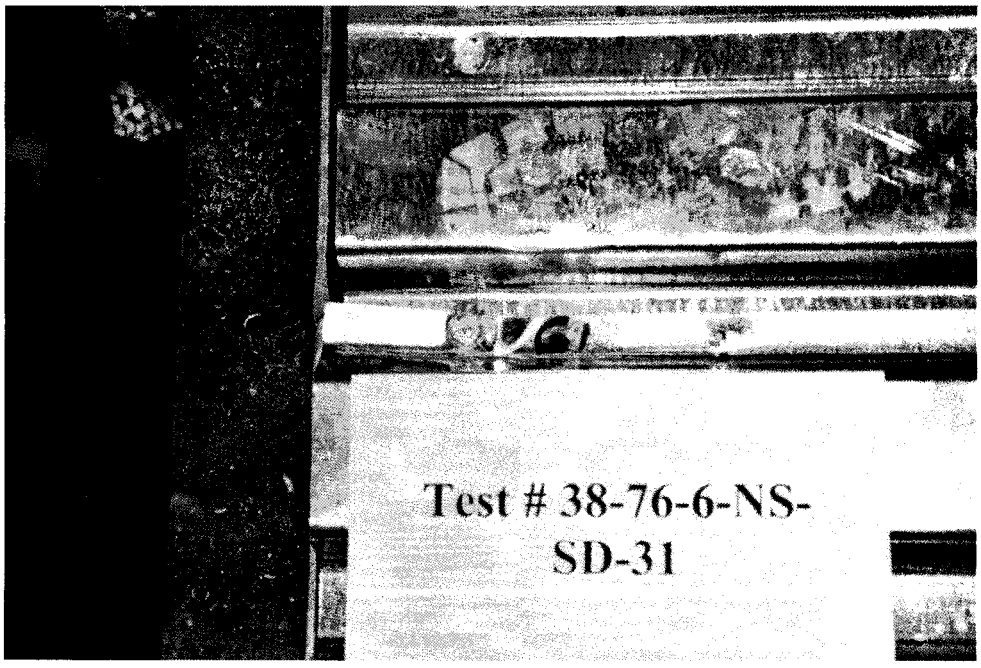

Figure 5.97 B1 failure mode at G1, Test 31

5.9 DATA ANALYSIS

A number of methods were used in order to evaluate quantitatively the ability of the diaphragm to sustain inelastic seismic distortion. The parameters can also be useful in the development of analytical hysteretical models of the diaphragm behaviour. The criteria used in the evaluation are presented along with the resulting data.

5.9.1 Selection of the performance criteria

Due to the differences between the SD and LD loading protocols, it was difficult to choose criteria that could be common to both protocols. For this reason, some of the selected parameters were therefore specific to each protocol. Two parameters that were used for all tests were the maximum force, S_u, and the initial stiffness G'.G' was calculated using a linear regression in the linear part of the first cycle at $0.4\gamma_u$. Both SD and LD loading protocols contained initial cycles at this amplitude. In monotonic tests, G' was found based on the approach described in Section 5.5.

Table 5.43 summarises the parameters selected for the SD protocol. These are illustrated in Figure 5.98. As indicated, the three main segments of the loading protocol were numbered I, II and II for simplicity: I for the East R_d =3.0, II for the West R_d =2.0, and III for the West R_d =3.0 segments. It must be restated here that the real West R_d =2.0 loading protocol in fact includes East R_d =3.0 and West R_d =2.0. Similarly, the protocol for R_d = 3.0 buildings located in western Canada corresponds to the entire loading protocol.

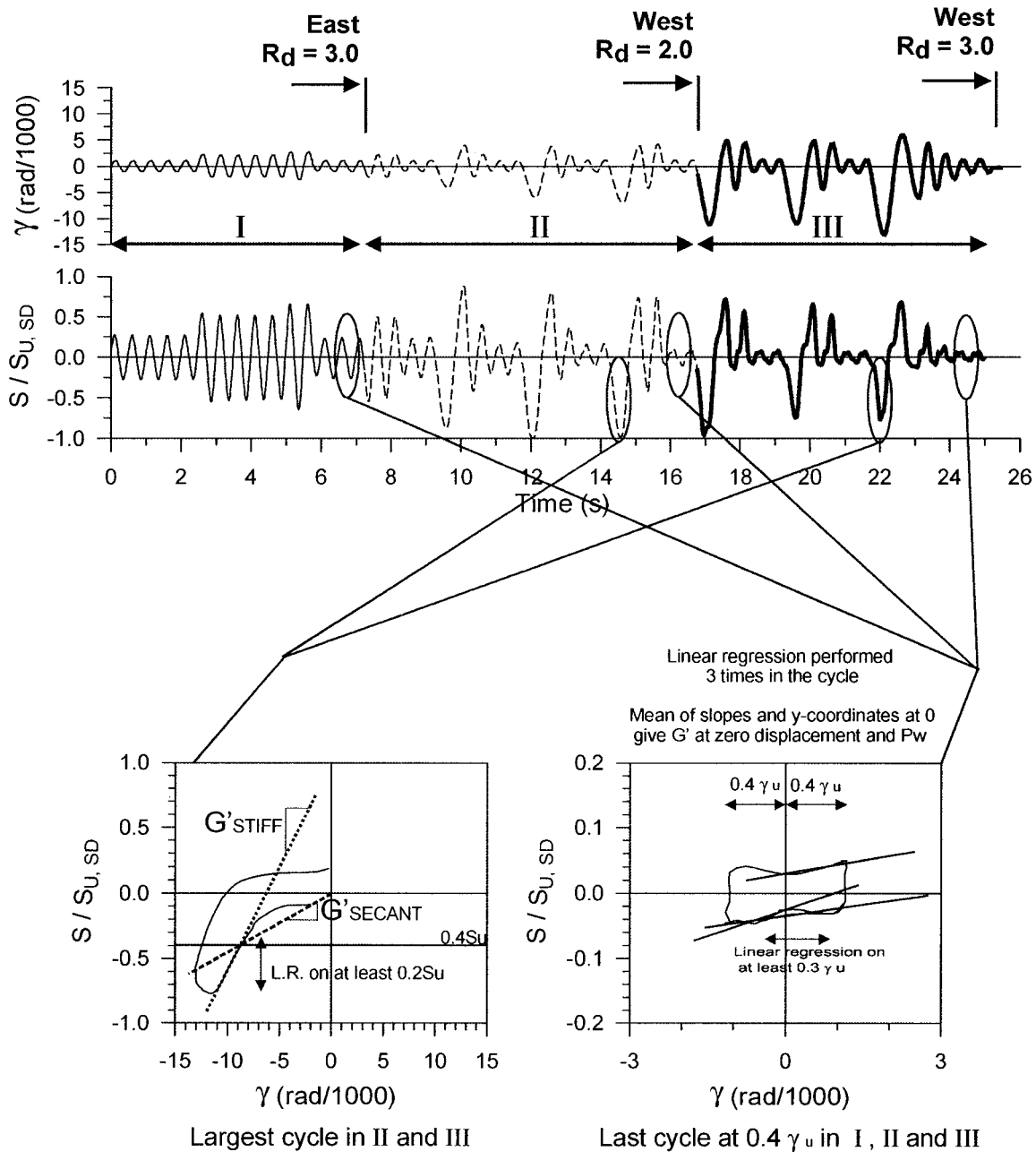

Figure 5.98 Parameters used to evaluate the hysteretic behaviour under the SD loading protocol

Table 5.43 List of hysteretic parameters used for the SD loading protocol

Criteria	Definition
Reference distortion used (rad/1000)	Reference distortion used in the loading protocol. See Section 5.5 for more information.
$S_i / S_{U, SD}$	Ratio of the maximum force in largest excursion in segment I, II or III to the maximum measured force in the total SD signal
S_L / S_{2L}	Ratio of the maximum force in the largest excursion in segment I, II and III to the maximum force in the 2nd largest excursion in the same time interval
$E_H / (S_{U,SD} . \Sigma (\Delta\gamma))$	Cumulated hysteretic energy in segment I, II or III normalised to the maximum force measured in the SD loading protocol and cumulated absolute distortion in same time interval
G'_{SECANT} / G'	Ratio of G'_{SECANT} to initial G'. G'_{SECANT} is a secant stiffness, measured in the largest excursion in segment II and III, from the origin to the intersection of shear-distortion curve and $0.4S_{U, SD}$
S_U, Run2/Run1	Ratio of maximum measured force in run 2 compared to maximum force in run 1
E_H, Run2/Run1	Ratio of the cumulative hysteretic energy in run 2 compared to run 1
G' i/G' at zero displacement	Ratio of the residual stiffness at zero displacement to initial stiffness. This stiffness is found in the last cycle at $0.4\gamma_u$ in segment I, II and III. To find the stiffness, a linear regression is performed at 3 locations in the cycle. The mean of these 3 slopes gives G'i. Each linear regression covers at least a 0.3 γ_u distortion range.
P_W / S_U	Ratio of the pinching width, P_W, to the maximum measured force in the SD loading protocol. P_W is calculated in the last cycle at $0.4\gamma_u$ in segment I, II and III.
G'_{STIFF} / G'	Ratio of G'_{STIFF} to initial G'. G'_{STIFF} represents the stiffness found when reloading of the deck occurs. This value is measured in the largest excursion in segment II and III. It is found from a linear regression on data covering at least 0.2 $S_{U, SD}$.

Pinching can be considered as the double change in curvature of the shear-distortion curve occurring within half a cycle. In order to better understand the extent of pinching throughout the signal, it was decided to use two criteria: P_W and G'i. P_W is the pinching width and G'i is the stiffness at zero deformation. These two values were calculated from cycles at $0.4\gamma_u$ at the end of each segment. They were obtained from three linear

regressions in one cycle of the shear-distortion curve. Each linear regression covered at least a $0.3\gamma_u$ distortion range. Figure 5.99 presents a typical cycle at $0.4\gamma_u$ with linear regressions.

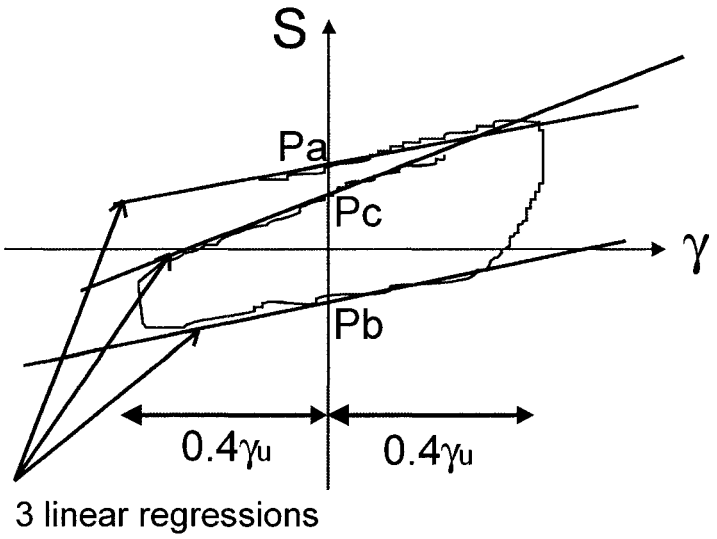

Figure 5.99 Linear regressions on cycles at 0.4 γ_u

G' is equal to the mean of the three slopes from the linear regressions. P_w comes from the y-coordinates at zero displacement as described by Essa *et al.* (2001). In this project, P_w from Essa *et al.* was modified since values from the linear regressions were used instead of local values taken on the curve. P_w is calculated with the following formula:

$$Pw = \frac{Pa + Pc}{4} + Pb/2 \qquad (5\text{-}2)$$

Other parameters, G'_{SECANT} and G'_{STIFF}, were developed to measure the extent of pinching. These 2 stiffnesses are calculated for the largest cycles of the West R_d =2.0 and West R_d =3.0 segments. To assess the residual stiffness under service loads, G'_{SECANT} was created. G'_{SECANT} is a slope starting from the origin (0,0) and reaching the

shear-distortion curve at $0.4S_u$. G'_{STIFF} was created to provide a measure of the stiffness attained when the specimen reaches large deformations and strength increases. A linear regression was performed on the shear-distortion curve on a range of at least $0.2S_u$.

For the LD loading protocol, other parameters were used to assess the hysteretic behaviour. The LD protocol was divided into segments to allow for comparison of different cycles during the loading (Figure 5.100). First, the loading protocol was divided in 2 halves. Second, the protocol was divided into 6 segments. Finally, the cycles at $(\gamma_u+\gamma_2)/2$ beside the peaks were numbered 1, 2, 3 and 4. After the LD loading protocol, a cyclic test called "additional loop" was performed to measure the residual capacity of the deck diaphragm. The specimen was pushed in one direction far enough to attain its maximum strength. At this time, the direction of displacement was reversed and the specimen was again pushed to its maximum strength.

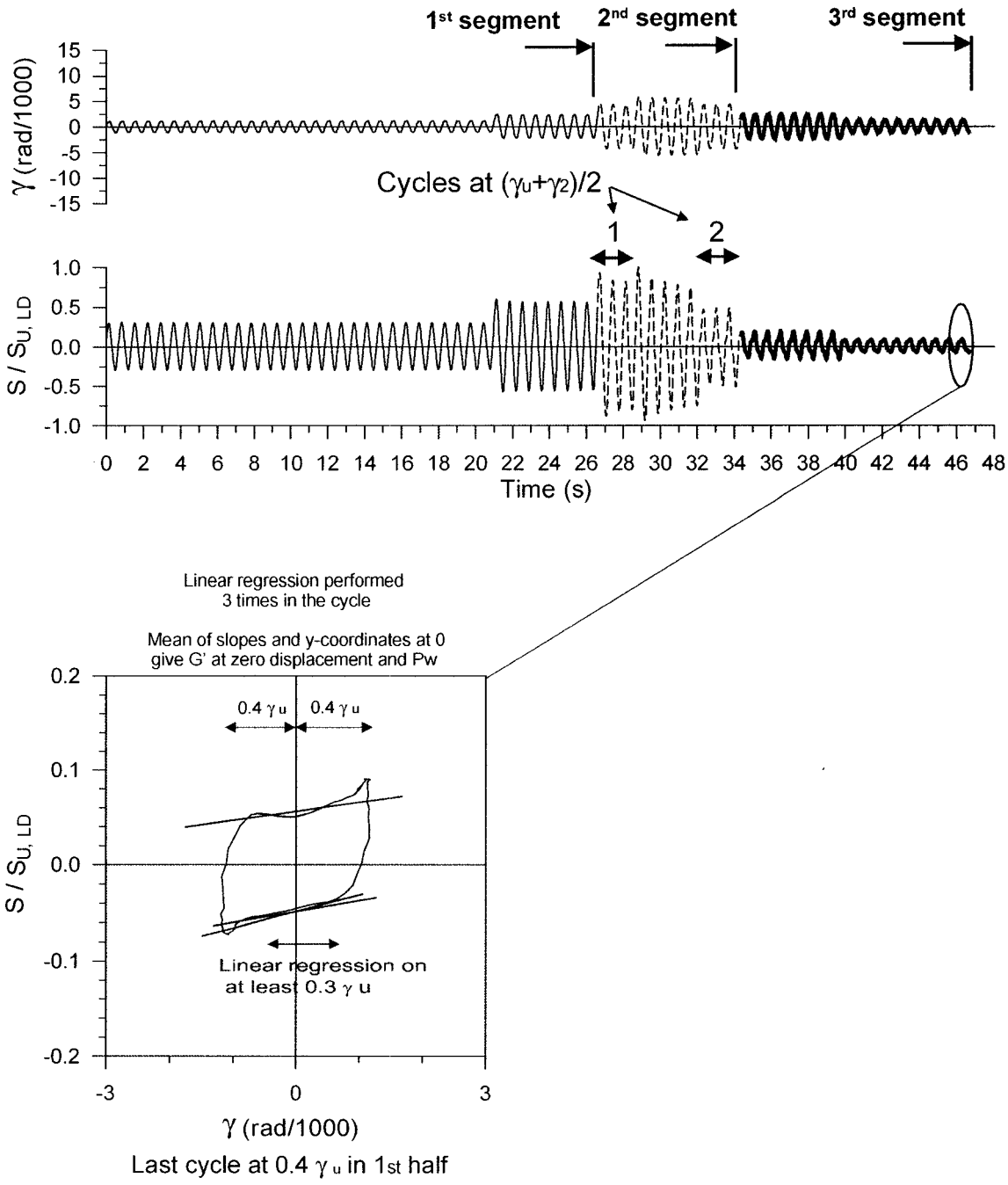

Figure 5.100 Parameters used to evaluate the hysteretic behaviour under the LD loading protocol

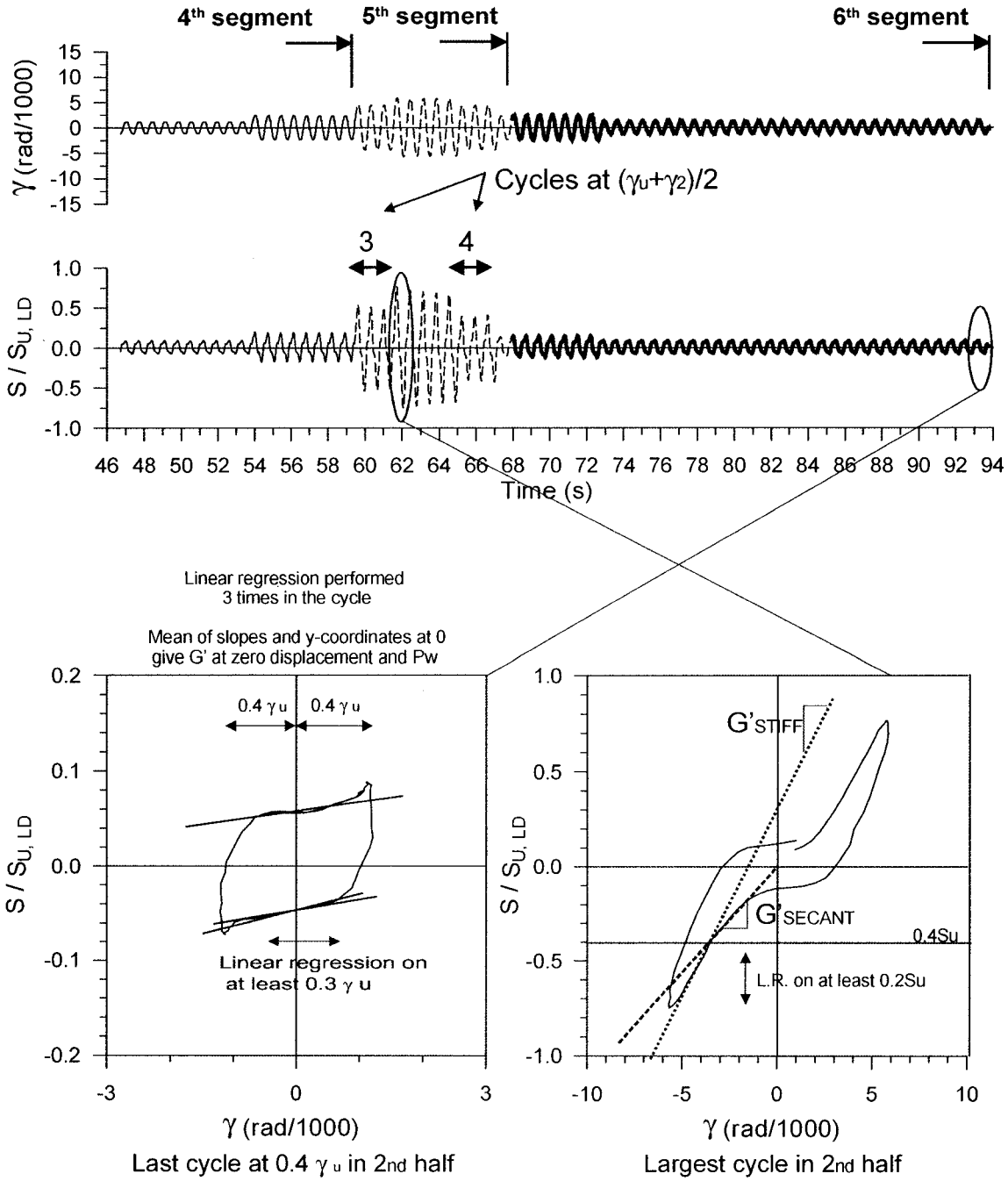

Figure 5.100 Parameters used to evaluate the hysteretic behaviour under the LD loading protocol (continued)

Table 5.44 List of hysteretic parameters used for the LD loading protocol

Criteria	Definition
Reference distortion used (rad/1000)	Reference distortion used in the LD loading protocol. See Section 5.5 for more information.
$S_i / S_{U, LD}$	Ratio of the maximum force in largest excursion in 1st and 2nd halves to the maximum measured force in the total signal
Strength degradation Cycles at $(\gamma_U+\gamma_2)/2$ $S1 / S_{U, LD}$, S2/ S1, S3/ S1, S4/ S1	Ratio of the maximum force in one cycle at $(\gamma_u+\gamma_2)/2$ to a reference force. S1 is the maximum force in the last cycle of the 1st set of cycles at $(\gamma_u+\gamma_2)/2$. S2 is the maximum force in the first cycle of the 2nd set of cycles at $(\gamma_u+\gamma_2)/2$. S3 is the maximum force in the last cycle of the 3rd set of cycles at $(\gamma_u+\gamma_2)/2$. S4 is the maximum force in the first cycle of the 4th set of cycles at $(\gamma_u+\gamma_2)/2$.
$E_H / (S_{U,LD} \cdot \Sigma(\Delta\gamma))$ (1st half)	Cumulative hysteretic energy in the 1st half of the loading protocol normalised to the maximum force measured in the LD loading protocol and cumulated absolute distortion in same time interval
Energy dissipation comparison ratio E_H 2nd half/ E_H 1st half E_H 5th seg./ E_H 2nd seg. EH2/EH1 EH3/EH1 EH4/EH1	Ratio of the hysteretic energy dissipated in one time interval to the energy dissipated in another time interval of same time duration and total distortion EH1: Hysteretic energy dissipated in the first set (1) of cycles at $(\gamma_u+\gamma_2)/2$ EH2: Hysteretic energy dissipated in the second set (2) of cycles at $(\gamma_u+\gamma_2)/2$ EH3: Hysteretic energy dissipated in the third set (3) of cycles at $(\gamma_u+\gamma_2)/2$ EH4: Hysteretic energy dissipated in the fourth set (4) of cycles at $(\gamma_u+\gamma_2)/2$
G'i/ G' at zero displacement	Ratio of the residual stiffness at zero displacement to initial stiffness. This stiffness is calculated in the last cycle at $0.4\gamma_u$ for 1st and 2nd halves of the loading protocol. To find the stiffness, a linear regression is performed at 3 locations in the cycle. The mean of these 3 slopes is G'i. Each linear regression covers at least a $0.3\gamma_u$ distortion range.
$P_W / S_{U, LD}$	Ratio of the pinching width, P_W, to the maximum measured force in the LD loading protocol. P_W is calculated in the last cycle at $0.4\gamma_u$ for 1st and 2nd halves of the loading protocol.
G'_{STIFF} / G'	Ratio of G'_{STIFF} to initial G'. G'_{STIFF} represents the stiffness found when reloading of the deck occurs. This value is measured in the

	largest excursion in 2nd half. It is found from a linear regression on data covering at least a range of $0.2S_{U, LD}$.
G'_{SECANT} / G'	Ratio of G'_{SECANT} to initial G'. G'_{SECANT} is a secant stiffness measured in the largest excursion of the 2nd half, from the origin (0,0) to the intersection of shear-distortion curve and $0.4S_{U, LD}$
Additional loop $S_{ADD} / S_{U,LD}$	Ratio of the maximum measured force in the additional loop to the maximum measured force in the LD loading protocol.
Additional loop $G'_{STIFF\ ADD} / G'$	Ratio of G'_{STIFF} to the initial G'. G'_{STIFF} represents the stiffness found in the additional loop when reloading of the deck occurs. It is found from a linear regression on data covering a range of at least $0.2S_{U, LD}$.

5.9.2 Performance of the diaphragms under the SD protocol

In this section the results from the data analysis are presented and comments are made for the SD loading protocols. In Table 5.45, the test values, ultimate loads and stiffnesses are displayed for all tests. Table 5.46 presents the parameters for the SD loading protocol.

Table 5.45 Test values for ultimate loads and stiffnesses

Test	Date of testing	Test values Su kN/m	G' kN/mm
38-91-6-WB-M-37	03/20/2002	12.6	3.32
38-91-6-WB-SD-21	02/15/2002	13.8	3.16
38-76-6-WB-SD-20	02/13/2002	9.81	2.44
38-76-6-WB-SD-36a(1)	03/19/2002	5.80	2.40
38-76-6-WB-SD-36b(1)		5.69	0.94
Mean (2)			
C.o.V. (2)			
38-91-6-W'W-M-22	02/20/2002	32.1	4.54
38-91-6-W'W-SD-23	02/22/2002	34.6	4.60
38-91-6-W'W-LD-24	02/27/2002	33.2	4.36
Mean			
C.o.V.			
38-91-6-NW-M-25	03/01/2002	22.5	4.33
38-91-6-NW-SD-26	03/04/2002	26.5	4.09
38-91-6-NW-LD-27	03/18/2002	26.2	3.64
Mean			
C.o.V.			
38-91-6-NS-M-19	02/08/2002	16.7	4.13
38-91-6-NS-SD-34	03/14/2002	17.0	4.01
38-91-6-NS-LD-35	03/15/2002	17.3	3.90
38-76-6-NS-SD-28	03/06/2002	14.1	2.45
38-76-6-NS-LD-29	03/07/2002	13.6	2.39
Mean			
C.o.V.			
38-91-6-NS-M-32	03/13/2002	34.4	18.3
38-91-6-NS-SD-33	03/14/2002	35.2	18.4
38-76-6-NS-M-30	03/08/2002	23.4	13.5
38-76-6-NS-SD-31	03/12/2002	26.5	15.0
Mean			
C.o.V.			

(1): Cycles at 0.4 γ_u and 0.6 γ_u were performed prior to the SD loading protocol.
a refers to the cyclic part, b to the SD loading protocol.
(2): Test 36 results are not included in the mean and C.o.V.

Table 5.46 Parameters for the SD cyclic tests

Test no.	Deck assembly type	Reference distortion used (rad/1000)		S_i/S_{USD}			S_L/S_{zL}			$E_H/(S_{USD}.\Sigma(\Delta\gamma))$			G'_{SECANT}/G'		S_U, Run 2/ Run 1	E_H, Run 2/ Run 1
		γ_u	γ_2	I	II	III	I	II	III	I	II	III	II	III		
21 (1)	WB	2.84	2.98	0.76	0.76	0.11	1.21	0.76	----	0.155	0.169	0.056	0.91	N/A	0.09	0.18
20	WB	5.33	5.60	0.85	0.14	0.05	1.08	0.50	----	0.232	0.082	0.028	N/A	N/A	0.10	0.23
36 (2)	WB	5.33	5.60	0.48	0.26	0.10	1.18	0.64	----	0.070	0.053	0.030	N/A	N/A	0.12	0.37
23 (1)	WW	6.08	8.64	0.62	1.00	0.43	1.22	1.02	0.83	0.069	0.097	0.110	0.84	0.24	0.34	0.39
26	NW	4.69	6.67	0.60	0.90	0.80	1.20	0.97	0.93	0.063	0.094	0.118	0.67	0.34	0.59	0.60
34	NS	3.23	6.60	0.66	0.99	0.77	1.26	0.99	1.03	0.063	0.112	0.133	0.57	0.19	0.64	0.55
28	NS	3.55	5.04	0.60	0.90	0.78	1.27	1.03	0.98	0.066	0.100	0.145	0.69	0.28	0.58	0.58
33	NS	1.22	5.50	0.46	0.98	0.75	1.29	0.99	1.16	0.045	0.151	0.148	0.33	0.10	0.67	0.45
31	NS	1.59	3.70	0.58	0.94	0.70	1.28	0.94	1.11	0.063	0.164	0.155	0.32	0.09	0.62	0.45

(1): In tests 21, 23 and 24, the loading references were not evaluated as intended.

(2): Test 36 was tested for fatigue under service loads prior to the execution of the SD loading protocol.

200 cycles at 0.4 γ_u and 2 cycles at 0.6 γ_u were performed.

Table 5.46 Parameters for the SD cyclic tests (continued)

Test no.	Deck assembly type	Reference distortion used (rad/1000)		G'_i/G' at zero displacement			P_W/S_U			G'_{STIFF}/G'	
		γ_u	γ_2	I	II	III	I	II	III	II	III
21 (1)	WB	2.84	2.98	0.95	0.39	0.06	0.11	0.05	0.01	0.35	N/A
20	WB	5.33	5.60	0.46	0.00	0.00	0.11	0.00	0.00	0.04	N/A
36 (2)	WB	5.33	5.60	0.20	0.07	0.02	0.03	0.02	0.02	N/A	N/A
23 (1)	WW	6.08	8.64	0.86	0.82	0.07	0.04	0.04	0.02	0.77	0.34
26	NW	4.69	6.67	0.87	0.60	0.31	0.05	0.04	0.03	0.78	0.58
34	NS	3.23	6.60	0.87	0.12	0.01	0.05	0.04	0.03	0.75	0.55
28	NS	3.55	5.04	0.83	0.46	0.08	0.05	0.04	0.03	0.92	0.59
33	NS	1.22	5.50	0.90	0.22	0.03	0.05	0.04	0.03	0.55	0.34
31	NS	1.59	3.70	0.83	0.14	0.02	0.05	0.04	0.03	0.38	0.28

(1): In tests 21, 23 and 24, the loading references were not evaluated as intended.

(2): Test 36 was tested for fatigue under service loads prior to the execution of the SD loading protocol. 200 cycles at 0.4 γ_u and 2 cycles at 0.6 γ_u were performed.

Parameters for the SD cyclic tests, displayed in Table 5.46, are discussed here. For simplicity, the abbreviations for the deck assembly types (W'B, W'W, NW and NS) may be used in the text instead of the full names. In addition, for clarity, the designations NS-305 and NS-152 are used in the text when it is necessary to distinguish between the two NS designs according to the spacing of their fasteners.

The following general remarks can be made regarding the results. Tests 21, 23 and 24 were not subjected to loading protocols based on their target loading references, as discussed in section 5.5. The results from these tests are printed with a grey background in the Table and have to be analysed accordingly. For the WB design, only test 20 may be considered as appropriate, as test 36 was subjected to 202 cycles prior to the SD loading protocol.

For the $S_i/S_{U,SD}$ ratios, WB was maximum in segment I whereas all other designs were at their maximum in segment II. For the W'W design (test 23), the degradation was significant since the ratio in segment III was equal to 0.43. For the NW and NS designs, the degradation in segment III was not as extensive as demonstrated by the ratios, which are between 0.70 and 0.80.

The S_L/S_{2L} ratios for all tests were greater than 1.0 in the segment I, showing that there was an increase in strength when an increased distortion was applied. In segment II, for the WB design, the strength degraded as the ratio of 0.50 demonstrates and in III, the system failed. For other designs (W'W, NW and NS) with 305 mm spacing in segment III, the ratios are between 0.83 and 1.03, which means that deterioration occurred. For the NS-152 diaphragms, the system continued to develop higher resistance as the applied displacement was increased in III.

For the $E_H/(S_{U,SD}.\Sigma(\Delta\gamma))$ parameter, in segment I, WB performed better than other systems since this deck assembly type could achieve a stable elliptical hysteretic behaviour without degradation. Other specimens exhibited a more linear response in segment I and, hence dissipated less energy. In segment II, the NS designs had values greater than 0.100. The NS-152 presented greater values than NS-305, and WB designs showed smaller values than the two other cases. In the NS-152 tests, the inelastic demand started earlier in the protocol, and hence this produced higher values in segment II for this system. In segment III, energy dissipation of the WB diaphragm was minimal. Other systems dissipated a higher amount of normalised energy, except the NS-152 for which the values slightly diminished.

For G'_{SECANT}/ G' ratios, under segment II, W'W and NS-305 were better than NS-152. In segment III, NW was higher than NS. For the NS systems in III, the ratios were higher for NS-305 compared to NS-152. From the results, it is possible to understand the situation. This parameter depended on 2 values: G'_{SECANT} and the initial stiffness G'. Figure 5.101 presents the G'_{SECANT} measured in the largest cycle of segment III for test 34 (305 mm c/c spacing) and test 33 (152 mm c/c spacing). On one hand, the initial stiffness of the NS-152 diaphragm (18.4 kN/mm) was around 5 times higher than the corresponding NS-305 specimen (4.01 kN/mm). On the other hand, the G'_{SECANT} measured for NS-152 (1.84 kN/mm) was 2 times higher than for NS-305 (0.78 kN/mm). Hence, the important difference in the initial value of the stiffness must be considered when interpreting the G'_{SECANT}/ G' parameter.

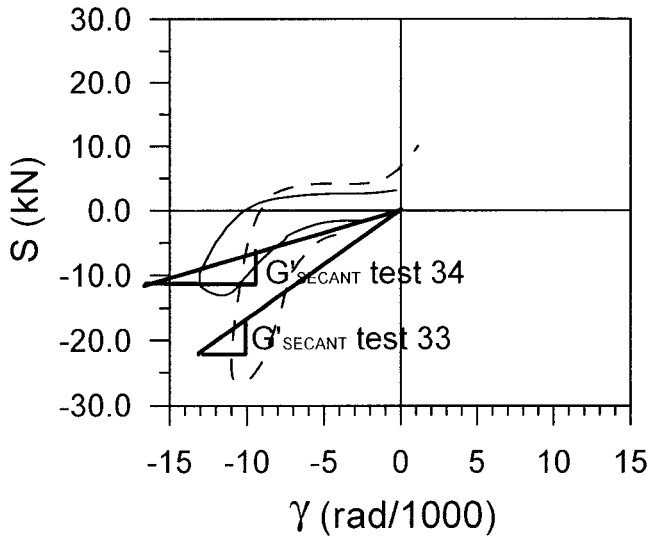

Figure 5.101 G'_{SECANT} in the last cycle of West Rd=3.0 for tests 34 and 33

Given the results of the S_U Run2/Run1 and E_H Run2/Run 1 comparison, the following comment can be made. The WB diaphragm had the poorest response and that all NW and NS specimens exhibited similar values. Test 23 with W'W design degraded to a greater extent in terms of shear capacity and energy dissipation compared with the NS designs, even though the specimen was not sufficiently displaced due to the error in the evaluation of loading references.

For G'_i/ G' ratios, in segment I, W'W, NW, and NS tests showed similar values, much greater than the WB designs. In segment II and III, WB had negligible stiffness. NW design was better than NS in II and III. This is due to the more severely pinched hysteretical behaviour exhibited by the NS diaphragms.

The P_W/S_U ratios are very small in all cases, varying between 0% and 5%. The values are generally lower for the WB design and slightly better for the NW and NS diaphragms. Essa *et al.* found higher values for similar specimens. However, it must be noted that the values presented herein represent lower bound estimate and that the

selection of a representative value should be done by careful examination of the shear-distortion curves.

For G'_{STIFF}/ G', the WB designs exhibited negligible values. For NS designs, the NS-152 results were smaller compared to the NS-305 ones. In the 152 mm c/c arrangement, the behaviour is more influenced by the screws, which represented a larger proportion of connections at sidelaps. At the end of the test, the screws in the 152 mm c/c specimen were completely fallen out so the ratios tend to be smaller. In the NS-305 specimens, the behaviour was more affected by nails and, in general, at the end of the test, the nails are more active than the screws and larger ratios were obtained.

Based on the parameters presented in this section, the sheet steel thickness was found not to have influenced the hysteretic capabilities for screw-nail designs. This was observed for all parameters. This result is not in line with the observations documented by Essa *et al.*: "Comparing tests 7 and 18 (with Hilti nails and screwed sidelaps) indicates that increasing the deck thickness from 0.76 mm to 0.91 mm (i.e. increasing the deck material by only 20%) results in a remarkable improvement in the energy dissipation capability of about 50%." It has to be mentioned that Essa *et al.* did not normalise energy values with the maximum load reached and the cumulated displacement, hence different conclusions were drawn. Table 5.47 presents the dissipated energy results based on the approach used by Essa *et al.* for 6 screw-nail dynamic tests of the present study. The energy units are kN/ m x rad/1000. The ratios of the energy dissipated for the 0.91 mm sheet steel thickness in comparison with the 0.76 mm sheet steel are also given.

Table 5.47 Comparison of the energy dissipated in screw-nail designs with 0.91 mm and 0.76 mm sheet steel thickness

Sheet steel nominal thickness	0.91 mm	0.76 mm	Ratio 0.91/0.76
Test no.	38-91-6-NS-SD-34	38-76-6-NS-SD-28	
Energy dissipated	829.3	722.6	1.15
Test no.	38-91-6-NS-LD-35	38-76-6-NS-LD-29	
Energy dissipated	1592.9	1240.9	1.28
Test no.	38-91-6-NS-SD-33	38-76-6-SD-31	
Energy dissipated	1122.4	997.9	1.12

The ratios of the energy dissipated (not normalised) for the 0.91 mm with regard to the 0.76 mm sheet steel thickness are all greater than 1.0, but are lower than the ratio of 1.50 that Essa *et al.* found. This cannot be directly explained by the ratio of the actual thickness and ultimate capacity of the sheet steel used in the studies, even though diaphragm energy dissipation capacities are deemed related to these properties. In Essa *et al.*, the ratio of thickness and ultimate strength (Eqn. 5-3) is 1.25 whereas in this study, the ratio is equal to 1.51.

$$\frac{t \times F_u(0.91\,mm\ sheet)}{t \times F_u(0.76\,mm\ sheet)} \qquad (5\text{-}3)$$

Based on these values, a higher dissipated energy ratio would have been expected in the present study as opposed to what was observed. However, the energy is not only related to t and Fu, which are strength related parameters. The imposed displacement also influences the amount of energy dissipated (energy = integral of force x displacement). In the tests by Essa *et al.*, the amplitude in the large displacement cycles (those in which a high proportion of the energy was dissipated) were a multiplier of delta 2 (1.0, 1.5 and 2 times delta 2). The ratio of delta 2 0.91 mm to delta 2 0.76 mm = 33/25= 1.32. This

factor, combined with the t and Fu ratios, must have contributed to the energy ratio of 1.50. In this study, the amplitude of the large amplitude cycles was nearly the same for both steel thicknesses as these amplitudes were obtained by adding constant γ_p values to slightly different values of γ_u (only γ_u was varying with t). This resulted in a relatively lower demand imposed on the 0.91 mm specimen.

5.9.3 Performance of the diaphragms under the LD protocol

Table 5.48 presents the parameters for the LD loading protocol. It should be mentioned that no LD loading protocol was performed with the WB deck assembly. It was deemed that performing a LD loading protocol on a WB deck assembly was not relevant since this deck assembly was not able to sustain the demand for Victoria R_d= 2.0 and R_d= 3.0.

Table 5.48 Parameters for the LD cyclic tests

Test no.	Reference distortion used (rad/1000)		S_i/S_{ULD}		Strength degradation Cycles at $(\gamma_u + \gamma_2)/2$				$E_H/(S_{ULD} \cdot \Sigma(\Delta\gamma))$	Energy dissipation comparison ratio				
												Cycles at $(\gamma_u + \gamma_2)/2$		
	γ_u	γ_2	1st half	2nd half	S1/S_{ULD}	S2/S1	S3/S1	S4/S1	1st half	2nd half/1st half	5th seg./2nd seg.	EH2/EH1	EH3/EH1	EH4/EH1
24 (1)	6.08	8.64	1.00	0.68	0.70	0.58	0.70	0.32	0.075	0.69	0.75	0.49	0.70	0.33
27	4.69	6.67	1.00	0.69	0.67	0.45	0.56	0.36	0.050	0.85	0.69	0.64	0.68	0.59
35	3.23	6.60	1.00	0.77	0.82	0.59	0.63	0.49	0.088	0.86	0.77	0.66	0.67	0.63
29	3.55	5.04	1.00	0.70	0.71	0.48	0.51	0.35	0.084	0.80	0.76	0.82	0.80	0.80

(1): In tests 21, 23 and 24, the loading references were not evaluated as intended.

Test no.	Deck assembly type
24	W'W
27	NW
35	NS
29	NS

Table 5.48 Parameters for the LD cyclic tests (continued)

Test no.	Reference distortion used (rad/1000)		G'_i/G' at zero displacement		P_W/S_{ULD}		G'_{STIFF}/G'	G'_{SECANT}/G'	Additional loop		
									S_{ADD}/S_{ULD}	$G'_{STIFF\,ADD}/G'$	
	γ_u	γ_2	1st half	2nd half	1st half	2nd half	2nd half	2nd half			
24 (1)	6.08	8.64	0.46	0.18	0.03	0.02	0.60	0.61	0.35	0.25	
27	4.69	6.67	0.20	0.25	0.04	0.03	0.77	0.56	0.76	0.67	
35	3.23	6.60	0.08	0.06	0.05	0.05	0.80	0.49	1.00	0.60	
29	3.55	5.04	0.14	0.10	0.04	0.04	0.72	0.58	0.84	0.57	

(1): In tests 21, 23 and 24, the loading references were not evaluated as intended.

Test no.	Deck assembly type
24	WW
27	NW
35	NS
29	NS

For the $S_i/S_{U,LD}$ ratios, similar values were found in all tests. The maximum loads all occurred in the 2nd segment of the signal (1st set of peaks at $2\gamma_u$).

For the strength degradation parameters obtained from cycles at $(\gamma_u+\gamma_2)/2$, the following observations could be made. The $S_{U,LD}$ values were obtained in the first excursion at $2\gamma_u$, which are the largest in the protocol. From the ratio S2/S1, we can see that there was degradation in the largest excursion at $2\gamma_u$, even if in some cases the actuator was not able to push as far as intended. From the ratio S3/S1, we can see there was no degradation between set 2 and set 3 of cycles at $(\gamma_u+\gamma_2)/2$, as the cycles at $0.4\gamma_u$ had a negligible influence on the specimen properties. For S2/S1, S3/S1 and S4/S1, the NS-305 had better results than NW and NS-152. W'W had similar results than NS-305, however these results were not representative since there was an error in the evaluation of the loading references for W'W.

$E_H/ (S_{U,LD} . \Sigma (\Delta\gamma))$ was given only for the 1st half of the loading protocol. For the 2nd half, a ratio of the energy dissipation of the 2nd half compared with the 1st half was given. From this ratio, we can see that W'W was more deteriorated compared to NW and NS.

The ratios of G'i/G' for the NW designs in the 1st and 2nd halves of the loading protocol were higher compared to the NS designs. As observed for the SD protocol, the difference is mainly due to the more severely pinched response of the NS specimens.

All of the $P_W/S_{U,LD}$ ratios were between 0.02 and 0.05. As said previously, these are lower bound values and the reader is invited to look at the hysteretic curves to found a more representative value.

In the additional loop, NS performed much better than welded designs for strength but were similar for stiffness. NS-305 seemed to be better (because lower demand on the fasteners due to larger elastic deformations).

5.9.4 Comparison between SD and LD protocols

The degradation in SD and LD loading protocols can be compared. LD tests nos. 24, 27, 35, and 29 are related to SD tests nos. 23, 26, 34, and 28, respectively. Tests 23 and 24 are less representative as they were not loaded with the correct values. Their values are then given in ( ).

LD was developed for structures located in the West with $R_d = 3.0$ and, hence, will then be compared to the entire SD loading protocol (Segment III), which applies to the same conditions. LD has a much larger number of cycles: total of 134, compared to 44 in SD. The amplitude of the largest cycles for LD was smaller: 2.0 γ_u for LD vs γ_u + 10 rad/1000 for SD. For the four specimens tested under the LD protocol, γ_u varied between 3.23 to 6.08 rad/1000. Hence, the peak amplitudes imposed in the LD protocol varied between 6.46 and 12.2 compared to 13.2 to 16.1 rad/1000 for the SD protocol (between 2.04 and 1.31 times larger). More important, in the LD tests, the applied peak deformation exceeded γ_2 in three tests only, by 2.06 to 3.52 rad/1000. Under the SD protocol, γ_2 was exceeded in all four tests by a deformation varying from 6.63 to 8.51 rad/1000. Thus, there is much more severe inelastic demand imposed during the SD protocol.

We can first compare the peak value reached in both tests to see if the small amplitude cycles applied prior to reaching S_U had a different impact: the ratio $S_{U,\,LD}/S_{U,\,SD}$ varies from 0.96 to 1.02 (0.96). Thus, there is no significant difference.

For strength degradation, we can examine $S_i/S_{U, LD}$ for the LD protocol. For the second half of the signal, this value varies between 0.69 and 0.77 (0.68). For the SD protocol, we can look at the ratio of $S_{U, RUN\ 2}$ / $S_{U, RUN\ 1}$ as a comparison. This value varies from 0.58 to 0.64 (0.34). Thus, SD is slightly more critical.

For stiffness, we can look at the G'_i/ G' ratio. For the LD protocol, the ratios in the second half for the four tests are 0.25, 0.06, and 0.10 (0.18), compared to 0.31, 0.01, and 0.08 (0.07) for the SD protocol. Thus SD is generally more critical.

The G'_{STIFF}/ G' ratios for the second half of the LD protocol vary from 0.72 to 0.80 (0.60), compared to 0.55 to 0.59 (0.34) for the SD protocol. Thus SD is slightly more critical.

The G'_{SECANT}/ G' ratios vary from 0.49 to 0.58 (0.61) for the second half of the LD loading history, compared to 0.19 to 0.34 (0.24) for the SD protocol. Thus SD is more critical.

Overall, the diaphragms can develop the same maximum capacity under both signals and the two loading histories produced a comparable level of strength and stiffness degradations. The SD loading protocol was slightly more critical than the LD protocol.

5.10 CONCLUSIONS AND RECOMMENDATIONS

Conclusions and recommendations for this chapter are presented in this section. Remarks are made on the test procedure and on the performance and design recommendations applicable to each deck assembly type (WB, W'W, NW and NS).

The design recommendations are made for western Canada and are applicable for both intra-plate and inter-plate seismic ground motions. The demand on diaphragms in eastern Canada was found to be less severe and design requirements could have been relaxed. However, this possibility was not considered herein. In addition, these design recommendations are valid for diaphragms for which the frame fasteners are spaced at every other rib in the direction perpendicular to the flutes, thus allowing deck warping deformation to take place. Higher inelastic demand is anticipated in the connections of diaphragms with more closely spaced fasteners and this aspect must be examined further before expanding the range of application of these recommendations to deck systems with closer fastener spacing.

5.10.1 Test procedure

The test frame set-up was adequate in its ability to distribute the applied displacements to the diaphragm panels. However, the actuator had difficulties in reaching the required imposed displacements for the long duration (LD) loading protocols due to an insufficient supply of hydraulic oil.

It was important to use dynamic tests instead of slow cyclic tests since the distribution of forces among fasteners and the strain-rate effects on material properties are influenced

by the rate of deformation. However, the dynamic tests did not allow for detailed observation of the sequence of failures in the fasteners and deck. Overall, no special effects that could have been attributed to dynamic effects, such as out-of-plane vibration of the deck between the joists or near the end fasteners due to local warping deformations, were observed. However, it is recommended that future tests be also carried out dynamically to better represent the effect of an earthquake.

The method used for measuring sidelap slip, in which two independent LVDT's per sidelap were mounted on the frame below the deck and an angle was fixed under the deck panel at each LVDT, was reliable.

The four deck panels placed over the test frame produced an undesirable behaviour. In most cases, the slips were forced at sidelaps 1,2 and 3,4, which are located beside the more rigid side connections to the North and South members of the test frame. It would be possible to diminish this effect by using edge panels that are half of the width of normal deck panels. Overall, five sheets would be installed, 3 regular panels and 2 half panels. This would work better since the 5 sidelaps would have similar stiffness and therefore they would experience similar slippage.

5.10.2 Button punch-weld design (WB)

Weld failures were observed below γ_u. The quality of welds at sidelap locations was questionable due to the oval shape of the interlock edge of the standard deck panels. At sidelaps, two types of connectors were found: welds and button punches. The fasteners were not compatible since the button punches are flexible compared with the welds. Furthermore, the more rigid welds are fragile whereas the flexible button punches are ductile. When the welds fail, all of the force in the sidelap is transferred to the button punches, which are not able to sustain the load.

From the test results, it is recommended that the system should remain elastic under seismic loading, i.e. $R_d = 1.0$ should be used in design. With regard to the overstrength related force modification factor, $R_o = R_\phi \cdot R_{yield} \cdot R_{sh} \cdot R_{size} \cdot R_{mech}$, it is believed that a value of $R_\phi = 1/\phi$ would be too high because the system is not ductile, as degradation in stiffness and shear capacity was observed at γ_u. In addition, there was an extensive variability in the fastener quality which means that it will be difficult to accurately predict the behaviour in terms of capacity, stiffness, etc. At this time, it is also proposed to adopt $R_{yield} = R_{size} = 1.0$ due to the lack of data on the actual properties of as-built metal deck diaphragms, and the analyses and tests confirmed that the parameters R_{sh} and R_{mech} must also be taken equal to 1.0. This is applicable to all diaphragms studied herein.

Given that a degradation in shear strength was observed in the 200 cycles at $0.6\gamma_u$ (test 36) and at γ_u in test 20, an intermediate measure in which R_d and R_o are equal to 1.0 would have to be used. To justify a higher value of R_o for use with R_d=1.0, a new loading protocol would be required. Additional tests of button punch – weld diaphragms with loading protocols in load-control would have to be made. The loading protocols would be based on building analyses with $R_d = 1.0$ and R_o which could vary between 1.0 and a desired value around 1.3. The stiffness and strength degradation under these loading protocols would have to be analysed and judgement would have to be made on the results to accept a higher R_o value.

The cause behind the strength degradation observed at $0.6\gamma_u$ should be examined further. Given the results obtained from the pseudo fatigue test that was carried out it is possible that repeated wind loading could affect the value of R_o used in design.

5.10.3 Weld with washer-weld with washer design (W'W)

The W'W design resulted in the highest shear strength for all of the diaphragm deck assemblies that were tested. The quality of fasteners was improved in comparison with the WB system connections. However, the behaviour of the W'W diaphragm had a limited ductility since the γ_u and γ_2 values were close and a steep degradation in shear capacity was observed beyond the peak load due to sudden weld failures or local buckling of the deck adjacent to the fasteners.

As discussed for the WB system, an overstrength related force modification factor equal to R_ϕ is recommended. This time, the parameter R_ϕ equal to $1/\phi$ could be used since the fastener properties were more reliable compared to the WB system and no failure was observed prior γ_2. A ductility related force modification factor, R_d, equal to 1.5 would be acceptable as γ_u and γ_2 were close and a steep degradation was observed beyond the peak load. Because of its high strength, this diaphragm design is suitable for regions of applications with high seismic loads. The designers must be warned, however, that proper weld quality along the sidelaps will require particular attention and skilled workmanship.

5.10.4 Weld with washer-nail design (NW)

In the diaphragms studied, the shear strength of the welded sidelap connections was comparable to that of the nailed connections along the North and South perimeter members of the test frame. In one case, inelastic response developed at the sidelaps, likely due to presence of weaker welds. For the two remaining specimens, the edge connections were the weaker link and the whole diaphragm responded as a single sheet

element. In this case, inelastic deformations were observed at nailed fasteners, which is a desirable failure mode. However, the bearing failures perpendicular to the flutes at the sheet ends, which are associated with such single-sheet behaviour, were not desirable. The single-sheet mode in a real building would result in deformations that would be too large at the diaphragm perimeter.

For this diaphragm system, observation of the two response modes suggest that inelastic response can be directed to the sidelaps by using a proper balance of strength in design between the sidelaps and the connections along the edge members. In this case, the seismic behaviour will become similar to that of the W'W design, i.e., controlled by the limited ductility response of the sidelap welds, and the same values of R_o and R_d would then apply.

Similarly to the W'W design, acceptable response of the NW system is dependant upon good quality welding.

5.10.5 Screw-nail design (NS)

Due to the behaviour of nail and screw connectors under shear loading, pinching occurred in the overall diaphragm load vs. displacement hysteresis, although the degradation in shear capacity was progressive. As a positive observation the deck fasteners (screws and nails) were highly reliable and do not require a high degree of operator skill for proper installation.

An overstrength related force modification factor, R_o, equal to $1/\phi$ could be used. As a minimum, a ductility related factor, R_d, equal to 2.0 could be taken. If the problem with pinching is resolved, an R_d equal to 3.0 could be employed. However, the analyses performed in this study indicated that the inelastic demand can increase rapidly when

using R_d = 3.0 is used in design in lieu of R_d = 2.0. Considering that only a limited number of analyses have been performed on simple, symmetric buildings, it is recommended that prior to obtaining a more thorough understanding of the effect of pinching on the seismic diaphragm performance, an intermediate measure with R_d equal to 2.0 be taken.

For the nail-screw designs, it was found that the sheet steel thickness had no influence on the hysteretic behaviour. As the spacing of the fasteners is reduced, however, the inelastic demand on the fasteners tend to increase and the behaviour becomes more dependant on the screw fasteners, i.e., with a more severely pinched hysteretic response. A sidelap fastener, which is not as susceptible to tilting as screws and that is less prone to disconnect, could be investigated to obtain a diaphragm behaviour which would exhibit less pinching.

CHAPTER 6

CONCLUSIONS AND RECOMMENDATIONS

6.1 SUMMARY

In this study, an evaluation of the inelastic response of steel roof deck diaphragms under simulated dynamically applied seismic loading was carried out. More specifically, the objectives were to evaluate the seismic demand on diaphragms designed to respond in the inelastic range, and to examine the response of various diaphragm designs subjected to that demand. Another objective was to recommend minimum design strength levels for the diaphragm systems that were studied. The conclusions are presented in three sections: building analysis, loading protocols, and diaphragm tests. Further, recommendations are proposed regarding the design approach, the analytical modelling, and for future experimental tests.

6.2 BUILDING ANALYSIS

An analytical study was performed to evaluate the inelastic demand on metal roof deck diaphragms of single-storey steel buildings in which the diaphragm is selected as the main energy dissipating element. The structures were designed according to the upcoming NBCC 2004 provisions and the CSA S16-2001 steel design standard with tentative R_d values of 2.0 and 3.0, with deck panels having screwed sidelap and nailed frame fasteners. Two different seismic regions of Canada were considered: Eastern (Quebec City, QC) and Western (Victoria, BC) and ensembles of ground motions were selected for the analysis for each site. For the Victoria site, the hazard from Cascadia subduction earthquakes was also considered separately. In addition, the seismic demand

on buildings with deck diaphragms that contain button punched sidelap and welded frame fasteners was studied. For this particular case, the design was carried out according to the current NBCC 1995 requirements which allow for the steel roof deck diaphragm to be unknowingly detailed as the weak element in the lateral load path. A system with ductile braced frames was used, allowing the use of a force modification factor, R, equal to 3.0. Nonlinear time step analyses of all structures were performed using the Ruaumoko program (Carr, 2000). The main findings from these analyses are presented in two parts: the observations for the screw-nail design with NBCC 2004 and the button punch-weld design with NBCC 1995.

NBCC 2004 designs:

For all models, the maximum dynamic deflection was smaller than the deflection found from the conventional design method, in which the building is uniformly loaded with the base shear force and the deflection multiplied by R_dR_o. In all cases, the maximum lateral deflection also met the NBCC lateral drift limit of 2.5% of the storey height. The results indicated that the buildings in Quebec experienced smaller deflections than in the West, mostly because these structures had significant reserve strength and stiffness due to design requirements. In addition, it is believed that the main periods of the ground motions were lower than the fundamental periods of the buildings, thus contributing to the smaller deflections that were obtained in the East.

Under intra-plate earthquakes, the buildings located in Victoria experienced peak inelastic shear deformations of up to 6.1 and 10.8 rad/1000 for R_d = 2.0 and 3.0, respectively. Typically, the roof deck panels that yielded most were located adjacent to the building end walls. This level of inelastic shear distortions is below or compares well with the acceptable range of 10 rad/1000 determined by Essa *et al.* (2001) for the screw-nail design. This allowable range was defined to ensure that the shear strength level of the diaphragm under cyclic loading does not degrade below 80% of the peak resistance.

Roof diaphragms of the structures located in Quebec City were not subjected to inelastic deformations. For Victoria, the Cascadia records produced less demand than intra-plate earthquakes in terms of distortion amplitudes. However, the Cascadia ground motions were of much longer duration in comparison to intra-plate earthquakes, and hence the total number of cycles was greater.

For all three cases, the observed performance indicated that the values of R_d that had been selected for design were feasible. The analyses for intra-plate earthquakes in Victoria showed, however, that the diaphragm inelastic shear distortion, γ_p, was not proportional to the seismic force modification factor, R_d, used in design. For instance, the level of inelastic demand did not seem to agree with the predictions based on the equal displacement principle, the demand increasing more rapidly than expected when an R_d factor of 3.0 was used instead of $R_d = 2.0$.

For the button punch-weld deck assemblies designed according to current 1995 provisions, inelastic deformations, γ_p, of up to 9.8 rad/1000 were computed and tests by Essa *et al.* showed that this deck system cannot sustain inelastic deformations. Hence, extensive damage with possible loss of structural integrity can be anticipated for this system under a major earthquake.

6.3 LOADING PROTOCOLS

Loading histories were developed such that the diaphragm demand obtained from the analytical investigation of this project could be imposed on the deck panel test specimens. A statistical analysis of the time histories was performed in order to evaluate the demand and two loading protocols were developed.

For intra-plate earthquakes, it was found that the buildings located in Victoria and designed with $R_d = 3.0$ experienced the greatest demand, followed by Victoria $R_d = 2.0$ and Quebec with $R_d = 3.0$. The demand for buildings in Quebec with $R_d = 2.0$ was too small and therefore was not considered. Also, it was observed that the demand for the button punch-weld deck assemblies for Victoria with R = 3.0 was similar to the screw-nail connection case for Victoria $R_d = 3.0$. However, for Cascadia earthquakes, it was found that the demand was completely different than that obtained for intra-plate earthquakes. The number of cycles under Cascadia earthquakes was much larger than under intra-plate earthquakes, whereas the level of distortion tended to be lower.

A statistical analysis was performed to obtain representative values of the demand parameters (distortion amplitudes, number of cycles, etc) under the different ground motions. From these results and visual inspections of the diaphragm deformation time histories, two loading protocols were developed: the short duration (SD) and the long duration (LD). The SD loading protocol applies to both the screw-nail deck designs and the button punch-weld deck assemblies. It includes three segments that are arranged sequentially to represent the cumulative demand on structures, i.e. respectively, in Quebec with $R_d = 3.0$, in Victoria with $R_d = 2.0$, and in Victoria with $R_d = 3.0$. The LD loading protocol was representative of the demand on structures located in Victoria and designed with an R_d of 3.0 when subjected to ground motions produced by Cascadia subduction earthquakes.

6.4 DIAPHRAGM TESTS

A total of 19 full-scale tests were performed on 3.6 m x 6.1 m diaphragm specimens that were made of four 6.1 m long x 914 mm wide deck sheets. A cantilever test frame with pinned connections at each corner and intermediate joists spaced at 1524 mm was used. A dynamic high capacity (1.5 MN) actuator was incorporated to apply realistic dynamic loading. Four different combinations of sidelap and frame fasteners were studied: button

punched sidelap with standard welded (no washer) frame connections (WB design), 16 mm diameter welds reinforced by a 3 mm thick circular washers for both the sidelap and frame connections (W'W design), the 16 mm welds with 3 mm thick washers for the sidelaps with Hilti X-EDNK22-THQ12 nails (NW design), and no.12 Hilti self-drilling screws with the same nailed deck-to-frame connectors (NS design).

For all systems, the thickness of the steel deck was 0.91 mm but deck diaphragms made of 0.76 sheet steel were also studied for the NS and WB systems. The spacing of the fasteners was 305 mm in all tests except that tests on the NS system were also performed with fasteners spaced at 152 mm. The diaphragms were subjected to monotonic or seismic loading. An additional monotonic test was performed on a NS diaphragm specimen. A weld-button punch (WB) diaphragm was subjected to low amplitude cycles prior to applying the seismic loading protocol in order to examine possible degradation of the structural properties due to wind loading over time prior to the occurrence of an earthquake.

The response of diaphragms was dominated by the connection behaviour. The WB assemblies exhibited a non-ductile behaviour and damage below γ_u. Under the short duration (SD) loading protocol, strength degradation started in the East R_d = 3.0 segment, after brittle failure occurred in the sidelap welds at joists, indicating very limited inelastic capability for this deck system. Complete sidelap separation occurred before the end of the West R_d = 2.0 segment.

The W'W deck assemblies had higher strength in comparison to other deck assembly types. However, its shear strength degraded significantly and rapidly after peak load was reached due to weld failure at sidelaps. Failure at sidelaps involved a non-ductile bond failure between the sheet metal and weld and/or local buckling of the sheet steel near the welds. Under the SD loading protocol, the connections remained nearly intact up to the

West R_d = 2.0 segment and strength degradation was observed in the West R_d = 3.0 segment.

In the seismic tests, the NW system developed a single-sheet mode behaviour in which the overall diaphragm acted as one piece with inelastic deformations developing only at the edges. This behaviour was ductile since it involved bearing of the sheet steel against the nails at the perimeter. However, it resulted in large inelastic demand along the edges. In the West R_d = 3.0 segment of the SD loading protocol, hole elongation extended into the deck webs in the direction perpendicular to the flutes, which resulted in the loss of structural integrity of these connectors. The behaviour was different in the monotonic test as failure occurred at sidelaps. This failure mode was not as ductile as it involved failures of welded with washer sidelap connections. The location of the inelastic demand depended upon the relative strength of the interior sidelaps versus the outer edge joints.

The NS design exhibited a ductile behaviour with pinching. The inelastic response essentially took place along the interior sidelap joints through tilting of the screws and bearing deformation of the sheet steel against the nails at the joists. In the West R_d =3.0 segment of the SD loading protocol, the deformation mode resulted in a severely pinched hysteretic response.

With the increase of the sheet steel thickness, the shear capacity of deck assemblies reached higher values. With the reduction of the fastener spacing, thus when increasing the number of connectors, the warping deformations were constrained. This produced a higher strength and stiffness but forced earlier and higher deformation demand on the fasteners at the sidelaps. Finally, the effect of the Cascadia earthquakes simulated by the LD loading protocol was different than intra-plate earthquakes simulated by the SD protocol. Both types of earthquakes had a similar impact, however the SD protocol had a slightly more detrimental effect on the deck assemblies in terms of damage and capacity reduction.

Values for the ductility related and overstrength related force modification factors, R_d and R_o, were established for each diaphragm system based on the results of the analytical program and the test program. They are presented in Section 6.5 Recommendations.

Dynamic tests were assumed to be more representative of the seismic demand in comparison with the slow reversed cyclic tests. However, in this test series, no dynamic effects such as out-of-plane vibrations between the joists or near the end fasteners due to local warping were noticed.

6.5 RECOMMENDATIONS

General recommendations have been provided for future studies which include: future field studies, improved analytical models and analyses, and future experimental tests. Thereafter, intermediate design recommendations are presented. These design recommendations need to be verified against improved analytical models and new testing that are presented together with the design recommendations.

6.5.1 Future studies

6.5.1.1 Future field studies

Field data on the dynamic properties (period, damping, etc) of low-rise steel buildings need to be collected. The demand levels obtained in this study depend heavily on assumed structural and dynamic properties and it is critical that these assumptions be verified.

6.5.1.2 Improved analytical models and analyses

Based on the test data generated in this study, hysteretic models could be improved to better represent the behaviour of each fastener-deck assembly, and hence, the assessment of the demand on diaphragms could be refined. The analytical study for eastern Canada could be extended to confirm that no inelastic demand is present in steel roof deck diaphragms. This could allow for a relaxation of the design recommendations. Additional analyses should be performed on a broader sampling of buildings for both eastern and western Canada to ensure that the findings are adequate for various types of structures: dimensions, shapes, location of bracing bents, variation of diaphragm properties over the roof area, non symmetrical buildings, etc. In addition, P-delta effects were neglected in the analysis and need to be taken into account.

6.5.1.3 Future experimental tests

The effects of non-structural elements (insulation, membrane, etc) on the diaphragm hysteretic behaviour (stiffness, resistance, degradation, etc) should be investigated. This could be done in parallel with field measurements. Additional diaphragm designs could be examined to produce enhanced seismic response. In addition, the influence of overlapping panel end joints and openings in the diaphragm need to be investigated. Moreover, the effect of fatigue loading prior to an earthquake needs to be studied under a load-control protocol.

The definition of γ_u used in this study for developing the loading protocols was based on an experimental value of G' and a theoretical value of S_u ($S_{u,\ SDI*}$). This led to some difficulty in the interpretation of the results. It would be preferable to have γ_u based on experimental values only, so that the specimens would be loaded according to their actual capacity.

The force path in the test frame is not truly representative of the force path present in the roof diaphragm of a real building subjected to an earthquake. Under ground motions, the inertia forces would develop in the roof deck diaphragm due to the mass of the diaphragm and the roofing material, and would then reach the frame via the fasteners. In the test program, the forces were applied to the frame by an actuator and then transmitted to the deck diaphragm. It is believed that what was learned in this study is still valid and applicable to the design of these buildings and is useful towards a better understanding of their seismic behaviour. However, a study investigating the effects of dynamic loads applied as real inertia forces should be performed.

6.5.2 Preliminary design recommendations and further related studies

Intermediate design recommendations were determined based on the analysis results and the response observed in tests. The recommendations were developed for western Canada and are applicable to both intra-plate and inter-plate ground motions. Some of the design requirements could probably be relaxed for eastern Canada, however this will be left for future studies. It is believed that further analytical studies on the response under eastern earthquakes should be performed before applying more permissive design recommendations for the east. In addition, these design recommendations are valid for diaphragms for which the frame fasteners are spaced at every other rib in the direction perpendicular to the flutes, thus allowing deck warping deformation to take place. Higher inelastic demand is anticipated in the connections of diaphragms with more closely spaced fasteners and this aspect must be examined further before expanding the range of application of these recommendations to deck systems with closer fastener spacing.

6.5.2.1 Button punch-weld (WB) design

It is recommended that the system be designed to remain elastic under seismic loading, i.e. R_d = 1.0 should be used in design. With regards to the overstrength related force modification factor, it is deemed that using R_o= 1/ϕ would not be adequate because the system is not ductile, as degradation in stiffness and shear capacity was observed at cyclic deformations with an amplitude of γ_u. In addition, both the sidelap and deck-to-frame connections are prone to a significant variability, which means that it would be difficult to accurately predict the behaviour in terms of ultimate capacity, stiffness, etc. Such variability can result in a concentration of the inelastic demand and complete failure at a localised position in a roof diaphragm, which would lead to a loss of the integrity of the lateral load resisting system. Thus, a value of 1.0 is suggested for R_o. This value could be increased if justified by further analytical and experimental studies. In order to better control the applied demand level on this diaphragm system, it is recommended that future tests be performed under load control instead of displacement control below γ_u.

6.5.2.2 Weld with washer-weld with washer (W'W) design

An overstrength related force modification factor, R_o, equal to 1/ϕ can be used for this system as the fastener properties were found to be more reliable compared to the button punch-weld system and no failure was observed prior to γ_2. This system is permitted for a weak-diaphragm design provided that the outer edge connections are stronger than the interior sidelaps such that inelastic response be distributed in the interior sidelaps and does not concentrate at the diaphragm edges. Although this system performed well under deformations corresponding to R_d = 2.0 in the seismic test, a ductility related force modification factor, R_d, equal to 1.5 is recommended. This R_d factor is considered appropriate because deformations γ_u and γ_2 were close, and in addition a steep

degradation was observed in shear capacity beyond the peak load due to the failure mode with limited ductility associated with welded sidelaps.

The test results are, however, directly related to the imposed demand that was obtained in the analysis assuming a screw-nail diaphragm model. Therefore, it would be appropriate to revise the demand based on a new hysteretic model adapted to represent the behaviour of the W'W deck assembly. Overall, this system exhibited a very high capacity and would be most appropriate in buildings located in high seismic regions with weak brace designs.

6.5.2.3 Weld with washer-nail (NW) design

For this system, there is also a limit on the ratio of sidelap to frame fastener strength that must be adhered to such that inelastic behaviour takes place at the interior sidelaps and not at the diaphragm edges. NW diaphragms so-designed would behave in a similar manner to the W'W system and, hence, a ductility related force modification factor, R_d, of 1.5 and an overstrength related factor, R_o, of $1/\phi$ are recommended.

6.5.2.4 Screw-nail (NS) design

An overstrength related force modification factor, R_o, equal to $1/\phi$ can be used in view of the reliability of mechanical fasteners. Considering the severe hysteretic pinching that was observed at deformation levels expected when using $R_d = 3.0$, it is recommended that a ductility related factor, R_d, equal to 2.0 be used for a weak-design diaphragm of this type. This value could be increased if it can be demonstrated by further analysis that pinching has no detrimental effect on the building response or if sidelap connectors with enhanced inelastic cyclic response are used. Again, provisions must be made for this system to ensure inelastic response will develop first in the interior sidelap joints.

REFERENCES

ADAMS, J., WEICHERT, D., HALCHUK, S. (1999). Trial Seismic Hazard Maps of Canada – 1999: 2%/50 Year Values for Selected Canadian Cities, Geological Survey of Canada Open File 3724. National Earthquake Hazards Program. Geological Survey of Canada, Natural Resources Canada, Ottawa, Ont.

AMERICAN IRON AND STEEL INSTITUTE (1996). Cold-Formed Steel Design Manual 1996 Edition. Washington, DC, USA.

AMERICAN IRON AND STEEL INSTITUTE (1997). 1996 Edition of the Specification for the Design of Cold-Formed Steel Structural Members. Washington, DC, USA.

AMERICAN SOCIETY FOR TESTING AND MATERIALS (2002). A370 Standard Test Methods and Definitions for Mechanical Testing of Steel Products. Philadelphia, PA, USA.

AMERICAN SOCIETY FOR TESTING AND MATERIALS (2002). A653 Standard Specifications for Steel Sheet, Zinc-Coated (Galvanized) or Zinc-Iron Alloy-Coated (Galvannealed) by the Hot-Dip Process. Philadelphia, PA, USA.

APPLIED TECHNOLOGY COUNCIL, ATC (1992). ATC24 – Guidelines for Cyclic Seismic Testing of Components of Steel Structures. Redwood City, CA, USA.

BEAULIEU, D., BRINDAMOUR, A. (1984). Étude des méthodes de calcul et des problèmes de fixations pour les diaphragmes métalliques. Université Laval, Québec, QC, Canada.

BERAIR, T. (1999). Étude expérimentale sur le comportement sismique de bâtiments d'un seul étage en acier avec diaphragme de toit flexible. École Polytechnique de Montréal, Montréal, QC, Canada.

BOND, W.F., ROGERS, C.A., TREMBLAY, R. (2001). Seismic Performance of Arc-Spot Weld Deck-to-Frame Connections. Proc. Third International Conference on Thin-Walled Structures, Cracow, Poland, 357-364.

BOUATAY, N. (2001). Étude du comportement sismique des contreventements ductiles en chevron munis de fusibles. École Polytechnique de Montréal, Montréal, QC, Canada.

BRUNEAU, M., UANG, C.-M., WHITTAKER, A. (1998). Ductile Design of Steel Structures. McGraw-Hill, New York, NY, USA.

BSSC (1997). NEHRP Guidelines for the Seismic Rehabilitation of Buildings. Federal Emergency Management Agency Report FEMA 273, Building Seismic Safety Council, Washington, DC, USA.

BSSC (1997). NEHRP Recommended Provisions for Seismic Regulations for New Buildings and Other Structures. Federal Emergency Management Agency Report FEMA 302, Building Seismic Safety Council, Washington, DC, USA.

CANADIAN NATIONAL COMMITTEE ON EARTHQUAKE ENGINEERING, CANCEE (2001). NBCC (2004) Part 4.1.9 – Markup by Task Group Chair Meeting, April 11-12, 2001.

CANADIAN STANDARDS ASSOCIATION, CSA (1992). CAN/CSA-G40.20/G40.21-92 General Requirements for Rolled or Welded Structural Quality Steel/Structural Quality Steels. Etobicoke, Ont., Canada.

CANADIAN STANDARDS ASSOCIATION, CSA (1994). CAN/CSA-S136 Cold Formed Steel Structural Members. Etobicoke, Ont., Canada.

CANADIAN STANDARDS ASSOCIATION, CSA (1994). CAN/CSA-S16.1 Limit States Design of Steel Structures. Etobicoke, Ont., Canada.

CANADIAN STANDARDS ASSOCIATION, CSA (2001). CAN/CSA-S16 Limit States Design of Steel Structures, Letter ballot no.48. Etobicoke, Ont., Canada

CANADIAN SHEET STEEL BUILDING INSTITUTE, CSSBI (1991). Design of Steel Deck Diaphragms. B13-91, Cambridge, Ont., Canada.

CARR, A.J. (2000). RUAUMOKO – Inelastic dynamic analysis, Version March 15th 2000. Dept. of Civil Eng., University of Canterbury, Christchurch, New Zealand.

CECM (1977). Convention Européenne de la Construction Métallique, The Stressed Skin Design of Steel Structures. Recommendations for Steel Construction. CECM-TC7.

CHOPRA, A.K. (2000). Dynamics of Structures: theory and applications to earthquake engineering. Prentice-Hall Inc., Upper Saddle River, NJ, USA.

DAVIES, J.M., BRYAN, E.R. (1982). Manual of Stressed Skin Diaphragm Design. John Wiley and Sons Inc., New York, NY, USA.

DE MATTEIS, G. (1998). The effect of cladding panels in steel buildings under seismic actions. Dottorato di Ricerca in Ingegneria delle Strutture, Facoltà di Ingegneria, Università degli Studi di Napoli Federico II, Napoli, Italia.

ESSA, H.S., TREMBLAY, R., ROGERS, C.A. (2001). Inelastic seismic behaviour of steel deck roof diaphragms under quasi-static cyclic loading. Report no. EPM/CGS-2001-11. Department of Civil, Geological and Mining Engineering, École Polytechnique de Montréal, Montréal, QC, Canada.

FLEISCHMAN, R.B., FARROW, K.T. (2001). Dynamic behavior of perimeter lateral-system structures with flexible diaphragms. Earthquake engineering and structural dynamics, 30: 745-763.

HILTI (2001). Hilti North America Product Technical Guide-2001 Edition. Hilti Corporation, Schaan, Principality of Liechstenstein.

JU, S.H., LIN, M.C. (1999). Comparison of Building Analyses Assuming Rigid or Flexible Floors. Journal of Structural Engineering, ASCE, 125, P.25-31.

MAZZOLANI, F.M., DE MATTEIS, G., LANDOLFO, R. (1997). Dynamic behaviour of sandwich diaphragms in simple pin-jointed steel frames. Proceedings, Behaviour of Steel Structures in Seismic Areas, STESSA 1997, Kyoto, Japan.

MEDHEKAR, M.S. (1997). Seismic Evaluation of Steel Buildings with Concentrically Braced Frames. Ph.D. Thesis, Dept. of Civil and Environmental Engineering, Univ. of Alberta, Edmonton, Alberta, Canada.

MEDHEKAR, M.S., KENNEDY, D.J.L. (1999). Seismic Evaluation of Single-storey Steel Buildings. Canadian Journal of Civil Engineering, 26 P.379- 394.

MITCHELL, D., TREMBLAY, R., KARACABEYLI, E., PAULTRE, P., SAATCIOGLU, M., ANDERSON, D.L. (2002). Seismic force modification factors for the proposed 2004 NBCC. Submitted to the Canadian Journal of Civil Engineering for review on May 9, 2002.

NEDISAN, C. (2002). Comportement sismique de bâtiments en acier d'un seul étage avec diaphragme de toit flexible. École Polytechnique de Montréal, Montréal, QC, Canada.

NRCC (1995). National Building Code of Canada 1995 (NBCC), 11th ed.. Canadian Commission on Building and Fire Codes, National Research Council of Canada, Ottawa, Ontario, Canada.

NRCC (2001). Proposed changes to NBCC 1995 - Part 4. National Research Council of Canada, Institute for Research in Construction, Ottawa, Ontario, Canada.

PEULER, M. (2002). Inelastic response of arc-spot welded deck-to-frame connections for steel roof deck diaphragms. Master's Degree Project Report, Department of Civil Engineering and Applied Mechanics, McGill University, Montreal, QC, Canada.

ROGERS, C.A., TREMBLAY, R. (2000). Inelastic seismic response of frame and side-lap fasteners for steel roof decks. Research Report No. EPM/CGS-2000-09, Department of Civil, Geological and Mining Engineering, École Polytechnique de Montréal, Montréal, QC, Canada.

SAC Joint Venture (2000). NEHRP Recommended Seismic Design Criteria for New Steel Moment-Frame Buildings. Federal Emergency Management Agency Report FEMA 350, Building Seismic Safety Council, Washington, DC, USA.

STEEL DECK INSTITUTE, SDI (1981). Diaphragm Design Manual. Canton, OH, USA.

STEEL DECK INSTITUTE, SDI (1987). Diaphragm Design Manual, Second Edition. Canton, OH, USA.

STEWART, W.G. (1987). The Seismic Design of Plywood Sheated Shear Walls. Ph.D. Thesis, Department of Civil Engineering, University of Canterbury, Christchurch, New Zealand.

TENA-COLUNGA, A., ABRAMS, D.P. (1996). Seismic Behavior of Structures with Flexible Diaphragms. Journal of Structural Engineering, ASCE, 122, P. 439,445.

TREMBLAY, R., STIEMER, S.F. (1996). Seismic Behavior of Single-storey Steel Structures with a Flexible Roof Diaphragm. Canadian Journal of Civil Engineering, 23 P.49-62.

TREMBLAY, R., BERAIR, T. (1999). Shake Table Testing of Low-Rise Steel building with Flexible Roof Diaphragm. Proc. 8th Can. Conf. on Earthquake Eng., Vancouver, B.C., 585-590.

TREMBLAY, R. (2001). Seismic Behaviour and Design of Concentrically Braced Steel Frames. AISC Eng. J., 38 (3), 148-166.

TREMBLAY, R., ATKINSON, G.M. (2001). Comparative Study of the Inelastic Seismic Demand of Eastern and Western Sites. Earthquake Spectra, 17(2): 333-358.

TREMBLAY, R., LACERTE, M. (2002). Influence of the properties of bracing members on the seismic response of concentrically braced steel frames. Proc. of the 12th European Conference on Earthquake Engineering, Oxford, Elsevier: Paper Reference 481.

TREMBLAY, R., ROGERS, C., NEDISAN, C. (2002). Use of Uniform Hazard Spectrum and Computed Period in the Seismic Design of Single-Storey Steel Structures. Proc. 7th U.S. National Conference on Earthquake Engineering, Boston, MA.

TRI-SERVICES TECHNICAL MANUAL (1982). Seismic Design for Buildings. Depts. of Army, Navy and Air Force, U.S. Government Printing Office, Philadelphia, PA. USA.

US ARMY CORPS OF ENGINEERS (1998). Seismic Design for Buildings. Engineering Division, Directorate of Military Programs, Washington, DC, USA. www.hnd.usace.army.mil/techinfo/ti.htm

APPENDIX A

STATISTICAL ANALYSES OF DECK DISTORTION TIME HISTORIES FROM RUAUMOKO

In this Appendix, the values from the statistical analyses performed on the deck distortion time histories are given. The results for the analyses with screw-nail designs (NBCC 2004) are presented first, then the results for button punch-weld designs (NBCC 1995) are displayed. For each distortion range in each direction, the number of peaks, n, the average amplitude of the peak distortions in rad/1000, AVE, and the standard deviation of the amplitude of the peaks in rad/1000, SD, are shown.

Statistical analysis of the deck distortion time histories

Victoria Rd=3
Small building (15 m x 30 m)
Screw- Nail connector pattern
gamma u= 2.73 rad / 1000

N.B.: Ave.and SD are deck distortions in rad / 1000

E/Q			0.2-0.6 gamma u	0.6-1.0 gamma u	1.0-1.465 gamma u	4.0 - 8.0 rad / 1000	> 8.0 rad / 1000	Total
A	Positive	n	4	2	1	0	0	7
		Ave.	0.97	1.96	3.13	N/A	N/A	
		SD	0.45	0.33	N/A	N/A	N/A	
	Negative	n	10	6	4	1	2	23
		Ave.	-0.99	-2.12	-3.46	-4.60	-10.52	
		SD	0.42	0.32	0.46	N/A	1.29	
B	Positive	n	8	6	2	3	0	19
		Ave.	1.01	2.13	3.48	4.90	N/A	
		SD	0.26	0.41	0.44	1.17	N/A	
	Negative	n	9	2	6	3	0	20
		Ave.	-0.93	-2.25	-3.30	-7.08	N/A	
		SD	0.29	0.51	0.38	1.07	N/A	
C	Positive	n	13	12	2	3	0	30
		Ave.	1.09	2.15	3.27	4.83	N/A	
		SD	0.36	0.30	0.33	1.24	N/A	
	Negative	n	12	11	5	0	0	28
		Ave.	-1.22	-2.22	-3.11	N/A	N/A	
		SD	0.26	0.34	0.35	N/A	N/A	
D	Positive	n	15	5	0	1	0	21
		Ave.	1.03	2.09	N/A	5.38	N/A	
		SD	0.28	0.29	N/A	N/A	N/A	
	Negative	n	8	2	1	0	0	11
		Ave.	-0.91	-2.04	-3.10	N/A	N/A	
		SD	0.27	0.25	N/A	N/A	N/A	
G	Positive	n	8	4	1	3	0	16
		Ave.	1.12	2.19	2.84	5.30	N/A	
		SD	0.34	0.31	N/A	0.82	N/A	
	Negative	n	12	9	4	6	3	34
		Ave.	-1.10	-2.15	-3.06	-6.85	-11.96	
		SD	0.36	0.26	0.06	1.43	1.40	
H	Positive	n	5	2	3	1	0	11
		Ave.	0.77	2.26	3.34	4.06	N/A	
		SD	0.14	0.27	0.39	N/A	N/A	
	Negative	n	6	10	5	3	2	26
		Ave.	-0.91	-2.11	-3.25	-5.72	-8.93	
		SD	0.39	0.32	0.43	1.95	0.59	

Comparison

0.2 gamma u	0.55 rad/1000
0.6 gamma u	1.64 rad/1000
1.0 gamma u	2.73 rad/1000
1.465 gamma u	4.00 rad/1000

Statistical analysis of the deck distortion time histories

Victoria Rd=3
Medium building (30 m x 60 m)
Screw- Nail connector pattern
gamma u= 0.84 rad/1000

N.B.: Ave.and SD are deck distortions in rad/1000

E/Q			0.2-0.6 gamma u	0.6-1.0 gamma u	1.0-1.42 gamma u	1.198-4.0 rad/1000	4.0 - 8.0 rad/1000	> 8.0 rad/1000	Total
A	Positive	n	3	1	0	7	0	0	11
		Ave.	0.23	0.52	N/A	1.64	N/A	N/A	
		SD	0.06	N/A	N/A	0.65	N/A	N/A	
	Negative	n	7	3	3	6	0	2	21
		Ave.	-0.39	-0.61	-0.92	-2.28	N/A	-9.34	
		SD	0.09	0.08	0.06	0.46	N/A	0.50	
B	Positive	n	8	5	1	6	0	0	20
		Ave.	0.37	0.65	0.91	2.33	N/A	N/A	
		SD	0.06	0.06	N/A	0.83	N/A	N/A	
	Negative	n	29	6	5	5	2	0	47
		Ave.	-0.32	-0.66	-1.13	-1.78	-4.56	N/A	
		SD	0.09	0.14	0.06	0.45	0.24	N/A	
C	Positive	n	10	8	6	5	0	0	29
		Ave.	0.29	0.68	1.09	1.99	N/A	N/A	
		SD	0.11	0.08	0.09	0.62	N/A	N/A	
	Negative	n	8	5	5	5	0	0	23
		Ave.	-0.37	-0.68	-0.94	-1.35	N/A	N/A	
		SD	0.10	0.10	0.09	0.15	N/A	N/A	
D	Positive	n	4	6	11	12	1	0	34
		Ave.	0.39	0.66	1.07	1.71	4.80	N/A	
		SD	0.09	0.13	0.09	0.70	N/A	N/A	
	Negative	n	4	5	2	0	0	0	11
		Ave.	-0.33	-0.61	-1.00	N/A	N/A	N/A	
		SD	0.11	0.08	0.21	N/A	N/A	N/A	
G	Positive	n	6	7	2	3	0	0	18
		Ave.	0.27	0.56	0.90	1.91	N/A	N/A	
		SD	0.07	0.04	0.02	0.91	N/A	N/A	
	Negative	n	4	0	0	29	4	2	39
		Ave.	-0.22	N/A	N/A	-3.21	-5.44	-10.82	
		SD	0.06	N/A	N/A	0.61	0.86	0.76	
H	Positive	n	7	2	3	5	0	0	17
		Ave.	0.30	0.69	0.96	3.04	N/A	N/A	
		SD	0.11	0.07	0.07	0.96	N/A	N/A	
	Negative	n	5	2	2	9	0	0	18
		Ave.	-0.38	-0.57	-0.87	-2.28	N/A	N/A	
		SD	0.10	0.01	0.02	0.77	N/A	N/A	

Comparison

0.2 gamma u	0.17 rad/1000
0.6 gamma u	0.51 rad/1000
1.0 gamma u	0.84 rad/1000
1.42 gamma u	1.20 rad/1000

Statistical analysis of the deck distortion time histories
Cascadia earthquakes

N.B.: Ave.and SD are deck distortions in rad/1000

Victoria Rd=3
Small building (15 m x 30 m)
Screw- Nail connector pattern
gamma u= 2.73 rad / 1000

E/Q			0.2-0.6 gamma u	0.6-1.0 gamma u	1.0-1.465 gamma u	4.0 - 8.0 rad/1000	> 8.0 rad/1000	Total
E	Positive	n	61	21	4	2	0	88
		Ave.	0.92	2.03	3.43	4.14	N/A	
		SD	0.33	0.28	0.35	0.15	N/A	
	Negative	n	52	14	3	0	0	69
		Ave.	-1.04	-2.00	-3.16	N/A	N/A	
		SD	0.33	0.29	0.28	N/A	N/A	
F	Positive	n	51	24	1	0	0	76
		Ave.	1.00	1.98	2.80	N/A	N/A	
		SD	0.31	0.28	N/A	N/A	N/A	
	Negative	n	87	31	1	0	0	119
		Ave.	-0.99	-1.99	-3.71	N/A	N/A	
		SD	0.29	0.27	N/A	N/A	N/A	

Victoria Rd=3
Medium building (30 m x 60 m)
Screw- Nail connector pattern
gamma u= 0.84 rad / 1000

E/Q			0.2-0.6 gamma u	0.6-1.0 gamma u	1.0-1.42 gamma u	1.198-4.0 rad/1000	4.0 - 8.0 rad/1000	> 8.0 rad/1000	Total
E	Positive	n	123	30	12	19	0	0	184
		Ave.	0.31	0.65	1.04	1.64	N/A	N/A	
		SD	0.08	0.09	0.10	0.40	N/A	N/A	
	Negative	n	36	21	5	2	0	0	64
		Ave.	-0.32	-0.60	-0.94	-1.44	N/A	N/A	
		SD	0.10	0.06	0.08	0.02	N/A	N/A	
F	Positive	n	55	23	7	0	0	0	85
		Ave.	0.32	0.66	0.94	N/A	N/A	N/A	
		SD	0.08	0.09	0.06	N/A	N/A	N/A	
	Negative	n	75	44	15	14	0	0	148
		Ave.	-0.34	-0.66	-1.01	-1.45	N/A	N/A	
		SD	0.10	0.09	0.09	0.21	N/A	N/A	

Statistical analysis of the deck distortion time histories

Quebec Rd=3
Small building (15 m x 30 m)
Screw- Nail connector pattern
gamma u= 2.73 rad/1000

N.B.: Ave.and SD are deck distortions in rad/1000

E/Q			0.2-0.6 gamma u	0.6-1.0 gamma u	>1.0 gamma u	Total
M	Positive	n	5	3		8
		Ave.	1.20	2.14		
		SD	0.38	0.42		
	Negative	n	4	3		7
		Ave.	-0.79	-2.23		
		SD	0.32	0.25		
N	Positive	n	14	2		16
		Ave.	1.00	1.90		
		SD	0.37	0.00		
	Negative	n	27	3		30
		Ave.	-0.90	-1.86		
		SD	0.28	0.30		
O	Positive	n	12	0		12
		Ave.	0.62	N/A		
		SD	0.07	N/A		
	Negative	n	7	0		7
		Ave.	-0.80	N/A		
		SD	0.23	N/A		
P	Positive	n	5	0		5
		Ave.	0.93	N/A		
		SD	0.32	N/A		
	Negative	n	4	1		5
		Ave.	-0.75	-1.81		
		SD	0.17	N/A		

Comparison

0.2 gamma u	0.55 rad/1000
0.6 gamma u	1.64 rad/1000
1.0 gamma u	2.73 rad/1000

Statistical analysis of the deck distortion time histories

Quebec Rd=3
Medium building (15 m x 30 m)
Screw- Nail connector pattern
gamma u= 1.64 rad/1000

N.B.: Ave.and SD are deck distortions in rad/1000

E/Q			0.2-0.6 gamma u	0.6-1.0 gamma u	>1.0 gamma u	Total
M	Positive	n	10	0	0	10
		Ave.	0.60	N/A	N/A	
		SD	0.14	N/A	N/A	
	Negative	n	12	0	0	12
		Ave.	-0.57	N/A	N/A	
		SD	0.14	N/A	N/A	
N	Positive	n	23	12	0	35
		Ave.	0.61	1.13	N/A	
		SD	0.21	0.12	N/A	
	Negative	n	13	11	0	24
		Ave.	-0.70	-1.09	N/A	
		SD	0.20	0.09	N/A	
O	Positive	n	13	3	0	16
		Ave.	0.56	1.12	N/A	
		SD	0.15	0.09	N/A	
	Negative	n	24	4	1	28
		Ave.	-0.62	-1.15	-1.70	
		SD	0.23	0.14	N/A	
P	Positive	n	3	0	0	3
		Ave.	0.51	N/A	N/A	
		SD	0.17	N/A	N/A	
	Negative	n	4	0	0	4
		Ave.	-0.46	N/A	N/A	
		SD	0.17	N/A	N/A	

Comparison

0.2 gamma u	0.33 rad/1000
0.6 gamma u	0.98 rad/1000
1.0 gamma u	1.64 rad/1000

Number of inelastic excursions in deck panels under ground motions
Screw-nail designs (NBCC 2004)

Victoria R_d= 2.0 Small building (15m x 30 m)

Ground motions	Number of inelastic excursions
A	2
B	6
C	5
D	1

Victoria R_d= 2.0 Medium building (30m x 60 m)

Ground motions	Number of inelastic excursions
A	3
B	3
C	1
D	2

Statistical analysis of the deck distortion time histories

Victoria R=3 NBCC 1995
Small building (15 m x 30 m)
Button punch-weld connector pattern
gamma u= 1.79 rad/1000

N.B.: Ave.and SD are deck distortions in rad/1000

E/Q			0.2-0.6 gamma u	0.6-1.0 gamma u	1.0-1.05 gamma u	1.879-4.0 rad/1000	4.0 - 8.0 rad/1000	> 8.0 rad/1000	Total
A	Positive	n	7	6	0	0	0	0	13
		Ave.	0.54	1.30	N/A	N/A	N/A	N/A	
		SD	0.20	0.17	N/A	N/A	N/A	N/A	
	Negative	n	14	7	0	2	0	0	23
		Ave.	-0.73	-1.37	N/A	-2.84	N/A	N/A	
		SD	0.20	0.21	N/A	0.13	N/A	N/A	
G	Positive	n	7	3	0	7	0	0	17
		Ave.	0.69	1.28	N/A	2.42	N/A	N/A	
		SD	0.21	0.16	N/A	0.30	N/A	N/A	
	Negative	n	6	2	0	10	10	1	29
		Ave.	-0.61	-1.56	N/A	-2.84	-6.27	-8.82	
		SD	0.22	0.26	N/A	0.69	0.89	N/A	
H	Positive	n	10	9	0	2	0	0	21
		Ave.	0.69	1.39	N/A	2.86	N/A	N/A	
		SD	0.17	0.21	N/A	0.34	N/A	N/A	
	Negative	n	6	6	3	4	6	0	25
		Ave.	-0.77	-1.44	-1.84	-2.65	-5.58	N/A	
		SD	0.24	0.15	0.04	0.46	0.75	N/A	

Comparison

0.2 gamma u	0.358 rad/1000
0.6 gamma u	1.074 rad/1000
1.0 gamma u	1.790 rad/1000
1.05 gamma u	1.879 rad/1000

Statistical analysis of the deck distortion time histories

Victoria R=3 NBCC 1995
Medium building (30 m x 60 m)
Button punch-weld connector pattern
gamma u= 1.17 rad/1000

N.B.: Ave.and SD are deck distortions in rad/1000

E/Q			0.2-0.6 gamma u	0.6-1.0 gamma u	1.0-1.05 gamma u	1.229-4.0 rad/1000	4.0 - 8.0 rad/1000	> 8.0 rad/1000	
A	Positive	n	6	1	1	0	0	0	8
		Ave.	0.49	1.14	1.23	N/A	N/A	N/A	
		SD	0.16	N/A	N/A	N/A	N/A	N/A	
	Negative	n	8	1	0	4	3	0	16
		Ave.	-0.48	-1.00	N/A	-2.87	-4.79	N/A	
		SD	0.11	N/A	N/A	0.82	0.46	N/A	
G	Positive	n	2	3	0	8	0	0	13
		Ave.	0.37	0.94	N/A	2.16	N/A	N/A	
		SD	0.01	0.19	N/A	0.77	N/A	N/A	
	Negative	n	3	0	0	6	6	2	17
		Ave.	-0.30	N/A	N/A	-2.72	-6.05	-10.41	
		SD	0.08	N/A	N/A	0.36	0.67	0.71	
H	Positive	n	5	1	1	4	0	0	11
		Ave.	0.39	0.84	1.19	1.75	N/A	N/A	
		SD	0.15	N/A	N/A	0.15	N/A	N/A	
	Negative	n	6	5	0	8	2	0	21
		Ave.	-0.39	-0.92	N/A	-2.53	-4.43	N/A	
		SD	0.11	0.16	N/A	0.94	0.17	N/A	

Comparison

0.2 gamma u	0.234 rad/1000
0.6 gamma u	0.702 rad/1000
1.0 gamma u	1.170 rad/1000
1.05 gamma u	1.229 rad/1000

APPENDIX B

COUPON TENSION TESTS

In this appendix, the results of the coupon tests performed for this project are presented and discussed.

Galvanised Grade 230 structural quality ASTM A653 (2002) sheet steels with a Z275 zinc coating were specified for the diaphragm test series. In addition, the 0.76 mm thick standard deck profile sheets from the investigation carried out by Essa *et al.* (2001a) were used in this study, and hence the mechanical properties were already available. However, no data was available for the other sheet profiles used in this study, i.e. 0.91 mm standard deck, 0.76 B-deck and 0.91 B-deck profiles. Hence, three coupons were cut from each of the profile types (from the bottom flute in the longitudinal direction) and tensile testing was conducted. The mill test certificates are also presented in Appendix C for further information.

The tension tests were performed according to the requirements of ASTM A370 (2002) with a 50 mm reference length. The cross-head speed used in testing was 0.5 mm/minute. The measured stress-strain graphs are given in Figures B.1, B.2 and B.3. Yield strength was determined directly from the curves as all materials showed a sharp-yielding behaviour. The thickness of the material was measured after removing the galvanised coating with a hydrochloric-water solution. The static yield strength was determined by stopping the movement of the cross-head of the testing machine for 60 seconds interval at several times during the test. During these stops, the elongation remained the same but the load decreased. The static yield strength was taken as the average of minimum values in the yielding plateau. This decrease was function of the strain-rate dependency of the material. The Young's modulus, E, was measured in tests where the coupon specimen exhibited no bending and the stress-strain curve remained

straight. The percentage of elongation at fracture was measured after failure so that the elastic rebound was removed.

The results are given in Table B.1. The uncorrected values of Fy and Fu are presented together with the corrected values. The corrected values were found by subtracting the strain-rate dependency from the uncorrected values. For the calculations in the project, the corrected, i.e. static, values were used.

Sheet steel thicknesses were found to meet the tolerances given in S136 (1994). The sheet steels were found to have 50 mm gauge length elongations and Fu / Fy ratios that meet the S136 (1994) and American Iron and Steel Institute (1997) material specifications. Both standards require that Fu/Fy be greater than 1.08 and the 50 mm gauge elongation be greater than 10%.

ASTM A653 Grade 230 specifies that the yield strength, Fy, should be at least equal to 230 MPa and the ultimate strength, Fu, 310 MPa. In addition, the elongation in a 50 mm gauge length has to be greater than 20%. Sheet steels tested were found to conform with these requirements.

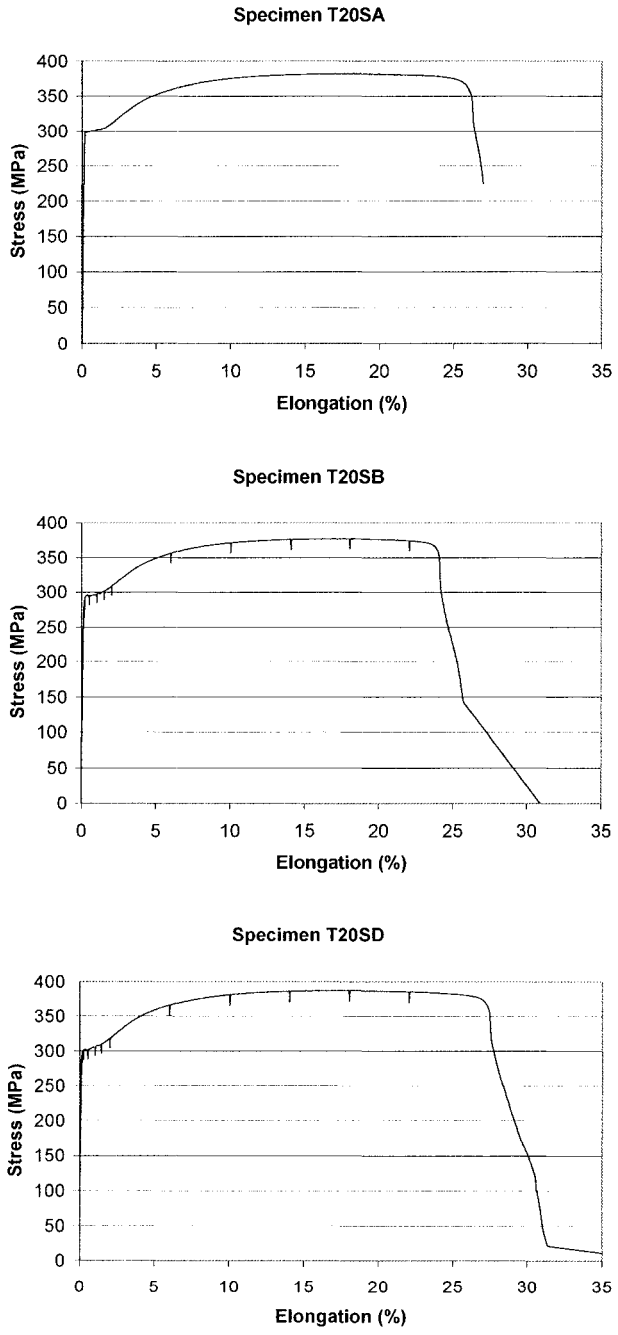

Figure B.1 Stress-strain curves for specimens from 0.91 mm nominal thickness standard deck sheets

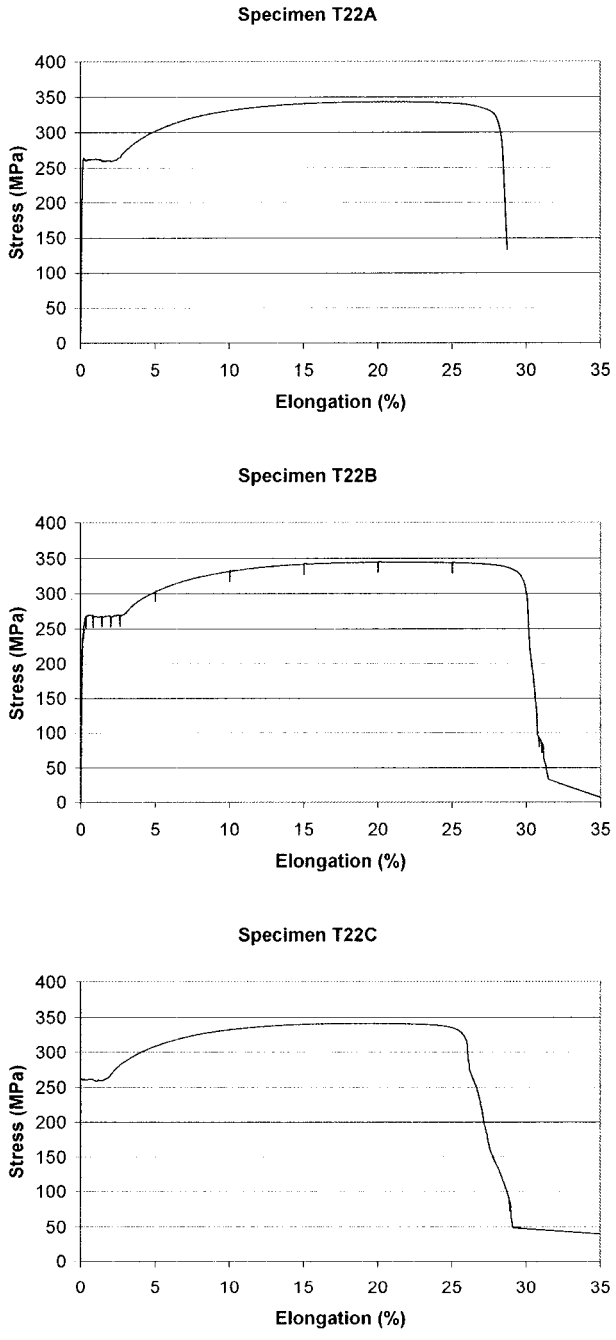

Figure B.2 Stress-strain curves for specimens from 0.76 mm nominal thickness B-deck sheets

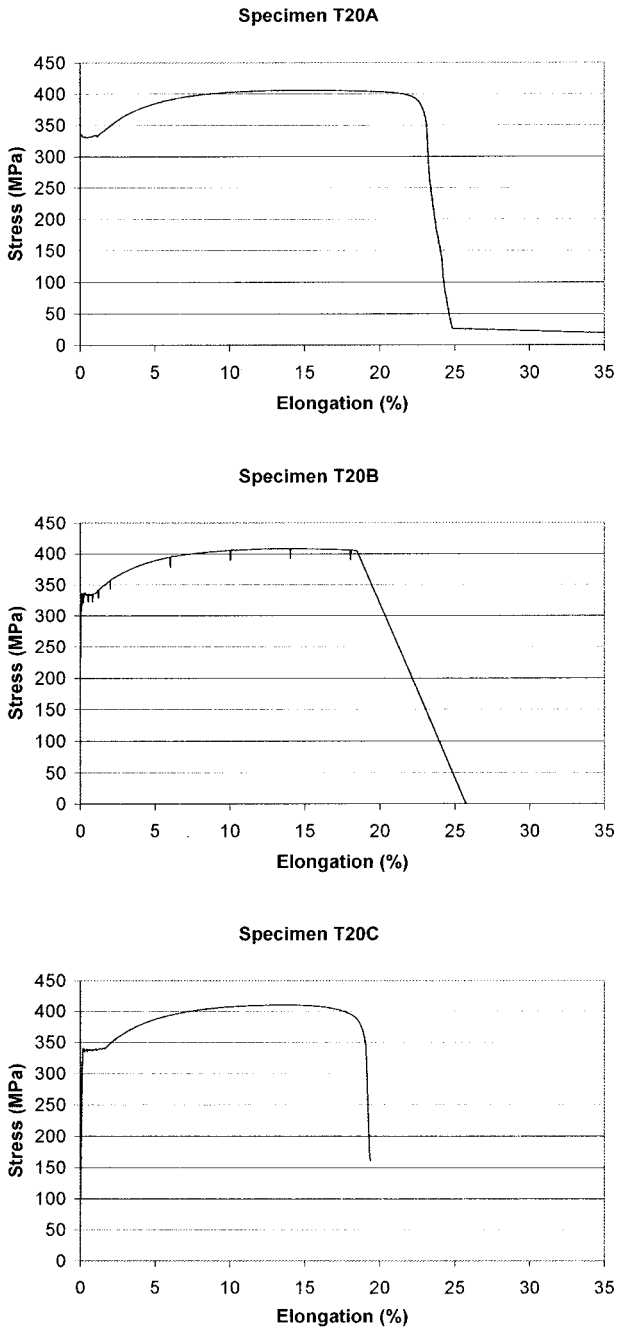

Figure B.3 Stress-strain curves for specimens from 0.91 mm nominal thickness B-deck sheets

Table B.1: Tension test results

P3615 Std 0.91 mm thickness	Coated thickness (mm)	Uncoated thickness (mm)	Uncorrected Fy (Mpa)	Uncorrected Fu (Mpa)	E (Mpa)	% Elongation
T20SA	0.89	0.86	300.1	382.3	198000	30.0
T20SB	0.89	0.87	295.9	376.9	N/A	28.0
T20SD	0.89	0.85	301.6	386.9	N/A	36.0
Mean	0.89	0.86	299.2	382.0	198000	31.3
Std dev			2.95	5.01		4.16
CoV			0.010	0.013		0.133
Strain-rate dependency		13.9 Mpa				
Corrected Fy		285 Mpa				
Corrected Fu		368 Mpa		Fu/Fy	1.29	

P3615 B 0.76 mm thickness	Coated thickness (mm)	Uncoated thickness (mm)	Uncorrected Fy (Mpa)	Uncorrected Fu (Mpa)	E (Mpa)	% Elongation
T22A	0.75	0.70	262.1	343.2	203433	30.0
T22B	0.75	0.70	267.2	343.8	204970	34.0
T22C	0.75	0.70	261.4	341.6	N/A	32.0
Mean	0.75	0.70	263.6	342.9	204202	32.0
Std dev			3.17	1.14	1087	2.00
CoV			0.012	0.003	0.005	0.063
Strain-rate dependency		15.6 Mpa				
Corrected Fy		248 Mpa				
Corrected Fu		327 Mpa		Fu/Fy	1.32	

P3615 B 0.91 mm thickness	Coated thickness (mm)	Uncoated thickness (mm)	Uncorrected Fy (Mpa)	Uncorrected Fu (Mpa)	E (Mpa)	% Elongation
T20A	0.92	0.88	331.4	406.1	N/A	26.5
T20B	0.92	0.88	332.5	408.8	N/A	24.0
T20C	0.91	0.89	337.9	410.3	210068	22.0
Mean	0.92	0.88	333.9	408.4	210068	24.2
Std dev			3.48	2.13		2.25
CoV			0.010	0.005		0.093
Strain-rate dependency		14.9 Mpa				
Corrected Fy		319 Mpa				
Corrected Fu		394 Mpa		Fu/Fy	1.23	

APPENDIX C

MILL TEST CERTIFICATES

In this appendix, information regarding the mill tests is presented. Figure C.1 and C.2 display the material properties listed on the mill test certificates for 0.91 and 0.76 mm nominal thickness B-deck profiles. In addition, comparisons between the results obtained from tension coupon tests and the mill tests are shown in Table C.1. We can see that the results from mill tests correspond to the results from the tension coupon tests.

Table C.1 Material properties from tension coupon tests and mill tests

		Thickness (mm)	Fy (MPa)	Fu (MPa)	E (MPa)	% Elongation
B-deck, 0.91 mm	Tension coupon	0.88	319	394	210000	24
Sorevco	Mill test	N/A	326	385	N/A	31
Coil no.: 147624	Ratio tension/mill	N/A	0.98	1.02	N/A	0.77
B-deck, 0.76 mm	Tension coupon	0.70	248	327	204000	32
Stelco	Mill test	N/A	271	352	N/A	32
Coil no.: 658104	Ratio tension/mill	N/A	0.92	0.93	N/A	1.00

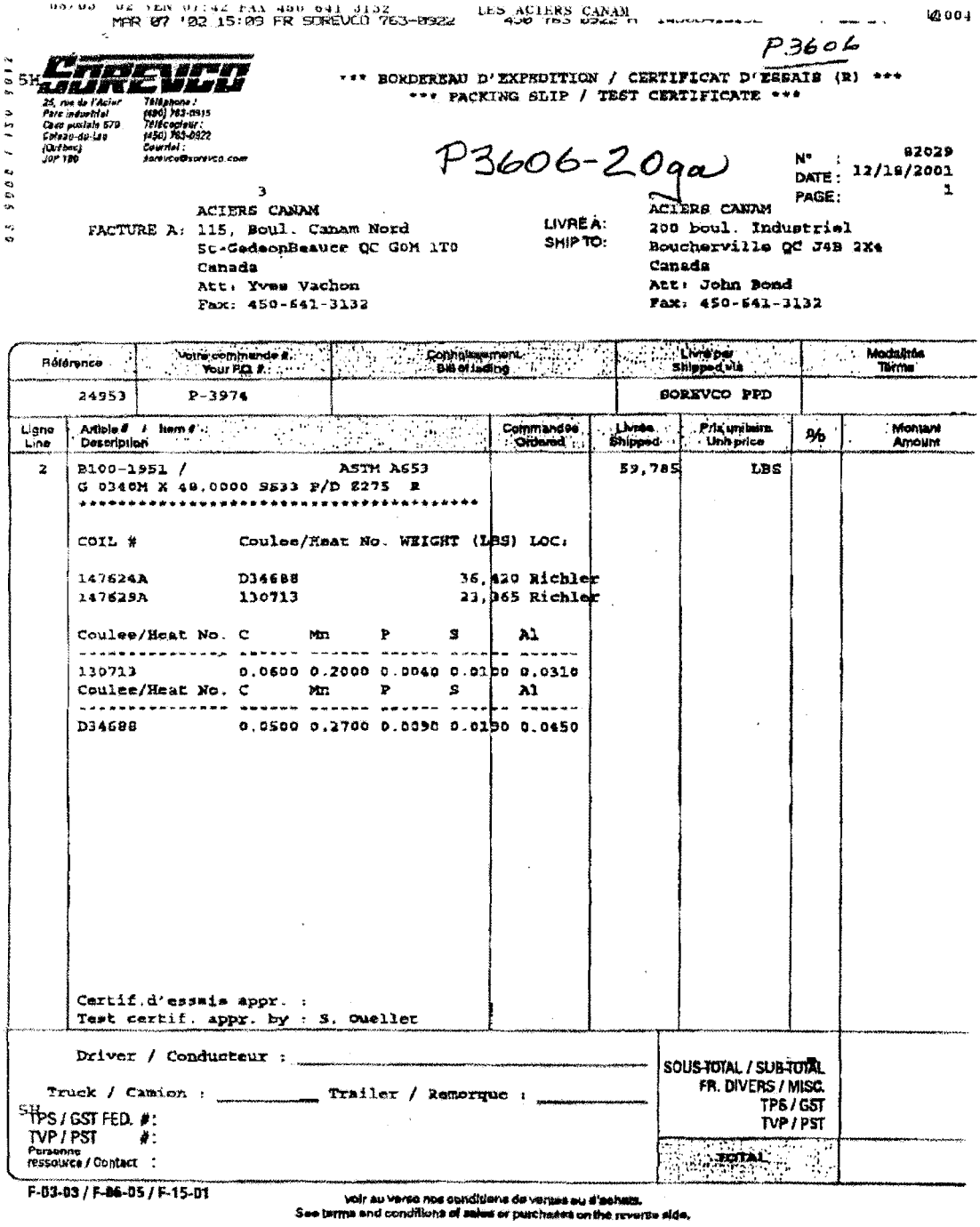

05/03 02 VEN 07:42 FAX 450 641 3132 LES ACIERS CANAM 004
MAR 07 '02 15:03 FR SOREVCO 763-8922

P.3606

SOREVCO
25, rue de l'Acier
Parc industriel
Case postale 579
Cdeau-du-Lac
(Québec)
J0P 1B0
Téléphone : (450) 763-0915
Télécopieur : (450) 763-0922
Courriel : sorevco@sorevco.com

*** BORDEREAU D'EXPEDITION / CERTIFICAT D'ESSAIS (R) ***
*** PACKING SLIP / TEST CERTIFICATE ***

P3606-20qa

N° : 82029
DATE : 12/18/2001
PAGE : 1

3

FACTURE A: ACIERS CANAM
115, Boul. Canam Nord
St-GedeonBeauce QC G0M 1T0
Canada
Att: Yves Vachon
Fax: 450-641-3132

LIVRÉ À: SHIP TO: ACIERS CANAM
200 boul. Industriel
Boucherville QC J4B 2X4
Canada
Att: John Bond
Fax: 450-641-3132

Référence	Votre commande # / Your PO # :	Connaissement / Bill of lading	Livré par / Shipped via	Modalités / Terms
24953	P-3974		SOREVCO PPD	

Ligne / Line	Article # / Item # : Description	Commandés / Ordered	Livrés / Shipped	Prix unitaire / Unit price	%	Montant / Amount
2	B100-1951 / ASTM A653 G 0346M X 49.0000 S533 P/D Z275 R **********		59,785	LBS		

COIL # Coulee/Heat No. WEIGHT (LBS) LOC:

147624A	D34688	36,620	Richler
147629A	130713	23,165	Richler

Coulee/Heat No.	C	Mn	P	S	Al
130713	0.0600	0.2000	0.0040	0.0100	0.0310
Coulee/Heat No.	C	Mn	P	S	Al
D34688	0.0500	0.2700	0.0090	0.0190	0.0450

Certif.d'essais appr. :
Test certif. appr. by : S. Ouellet

Driver / Conducteur : _____

Truck / Camion : _____ Trailer / Remorque : _____

TPS / GST FED. #:
TVP / PST #:
Personne ressource / Contact :

SOUS-TOTAL / SUB-TOTAL
FR. DIVERS / MISC.
TPS / GST
TVP / PST
TOTAL

F-03-03 / F-86-05 / F-15-01

Voir au verso nos conditions de ventes ou d'achats.
See terms and conditions of sales or purchases on the reverse side.

Figure C.1 Certificate for 0.91 mm nominal thickness B-deck profiles

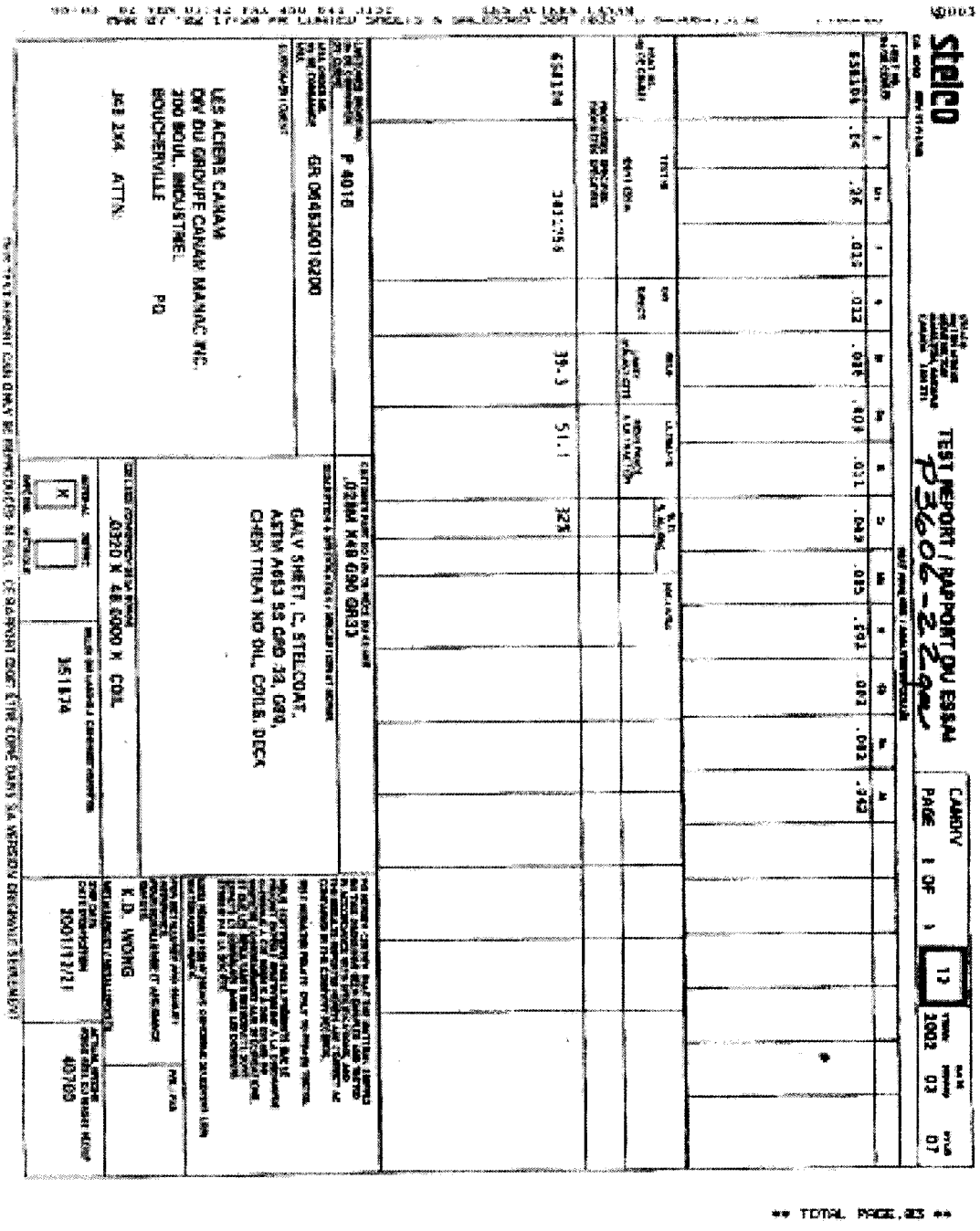

Figure C.2 Certificate for 0.76 mm nominal thickness B-deck profiles

APPENDIX D

SIDELAP CONNECTION TESTS

D.1 GENERAL

A new design with robust welded sidelap connections using B-deck profiles was envisaged. Prior to the initiation of this research project, no information was available on the welded sidelap connections with B-deck profiles. For this reason two types of connections were tested as a subtopic of this investigation, from which the more robust was chosen for use in the full-scale diaphragm tests: slotted welds and welds with washer. In addition, screwed sidelap connections were tested for comparison. General comments and test results are presented in this Appendix.

The test specimens were prepared in the same fashion as used by Rogers and Tremblay (2000). They were made of two adjoining 300 mm long deck sections connected with one or two connections. The dimensions of the specimens with 2 connections are presented in Rogers and Tremblay (2000). For specimens with one connection, the same dimensions were used, however the connection was located at the mid-position of the specimen. Specimens were cut from P3615 B-deck 0.91 mm nominal thickness sheets.

As said, three types of connections were studied. The first type was the welded with washer connection. The washer had an outer diameter of 35 mm, an inner diameter of 14 mm and a thickness of 2.5 mm. The welder started the weld at the centre of the washer and punched a hole through the two layers of sheet steel. Thereafter, the electrode was moved in a circular pattern around the washer inner diameter. An E6010 electrode of 3.2 mm diameter was used under a direct current of 115 Amp.

The second type of tested connection was the slot weld. A slotted hole is made through the two steel sheets. The connection is made through the fusion of the sheet steels and the deposition of weld metal around the perimeter of this slot. An E6010 3.2 mm diameter electrode was used under a direct current of 115 Amp. The choice of slot length was based on the following equation from the Manual of Stressed Skin Diaphragm Design (Davis and Bryan, 1982). The formula was developed for single flare vee welds and arc seam welds at sidelaps with interlock.

$$F'_s = 0.55 L_w t \sigma_u$$

where

F'_s : Ultimate strength (kN)
L_w : Length of weld (mm)
t : net sheet thickness (mm)
σ_u : Ultimate strength of plate material (kN/mm^2)

A weld length of 38 mm was chosen with the intent of matching the weld resistance obtained from Rogers and Tremblay (2000) of about 7.0 kN for the standard deck profile welded sidelap connections. For a thickness of 0.91 mm and a tensile resistance of 400 MPa, it was anticipated that a weld length of 38 mm would provide a shear resistance , F'_s, equal to 7.6 kN.

In addition, screwed sidelap connections were tested. TEK 12 - 14 x 1 HWH Tek/3 Climaseal screws from Buildex were used.

The test set-up was designed by Rogers according to the recommendations provided in the AISI Design Manual (1996). For the current series of tests, the set-up was modified

such that it could be installed vertically in an MTS Sintech 30/G universal testing machine (Figure D.1). A 150 kN MTS load cell was used to measure load that developed upon imposing a shear deformation on the test specimen. The cross-head speed was equal to 1mm/min. Friction forces of the set-up were found to be around 0.02 kN when the cross-head was moved upwards, whereas they were around 0.01 kN when moving downwards. Figure D.2 shows a typical specimen deformed by shear. In the cyclic tests, the specimens were displaced far enough to reach the maximum load and to start the load degradation, then the direction of the imposed displacement was inverted and the maximum load was obtained in the other direction.

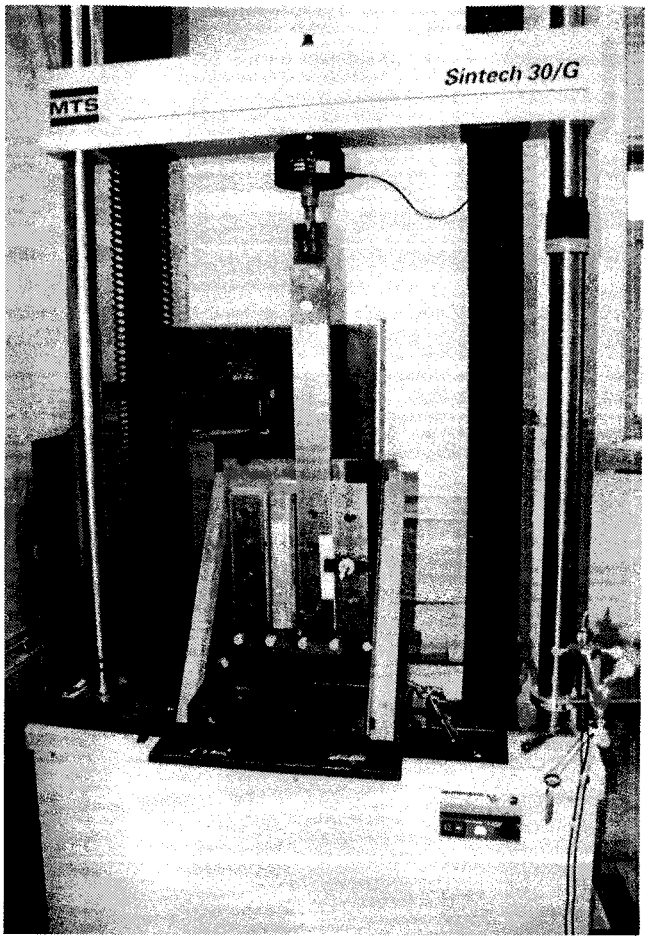

Figure D.1 Sidelap connection test set-up

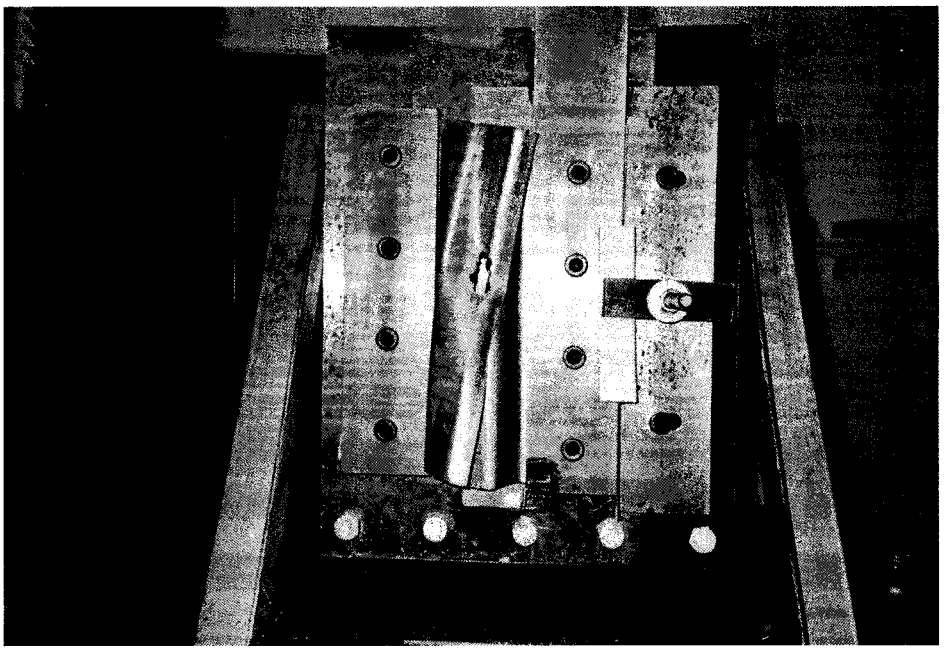

Figure D.2 Slot welded connection specimen deformed by shear

D.2 TEST RESULTS

All test results are presented in Table D.2 and Table D.3. In addition, load-displacement curves for all tests are shown in Figure D.6 and Figure D.7. Figures D.3 to D.5 present test specimens prior or after testing.

For both weld types, the behaviour depended mainly on the weld connectivity. From test curves, two families of welded specimens were found: those with a high degree of connectivity and those with poor connectivity. The high connectivity welds sustained much larger deformation and developed higher strengths in comparison to poor welds. The weld connectivity depended mainly on the gap between the sheets at the time of welding. As the gap increased the connectivity decreased. Figure D.8 presents the relationship between connectivity and strength whereas Figure D.9 shows the relationship for stiffness for welded with washer connections. The connection strengths tend to be related strongly to connectivity whereas the stiffnesses are not.

Both types of weld developed similar strengths when the welds were of good quality. However, welded with washer connections sustained higher deformations than slot welded connections (up to 18 mm compared to 10 mm) prior to deterioration in the load carrying capacity.

Because of their robustness, welded with washer sidelap connections were chosen for the diaphragm experiments. The measured connection strengths and stiffness that were later used in the evaluation of the full-scale diaphragm tests are shown in Table D.1. The values were rounded to 1 significant digit because of the high variability in the measured results and the relatively low number of samples.

Table D.1 Strengths and stiffnesses of welded with washer sidelap connections

	Strength (kN)	Stiffness (kN/mm)
	Test	Test
Welds with washers (0.91 mm)	8.00	4.00

Figure D.3 Welded with washer connection specimen prior to testing

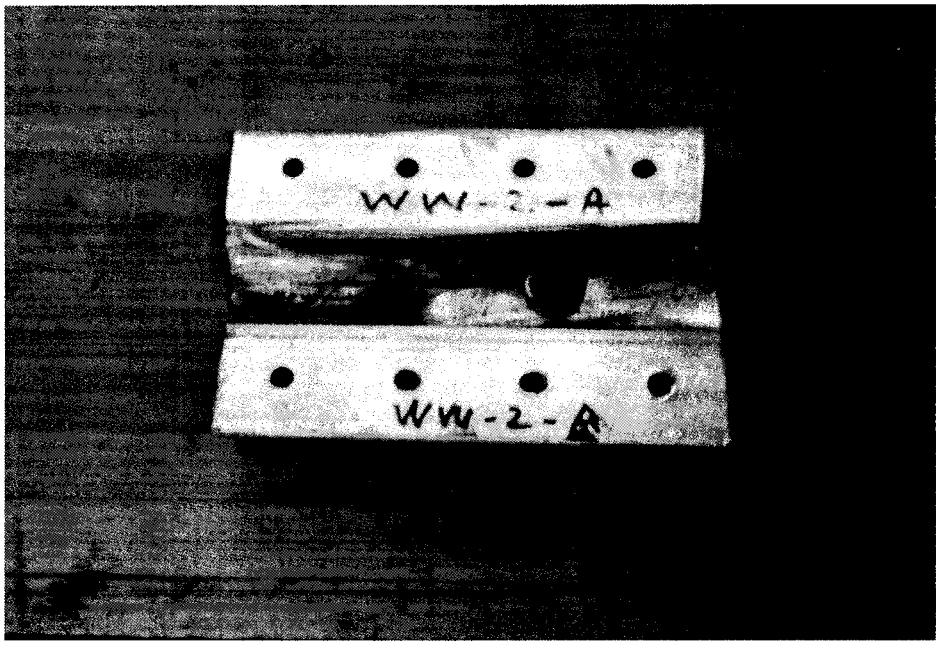

Figure D.4 Welded with washer connection specimen after testing

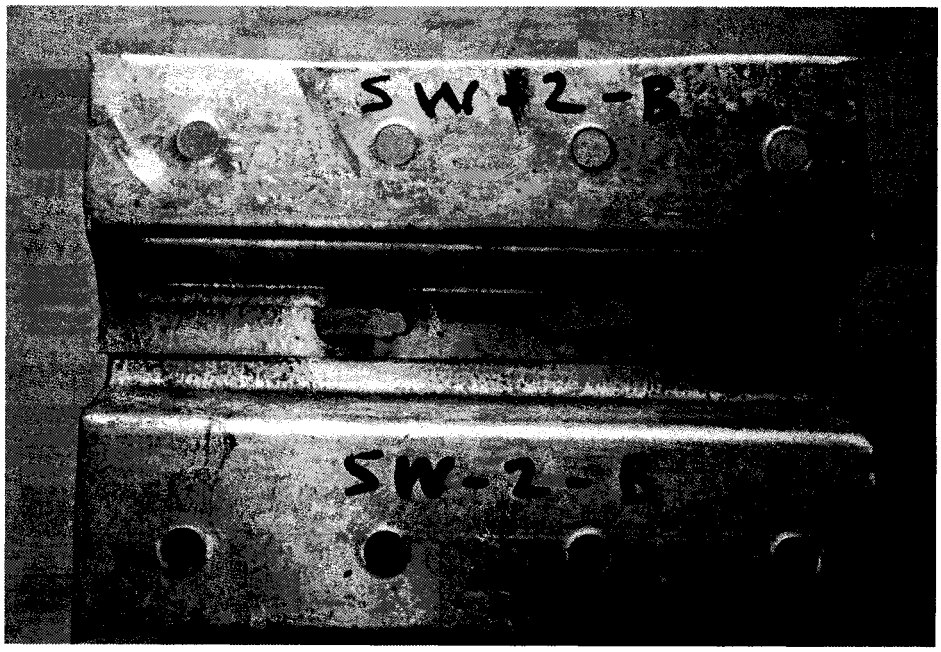

Figure D.5 Slot welded connection specimen prior to testing

Table D.2 Test results for single connection specimens

Welds with washer

	Pu+ (kN)	Pu- (kN)	Ratio Pu-/Pu+	K (kN/mm)	By visual inspection Diameter (mm)	Connectivity (%)
WW-1-A	5.47	1.50	0.27	4.87	19	40
WW-1-B	6.48	3.77	0.58	2.78	17	40
WW-1-C	11.9	12.2	1.03	3.35	15	90
WW-1-D	4.68	1.89	0.40	2.96	14	40
WW-1-E	7.66	7.51	0.98	4.65	13	80
WW-1-F	8.28	6.95	0.84	3.71	14	80
Average	7.13	4.84	0.57	3.49		
S.D.	3.26	5.01	0.33	0.95		
C.O.V.	0.46	1.03	0.58	0.27		

Slot welds

	Pu+ (kN)	Pu- (kN)	Ratio Pu-/Pu+	K (kN/mm)	By visual inspection Length (mm)	Width (mm)	Connectivity (%)
SW-1-A	6.20	5.32	0.86	5.58	35	12	20
SW-1-B	6.89	5.74	0.83	4.47	33	9	50
SW-1-C	12.8	8.24	0.64	3.90	28	8	100
SW-1-D	10.9	8.61	0.79	3.39	30	8	80
Average	9.19	6.98	0.78	4.33			
S.D.	3.16	1.69	0.10	0.94			
C.O.V.	0.34	0.24	0.13	0.22			

Table D.3 Test results for double connection specimens

Welds with washer

	Pu+ (kN)	Pu- (kN)	Ratio Pu-/Pu+	K (kN/mm)	By visual inspection Diameter (mm)	Connectivity (%)
WW-2-A	18.3	18.2	1.00	3.51	15	90
WW-2-B	16.6	10.4	0.63	3.22	12	78
Average	17.4	14.3	0.82	3.37		
S.D.	1.22	5.52	0.26	0.21		
C.O.V.	0.07	0.38	0.32	0.06		

Slot welds

	Pu+ (kN)	Pu- (kN)	Ratio Pu-/Pu+	K (kN/mm)	By visual inspection Length (mm)	Width (mm)	Connectivity (%)
SW-2-A	13.9	11.2	0.80	5.02	36	10	55
SW-2-B	11.1	13.5	1.22	3.66	34	10	70
Average	12.5	12.4	1.01	4.34			
S.D.	2.01	1.64	0.30	0.96			
C.O.V.	0.16	0.13	0.29	0.22			

Screwed (Tek 12-14x1 HWH Tek/3 Climaseal)

	Pu+ (kN)	Pu- (kN)	Ratio Pu-/Pu+	K (kN/mm)
S-2-A	7.16	5.12	0.71	4.30
S-2-B	5.79	5.02	0.87	4.28
S-2-C	7.08	4.81	0.68	4.25
Average	6.48	5.07	0.79	4.29
S.D.	0.97	0.07	0.11	0.02
C.O.V.	0.15	0.01	0.14	0.00

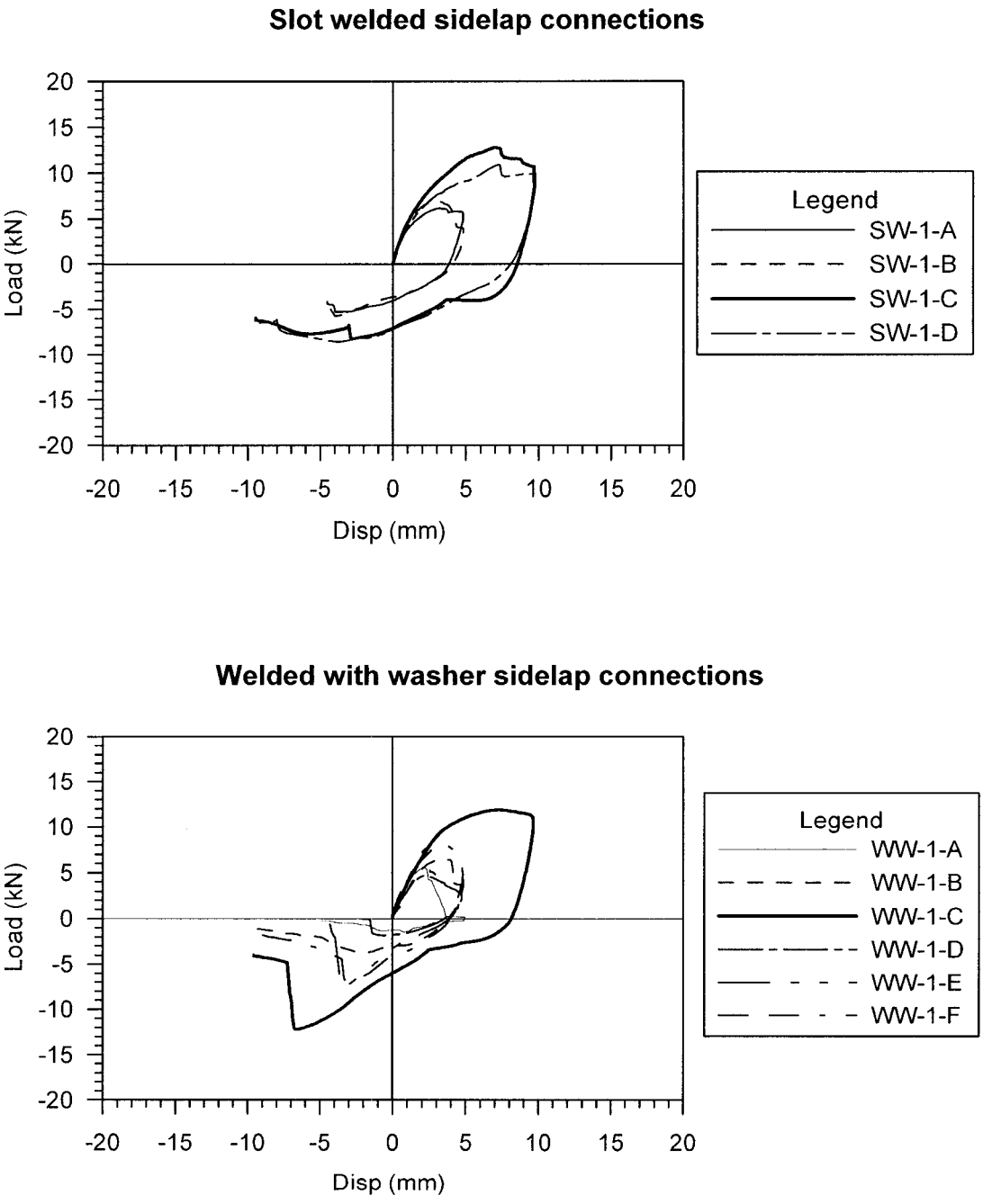

Figure D.6 Load-displacement curves for single connection specimens

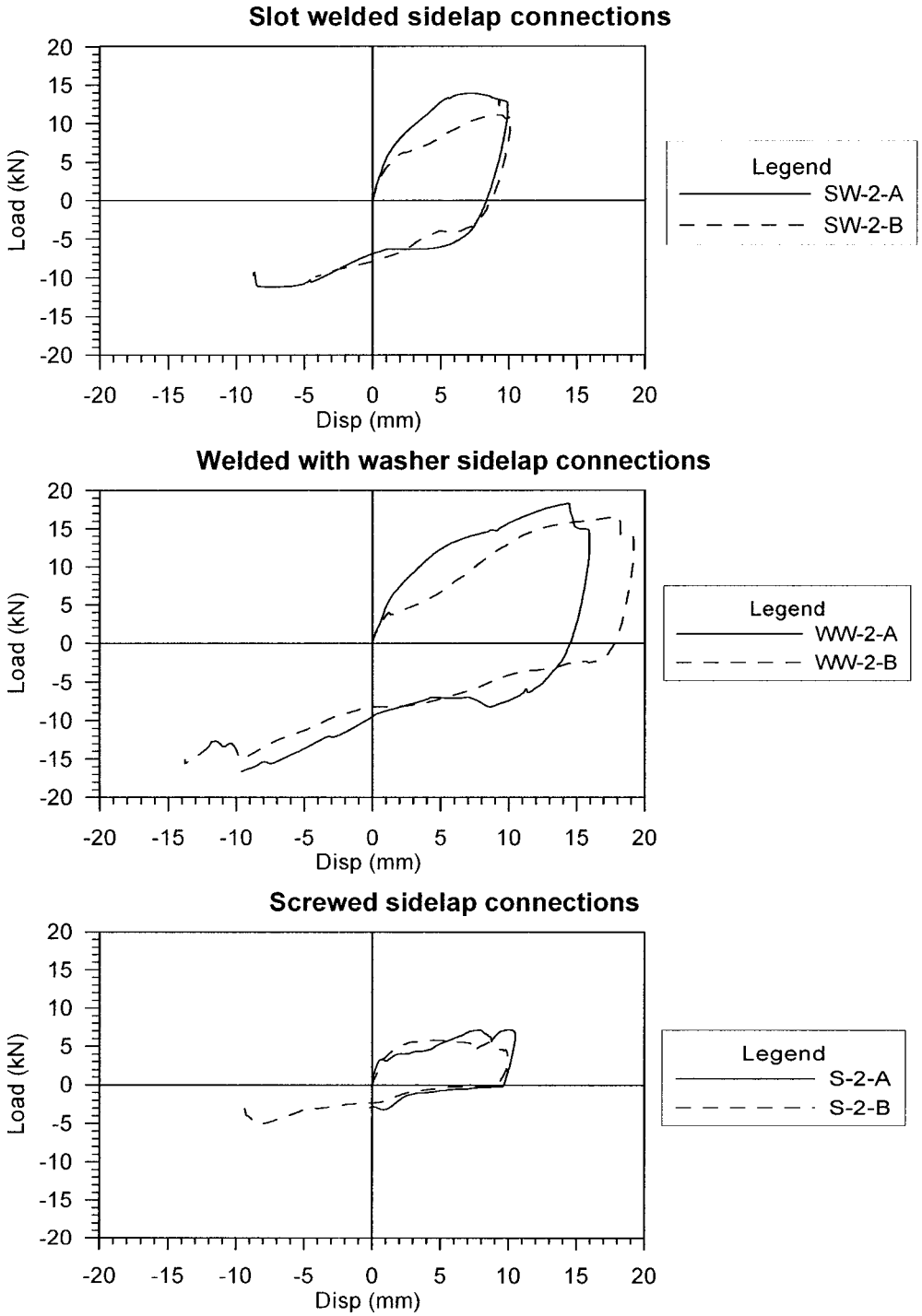

Figure D.7 Load-displacement curves for double connection specimens

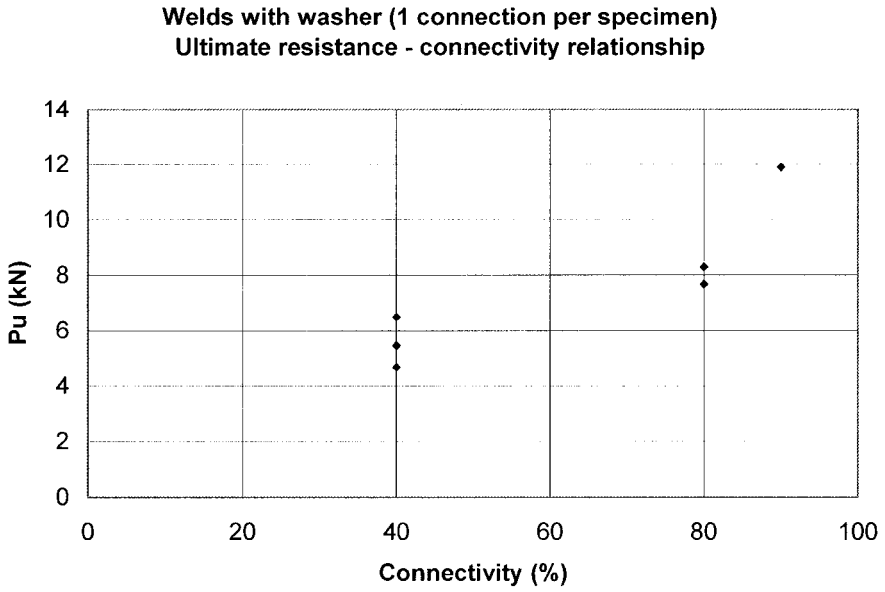

Figure D.8 Ultimate resistance-connectivity relationship for welds with washer

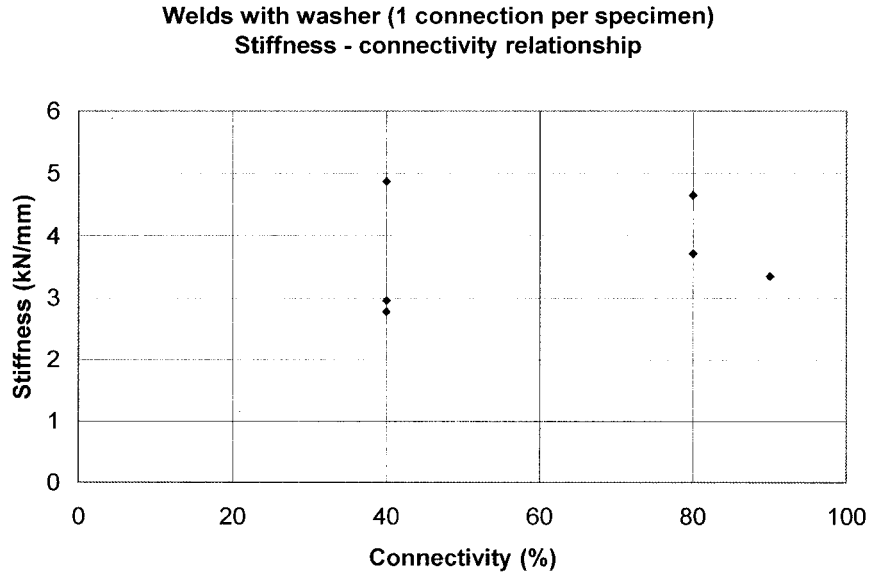

Figure D.9 Stiffness-connectivity relationship for welds with washer connections

APPENDIX E

MEASUREMENTS OF NAIL STAND-OFF

This Appendix presents the measured nail stand-offs for all diaphragm test specimens. For the connectors, two spacing patterns were used. Tests 19, 25, 26, 27, 28, 29, 34 and 35 involved a 305 mm (1 ft) spacing for both connector types (nailed deck-to-frame and screwed sidelap fasteners) whereas tests 30, 31, 32 and 33 were conducted with a 152 mm (6 inches) spacing. The test specimens are presented in their chronological order in the next pages.

The nail stand-off is defined as the distance from top of nail to top of sheet steel. In case of a double sheet thickness configuration, the stand-off is also measured to the top sheet steel. Figure E.1 presents a schematic of the nail stand-offs for the single sheet and double sheet configurations.

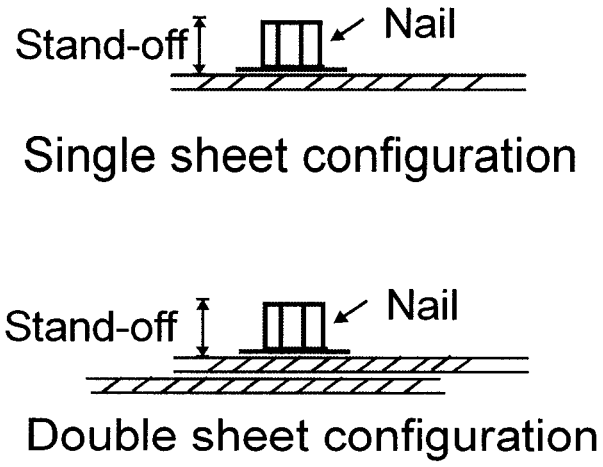

Figure E.1 Nail stand-off

Test 38-91-6-NS-M-19
Nail stand-off in mm

	1	2	3	4	5	6	7	8	9	10	11	12	13	14	15	16	17	18	19	20	21
A	9.06	6.86	6.31	5.24	6.85	5.75	8.07	6.06	6.49	8.68	8.02	8.02	6.82	9.07	7.44	8.07	8.36	7.49	8.92	9.66	10.15
B	7.98					8.55					7.23					7.58					6.40
C	6.95					8.45					6.42					8.84					6.85
D	7.08					7.82					8.92					8.90					6.40
E	7.21					8.51					8.66					9.79					6.44
F	8.85					8.94					9.07					7.88					5.96
G	9.17					7.23					9.55					7.83					6.28
H	8.86					6.91					8.65					7.50					5.20
I	8.53					6.46					8.14					9.05					5.41
J	9.49					7.61					8.29					8.92					9.09
K	9.23					8.83					8.86					7.85					6.54
L	5.88					6.53					6.39					6.84					6.90
M	10.25	7.31	8.99	8.34	8.92	7.65	9.02	6.05	7.78	7.86	6.62	8.32	7.98	7.39	7.58	6.56	7.11	5.83	7.08	7.03	7.66
Ave.	7.74	mm		At sidelaps		Ave.	8.17	mm		Except sidelaps			Ave.	7.66	mm						
S.D.	1.18	mm				S.D.	1.09	mm					S.D.	1.18	mm						
C.o.V.	0.15					C.o.V.	0.13						C.o.V.	0.15							

Test 38-91-6-NW-M-25
Nail stand-off in mm

	1	2	3	4	5	6	7	8	9	10	11	12	13	14	15	16	17	18	19	20	21
A	8.90	7.61	6.88	7.01	7.90	7.22	6.88	7.17	7.14	7.31	7.70	7.62	14.61	8.01	4.73	7.85	8.06	6.74	6.26	6.60	5.22
B	9.06					6.46					6.32					6.36					6.30
C	11.26					7.22					5.92					6.02					6.15
D	7.62					6.69					6.34					6.32					6.60
E	6.85					6.02					7.47					11.24					5.62
F	6.77					6.45					12.81					5.80					5.93
G	4.87					8.03					6.05					6.05					7.31
H	10.30					5.38					5.95					5.15					6.77
I	8.60					5.43					5.55					5.67					5.50
J	5.64					5.42					6.56					7.18					6.50
K	8.20					6.80					6.41					8.43					5.47
L	9.36					5.64					5.26					7.15					6.17
M	7.08	9.03	8.68	9.38	7.01	8.34	6.30	9.28	7.56	7.31	8.00	9.63	6.24	7.60	7.90	6.28	7.32	5.84	5.27	6.42	6.24
Ave.	7.12	mm		At sidelaps		Ave.	6.48	mm		Except sidelaps			Ave.	7.24	mm						
S.D.	1.63	mm				S.D.	0.84	mm					S.D.	1.72	mm						
C.o.V.	0.23					C.o.V.	0.13						C.o.V.	0.24							

Test 38-91-6-NW-SD-26
Nail stand-off in mm

	1	2	3	4	5	6	7	8	9	10	11	12	13	14	15	16	17	18	19	20	21
A	5.75	8.57	6.99	5.52	5.05	5.80	5.70	4.85	5.79	6.08	5.50	5.49	5.85	5.69	5.66	6.47	6.15	6.61	5.93	5.63	7.85
B	5.54					5.59					6.15					5.74					4.53
C	5.14					5.80					5.38					5.85					10.74
D	5.67					5.30					6.92					6.86					5.41
E	6.10					5.81					6.17					5.70					5.81
F	5.13					5.09					5.43					5.20					9.72
G	6.95					6.38					7.20					7.86					7.81
H	5.33					5.72					6.01					5.27					5.18
I	4.76					5.07					5.90					6.64					7.70
J	5.76					5.92					9.05					6.94					7.07
K	5.26					5.86					5.56					5.55					4.83
L	5.52					4.95					6.20					5.47					4.99
M	6.38	5.47	5.31	6.17	5.80	5.81	5.68	6.18	5.41	5.45	5.50	5.80	5.60	6.63	6.40	11.37	5.17	5.19	5.72	5.01	5.35
Ave.	6.04	mm		At sidelaps		Ave.	6.74	mm		Except sidelaps			Ave.	5.91	mm						
S.D.	1.15	mm				S.D.	1.03	mm					S.D.	1.14	mm						
C.o.V.	0.19					C.o.V.	0.15						C.o.V.	0.19							

Test 38-91-6-NW-LD-27
Nail stand-off in mm

	1	2	3	4	5	6	7	8	9	10	11	12	13	14	15	16	17	18	19	20	21
A	8.80	6.29	7.23	7.22	6.54	6.79	7.19	7.15	5.89	7.33	9.56	6.52	6.98	7.26	7.20	6.65	7.21	6.94	7.19	7.45	7.37
B	7.26					8.16					6.99					7.00					6.59
C	7.66					6.86					7.26					6.57					7.69
D	7.81					7.14					8.41					7.25					7.95
E	7.13					7.61					7.46					7.08					6.90
F	6.66					6.96					6.90					7.42					6.78
G	7.29					8.13					7.81					8.21					7.30
H	6.98					6.63					7.26					7.21					7.19
I	8.96					7.01					6.72					7.02					7.21
J	8.77					7.79					7.50					8.57					7.31
K	7.53					7.00					7.57					10.32					7.19
L	7.36					6.48					7.44					7.30					7.19
M	7.45	7.00	6.42	8.46	7.70	9.53	7.09	8.81	7.51	8.47	6.86	6.50	6.87	7.70	7.93	8.36	6.67	6.52	7.95	6.15	8.36
Ave.	7.39	mm		At sidelaps		Ave.	7.82	mm		Except sidelaps			Ave.	7.31	mm						
S.D.	0.76	mm				S.D.	0.52	mm					S.D.	0.77	mm						
C.o.V.	0.10					C.o.V.	0.07						C.o.V.	0.11							

Test 38-76-6-NS-SD-28
Nail stand-off in mm

	1	2	3	4	5	6	7	8	9	10	11	12	13	14	15	16	17	18	19	20	21
A	6.58	5.96	5.23	4.94	4.91	5.14	5.80	5.43	4.96	5.75	5.53	5.57	7.12	5.78	5.24	6.01	5.84	5.44	5.78	5.35	5.70
B	5.63					5.52					4.72					4.26					5.84
C	4.91					4.54					4.54					4.54					5.71
D	8.56					5.74					5.46					5.00					6.41
E	5.05					4.20					4.55					4.45					5.14
F	5.15					4.85					4.72					4.62					6.01
G	6.83					5.64					5.61					4.96					5.92
H	5.80					5.01					4.30					4.78					5.56
I	4.50					4.58					4.72					4.80					5.28
J	5.87					5.24					6.30					5.09					6.44
K	6.06					4.69					9.73					4.66					6.34
L	5.49					4.99					4.78					4.62					7.02
M	6.50	8.48	5.72	5.79	5.47	5.66	6.05	5.78	5.66	5.77	6.70	6.30	5.27	6.06	5.61	5.29	5.82	5.90	5.35	5.54	5.84
Ave.	5.55	mm		At sidelaps		Ave.	5.94	mm		Except sidelaps			Ave.	5.48	mm						
S.D.	0.88	mm				S.D.	0.92	mm					S.D.	0.86	mm						
C.o.V.	0.16					C.o.V.	0.15						C.o.V.	0.16							

Test 38-76-6-NS-LD-29
Nail stand-off in mm

	1	2	3	4	5	6	7	8	9	10	11	12	13	14	15	16	17	18	19	20	21
A	5.85	5.07	5.20	4.62	5.28	5.26	4.87	5.54	5.40	5.85	5.10	5.67	5.27	5.54	5.20	5.42	5.75	6.16	5.26	5.73	7.44
B	4.02					6.66					7.66					7.67					5.82
C	5.90					6.13					7.45					6.55					5.67
D	6.10					5.67					6.11					7.09					6.65
E	5.65					7.60					7.32					6.75					5.40
F	5.70					6.75					6.93					6.65					5.65
G	5.98					6.00					6.96					6.62					6.40
H	6.12					7.20					7.41					8.63					5.36
I	7.10					5.00					6.56					8.02					6.78
J	6.28					6.33					6.12					6.94					6.82
K	7.82					5.83					7.27					7.50					6.10
L	7.44					11.53					7.03					7.42					5.83
M	6.30	5.76	5.51	6.03	5.66	6.23	6.48	6.08	6.25	6.52	5.43	5.37	5.56	5.92	5.84	5.69	7.65	5.67	6.91	8.30	6.11
Ave.	6.30	mm		At sidelaps		Ave.	6.40	mm		Except sidelaps			Ave.	6.28	mm						
S.D.	1.02	mm				S.D.	0.42	mm					S.D.	1.10	mm						
C.o.V.	0.16					C.o.V.	0.07						C.o.V.	0.17							

Test 38-76-6-NS-M-30
Nail stand-off in mm

	1	1'	2	2'	3	3'	4	4'	5	5'	6	6'	7	7'	8	8'	9	9'	10	10'	11
A	5.93	5.27	5.27	5.42	5.44	4.52	5.49	6.75	6.17	7.39	5.76	5.40	5.93	5.51	5.43	5.35	7.10	6.27	6.47	5.40	8.25
A'	6.33										6.11										5.50
B	5.25										5.38										5.17
B'	5.45										5.39										5.61
C	6.63										6.04										5.23
C'	6.05										5.24										5.33
D	7.01										5.95										6.35
D'	5.78										5.47										5.83
E	6.39										5.23										5.33
E'	6.76										5.20										5.90
F	6.25										5.26										5.31
F'	6.62										5.22										5.20
G	7.78										6.67										6.45
G'	7.78										8.10										7.35
H	7.97										6.06										5.38
H'	9.24										6.47										6.23
I	8.81										5.49										6.96
I'	6.81										6.02										6.07
J	8.50										6.02										5.19
J'	9.08										6.71										6.59
K	7.44										5.55										5.19
K'	5.47										7.06										6.88
L	6.30										7.89										5.64
L'	6.01										8.53										7.07
M	7.84	6.16	5.01	6.04	5.35	5.99	5.18	5.79	6.50	4.94	5.10	5.82	5.16	6.23	5.05	4.58	5.74	6.85	6.55	6.03	4.41
Ave.	6.00	mm		At sidelaps		6.53	mm		Except sidelaps			5.96	mm								
S.D.	2.09	mm				2.61	mm					2.04	mm								
C.o.V.	0.35					0.40						0.34									

Test 38-76-6-NS-M-30
Nail stand-off in mm

	11'	12	12'	13	13'	14	14'	15	15'	16	16'	17	17'	18	18'	19	19'	20	20'	21
A	6.25	5.60	6.20	6.05	5.90	6.59	5.05	4.91	5.85	5.70	6.79	4.80	6.60	6.50	5.40	4.96	5.88	5.60	5.84	6.01
A'										5.85										5.93
B										5.48										5.29
B'										5.10										5.07
C										5.32										5.22
C'										4.76										6.51
D										6.88										5.69
D'										5.26										5.05
E										5.40										5.30
E'										5.24										5.46
F										5.21										7.09
F'										5.02										5.44
G										6.66										6.21
G'										4.97										5.09
H										5.11										5.88
H'										6.00										5.79
I										6.63										6.61
I'										6.19										5.20
J										6.33										6.31
J'										6.08										5.54
K										6.19										4.64
K'										7.55										6.29
L										5.84										4.89
L'										6.42										7.32
M	6.72	7.29	6.21	5.28	5.72	5.71	6.20	5.04	5.18	5.57	5.32	5.23	5.49	5.25	6.70	7.31	8.53	5.03	5.77	5.42

Test 38-76-6-NS-SD-31
Nail stand-off in mm

	1	1'	2	2'	3	3'	4	4'	5	5'	6	6'	7	7'	8	8'	9	9'	10	10'	11
A	7.03	5.85	7.23	5.20	5.80	5.38	6.74	5.83	6.04	6.51	8.82	7.11	5.89	8.11	5.52	5.82	5.76	5.83	6.48	5.81	6.67
A'	6.86										5.55										5.88
B	7.19										5.85										7.42
B'	5.83										5.87										4.95
C	5.82										5.16										5.80
C'	5.25										5.37										5.29
D	6.76										6.25										6.40
D'	6.09										5.66										5.82
E	7.15										5.59										5.17
E'	7.28										6.32										6.40
F	5.78										5.28										4.46
F'	6.06										5.48										5.24
G	7.20										6.04										6.51
G'	8.56										5.54										5.92
H	6.08										6.43										5.28
H'	5.77										5.88										5.40
I	6.87										6.87										5.68
I'	5.75										6.12										5.53
J	7.16										6.35										6.96
J'	7.68										6.92										7.58
K	5.95										7.32										5.51
K'	9.01										5.15										6.81
L	6.83										6.97										6.26
L'	7.38										6.35										10.55
M	8.05	11.73	7.30	7.61	6.70	6.05	7.78	5.42	5.29	7.46	5.84	5.05	4.66	5.35	4.87	5.05	5.41	5.12	6.96	6.78	5.58
Ave.	5.96	mm		At sidelaps		6.19	mm		Except sidelaps			5.94	mm								
S.D.	2.12	mm				2.48	mm					2.09	mm								
C.o.V.	0.36					0.40						0.35									

Test 38-76-6-NS-SD-31
Nail stand-off in mm

	11'	12	12'	13	13'	14	14'	15	15'	16	16'	17	17'	18	18'	19	19'	20	20'	21
A	5.80	6.61	6.13	7.02	5.79	4.81	5.22	5.09	5.66	4.77	4.48	4.80	4.72	6.48	4.74	5.63	5.54	5.33	5.36	5.99
A'										6.19										5.00
B										5.87										5.11
B'										6.05										5.55
C										5.78										5.13
C'										5.96										4.80
D										6.60										5.23
D'										5.59										5.09
E										5.05										4.51
E'										5.85										5.45
F										5.71										5.56
F'										5.47										5.38
G										6.58										4.85
G'										5.95										4.96
H										5.88										5.05
H'										6.04										5.33
I										6.09										4.45
I'										5.94										4.49
J										4.72										5.19
J'										5.44										4.28
K										5.57										4.06
K'										5.89										5.12
L										6.15										5.07
L'										7.00										5.87
M	4.88	4.89	4.86	5.79	5.36	5.02	7.04	6.23	5.96	6.35	5.30	4.97	5.39	6.41	6.63	5.26	5.07	5.62	6.02	5.85

Test 38-91-6-NS-M-32
Nail stand-off in mm

	1	1'	2	2'	3	3'	4	4'	5	5'	6	6'	7	7'	8	8'	9	9'	10	10'	11
A	6.50	6.00	5.80	5.74	5.88	6.13	5.17	6.45	5.40	6.37	6.25	5.35	5.93	6.10	7.03	5.91	6.02	6.26	5.68	6.17	5.85
A'	7.15										6.17										6.16
B	7.04										5.38										5.72
B'	7.31										5.97										4.02
C	7.18										5.47										5.72
C'	6.43										6.61										5.79
D	6.35										8.20										8.33
D'	9.69										6.25										6.05
E	6.82										5.93										6.14
E'	6.51										6.97										5.45
F	7.14										7.08										7.30
F'	6.17										6.43										6.19
G	8.39										7.14										6.74
G'	7.94										7.30										6.62
H	8.81										7.11										6.81
H'	5.78										6.41										5.93
I	7.59										7.43										6.29
I'	5.98										5.77										5.57
J	8.05										7.58										7.99
J'	6.73										5.92										6.25
K	6.71										6.50										6.08
K'	6.40										6.44										5.65
L	7.44										6.26										5.64
L'	7.41										10.18										7.90
M	7.45	5.80	6.71	6.10	6.74	6.54	6.66	5.91	7.05	5.52	7.03	6.15	5.51	5.79	6.06	8.01	7.17	5.48	5.26	6.29	6.04
Ave.	6.40	mm		At sidelaps		7.70	mm		Except sidelaps			6.29	mm								
S.D.	2.20	mm				3.06	mm					2.11	mm								
C.o.V.	0.34					0.40						0.34									

Test 38-91-6-NS-M-32
Nail stand-off in mm

	11'	12	12'	13	13'	14	14'	15	15'	16	16'	17	17'	18	18'	19	19'	20	20'	21
A	5.58	6.22	5.94	6.06	5.97	6.02	5.78	5.53	5.72	5.52	5.90	5.39	5.38	5.69	5.26	5.52	6.01	5.94	6.09	6.18
A'										6.84										6.50
B										6.51										6.08
B'										6.00										5.70
C										6.82										5.65
C'										6.42										6.42
D										7.30										6.20
D'										6.40										5.50
E										9.84										5.95
E'										6.59										6.78
F										7.93										6.40
F'										6.30										5.70
G										8.97										9.19
G'										5.71										5.61
H										5.95										5.79
H'										5.63										5.67
I										6.16										7.21
I'										5.99										5.86
J										6.85										8.17
J'										6.17										6.04
K										5.82										5.66
K'										6.33										5.53
L										6.47										5.77
L'										6.92										7.10
M	5.75	6.66	5.24	5.60	6.06	6.67	7.18	6.70	5.63	9.28	5.79	5.83	5.67	5.83	5.73	6.25	5.61	5.83	5.42	7.01

Test 38-91-6-NS-SD-33
Nail stand-off in mm

	1	1'	2	2'	3	3'	4	4'	5	5'	6	6'	7	7'	8	8'	9	9'	10	10'	11
A	6.62	6.39	6.49	6.14	5.86	7.10	6.49	7.00	6.39	6.59	6.53	8.10	6.39	6.06	6.16	6.27	5.95	6.08	6.14	6.32	6.61
A'	7.35										6.53										6.00
B	6.26										6.76										6.74
B'	7.14										6.03										6.55
C	6.87										6.53										8.25
C'	6.08										6.21										6.07
D	7.48										6.26										7.04
D'	6.11										6.74										6.45
E	6.07										6.30										6.33
E'	5.61										6.25										9.04
F	6.53										6.86										7.22
F'	6.64										6.07										6.67
G	6.29										7.61										7.40
G'	7.23										6.23										6.56
H	6.50										6.93										5.83
H'	5.46										7.12										6.58
I	7.27										6.76										6.70
I'	6.97										7.14										6.92
J	7.07										8.87										6.79
J'	5.77										5.92										7.46
K	5.58										6.67										6.55
K'	5.95										6.31										6.73
L	5.94										6.79										6.72
L'	7.04										11.77										6.96
M	6.85	6.17	6.56	5.92	5.82	5.85	5.61	6.77	6.56	6.56	7.19	5.96	6.10	6.83	5.66	6.25	6.01	6.12	5.87	6.09	6.06
Ave.	6.60	mm		At sidelaps		7.25	mm		Except sidelaps			6.55	mm								
S.D.	2.26	mm				2.85	mm					2.21	mm								
C.o.V.	0.34					0.39						0.34									

Test 38-91-6-NS-SD-33
Nail stand-off in mm

	11'	12	12'	13	13'	14	14'	15	15'	16	16'	17	17'	18	18'	19	19'	20	20'	21
A	7.03	6.52	6.02	6.18	6.38	6.05	6.56	5.64	6.00	5.57	7.20	6.33	6.70	6.22	6.84	6.11	7.37	6.81	6.75	7.03
A'										6.48										7.17
B										5.82										6.29
B'										6.20										5.91
C										7.76										5.66
C'										6.37										7.15
D										7.90										6.90
D'										6.51										6.31
E										6.18										5.99
E'										7.00										6.29
F										7.10										7.00
F'										7.00										6.43
G										6.57										7.80
G'										6.31										6.83
H										6.52										5.95
H'										9.24										5.68
I										6.77										6.33
I'										6.38										6.43
J										7.05										7.76
J'										6.31										6.31
K										6.52										5.63
K'										6.04										8.40
L										7.42										6.46
L'										6.75										6.94
M	6.74	5.68	6.34	6.02	13.94	6.76	6.43	6.60	5.55	6.11	6.28	5.63	6.88	5.73	5.49	6.62	6.03	5.56	5.62	7.85

Test 38-91-6-NS-SD-34
Nail stand-off in mm

	1	2	3	4	5	6	7	8	9	10	11	12	13	14	15	16	17	18	19	20	21
A	7.14	7.07	6.41	6.01	6.66	6.32	6.71	6.14	6.83	10.15	6.91	7.56	6.49	7.14	7.09	6.28	6.64	7.10	6.95	6.55	7.62
B	6.91					6.64					6.57					7.21					7.11
C	6.61					6.65					6.60					6.55					6.66
D	7.43					6.54					7.84					8.18					7.52
E	8.26					6.28					7.27					6.88					7.66
F	5.95					6.73					5.96					6.45					6.46
G	7.50					10.38					7.93					9.00					7.02
H	6.06					6.38					7.14					6.65					6.54
I	7.10					6.78					7.42					6.89					6.87
J	8.35					9.05					7.55					10.94					6.82
K	6.81					7.11					7.13					6.93					6.16
L	6.09					6.58					6.37					6.50					8.01
M	8.71	6.02	6.03	5.97	6.09	6.06	6.26	6.14	6.19	6.40	6.90	5.77	7.32	5.98	6.24	7.24	7.41	6.47	6.88	5.85	8.36
Ave.	6.98	mm		At sidelaps		Ave.	8.14	mm		Except sidelaps			Ave.	6.77	mm						
S.D.	0.94	mm				S.D.	1.25	mm					S.D.	0.69	mm						
C.o.V.	0.13					C.o.V.	0.15						C.o.V.	0.10							

Test 38-91-6-NS-LD-35
Nail stand-off in mm

	1	2	3	4	5	6	7	8	9	10	11	12	13	14	15	16	17	18	19	20	21
A	7.19	6.97	6.60	6.55	5.77	6.88	6.82	7.06	6.47	7.67	6.26	6.40	6.86	6.42	6.42	6.86	6.35	6.57	6.93	6.66	8.03
B	7.09					6.66					6.21					6.19					5.94
C	6.61					6.55					6.23					6.59					6.06
D	7.52					7.14					6.41					7.40					7.28
E	6.80					6.34					6.72					6.66					5.80
F	6.94					6.07					6.22					10.55					5.41
G	7.21					7.31					7.62					7.33					6.35
H	6.88					6.13					6.17					5.87					5.24
I	10.87					7.26					6.82					6.55					5.78
J	7.16					6.90					7.90					6.75					9.34
K	9.34					6.92					11.12					6.10					6.46
L	6.05					6.12					6.45					6.60					6.16
M	10.78	6.36	6.44	6.84	6.79	6.96	7.52	7.25	7.37	7.47	7.28	5.68	6.20	7.21	6.86	5.68	6.61	11.66	5.87	6.23	7.56
Ave.	6.93	mm		At sidelaps		Ave.	7.31	mm		Except sidelaps			Ave.	6.86	mm						
S.D.	1.17	mm				S.D.	0.70	mm					S.D.	1.22	mm						
C.o.V.	0.17					C.o.V.	0.10						C.o.V.	0.18							

APPENDIX F

WELD DIMENSIONS

This Appendix presents the weld dimensions for all of diaphragm test specimens with welded deck-to-frame connections. The average weld dimensions for each test specimens are listed in Table F.1. On the following pages, the measured weld dimensions for each connection are shown. Two types of welds were present and measured: typical round welds and welds at sidelap (slotted welds). Figure F.1 presents a schematic of the dimensions measured for the two types of welds. The weld limits are not regular, thus the dimensions given are the dimensions deemed average by the author.

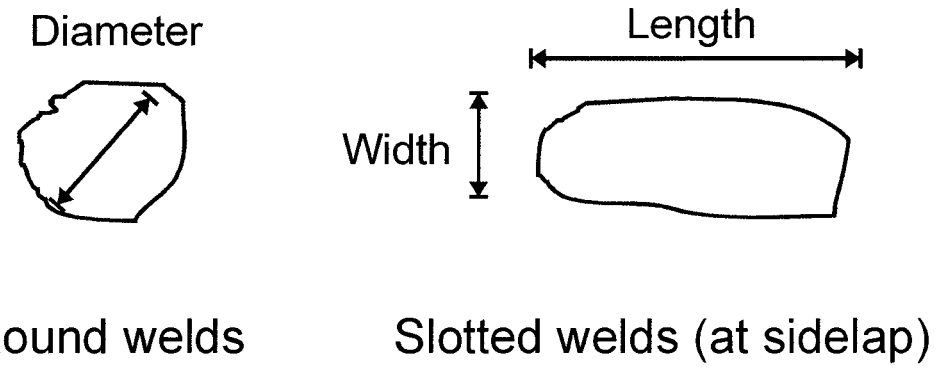

Figure F.1 Schematic of the measured dimensions

Table F.1: Weld dimensions in test specimens

Test	Round welds		Slotted welds			
	Diameter (mm)		Length (mm)		Width (mm)	
	Average	CoV	Average	C.o.V.	Average	C.o.V.
38-91-6-WB-M-37	16.6	0.03	18.0	0.00	10.0	0.00
38-91-6-WB-SD-21	16.1	0.06	20.0	0.25	10.0	0.00
38-76-6-WB-SD-20	16.1	0.04	22.5	0.12	10.0	0.00
38-76-6-WB-SD-36	16.5	0.08	15.3	0.05	10.0	0.00

Test 38-91-6-WB-M-37 Weld dimensions

Diameter
Circular welds only
Welds not located at sidelaps

	1	2	3	4	5	6	7	8	9	10	11	12	13	14	15	16	17	18	19	20	21
A																					
B																					17
C						16															16
D																					
E											16										
F											16										
G																					
H																					
I																					
J																					
K																17					17
L																17					17
M																					
Ave.	16.6																				
S.D.	0.53																				
C.O.V.	0.03																				

Length
Welds located at sidelaps

	1	2	3	4	5	6	7	8	9	10	11	12	13	14	15	16	17	18	19	20	21
A																					
B																					
C																					
D						18															18
E																					
F																					
G											18										18
H																					
I																					
J																					
K																					
L																					
M																					
Ave.	18.0																				
S.D.	0.00																				
C.O.V.	0.00																				

Width
Welds located at sidelaps

	1	2	3	4	5	6	7	8	9	10	11	12	13	14	15	16	17	18	19	20	21
A																					
B																					
C																					
D						10															10
E																					
F																					
G											10										10
H																					
I																					
J																					
K																					
L																					
M																					
Ave.	10.0																				
S.D.	0.00																				
C.O.V.	0.00																				

Test 38-91-6-WB-SD-21 Weld dimensions

Diameter
Circular welds only
Welds not located at sidelaps

	1	2	3	4	5	6	7	8	9	10	11	12	13	14	15	16	17	18	19	20	21
A																					
B	17										15										15
C						16					17										16
D																					
E						18					15					16					
F											15										
G																					
H																					16
I	16					17										16					15
J																					
K																15					
L	17					18										15					
M																					
Ave.	16.1																				
S.D.	1.03																				
C.O.V.	0.06																				

Length
Welds located at sidelaps

	1	2	3	4	5	6	7	8	9	10	11	12	13	14	15	16	17	18	19	20	21
A																					
B																					
C																					
D						25															15
E																					
F																					
G																					
H																					
I																					
J																20					
K																					
L																					
M																					
Ave.	20.0																				
S.D.	5.00																				
C.O.V.	0.25																				

Width
Welds located at sidelaps

	1	2	3	4	5	6	7	8	9	10	11	12	13	14	15	16	17	18	19	20	21
A																					
B																					
C																					
D						10															10
E																					
F																					
G																					
H																					
I																					
J																10					
K																					
L																					
M																					
Ave.	10.0																				
S.D.	0.00																				
C.O.V.	0.00																				

Test 38-76-6-WB-SD-20 Weld dimensions

Diameter
Circular welds only
Welds not located at sidelaps

	1	2	3	4	5	6	7	8	9	10	11	12	13	14	15	16	17	18	19	20	21
A																					
B	16					17										16					
C	16					15					16					17					
D																					
E											16					16					
F																					
G																					
H						16															
I	16					16															
J																					
K	15										17					16					
L	16					15					17										
M																					
Ave.	16.1																				
S.D.	0.64																				
C.O.V.	0.04																				

Length
Welds located at sidelaps

	1	2	3	4	5	6	7	8	9	10	11	12	13	14	15	16	17	18	19	20	21
A						25			20												
B																					
C																					
D																25					
E																					
F																					
G	20																				
H																					
I																					
J											25										
K																					
L																					
M						20															
Ave.	22.5																				
S.D.	2.74																				
C.O.V.	0.12																				

Width
Welds located at sidelaps

	1	2	3	4	5	6	7	8	9	10	11	12	13	14	15	16	17	18	19	20	21
A						10			10												
B																					
C																					
D																10					
E																					
F																					
G	10																				
H																					
I																					
J											10										
K																					
L																					
M						10															
Ave.	10.0																				
S.D.	0.00																				
C.O.V.	0.00																				

Test 38-76-6-WB-SD-36 Weld dimensions

Diameter
Circular welds only
Welds not located at sidelaps

	1	2	3	4	5	6	7	8	9	10	11	12	13	14	15	16	17	18	19	20	21
A																					
B	16					15					15					16					18
C	16					15					17					15					18
D																					
E	15					17					15					17					17
F	15					17					17					18					18
G																					
H	15					17					15					16					16
I	15					17					17					16					18
J																					
K	15					16					18					16					20
L	15					16					17					17					20
M																15					18
Ave.	16.5																				
S.D.	1.35																				
C.O.V.	0.08																				

Length
Welds located at sidelaps

	1	2	3	4	5	6	7	8	9	10	11	12	13	14	15	16	17	18	19	20	21
A																15					15
B																					
C																					
D						15					15					15					18
E																					
F																					
G	15					15					15					15					15
H																					
I																					
J	16					15					15					15					16
K																					
L																					
M																					
Ave.	15.3																				
S.D.	0.79																				
C.O.V.	0.05																				

Width
Welds located at sidelaps

	1	2	3	4	5	6	7	8	9	10	11	12	13	14	15	16	17	18	19	20	21
A																					
B																					
C																					
D						10				10						10					10
E																					
F																					
G	10					10				10						10					10
H																					
I																					
J	10					10				10						10					10
K																					
L																					
M																					
Ave.	10.0																				
S.D.	0.00																				
C.O.V.	0.00																				